

SOLAR-HYDROGEN COMBINED HEAT AND POWER SYSTEMS FOR REMOTE AREA POWER SUPPLY

**A thesis submitted in fulfilment of the requirements for the degree of
Doctor of Philosophy**

Bahman Shabani
M.Sc. Eng.

School of Aerospace, Mechanical and Manufacturing Engineering
College of Science, Engineering and Health
RMIT University
July 2010

Dedicated to my wife, Nafise, for her loving support

ACKNOWLEDGMENTS

This PhD program was a fantastic opportunity for me to engage with high calibre individuals at RMIT University. In particular, the invaluable guidance and advice given by my first supervisor, Associate Professor John Andrews, were the most precious part of the program that truly defies description. I would like to extend my utmost gratitude to him wholeheartedly for all his kind and continuous support, encouragement, mentorship and friendship. My special thanks goes to Professor Simon Watkins my second supervisor for all his encouragement and valuable comments, particularly in completion of this dissertation. He was my first point of contact to RMIT and I would always remember him for changing my life journey in the best possible way. I was also honoured to be advised by Professor Aliakbar Akbarzadeh from RMIT University, who is a highly-recognised and globally-distinguished expert in the area of renewable energy. His exemplary kind and friendly character, etched in his face, gives you a lovely first impression as if he is an old friend from the past. My special thanks also goes to Dr Sukhvinder Badwal, Chief Research Scientist, CSIRO Energy Technology, for his valuable support and his fruitful comments on preparing this dissertation and the associated papers.

I would also express my loving appreciation to the angel of my life, my wife, Nafise Parsapour for her unconditional support, patience, and self-abnegation. She has always proven to be the friend of my rainy days and not only a fair-weather friend.

I also like to thank the staff of workshop at RMIT Bundoora East Campus, in particular Patrick Wilkins and David Goodie, who greatly helped me in construction and installation of the experimental rig used for this study. My salute to my fellow researchers at RMIT Energy CARE group: particularly Bidyut Paul, Randeep Singh, Abhijit Date, Arum Kumar Doddathimmaiah, and Suhaib Ali for their support and sharing of their knowledge with me.

I am indebted to the CSIRO for financial support for this project including my PhD scholarship within the National Hydrogen Materials Alliance by the CSIRO Flagship Collaboration Fund under the Energy Transformed Flagship Award.

DECLARATION

I, Bahman Shabani, hereby submit the thesis entitled “Solar-Hydrogen Combined Heat and Power Systems for Remote Area Power Supply” for the degree of Doctor of Philosophy, and certify that except where due acknowledgement has been made, the work is that of the author alone; the work has not been submitted previously, in whole or in part, to qualify for any other academic award, and the content of the thesis is the result of work that has been carried out since the official commencement date of the approved research program.

Bahman Shabani
July 2010

TABLE OF CONTENTS

ACKNOWLEDGMENTS	III
DECLARATION	IV
TABLE OF CONTENTS	V
ACRONYMS	IX
NOMENCLATURE	XI
LIST OF FIGURES	XV
LIST OF TABLES	XXIII
EXECUTIVE SUMMARY	XXVI
PUBLICATIONS FROM THIS RESEARCH PROGRAM	XXXVI
1 INTRODUCTION	1
1.1 Background.....	1
1.1.1 The problems with fossil fuels.....	1
1.1.2 Fossil fuels and Australia.....	3
1.1.3 Renewable energy as an alternative to fossil fuels	5
1.1.4 Australia’s support for renewable energy	6
1.1.5 Hydrogen as the prospective energy store and carrier for renewable energy	7
1.2 Solar-hydrogen systems.....	10
1.2.1 Solar-hydrogen generation.....	10
1.2.2 Stand-alone solar-hydrogen systems	12
1.2.3 Hurdles facing solar-hydrogen systems	14
1.3 Solar-hydrogen CHP system	16
1.4 Objectives and scope of the thesis	17
1.4.1 Objectives	17
1.4.2 Scope of thesis	18
1.5 Research questions	19
1.6 Method.....	20
1.7 Outcomes	21
1.8 Thesis structure.....	23
2 SOLAR-HYDROGEN CHP SYSTEMS FOR RAPS	24
2.1 Introduction	24
2.2 Hydrogen as an alternative energy storage in PV-based RAPS	25
2.3 Solar-hydrogen systems for RAPS	27
2.3.1 The basic solar-hydrogen system for RAPS	27
2.3.2 Current state of development of solar-hydrogen systems.....	29
2.3.2.1 Modelling and demonstration	29
2.3.2.2 System modelling	30
2.3.2.3 System Demonstration.....	35
2.3.2.4 Challenges facing solar-hydrogen RAPS systems.....	37
2.4 Solar-hydrogen CHP systems	40
2.4.1 The origin of the idea.....	40
2.4.2 History and state of the art review	40
2.5 Focus of this thesis	44
3 SYSTEM MODELLING	46
3.1 Introduction	46
3.1.1 Aims.....	46
3.1.2 The major features of the model.....	46
3.2 The overall structure of the model.....	48
3.3 Solar geometry and PV modelling.....	51
3.3.1 Terminology	51

3.3.2	The basic solar geometry used in the model	51
3.3.3	PV module modelling	54
3.3.3.1	Key parameters	54
3.3.3.2	PV sub-model description	56
3.3.3.3	PV sub-model validation	65
3.4	Hydrogen storage modelling	68
3.5	Fuel cell modelling	70
3.5.1	Fuel cell reaction.....	70
3.5.2	Reactant flow rates	70
3.5.3	Maximum EMF and open circuit voltage	73
3.5.4	Modified Butler-Volmer equations.....	78
3.5.5	Fuel cell heat generation and CHP concept.....	86
3.5.6	PEM fuel cell water management and relative humidity.....	88
3.6	Electrolyser modelling.....	91
3.7	Solar-hydrogen system analysis and sizing	92
3.7.1	An overview of system sizing.....	92
3.7.2	Solar-hydrogen system sizing for an unconstrained hydrogen storage.....	94
3.7.3	Solar-hydrogen system sizing for a constrained hydrogen storage.....	97
3.8	Modelling system economics	101
4	USE OF MODEL FOR A CASE STUDY OF A SOLAR-HYDROGEN COMBINED HEAT AND POWER SYSTEM.....	102
4.1	An introduction to the case study	102
4.1.1	Location	102
4.1.2	Electrical demand profile.....	102
4.1.3	Solar irradiance profile	103
4.1.4	Wind speed and ambient temperature profiles	104
4.2	System components used in the case study	105
4.2.1	BP275 PV module and its performance.....	105
4.2.2	StaXX 7 electrolyser and its performance	107
4.2.3	500 W PEM fuel cell and its performance.....	108
4.3	System sizing and economy	110
4.3.1	Minimum size of fuel cell, unconstrained hydrogen storage.....	110
4.3.2	Minimum size of fuel cell, constrained hydrogen storage.....	117
4.3.3	System optimisation based on unit cost of electricity.....	121
4.3.3.1	Cost minimisation.....	121
4.3.3.2	Load management	121
4.3.3.3	Oversized fuel cell condition.....	125
4.3.3.4	Sensitivity analysis	129
4.4	Solar-hydrogen CHP system	135
4.4.1	Potential for conversion to a CHP system	135
4.4.2	Cumulative annual fuel cell cooling load	140
4.4.2.1	Cooling load with minimum fuel cell size.....	140
4.4.2.2	Cooling load with optimal fuel cell size	141
4.4.2.3	Cooling load: system with unconstrained/constrained tank	143
4.4.2.4	Cooling load and electrical load management in the solar-hydrogen system.....	144
4.4.3	Using fuel cell heat and excess hydrogen for domestic hot water supply	145
4.4.3.1	System configuration.....	145
4.4.3.2	Assumptions	145
4.4.3.3	Results	147
4.4.4	System optimisation based on overall economics of CHP system	150
4.5	Conclusion.....	152
5	EXPERIMENTAL INVESTIGATION INTO A FUEL CELL COMBINED HEAT AND POWER SYSTEM	155
5.1	Introduction	155

5.2	Experimental setup	155
5.2.1	Overall system studied.....	155
5.2.2	Hydrogen supply line.....	157
5.2.2.1	Overall plan	157
5.2.2.2	Hydrogen bottle	157
5.2.2.3	Piping and fittings.....	158
5.2.2.4	Safety setup	158
5.2.2.5	Measuring instruments	164
5.2.3	Air line	166
5.2.3.1	Overall plan	166
5.2.3.2	Air compressor	166
5.2.3.3	Air bottle.....	167
5.2.3.4	Piping and connectors.....	167
5.2.3.5	Gas dryer	167
5.2.3.6	Regulator, measurement, and monitoring instrument.....	168
5.2.4	Cooling system	170
5.2.4.1	Overall plan	170
5.2.4.2	Water pump	171
5.2.4.3	Heat exchanger	171
5.2.4.4	Measurement instrument	172
5.2.4.5	Reserve tank	174
5.2.4.6	Tubing, valves, and connectors	175
5.2.4.7	Insulation	175
5.2.5	Fuel cell	176
5.2.5.1	General introduction.....	176
5.2.5.2	Manufacturer's polarisation curve.....	178
5.2.5.3	Air flow rates.....	178
5.2.6	Electronic load.....	179
5.3	Method.....	179
5.3.1	An overview on the experimental plan and procedure	179
5.3.2	Restrictions imposed by the measurement instruments	182
5.3.3	Uncertainties associated with the experimental measurements	183
5.4	Experimental results and analysis.....	185
5.4.1	Polarisation curve	185
5.4.2	Cooling load curve.....	186
5.4.3	The effect of operating temperature and air stoichiometry on cooling load and power 189	
5.4.4	Energy efficiency and fuel utilisation coefficient.....	197
5.4.5	Solar-hydrogen CHP system overall energy efficiency.....	199
5.4.6	Rerunning the model using the experiment fuel cell polarisation curve.....	201
5.5	Conclusions	202
6	COMPARISON OF A SOLAR-HYDROGEN CHP SYSTEM WITH OTHER ALTERNATIVES	205
6.1	Introduction	205
6.2	System arrangement, sizing and operation	206
6.2.1	Solar-hydrogen system alone and with CHP	206
6.2.2	ICE generators	208
6.2.3	Solar PV-battery-ICE generator systems.....	209
6.2.4	Solar- hydrogen-battery system.....	211
6.3	Triple bottom line comparison	213
6.3.1	Economics.....	213
6.3.2	Environmental.....	217
6.3.3	Social	220
6.4	Conclusion.....	221

7	CONCLUSIONS AND RECOMMENDATIONS	224
7.1	Response to the research questions	224
7.1.1	Introduction.....	224
7.1.2	What are the main factors affecting the performance of solar-hydrogen CHP system? 224	
7.1.3	To what extent can the overall energy efficiency and hence economic viability of a solar-hydrogen system for remote applications be improved by utilising the waste heat from fuel cell operation for water or space heating?.....	226
7.1.4	What is the economically-optimal size of a solar-hydrogen CHP system for a remote household with given electrical and hot water demand?.....	228
7.1.5	How does a solar-hydrogen CHP system compare on a triple bottom line basis with conventional alternatives?	229
7.1.5.1	Economic benefits	229
7.1.5.2	Environmental benefits.....	231
7.1.5.3	Social benefits	231
7.1.6	Which components of a solar-hydrogen CHP system require further research and development to enable such systems to compete with conventional alternatives?.....	232
7.2	Conclusions	235
7.3	Recommendations	242
	REFERENCES	245
	APPENDICES	259
	APPENDIX 1: THE RSHAP USER MANUAL	260
	APPENDIX 2: EXPERIMENTAL MEASUREMENTS, 500 W BCS PEM FUEL CELL	311
	APPENDIX 3: EQUIPMENT DATASHEETS	359
	APPENDIX 4: SOLAR GEOMETRY ANGLES	363
	APPENDIX 5: THERMODYNAMIC PROPERTIES AS FUNCTIONS OF TEMPERATURE	364
	APPENDIX 6: ERROR ANALYSIS	365
	APPENDIX 7: COMPONENTS USED IN THE 500-W FUEL CELL EXPERIMENTAL RIG	369

ACRONYMS

<i>A</i>	Amp
<i>AFC</i>	Alkaline Fuel Cell
<i>BOM</i>	Bureau Of Metrology
<i>BV</i>	Butler Volmer
<i>BCSE</i>	BCSE Business Council for Sustainable Energy
<i>CHP</i>	Combined Heat and Power
<i>CNG</i>	Compressed Natural Gas
<i>DOE</i>	Department of Energy
<i>DMFC</i>	Direct Methanol Fuel Cell
<i>EMF</i>	Electromotive Force
<i>EIA</i>	Energy Information Administration
<i>EXP</i>	Experimental
<i>FC</i>	Fuel Cell
<i>GHG</i>	Greenhouse gas
<i>HHV</i>	High Heating Value
<i>HT-PEMFC</i>	High Temperature PEM Fuel Cell
<i>ICE</i>	Internal Combustion Engine
<i>IEA</i>	International Energy Agency
<i>IPCC</i>	Intergovernmental Panel on Climate Change
<i>IASTED</i>	The International Association of Science and Technology for Development
<i>LPG</i>	Liquid Propane Gas
<i>LAB</i>	Lead Acid Battery
<i>MRET</i>	Mandatory Renewable Energy Target
<i>MPPT</i>	Maximum Power Point Tracker
<i>MCFC</i>	Melton Carbonate Fuel Cell
<i>MP</i>	Maximum Power
<i>MHCoE</i>	Metal Hybrid Centre of Excellence
<i>Mod</i>	Model
<i>MSDS</i>	Material Safety Data Sheet
<i>Nm³</i>	Normal Cubic Metre; measured at 1 atm and 273.15 °K
<i>NPV</i>	Net Present Value
<i>OC</i>	Open Circuit
<i>O&M</i>	Operation and Maintenance
<i>OCV</i>	Open Circuit Voltage
<i>ORER</i>	Office of the Renewable Energy Regulator
<i>PAFC</i>	Phosphoric Acid Fuel Cell
<i>PEM</i>	Proton Exchange Membrane

<i>PV</i>	Photovoltaic
<i>PVC</i>	Polyvinyl Chloride
<i>RAPS</i>	Remote Area Power Supply
<i>RAD</i>	Rapid Application Development
<i>REL</i>	Renewable Energy Laboratory
<i>RH</i>	Relative Humidity
<i>RSHAP</i>	RMIT Solar-Hydrogen Analysis Program
<i>SC</i>	Short Circuit
<i>SI</i>	Spark Ignition
<i>slpm</i>	Standard Litre Per Minute
<i>SOFC</i>	Solid Oxide Fuel Cell
<i>STC</i>	Standard test Condition
<i>TBL</i>	Triple Bottom Line
<i>URFC</i>	Unitised Regenerative Fuel Cell
<i>V</i>	Volt
<i>VCL</i>	Visual Component Library
<i>WELS</i>	Water Efficiency Labelling and Standards

NOMENCLATURE

A	Completion factor
a_p	Array azimuth angle
\bar{c}_p	Molar specific heat
C_p	Thermal capacity
D	Diode diffusion factor
Day	Number of days (counted from 1 Jan)
f	Modulation function
E	Modified maximum electromotive motive force (EMF)
EC_i	Energy content factor of fuel type (i) (gigajoules per kilolitre)
EF_{ijoxec}	Emission factor for each gas type (j) (which includes the effect of an oxidation factor) for fuel type (i) (kilograms CO ₂ -e per gigajoule)
E_0	Maximum electromotive motive force (EMF)
E_{ij}	Emissions of gas type (j), (carbon dioxide, methane or nitrous oxide), from fuel type (i) (CO ₂ -e kg)
F	Faraday constant, 96485 Coulomb/mol
G	Radiation
\bar{g}_f	Gibbs free energy
$\bar{g}_{f,T}$	Gibbs free energy at temperature of T
$G_{dif,tilt}$	Diffused radiation on the tilted surface
G_d	Direct radiation
G_H	Horizontal radiation
$G_{H,total}$	Total global irradiance on the horizontal surface
G_p	Normal radiation
$G_{refl,tilt}$	Ground reflection on the tilted surface
H	Enthalpy
\bar{h}_f	Enthalpy of formation
$\bar{h}_{f,T}$	Enthalpy of formation at temperature of T
I	Photovoltaic cell current
I_0	Reverse diode saturation current
I_D	Diode current
J	Fuel cell/electrolyser current
j	Fuel cell/Electrolyser current density (current divided by membrane effective area)

j_0	Exchange current density
I_L	Light current
k	Boltzmann constant, 1.31×10^{-23} (J/K)
L	Local latitude angle/membrane thickness
V	Voltage
m	Mass
\dot{m}	Hydrogen/oxygen mass flow rate
M	Molar mass
n	Number of cell in a/an fuel cell/electrolyser stack/Number of measurements
N	Number of consumed moles of hydrogen or oxygen
N_A	Avogadro's Number 6.022×10^{23}
NP	Number of PV modules in parallel
NS	Number of PV modules in series
NCS	Number of cells in series
P	Power/Pressure
q	Electron charge 1.602×10^{-19} (C)
Q	Electrical charge
\dot{Q}	Heat generation/transfer rate
Q_i	Quantity of type (i) (kilolitre) combusted for stationary energy purposes
R	Universal gas constant
R_e^O	Oxygen electrode ohmic resistance against flow of electrons
R_e^H	Hydrogen electrode ohmic resistance against flow of electrons
$R_m^{H^+}$	Membrane resistance against hydrogen ions
R_S	Series resistance of the PV module
$R_{s,tot}$	Total series resistance of the PV array
S	Membrane effective area
\bar{s}	Molar entropy
\bar{s}_T	Molar entropy at temperature T
T	Temperature
t	Time
u	Standard deviation of the mean

x	An experimentally-measured value
\bar{x}	Mean of a set of experimentally-measured values

Greek Symbols

δ	Declination angle
α	Solar altitude angle/Charge transfer coefficient
β	Array tilt angle
ω	Hour angle/ Humidity ratio
γ	Shape factor
γ_e	Total electrode resistance per unit area
θ_i	Incidence angle
ε_G	Material band gap energy
λ	Stoichiometry factor
η	Efficiency/Activation overpotential
φ	Relative humidity
μ_{VOC}	Open circuit voltage temperature coefficient
μ_{ISC}	Short circuit current temperature coefficient
μ_f	Hydrogen utilisation coefficient /Faraday efficiency
$\rho_m^{H^+}$	Membrane's specific resistance to the ions
$\sigma_m^{H^+}$	Electrical conductivity of the membrane to ionic current
$\sigma_m^{e^-}$	Electrical conductivity of the membrane to electron current

Subscripts and superscripts

<i>air</i>	Air
<i>exp</i>	Experimental
<i>w</i>	Water
<i>C</i>	Photovoltaic cell
<i>Cell</i>	Fuel cell/electrolyser cell
<i>E</i>	Electrolyser
<i>FC</i>	Fuel cell
<i>max</i>	Maximum
<i>min</i>	Minimum

<i>mod</i>	Model
<i>O</i>	Oxygen side
<i>H</i>	Hydrogen side
<i>hydrogen</i>	Hydrogen
<i>OC</i>	Open circuit
<i>SC</i>	Short circuit
<i>ref</i>	Reference condition (also called standard test condition)
<i>tot</i>	Total
<i>int</i>	Internal

LIST OF FIGURES

Figure 1-1. World energy consumption, history and projections (IEA 2009)	1
Figure 1-2. Historical trends for the price of crude oil (IEA 2009)	2
Figure 1-3. The history of annual carbon dioxide production from fossil fuels (IEA 2009)	2
Figure 1-4. Global mean temperature rising (IPCC 2007)	3
Figure 1-5. The history of oil production and consumption in Australia (EIA 2009)	4
Figure 1-6. The history of coal production and consumption in Australia (EIA 2009)	4
Figure 1-7. World electricity generation by fuel (EIA 2009)	5
Figure 1-8. Prediction of global electricity generation from hydrogen-based fuel cells (Barreto <i>et al.</i> 2003) .	10
Figure 1-9. The simple schematic of the solar-hydrogen system diagram used in the study conducted by Shapiro, Duffy <i>et al.</i> (2005).....	12
Figure 2-1. Simplefied schematic of a typical solar-hydrogen system (Shabani <i>et al.</i> 2010).....	28
Figure 2-2. Stand-alone solar-hydrogen system investigated by Santarelli and Macagno (2004).....	33
Figure 2-3. PEM fuel cell CHP configuration suggested by Ferguson and Ismet Ugursal (2004) for supplying both heat and power demand of a building.....	42
Figure 2-4. Use of fuel cell heat to discharge hydrogen from a metal hydride (Varkaraki <i>et al.</i> 2003)	43
Figure 2-5. Modelling of PEM fuel cell including thermal coupling between the fuel cell stack and hydrogen metal hydride storage tank done by Graf <i>et al.</i> (2006)	43
Figure 3-1. An overview on the structure of the model (RSHAP)	49
Figure 3-2. The main panel of the solar-hydrogen modelling tool, RSHAP	50
Figure 3-3. Solar-hydrogen system analysis panel	50
Figure 3-4. From left to right: PV cell, PV module, and PV array	51
Figure 3-5. Equivalent electrical circuit of a PV module used for PV modelling (Chenni <i>et al.</i> 2007)	56
Figure 3-6. The procedure of finding series resistance, shape factor, completion factor, and reference reverse diode saturation current of a PV module	62
Figure 3-7. The procedure of finding current and voltage at the maximum power point of a PV module	63
Figure 3-8. The PV sub-model output, showing the effect of cell's temperature on the performance of a PV array of 4 BP275 modules receiving 880 W/m ² irradiance	65
Figure 3-9. The PV sub-model output showing the effect of irradiance on the performance of a BP275 PV module while its temperature is assumed to be kept at 40 °C	65
Figure 3-10. Experimental and model power curves for a BP SX320 module at 40 °C cell temperature and 945 W/m ² irradiance (left) BP SX320 module (right)	66
Figure 3-11. Theoretical analysis showing the effect of temperature on the maximum power point of an array of four BP275 modules while receiving 880 W/m ² incident solar irradiance.....	68
Figure 3-12. Hydrogen density estimation as a function of pressure using different equations of state (DOE 2001).....	69
Figure 3-13. The effect of temperature on reversible open circuit voltage of a single-cell fuel cell as predicted by the model	76
Figure 3-14. Fuel cell inlet and exit air and hydrogen stream	77
Figure 3-15. The effect of hydrogen supply pressure on the reversible open circuit voltage of a fuel cell performance (32-cell 500 W PEM BCS fuel cell stack) using the Nernst equation in the fuel cell model	78
Figure 3-16. Typical voltage drop trend in a fuel cell (polarisation curve)	78
Figure 3-17. Equivalent circuit of a fuel cell used for applying the BV equations in fuel cell modelling.....	81
Figure 3-18. The typical effect of temperature on PEM fuel cell polarisation curve; theoretical analysis using modified Butler-Volmer equations; operating condition as shown in table 3-3; temperatures are all in °C.....	83
Figure 3-19. Least squares method used for curve fitting	85
Figure 3-20. An example to show fuel cell polarisation curve fitting using the least squares method and Butler-Volmer equations; operating condition as given in table 3-3; saturation current density 0.6 A/cm ²	85
Figure 3-21. PEM fuel cell performance and relative humidity (Zhang <i>et al.</i> 2008).....	89
Figure 3-22. Membrane conductivity as a function of current density (Zhang <i>et al.</i> 2008)	89
Figure 3-23. Equivalent circuit of an electrolyser used for applying the Butler-Volmer equations in electrolyser modelling (Doddathimmaiah and Andrews 2008)	92
Figure 3-24. Solar-hydrogen system sizing procedure for unconstrained hydrogen tank.....	96
Figure 3-25. Typical annual variation of hydrogen stored in an unconstrained tank in a solar-hydrogen system	97
Figure 3-26. Solar-hydrogen system sizing procedure for constrained hydrogen tank.....	99
Figure 3-27. Part 'B'. Solar-hydrogen system sizing procedure for a constrained hydrogen tank	100
Figure 3-28. Typical annual variation of hydrogen level in a constrained tank in a solar-hydrogen system..	101
Figure 4-1. Demand profile used for the case study (Ali 2007)	103

Figure 4-2. Irradiance on the surface tilted at local latitude of Melbourne (38.7°- South).....	104
Figure 4-3. BP 275 modules at RMIT Renewable Energy Laboratory (REL), RMIT Bundoora East Campus	106
Figure 4-4. Power input and predicted output for a BP275 module (half-hourly) based on Melbourne irradiance, ambient temperature and wind speed profile	107
Figure 4-5. StaXX 7 PEM electrolyser (left) from Fuel cell store website (Fuelcellstore 2009)-typical polarisation (V-I) curve of a PEM electrolyser (right); the characteristics curve (right) is an experimental measurement done by Paul and Andrews (2008) on StaXX 7 PEM electrolyser stack.....	107
Figure 4-6. Comparing the theoretical (using Butler-Volmer equations) and experimental P-I curves of the 50W StaXX7 PEM electrolyser stack.....	108
Figure 4-7. 500 W PEM BCS fuel cell stack (BCS 2009).....	109
Figure 4-8. 500 W PEM BCS fuel cell polarisation curve (BCS 2009)	109
Figure 4-9. 500 PEM BCS theoretical polarisation curve fitted on the experimental curve using least-squares method and based on the Butler-Volmer equations.....	110
Figure 4-10. Solar-hydrogen system sizing results (for fuel cell minimum size and unconstrained tank)	111
Figure 4-11. Case study: annual hydrogen production rate by the electrolyser; unconstrained tank and minimum fuel cell size	113
Figure 4-12. Case study: annual hydrogen level variation in the tank (half hourly basis); unconstrained tank and minimum fuel cell size.....	115
Figure 4-13. Case study: An example to show the short-term hydrogen variation (end of July); unconstrained tank and minimum fuel cell size.....	115
Figure 4-14. The detail of cost analysis on the solar-hydrogen system, with minimum size of the fuel cell and unconstrained tank.....	116
Figure 4-15. The effect of constrained size of hydrogen tank on the PV array size	118
Figure 4-16. The effect of using constrained hydrogen tank on the electrolyser size and its total annual hours of operation.....	118
Figure 4-17. The detail of cost analysis of the solar-hydrogen system when the minimally-sized fuel cell (~0.3 kW) and a 3-kg constrained hydrogen tank are used	118
Figure 4-18. Case study: annual hydrogen level variation in a 3-kg constrained hydrogen tank	119
Figure 4-19. Case study: non-utilised capacity of electrolyser when using constrained hydrogen tank.....	120
Figure 4-20. Changing the peak of the daily load profile while the total daily demand remains constant (Shabani <i>et. al.</i> 2009).....	121
Figure 4-21. Case study: the effect of varying the peak demand on the size of the components	122
Figure 4-22. Case study: the effect of varying the peak demand on the overall cost of the system	122
Figure 4-23. Case study: the effect of peak load on the average annual electrical energy efficiency of the fuel cell (based on minimum size of fuel cell required)	123
Figure 4-24. The effect of using uniform demand profile and avoiding the peak load (unconstrained tank and minimum fuel cell sizing strategy was applied)	124
Figure 4-25. The effect of load profile scale on the system's overall sizing and economy (Shabani <i>et. al.</i> 2009).....	124
Figure 4-26. The effect of the fuel cell size on the average annual efficiency of this component when it is operated in the system of the case studied.....	126
Figure 4-27. The effect of the fuel cell size on the size of the PV array.....	126
Figure 4-28. Left: The effect of fuel cell size on the size of the electrolyser; right: the effect of the fuel cell size on the size of the storage tank	126
Figure 4-29. Left: The effect of the fuel cell size on the unit cost of the electricity (the idea of the fuel cell optimum size); right: The details of cost analysis on the solar-hydrogen system when the optimally-sized fuel cell, 1 kW, and unconstrained tank were used.....	127
Figure 4-30. Solar-hydrogen system sizing results (for the optimally-sized fuel cell and unconstrained tank)	128
Figure 4-31. The effect of financial assumptions on the unit cost of electricity (left: the effect of discount rate in an assessment period of 30 years right: the effect of assessment period at the discount rate of 5%)	130
Figure 4-32. The effect of cost assumptions for the major components of the system on the unit cost of electricity generated; the future price and the maintenance costs are assumed to be varied proportionately; the cost of one component varies at a time and the costs of the others are based on table 4-5.....	131
Figure 4-33. The effect of components' lifetime assumptions on the unit cost of electricity	132
Figure 4-34. The effect of hydrogen stoichiometry on the PV array size in the case study (5 kWh daily demand peaked at 0.3 kW in south-eastern Australia)	133
Figure 4-35. The effect of hydrogen stoichiometry on the hydrogen tank size in the case study (5 kWh daily demand peaked at 0.3 kW in south-eastern Australia)	134

Figure 4-36. The effect of hydrogen stoichiometry on the electrolyser size in the case study (5 kWh daily demand peaked at 0.3 kW in south-eastern Australia)	134
Figure 4-37. The effect of hydrogen stoichiometry on the unit cost of electricity generated by the solar-hydrogen system designed in the case study (5 kWh daily demand peaked at 0.3 kW in south-eastern Australia)	134
Figure 4-38. Improvement in the performance of a single cell of the 500W PEM fuel cell which was used for the case study.....	135
Figure 4-39. The results of the theoretical analysis to compare the heat and power generations of the 500 W PEM BCS fuel cell; operating condition: as shown in table 3-3, inlet air relative humidity 50%.....	136
Figure 4-40. How the generated heat is removed from the 500 W (540 W) PEM BCS fuel cell; operating condition as shown by table 3-3	137
Figure 4-41. Theoretical investigation on the 500W (540 W maximum power) BCS PEM fuel cell stack, heat generation; operating condition as shown by table 3-3(Shabani <i>et al.</i> 2010)	137
Figure 4-42. Typical Sankey diagram for a PEM fuel cell	138
Figure 4-43. The effect of air stoichiometry on the heat removal from a 500 W BSC fuel cell at 130 W power point at operating condition shown in table 3-3	139
Figure 4-44. The cumulative annual energy flow of the solar-hydrogen system of the case study (fuel cell minimum size and unconstrained tank)	141
Figure 4-45. Daily variation of the fuel cell heat, cooling load, and power generation when it is operated in the solar-hydrogen system of the case study (fuel cell minimum size and unconstrained tank).....	141
Figure 4-46. The cumulative annual energy flow of the solar-hydrogen system of the case study (optimally-sized fuel cell and unconstrained tank).....	142
Figure 4-47. Daily variation of the fuel cell heat, cooling load, and power generation when it is operated in the solar-hydrogen system of the case study (optimally-sized fuel cell and unconstrained tank)	142
Figure 4-48. The cumulative annual energy flow of the solar-hydrogen system of the case study (fuel cell minimum size and a 3-kg constrained tank)	143
Figure 4-49. Daily variation of the fuel cell heat, cooling load, and power when it is operated in the solar-hydrogen system of the case study (fuel cell minimum size and a 3-kg constrained tank)	143
Figure 4-50. The cumulative annual energy flow of the solar-hydrogen system of the case study (fuel cell minimum size, unconstrained tank, and managed peak load).....	144
Figure 4-51. Fuel Daily variation of the fuel cell heat, cooling load, and power when it is operated in the solar-hydrogen system of the case study (cell minimum size, unconstrained tank, and managed peak load)	144
Figure 4-52. Suggested simplified configuration for a solar-hydrogen CHP system; left: no CHP application; right: fuel cell heat is used for boosting the hot water system (Shabani <i>et al.</i> 2009).....	145
Figure 4-53. Fuel cell annual cooling load and energy demand for hot water supply, on daily basis	150
Figure 4-54. Economics of solar-hydrogen CHP system when using the fuel cell minimum size and optimally-sized fuel cell (based on power only application) and considering the value of fuel cell heat recovery	151
Figure 4-55. Economics of solar-hydrogen CHP system when using different sizes of fuel cells and considering the value of fuel cell heat recovery	152
Figure 5-1. An overview of the experimental rig	156
Figure 5-2. An overall view of the hydrogen line	157
Figure 5-3. 13.7-MPa hydrogen bottle with a regulator preset to maximum output of 1700 kPa	158
Figure 5-4. Hydrogen flammability level (DOE 2001)	159
Figure 5-5. A schematic of the safety interlock system used for the experimental study on the 500 W PEM BCS fuel cell	160
Figure 5-6. Regulator and flashback arrestor arrangement in the hydrogen storage unit	161
Figure 5-7. Hydrogen storage cabinet	162
Figure 5-8. Fume cupboard for doing hydrogen-related experiments	164
Figure 5-9. A schematic diagram showing how the mass flow meter and pressure gauge are installed in the hydrogen line	165
Figure 5-10. A schematic of the air supply line for the fuel cell	166
Figure 5-11. LPG camping gas cylinder used as a buffer between the air compressor and air regulator	167
Figure 5-12. Gas dryer used for capturing the moisture in the air before it enters the fuel cell.....	168
Figure 5-13. The air regulator and release valve set-up, as part of 500 W fuel cell air supply line (see figure 5-10)	168
Figure 5-14. Schematic diagram of the mass flow meter and pressure gauge installed in the air side	169
Figure 5-15. A schematic of the fuel cell cooling system.....	170
Figure 5-16. Exergy LLC miniature heat exchanger, model: 10 series 00268-2 (Exergy 2009)	172
Figure 5-17. Temperature and water flow meters displays.....	174

Figure 5-18. The water reserve tank to supply the fuel cell cooling system with water	175
Figure 5-19. Fuel cell and its cooling system before and after insulation	176
Figure 5-20. The 500 W PEM BCS fuel cell used in the experimental setup.....	177
Figure 5-21. The fuel cell control box	177
Figure 5-22. Solenoid valve for controlling the hydrogen purging	177
Figure 5-23. 500 W PEM fuel cell cooling load and power curves at 10 A operating point; operating temperature ~50 °C, exit air pressure 30 kPa, inlet hydrogen pressure 20-30 kPa, air stoichiometry 2.....	182
Figure 5-24. Experimental and manufacturer’s predicted polarisation and power curves for the 500 W BCS PEM fuel cell; operating temperature 60 °C; exit air pressure 30 kPa; air stoichiometry 2; inlet hydrogen pressure 20-30 kPa	186
Figure 5-25. 500 W PEM BCS fuel cell cooling load curve; operating temperature 60 °C; exit air pressure 30 kPa; air stoichiometry 2; inlet hydrogen pressure 20-30 kPa	188
Figure 5-26. 500 W BCS PEM experimental power and cooling load curves; operating temperature 60 °C; exit air pressure 30 kPa; air stoichiometry 2; inlet hydrogen pressure 20-30 kPa.....	188
Figure 5-27. The effect of the operating temperature on the polarisation curve of the 500 W PEM BCS fuel cell predicted by the model; the relative humidity of the cell is controlled to be within its recommended range while changing the operating temperature.....	189
Figure 5-28. Experimental polarisation curves for the 500 W PEM BCS fuel cell at different fuel cell; operating temperatures; exit air pressure 30 kPa, air stoichiometry 2, and inlet hydrogen pressure 20-30 kPa	190
Figure 5-29. The effect of air stoichiometry and cell operating temperature on the exit air relative humidity for the 500 W BCS PEM fuel cell as predicted by the simulation model.....	191
Figure 5-30. The effect of air stoichiometry on the performance of an already flooded 500 W fuel cell; operated at low temperatures; exit air pressure 30 kPa, and inlet hydrogen pressure 20-30 kPa	192
Figure 5-31. 500 W PEM BCS fuel cell measured cooling load at different operating temperatures compared with the cooling load curve predicted by the model at 60 °C; exit air pressure 30 kPa; air stoichiometry 2; inlet hydrogen pressure 20-30 kPa	194
Figure 5-32. 500 W PEM BCS fuel cell cooling load; operating temperature 50 °C; air stoichiometries 2 and 4; exit air pressure 30 kPa; inlet hydrogen pressure 20-30 kPa	194
Figure 5-33. 500 W fuel cell Sankey diagram at 5A operating point, theoretical and experimental study ...	196
Figure 5-34. The measured hydrogen utilisation coefficient of 500-W BCS PEM fuel cell; operating temperature 60 °C; exit air pressure 30 kPa; air stoichiometry 2 & 4; inlet hydrogen pressure 20-30 kPa....	198
Figure 5-35. 500 W PEM BCS fuel cell energy efficiency; operating temperature 60 °C; exit air pressure 30 kPa; air stoichiometry 2; inlet hydrogen pressure 20-30 kPa	199
Figure 5-36. 500 W PEM BCS fuel cell CHP (overall) energy efficiency; operating temperature 60 °C; exit air pressure 30 kPa; air stoichiometry 2 and 4; inlet hydrogen pressure 20-30 kPa	200
Figure 5-37. The fuel cell average electrical and CHP efficiencies at low and high operating temperatures; operating temperatures 40 °C and 60 °C; exit air pressure 30 kPa; air stoichiometry 2; inlet hydrogen pressure 20-30 kPa	201
Figure 6-1. Solar-hydrogen system configuration studied using HOMER	207
Figure 6-2. Petrol generator configuration for supplying the load simulated by HOMER	208
Figure 6-3. Petrol generators-battery system analysed by HOMER.....	209
Figure 6-4. Solar PV-battery-ICE generator system analysed by HOMER.....	210
Figure 6-5. The battery hourly state of charge throughout the year for the solar PV-battery-ICE generator system for the case studied in Chapter 4.....	211
Figure 6-6. CHP solar-hydrogen-battery system analysed using HOMER	212
Figure 6-7. The battery bank charge status for the solar-hydrogen-battery system when it is sized for about 10 days of autonomous operation (case study chapter 4)	213
Figure 6-8. Left: Yamaha ET650 petrol generator (Macfarlane 2008); Right: The cost of the solar-hydrogen system Vs IC generator	215
Figure 6-9. The breakdown of the total cost for a solar-hydrogen battery RAPS system used for the case study described in Chapter 4	216
Figure 7-1. The experimentally-measured electrical, thermal (based on the cooling load extracted and not the total heat generated), and CHP energy efficiency of 500-W BCS PEM fuel cell; operating temperature 60 °C; exit air pressure 30 kPa; air stoichiometry 2; inlet hydrogen pressure 20-30 kPa.....	226
Figure A- 1. The simulation code opening panel.....	260
Figure A- 2. Photovoltaic array analysis modes	261
Figure A- 3. The PV array ‘Single Point Analysis’ mode	262
Figure A- 4. ‘Radiation Data’ panel	263

Figure A- 5. An example to show how the program rejects an unacceptable input.....	263
Figure A- 6. Entering the PV array orientation data.....	264
Figure A- 7. Calculating the cell temperature using an empirical formula.....	265
Figure A- 8. Entering the cell temperature which comes directly from an actual measurement	265
Figure A- 9. Entering the PV module specifications	267
Figure A- 10. Starting the PV array analysis.....	268
Figure A- 11. ‘Show Results’ button to see the PV module analysis results.....	268
Figure A- 12. Key solar angles	269
Figure A- 13. The PV array analysis while it is tracking the sun	269
Figure A- 14. Irradiance and cell temperature	270
Figure A- 15. Module/Array outputs	271
Figure A- 16. The button used to show the performance curves of the PV array.....	271
Figure A- 17. The effect of temperature and irradiance on the performance of the PV array	272
Figure A- 18. The PV array ‘Yearly Analysis’ mode.....	272
Figure A- 19. Input data, site location	273
Figure A- 20. Input data, array orientation	274
Figure A- 21. Input data, radiation profile.....	275
Figure A- 22. Input data, Ambient/Cell Temp.....	276
Figure A- 23. Input data, ambient temperature profile	277
Figure A- 24. The right format for arranging a compatible temperature data file to be loaded into the program.	277
Figure A- 25. Input data, the wind speed profile	278
Figure A- 26. Results button, press to see the PV array yearly analysis results	279
Figure A- 27. Results, daily input and output.....	280
Figure A- 28. Electrolyser input data, electrolyser size and operating condition	281
Figure A- 29. Electrolyser analysis mode.....	282
Figure A- 30. Fuel cell analysis main page	283
Figure A- 31. Fuel cell analysis, ‘Single Point Analysis’ mode	283
Figure A- 32. Entering the fuel cell stack operating data	284
Figure A- 33. Entering the data related to the air side of the fuel cell	284
Figure A- 34. Hydrogen reactant specifications	285
Figure A- 35. Ambient condition, used for the fuel cell analysis	285
Figure A- 36. The results of the Fuel cell analysis provided in four categories	286
Figure A- 37. The fuel cell water management results.....	287
Figure A- 38. The fuel cell analysis results: thermal management.....	288
Figure A- 39. The air and hydrogen inlet/exit/consumption flow rates	288
Figure A- 40. Fuel cell analysis results: Efficiencies	289
Figure A- 41. Start page for Stack Characteristic Curve Recognition.....	290
Figure A- 42. Fuel cell identification strategy	291
Figure A- 43. Introducing the experimental fuel cell polarisation curve.....	291
Figure A- 44. Fuel cell graphs	292
Figure A- 45. Fuel cell operating data provided in the table	292
Figure A- 46. Editing the given data	293
Figure A- 47. Curve fitting on the fuel cell experimental polarisation curve based on Butler-Volmer equations and using the least squares method.....	293
Figure A- 48. Fuel cell performance curve identification by direct use of the Butler-Volmer equations.....	294
Figure A- 49. Solar-hydrogen system analysis	294
Figure A- 50. The main panel of solar-hydrogen system analysis.....	295
Figure A- 51. Initial suggestion for PV panel size for doing solar-hydrogen system analysis.....	295
Figure A- 52. Calling the demand profile file	296
Figure A- 53. Hydrogen storage tank definition for solar-hydrogen system analysis	297
Figure A- 54. The system is sized when ‘A’ and ‘B’ are equal to zero	298
Figure A- 55. The power surplus/deficit graph for the entire year	298
Figure A- 56. The graph showing the hydrogen production rate on hourly or half-hourly basis	299
Figure A- 57. Hydrogen consumption	299
Figure A- 58. Extra capacity of the electrolyser in hydrogen production (in this graph this extra capacity is zero as it is for a system with an unconstrained tank)	300
Figure A- 59. The fuel cell yearly heat and power generation profile (on daily basis)	300
Figure A- 60. Energy flow diagram of solar-hydrogen system	301
Figure A- 61. Table of half-hourly results.....	301

Figure A- 62. The yearly performance of the solar-hydrogen system and its components	302
Figure A- 63. Hydrogen tank yearly performance results	302
Figure A- 64. Yearly performance results for the electrolyser	303
Figure A- 65. Fuel cell performance parameters	303
Figure A- 66. Solar-hydrogen system performance results	304
Figure A- 67. The cost analysis panel	304
Figure A- 68. The panel for entering the key parameters to do economic analysis on the solar-hydrogen system.....	305
Figure A- 69. The page for entering the cost data of the PV array	306
Figure A- 70. The panel for entering the cost data of the electrolyser.....	306
Figure A- 71. The panel for entering the cost data of the hydrogen storage tank.....	307
Figure A- 72. The panel for entering the cost data of the fuel cell	307
Figure A- 73. The balance cost of the system.....	308
Figure A- 74. The unit cost of the electricity generated by the solar-hydrogen system	308
Figure A- 75. Hot water supply analysis mode	309
Figure A- 76. The results of the hot water supply analysis	310
Figure A- 77. 500 W BSC PEM fuel cell power measurements at 5 A; Operating temperature ~40 °C, exit air 30 kPa, air stoichiometry 2, inlet hydrogen ~20-30 kPa.....	311
Figure A- 78. 500 W BSC PEM fuel cell cooling load measurements at 5 A; Operating temperature ~40 °C, exit air 30 kPa, air stoichiometry 2, inlet hydrogen ~20-30 kPa.....	312
Figure A- 79. 500 W BSC PEM fuel cell power measurements at 5 A; Operating temperature ~40 °C, exit air 30 kPa, air stoichiometry 4, inlet hydrogen ~20-30 kPa.....	313
Figure A- 80. 500 W BSC PEM fuel cell cooling load measurement at 5 A; Operating temperature ~40 °C, exit air 30 kPa, air stoichiometry 4, inlet hydrogen ~20-30 kPa.....	314
Figure A- 81. 500 W BSC PEM fuel cell power measurements at 5 A; Operating temperature ~50 °C, exit air 30 kPa, air stoichiometry 2, inlet hydrogen ~20-30 kPa.....	315
Figure A- 82. 500 W BSC PEM fuel cell cooling load measurements at 5 A; Operating temperature ~50 °C, exit air 30 kPa, air stoichiometry 2, inlet hydrogen ~20-30 kPa.....	316
Figure A- 83. 500 W BSC PEM fuel cell power measurements at 5 A; Operating temperature ~50 °C, exit air 30 kPa, air stoichiometry 4, inlet hydrogen ~20-30 kPa.....	317
Figure A- 84. 500 W BSC PEM fuel cell cooling load measurements at 5 A; Operating temperature ~50 °C, exit air 30 kPa, air stoichiometry 4, inlet hydrogen ~20-30 kPa.....	318
Figure A- 85. 500 W BSC PEM fuel cell power measurements at 5 A; Operating temperature ~60 °C, exit air 30 kPa, air stoichiometry 2, inlet hydrogen ~20-30 kPa.....	319
Figure A- 86. 500 W BSC PEM fuel cell cooling load measurements at 5 A; Operating temperature ~60 °C, exit air 30 kPa, air stoichiometry 2, inlet hydrogen ~20-30 kPa.....	320
Figure A- 87. 500 W BSC PEM fuel cell power measurements at 5 A; Operating temperature ~60 °C, exit air 30 kPa, air stoichiometry 4, inlet hydrogen ~20-30 kPa.....	321
Figure A- 88. 500 W BSC PEM fuel cell cooling load measurements at 5 A; Operating temperature ~60 °C, exit air 30 kPa, air stoichiometry 4, inlet hydrogen ~20-30 kPa.....	322
Figure A- 89. 500 W BSC PEM fuel cell power measurements at 10 A; Operating temperature ~40 °C, exit air 30 kPa, air stoichiometry 2, inlet hydrogen ~20-30 kPa	323
Figure A- 90. 500 W BSC PEM fuel cell cooling load measurements at 10 A; Operating temperature ~40 °C, exit air 30 kPa, air stoichiometry 2, inlet hydrogen ~20-30 kPa.....	324
Figure A- 91. 500 W BSC PEM fuel cell power measurements at 10 A; Operating temperature ~40 °C, exit air 30 kPa, air stoichiometry 4, inlet hydrogen ~20-30 kPa	325
Figure A- 92. 500 W BSC PEM fuel cell cooling load measurements at 10 A; Operating temperature ~40 °C, exit air 30 kPa, air stoichiometry 4, inlet hydrogen ~20-30 kPa.....	326
Figure A- 93. 500 W BSC PEM fuel cell power measurements at 10 A; Operating temperature ~50 °C, exit air 30 kPa, air stoichiometry 2, inlet hydrogen ~20-30 kPa	327
Figure A- 94. 500 W BSC PEM fuel cell cooling load measurements at 10 A; Operating temperature ~50 °C, exit air 30 kPa, air stoichiometry 2, inlet hydrogen ~20-30 kPa.....	328
Figure A- 95. 500 W BSC PEM fuel cell power measurements at 10 A; Operating temperature ~50 °C, exit air 30 kPa, air stoichiometry 4, inlet hydrogen ~20-30 kPa	329
Figure A- 96. 500 W BSC PEM fuel cell cooling load measurements at 10 A; Operating temperature ~50 °C, exit air 30 kPa, air stoichiometry 4, inlet hydrogen ~20-30 kPa.....	330
Figure A- 97. 500 W BSC PEM fuel cell power measurements at 10 A; Operating temperature ~60 °C, exit air 30 kPa, air stoichiometry 2, inlet hydrogen ~20-30 kPa	331
Figure A- 98. 500 W BSC PEM fuel cell cooling load measurements at 10 A; Operating temperature ~60 °C, exit air 30 kPa, air stoichiometry 2, inlet hydrogen ~20-30 kPa.....	332

Figure A- 99. 500 W BSC PEM fuel cell power measurements at 10 A; Operating temperature ~60 °C, exit air 30 kPa, air stoichiometry 4, inlet hydrogen ~20-30 kPa	333
Figure A- 100. 500 W BSC PEM fuel cell cooling load measurements at 10 A; Operating temperature ~60 °C, exit air 30 kPa, air stoichiometry 4, inlet hydrogen ~20-30 kPa	334
Figure A- 101. 500 W BSC PEM fuel cell power measurements at 15 A; Operating temperature ~40 °C, exit air 30 kPa, air stoichiometry 2, inlet hydrogen ~20-30 kPa	335
Figure A- 102. 500 W BSC PEM fuel cell cooling load measurements at 15 A; Operating temperature ~40 °C, exit air 30 kPa, air stoichiometry 2, inlet hydrogen ~20-30 kPa	336
Figure A- 103. 500 W BSC PEM fuel cell power measurements at 15 A; Operating temperature ~40 °C, exit air 30 kPa, air stoichiometry 4, inlet hydrogen ~20-30 kPa	337
Figure A- 104. 500 W BSC PEM fuel cell cooling load measurements at 15 A; Operating temperature ~40 °C, exit air 30 kPa, air stoichiometry 4, inlet hydrogen ~20-30 kPa	338
Figure A- 105. 500 W BSC PEM fuel cell power measurements at 15 A; Operating temperature ~50 °C, exit air 30 kPa, air stoichiometry 2, inlet hydrogen ~20-30 kPa	339
Figure A- 106. 500 W BSC PEM fuel cell cooling load measurements at 15 A; Operating temperature ~50 °C, exit air 30 kPa, air stoichiometry 2, inlet hydrogen ~20-30 kPa	340
Figure A- 107. 500 W BSC PEM fuel cell power measurements at 15 A; Operating temperature ~50 °C, exit air 30 kPa, air stoichiometry 4, inlet hydrogen ~20-30 kPa	341
Figure A- 108. 500 W BSC PEM fuel cell cooling load measurements at 15 A; Operating temperature ~50 °C, exit air 30 kPa, air stoichiometry 4, inlet hydrogen ~20-30 kPa	342
Figure A- 109. 500 W BSC PEM fuel cell power measurements at 15 A; Operating temperature ~60 °C, exit air 30 kPa, air stoichiometry 2, inlet hydrogen ~20-30 kPa	343
Figure A- 110. 500 W BSC PEM fuel cell cooling load measurements at 15 A; Operating temperature ~60 °C, exit air 30 kPa, air stoichiometry 2, inlet hydrogen ~20-30 kPa	344
Figure A- 111. 500 W BSC PEM fuel cell power measurements at 15 A; Operating temperature ~60 °C, exit air 30 kPa, air stoichiometry 4, inlet hydrogen ~20-30 kPa	345
Figure A- 112. 500 W BSC PEM fuel cell cooling load measurements at 15 A; Operating temperature ~60 °C, exit air 30 kPa, air stoichiometry 4, inlet hydrogen ~20-30 kPa	346
Figure A- 113. 500 W BSC PEM fuel cell power measurements at 20 A; Operating temperature ~40 °C, exit air 30 kPa, air stoichiometry 2, inlet hydrogen ~20-30 kPa	347
Figure A- 114. 500 W BSC PEM fuel cell cooling load measurements at 20 A; Operating temperature ~40 °C, exit air 30 kPa, air stoichiometry 2, inlet hydrogen ~20-30 kPa	348
Figure A- 115. 500 W BSC PEM fuel cell power measurements at 20 A; Operating temperature ~50 °C, exit air 30 kPa, air stoichiometry 2, inlet hydrogen ~20-30 kPa	349
Figure A- 116. 500 W BSC PEM fuel cell cooling load measurements at 20 A; Operating temperature ~50 °C, exit air 30 kPa, air stoichiometry 2, inlet hydrogen ~20-30 kPa	350
Figure A- 117. 500 W BSC PEM fuel cell power measurements at 20 A; Operating temperature ~60 °C, exit air 30 kPa, air stoichiometry 2, inlet hydrogen ~20-30 kPa	351
Figure A- 118. 500 W BSC PEM fuel cell cooling load measurements at 20 A; Operating temperature ~60 °C, exit air 30 kPa, air stoichiometry 2, inlet hydrogen ~20-30 kPa	352
Figure A- 119. 500 W BSC PEM fuel cell power measurements at 25 A; Operating temperature ~40 °C, exit air 30 kPa, air stoichiometry 2, inlet hydrogen ~20-30 kPa	353
Figure A- 120. 500 W BSC PEM fuel cell cooling load measurements at 25 A; Operating temperature ~40 °C, exit air 30 kPa, air stoichiometry 2, inlet hydrogen ~20-30 kPa	354
Figure A- 121. 500 W BSC PEM fuel cell power measurements at 25 A; Operating temperature ~50 °C, exit air 30 kPa, air stoichiometry 2, inlet hydrogen ~20-30 kPa	355
Figure A- 122. 500 W BSC PEM fuel cell cooling load measurements at 25 A; Operating temperature ~50 °C, exit air 30 kPa, air stoichiometry 2, inlet hydrogen ~20-30 kPa	356
Figure A- 123. 500 W BSC PEM fuel cell power measurements at 25 A; Operating temperature ~60 °C, exit air 30 kPa, air stoichiometry 2, inlet hydrogen ~20-30 kPa	357
Figure A- 124. 500 W BSC PEM fuel cell cooling load measurements at 25 A; Operating temperature ~60 °C, exit air 30 kPa, air stoichiometry 2, inlet hydrogen ~20-30 kPa	358
Figure A- 125. Declination angle	363
Figure A- 126. Solar altitude and azimuth.....	363
Figure A- 127. Array azimuth and slope angles	363
Figure A- 128. Swagelok parts used for putting the hydrogen line together (Swagelok 2008).....	369
Figure A- 129. Stainless steel 24V AC/DC, 0-1000 kPa intrinsically safe solenoid valve, type 6013 ATEX - Supplier: RS Australia, RS stock number: 410-5165 (RSAustralia 2009)	369
Figure A- 130. Handheld hydrogen detector to check the hydrogen line for leakage (Fuelcellstore 2009) ..	370
Figure A- 131. Oil-free Swagelok pressure gauge (Swagelok 2008) - Part No: PGI-50M-PG30-LAOX.....	370

Figure A- 132. C100 model mass flow controller from Procon Instrument Technology (Sierra) used in the hydrogen line (C100 user manual)	370
Figure A- 133. Cole-Parmer oil-less air compressor , model : CZ-07054-23 used for supplying air to the 500 W fuel cell (ColeParmer 2009).....	371
Figure A- 134. 810C model Procon Instrument Technology (Sierra) mass flow meter and controller used in the air line (McMillan 2009)	371
Figure A- 135. The water pump (Cole Parmer Catalogue: 72008-30), used in the fuel cell cooling system (ColeParmer 2009)	371
Figure A- 136. Flow meters for measuring the fluid flow rates of the heat exchanger (left) (ColeParmer 2009) and 220 Mcmillan model display (right) (McMillan 2009).....	372
Figure A- 137. Pt100 temperature probe (left); Kubler temperature display (right); used for temperature reading (RSAustralia 2009).....	372
Figure A- 138. Kikusui PLZ1004W electronic load.....	372

LIST OF TABLES

Table 3-1. BP SX320 technical data provided in the manufacturer’s catalogue.....	67
Table 3-2. Comparing the maximum power outputs of a BP SX320 PV module at different operating conditions	67
Table 3-3. Air and hydrogen flow rates for a BCS 500 W PEM fuel cell predicted by the model and compared with values provided by the manufacturer.....	73
Table 3-4. Enthalpy of formation for water, hydrogen, oxygen and nitrogen at 298.15 °K	75
Table 4-1. Monthly average wind velocity for Melbourne (BOM 2009)	104
Table 4-2. Average daily minimum and maximum temperature for Bundoora (Victoria 3083, Australia), recorded at Latrobe University, and based on statistical information from 1979 to 2008 (BOM 2009).	105
Table 4-3. BP275 PV module technical specifications; the symbols used in this table were defined earlier in section 3.3.....	106
Table 4-4. Solar-hydrogen system sizing results (for fuel cell minimum size and unconstrained tank)	112
Table 4-5. Solar-hydrogen system components’ costs and lifetimes	116
Table 4-6. The effect of the constrained size of hydrogen tank on the size and the performance of the other components and the unit cost of the electricity generated	119
Table 4-7. Solar-hydrogen system sizing results (for fuel cell optimum size and unconstrained tank).....	129
Table 4-8. The effect of a 10% improvement in fuel cell performance on the system’s sizing and economics for an unconstrained tank analysis.....	135
Table 4-9. 500 W BCS PEM fuel cell heat and power generation details for air stoichiometries of 2 and 4; water product has been assumed to be in vapour form	139
Table 4-10. Cold water monthly average temperature for Melbourne (BOM 2009).....	146
Table 4-11. The results of analysis on using fuel cell heat and excess hydrogen for domestic hot water supply	149
Table 5-1. Code description for C100 mass flow controller used for the hydrogen line	165
Table 5-2. Operating limitations of the heat exchanger, used in the fuel cell cooling system (Exergy 2009).....	172
Table 5-3. Specifications of the ColeParmer flow meters used in the fuel cell cooling system (ColeParmer 2009).....	173
Table 5-4. Technical specifications of the Pt 100 temperature probe (RSAustralia 2009).....	174
Table 5-5. 500 W BCS fuel cell air flow rates (slpm) at different currents and air stoichiometries	178
Table 5-6. Specifications of the Kikusui electronic load	179
Table 5-7. 500 W fuel cell: the average of the experimentally-measured cooling load at different operating points and conditions in compared with the model predictions; exit air pressure 30 kPa; inlet hydrogen pressure 20-30 kPa	197
Table 5-8. Average experimentally-measured values for the hydrogen utilisation coefficient for the 500 W BCS PEM fuel cell; exit air pressure 30 kPa; inlet hydrogen pressure 20-30 kPa; air stoichiometry 2	198
Table 5-9. Average experimentally-measured values for the hydrogen utilisation coefficient for the 500 W BCS PEM fuel cell; exit air pressure 30 kPa; inlet hydrogen pressure 20-30 kPa; air stoichiometry 4	198
Table 5-10. Comparing the size of the components when the experimental and manufacturer’s polarisation curves and hydrogen utilisation coefficient s are used by the program	201
Table 6-1. Solar-hydrogen system sizing by HOMER and RSHAP for the case study in Chapter 4 (5 kWh daily demand in south-eastern Australia)	207
Table 6-2. Comparing solar-hydrogen & solar-hydrogen-battery systems using HOMER for the case studied in Chapter 4	212
Table 6-3. Comparing the RAPS alternatives from the techno-economics point of view (30 year assessment period) for the case study in Chapter 4.....	217
Table 6-4. Comparing the RAPS alternatives from the environment point of view for the case study	219
Table 6-5. Overview of TBL-based comparison of RAPS alternatives for the case study conducted.....	223
Table A- 1. 500 W BSC PEM fuel cell power and hydrogen consumption measurement at 5 A; Operating temperature ~40 °C, exit air 30 kPa, air stoichiometry 2, inlet hydrogen ~20-30 kPa	311
Table A- 2. 500 W BSC PEM fuel cell cooling load measurements at 5 A; Operating temperature ~40 °C, exit air 30 kPa, air stoichiometry 2, inlet hydrogen ~20-30 kPa	312
Table A- 3. 500 W BSC PEM fuel cell power and hydrogen consumption measurement at 5 A; Operating temperature ~40 °C, exit air 30 kPa, air stoichiometry 4, inlet hydrogen ~20-30 kPa	313
Table A- 4. 500 W BSC PEM fuel cell cooling load measurements at 5 A; Operating temperature ~40 °C, exit air 30 kPa, air stoichiometry 4, inlet hydrogen ~20-30 kPa	314

Table A- 35. 500 W BSC PEM fuel cell power and hydrogen consumption measurement at 15 A; Operating temperature ~60 °C, exit air 30 kPa, air stoichiometry 4, inlet hydrogen ~20-30 kPa	345
Table A- 36. 500 W BSC PEM fuel cell cooling load measurements at 15 A; Operating temperature ~60 °C, exit air 30 kPa, air stoichiometry 4, inlet hydrogen ~20-30 kPa.....	346
Table A- 37. 500 W BSC PEM fuel cell power and hydrogen consumption measurement at 10 A; Operating temperature ~40 °C, exit air 30 kPa, air stoichiometry 2, inlet hydrogen ~20-30 kPa	347
Table A- 38. 500 W BSC PEM fuel cell cooling load measurements at 20 A; Operating temperature ~40 °C, exit air 30 kPa, air stoichiometry 2, inlet hydrogen ~20-30 kPa.....	348
Table A- 39. 500 W BSC PEM fuel cell power and hydrogen consumption measurement at 20 A; Operating temperature ~50 °C, exit air 30 kPa, air stoichiometry 2, inlet hydrogen ~20-30 kPa	349
Table A- 40. 500 W BSC PEM fuel cell cooling load measurements at 20 A; Operating temperature ~50 °C, exit air 30 kPa, air stoichiometry 2, inlet hydrogen ~20-30 kPa.....	350
Table A- 41. 500 W BSC PEM fuel cell power and hydrogen consumption measurement at 20 A; Operating temperature ~60 °C, exit air 30 kPa, air stoichiometry 2, inlet hydrogen ~20-30 kPa	351
Table A- 42. 500 W BSC PEM fuel cell cooling load measurements at 20 A; Operating temperature ~60 °C, exit air 30 kPa, air stoichiometry 2, inlet hydrogen ~20-30 kPa.....	352
Table A- 43. 500 W BSC PEM fuel cell power and hydrogen consumption measurement at 10 A; Operating temperature ~40 °C, exit air 30 kPa, air stoichiometry 2, inlet hydrogen ~20-30 kPa	353
Table A- 44. 500 W BSC PEM fuel cell cooling load measurements at 25 A; Operating temperature ~40 °C, exit air 30 kPa, air stoichiometry 2, inlet hydrogen ~20-30 kPa.....	354
Table A- 45. 500 W BSC PEM fuel cell power and hydrogen consumption measurement at 25 A; Operating temperature ~50 °C, exit air 30 kPa, air stoichiometry 2, inlet hydrogen ~20-30 kPa	355
Table A- 46. 500 W BSC PEM fuel cell cooling load measurements at 25 A; Operating temperature ~50 °C, exit air 30 kPa, air stoichiometry 2, inlet hydrogen ~20-30 kPa.....	356
Table A- 47. 500 W BSC PEM fuel cell power and hydrogen consumption measurement at 25 A; Operating temperature ~60 °C, exit air 30 kPa, air stoichiometry 2, inlet hydrogen ~20-30 kPa	357
Table A- 48. 500 W BSC PEM fuel cell cooling load measurements at 25 A; Operating temperature ~60 °C, exit air 30 kPa, air stoichiometry 2, inlet hydrogen ~20-30 kPa.....	358
Table A- 49. Molar specific heat functions for water, hydrogen, oxygen and nitrogen (Sonntag <i>et al.</i> 2003)	364
Table A- 50. Enthalpy of formation functions for water, hydrogen, oxygen and nitrogen (Sonntag <i>et al.</i> 2003)	364
Table A- 51. Molar entropy of the contributing components water, hydrogen, and oxygen (Sonntag <i>et al.</i> 2003).....	364
Table A- 52. Measured values to calculate the cooling load of the fuel cell at 5A operating point when the operating temperature is about 40 °C, the exit air pressure is 30 kPa, the air stoichiometry is 4, and the inlet hydrogen pressure is 20-30 kPa.....	366

EXECUTIVE SUMMARY

Global energy supply and demand are increasingly dominated by major concerns about multiple factors, most notably climate change, shortage of oil supply and price increase, and rising population levels and per capita energy consumption. Hence it is critically important to find an alternative to fossil fuels, in particular petroleum fuels, from economic, environmental and social perspectives. Renewable energy sources with near zero-emissions such as solar energy, wind, wave, hydro, and biomass energy offer such an alternative. However, renewables such as solar energy are inherently variable and intermittent and cannot alone provide round-the-clock constant energy supply. Hence a suitable energy storage medium is required to overcome the intermittency of renewable energy and for load levelling. Hydrogen is one of the most attractive options for energy storage to be used in conjunction with renewables since it can store energy both for short durations, and for much longer periods of weeks, months and most importantly from season to season.

Stand-alone solar-hydrogen systems, including the photovoltaic (PV) arrays and a hydrogen energy storage sub-system (electrolyser, hydrogen storage tank, and fuel cell), promise to be a reliable renewable solution for uninterrupted Remote Area Power Supply (RAPS) to meet electrical load demand independent of grid electricity. The capability of flexible storage from season to season in such a system allows a much smaller PV array to be employed than would otherwise be the case, and obviates the need for a diesel or petrol generator back-up as normally required in a solar PV-battery system. However, the relatively low round-trip energy efficiency of the hydrogen production, storage and reuse sub-system (typically in the range 20-40%) is one of the major hurdles facing solar-hydrogen systems. Although the overall conversion efficiency of solar to usable energy (electricity) is better than batteries in long-term storage applications, this efficiency still needs further improvement.

The relatively high capital cost of solar-hydrogen systems is the second major hurdle facing these systems. Some efforts have been made so far to address these problems: such as using low-cost hydrogen storage tanks, direct coupling of PV arrays to electrolysers to eliminate electronic interfaces such as DC-to-DC convertors, and using unitised

regenerative fuel cells (a single unit operating in both electrolyser and fuel cell modes) in the system.

The present thesis seeks to make a contribution towards surmounting these two hurdles in the path towards commercialisation of solar-hydrogen RAPS systems by exploring the potential for converting the basic system to Combined Heat and Power (CHP) operation. By recovering the waste heat from the fuel cell and using it for domestic water heating or applications requiring low-temperature heat, there is an opportunity to raise the overall energy efficiency substantially and enhance the economic competitiveness of the system.

Hence the objectives of this thesis are to:

- review previous work on solar-hydrogen and fuel cell CHP systems;
- develop a computer model of a stand-alone solar-hydrogen CHP system based on a PEM electrolyser and fuel cell for remote area applications;
- investigate the energy efficiency and sizing of components via the model;
- perform optimisation analysis on the system by using the model;
- design, construct, and measure the performance of a laboratory rig of a CHP fuel cell system with heat used for water heating, and hence validate the computer model of the system;
- compare the solar-hydrogen CHP system with conventional remote area power supply systems in terms of technical performance, and triple bottom line (that is, economic, environmental and social) impacts; and
- identify priorities for further research and development to enhance the competitiveness of such systems.

Based on these objectives, the following research questions were posed to be answered by a combination of theoretical, computer modelling and experimental investigations:

- What are the main factors affecting the performance of a solar-hydrogen CHP system?
- To what extent can the overall energy efficiency and hence economic viability of a solar-hydrogen system for remote applications be improved by utilising the waste heat from fuel cell operation for water or space heating?

- What is the economically-optimal size of a solar-hydrogen CHP system for a remote household with given electrical and hot water demand?
- How does a solar-hydrogen CHP system compare on a triple bottom line basis with conventional alternatives such as diesel or petrol generators and PV-battery systems?
- Which components of a solar-hydrogen CHP system require further research and development to enable such systems to compete with conventional alternatives?

In addressing these objectives and research questions, the research program has led to the following main original outcomes and findings:

- *Development of a comprehensive state-of-the-art computer simulation program in a visual-based environment for solar-hydrogen CHP system analysis.*

A state-of-the-art computer model, named the RMIT Solar-Hydrogen Analysis Program (RSHAP), has been developed. RSHAP is able to perform techno-economic analysis on solar-hydrogen CHP systems. This comprehensive model is able to simulate the solar-hydrogen systems in both power-only and combined heat and power modes operation. The model is structured on a visual-based platform (Delphi), which offers a friendly environment to users. The structure of the program allows further computational modules and procedures to be added in the future if required. The user can analyse the overall performance of a solar-hydrogen system as well as the performance of individual components. The sub-models are all based on recently-developed mathematical models for the individual components and have been validated as a part of this study before being linked to the other sub-models to form the entire simulation program. The PV array was simulated using a series diode-resistance model. Both electrolyser and fuel cell were modelled using the newly-introduced modified Butler-Volmer equations developed at RMIT University. This modified Butler-Volmer model has proven to be extremely accurate in fitting theoretical curves to existing sets of experimental data for the electrolyser and fuel cell performance (polarisation) curves.

- *'Oversizing' the fuel cell in a solar-hydrogen RAPS system above the peak demand can lead to net system economic benefits*

A solar-hydrogen system for a remote household in southeast Australia with a total daily demand of 5 kWh peaked at 0.3 kW has been studied in detail using RSHAP. Initially the

fuel cell was sized to its minimum requirement (0.31 kW), that is, meeting the peak of the demand without receiving any input from the PV panel when no heat recovery from the fuel cell was considered. Then increasing the size of the fuel cell above its minimum size was studied. This strategy led to the fuel cell performing at a higher annual average efficiency as it was mostly operated at lower power than its rated one. This improved efficiency caused a reduction in the cumulative annual hydrogen consumption of this component, and hence to a smaller required size of hydrogen tank, electrolyser and PV array. Oversizing the fuel cell up to 1 kW yielded a 12% reduction in the overall cost of the system and hence in the unit cost of electricity (from 1.06 US\$/kWh to 0.94 US\$/kWh). However, further oversizing the fuel cell above 1 kW led to increasing the overall cost of the system again.

For this basic system, constraining the hydrogen tank to smaller sizes was also investigated and not found to be effective in reducing the cost of the system.

- *Adding a CHP capability to a solar-hydrogen system for a remote household can lead to significant net economic benefits*

The possibilities of recovering the heat generated by the fuel cell, and also using the heat extracted from burning the excess hydrogen (in the exit hydrogen stream of the fuel cell), that is, operating the solar-hydrogen system in CHP mode, were investigated using the RSHAP model. The heat extracted from the system was assumed to be utilised for boosting a LPG hot water system. The model predicted an increase from 33% to 63% in the average annual efficiency of the fuel cell when fuel cell heat recovery was performed in the RAPS case study investigated. Recovering this heat while using the fuel cell minimum size in the system led to about a 35% saving in LPG consumption for domestic hot water supply to the remote household. This saving was equivalent to about 15% of the overall cost of the system over an assessment period of 30 years when a 4% annual increase in the real cost of LPG is assumed, and an 8% reduction in total system costs if the real LPG price stays constant.

For the hydrogen stoichiometry of 1.2 assumed for this case study, recovering the excess hydrogen (above 15 kg per year) exiting the fuel cell and burning this in a 90% efficient burner to supply further heat for water heating gave an LPG saving almost the same as for

fuel cell heat recovery. Hence the model estimated that a saving of about 70% on LPG for water heating is achievable if both fuel cell heat and waste hydrogen recovery are performed. This saving in LPG is equivalent to about 30% of the overall cost of the system (at a 4% annual increase in the real cost of LPG). Recycling the excess hydrogen (collected from the exit hydrogen stream of the fuel cell) back to the hydrogen tank to be reused in the fuel cell is another possible option that needs a detailed investigation to measure if it is economically viable or not. This option has not been considered to be studied in this thesis.

The possibility of heat and excess hydrogen recovery from the fuel cell was also investigated for a solar-hydrogen system with an economically-optimised fuel cell size. In this case the savings in LPG (used for water heating) were 20% and 26% by heat and excess hydrogen recovery respectively.

Operating the solar-hydrogen system in CHP mode (heat recovery only) improved the round-trip efficiency of the hydrogen energy storage sub-system from ~24% (for the system with fuel cell minimum size) and ~30% (for the system with optimally-sized fuel cell) to about 45%. It is noteworthy that in CHP mode the economics of the system also depends on the assumed annual rise in the real cost of LPG. However, the RSHAP modelling showed that the already optimally-sized system (based on the unit cost of electricity only) still proves to be optimal (in CHP mode operation) if the annual rise in the real cost of LPG is less than 4%.

- *Experimental confirmation of doubling of efficiency of a PEM fuel cell when operated in CHP mode*

The case study analysed using the RHAP model was followed by an experimental investigation on a 500 W PEM BCS fuel cell, set up for heat and power measurement. After setting a safe stage to conduct the experiments, the fuel cell heat and power were measured under different operating condition (e.g. varying the operating temperature and air flow rates). The experimental results confirmed the central findings from the simulation modelling about the economic benefits and the performance improvement achieved by performing the fuel cell heat recovery. Previously, using the manufacturer's polarisation curve of the fuel cell and RSHAP the average efficiency of the fuel cell in CHP mode operation was estimated to be 63%. After inputting the polarisation curve obtained from

the experiment into RSHAP, this estimation was amended to 68%. The CHP efficiency was measured experimentally to be 72% on average, close to that obtained from the model. The relatively small remaining difference between model predictions and experimental results was identified as being due mainly to the experimentally-measured hydrogen utilisation coefficient (on average 95%) being about 10% points higher than that assumed in the model.

If the fuel cell characteristics in the model are amended to take account of this improved efficiency, the calculated unit cost of electricity in the case study (optimal fuel cell size) falls from 0.94 US\$/kWh to 0.85 US\$/kWh.

The overall CHP energy efficiency is not a function of the electrical performance of the fuel cell according to the experimental results, as expected from the conservation of energy since as less electricity is generated, more heat is produced. This independence of the CHP efficiency may be regarded as a positive feature since as the electrical performance of the fuel cell drops with age, correspondingly more heat becomes available for the heating application.

The experimentally-measured cooling load of the fuel cell was compared to that predicted by the model. At currents above 20 A, the experimentally-measured cooling loads were very close to those estimated by the model. At currents less than 20 A, up to 17% differences between the model and the experiment were observed. However, this difference can be reduced to less than 7% if the experimentally-obtained polarisation curve is used in the model to estimate the fuel cell cooling load curve.

- *The experimental study found strong connections between the fuel cell CHP capability and its water management.*

The heat and power generated by the fuel cell are strongly influenced by how the water produced inside the fuel cell is managed. In turn, water management is greatly affected by the operating temperature and the air stoichiometry. The formation of liquid water inside the fuel cell at low operating temperatures (mainly lower than that recommended by the manufacturer) can increase the collectable cooling load of the fuel cell (no heat is absorbed internally for water evaporation). Increasing the fuel cell heat by decreasing the operating

temperature of the fuel cell is at the expense of increasing the fuel cell overpotentials or decreasing the electrical energy efficiency, making the fuel cell unstable in continuous uniform power generation, and hence worsening the overall economics of the solar-hydrogen system. When the fuel cell is operated at lower than its design temperature, increasing the air stoichiometry can partly reduce the negative effect of this low temperature operation on performance, by enhancing the electrical energy efficiency and suppressing its thermal output. For example, when the fuel cell was operated at 50 °C, by raising the air stoichiometry to 4 increased the power output by 6-8%, and reduced the available cooling load by 30-50%, depending on the operating point of the fuel cell, compared to the performance at an air stoichiometry of 2.

- *A solar-hydrogen CHP system for RAPS in south-eastern Australia can be economically competitive with petrol/diesel generators over assessment periods of less than 20 years, and at the same time yield significant greenhouse gas emission reduction and social benefits.*

The solar-hydrogen combined heat and power system has also been compared with the main RAPS alternatives from a triple bottom line (TBL) point of view. The nature of the load, local environmental condition, cost, and the degree of reliability are important factors to be considered when choosing a stand-alone power supply system for a remote application. Using HOMER software and RSHAP, petrol/diesel generators, solar PV-battery-generator systems, and solar-hydrogen-battery systems were all compared with a solar-hydrogen system with and without CHP in the case study situation (that is, a remote household with a 5 kWh daily demand in south-eastern Australia). The analysis showed that the solar-hydrogen system is competitive to petrol/diesel generators over assessment periods of 20 years and above. Taking into account the economic benefit of fuel cell heat recovery this figure can be reduced to at least 18 years. Solar PV-battery systems did not prove economic compared to the other systems for this case. The results also showed that using relatively-low energy capacity battery storage system in conjunction with hydrogen storage (solar-hydrogen-battery CHP system) can further improve the economics of the solar-hydrogen CHP system by about 10%. However, using battery storage can reduce the heat recovery potential from the system by more than 50%.

From the environmental point of view, solar-hydrogen systems (with and without CHP) have zero greenhouse gas emissions while operating. If these systems replaced petrol/diesel generators in the case study, more than 1500 kg CO₂-e/year can be avoided. By utilising the fuel cell heat to save on LPG for the hot water system another 140 kg CO₂-e/year can be eliminated. In the solar PV-battery systems with back-up generator in the case study the annual emissions were just above 200 CO₂-e/year. The end-of-life waste management of batteries is another environmental impact avoided when using hydrogen-based energy storage systems.

Social benefits of using solar-hydrogen systems include more reliable energy supplies for remote communities and households, and greater energy security and independence compared to reliance on imported fossil fuels. The manufacture and installation of such systems can lead to industry development and employment creation opportunities. Improving health standards through reducing the harmful emissions normally associated with traditional systems (e.g. generators and battery-based systems) is another social benefit of using solar-hydrogen systems. There are a lot of misunderstandings about the level of risks involved in using hydrogen as a fuel, and a lack of agreed safety standards. The benefits of hydrogen including its safety advantages compared to the conventionally-used fossil fuels must therefore be explained to the public and industry. Hydrogen safety standards are now being more developed and these will help create a more promising future for hydrogen in terms of acceptability by the public.

On the basis of the theoretical and experimental investigations conducted in this research program, the following key recommendations are made:

- Further technological development and demonstrations of solar-hydrogen systems should be conducted to prepare the ground for the commercial deployment of these systems in suitable RAPS and other stand-alone applications. Priority areas for technological development include:
 - extending the lifetimes of PEM electrolysers,
 - improving the electrical energy efficiency of PEM fuel cells used in RAPS systems,
 - developing solid-state hydrogen storage systems (metal hydride or others) with very high round-trip energy efficiencies for use in solar-hydrogen RAPS systems,

- developing an overall control unit for a solar-hydrogen system that can regulate and optimise the performance of all the components (PV array, electrolyser, hydrogen storage, and fuel cell, including water management in the fuel cell and electrolyser) at all times, and
 - incorporating a small-energy capacity battery bank into the system to meet peak demands and provide short-duration storage at high round-trip energy efficiency while hydrogen provides the required longer-duration storage.
- Fuel cell heat recovery should be integrated into a solar-hydrogen system whenever there is a suitable use for the low-temperature heat in order to increase the overall energy efficiency of the system and enhance its economic competitiveness:
- Potential uses for the recovered heat to be considered include domestic water heating, space heating, and supply of heat to metal hydride storages to increase discharge rates and amounts.
 - The body of the fuel cell should be well insulated, so that no heat is wasted through convection between the outer surfaces of the fuel cell and surrounding atmosphere, hence the maximum amount of heat generated by the fuel cell is transferred to the cooling system.
 - A complete demonstration in the field of a solar-hydrogen CHP system in an appropriate RAPS application requiring both electricity and heat should be conducted for extended periods (at least 1-3 years) to acquire the data and experience necessary to commercialise zero-emission cogeneration systems of this kind.
- Sizing of a solar-hydrogen system (with or without CHP) using the RSHAP or equivalent model and based on minimising the average unit cost of electricity produced over the system lifetime as introduced in this study, is recommended. The recommended procedure would thus include:
- increasing the size of the fuel cell above the minimum needed to meet the peak load until the economically optimal size is found that takes full advantage of the energy efficiency gains of operating the cell at less than its maximum power,
 - investigation of both unconstrained and constrained hydrogen storage tank capacities for the particular application being considered, and

- allowing for some drop in the fuel cell hydrogen utilisation coefficient, and an additional contingency capacity in the hydrogen storage, so that the system is able to maintain its continuous supply even after the performance of the fuel cell and other components falls slightly with age, and in the event of atypical patterns of solar radiation and demand in certain years.
- Full Life Cycle Analyses (LCA) should be conducted to compare solar-hydrogen systems with petrol/diesel generators, and solar PV-battery- ICE generator systems for RAPS applications in terms of cradle-to-grave greenhouse gas emissions and other environmental impacts.

The following additions and extensions of the RSHAP model developed in this study are recommended:

- Incorporation into the model of a more detailed and realistic model of the hydrogen storage sub-system, including compressed gas and metal hydride options allowing for round-trip efficiencies of less than 100%.
- Allowing for a more detailed breakdown of costs and lifetimes of all the components of the system to be input, including, for example, the costs of installation and commissioning, a control system, a MMPT (if needed), the cooling system, and a humidifier/dehumidifier.
- Extension of the model to represent the transient behaviour of the fuel cell when exposed to a variable load, or restarted after a period of being in operation, rather than assuming steady-state operation at all times.
- Adding the capability to the economic analysis program of taking into account government rebates or other financial incentives to encourage use of renewable sources of energy and to reduce the carbon footprint.
- Extending the model to cover the potentially-attractive combination of a solar-hydrogen system with a solar water heater to supply a remote household with both its electricity and domestic hot water needs with zero greenhouse gas emissions.

PUBLICATIONS FROM THIS RESEARCH PROGRAM

Conference Papers:

- 1- Mac E., Gray A., Webb C.J., Andrews J., **Shabani B.** *et al.*, Hydrogen storage for off-grid power supply, 3rd International Symposium on Hydrogen in Matter 13-16 Dec. 2009, Chennai, India
- 2- **Shabani B.**, Andrews J., Badwal S.P.S., Theoretical and experimental investigation into using a PEM fuel cell to supply combined heat and power in a solar-hydrogen system, Sustainable Energy Technology Conference (SET 2009), 31 Aug.-3 Sept. 2009, Aachen, Germany
- 3- **Shabani B.**, Andrews J., Badwal S.P.S., Fuel-cell heat recovery, electrical load management, and the economics of solar-hydrogen systems, 3rd IASTED, Asian Conference on power and energy systems, 12-14 Oct. 2009, Beijing, China
- 4- **Shabani B.**, Andrews J., Modelling of a solar-hydrogen combined heat and power system for remote power supply, 17th World Hydrogen Energy Conference (WHEC), 16-19 June 2008, Brisbane, Australia

Journal Papers:

- 1- **Shabani B.**, Andrews J., Watkins S. 2010, Energy and cost analysis of a solar-hydrogen combined heat and power system for remote area power supply using a computer simulation, *International Solar Energy Journal*, 84 (1) 144-155
- 2- Gray E.MacA., Webb C.J., Andrews J., **Shabani B.**, Tsai P.J., Chan S.L.I. 2010, Hydrogen storage for off-grid power supply, *International Journal of Hydrogen Energy*, In Press Corrected Proof, Available online 16 October 2010.
- 3- **Shabani B.**, Andrews J., Badwal S. 2010, Fuel-cell heat recovery, electrical load management, and the economics of solar-hydrogen systems, *International Journal of Power and Energy Systems*, 30 (4) (*this paper was originally submitted to the 3rd IASTED conference in China 2009 and later was selected by IASTED to be published in this journal*).
- 4- **Shabani B.**, Andrews J. 2010, An experimental investigation of a PEM fuel cell to supply both heat and power in a solar-hydrogen RAPS system, *International Journal of Hydrogen Energy*, *under review*.

1 Introduction

1.1 BACKGROUND

1.1.1 The problems with fossil fuels

Global energy supply and demand are increasingly dominated by major concerns about climate change, shortage of oil supply and price increase, rising population levels and per capita energy consumption, air pollution, availability of fresh water resources, coastal pollution, deforestation, and biodiversity losses (Lior 2008). The major part of the world's energy demand is supplied by fossil fuels (Moriarty and Honnery 2007), implying a strong connection between the global economic indices and the prices of these fossil fuels. IEA (2009) predicts a 40% increase in global energy consumption, mostly from fossil fuels, by 2030 compared to 2007 (figure 1-1). This ever-increasing consumption of such fuels calls their future availability into question. It is widely accepted by scientists and statistical reports that fossil fuel resources, especially crude oil and natural gas, will be severely depleted in the foreseeable future (Veziroglu and Sahin 2008; Shafiee and Topal 2009). This depletion trend together with the current conflicts in oil-producing countries are causing oil prices to remain high and a likelihood of rises in the future (figure 1-2). Such a condition will have a continuing adverse impact on the world economy as many researchers have found strong links between the latest world economic crisis and the rising oil price during the last decade (Shafiee and Topal 2009). Hence it is critically important to find an alternative to petroleum fuels from an economic point of view, over and above the environmental imperative of reducing greenhouse gas emissions.

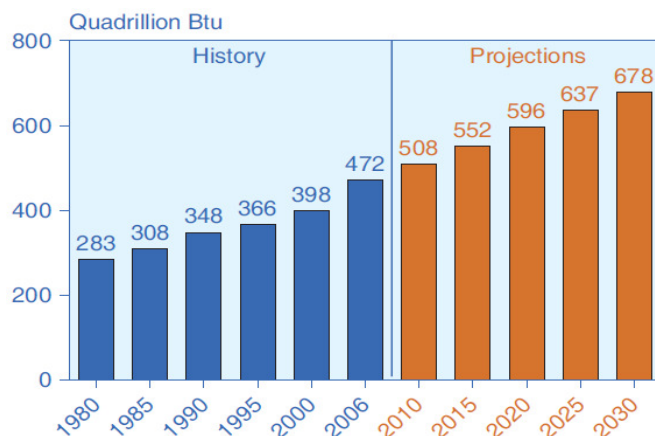


Figure 1-1. World energy consumption, history and projections (IEA 2009)

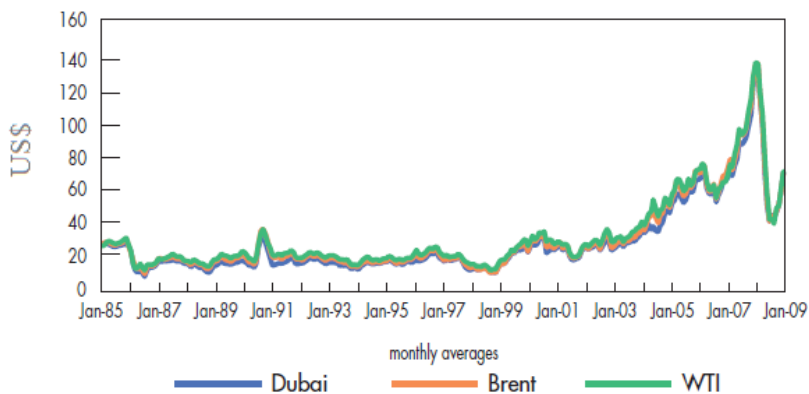


Figure 1-2. Historical trends for the price of crude oil (IEA 2009)

Environmental and social impacts of using fossil fuels linked to global warming during the past decades are another major concern. Large populations in many developing countries are particularly vulnerable to the impacts of climate change, such as rising sea levels and altered rainfall patterns, even though they have contributed little to global greenhouse gas (GHG) emissions.

A report published by IEA (2009) discussed the global carbon dioxide emission production from fossil fuel combustion using the data originally delivered by the Carbon Dioxide Information Analysis Centre (DOE 2007). These data (figure 1-3) clearly show that since 1870 CO₂ emissions from fossil fuel combustion have risen exponentially. This report predicts over 40 Gt/year of carbon dioxide emission production (only from the combustion of fossil fuels) by 2030.

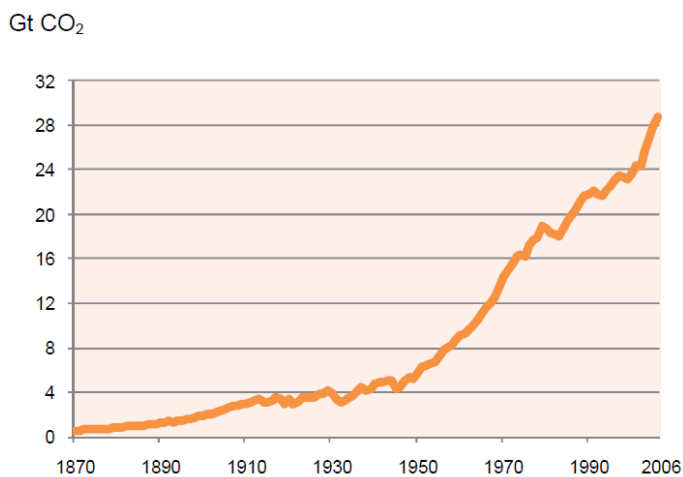


Figure 1-3. The history of annual carbon dioxide production from fossil fuels (IEA 2009)

Carbon dioxide is one of the main reasons for global warming by acting like a greenhouse shield around the atmosphere of the earth and trapping the heat gained by the earth through the solar radiation (Hoffmann 2001). The Fourth Assessment Report released by the Intergovernmental Panel on Climate Change (IPCC 2007) showed that the global average surface temperature has considerably increased in the last 100 years (figure 1-4), leading to a range of adverse environmental and social issues impacts (Florides and Christodoulides 2009). IPCC (2007) also predicted a worst-case scenario of a 2.4 °C to 6.4 °C increase in the mean global surface temperature of the earth by 2100. This continuing global warming trend will severely impact the availability of fresh water resources, the stability of ecosystems, food production, and human health (Hoffmann 2001).

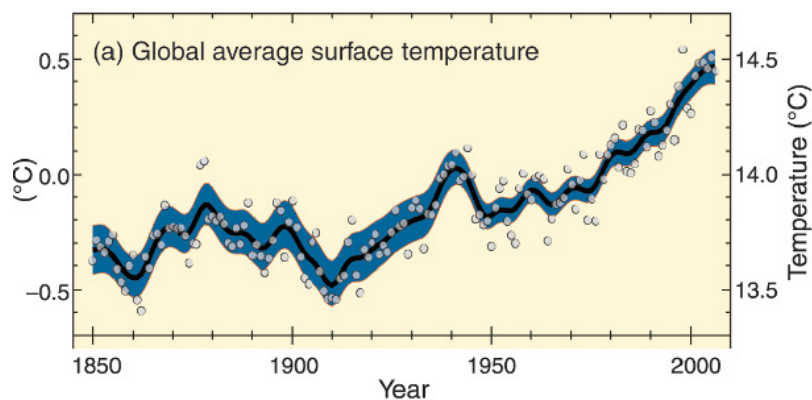


Figure 1-4. Global mean temperature rising (IPCC 2007)

1.1.2 Fossil fuels and Australia

Australia's level of greenhouse gas emissions per capita is among the highest in the world (Saddler *et al.* 2007). Thus to meet national and international targets for reducing emissions, there is a necessity to move towards cleaner or zero-emission energy sources. The Australian economy, like the rest of the world, will also be strongly affected by the inevitable rise of oil, natural gas and other energy prices as fossil fuel reserves are depleted.

Domestic production of oil in Australia is not enough to supply the demand and the Energy Information Administration (EIA 2009) calculated that the gap between production and consumption of oil has increased particularly during the last decade (figure 1-5).

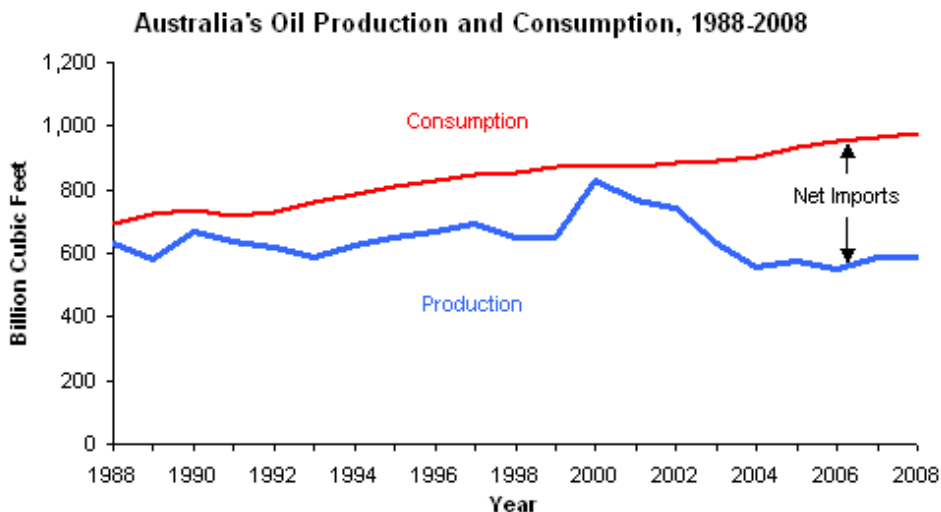


Figure 1-5. The history of oil production and consumption in Australia (EIA 2009)

Coal provides around 80% of Australia’s total electricity, and accounts for around 32% of Australia's total greenhouse gas emissions. Coal is the Australia’s biggest single export earner (around \$43 billion in 2008-09) and is clearly important in the global energy mix (Minister for Resources and Energy, 2008). While depletion of coal reserves may not be an issue for Australia in the near future due to the vast reserves (figure 1-6), the greenhouse gas emissions from continued use of coal is a major concern.

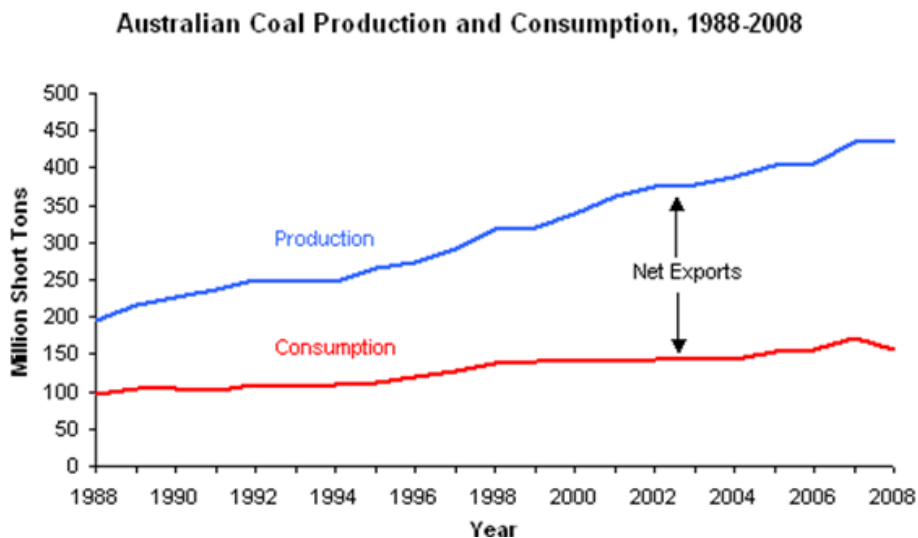


Figure 1-6. The history of coal production and consumption in Australia (EIA 2009)

1.1.3 Renewable energy as an alternative to fossil fuels

For all the reasons discussed in the previous section, renewable energy sources with near zero-emissions must be developed as alternatives to fossil fuels over the coming decades. Solar energy, the primary source of renewable energy, appears in different forms including wind, wave, hydro, and biomass energy, and in principle has the potential of meeting the global energy demand many times over. The world is now moving towards renewable alternatives to some degree; for example using photovoltaic system to convert solar energy to electricity has shown a 30% of growth during past decade (Moriarty and Honnery 2007).

Figure 1-7, the forecast released by EIA (2009), shows that renewable energy will play an increasing role in the world electricity generation over the next few decades.

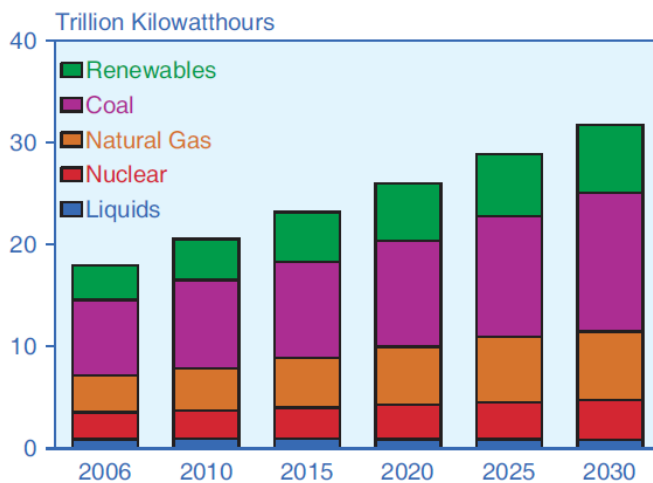


Figure 1-7. World electricity generation by fuel (EIA 2009)

The most important barrier to renewable energy deployment is the high cost. Many renewable energy technologies are still under development and not yet at the stage of mass production, which often keeps the price of renewable energy systems high. However, things are now changing and the cost is predicted to drop in a near future, while the cost of energy supply sourced by fossil fuel is on the increase. For instance the cost of solar electricity is predicted to reduce by more than 30% by 2020 (IEA 2001). Although renewable energy options such as solar energy are still expensive, they are already relatively competitive in remote area power supply due to higher cost of fossil fuel-based power supplied to these areas because of the added fuel transportation costs. Needless to say the ever-increasing cost of fossil fuels and further development in renewable energy

technologies (e.g. photovoltaic) will enhance the competitiveness of renewable energy-based options relative to the traditional fossil-fuel-based technologies.

1.1.4 Australia's support for renewable energy

Ratifying the Kyoto protocol as the first official act by the Labour Government of Australia in 2008 sent a clear message that Australia is now moving towards cleaner energies. The \$500 million renewable energy fund, the AU\$150 million energy innovation fund (AU\$100 million for research on solar energy and AU\$50 million for other energy innovation including energy storage for hydrogen), and the AU\$500 million national clean coal fund were in the 2008-09 budget allocation (Minister for Resources and Energy, 2008); this indicates a firm commitment by the Australian Government to tackle the climate change issue. The report released by Australian Minister for Resources and Energy (2008) expressed the aims of allocating such budgets as necessary to restore and maintain Australia's world leadership in solar energy research and development; to develop and advance Australia's research and development capabilities and intellectual property in clean energy technologies; to increase the level of collaboration within Australia and internationally on clean energy research and development; and to create clean energy technology development, growth and export opportunities for Australian businesses. The report indicates that the Australian Government's commitment to reduce Australia's greenhouse gas emissions by 60 per cent on 2000 levels by 2050 will require substantial greenhouse gas reductions through greater energy efficiency and cleaner energy technologies in association with a national emissions trading scheme.

The Mandatory Renewable Energy Target (MRET) set by the Australian Government is another measure to broaden the efforts to protect the environment. According to the Office of the Renewable Energy Regulator (ORER 2009), this target is a consistent progress towards achieving the additional production of 9,500 GWh of renewable energy by 2010 and 45,000 GWh by 2020.

Another step taken by the Australian Government through Department of the Environment, Water, Heritage and the Arts (DEWHA 2009) is allocating a cash rebate for residential photovoltaic panel installation under Solar Homes and Communities Plan. Also

government provides a special financial support aimed at developing the use of renewable energy in remote areas, the focal point of this study. Replacing fossil fuels with renewable generation such as solar and wind power not only benefits the environment, but can also improve the lifestyle of Australians living in remote parts of the country, giving them greater access to electricity, reducing noise and air pollution and reducing the need to transport fuel over long distances (DEWHA 2009). The program has funding available from 2011.

As mentioned earlier the sun is the primary source of different kinds of renewable energy sources. Australia in particular has a great capacity for solar energy deployment; the solar regime in the northern and central region of Australia is among the highest in the world (Lowe and Lloyd 2001). This fact is an endorsement to the Australian government policy in supporting renewable energy alternatives, and in particular solar energy.

1.1.5 Hydrogen as the prospective energy store and carrier for renewable energy

Renewable energy sources, such as solar energy, that are inherently variable and intermittent cannot alone provide round-the-clock constant energy supply. The energy available from most renewables depends randomly on climate and weather conditions, and typically has diurnal and seasonal patterns of variability. In particular, direct solar energy varies from summer to winter and cannot provide power during the night time. Hence renewable energy sources need a suitable medium to play the role of energy storage. Rechargeable batteries are an immediate and traditional storage solution for electrical energy for cases where the times between charging and discharging are relatively short – in the order of days or at most weeks. Hydrogen provides an energy storage option that is particularly suited to longer-term storage, that is, from weeks to months and including most notably from season to season as will be required by any renewable energy sources (Shabani *et al.* 2010). It is important to note here that hydrogen is not a primary energy source like natural gas, or crude oil; rather it is just an energy carrier and storage medium that has to be manufactured using a primary energy input, such as solar or wind energy (Hoffmann 2001). In its role as energy carrier, hydrogen is similar to electricity, which also has to be generated using primary energy sources. Nevertheless hydrogen has a great potential role as an energy store and carrier as the contribution of variable renewable

energy sources increases and the world makes the transition towards a truly sustainable energy economy (Schoots *et al.* 2008).

Hydrogen can be produced using a variety of methods such as electrolysis, steam reforming and biological process (Larminie and Dicks 2003). The fact that there are so many different methods and sources available for its production is seen as a unique feature and advantage of hydrogen (Verhelst and Wallner 2009). In particular, the production of hydrogen by electrolysis of water can be powered by renewable energy technologies like solar photovoltaic arrays and wind powered generators, which can be employed in many locations rather than just in large centralised facilities. The hydrogen produced can then be stored as a compressed gas, liquid, or as an integral component in certain alloys known as metal hydrides (Hoffmann 2001; Larminie and Dicks 2003).

The energy stored in hydrogen can be regained through combustion or in an electrochemical reaction in a fuel cell (Hoffmann 2001). Combustion of hydrogen is a very low emission process as the product is water, plus a small amount of NO_x (oxides of nitrogen) if it is burned with air rather than pure oxygen (Heffel 2003). For the case of Spark Ignition (SI) Internal Combustion Engines (ICEs), hydrogen engines can be potentially much more efficient than gasoline ICEs, particularly if a hydrogen-dedicated engine is used to burn hydrogen. Theoretically speaking, this higher efficiency is basically because of the higher octane number of hydrogen compared to other fuels used in SI ICEs, which allows higher compression ratios without deleterious knocking.

Another method of drawing on the energy stored in hydrogen is the electrochemical reaction of recombining hydrogen and oxygen in a fuel cell to form water. This is the reverse reaction to that in an electrolyser. Such a method of releasing the hydrogen energy is considerably more efficient than the combustion method, this can be above twice as efficient as a hydrogen-based ICE (Hoffmann 2001) after being converted to mechanical power; this is the main reason for the global interest in fuel cell-based engines (Marbán and Valdés-Solís 2007). The reaction in a fuel cell has absolutely zero emissions, since the only product is water with no other pollutants and this is another key advantage of fuel cells over ICEs.

The major automotive companies, such as:

- Toyota and Honda: reported by Fuel Cells Bulletin (2003);
- BMW: Hydrogen 7 (Brunner and Kircher 2008; Verhelst and Wallner 2009);
- GM: GM2001(Ahluwalia *et al.* 2004);
- Ford: P2000 (Verhelst and Wallner 2009); and
- Chrysler: Luxury fuel cell-based model reported by Fuel Cells Bulletin (2008)

have all shown their interest in hydrogen cars (either fuel cell or hydrogen ICEs) by developing demonstration models of their popular products running on hydrogen. Such efforts made by these globally-recognised automotive companies are still being continued aimed at taking hydrogen cars to the mass production stage. For instance, the Green Car Congress website (2009) reported on Toyota's plan to have its first limited consumer sales of hydrogen fuel-cell vehicles by 2015.

Stationary applications, powered by either hydrogen ICEs-based generators or fuel cells, such as supplying power to remote areas, or other applications where independence from transported fossil fuels or the main electricity grid is required, are another prospective market for hydrogen energy systems used in conjunction with renewables. Some examples of these remote or stand-alone applications are:

- remote household, community or island power supply;
- remote construction projects;
- remote telecommunication sites;
- power supply to remote industrial and agricultural facilities; and
- hydrogen fuelling stations.

The relatively high energy content per unit mass of hydrogen is counted as an advantage. However, despite this positive fact about the hydrogen's heating value, when it comes to volumetric energy density, hydrogen is not in such a good position compared to other conventional liquid fossil fuels such as gasoline, diesel fuel, and compressed natural gas (CNG). This is because of the lightness of hydrogen molecules: even a litre of liquid hydrogen weighs as much as 0.01 of a litre of gasoline. Obviously high volumetric energy density is a basic requirement for a fuel which is to be carried on-board a vehicle, that is

why this matter still has remained a challenge for replacing hydrogen with conventional fuels to be used for transport purposes (Marbán and Valdés-Solís 2007). However, for a remote area application where plenty of space is often available for hydrogen storage this low volumetric energy density would not be counted as a considerable disadvantage of hydrogen storage.

Hydrogen is a strong alternative to liquid fossil fuels that can help the automotive sector to meet future greenhouse gas and other emission reduction targets as well as providing energy security (White *et al.* 2006). Hydrogen can play a similar role in the stationary energy sector by supplying continuous clean energy to this market for the centuries to come. Hydrogen produced from renewables can be a driving factor to push the global energy supply system to a sustainable path (Barreto *et al.* 2003) and obviously this role will be more pronounced in the foreseeable future when the share of fossil fuel sources becomes less in global energy supply. For example the global energy model developed by Marbán and Valdés-Solís (2007) shows a rapid increase of using hydrogen fuel cells for both stationary and mobile applications in the next few decades (figure 1-8).

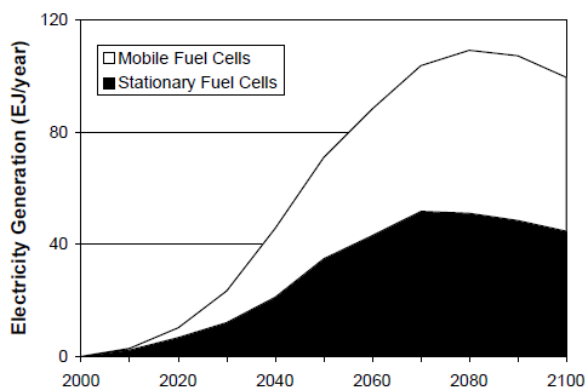


Figure 1-8. Prediction of global electricity generation from hydrogen-based fuel cells (Barreto *et al.* 2003)

1.2 SOLAR-HYDROGEN SYSTEMS

1.2.1 Solar-hydrogen generation

Hydrogen can be generated using both renewable and non-renewable sources of energy. In the present project the focus is on renewable methods, and in particular solar electricity captured by photovoltaic (PV) arrays, to ensure a zero-emission source of hydrogen. The electrical output of PV arrays can power electrolyzers to split water into its basic elements:

hydrogen and oxygen. The hydrogen can be stored for later reuse for the application in mind. Hydrogen can either be used as a raw material for many industrial applications or as a fuel for power production in ICEs or fuel cells, both in mobile and stationary applications as discussed earlier. Solar-hydrogen refueling stations (either public or domestic) are examples of one of the prospective applications of such a method of hydrogen production (Bilgen 2004).

However, the cost of hydrogen production using a renewable energy source, and in particular solar PV systems, by electrolysis remains high compared to electricity supplied by the grid (Levene *et al.* 2007). Paul (2009) gave an indicative figure of about 22 US\$/kg for the cost of hydrogen production when an optimal coupling between PV arrays and electrolyzers are used and the maximum power point tracker (MPPT) that sits between the PV array and electrolyser is eliminated. The high cost is the reason that solar-hydrogen production in conjunction with electrolysis is not normally chosen by industry to be widely practiced (Hoffmann 2001; Levene *et al.* 2007). However, the widespread availability of renewable energy sources and near zero-emission production process, together with technological development and higher volume production of components, can potentially make this method of hydrogen generation attractive in the near future.

Solar-hydrogen production is being studied or practiced by many countries, especially those with proven high levels of solar radiation. A proposed solar-hydrogen system concept for Spain developed by Contreras *et al.* (1999) shows such a system can effectively reduce the dependency of Spain on imported fossil fuels; this study even predicted that Spain could become an energy-exporting country if solar-hydrogen production is widely practiced in unproductive parts of the country. A similar study was done for Egypt by Abdallah *et al.* (1999) showing that a solar-hydrogen production system would substantially extend the available fossil fuels in this country. The study done by Kazim and Veziroglu (2001) for UAE is another example of this kind, suggesting a promising future for the energy market of UAE in both domestic and international scale if solar-hydrogen systems are introduced. Almogren and Veziroglu (2004)'s similar model for Saudi Arabia showed that the oil production of Saudi Arabia will not be able to supply the domestic and export demand from years between 2030 and 2040 onwards, and that a solar-hydrogen production system has the potential of allowing Saudi Arabia to become an exporter of hydrogen in the future. Italy is also another leading country on doing research

on solar-hydrogen production. An example of this is a completely stand-alone solar-hydrogen system demonstration in Italy, Galli and Stefanoni (1997). The system was erected and successfully demonstrated as the result of a hydrogen project taken up by the Italian National Agency for New Technologies. This solar-hydrogen system included a PV array, high pressure alkaline electrolyser, metal hydride alloy storage for hydrogen, and a solid polymer fuel cell.

1.2.2 Stand-alone solar-hydrogen systems

A stand-alone solar-hydrogen system is used for uninterrupted power supply to an electrical demand independently from grid electricity. The system includes the solar-hydrogen production/storage sub-system, similar to that described in section 1.2.1, and a fuel cell to generate electricity by drawing on the stored hydrogen (figure 1-9). PV arrays are primarily used to supply the demand directly as much as possible. The surplus of the PV power over the demand is used by the electrolyser to produce hydrogen for storage (if there is any space left in the hydrogen storage tank). The fuel cell then consumes this stored hydrogen to produce electricity when the demand is not fully supplied by the PV arrays.

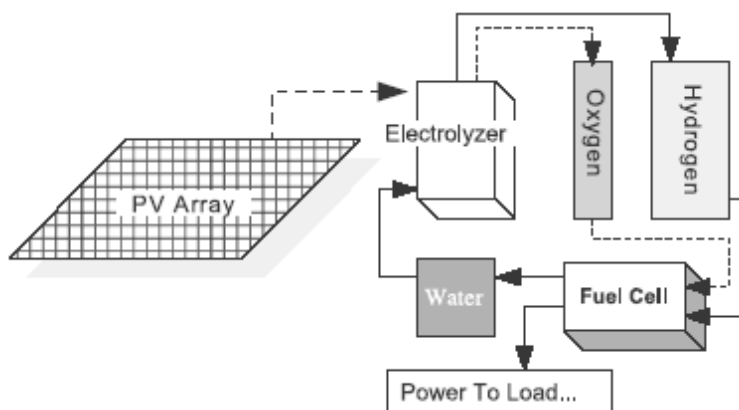


Figure 1-9. The simple schematic of the solar-hydrogen system diagram used in the study conducted by Shapiro, Duffy *et al.* (2005)

The hydrogen energy storage sub-system is an integral part of a stand-alone solar-hydrogen power supply system, since the intermittent source of energy, solar radiation, is not available round the clock. Battery systems, in particular lead-acid batteries, have traditionally been used in conjunction with PV systems for storing electrical energy. In a

solar-hydrogen storage system, the combination of the electrolyser, hydrogen storage tank, and fuel cell basically replaces the battery storage allowing electrical energy to be stored and supplied again at a later time when required.

The use of hydrogen in a solar-hydrogen power supply system provides the capability of both long and short-term energy storage. Most importantly long-term storage allows surplus solar energy in summer to be stored until winter when solar radiation is much lower in most locations. The capability of storage from season to season in this way allows a much smaller PV array to be employed than would otherwise be the case, and obviates the need for a diesel or petrol generator back-up. For example in a telecommunication site, located in a truly remote area, a reliable uninterruptable power supply is essential. The battery systems commonly used currently are suitable for short-term energy storage but cannot provide longer-term season-to-season storage. Hence PV systems with battery storage normally require a back-up diesel/petrol generator to ensure continuity and reliability of supply throughout the year, adding to the cost of the system and the annual operating and maintenance requirements.

The principal potential advantages of hydrogen energy storage compared to batteries are relatively higher round-trip efficiency than batteries in long-term storage applications (season-to-season storage), and flexibility in terms of production from both renewable (nearly available everywhere) and non-renewable sources of energy. Also, from the cost point of view, solar-hydrogen systems have a strong prospect of becoming competitive against the traditional and mostly non-sustainable systems as the cost of fossil fuels increases. The ever-increasing costs of diesel and petrol, as well as the high cost of transporting these fuels to a remote area, and the greenhouse emissions associated with their consumption are all reasons to stop their use in RAPS applications. Also the costs of the components of solar-hydrogen systems are dropping due to technological development and their mass production.

Such advantages have been encouraging many researchers to conduct studies on solar and/or wind hydrogen systems for stand-alone power supply applications, for example: a stand-alone solar-hydrogen system in Mexico reported by Torres *et al.* (1998); stand-alone power supply to remote telecommunication units (Martínez Chaparro *et al.* 2003; Varkaraki *et al.* 2003); the system erected in a valley of the Alps in Italy (Santarelli and

Macagno 2004); the one in North America, New Jersey, reported by Fuel Cells Bulletin (2006); stand-alone solar-hydrogen system for remote households (Santarelli and Macagno 2004; Ali and Andrews 2005; Gibril 2008); small scale solar-hydrogen system practiced in China (Liu *et al.* 2009). In the European energy market the research done by Zoulias *et al.* (2006) on stand-alone hydrogen systems is being used by European Governments to prepare the ground for regulatory changes to facilitate alternatives to grid solutions.

Remote Area Power Supply (RAPS) is one of the prime target markets for stand-alone solar-hydrogen systems in the near future. The main reasons for this are: the very high reliability of supply particularly for long-term storage applications potentially obtainable from solar-hydrogen systems, and their expected economic competitiveness as component costs are reduced.

Solar-hydrogen systems can be also used in grid-connected areas (operated independently and in parallel to the grid electricity) for handling sharp peaks of the demand (Barbir 2005; Maclay *et al.* 2006) or providing back-up power to cases like telecommunication or medical facilities (Shapiro *et al.* 2005).

A detailed review of the findings of the studies to date on solar-hydrogen systems for RAPS applications is provided in Chapter 2 of this thesis.

1.2.3 Hurdles facing solar-hydrogen systems

There are a number of critical hurdles that need to be cleared before solar-hydrogen RAPS systems can become a commercially-available technology that is widely deployed.

The first hurdle is low round-trip efficiency of the hydrogen production, storage and reuse sub-system. Although the overall conversion efficiency of solar to usable energy (electricity) is relatively better than battery in long-term storage application, this efficiency still needs further improvement. The round-trip efficiency of battery for a short-term storage case is normally above 80% (Maclay *et al.* 2006); however, for a long-term application the round-trip efficiency can drop down to nearly zero if the battery does not receive any charge for a few weeks. For the case of a hydrogen energy storage system, the

round-trip energy efficiency is the product of the individual energy efficiencies of the electrolyser (in hydrogen production), the hydrogen storage tank (from the leakage point of view and the external energy inputs needed for charging and discharging), and the fuel cell (in electricity generation by using this hydrogen). Even assuming optimistically no net energy losses in the hydrogen storage tank, the overall round-trip efficiency of the systems constructed to date has generally been found to be in the range of 20-40% (Barbir 2005; Shapiro *et al.* 2005). This range is broadly consistent with expectations based on typical efficiencies of an electrolyser and a fuel cell: for example if an electrolyser operates at 80% efficiency point (delivering hydrogen at low pressure, suitable for a RAPS application) and a fuel cell generates electricity at its 40% efficiency point, the round-trip efficiency is 32%. Obviously for short-term energy storage applications batteries perform much better than hydrogen storage systems, but when it comes to longer-term storage application (season-to-season), the preferable option in terms of round-trip efficiency is hydrogen.

The second major hurdle is the relatively high capital cost of solar-hydrogen systems. For example a half-a-kilowatt petrol generator can be purchased for only about US\$500 (Macfarlane 2008); and due to the maturity of the technology, the installation cost of such a system is also quite reasonable. But the cumulative operation (mainly fuel) and maintenance (oil, filter, and periodic overhaul) costs of the system over its normal lifetime (20-30 years) are relatively high. The same size solar-hydrogen system costs above US\$50000 over an assessment periods of 20-30 years (Shabani *et al.* 2010), comprised mainly of the set-up capital cost of the system. Depending upon the operation and maintenance-related costs of the petrol/diesel based systems, they may turn to be more expensive than the solar-hydrogen system in a long-term operation, e.g. 20-30 years (Shabani *et al.* 2010). Nevertheless, the high initial investment costs of solar-hydrogen system remain a major hurdle deterring users from going for this option. Although there are promising predictions of cost reduction for the different components of the solar-hydrogen system in the next 10 to 15 years (Zoulias and Lymberopoulos 2007; Beccali *et al.* 2008; Lagorse *et al.* 2008), the system capital and set-up (if not the overall cost over a reasonable assessment period) costs are considerably more expensive at the present time compared to some of the existing alternatives such as petrol/diesel generators (Cuoco *et al.* 1995; Barbir 2005; Liu *et al.* 2009). This issue has encouraged many research studies on employing either new techniques or new technologies for reducing the cost of the solar-hydrogen system. The examples of these are the research done on eliminating elements like the DC-

to-DC converter of the system (Solmecke *et al.* 2000; Shapiro *et al.* 2005; Arriaga *et al.* 2007; Paul and Andrews 2008; Clarke *et al.* 2009), the cost reduction projects on the hydrogen storage tank by Ali and Andrews (2005), and the idea of using the same unit operated in both electrolyser and fuel cell mode or unitised regenerative fuel cell (Maclay *et al.* 2006; Doddathimmaiah and Andrews 2009).

1.3 SOLAR-HYDROGEN CHP SYSTEM

The present thesis seeks to make a contribution towards addressing the twin hurdles of low round-trip energy efficiency, and the need for improving the economics of stand-alone solar-hydrogen systems, as discussed in the previous section. Typically more than 50% of the energy content of the input hydrogen to the fuel cell is lost as waste heat (Larminie and Dicks 2003). Hence the opportunity explored by this thesis is to recover as much as possible of this heat and make use of it in a value adding or cost reducing way. This heat, for example, can be employed for either domestic hot water supply or space heating (Ferguson and Ismet Ugursal 2004) or even stimulating hydrogen discharging from metal hydride hydrogen storage (Varkaraki *et al.* 2003; Graf *et al.* 2006) if this type of storage is used in the system. The energy efficiency of fuel cells in power only applications (~30-50%) can be improved to more or less about 80% (Hawkes and Leach 2005; Hawkins *et al.* 2005) when it is used for CHP supply purposes. In turn the overall energy efficiency of the fuel cell and hence the overall round-trip efficiency of the whole solar-hydrogen system can be greatly enhanced by using both the electrical output and a substantial heat generated as the result of fuel cell operation.

The study in this thesis is mainly focussed on recovering this waste heat from the fuel cell to boost the remote area hot water system, as in many RAPS applications there is also a need to supply domestic hot water. The required heat may be at least in part supplied by the heat generated by the fuel cell, while the solar-hydrogen system is primarily designed and sized for meeting the electrical demand. This heat recovery would thus lead to cost saving, greenhouse gas (GHG) emission reduction, and reducing the inputs of conventional fuel used for water heating. Even solar water heaters can only supply part of the demand depending on the location (about 60% in Victoria, Australia), with the rest still having to be supplied by a fossil fuel-based boosting system.

Combined Heat and Power (CHP) fuel cell systems have been studied or demonstrated by a few researchers to date, for example: Gibbs and Steel (1992); Wallmark and Alvfors (2002); Colella (2003); Ferguson and Ismet Ugursal (2004); Gigliucci *et al.* (2004); Jalalzadeh-Azar (2004); Hawkes and Leach (2005); König *et al.* (2005). However, in all these investigations, the fuel cell has been studied as an isolated unit in heat and power production. By contrast the present thesis investigates fuel cell heat recovery in the context of the complete solar-hydrogen system. Modes of operation and the potential for fuel cell heat recovery are hence identified with the prime aim in mind of improving the performance and the economics of the whole system.

Bilgen (2001) investigated optimisation the hydrogen production sub-system. However, little work has been reported to date on optimisation of the entire solar-hydrogen CHP system, taking the economic benefit of the fuel cell heat recovery fully into account. Moreover, the present study follows a new approach to system optimisation in which the overall ‘net cost’ of the system is minimised after including the economic benefits of fuel cell heat recovery. In another words, this system optimisation approach is not just limited to the power supply mode of a solar-hydrogen system, but also incorporates CHP mode operation.

1.4 OBJECTIVES AND SCOPE OF THE THESIS

1.4.1 Objectives

The present PhD thesis thus focusses on computer modelling, design, optimisation, and evaluation of a stand-alone solar-hydrogen CHP system for supplying both electricity and heat for a remote application. The main challenge addressed is to improve the economics of the overall system by harnessing the thermal load of the fuel cell to meet other heat demands (e.g. domestic hot water) that would otherwise require purchase fuels to supply.

Specifically the objectives of the research program were to:

- review previous work on solar-hydrogen and fuel cell CHP systems;
- develop a computer model of a stand-alone solar-hydrogen CHP system based on a PEM electrolyser and fuel cell for remote area applications;

- investigate the energy efficiency and sizing of components via the model;
- perform optimisation analysis on the system by using the model;
- design, construct, and measure the performance of a laboratory rig of a CHP fuel cell system with heat used for water heating, and hence validate the computer model of the system;
- compare the solar-hydrogen CHP system with conventional remote area power supply systems in terms of technical performance, and triple bottom line (that is, economic, environmental and social) impacts; and
- identify priorities for further research and development to enhance the competitiveness of such systems.

1.4.2 Scope of thesis

The thesis focusses on stand-alone solar-hydrogen systems for supplying remote applications without a connection to the main electricity grid. The use of solar-hydrogen systems connected the main grid is outside of the scope of the present work. The standard system configuration studied comprises a PV array, a PEM electrolyser, a PEM fuel cell, and a hydrogen storage tank. Additional equipment such as DC-to-DC converters, DC-to-AC inverters, hydrogen humidifiers and dehumidifiers/driers, wiring, and control systems have not been considered in detail in the thesis, although an estimation of their overall cost in the system has been used for performing economic analysis.

The system considered is for supplying continuous electrical power to a remote household or other remote application with no grid connection and conservative electricity usage. The PV array is chosen as the main renewable energy supply for this remote application and the other components together play the role of the energy storage in the system. The PV array is analysed and modelled mathematically with hourly or half-hourly solar radiation data as the input. Wind generators are another possible renewable input to such a system, but are outside the scope of the present study.

A PEM electrolyser is used in the solar-hydrogen system studied in this thesis. Simplicity, high efficiency, and the possibility of delivering already-pressurised hydrogen are the principal advantages of this type of electrolyser over alkaline or solid oxide electrolysers

in RAPS applications (Paul and Andrews 2008). This component is modelled mathematically using a very recent theoretical analysis introduced by Doddathimmaiah and Andrews (2009).

The simplifying assumption is made of no energy penalty for storing hydrogen as a low-pressure gas and reusing it in a fuel cell, as it is assumed to be stored at near atmospheric pressure. Relatively large hydrogen storage cylinders are in principle feasible in remote areas since there is usually little restriction on the space available. Assuming hydrogen at low pressure allows the ideal gas law for hydrogen to be employed, which is the simplest assumption for modelling the hydrogen storage tank. Metal hydride and high pressure hydrogen storage tank are not within the scope of this study, although these alternative storage media could be modelled without too much modification of the main model.

The fuel cell in a solar-hydrogen system is at the focal point of this research, so it has been studied and modelled in the greatest depth. Only PEM fuel cells are investigated here due to their simplicity, quick response to variable loads, quick start up, and flexibility to be converted to a combined heat and power production unit (Larminie and Dicks 2003). This component has been concentrated upon as a prime opportunity to improve the system's economics by using it as a CHP unit. Water and space heating, and discharging hydrogen from a metal hydride, are all possible applications of the heat collected from the fuel cell while generating electrical power. This thesis concentrates in particular on using this waste heat for domestic hot water supply.

The study includes both theoretical analysis and experimental research. The theoretical part includes development and application of a general computer simulation model of a solar-hydrogen combined heat and power system. The experimental part focusses solely on the heat recovery potential of the fuel cell rather than the performance of the whole solar-hydrogen system.

1.5 RESEARCH QUESTIONS

The principal research questions addressed by this thesis are the following:

- What are the main factors affecting the performance of a solar-hydrogen CHP system?

- To what extent can the overall energy efficiency and hence economic viability of a solar-hydrogen system for remote applications be improved by utilising the waste heat from fuel cell operation for water or space heating?
- What is the economically-optimal size of a solar-hydrogen CHP system for a remote household with given electrical and hot water demand?
- How does a solar-hydrogen CHP system compare on a triple bottom line basis with conventional alternatives such as diesel or petrol generators and PV-battery systems?
- Which components of a solar-hydrogen CHP system require further research and development to enable such systems to compete with conventional alternatives?

1.6 METHOD

These research questions have been addressed using a combination of literature review, theoretical analysis and computer simulation modelling, and experimental investigations. The experimental results were compared with model predictions both to check their accuracy, and the validity of the model.

Specifically the main activities conducted within the overall project were as follows:

- *Literature review.* This activity included collecting and reviewing relevant scientific, technical and commercial product literature and other sources to find out the current ‘state of the art’ of solar-hydrogen systems in general and solar-hydrogen CHP systems in particular. The literature review and analysis on the reported data in effect constructed a platform from which the present project could be launched. It also provided initial answers to the first two research questions.
- *Mathematical modelling.* This work was about developing a mathematical model of all the components and the system as a whole to simulate the system behaviour. The model is flexible enough to accept new components. The PEM fuel cell was at the focal point of the model as its thermal load was to be investigated in particular. The simulation was built up in a visual base platform, Delphi, on the basis of Pascal programming language. This step created the possibility to answer all the research questions at a theoretical level.

- *Case study, system sizing and optimisation.* A case study relating to a remote household in south-eastern Australia was conducted using the simulation model to prove the ability of the simulation code in analysing a real case, finding the best sizing strategy to minimise the cost of the system and system optimisation, and also estimating the potential of the system for used as a CHP unit.
- *Setting up an experimental CHP fuel cell rig and model validation.* An experimental rig based on a 500 W PEM fuel cell and the available facilities in the RMIT Renewable Energy Laboratory (REL) was set up to evaluate the model in terms of recoverable heat predicted for the fuel cell. The experimental part of the project investigated the importance of some parameters that have to be considered and controlled carefully when running the fuel cell.
- *Triple bottom line evaluation.* The solar-hydrogen CHP system was then compared with other possible alternative systems and evaluated from social, environmental, and economic aspects using both the new model developed in the present work, and for certain cases the HOMER model (HOMER 2009).
- *Conclusions and recommendations.* Answers to all the research questions posed at the beginning of the thesis are provided on the basis of all the work conducted. Key factors that need to be considered when designing a solar-hydrogen CHP system are identified. Aspects that may need further investigations are listed. Conclusions on how a solar-hydrogen CHP system compares on a triple bottom line basis with conventional systems are drawn. Recommendations for further work and next steps are formulated.
- *Thesis preparation and publications.* Preparation of this dissertation as currently presented was the last task in of the project to report fully and reflect on the findings of this research. A number of conference and journal publications were also prepared as key outputs of this research.

1.7 OUTCOMES

The original deliverables set for this research project are listed as follows:

- A comprehensive state-of-the-art computer simulation program in a visual based environment for solar-hydrogen CHP system analysis.
- More in-depth knowledge on solar-hydrogen system design, sizing, and optimisation established through applying the model to a case study.
 - A comprehensive research on different sizing methods for the solar-hydrogen system
 - A novel technique for system sizing optimisation and cost minimisation was introduced
 - The heat recovery potential of the fuel cell and its associated economic advantage in the context of a RAPS solar-hydrogen system were studied. This investigation on solar-hydrogen system to use it for both heat and power generation was another step forwards to push the borders of knowledge on such a systems
 - The components with further need for research and development to improve the economics index of the system were identified
 - Sensitivity analysis showed how the system sizing and optimisation can be affected by following different economic and technical assumptions
- Development of an experimental PEM fuel cell CHP system to do experimental investigation on such a system.
 - Feasibility study on the fuel cell to find out about its potential for being used as a CHP unit and to show to what extent the predictions by the model agree with what happens in practice
 - The fuel cell controlling parameters that affect its heat and power output were identified
 - An investigation to show how the model is reliable for performing future analyses
- Research publication
 - Four conference papers and a journal paper are the up-to-date publications out of this research. Another journal paper, recently submitted, is now under review for publication.

1.8 THESIS STRUCTURE

Following this introductory chapter, Chapter 2 gives a more comprehensive and detailed introduction to the solar-hydrogen system, including a more extensive literature review of previous work in this area. Chapter 3 presents the new mathematical simulation model developed in this study for analysing solar-hydrogen combined heat and power systems. The theoretical basis of the model is presented for each component and the system as a whole. The structure of the corresponding simulation code, introduced with an operational guide, is provided in Appendix 1. Chapter 4 describes a case study conducted using the simulation model created of a stand-alone solar-hydrogen system to meet the energy needs of a remote household in south-eastern Australia with no access to grid electricity. On the basis of this case study, the potential for converting the solar-hydrogen into a combined heat and power system is investigated, and the economic advantage of such a CHP system is studied. A novel sizing method to optimise a solar-hydrogen system is identified and introduced as a result of this case study. Chapter 5 is a report of the whole experimental part of the research on a 500 W PEM combined heat and power fuel cell including the details of the rig development and the experimental results. The experimental results are compared to the outputs of the simulation model to see how reliable the model is in estimating the capacity of the solar-hydrogen system to be used as a CHP unit. Chapter 6 compares the solar-hydrogen CHP system studied in Chapter 4 with possible alternative RAPS systems such as diesel/petrol generator system, solar PV-battery system, and solar-hydrogen-battery system on the basis of triple bottom line – economic, environmental and social – assessment criteria. Finally Chapter 7 is dedicated to conclusions and recommendations.

2 Solar-hydrogen CHP systems for RAPS

2.1 INTRODUCTION

In vast countries such as Australia, there are many areas located far from the centralised electricity grid and gas distribution network that have to be provided with power. Therefore Remote Area Power Supply (RAPS) systems have been developed to meet the energy needs of such areas. Remote households, remote industrial and agricultural activities, remote communities, and remote telecommunication sites are some of the best examples of RAPS applications. A range of renewable and non-renewable systems such as diesel/petrol generator, and solar/wind battery/hydrogen systems are used for RAPS purposes. Factors including the local availability of renewable sources (such as solar radiation levels and wind speed regimes), the nature of the electrical load to be supplied, and the degree of reliability required for power supply, together with relative capital costs, usually determine which system is chosen for a particular case.

Solar-hydrogen systems offer a completely renewable and nearly zero-emission system for RAPS applications. While currently such systems are at an embryonic stage of development and hence expensive, they have great potential of becoming a cost-effective option in the near future as further system and technological development take place, and the main components are manufactured in much higher volumes (Ghosh *et al.* 2003; Beccali *et al.* 2008; Paul 2009).

In the present chapter, the basic stand-alone solar-hydrogen system to be used for RAPS is introduced and its potential advantages over conventional RAPS systems are identified. The main components of the system and how they interact to give the system its functionality are described. A literature review on the current state of development and know-how of solar-hydrogen RAPS systems is presented. Barriers in the way of commercialisation of such systems, and potentials for improvement are identified. In particular, the potential of solar-hydrogen systems to be used in a combined heat and power mode – one of the prime opportunities to improve the systems economics and competitiveness – is discussed.

2.2 HYDROGEN AS AN ALTERNATIVE ENERGY STORAGE IN PV-BASED RAPS

Photovoltaic arrays can be used for supplying the electrical demand for a remote application. However, the PV system is not able to meet the demand all the time, as a result of variable sunlight during each day, from season to season, and of course the absence of any solar radiation at night. Hence some form of energy storage is a necessary part of a PV system that has to supply power continuously throughout each year.

Basically the PV arrays are sized to generate more power than demand when they are exposed to enough solar radiation to do so. This surplus is stored to be used for those cloudy days or night time when the output of the PV array is either insufficient or zero to meet the demand all by itself. Batteries are a very common and conventional storage system for such an application. In a solar PV-battery system the PV arrays are sized for the month with lowest solar radiation (usually in winter) and this causes the system to be oversized for the summertime (Richards and Conibeer 2007). This leads to a substantial proportion of the output being wasted during the sunny summer days. Hence a solar PV-battery system for a reliably-continuous supply usually needs a back-up diesel-petrol generator to avoid a very large PV area or battery storage capacity that would be needed if only battery storage is used. Moreover, a few other problems are common with battery storage system, which triggers the idea of seeking alternative energy storage systems to avoid them. Maclay *et al.* (2006) listed the following problems associated with battery storage systems:

1. Relatively long battery recharging duration
2. Operational limitations such as depth of discharge and low charge and discharge rates
3. The requirement of frequent maintenance of the electrolyte level
4. Disulphation of the electrodes
5. Relatively short lifetime of the battery when a residential load is being supplied
6. Hazardous waste handling during disposal
7. Being only suitable for short-term application and considerable lost of charge when used for long-term storage applications
8. The need to be kept away from deep discharge to save the lifetime of the battery

In the light of these problems it is generally preferred to limit strongly the capacity of the battery energy storage.

Hydrogen-based energy storage systems are a strong alternative to battery systems in RAPS applications for the following main reasons:

1. *Long-term energy storage:* Unlike batteries, hydrogen can be used as a long-term energy storage. In long-term energy storage applications, that is, periods longer than a few weeks, batteries lose charge considerably, whereas hydrogen retains its energy content inside a storage tank as long as it is not being used. Hence, most importantly hydrogen, provides the flexibility of season-to-season storage with no problem of losing charge usually associated with battery system in long-term storage applications (Ali and Andrews 2005).
2. *Energy density:* The mass energy density (Wh/kg) of a hydrogen storage system can be higher than a lead-acid battery particularly if hydrogen is stored at relatively high pressure (Ulleberg and Mørner 1997). DOE (2009) reported that the maximum hydrogen storage capacity of 4.4 wt% (equivalent to above 1.5 kWh/kg mass energy density) has been achieved for high pressure hydrogen storage (70 Mpa). However, the mass energy density of different types of commercially-available batteries ranges from ~0.04 kWh/kg to ~0.75 kWh/kg (Nexergy, 2010), considerably less than the figure achieved for high-pressure hydrogen tanks.
3. *Flexibility of production:* Although hydrogen is not usually found in pure form on the earth (due to its high chemical reactivity), it is the most abundant element in the universe accounting for more than 75% of the total mass of universe (Contreras *et al.* 1999). Such availability, in conjunction with the presence of some renewable sources of energy nearly everywhere, create a great flexibility of hydrogen generation as an energy carrier over almost all the world.
4. *Simplicity of production using renewable sources:* Hydrogen can be readily produced by electrolysis of water using electricity generated by renewable energy sources such as solar and wind power (Nowotny *et al.* 2005).

5. *End-of-life disposal emission:* Disposal of a lead-acid battery at the end of its life is a serious environmental issue due to the toxic materials involved (Ro and Rahman 1998), while such a problem for the case of hydrogen storage systems can be avoided.

It is important to be noted that despite these problems associated with batteries, they show a good round-trip efficiency (about 80-90%) when used as a short-term storage (e.g. daily periods) (Maclay *et al.* 2006). This has encouraged many researchers to use both hydrogen-based energy storages and batteries together to meet both long-term and short-term energy storage requirements respectively (Ulleberg and Mørner 1997; Torres *et al.* 1998; Ghosh *et al.* 2003; Martínez Chaparro *et al.* 2003; Lagorse *et al.* 2008).

2.3 SOLAR-HYDROGEN SYSTEMS FOR RAPS

2.3.1 The basic solar-hydrogen system for RAPS

There is increasing interest in the use of solar-hydrogen systems for RAPS or other stand-alone applications (Gibril 2008). The main attractions of such systems are zero greenhouse gas emissions, complete stand-alone operation over extended periods of time, and low maintenance. As mentioned before, the use of hydrogen for energy storage rather than batteries has the potential to allow season-to-season storage of energy and hence a much lower photovoltaic array area (particularly in regions with highly variable seasonal irradiance), and no need for a back-up diesel generator. A typical solar-hydrogen system for stand-alone power supply to a remote application comprises an array of photovoltaic modules, a Proton Exchange Membrane (PEM) electrolyser, a storage tank for the hydrogen produced, and a PEM fuel cell to convert the hydrogen back to electricity when required. As schematically shown in figure 2-1, the electricity supplied by PV array is used to meet the demand directly to the maximum extent possible.

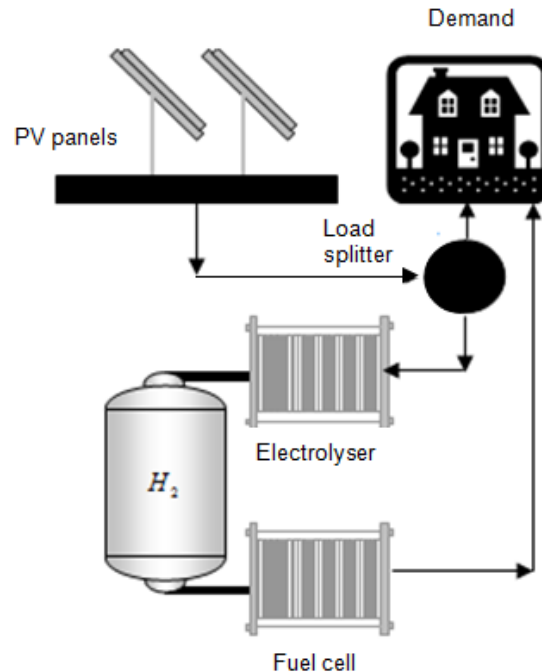


Figure 2-1. Simplified schematic of a typical solar-hydrogen system (Shabani *et al.* 2010)

If there is any surplus PV power over demand, and empty space left in the tank for accommodating additional hydrogen, this surplus power is supplied to the electrolyser to produce hydrogen for storage. Water can be broken into its basic components, oxygen and hydrogen, by passing electric current between two electrodes of the electrolyser located in an aqueous electrolyte (Uzunoglu *et al.* 2009). The efficiency of this conversion can be quite high-about 90% (Clarke *et al.* 2009). Alkaline and PEM electrolysers are the two commercially-available types of electrolyser. Electrolysis systems based on PEM have a number of advantages in comparison with traditional water-alkaline electrolysers, including ecological cleanliness, considerably smaller mass-volume characteristics and power costs, a high degree of gas purity, an opportunity of compressed gases obtaining directly in the installation, and the increased level of safety (Pahomov and Fateev 1990). Electrolysers can either deliver hydrogen at low or high pressure, depending on the pressure that the hydrogen is needed to be stored. High-pressure, up to several hundred bar, are mostly needed for the industrial market for hydrogen (Grigoriev *et al.* 2009). Pressurising of hydrogen through the electrolyser has the advantage of eliminating mechanical losses through a typical mechanical compressor (Dunlop 2004; Shapiro *et al.* 2005; Marangio *et al.* 2009). In the present study, where hydrogen is used in a RAPS

application, the availability of space is not an issue normally, and hydrogen can be generated and stored at a low pressure.

The last piece of the solar-hydrogen system circuit is the fuel cell which is a power supply device running on hydrogen and oxygen. Fuel cells can be used for a range of applications from stationary and portable power generation to automobiles (Sammes and Coors 2006). When the output of the PV array is not sufficient to supply the demand, the fuel cell draws on hydrogen from the storage and produces electricity to meet the supply deficit. The type of the fuel cell the present research focuses on is based on proton exchange membranes (PEM). The unique features of this type of fuel cell are its inherent simplicity, low cost, high power density, high electrical efficiency, low operating temperature, and safe operation. PEM fuel cells operate at relatively low temperatures in the range of 30-100 °C (Larminie and Dicks 2003), a feature which yields a very short start-up time and quick response to a changing load (Zhang *et al.* 2004). Also common materials and technologies between the PEM electrolyser and fuel cell are used (for example, similar membranes, and platinum catalysts are used and similar techniques of catalyst synthesis are applied), so that technological and production improvements in one can help the market competitiveness of the other (Grigoriev *et al.* 2006).

2.3.2 Current state of development of solar-hydrogen systems

2.3.2.1 Modelling and demonstration

Solar-hydrogen systems, either a particular section of them (e.g. just the hydrogen generation including the PV array and electrolyser) or the entire system, including stand-alone RAPS system, have been investigated by many researchers using theoretical models (Hollenberg *et al.* 1995; Vanhanen *et al.* 1996; Ulleberg and Mørner 1997; Tani *et al.* 2000; Ghosh *et al.* 2003; Martínez Chaparro *et al.* 2003; Ali 2007; Lagorse *et al.* 2008), and/or experimental studies and demonstrations (Galli and Stefanoni 1997; Agbossou *et al.* 2001; Miland and Ulleberg 2008; Liu *et al.* 2009). Some modelling and demonstrations have used batteries coupled to the hydrogen energy storage system to take the advantage of the high round-trip efficiency of batteries for short-term energy storage.

Also many countries such as Spain (Contreras *et al.* 1999), Egypt (Abdallah *et al.* 1999), UAE (Kazim and Veziroglu 2001), and Saudi Arabia (Almogren and Veziroglu 2004) have performed a variety of research studies on renewable production of hydrogen, in particular using solar energy to reduce their demand on fossil fuels. It should be noted that solar-hydrogen production is a part of the stand-alone solar-hydrogen system being discussed and investigated by this research. Stand-alone power supply has also been targeted and investigated by many technologically-advanced countries. For example, the research done by Zoulias *et al.* (2006) on stand-alone hydrogen is to be used by European Governments to prepare the ground for regulatory changes to facilitate alternative grid solutions.

Some other research studies have also been conducted on applying solar-hydrogen systems for automotive applications, for example: Dunlop (2004); however, they are not discussed and reviewed here as transport applications are outside of the scope of this study.

2.3.2.2 System modelling

Hollenberg, Chen *et al.* (1995) did research on a renewable solar-hydrogen system by developing a computer model for analysing the system. The system modelled and studied by this research included an array of 150 W photovoltaic modules and a three-cell electrolyser stack (6.8 V, 14 A) with a maximum hydrogen production capacity of 225 Ncm³/min. They also investigated a metal hydride system for hydrogen storage as a safe, low maintenance cost system with high volumetric density.

Vanhanen *et al.* (1996) conducted a feasibility study in particular on using metal hydride storage in a self-sufficient solar-hydrogen system employing a pressurised electrolyser to charge the metal hydride directly. A 1 Nm³ (measured at 1 atm and 273 °K) commercially manufactured Hydralloy C15 metal hydride was used for this study. The study suggested low-temperature metal hydrides could become economically and technically viable hydrogen storage solutions for small-scale stand-alone solar-hydrogen systems. A few other metal hydride alloys were also investigated by this research.

Ulleberg and Mørner (1997) developed a model using TRNSYS for performing transient simulation on solar-hydrogen-battery systems. The model was then used to study and size

such a system at three different locations in north hemisphere, and it also investigated the effect of yearly electrical demand on the system sizing. The model considered a pressurised electrolyser (3000 kPa) and a PEM type of fuel cell for the system studied.

A solar-hydrogen-battery system was modelled for Mexico by Torres *et al.* (1998). The results of solar-hydrogen hybrid system simulation were reported for different locations in Mexico. This study suggested that the voltage of the PV array and the fuel cell must be high enough to charge the battery, and the voltage of the electrolyser must be low enough for the battery to power it during periods of low insolation. This research also illustrated that the sizes of the components have a high degree of dependency on the location where the solar-hydrogen system is installed.

Tani *et al.* (2000) developed a mathematical model and a small-scale solar-hydrogen production rig. They also performed a system optimisation based on the cost of the hydrogen produced by the system. The system modeled contained PV modules rated at 3.4 V and 27.75 A (12.75% conversion efficiency at STC) connected to a PEM electrolyser. This study also commented on the effect of PV cells' temperature, solar irradiance, and electrolyser operating temperature on the performance of the PV array and electrolyser and hence on the cost of hydrogen production.

Rzayeva *et al.* (2001) worked on a mathematical model to study the economic viability of solar-hydrogen production. The case studied by this model was a solar-hydrogen production plant in Baku where the maximum solar irradiance is about 900 W/m² in July. This research was followed by an experimental investigation on the negative impact of the dynamic output of the PV array and some comments on matching the size of the electrolyser with this variable PV output to optimise the system.

Solar-hydrogen-battery systems for stand-alone remote telecommunication application were modeled and studied by Martínez Chaparro *et al.* (2003). The system that was later installed for testing in Madrid, Spain had to supply an electrical load with a peak of 200 W. A 1.4 kW PV array (15.8 m²) was chosen to be used in this system with an average efficiency of 9.9%. 65-69% of the PV output was directly used by the load and 30% of it fed into a 76% efficient 1 kW PEM electrolyser (a stack of 30 cells) with an average daily hydrogen production of 0.33 Nm³. 1-5% of the PV output was also considered to be used

by the electronic control system. The conversion efficiency of the 450 W 48-cell PEM fuel cell stack (Nuvera) used in the system was assumed to be 50% on average (based on HHV of hydrogen). Seven metal hydride tanks (La-Ce-Ni-Al-Sn alloy) were used to store hydrogen at about 3 MPa.

Varkaraki *et al.* (2003) modeled a hydrogen-based emergency back-up system for telecommunication applications. The system comprised a 35% efficient PEM fuel cell (on average) to supply 5 kW power for 5 hours; an 82% efficient PEM electrolyser stack with a capacity of 0.5 Nm³/h of hydrogen production with the purity of 99.999 vol.% at 1000 kPa of pressure; a metal hybrid tank to accommodate 15 Nm³ of hydrogen; and a medium pressure 1 m³ conventional hydrogen tank with the capacity of 6 Nm³ of hydrogen just to start up the fuel cell. The fuel cell draws on hydrogen from the conventional tank to start up, and thereafter the heat generated by the fuel cell is conducted to the metal hydride to help discharge the hydrogen to the fuel cell and hence keep the system going. This study showed that the most critical part of the system that needed to be improved is the fuel cell. It was illustrated that using oxygen instead of air in the fuel cell could potentially increase its efficiency from the average of 35% to about 50%.

Ghosh *et al.* (2003) conducted a modelling study to compare a solar-hydrogen-battery system with a diesel generator. The study showed the system was expensive at that time compared to a diesel generator, due to the high cost of the fuel cell and electrolyser; however, it was expected to become competitive to a diesel generator in the near future when a target cost of about 3000 €/kW for these components is achieved. The round-trip efficiency of the battery and the hydrogen energy storage systems were assumed to be 93% and 40% respectively in this study and a nominal discount rate of 7% and an inflation rate of 5% were used for doing the economic analysis.

An hourly-based analysis of a household located in a valley of the Alps in Italy by Santarelli and Macagno (2004) is another example of a theoretical study of solar-hydrogen RAPS systems. This analysis included a detailed investigation on the economics of the system. Figure 2-2 shows the configuration used in the research done by Santarelli and Macagno (2004). The system investigated by this study comprised a PV array, composed of 75 modules with the total surface of 47 m², and another alternative PV array including 21 S_μHHES modules with the total surface of 15 m²; three small electrolysers (1 kW

Ali and Andrews (2005) developed a very useful spreadsheet model to simulate a stand-alone solar-hydrogen system for RAPS, with the main focus on the storage tank to minimise the cost of the system. This research also studied the effect of using an unconstrained hydrogen tank as a potential solution for reducing the cost of the system in some cases. Experimental investigations were conducted into the possibility of using low cost hydrogen storage options such as acrylic cylinders; fibre reinforced plastic water tanks; composite cylinders; and low-carbon steel (up to 2000 kPa) cylinders for a low pressure stand-alone solar-hydrogen system for RAPS applications.

The MATLAB/SIMULINK based computer model developed by Maclay *et al.* (2006) has been used for modelling stand-alone solar-hydrogen systems; the system simulated included a battery for short-term storage and hydrogen was just considered as a long-term energy storage option. This research also studied the viability of using a regenerative fuel cell in the system. The results revealed that, although using battery coupled with the system can enhance the PV power output utilisation, it can increase the size of the solar-hydrogen system and reduce the average efficiency of the fuel cell. The use of a battery for covering the peak demand was recommended by this study.

The model developed by Lagorse *et al.* (2008) is another MATLAB/SIMULINK model that looked at different configurations, including a solar-hydrogen system with and without battery storage and a solar PV-battery system. The comparison was done based on the economics of these systems. Lagorse *et al.* (2008) also tried to predict the future of these technologies, when components such as the fuel cell become more affordable, using the results generated by the model. The case studied was a site with total annual solar energy of about 1.6 MWh/m². The average efficiency of the polycrystalline PV modules used was roughly 10% and thus a total annual output of 160 kWh/m² from the PV array was fed into the model. The PEM fuel cell used by the model was assumed to have an average annual energy efficiency of 40% with 95-98% hydrogen utilisation.

2.3.2.3 *System Demonstration*

Studies on solar-hydrogen systems have not been just limited to modelling and simulation studies, and several demonstrations have also been set up so far to look at the practical side of the system. Some examples of these demonstrations are the following:

A completely-stand-alone solar-hydrogen system was demonstrated in Italy and reported and analysed by Galli and Stefanoni (1997). The system was composed of a 5.6 kW PV array directly coupled to an Alyzer-0100 5 kW alkaline pressurised electrolyser (Max 2000 kPa). The electrolyser was a stack of 17 cells operated at 80 °C. The possibilities of using a conventional hydrogen tank and metal hydride alloy storage were both considered. A 3 kW PEM fuel cell, manufactured by Ballard Power System Inc. (Canada) and operated at 72 °C, was used to complete the stand-alone solar-hydrogen system. The efficiency of this fuel cell was measured to be 53.6% at maximum operating condition based on LHV of hydrogen when hydrogen/air were supplied at 207 kPa and air stoichiometry of 2 was used. The maximum output power of the fuel cell showed only about 8% drop after two years of operation in the system.

Agbossou *et al.* (2001) reported on an integrated solar-wind-hydrogen system for supplying continuous power to a telecommunication station. The system studied by this research used two sources of renewable energy: a 10 kW wind turbine and a 1 kW PV array. The hydrogen was produced through the excess available renewable energy fed into an electrolyser (71% efficiency at 55 °C) and then pressurised using an external compressor. A 5 kW 35-cell PEM fuel cell stack (Ballard MK5E) with an average efficiency of above 40% was used to complete the solar-hydrogen system circuit. This study also commented on the positive effect of increasing the operating temperatures of the fuel cell and electrolyser, on the performance of the system. The results of the study suggested using pure oxygen instead of air for running the fuel cell at considerably higher energy efficiency.

A study and demonstration of the technical feasibility of a hybrid stand-alone energy supply system, based on a photovoltaic array, a battery and hydrogen fuel cell system were performed by Ghosh *et al.* (2003). The battery was used for short-term energy storage (up

to three days) and supplied slightly above 50% of the annual demand. A hydrogen-fuel cell system was used as the long-term storage and supplied 20-25% of the annual demand.

Ghosh *et al.* (2003) reported on a demonstration solar-hydrogen-battery system supplying part of the energy demand of a library in Forschungszentrum Jülich, Germany, for ten years. The system consisted of PV arrays with the maximum output of 43 kW; a 110-cell lead acid battery bank with the capacity of 303 kWh at 10 A; a 26 kW alkaline electrolyser operated at maximum pressure of 700 kPa. The system was tried with two types of fuel cell separately: initially a 6.5 kW alkaline fuel cell and then a 5 kW PEM fuel cell. Operation of the system between 1997 and 2001 showed that 20-25% of the annual demand was supplied directly by the PV arrays, almost the same percentage was supplied by the fuel cell and the battery system had the biggest share of supply, by providing above 50% of the energy requirement.

The first solar-hydrogen home in North America, New Jersey, was reported by Fuel Cells Bulletin (2006). The hydrogen produced by the electrolyser was stored in propane tanks exactly at the same pressure that propane is normally stored in them. The PV array directly provided 60% of the electricity during the winter time with the remaining coming from the stored hydrogen reacted with oxygen from the air inside a fuel cell. The power, heat, and fresh water from the fuel cell were all utilised.

Miland and Ulleberg (2008) studied a hybrid solar-hydrogen system in which a 300 Ah lead-acid battery bank was employed. They also used an air-cooled metal hydride in their solar-hydrogen demonstration which was not reliable from heat transfer point of view (sufficient cooling rate is required for a proper hydrogen discharge). The system studied consisted of a 4.8 kW programmable power supply; a 1.5 kW electrolyser; a hydrogen purification unit (99.999%); a 14 Nm³ metal hydride storage; a 0.5 kW fuel cell; a 300 Ah battery; and a 0.6 kW programmable load. In this study the electrolyser and the fuel cell showed an average of 60% and 47% efficiency respectively.

One of the latest solar-hydrogen demonstrations in which a battery bank was also used was the first hybrid solar-hydrogen system in China (Liu *et al.* 2009). The system was not completely stand-alone and just above 30% of the demand was supplied through the PV array (directly or through the fuel cell), and the rest was provided by the AC supply. The

system comprised a 2 kW PV array; an electrolyser with a capacity of 0.5 Nm³ per hour; a 200 W hydrogen/air PEM fuel cell; a 10 Nm³ LaNi₅ alloy hydrogen storage tank; and a 300 Ah lead-acid battery. The system was installed by the Institute of Nuclear and New Energy Technology (INET) of Tsinghua University and was operated for several months. Both PEM and alkaline electrolysers were tried by this study. The conversion efficiency between the input to the PV array and the hydrogen output from of the electrolyser was calculated to be between 6-8% for the alkaline electrolyser and above 12% for the PEM electrolyser. However, it was suggested by the report that still better energy conversion efficiency is needed to make the system economically attractive.

2.3.2.4 Challenges facing solar-hydrogen RAPS systems

Solar-hydrogen systems, as just described, have the potential to become a dominant technology in RAPS applications and perhaps in more general applications over the coming decades. However, the previous review has identified some critical challenges facing these systems if their full promise is to be released (Nowotny *et al.* 2005). These critical challenges are:

- improving round-trip energy efficiency,
- reducing the high cost of the system, and
- fresh water supply.

Round-trip energy efficiency of the hydrogen storage sub-system is the percentage of the cumulative electrical energy supplied by the fuel cell to the electrical energy used by the electrolyser to produce hydrogen (that is recovered later by consuming the hydrogen produced in a fuel cell). The relatively low round-trip energy efficiency of the hydrogen storage sub-system can be a significant impediment in many applications, both in RAPS and more generally (Zoulias *et al.* 2006). This round-trip energy efficiency can theoretically be above 70%, although in practice it is much lower. For a unitised regenerative fuel cell (single unit for both electrolyser and fuel cell) known as URFC, the maximum achievable round-trip efficiencies have been reported to be in the range of 20-30% (Doddathimmaiah 2008). However, for systems in which separate units for electrolyser and fuel cell are used this figure can be higher than this range. The round-trip

efficiency of the system studied by Barbir (2005) was calculated above 30% whereas Shapiro *et al.* (2005) reported 25%. For the case of a solar-hydrogen system it is not guaranteed that the system works at its maximum round-trip efficiency point as the operational point of the fuel cell is dictated by the electrical load to which it is connected. That is why the average round-trip efficiency of the system over a year of operation can be quite low. For example, for the case study discussed in detail later in this thesis, the average annual round-trip efficiency is as low as 24%. These figures for round-trip efficiency are quite low compared with batteries for short-term energy storage but still higher over periods of several months or more. Hence unlike batteries, the hydrogen system can be used for both long and short-term energy storage applications (normally more than a few weeks) with almost the same range of round-trip efficiency whereas this efficiency in batteries drops dramatically, even down to nearly zero, if they are used for long-term storage purposes (e.g. season-to-season).

Cuoco *et al.* (1995), performed a case study on the economic viability of a PV-hydrogen system against using traditional fossil fuels. The results of this study showed no promising economic viability for the PV-hydrogen system against fossil fuel-based systems until about 2025. The cost of the solar-hydrogen systems has always been a challenging issue which needs further improvement before such systems can be a strong alternative to the existing technologies or competitive to the grid electricity (Liu *et al.* 2009). The reason for the current lack of competitiveness is the high-cost of the individual components used in solar-hydrogen systems. They are expensive mainly due to their relatively early stage of technological development and the low volumes of production. Many studies have been conducted on different aspects and parts of the system to improve its economics. Solar-hydrogen systems have been described an expensive technology by Barbir (2005) at the time that his research was done; however, this researcher saw a promising perspective for using this system at an economically acceptable cost for applications like RAPS where the cost of transporting fossil fuel to these areas is relatively high. He also investigated possible measures for increasing the efficiency of the system to improve the cost of the electricity produced.

Although the costs of current solar-hydrogen systems – mainly experimental and early-stage demonstrations units – are high, the competitiveness of such systems is likely to improve over the next decade as the cost of diesel, petrol or LPG rise, and the cost of

transporting these to rural areas also escalate. In addition the solar-hydrogen system costs are likely to fall with further technological development and larger-volume production of key components such as electrolyzers, fuel cells and hydrogen storage systems.

Low-cost hydrogen storage options, particularly for remote area applications were investigated by Ali and Andrews (2005). Another cost-reduction opportunity is to eliminate the cost of a DC-to-DC converter and maximum power point tracker by directly coupling suitably-configured PV arrays and electrolyzers (Solmecke *et al.* 2000; Shapiro *et al.* 2005; Arriaga *et al.* 2007). This possibility was investigated theoretically and demonstrated experimentally by Paul and Andrews (2008) and Paul (2009). A further experimental confirmation of the viability of the direct-coupling concept has been provided by Clarke *et al.* (2009) for a 2-kW PEM electrolyser developed by CSIRO Australia. However, to date direct PV-electrolyser coupling has been investigated only for the case in which all the output of the PV array is fed to the electrolyser at all times, rather than just the excess of PV output over the load, which is the much more desirable system configuration from an energy efficiency perspective.

Unitised regenerative fuel cells (URFCs) – a single cell that can operate reversibly in either electrolyser or fuel cell mode as required – is a further option that is being investigated to reduce the cost of solar-hydrogen systems. Maclay *et al.* (2006) used a unitised regenerative fuel cell in a solar-hydrogen system and described it a viable option to reduce the system cost. Doddathimmaiah (2008) and Doddathimmaiah and Andrews (2009) conducted comprehensive research on this option for remote area applications. This research resulted in a novel mathematical model for URFCs based on modified Butler-Volmer equations at both electrodes. They also conducted experimental tests to identify the best-performing catalysts for the oxygen-side.

Opportunities to reduce the cost of solar-hydrogen systems by optimising the system configuration and component sizes have been investigated by Bilgen (2001). The present study follows up this work and presents a new approach to system optimisation in Chapter 4.

PEM electrolyzers require deionised water and supplying this water might be an issue for some remote or stand-alone power applications. In a stand-alone solar-hydrogen system,

the pure water product of the fuel cell can be recycled to be used by the electrolyser, so that the demand for ongoing deionised water supply to the electrolyser is minimised. Some researchers have assumed 100% of the water supply to the electrolysers can be obtained by recycling the water produced by the fuel cell, given that in an ideal system with zero hydrogen losses the mass of end-product water is equal to the water input to the electrolysers. (Shapiro *et al.* 2005). Other studies have sought to take into account the hydrogen and water losses in actual systems, for example, Barbir (2005). 1 litre of water theoretically yields 1.24 Nm³ of hydrogen. Both gaseous hydrogen and oxygen leave the electrolyser slightly wet, leading to some water losses. In addition, all the water produced in the fuel cell cannot be in practice recovered. Typically the net losses are about a quarter of the water consumed even with recycling of the water from the fuel cell back to the electrolyser (Barbir 2005).

2.4 SOLAR-HYDROGEN CHP SYSTEMS

2.4.1 The origin of the idea

Under theoretically ideal conditions, and based on the second law of thermodynamics, the efficiency of a fuel cell in electrical power production varies from 62% to 83% for operating temperatures between 1000 °C and 25 °C. Fuel cell efficiencies in practice are less than these due to irreversibilities in both the electrochemical reactions and electrical processes (Larminie and Dicks, 2003). This lowering of energy efficiency below 100% occurs mainly because part of the input hydrogen energy content is converted to heat as the hydrogen reacts with the oxygen in the fuel cell. Herein is where the idea of a combined heat and power fuel-cell system originates: utilising the heat as well as the electricity generated by the fuel cell can greatly enhance the solar-hydrogen system's overall energy efficiency. In addition, by supplying both electricity and heat to end-use applications there is a potential to improve the overall economics of a solar-hydrogen system.

2.4.2 History and state of the art review

The concept of a fuel-cell CHP system was first proposed by Gibbs and Steel (1992). Packer (1992) described combined heat and power or cogeneration as an ideal application

for the fuel cell as a result of his study on commercialisation of fuel cells for small-scale applications. Drenckhahn (1996) focused on solid-oxide fuel cells and their application for combined heat and power plants. The first commercial fuel cell for producing both electricity (200 kW_e) and heat in Australia (made by UTC Power Manufacturing Company as a part of U.S. Department of Defense climate change fuel cell program) came on stream in the Australian Technology Park, Sydney, in 1999. This phosphoric acid fuel cell had an overall thermal and electrical efficiency of 80%, and used natural gas for producing hydrogen. The first fuel-cell CHP project in the UK was completed in December 2001 with the system providing heat and power for a swimming pool and leisure centre. Research done by Wallmark and Alvfors (2002) revealed that most of the heat and power requirement of a building in Sweden could be supplied by using a fuel cell in a combined heat and power application. Colella (2003) conducted a number of case studies on fuel cell CHP systems to show how this cogeneration arrangement could help fuel cells become economically competitive against conventional petrol/diesel generators. Study done by Gigliucci *et al.* (2004) on a residential CHP system demonstration based on PEM fuel cells is another example of demonstration of a residential CHP system of this kind. The result of the study conducted by Gigliucci *et al.* (2004) was also a mathematical tool for analysing fuel cell CHP systems for prediction of system performances and operating parameters. Ferguson and Ismet (2004) reported on the development of a PEM fuel-cell simulation model incorporating both electrical and heating loads of a building (space heating and hot water supply) as shown by figure 2-3. This model estimated fuel-cell performance in response to a varying building energy demand, and showed that fuel cell capacity and operating strategy are critical factors affecting this performance. Heat recovery methods from low-temperature PEM fuel cells and the associated challenges were investigated by Jalalzadeh-Azar (2004). In this research a number of fuel cell heat recovery methods for building applications were assessed from the thermodynamics point of view. The simulation done by Hawkes and Leach (2005) on a UK household showed a potential of 80-90% overall energy efficiency for a solid-oxide fuel cell providing both heat and power in this application. Another example was a prototype PEM fuel cell CHP system for decentralised energy supply in domestic applications installed in the Fuel Cell Testing Laboratory at the Institut für Werkstoffe der Elektrotechnik (IWE), Universität Karlsruhe (TH), reported by König *et al.* (2005). In a report released by UKSHEC Social Science (Hawkins *et al.* 2005), the overall efficiency of PEM fuel cell in both heat and power

generation was reported as 75%, slightly less than the efficiency given by Hawkes and Leach (2005) but still of the same order.

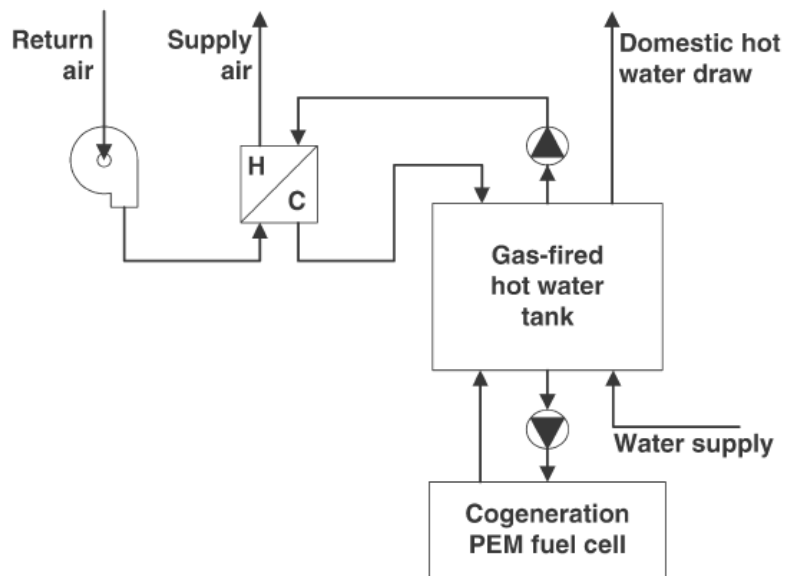


Figure 2-3. PEM fuel cell CHP configuration suggested by Ferguson and Ismet Ugursal (2004) for supplying both heat and power demand of a building

The heat generated by the fuel cell during operation was also suggested to be used to boost hydrogen release from a solid-state metal hydride (material-based) hydrogen storage canister (Varkaraki *et al.* 2003; DOE 2009). To start the discharge process in the first place, an electrical heating element might be used; or the fuel cell can be initially run on hydrogen coming from a conventional compressed gas tank with supply shifted to the metal hydride hydrogen storage tank when thermal load of the fuel cell rises to a sufficient level to drive the hydrogen discharging process. Such a design concept has been used by Varkaraki *et al.* (2003) in a hydrogen-based emergency back-up system for telecommunication applications. The schematic for this arrangement is shown in figure 2-4. Jiang *et al.* (2005) developed a simulation model to investigate the idea of using the fuel cell heat for extraction of hydrogen from the metal hydride storage tank. This idea was also proposed by Graf *et al.* (2006) as a result of their theoretical/experimental study on the heat generation side of a PEM fuel cell. Using this heat for hydrogen extraction from the metal hydride was described as a technique that provides trouble-free operation of the fuel cell when fed with hydrogen through a metal hydride hydrogen tank (figure 2-5). This idea was further followed by other researchers such as Førde *et al.* (2009).

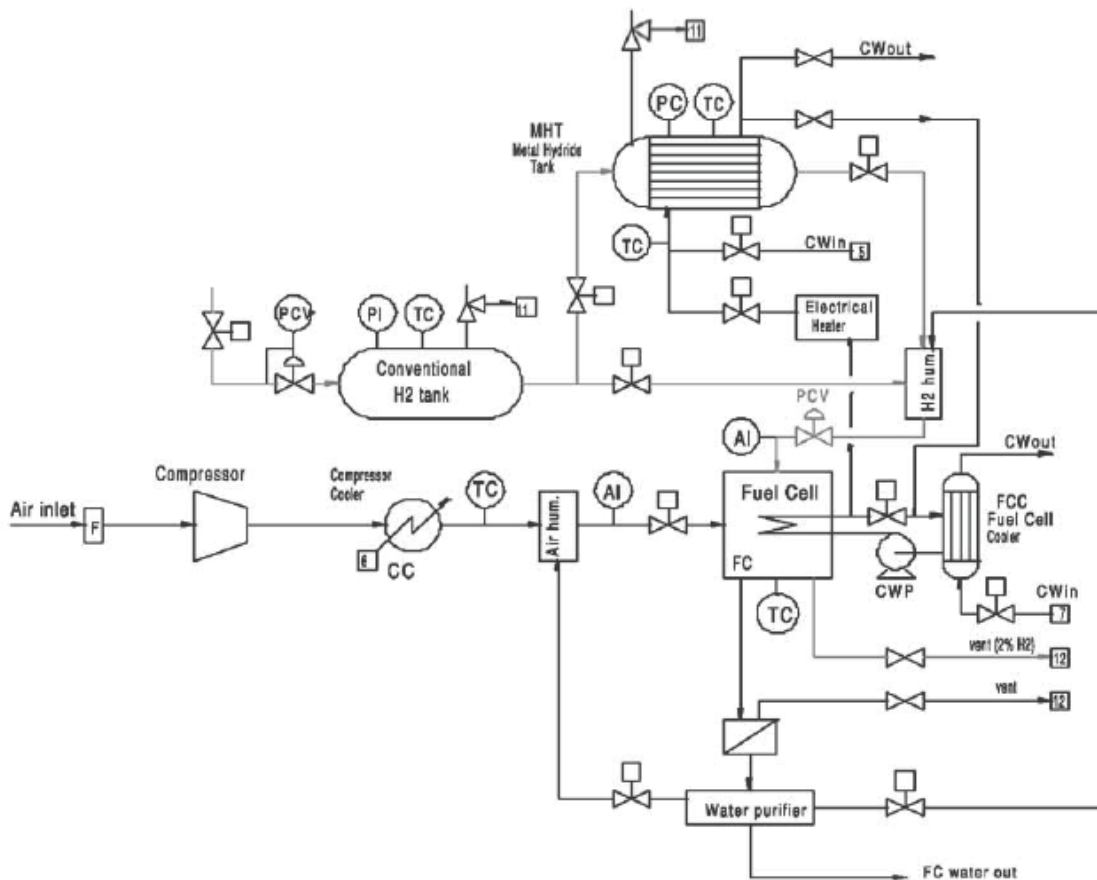


Figure 2-4. Use of fuel cell heat to discharge hydrogen from a metal hydride (Varkaraki *et al.* 2003)

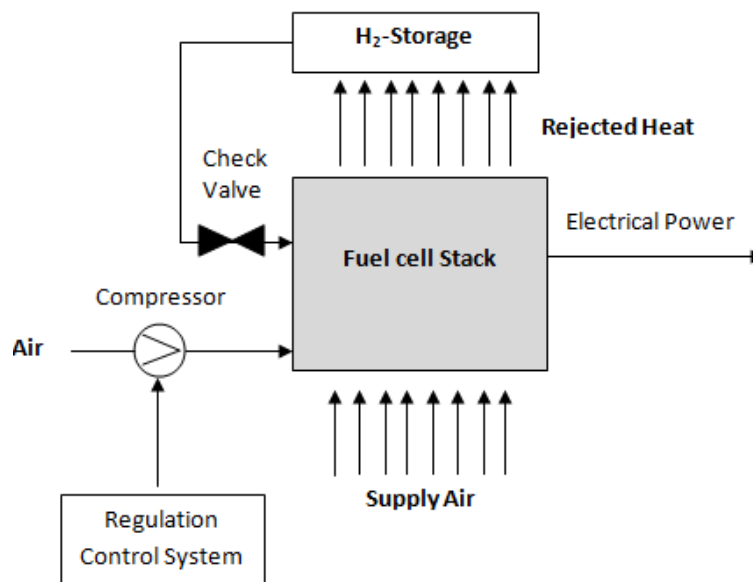


Figure 2-5. Modelling of PEM fuel cell including thermal coupling between the fuel cell stack and hydrogen metal hydride storage tank done by Graf *et al.* (2006)

Extra hydrogen and air (above the amount required by the standard chemical) has to be fed into the fuel cell to increase the probability of reactions at both electrodes. The heat generated by burning this excess hydrogen, collected from the hydrogen exit stream of the fuel cell, can be added to the heat generated by the fuel cell while producing power. This idea has also proposed by Hawkes and Leach (2005) where they suggested mixing the residual hydrogen (determined by the fuel cell hydrogen utilisation) with the air exhaust stream and then burning the hydrogen in a burner to capture its energy in the form of heat.

2.5 FOCUS OF THIS THESIS

In the research program for the present thesis, a comprehensive theoretical model of a solar-hydrogen RAPS system has been developed that can also simulate combined heat and power mode operation. The model is intended to be a general modelling tool, incorporating improved sub-models based on recently-developed theoretical analysis for the components, and not just dedicated to analyse a special case. The new model can be run on any operating platform (XP, Vista, or windows 7) with no dependency on particular supporting software such as Microsoft Excel, TRNSYS, or MATLAB, as has been the case for earlier models such as those developed by Ulleberg and Mørner (1997), Ali and Andrews (2005), and Maclay *et al.* (2006).

As reviewed in the previous section, a small number of modelling programs for simulation of combined heat and power operation of fuel cells have already been reported in the literature. Some of these concentrate on extraction of the heat generated out of the reaction between oxygen and hydrogen inside the fuel cell, like Ferguson and Ismet's (2004) study on a PEM fuel cell. Others look at other types of the fuel cell (e.g. solid-oxide) and basically heat recovery from the hydrogen reformer (Hawkes and Leach 2005). The common feature of these previous models is that they consider the fuel cell CHP system individually. Most work to date has thus focussed on fuel cell CHP systems operated using a provided supply of hydrogen, whether from a bottled gas or via steam reforming of natural gas. The important advance in the simulation model presented in this thesis is to treat CHP operation of the fuel cell as an integral part of the overall solar-hydrogen system, and assess total system performance on a yearly basis taking into account the variation in input solar energy. Hence the economics of the solar-hydrogen CHP system as a whole can

be investigated, rather than the PEM fuel cell CHP system. The prime aims are to investigate the potential of adding CHP mode operation to the standard solar-hydrogen system to raise the overall system energy efficiency, and thus enhance its economic viability.

The PEM fuel cell is used by this study that has been described an ideal option for domestic-scale CHP applications by Larminie and Dicks (2003). The heat extracted from the PEM fuel cell is potentially useable for a range of low-temperature (~60 °C) heating applications, such as domestic hot water supply, space heating for a remote household or other building, or enhancing discharge of hydrogen from a solid-state metal hydride storage. In the present thesis, the use of the heat extracted from the PEM cell by its cooling system to supply part of the energy required for producing hot water in a domestic application is considered in detail.

Some previously-created models have sought to optimise the system based on the cost of hydrogen produced (Tani *et al.* 2000). The model presented here by contrast performs system optimisation on the basis of minimising the average unit cost of electricity over the system lifetime, and takes into account the potential economic benefits of fuel cell heat recovery.

The new simulation model for solar-hydrogen CHP systems developed is presented in detail in the next chapter.

3 System modelling

3.1 INTRODUCTION

3.1.1 Aims

A simulation program has been developed as one of the main parts of this research study and aimed at performing the following tasks relating to solar-hydrogen CHP systems for remote applications:

- 1- Solar geometry analysis
- 2- Mathematical simulation of PV module to predict the performance at any given PV cell temperature and effective incoming solar radiation.
- 3- Mathematical simulation of fuel cell and electrolyser to conduct comprehensive performance analysis
- 4- Comprehensive mathematical modelling of solar-hydrogen system to analyse the performance, outputs, and the energy flow
- 5- Solar-hydrogen CHP system analysis and hydrogen waste recovery analysis
- 6- Solar-hydrogen system sizing and economic optimisation
- 7- Economic analysis of solar-hydrogen systems with and without performing waste recovery

This simulation program has been named the RMIT Solar-Hydrogen Analysis Program (RSHAP).

3.1.2 The major features of the model

RSHAP is supported by 20 000 plus lines of programming and separate procedures for handling individual computational tasks. RSHAP has the following additional features and capabilities compared to existing models:

- Unlike many other previous models (Hollenberg *et al.* 1995; Tani *et al.* 2000; Ali and Andrews 2005; Lagorse *et al.* 2008), RSHAP is built using a visually-based and a user-

friendly environment making it easy to learn how to use, and providing flexibility to add new modules if required.

- RSHAP is a stand-alone simulation program with no dependency on any particular operating platform (Such as Windows 1997-2003, Windows XP, Windows Vista, or Windows 7) or supporting primary software tools (such as Microsoft Excel, TRNSYS, or MATLAB) (Ulleberg and Mørner 1997; Ali and Andrews 2005; Maclay *et al.* 2006).
- Many models created so far are dedicated to analyse a special case (Martínez Chaparro *et al.* 2003; Varkaraki *et al.* 2003) whereas RSHAP is a more general modelling tool. It can flexibly receive variety of inputs and analyse different cases and scenarios; with new modules easily added with minor modifications to the main program.
- Solar geometry has been incorporated into the model so that new aspects such as the effect of using tracking PV arrays on the economy of the solar-hydrogen system can be investigated (although this aspect is not addressed in this research project). In many models developed for solar-hydrogen system analysis, the incident solar radiation is just an input to the model, and not the result of solar geometry analysis done within the model itself for a particular collector configuration (Santarelli and Macagno 2004; Ali and Andrews 2005).
- Economic analysis is an integral part of many existing solar-hydrogen system models (Rzayeva *et al.* 2001; Ali and Andrews 2005; Lagorse *et al.* 2008), but RSHAP links the economic analysis tool to the technical details of the components and component sizing, allowing it to perform integrated techno-economic analysis on a solar-hydrogen system.
- The sub-models of the program in RSHAP for simulating the PV array (Chenni *et al.* 2007), electrolyser and fuel cell (Doddathimmaiah and Andrews 2009) are based on improved theoretical formulations recently published in the literature. The electrolyser and fuel cell models are based on modified Butler-Volmer equations in which saturation behaviour is taken into account in the characteristic performance curve of these elements. These sub-models give greater accuracy to the results compared to previous models.

- RSHAP is able to analyse the potential of fuel cell heat recovery in the context of a solar-hydrogen system on a yearly basis when particular solar-radiation and demand profiles are the determining inputs for system sizing and performance. The option of heat recovery from the fuel cell and its use for some beneficial purpose such as domestic water heating in a stand-alone power supply application can therefore be investigated through both energy and economic analyses.
- The program is able to perform a comprehensive optimisation of system sizing based on minimising the unit cost of the electricity generated and the economic benefit of fuel cell heat recovery over a stipulated lifecycle assessment period. Thus it gives the possibility of choosing the best combination of all the components in terms of size to yield the minimum possible cost while the basic requirement of the system, continuous power supply to a given demand, is satisfied. Some previously created models (Tani *et al.* 2000) performed system optimisation based on the cost of hydrogen produced, not the overall cost of the electricity delivered.

RSHAP has been established based on the Visual Pascal language, Delphi, version 7, the eleventh and the latest version of the software (2008). Delphi provides the possibility of developing the simulation code in a very user friendly environment such that following up the design and simulation procedure on the created code is self-explanatory for a new user. Delphi is mainly used for the development of desktop and enterprise database applications, but it is a general-purpose software development tool suitable for most software projects.

3.2 THE OVERALL STRUCTURE OF THE MODEL

The overall structure of the model including a brief overview on the inputs and outputs is provided in figure 3-1. This figure only highlights the key outputs of each sub-model; however, these sub-models have much more detailed outputs and flexibilities. These details are given in the appendix 1 of this thesis, which is written in the form of a user manual.

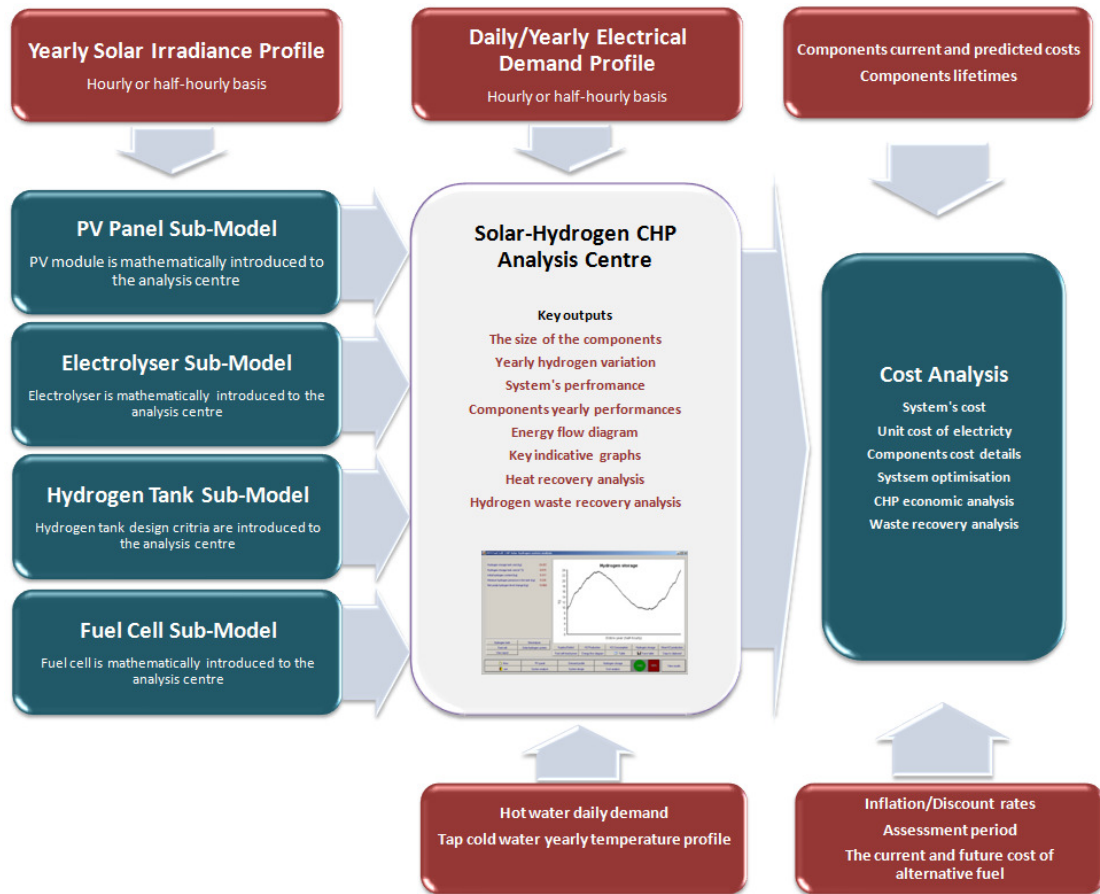


Figure 3-1. An overview on the structure of the model (RSHAP)

The RSHAP includes the sub-models of the system's components and the outputs of these sub-models become the inputs for the solar-hydrogen (CHP) model. The main solar-hydrogen system model does not work unless all the components have already been analysed by the sub-models and introduced to the main model. Each of these sub-models can create meaningful analytical outputs and graphs; thus a sub-model can be used for performing individual analysis on a particular component. Figure 3-2 shows the main panel of RSHAP. The user needs to go first to the components sections and complete the sub-models analyses before the solar-hydrogen system analysis button can be activated. As shown in the overall structure of the program (figure 3-1), completion of solar-hydrogen system analysis is the prerequisite of starting the economic analysis and system optimisation process (figure 3-3). This iterative optimisation process is completed by the program to minimise the overall cost of the system.

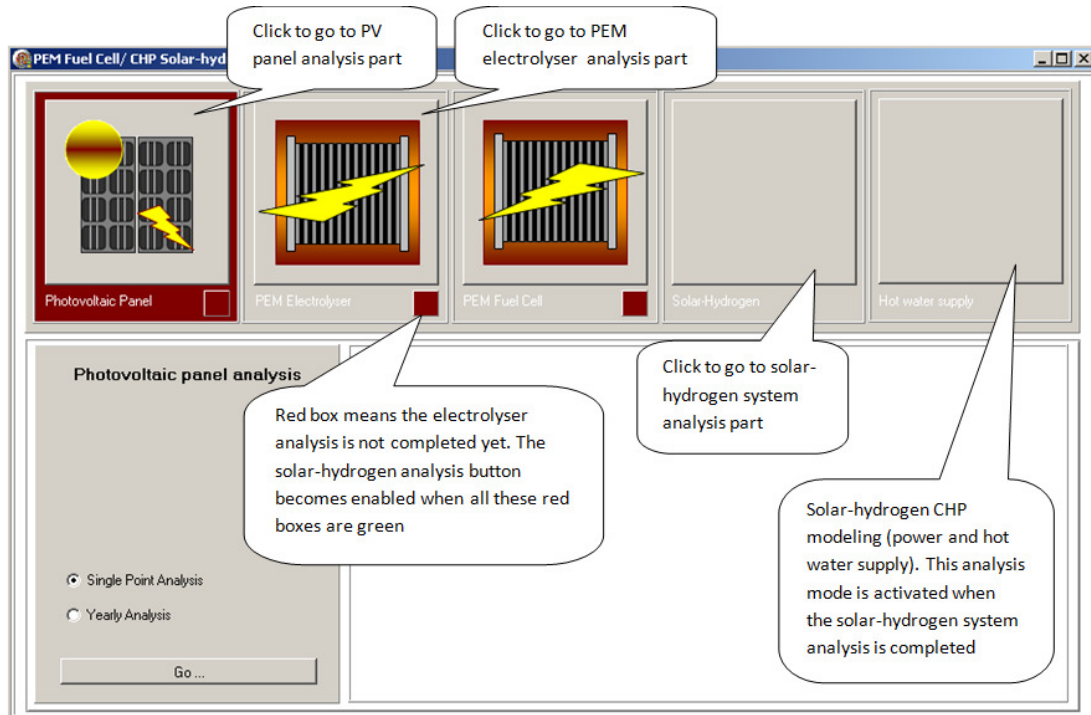


Figure 3-2. The main panel of the solar-hydrogen modelling tool, RSHAP

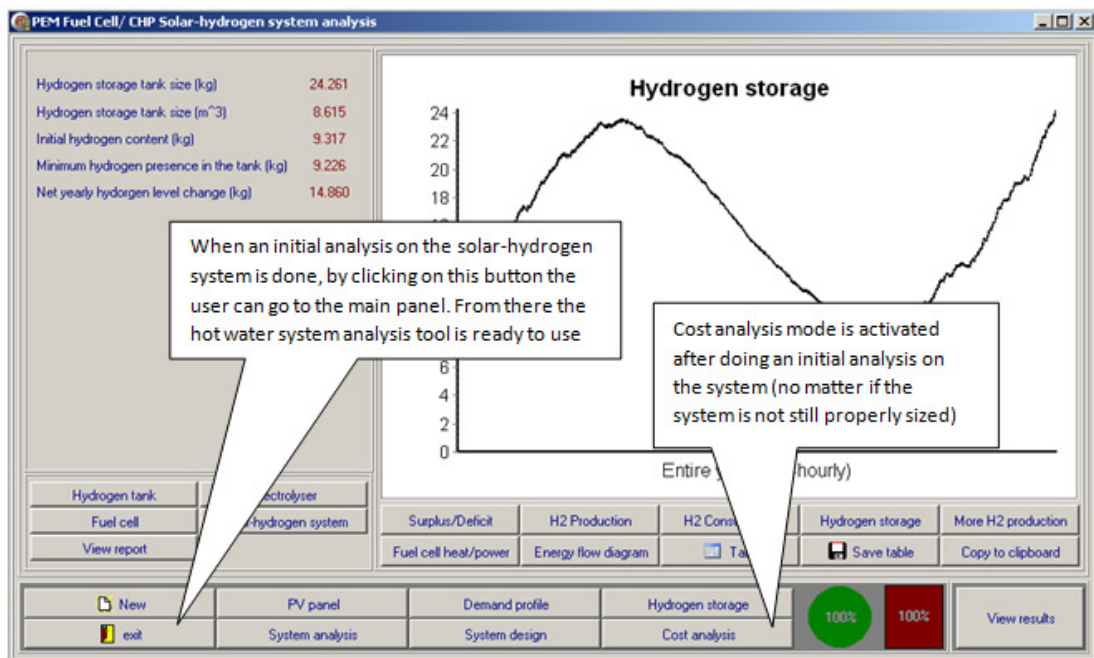


Figure 3-3. Solar-hydrogen system analysis panel

3.3 SOLAR GEOMETRY AND PV MODELLING

3.3.1 Terminology

The PV cell, PV module, and PV array are three terms used frequently in this thesis, so here these terms are defined. *PV cell* is the smallest segment of the photovoltaic converter to obtain electrical energy out of solar radiation; *PV module* is an assembly of PV cells normally connected in series; and PV array is a series/parallel assembly of PV modules (figure 3-4).

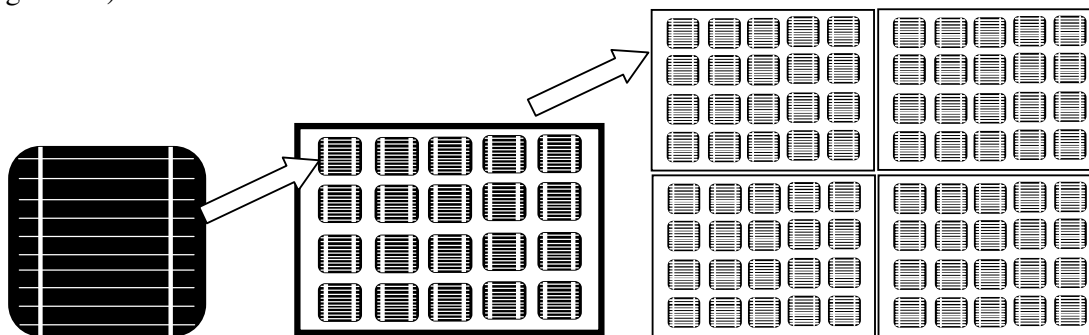


Figure 3-4. From left to right: PV cell, PV module, and PV array

3.3.2 The basic solar geometry used in the model

To find out the electrical output of the PV array at its maximum power point under any operating condition, both solar geometry and the electrical circuit of PV cells have to be modelled.

The first step is to calculate the solar radiation incident on the PV module at any given time of the day and angle of orientation of the panels. Some basic solar geometry has been incorporated into the simulation code to undertake these calculations. The incident solar radiation profile can be considered by the model in two different ways:

1. A time series of half-hourly or hourly array of total solar radiation incident on PV arrays over a full year when oriented at a particular angle. For instance, often statistical data of the annual solar radiation profile at the local latitude are directly available. Hence if the panels face north and are tilted to the horizontal at such an angle, there is no need for doing any additional solar geometry calculations to find out the perpendicular solar radiation on such panels.

2. A half-hourly or hourly array of horizontal solar radiation. These data are used when the irradiance profile for a particular angle are not available. Here is where the perpendicular radiation on the array has to be estimated using the available solar-geometry relations.

The angles used in the model for solar geometry modelling are the following:

- **Declination angle:** The angle between the line joining the centre of the sun to the centre of the earth and the equatorial plane is called the declination angle. This angle depends on the day of the year. The following equation gives a fairly good approximation for the declination angle δ (Akbarzadeh 1992) and is employed in the model:

$$\delta = 23.45 \sin [360(\text{Day} + 284) / 365] \quad (3-1)$$

where 'Day' is the number of days counted from 1 January ($\text{Day}=1$) to the end of December ($\text{Day}=365$).

- **Local latitude angle:** Local latitude angle, L , indicates the location of a place on the earth with respect to the equator where the local latitude angle is zero. This angle is taken as positive in the northern hemisphere ($+90^\circ$ for the North Pole) and negative in the southern hemisphere (-90° for the South Pole). For instance, the local latitude angle of Melbourne, located in south hemisphere, is -37.8° .
- **Solar azimuth and altitude angles:** Solar altitude angle, α , is the angle between the sun's rays and the horizontal plane of the location, and the solar azimuth angle, a , is the angle between the projection of the sun's rays on the horizontal plane and the north direction measured clockwise (Akbarzadeh 1992). These two angles locate the position of the sun in the sky. The solar altitude angle is calculated in the model using the formula (Akbarzadeh 1992):

$$\alpha = \sin^{-1}(\sin L \cdot \sin \delta + \cos L \cdot \cos \delta \cdot \cos \omega) \quad (3-2)$$

where L is the local latitude and ω is the solar hour angle (the number of hours from the solar noon time). Hour angle is 15° per hour and positive when moving towards the afternoon and negative for hours before the solar noontime (Akbarzadeh 1992).

Solar azimuth, a , is then calculated using (Akbarzadeh 1992):

$$a = \text{Sin}^{-1}(-\text{Cos}\delta \cdot \text{Sin}\omega / \text{Cos}\alpha) \quad (3-3)$$

- **Array slope and array azimuth angles:** The slope of the array with respect to horizontal surface, β , and the angle between the projection of the normal to the array onto the horizontal surface and the north direction (clockwise positive), the so-called panel azimuth angle, a_p , are the two key angles used in the solar-geometry model.
- **Incidence angle:** The incidence angle, θ_i , is the angle between the sun's rays and the normal to the surface of the panel, and is determined in the model from the following equations (Akbarzadeh 1992):

For south hemisphere:

$$\begin{aligned} \text{Cos}\theta_i = & \text{Sin}\delta \cdot \text{sin}L \cdot \text{Cos}\beta + \text{Sin}\delta \cdot \text{Cos}L \cdot \text{Sin}\beta \cdot \text{Cosa}_p + \text{Cos}\delta \cdot \text{Cos}L \cdot \text{Cos}\beta \cdot \text{Cos}\omega \\ & - \text{Cos}\delta \cdot \text{Sin}L \cdot \text{Sin}\beta \cdot \text{Cosa}_p \cdot \text{Cos}\omega - \text{Cos}\delta \cdot \text{Sin}\beta \cdot \text{Sina}_p \cdot \text{Sin}\omega \end{aligned} \quad (3-4)$$

For north hemisphere:

$$\begin{aligned} \text{Cos}\theta_i = & \text{Sin}\delta \cdot \text{Sin}L \cdot \text{Cos}\beta - \text{Sin}\delta \cdot \text{Cos}L \cdot \text{Sin}\beta \cdot \text{Cosa}_p + \text{Cos}\delta \cdot \text{Cos}L \cdot \text{Cos}\beta \cdot \text{Cos}\omega \\ & + \text{Cos}\delta \cdot \text{Sin}L \cdot \text{Sin}\beta \cdot \text{Cosa}_p \cdot \text{Cos}\omega - \text{Cos}\delta \cdot \text{Sin}\beta \cdot \text{Sina}_p \cdot \text{Sin}\omega \end{aligned} \quad (3-5)$$

The incidence angle can be used to calculate the irradiance on the array's surface from data on irradiation on a horizontal surface as follows. Having the direct horizontal irradiance data G_H it follows from the definition of solar altitude angle, and the direct radiation on the array G_d (the solar rays striking the array directly from the sun) is:

$$G_d = G_H / \text{Sin}\alpha \quad (3-6)$$

The effective part of this direct radiation, G_p , which is perpendicular to the array, is calculated as below:

$$G_p = G_d \cdot \text{Cos}\theta_i = G_H \cdot \text{Cos}\theta_i / \text{Sin}\alpha \quad (3-7)$$

The global irradiance G on an array tilted at an angle of β to the horizontal surface, is found from the following equation:

$$G = G_p + G_{dif,tilt} + G_{ref,tilt} \quad (3-8)$$

where $G_{dif,tilt}$ and $G_{ref,tilt}$ are the diffusion and the ground reflection parts of radiation on the tilted surface respectively. Diffuse irradiance is found using the following equation (Klucher 1979):

$$G_{dif,tilt} = G_H \left(\frac{1 + \cos\beta}{2} \right) \cdot (1 + f \sin^3 \frac{\beta}{2}) \cdot (1 + f \cos^2 \theta_i \cdot \sin^3 (90 - \alpha)) \quad (3-9)$$

f in this equation is called the modulating function (Klucher 1979):

$$f = 1 - \left(G_{dif,hor} / G_{H,total} \right)^2 \quad (3-10)$$

where $G_{dif,hor}$ and $G_{H,total}$ are diffuse irradiance and total global irradiances on the horizontal surface respectively. For example under overcast conditions, the ratio of these two is unity since the global irradiance on the horizontal surface is mainly diffuse insolation in the absence of direct radiation (Klucher 1979).

The ground reflection $G_{refl,tilt}$ on a surface titled at angle of β to the horizontal surface is calculated using the following equation (Quaschnig 2005):

$$G_{refl,tilt} = 0.2 G_{H,total} \cdot \left(\frac{1 + \cos\beta}{2} \right) \quad (3-11)$$

3.3.3 PV module modelling

3.3.3.1 Key parameters

The performance of a PV array is primarily influenced by two main parameters – cell temperature and solar irradiance – and the purpose of this modelling is to find the maximum power point of the array as a function of these two parameters.

The cell temperature has a considerable effect on the output power of a PV module. Solar cells are generally exposed to temperatures different from the temperature at which the initial tests have been performed. In order to be able to predict the performance of solar cells in different environments, it is thus essential to take into account the effect of temperature on the cells' performance (Akbarzadeh 1992). Increasing the cell temperature leads to a decrease in open circuit voltage and increase in short circuit current, but the

increase in the latter is much less than the decrease in the former. The effect of cell temperature, T_c , on open circuit voltage (V_{OC}) and short circuit current (I_{SC}) of a PV module is usually provided by manufactures under the reference (ref) condition (also called standard test condition shown by STC). The coefficients used by manufacturers for this purpose are the open circuit temperature coefficient (μ_{VOC}) and the short circuit temperature coefficient (μ_{ISC}) defined as:

$$\mu_{VOC} = \frac{\partial V_{OC,ref}}{\partial T_{c,ref}} \quad (3-12)$$

$$\mu_{ISC} = \frac{\partial I_{SC,ref}}{\partial T_{c,ref}} \quad (3-13)$$

Basically the model calculates the performance of a PV module, assuming all cells on the module perform equally, at every given or estimated temperature using the module's performance characteristics at STC.

Solar radiation, ambient temperature and wind speed are the principal external parameters that determine cell temperature. The following empirical equation connects these parameters to the cell temperature (Chenni *et al.* 2007).

$$T_c = 0.943T_{ambient} + 0.028(Irradiance) - 1.528(wind\ speed) + 4.3 \quad (3-14)$$

where ambient temperature, $T_{ambient}$, and cell temperature, T_c , are given and obtained in $^{\circ}C$, Irradiance is in W/m^2 and wind speed is in m/s .

Solar irradiance varies from sunrise to sunset as well as from season to season, and is also affected by the daily ambient environmental conditions. The effect of variation in irradiance is much larger than that of the cell temperature. Any increase in irradiance results in the array delivering more electrical power. In addition, the higher the solar irradiance, the higher the cell temperature will be, the other factors remaining constant. Although cell temperature inversely affects the output power, the positive effect of irradiance on the module's output power still dominates. On the I-V curve, the effect of module temperature on the short-circuit current is more than the open circuit voltage. The short-circuit current variation with solar radiation is almost linear (Akbarzadeh 1992).

3.3.3.2 PV sub-model description

Three key points of a PV module are open circuit voltage (zero current), short circuit current (zero voltage), and the maximum power points, each occur just once in the entire range of PV array's operational curves. These points are normally provided by the manufacturer at a standard test condition (STC) (e.g. the irradiance is normalised to 1000W/m^2 , and the cell temperature of $25\text{ }^\circ\text{C}$) (Chenni *et al.* 2007). To get the maximum benefit out of a PV array it has to be operated at its maximum power point. In conventional systems a device named maximum power point tracker (MPPT) ensures the PV arrays operate close to this point, thus it matches the load and the PV arrays output by separating them from each other. Usually the efficiency of MMPT is more than 80% which makes it attractive in terms of system energy efficiency. For the case of solar-hydrogen system, the electrolyzers which are connected to the PV modules act as an electrical load. For connecting PV modules to electrolyzers, a novel parallel-series PV module and electrolyser direct coupling technique has been recently investigated experimentally. This technique has been suggested to avoid the need for a MPPT and hence reduce the system's overall cost and slightly improve its efficiency (Paul and Andrews 2008).

The model introduced by Chenni, *et al.* (2007) is used in the PV sub-model of RSHAP. The main purpose of modelling the PV module is finding its maximum power point and it is supposed to be operated at that point when used in solar-hydrogen system. To find out the maximum output power of the PV module at any given irradiance and cell temperature, the equivalent internal electrical circuit shown in figure 3-5 has been used for the PV module.

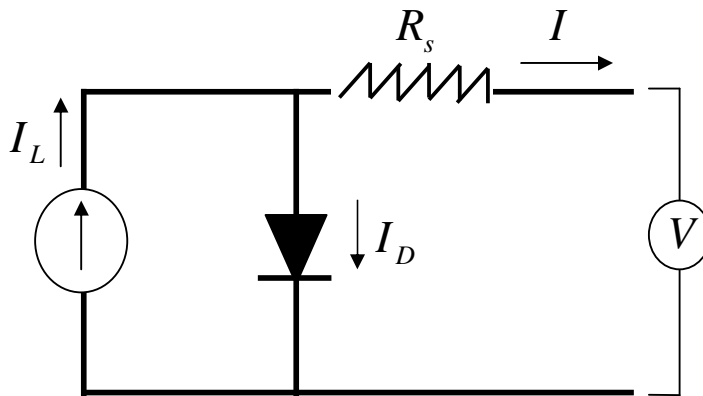


Figure 3-5. Equivalent electrical circuit of a PV module used for PV modelling (Chenni *et al.* 2007)

In figure 3-5, I_L is the light current that depends on both irradiance and temperature. It is measured at some reference condition and using the following formula it is possible to calculate I_L at any solar irradiation and cell temperature.

$$I_L = \left(\frac{G}{G_{ref}} \right) \left(I_{L,ref} + \mu_{ISC} (T_c - T_{c,ref}) \right) \quad (3-15)$$

G in this equation is the actual incident global irradiance and G_{ref} is the reference irradiance provided by the manufacturer (both in W/m^2), $I_{L,ref}$ is the light current at reference condition (A), T_c is the cell temperature, which is found from ambient temperature, irradiance and wind speed using equation (3-14), $T_{c,ref}$ is the reference temperature at which the cell characteristics are provided by the manufacturer, and μ_{ISC} (the short circuit temperature coefficient) has been introduced earlier by equation (3-13). In all these equations the index 'ref' stands for the reference or standard test condition (STC) given by the manufacturer.

I_D in figure 3-5 is the diode current, which is given by the Shockley equation:

$$I_D = I_0 \left[e^{\left(\frac{q(V+IR_s)}{\gamma k T_c} \right)} - 1 \right] \quad (3-16)$$

where:

V = terminal voltage (V)

I_0 = reverse diode saturation current (A)

γ = shape factor

R_s = series resistance (Ω)

q = electron charge 1.602×10^{-19} C

k = Boltzmann constant, 1.31×10^{-23} J/K.

I_L is a function of both irradiance and cell temperature; however, I_0 is only a function of temperature as shown in the following equation:

$$I_0 = D T_c^3 \cdot e^{\left(\frac{-q \mathcal{E}_G}{A k T_c} \right)} \quad (3-17)$$

where D is the diode diffusion factor, ε_G is the material band gap energy (1.12 eV for Si, 1.35 eV for GaGs), and A is the completion factor. By considering the ratio of reverse diode saturation current at two different temperatures, the factor D can be eliminated from equation (3-17). Hence applying this equation at the reference temperature and cell temperature, the reverse diode saturation current for an arbitrary cell temperature can be expressed in terms of $I_{0,ref}$ as follows:

$$I_0 = I_{0,ref} \left(\frac{T_c}{T_{c,ref}} \right)^3 . e^{\left[\frac{-q\varepsilon_G}{Ak} \left(\frac{1}{T_{c,ref}} - \frac{1}{T_c} \right) \right]} \quad (3-18)$$

The shape factor, γ , is assumed to be constant and is calculated as below:

$$\gamma = A.NCS \quad (3-19)$$

NCS is the number of cells connected in series per module. Based on Kirchoff's law and regarding the circuit given in figure 3-5, $I = I_L - I_D$; substituting I_D from equation (3-16) yields:

$$I = I_L - I_0 \left(e^{\left(\frac{q(V+IR_s)}{\gamma k T_c} \right)} - 1 \right) \quad (3-20)$$

Then by substituting for I_L and I_0 :

$$I = \left(\frac{G}{G_{ref}} \right) (I_{L,ref} + \mu_{ISC} (T_c - T_{c,ref})) - I_{0,ref} \left(\frac{T_c}{T_{c,ref}} \right)^3 . e^{\left[\frac{-q\varepsilon_G}{Ak} \left(\frac{1}{T_{c,ref}} - \frac{1}{T_c} \right) \right]} \left(e^{\left(\frac{-q(V+IR_s)}{\gamma k T_c} \right)} - 1 \right) \quad (3-21)$$

Considering the reference condition, open circuit ($I=0$), and substituting the corresponding values in the equation (3-21) the reference diode saturation current expressed in terms of the open circuit voltage in the reference condition:

$$I_{0,ref} = I_{L,ref} . e^{\left(\frac{-qV_{OC,ref}}{\gamma k T_{c,ref}} \right)} \quad (3-22)$$

Under the reference condition, applying equation (3-21) for the short circuit point, and also assuming the reverse saturation current (at reference condition) is small:

$$I_{L,ref} \approx I_{SC,ref} \quad (3-23)$$

Hence we can simplify the equation (3-22):

$$I_{0,ref} = I_{SC,ref} \cdot e^{\left(\frac{-qV_{OC,ref}}{k\gamma T_{c,ref}}\right)} \quad (3-24)$$

Using the approximate equation (3-23) and applying the equation (3-21) at the maximum power point, it can be shown that the shape factor can be expressed as:

$$\gamma = \frac{q(V_{MP,ref} + I_{MP,ref}R_s - V_{OC,ref})}{k.T_{c,ref} \cdot \text{Ln}\left(1 - \left(\frac{I_{MP,ref}}{I_{SC,ref}}\right)\right)} \quad (3-25)$$

Also equation (3-24) can be rearranged to give the open circuit voltage in reference condition:

$$V_{OC,ref} = \frac{\gamma k T_{c,ref}}{q} \ln\left(\frac{I_{SC,ref}}{I_{0,ref}}\right) \quad (3-26)$$

Then the open circuit temperature coefficient defined by equation (3-12), is given by:

$$\mu_{voc} = \frac{\partial V_{OC,ref}}{\partial T_{c,ref}} = \frac{\gamma k}{q} \left[\ln\left(\frac{I_{SC,ref}}{I_{0,ref}}\right) + \frac{\mu_{ISC} \cdot T_{c,ref}}{I_{SC,ref}} - \left(3 + \frac{q\mathcal{E}_G}{AkT_{c,ref}}\right) \right] \quad (3-27)$$

Using this analytical value for the open circuit temperature coefficient at the reference condition, we can define a procedure for finding the module series resistance and hence calculate the maximum power at any given cell temperature and irradiance.

As mentioned before, at any irradiance received by the PV module, there is only one point over the entire associated I-V curves that the module operates at the highest efficiency. At this maximum power point:

$$\frac{\partial P}{\partial V} = \frac{\partial (IV)}{\partial V} = I + V \frac{\partial I}{\partial V} = 0 \quad (3-28)$$

Substituting equation (3-20), the general expression that was developed for cell current, the partial derivative of I with respect to V is:

$$\frac{\partial I}{\partial V} = -I_0 e^{\left[\frac{q(V+IR_s)}{k\gamma T_{c,ref}}\right]} \cdot \frac{q}{kT_{c,ref}} \left(1 + R_s \frac{\partial I}{\partial V}\right) \quad (3-29)$$

After obtaining an explicit expression for $\partial I / \partial V$ and substituting into equation (3-28) with $V=V_{MP}$ and $I=I_{MP}$, the voltage and current at the maximum power point respectively, we have:

$$I_L + I_0 e^{-\left[\frac{q(V_{MP} + I_{MP} R_s)}{\gamma k T_{C,ref}} \right]} \times \left(1 + \frac{\frac{q V_{MP}}{\gamma k T_{C,ref}}}{1 + \frac{q R_s I_0}{\gamma k T_{C,ref}} e^{-\left[\frac{q(V_{MP} + I_{MP} R_s)}{\gamma k T_{C,ref}} \right]}} \right) = 0 \quad (3-30)$$

Equation (3-30) can be applied for the maximum power point, and also using the general I-V relationship shown by equation (3-20) at this point, derived in equation (3-31) it is possible to express V_{MP} in terms of just I_{MP} , and hence get an explicit equation for the current at maximum power point:

$$V_{MP} = \frac{\gamma k T_{C,ref}}{q} \ln \left(\frac{I_L - I_{MP}}{I_0} + 1 \right) - I_{MP} R_s \quad (3-31)$$

$$I_{MP} + \frac{(I_{MP} - I_L - I_0) \left[\ln \left(\frac{I_L - I_{MP}}{I_0} + 1 \right) - \frac{q I_{MP} R_s}{\gamma k T_{C,ref}} \right]}{1 + (I_L - I_{MP} + I_0) \frac{q I_{MP} R_s}{\gamma k T_{C,ref}}} = 0 \quad (3-32)$$

Chenni *et al.* (2007) have suggested using the Newton-Raphson method to solve equation (3-32) for I_{MP} , with the following trial solution to start off the iteration:

$$I_{MP,guess} = \left(\frac{G}{G_{ref}} \right) \left(I_{MP,ref} + \mu_{ISC} (T_c - T_{c,ref}) \right) \quad (3-33)$$

However, before the iteration can start, we need a value for the series resistance of R_s to substitute in the equation. The method used in the present PV sub-model to find R_s was suggested originally by Townsend (1989) and it has been also used by Chenni *et al.* (2007) for this PV cell modelling. The temperature coefficient of open circuit voltage often supplied by manufacturers is one of the basic parameters used in this method. The process is an iterative search of this resistance using a bisection method that needs a lower and upper limit for the convergence parameter; here the latter is the module series resistance. Using the lower and upper limit of R_s to calculate its average value, an analytical value for μ_{VOC} is calculated and compared with the value introduced by the manufacturer. Then

based on the difference between these two and the targeted level of accuracy chosen for the iteration it is possible to decide whether to continue the iteration or accept the current value of R_s as the answer.

The lower limit for series resistance is clearly 0Ω since it cannot be less than zero. As for the upper limit of R_s , the points of maximum power, short circuit and open circuit voltage are independent points influenced by the series resistance, and their variations in turn determine the curve shape factor of γ . In other words the shape of the I-V curve is influenced by the module series resistance. Progressively higher values of R_s result in progressively lower values of γ (Chenni *et al.* 2007). The completion factor A has a minimum value of 1.0 so given the basic relation between completion factor and shape factor the minimum value for γ is equal to the number of cells in series (NCS) which determines the maximum value of R_s . By substituting $\gamma = NCS$ into equation (3-25) and rearranging the equation for series resistance, $R_{s,max}$ is obtained as follows:

$$R_{s,max} = \frac{1}{I_{MP,ref}} \left[\frac{k.T_{C,ref} \cdot NCS}{q} \ln \left(1 - \frac{I_{MP,ref}}{I_{SC,ref}} \right) + V_{OC,ref} - V_{MP,ref} \right] \quad (3-34)$$

Figure 3-6 shows the step-by-step procedure for finding R_s (named procedure **A** for simplicity) and the maximum power point of the module under an arbitrary irradiance and temperature. This R_s can be found through iteration by setting an accuracy target (% error) for the expected answer. Once the difference between the calculated and measured open circuit temperature coefficients fall within this accuracy target the iteration process stops and the series resistance corresponding to the calculated open circuit temperature coefficient is recorded as the answer for this parameter.

After finding the module's series resistance the iteration process for finding current, voltage and power of the maximum power point can be launched. This procedure, shown schematically in figure 3-7 and named procedure **B**, includes using the Newton-Raphson method for solving the target equation. This method is just a numerical method for finding the root(s) of an equation or the zero(s) of a function. These two procedures (**A** and **B**) are

entirely based on the PV model developed by Chenni *et al.* (2007) that was briefly introduced in this chapter.

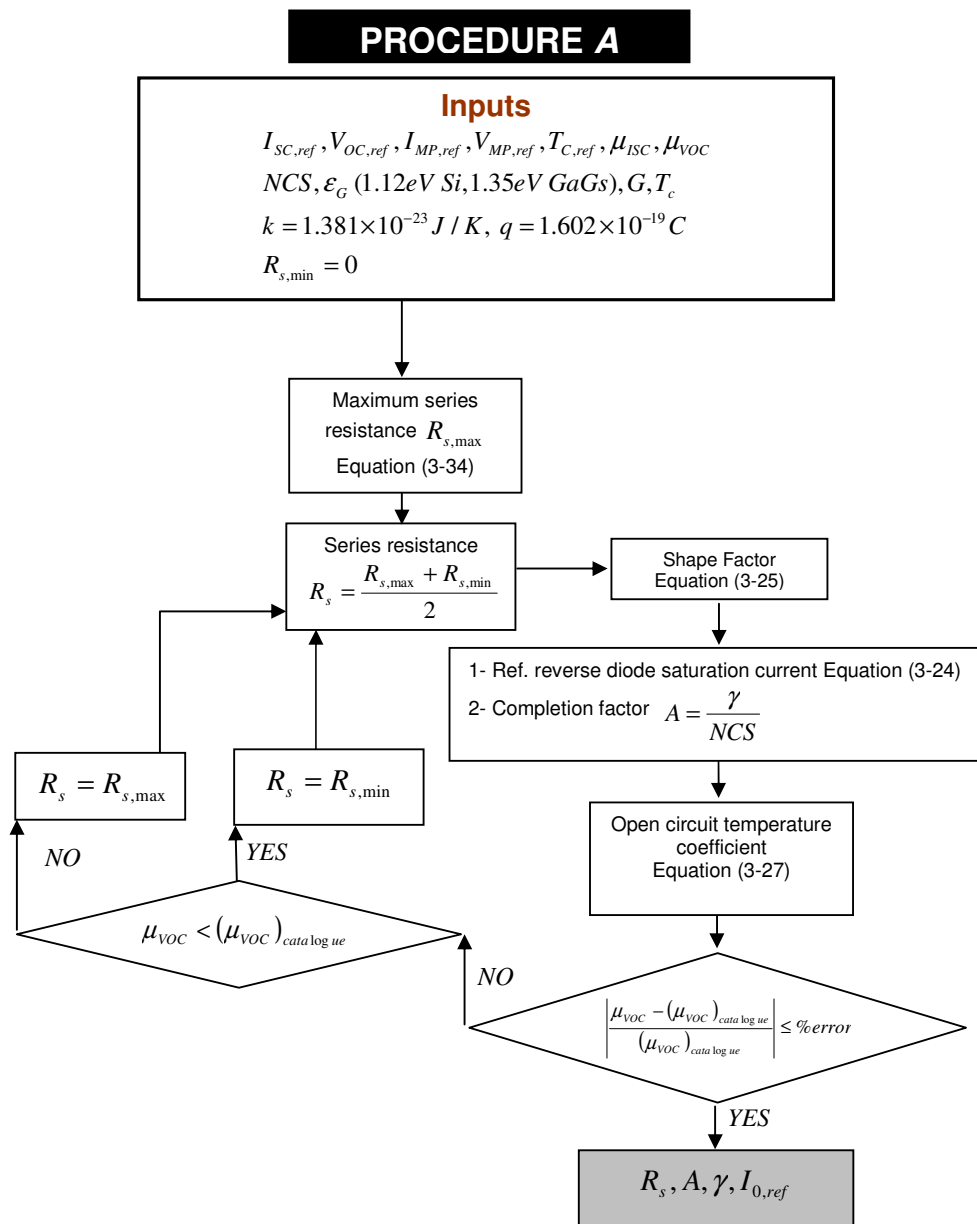


Figure 3-6. The procedure of finding series resistance, shape factor, completion factor, and reference reverse diode saturation current of a PV module

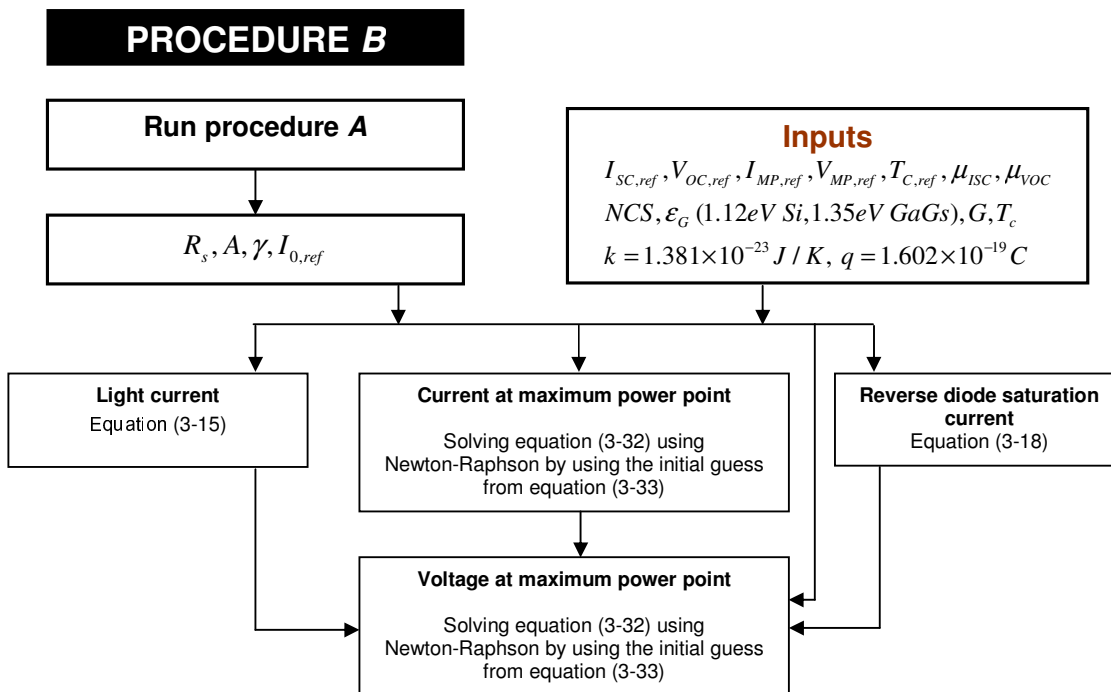


Figure 3-7. The procedure of finding current and voltage at the maximum power point of a PV module

The final stage of the PV module modelling is the application of some de-rating correction factors to the results of the theoretical analysis so that its outputs respectively fit the actual performance of the module performance and make them more realistic. Some or all of the following de-rating factors are thus applied in the model, according to the application condition, taken from Business Council for Sustainable Energy (BCSE 2009):

- 0.9-0.95: Manufacturer’s output tolerance. The products of a manufacturer are not all identical and there is no guarantee of identical performance. Hence the output power might be slightly different from the one given in the manual under the same test condition as used by the manufacturer. This tolerance factor is normally provided in the product’s manual.
- 0.95: Cable losses (if applicable). This factor can be slightly more or less regarding the length of the cable between module and load. Sometimes the short length of the cable, the size of the current, the electrical resistance and diameter of the cable suggest neglecting these losses.

For system sizing purposes another two de-rating factors are to be used:

- 0.9: Inverter efficiency (if applicable)
- 0.95: Dirt factor. Over the passage of time, dirt (e.g. dust) that collects on the surface of the module can slightly affect its performance. This dirt is supposed to be washed away from the module(s) periodically as a part of maintenance procedure between cleaning times.

By finding the maximum power point specifications of a single module it is possible to calculate these specifications for an array of a number of modules, arranged in series or parallel.

$$I_{MP,tot} = NP.I_{MP} \quad (3-35)$$

$$V_{MP,tot} = NS.V_{MP} \quad (3-36)$$

where NS and NP are the number of modules arranged in series and in parallel respectively.

For the total series resistance of a array, $R_{s,tot}$, we can also say:

$$R_{s,tot} = \frac{NS}{NP} R_s \quad (3-37)$$

This model now allows us to predict the output of the array on an hourly or half-hourly basis from input data for the solar irradiance profile, ambient temperature profile, wind speed profile, array technical data, and its orientation. Irradiance, temperature, and wind speed profiles for many locations in Australia are obtainable from the Australian Bureau of Meteorology (BOM 2009) and the specifications of most of the PV modules can be found from an online database of photovoltaic modules (Sandia 2009). The PV model also provides the flexibility of analysing full-tracking PV arrays simply by some minor modifications in the simulation code.

Figure 3-8 and figure 3-9 are the examples to show how the PV sub-model can predict the performance of a BP275 PV module/array (see the technical specifications given in appendix 3) at different cell temperatures and income irradiances.

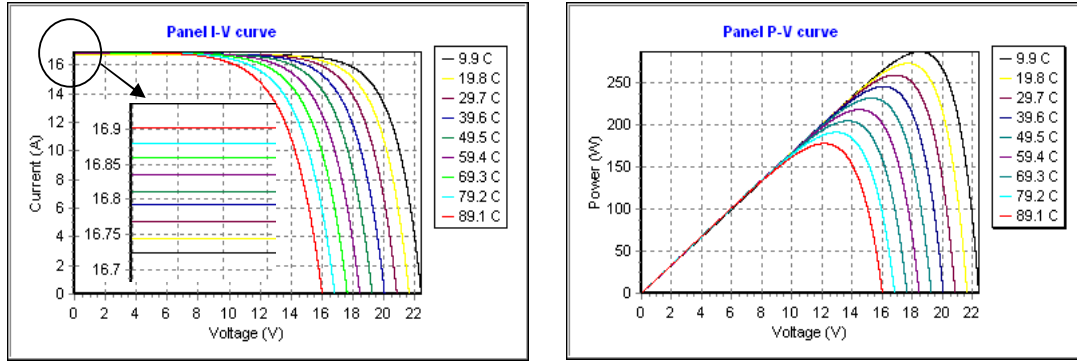


Figure 3-8. The PV sub-model output, showing the effect of cell's temperature on the performance of a PV array of 4 BP275 modules receiving 880 W/m^2 irradiance

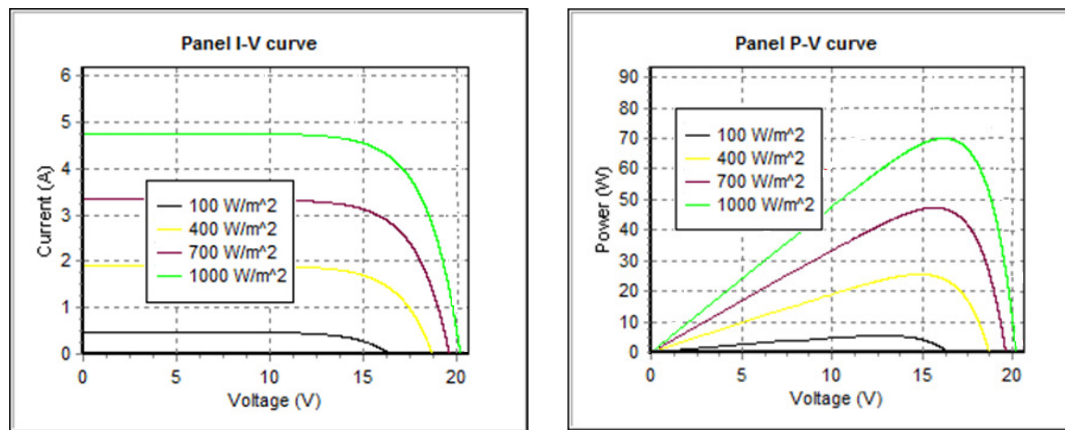


Figure 3-9. The PV sub-model output showing the effect of irradiance on the performance of a BP275 PV module while its temperature is assumed to be kept at $40 \text{ }^\circ\text{C}$

3.3.3.3 PV sub-model validation

The PV model explained so far was validated before incorporating it into the solar-hydrogen combined heat and power simulation code. For this purpose a 20-W silicon nitride multicrystalline silicon PV module, BP SX320 (table 3-1) and also a BP275 module (table 4-3) were experimentally investigated. Details of the technical specifications of these modules are given in appendix 3.

The normal operating condition at which the BP SX320 module is tested by the manufacturer is $20 \text{ }^\circ\text{C}$ of ambient temperature, 0.8 kW/m^2 module income irradiance, and 1 m/s wind speed. Under such conditions the cell temperature is $47 \pm 2 \text{ }^\circ\text{C}$ according to table 3-1 provided by the manufacturer. Alternatively, if equation (3-14) is used to estimate the cell temperature, at such a given operating condition, this temperature is predicted to be

44°C which is reasonably close to the temperature given by the manufacturer's manual. Hence, the error of the experimental formula used to estimate the module's temperature is just above 2% which is a quite acceptable as the impact of such an error on the final output of the module predicted by the model is negligible (~0.5%).

A 0.9 de-rating correction factor was applied to the model to predict the performance of the BP SX320 module. The load was just connected to the module with a very short cable so the losses normally associated with the cable were neglected. No MPPT (DC-to-DC converter) was used for this experimental investigation and hence this de-rating factor does not reflect such losses. The module used in this experiment was brand new and quite clean with no dust on the surface, so no dirt factor was included. This 90% de-rating factor is only the product performance tolerance given as a maximum of $\pm 10\%$ by the manufacturer (table 3-1). A comparison between the manufacturer's curve and the one generated by the model suggests that the de-rating factor used in this case does lead to a good match between the two curves (figure 3-10). The difference between the experimental curve and the model, shown in figure 3-10, is less than 2% at the maximum power point. The error associated with the power measurement instrument used for the test was $\pm 0.6\%$ as stated by the manufacturer. Using the same de-rating factor (90%) in a separate investigation, the maximum power points of the BP SX320 module at three different cell temperatures and income irradiances were experimentally measured and compared with the model predictions (table 3-2). The differences between the experimentally-measured maximum powers and the ones suggested by the model were all around 1-2%.

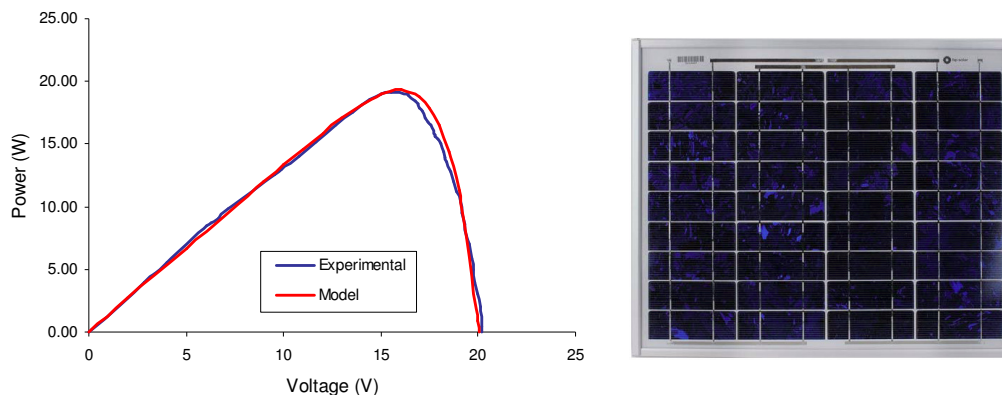


Figure 3-10. Experimental and model power curves for a BP SX320 module at 40 °C cell temperature and 945 W/m² irradiance (left) BP SX320 module (right)

Maximum power (P_{max})	20 W
Warranted minimum P_{max}	18 W
Power tolerance	$\pm 10\%$
Voltage at P_{max} (V_{MP})	16.8 V
Current at P_{max} (I_{MP})	1.19 A
Short-circuit current (I_{SC})	1.29 A
Open-circuit voltage (V_{OC})	21.0 V
Temperature coefficient of I_{SC}	$(0.065 \pm 0.015)\%/^{\circ}\text{C}$
Temperature coefficient of V_{OC}	$-(80 \pm 10) \text{ mV}/^{\circ}\text{C}$
Temperature coefficient of power	$-(0.5 \pm 0.05)\%/^{\circ}\text{C}$
Single cell area	38 mm \times 114 mm
Number of series cell in module	36
Normal operating condition test	Air 20 $^{\circ}\text{C}$; Sun 0.8 kW/m^2 ; wind 1 m/s Cell: 47 ± 2 $^{\circ}\text{C}$

Table 3-1. BP SX320 technical data provided in the manufacturer's catalogue

Module temperature ($^{\circ}\text{C}$)	Irradiance received by the module (W/m^2)	Measured module maximum power (W)	Maximum power estimated by the model (W)
40	945	19.17	19.34
42	533	10.69	10.51
53	840	15.67	15.93

Table 3-2. Comparing the maximum power outputs of a BP SX320 PV module at different operating conditions

For validating the model, especially investigating the effect of temperature on the PV performance, a BP275 PV module (see figure 4-3, table 4-3, and appendix 3) was also investigated. The specifications of the array were extracted from the manual (appendix 3) and an online photovoltaic database (Sandia 2009) to enter into the simulation code. As shown in figure 3-11 generated by the model, the maximum power drops by increasing the cell temperature in a linear fashion; it shows that for each 5 $^{\circ}\text{C}$ increase in temperature, the maximum power drops down by approximately 2.7%. This figure closely agrees with the figure of 2.5% given by previous studies (Akbarzadeh 1992).

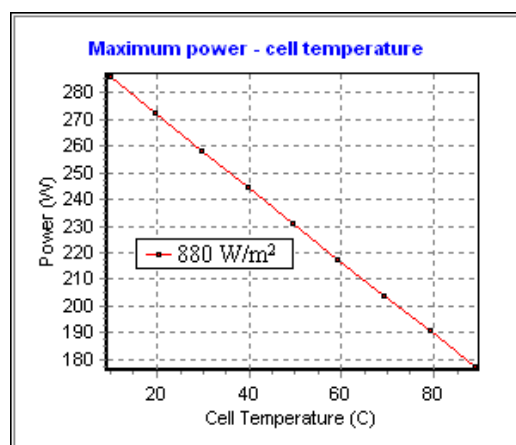


Figure 3-11. Theoretical analysis showing the effect of temperature on the maximum power point of an array of four BP275 modules while receiving 880 W/m^2 incident solar irradiance

The validity of the PV sub-model was further checked by applying the model to an array of four BP275 modules connected in parallel. Since the array was a number of years old it was not possible to compare the absolute values of power as supplied by manufacturer with those predicted by the model, so the rate of variation of the maximum power by varying solar radiation and cell temperature was measured and compared with the corresponding values predicted by the model. The model prediction shows that the maximum power output of the array with incident solar irradiance on the modules of 760 W/m^2 and a cell temperature of $27.3 \text{ }^\circ\text{C}$ is 15.9% lower than that at 882 W/m^2 and $30.1 \text{ }^\circ\text{C}$. This result agrees well with a 14.4% difference in the experimental results.

3.4 HYDROGEN STORAGE MODELLING

High and low pressure hydrogen storage systems (gaseous hydrogen), liquid hydrogen storage and material-based hydrogen storage are proven technologies for storing hydrogen. High pressure hydrogen and storing it in liquid form are suggested for on-board storage applications where the mass energy density of hydrogen has to be enhanced. The example of this is using liquid hydrogen for hydrogen 7 project by BMW (Brunner and Kircher 2008). Material-based hydrogen storages (e.g. metal-based or chemical-based materials) are the result of hydrogen reaction at high temperatures with many transition materials (Züttel 2003; Sakintuna *et al.* 2007). Safety and high volumetric storage have always been addressed as the inherent advantages of storing hydrogen in the form of metal hydride

(Santos and Huot 2009). This is due to the relatively low hydrogen charge/discharge pressure of metal hydride, when the hydrogen is kept inherently in atomic form (Tzimas *et al.* 2003).

Since the modelling has a focus on RAPS applications, availability of space is generally not an issue for hydrogen storage. Hence here it is basically assumed that the hydrogen is stored in gaseous form and at relatively low pressure (directly supplied by the electrolyser). The hydrogen content of the storage tank varies between a minimum and a maximum level during a typical year. Its maximum level determines the volume of the tank needed for storing hydrogen at a particular pressure. If the produced hydrogen is stored in gaseous form at low pressure and near ambient temperature, the ideal (perfect) gas model is the easiest and the best approach to calculate the needed volume. As shown in figure 3-12, for pressures below 2000 kPa, hydrogen follows the ideal gas behaviour closely, and applying the ideal gas model for such pressures is accurate enough to use in the solar-hydrogen system modelling when using gaseous hydrogen storage.

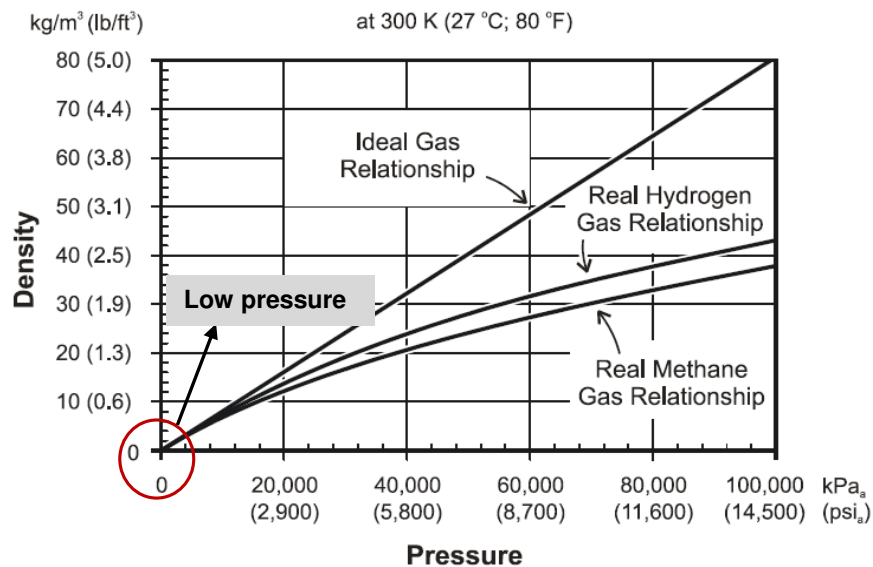


Figure 3-12. Hydrogen density estimation as a function of pressure using different equations of state (DOE 2001)

Round-trip energy efficiency of the hydrogen storage tank is assumed to be 100% in this study (no external compression, no leakage). However, depending on the storage type and the possible hydrogen losses through connectors (that is, leakage) it might be a few percent less than this figure in practice, and the model allows any given efficiency of the storage system to be used as necessary.

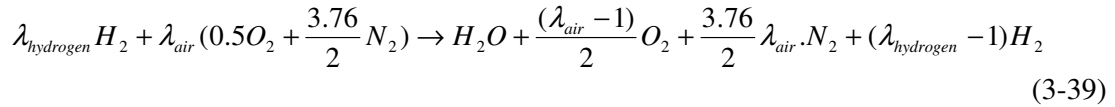
3.5 FUEL CELL MODELLING

3.5.1 Fuel cell reaction

The operational principle of a fuel cell is very similar to the reverse operation of an electrolyser. Here is the electrochemical reaction between hydrogen and oxygen in the fuel cell that leads to water, power, and heat:



Introducing a realistic chemical equation for the reaction taking place in a real fuel cell is the first step in constructing the fuel cell model. The core chemical reaction between hydrogen and oxygen in a fuel cell given in equation (3-38) is expanded in the model to take account of the real case when air is used instead of oxygen, and extra air and hydrogen, above the stoichiometric quantities, are fed into the fuel cell. Equation (3-39) is the resulting expanded equation (Shabani and Andrews 2008).



where λ_{air} and $\lambda_{hydrogen}$ are the air and hydrogen stoichiometric coefficients respectively. The extra hydrogen and air (mainly nitrogen), leave the fuel cell without taking part in the reaction. These gases just absorb heat and transfer it out of the fuel cell. This heat transfer is considered in the fuel cell thermal simulation in the model.

3.5.2 Reactant flow rates

In the basic fuel cell reaction shown in equation (3-38), two electrons pass round the external circuit for each water molecule produced and each hydrogen molecule used. So for one mole of hydrogen used, $2N_A$ electrons pass round the external circuit, where N_A is Avogadro's number. With the electronic charge being q , the Faraday constant, F , is defined as (Larminie and Dicks 2003):

$$F = q \times N_A = 6.022 \times 10^{23} \times 1.602 \times 10^{-19} C = 96485 C / mol \quad (3-40)$$

The electrical charge passing round the circuit is thus $-2F$ when the cell consumes a mole of hydrogen and 0.5 mole of oxygen. Disregarding the sign of the charge we can say the amount of this charge, Q , is obtained from the following equation:

$$|Q| = zFN \quad (3-41)$$

where N is the number of consumed moles (of hydrogen or oxygen), and z is 2 when hydrogen consumption is considered, or 4 when the calculation is based on oxygen. Hence:

$$|Q| = 2FN_{hydrogen} = 4FN_{oxygen} \quad (3-42)$$

The cell current, J_{cell} , is the rate of flow of electrical charge and is thus given by (Ryan O'Hayre *et al.* 2008):

$$J_{cell} = \frac{dQ}{dt} = zF \frac{dN}{dt} \quad (3-43)$$

Rearranging this equation gives (Ryan O'Hayre *et al.* 2008):

$$\frac{dN}{dt} = \frac{J_{cell}}{zF} \quad (3-44)$$

where, ' dN/dt ' is the rate of the electrochemical reaction (*mole/s*) for each single cell, and J_{cell} is the current passing through the external circuit of a single cell. For a stack of n cells in series, the rate of the electrochemical reaction (*mole/s*) in fuel cell stack becomes (Ryan O'Hayre *et al.* 2008):

$$\frac{dN}{dt} = \frac{nJ_{cell}}{zF} \quad (3-45)$$

This equation can also be expressed in terms of mass flow rate instead of mole flow rate. For every contributing substance in the chemical reaction with a mass of M , and a mass flow rate of \dot{m} :

$$\frac{dN}{dt} = \frac{1}{M} \cdot \dot{m} \quad (3-46)$$

By substituting equation (3-46) into equation (3-45) we have:

$$\dot{m} = \frac{M}{zF} \cdot nJ_{cell} \quad (3-47)$$

The hydrogen and oxygen reaction rates, and the water production rate, are then given by:

$$\left(\dot{m}_{hydrogen}\right)_{reaction} = \frac{2.02 \times 10^{-3}}{2 \times 96485} \cdot nJ_{cell} = 1.05 \times 10^{-8} nJ_{cell} \text{ (kg / s)} \quad (3-48)$$

$$\left(\dot{m}_{\text{oxygen}}\right)_{\text{reaction}} = \frac{32 \times 10^{-3}}{4 \times 96485} \cdot nJ_{\text{cell}} = 8.29 \times 10^{-8} nJ_{\text{cell}} \text{ (kg / s)} \quad (3-49)$$

$$\left(\dot{m}_{\text{H}_2\text{O}}\right)_{\text{produced}} = \frac{18.02 \times 10^{-3}}{2 \times 96485} \cdot nJ_{\text{cell}} = 9.34 \times 10^{-8} nJ_{\text{cell}} \text{ (kg / s)} \quad (3-50)$$

These equations can be expressed in terms of stack power, P_{stack} , and cell voltage, V_{cell} , instead of current, J_{cell} , and the number of cells, n , using:

$$P_{\text{stack}} = V_{\text{cell}} \times J_{\text{cell}} \times n \Rightarrow nJ_{\text{cell}} = P_{\text{stack}} / V_{\text{cell}} \quad (3-51)$$

The mass flow rates of hydrogen and air, into and out from the fuel cell are then obtained using equation (3-39), to take account of the actual air and hydrogen stoichiometries:

$$\left(\dot{m}_{\text{hydrogen}}\right)_{\text{in}} = n \times 1.05 \times 10^{-8} \cdot \lambda_{\text{hydrogen}} \cdot J_{\text{cell}} \text{ (kg / s)} \quad (3-52)$$

$$\left(\dot{m}_{\text{hydrogen}}\right)_{\text{out}} = n \times (\lambda_{\text{hydrogen}} - 1) \cdot 1.05 \times 10^{-8} \cdot J_{\text{cell}} \text{ (kg / s)} \quad (3-53)$$

$$\left(\dot{m}_{\text{air}}\right)_{\text{in}} = n \times 3.57 \times 10^{-7} \cdot \lambda_{\text{air}} \cdot J_{\text{cell}} \text{ (kg / s)} \quad (3-54)$$

$$\left(\dot{m}_{\text{air}}\right)_{\text{out}} = n \times (3.57 \times 10^{-7} \cdot \lambda_{\text{air}} - 8.29 \times 10^{-8}) \cdot J_{\text{cell}} \text{ (kg / s)} \quad (3-55)$$

By using an appropriate equation of state, e.g. the perfect gas law at low pressures, and given the inlet and exit pressures and temperatures of the reactants, it is possible to represent the flow rates on a volumetric instead of a mass basis. It is also noteworthy that the composition of the air leaving the fuel cell is not the same as that of the inlet air (approximately 79% nitrogen and 21% oxygen), since the oxygen is partly consumed by the fuel cell, and some water is added to the departing air instead.

The validity of these equations, using the ideal gas law for volumetric flow rates, was checked by applying them to a 500 W BCS PEM fuel cell and comparing the results with the values provided by the manufacturer at an air stoichiometry of 2 and hydrogen stoichiometry of 1.2 (table 3-3). The agreement between the theoretical predictions and manufacturer's values is within 5% for air and around 10% for hydrogen. Later in the experimental part of this study it will be shown that the predicted hydrogen flow rates obtained from these equations agree even more closely (within a few percent) with the actual experimental measurements.

Fuel cell type	PEM		Air stoichiometry	2		
Manufacturer/model	BCS/ FCS 6432		Exit air pressure	30k Pa		
Number of cells	32		Hydrogen inlet pressure	25 kPa		
Operating temperature	65 °C		Ambient pressure	100 kpa		
Ambient temperature	30 °C					
Current (A)	Air flow rate (slpm)		Accuracy	Hydrogen flow rate (slpm)		Accuracy
	model	manufacturer's manual		model	manufacturer's manual	
5	5.79	5.6	96.8%	1.47	1.3	89%
10	11.58	11.2	96.7%	2.94	2.7	92%
15	17.37	16.7	96.2%	4.4	4	91%
20	23.16	22.3	96.3%	5.87	5.3	91.3%
25	28.95	27.8	96%	7.34	6.7	91.3%
30	34.74	33.4	96.1%	8.8	8	91%

Table 3-3. Air and hydrogen flow rates for a BCS 500 W PEM fuel cell predicted by the model and compared with values provided by the manufacturer

3.5.3 Maximum EMF and open circuit voltage

The maximum electromotive force (EMF) is another parameter that has to be calculated for modelling the fuel cell. EMF and Open Circuit Voltage (OCV) calculations are done using the equation (3-39), after splitting it into equations (3-38) and (3-56):

$$\begin{aligned}
 & \left\{ \frac{(\lambda_{air} - 1)}{2} O_2 + \frac{3.76}{2} \lambda_{air} N_2 + (\lambda_{hydrogen} - 1) H_2 \right\}_{\text{Cell inlet temperature and pressure}} \\
 \rightarrow & \left\{ \frac{(\lambda_{air} - 1)}{2} O_2 + \frac{3.76}{2} \lambda_{air} N_2 + (\lambda_{hydrogen} - 1) H_2 \right\}_{\text{Cell outlet temperature and pressure}} \quad (3-56)
 \end{aligned}$$

It is notable that equation (3-39) is obtained by combining equation (3-38) and equation (3-56). Equation (3-56) does not represent a chemical reaction; it just shows the extra hydrogen, oxygen, and nitrogen entering the stack at the inlet pressure and temperature and leaving the stack at a different pressure and temperature. As discussed before, the main electrochemical reaction that leads to heat and power production is equation (3-38). The electromotive force of an ideal (100% efficient) cell, $EMF_{(100\% \text{ efficient cell})}$, is the electricity generated by the fuel cell when all the energy content of hydrogen is converted to electricity. Obviously this maximum electromotive force is ideally achievable if no loss happens in the fuel cell and the exit water is in liquid form (no energy is absorbed by water to be evaporated). Changes in the enthalpy of formation ($\Delta \bar{h}_f$), corresponding to the

hydrogen HHV (water outlet is in liquid form), are used to determine the maximum electromotive force of the cell:

$$EMF_{(100\% \text{ efficient cell})} = \frac{(-\Delta \bar{h}_f)_{\text{liquid water}}}{2F} = \frac{-(-285840)}{2 \times 96485} = 1.48 \text{ V} \quad (3-57)$$

Hence, the fuel cell efficiency (based on *HHV*) is obtained by having the actual fuel cell voltage, $V_{\text{Single cell}}$ (for just one cell, given in Volt), as follows:

$$\eta_{\text{energy}} = \mu_f \cdot V_{\text{Single cell}} / 1.48 \quad (3-58)$$

where, μ_f is the hydrogen utilisation coefficient, reflecting the fact that cells must be fed with more hydrogen than theoretically needed for producing a certain amount of electrical potential (Larminie and Dicks 2003):

$$\mu_f = \frac{\text{mass of the fuel reacted in stack}}{\text{Actual mass of the fuel input to the stack}} = \frac{\text{Volume of the fuel reacted in stack}}{\text{Actual volume of the fuel input to the stack}} \quad (3-59)$$

For finding the theoretical maximum theoretical open circuit voltage (OCV) of the fuel cell (not 100% efficient fuel cell), shown here by E_0 , the following equation (based on Gibbs free energy function rather than the enthalpy of formation) is used (Larminie and Dicks 2003):

$$E_0 = \frac{-\Delta \bar{g}_f}{2F} \quad (3-60)$$

To apply this equation in the model, the enthalpy of formation and the molar Gibbs free energy of formation of all the contributing components have to be represented as mathematical functions to be calculated at any given temperature. At low pressures the ideal gas assumption is in practice applicable for the contributing substances; hence their molar specific heats (\bar{c}_p) are only functions of temperature and independent of pressure. These functions are given by Sonntag *et al.* (2003) and provided in the appendix 5 of this thesis. The following equations show how the specific heats of the contributing components connect to their enthalpy of formation and Gibbs free energy (Sonntag *et al.* 2003).

Relation between enthalpy and specific heat:

$$d\bar{h}_{f,T} = \bar{c}_p \cdot dT \Rightarrow \bar{h}_{f,T} = \int_0^T \bar{c}_p \cdot dT \Rightarrow \bar{h}_{f,T} = \bar{h}_{f,298.15} + \int_{298.15}^T \bar{c}_p \cdot dT \quad (3-61)$$

Relation between entropy and specific heat:

$$\bar{g}_{f,T} = \bar{h}_{f,T} - T \left(\bar{s}_{298.15} + \int_{298.15}^T \frac{1}{T} \bar{c}_p \cdot dT \right) \quad (3-62)$$

where T is temperature in $^{\circ}\text{K}$; $\bar{h}_{f,T}$ is molar enthalpy of formation at temperature of T in J/mol ; $\bar{h}_{f,298.15}$ is the molar enthalpy of formation at 298.15°K (table 3-4); $\bar{g}_{f,T}$ is the molar Gibbs free energy at temperature of T in J/mol ; and $\bar{s}_{298.15}$ is molar entropy at 298.15°K in J/mol.K (table 3-4).

	Enthalpy of formation at 298.15°K (J/mol)	Molar entropy at 298.15°K (J/mol.K)
Water (Steam)	-241827	188.83
Water (Liquid)	-285838	70.05
Hydrogen	0	130.59
Oxygen	0	205.14
Nitrogen	0	<i>Not used in the calculation</i>

Table 3-4. Enthalpy of formation for water, hydrogen, oxygen and nitrogen at 298.15°K (Sonntag *et al.* 2003)

Hence it is possible to obtain the enthalpy of formation and molar entropy of the components as functions of temperature. As the assumption of an ideal gas is not a 100% accurate assumption, the change in Gibbs free energy used for finding the *OCV* can be obtained here at atmospheric pressure, and can be modified for other operating pressures using the Nernst equation, as will be discussed later in this section. The molar entropy of nitrogen is not used for the fuel cell-related calculations because nitrogen does not take part in the main reaction shown in equation (3-38).

Substituting the Gibbs functions, defined by equation (3-62) into equation (3-60), it is possible to find the *OCV* as a function of temperature at 1 atm. The higher the temperature the lower this open circuit voltage will be (figure 3-13). However, later it will be shown that the voltage drops in a fuel cell with higher operating temperatures, when loads are

connected and current is drawn, are less than those at lower operating temperatures, resulting in a better overall performance of the cell at higher temperatures, up to its operating limit.

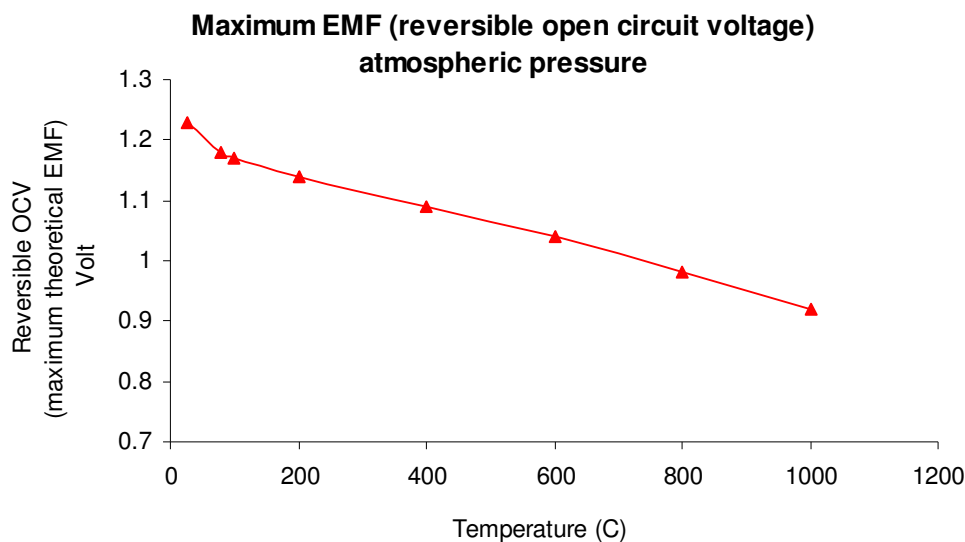


Figure 3-13. The effect of temperature on reversible open circuit voltage of a single-cell fuel cell as predicted by the model

The maximum theoretical open circuit voltage (E_0), obtained from equation (3-60), has to be modified (E) for applied pressures other than 1 atm. The Nernst equation, as discussed in detail by Larminie and Dicks (2003), is used for this purpose:

$$E = E_0 + \frac{RT}{2F} \ln\left(\frac{P_{H_2} \cdot P_{O_2}^{0.5}}{P_{H_2O}}\right) \quad (3-63)$$

where T is fuel cell operating temperature in $^{\circ}K$, F is the Faraday constant (96485 C/mol), R is the universal gas constant (8.314 J/mol.K) and pressures are all the partial gauge pressures in the inlet and exit streams of the fuel cell given in bar. Equation (3-39) is used for finding the partial pressures of water, oxygen, and hydrogen when the inlet and exit pressures are given. It is important to note that water appears in the exit air stream and only the water, oxygen, and nitrogen molecules, in the right hand side of equation (3-39), have to be taken into account for calculating the partial pressure of water; the extra hydrogen leaves the stack from a separate channel.

If P_{inlet,H_2} is the inlet pressure in the hydrogen stream, $P_{exit,air}$ is the exit pressure in the air stream, and $P_{inlet,air}$ is the inlet pressure in the air stream, these pressures are given by:

$$\begin{aligned}
 P_{H_2} &= \frac{\lambda_{hydrogen}}{\lambda_{hydrogen}} P_{inlet,H_2} = P_{inlet,H_2} \\
 P_{O_2} &= \frac{0.5\lambda_{air}}{\left(0.5 + \frac{3.76}{2}\right)\lambda_{air}} = \frac{1}{4.76} P_{inlet,air} \\
 P_{H_2O} &= \frac{1}{1 + \frac{(\lambda_{air} - 1)}{2} + \frac{3.76}{2}\lambda_{air}} P_{exit,air} = \frac{0.42}{0.21 + \lambda_{air}} P_{exit,air}
 \end{aligned} \tag{3-64}$$

In practice the inlet air contains some water due to its relative humidity. The effect of this inlet air relative humidity on the oxygen partial pressure is negligible, particularly when the relative humidity is above 50% (Zhang *et al.* 2008); however, the partial pressure of water has to be modified when the effect of inlet air relative humidity is taken into account. This modified equation will be shown later where the fuel cell water management is discussed (section 3.5.6).

In calculating the partial pressures using equation (3-39) it must be borne in mind that the excess hydrogen leaves the fuel cell in a separate channel from the excess air and the produced water, and also that hydrogen and air get into the fuel cell from separate channels (figure 3-14). In practice some of the produced water is dragged into the membrane and does not appear in the exit stream, a factor that is neglected when finding the partial pressure of water in equation (3-64).

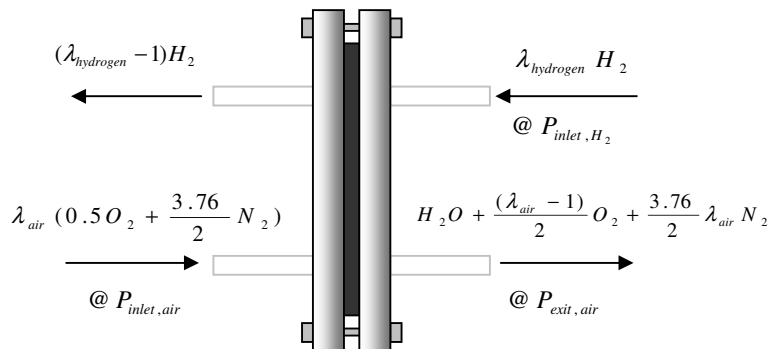


Figure 3-14. Fuel cell inlet and exit air and hydrogen stream

As an example of the use of the foregoing equations in the fuel cell model, figure 3-15 shows the effect of hydrogen supply pressure on the reversible OCV of the fuel cell using the Nernst equation (3-63), keeping the values of the other parameters to those shown in table 3-3.

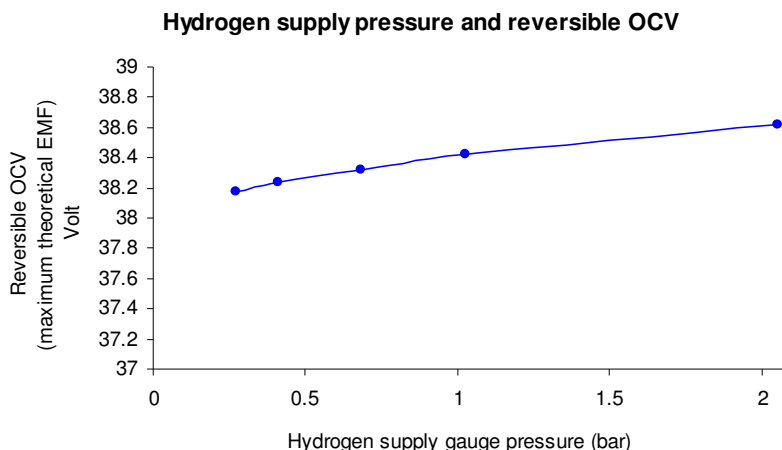


Figure 3-15. The effect of hydrogen supply pressure on the reversible open circuit voltage of a fuel cell performance (32-cell 500 W PEM BCS fuel cell stack) using the Nernst equation in the fuel cell model

3.5.4 Modified Butler-Volmer equations

In practice, when a load is connected to a fuel cell, its output voltage falls below the theoretical reversible open circuit voltage. As shown by figure 3-16 this voltage drop depends on the size of the load and consequently the current drawn from the fuel cell. The relationship between the current and the output voltage of a fuel cell, the so-called polarisation curve, is the crux of fuel cell modelling.

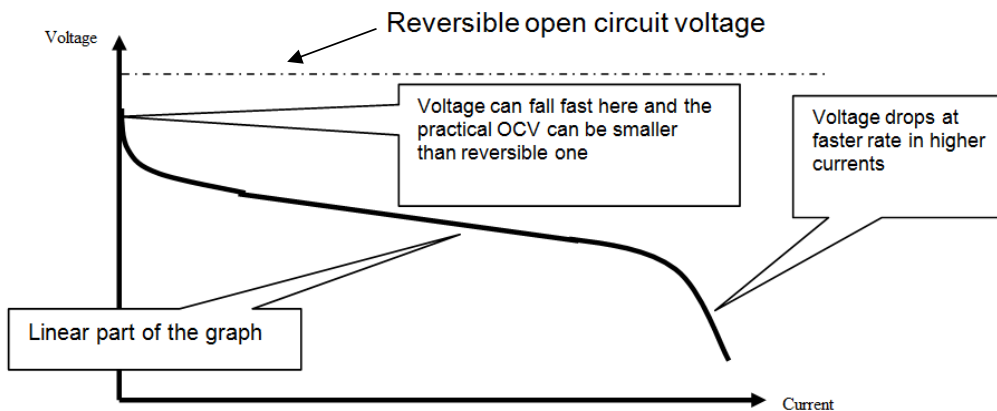


Figure 3-16. Typical voltage drop trend in a fuel cell (polarisation curve)

The shape of the polarisation curve is determined by four different kind of losses (Larminie and Dicks 2003):

- *Fuel crossover (internal current)*: This happens specially in low-temperature fuel cells whereas in higher-temperature fuel cells it is usually negligible (Larminie and Dicks 2003). When no load is connected to fuel cell, the open circuit voltage is smaller than the reversible OCV. It indicates that an internal current (J_{int}) is there even before any actual load is connected to the cell. The effect of this internal current can be assumed equivalent to fuel wastage through fuel crossover through the membrane from one electrode to the other without reaction (Larminie and Dicks 2003).
- *Activation overpotential*: This loss is caused by the limitations on the rates of the reactions taking place on the surface of the oxygen and hydrogen electrodes (Larminie and Dicks 2003). In the present chapter, these losses are represented by the overpotentials, η^O and η^H , on oxygen and hydrogen electrodes respectively. This kind of polarisation occurs in the first part of the polarisation curve from the left as shown in figure 3-16 (Aurora 2003).
- *Ohmic losses*: These losses are basically due to the resistance against the flow of ions through the membrane or electrons through electrodes, interconnections, and bipolar plates. The associated voltage drops obey Ohm's law and are linearly proportional to fuel cell current. These losses are the dominant influence in the middle (linear) part of the polarisation curve.
- *Mass transport losses*: As a reactant is consumed at the electrode by the electrochemical reaction, there is a drop in voltage due to the limitations on the rate of transport of reactants/products to/from the electrochemical reaction site. This drop is termed the 'concentration overvoltage' (Aurora 2003) or 'mass transport loss' (Larminie and Dicks 2003). Concentration loss becomes dominant as higher currents are drawn from fuel cell, as shown on the far right of the polarisation curve in figure 3-16.

These types of loss are not all independent. For example, one effective and straightforward way to reduce membrane resistance is to use a thinner membrane (Cheng *et al.* 2007). In early fuel cell development, Nafion 117 with the thickness of 175-173 μm was widely used, and most recently Nafion 211 or 111 with the thickness of 25 μm has been employed. However, with decreasing membrane thickness, another loss, hydrogen fuel crossover, may become the key factor especially when the fuel cell operates at low current densities and higher temperatures (Cheng *et al.* 2007).

The present fuel cell model employs modified Butler-Volmer (BV) equations and modelling approach recently developed by Doddathimmaiah and Andrews (2008) to represent mathematically the voltage-current characteristic curve. The various voltage drops in a typical fuel cell can be expressed as follows (Doddathimmaiah and Andrews 2008):

$$V_{cell} = E - J_{cell} \cdot (R_e^O + R_e^H) - |\eta^O| - |\eta^H| - (|j_{cell}| + |j_{int}|) \cdot S \cdot R_m^{H^+} \quad (3-65)$$

where:

E is the reversible OCV calculated from (3-63),

$J_{cell} \cdot (R_e^O + R_e^H)$ is the total ohmic potential loss on the oxygen and hydrogen electrodes,

η^O and η^H are the activation overpotentials on the oxygen and hydrogen sides respectively,

$(|j_{cell}| + |j_{int}|) \cdot S \cdot R_m^{H^+}$ is the internal current loss and ohmic loss in the electrolyte membrane,

j_{cell} is the current density (cell current divided by the cell's effective area),

j_{int} is the internal current density,

S is the cell's effective area,

$R_m^{H^+}$ is the membrane's ohmic resistance against the flow of ions,

R_e^O is the oxygen electrode's resistance against the flow of electrons,

R_e^H is the hydrogen electrode's resistance against the flow of electrons, and

J_{cell} is the cell's current.

The equivalent circuit of a fuel cell on which equation (3-65) is applied is shown in figure 3-17.

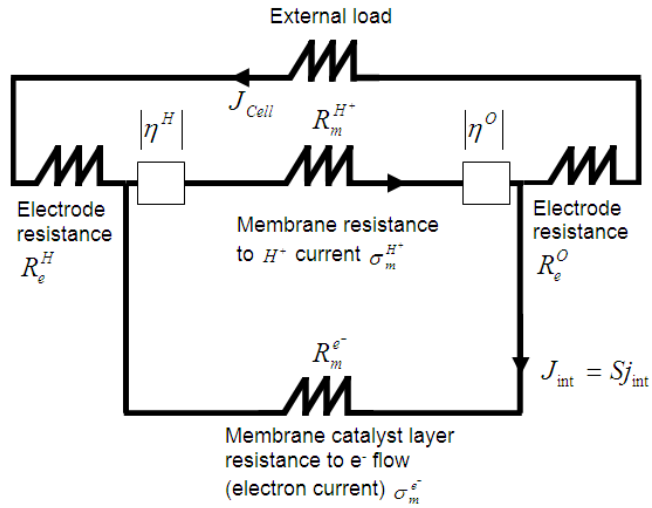


Figure 3-17. Equivalent circuit of a fuel cell used for applying the BV equations in fuel cell modelling (Doddathimmaiah and Andrews 2008)

The electrical conductivity of the membrane to ionic current, $\sigma_m^{H^+}$, is the inverse of the membrane's specific resistance to the ions, $\rho_m^{H^+}$. This specific resistance is actually the resistance per unit area, per unit length, so having the cell's area, S , and the membrane thickness, L , this conductivity can be related to the cell resistance against the flow of ions as below (Doddathimmaiah and Andrews 2008):

$$\sigma_m^{H^+} = 1 / \rho_m^{H^+} \quad (3-66)$$

$$\rho_m^{H^+} = \frac{S}{L} \cdot R_m^{H^+} \quad (3-67)$$

$$L / \sigma_m^{H^+} = S \cdot R_m^{H^+} \quad (3-68)$$

The same definition is applied to the membrane conductivity to the flow of electrons. Given that the potential difference across the membrane resistance to the electrons, $R_m^{e^-}$, is V_{cell} , the internal current density, j_{int} , can be expressed as:

$$j_{int} = \frac{\sigma_m^{e^-} \cdot V_{cell}}{L} \quad (3-69)$$

where $\sigma_m^{e^-}$ is the electronic conductivity of the membrane.

A new parameter, γ_e , the total electrode resistance per unit area, can be defined as:

$$\gamma_e = \frac{(R_e^H + R_e^O)}{S} \quad (3-70)$$

Thus equation (3-65) can be rearranged to (Doddathimmaiah and Andrews 2008):

$$V_{cell} = E - S \cdot J_{cell} \cdot \gamma_e - |\eta^O| - |\eta^H| - \left(|j_{cell}| + \frac{\sigma_m^{e-} \cdot V_{cell}}{L} \right) \cdot \frac{L}{\sigma_m^{H+}} \quad (3-71)$$

The overpotentials on the oxygen and hydrogen sides, $|\eta^O|$ and $|\eta^H|$, must be found to determine V_{cell} at any given J_{cell} . That is where the modified Butler-Volmer (BV) equations come in. A number of ways of modifying the BV equations to take the mass transport losses into account have been proposed, but these essentially involve adding ad hoc algebraic terms to the basic BV equations (Doddathimmaiah 2008). The modified version of the BV equations introduced by Doddathimmaiah and Andrews (2009) employs a logistic type of function to represent the saturation behaviour at high current densities inherent in the fuel cell; a parameter that first increases exponentially and then changes slowly until a saturation value is obtained. The modified BV equations used in the model for the oxygen and hydrogen electrodes, and incorporating logistic-type functions as proposed by Doddathimmaiah and Andrews (2009), are the following:

$$j_{cell} - \frac{\sigma_m^{e-} \cdot V_{cell}}{L} = j_0^O \frac{\left[\exp\left(\frac{\eta^O \alpha^O 2F}{RT_{cell}}\right) - \exp\left(\frac{-(1-\alpha^O)2F\eta^O}{RT_{cell}}\right) \right]}{\left(1 + \frac{\exp\left(\frac{-\eta^O(1-\alpha^O)2F}{RT_{cell}}\right)}{\left(\frac{j_{sat}^{FC}}{j_0^O}\right)} \right)} \quad (3-72)$$

$$j_{cell} - \frac{\sigma_m^{e-} \cdot V_{cell}}{L} = j_0^H \frac{\left[\exp\left(\frac{-\eta^H \alpha^H 2F}{RT_{cell}}\right) - \exp\left(\frac{(1-\alpha^H)2F\eta^H}{RT_{cell}}\right) \right]}{\left(1 + \frac{\exp\left(\frac{\eta^H(1-\alpha^H)2F}{RT_{cell}}\right)}{\left(\frac{j_{sat}^{FC}}{j_0^H}\right)} \right)} \quad (3-73)$$

F is the Faraday constant (96485 C/mol); α^O and α^H are charge transfer coefficients of oxygen and hydrogen sides; j_0^O and j_0^H are exchange current densities on oxygen and hydrogen sides; j_{sat}^{FC} is the saturation exchange current density of the fuel cell; T_{cell} is the cell operating temperature; and R is the universal gas constant (8.314 J/mol.K).

The value of the charge transfer coefficient depends on the reaction and the material the electrode is made from. It must be in the range of 0 to 1.0, and for the hydrogen electrode,

its value is about 0.5 for a great variety of electrode materials (Larminie and Dicks 2003). At the oxygen electrode the charge transfer coefficient shows more variation (Larminie and Dicks 2003). The charge transfer coefficient is also assumed to be independent of temperature (Zhang *et al.* 2006). The exchange current densities on both the oxygen and hydrogen sides, and also the membrane ionic conductivity depend on temperature. Empirical relationships for this dependency have been found experimentally in a particular case by Harrison (2006) as follows:

$$j_0^O = 2 \times 10^{-6} \cdot e^{0.043T_{cell}} \quad (A/cm^2) \quad (3-74)$$

$$j_0^H = 0.12 \cdot e^{0.026T_{cell}} \quad (A/cm^2) \quad (3-75)$$

$$\sigma_m^{H^+} = 0.001 \cdot T_{cell} + 0.03 \quad (S/cm) \quad (3-76)$$

If j_0^H , j_0^O , and $\sigma_m^{H^+}$ are assumed to be constant and independent of temperature, the BV equations suggest a decrease in overpotential with increasing cell operating temperature. However, the dependency of these parameters on temperature actually reverses this relationship: the higher the temperature the less the overpotential (Larminie and Dicks 2003). Despite the higher operating temperature resulting in lower reversible open circuit voltage, the overall effect of increasing the temperature on the whole polarisation curve is improvement in the performance of the fuel cell. This behaviour is shown in the theoretical curve of figure 3-18 produced using the present model on a 500 W PEM BCS fuel cell and in (Zhang *et al.* 2006)'s experimental investigations. Such behaviour has put the high temperature PEM fuel cells (HT-PEMFCs) in a promising perspective and encouraged many research studies conducted on high temperature (above 100 °C) PEM fuel cells (Coppo *et al.* 2006; Zhang *et al.* 2006; Cheng *et al.* 2007; Shamardina *et al.* 2009).

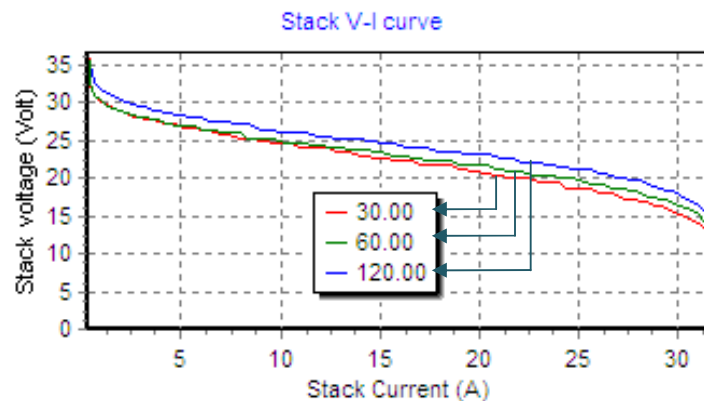


Figure 3-18. The typical effect of temperature on PEM fuel cell polarisation curve; theoretical analysis using modified Butler-Volmer equations; operating condition as shown in table 3-3; temperatures are all in °C

Increasing the temperature can weakly increase the charge transfer coefficients (Coppo *et al.* 2006); however, for simplicity this parameter has been assumed to be independent of temperature in the model (Zhang *et al.* 2006). Experimental results show that conditions such as air relative humidity slightly affect exchange current densities and membrane conductivities (Zhang *et al.* 2008). As these effects are quite small, hence to keep the model simple, these functions have not been taken into account. The reactants pressure can affect both the fuel cell *OCV* and overpotentials. This effect on overpotentials is quite small; that is why the model considered it only for the fuel cell *OCV* using equation (3-63), the Nernst equation.

The modified Butler-Volmer equations (3-72) and (3-73), along with equation (3-71), must be solved simultaneously using an iterative process to find the V_{cell} for a series of J_{cell} values and hence obtain the polarisation curve (Doddathimmaiah 2008). The Butler-Volmer polarisation curve of the fuel cell (a key input for solar-hydrogen system analysis) is introduced to the simulation code in two ways:

1. Using the experimental polarisation curve:

Usually the polarisation (voltage-current) curve of an electrolyser or fuel cell is provided by the manufacturer in the user manual. When such a curve is available, the model employs a least-squares method to find the theoretical curve based on the modified BV equations (3-72) and (3-73) that best fits the experimental performance curve. Values for the fuel cell parameters, such as charge transfer coefficients, are found by an iterative process, so that the theoretical curve fits the experimental one to within a predefined level of accuracy. The membrane conductivities and exchange current densities are calculated using equations (3-74) to (3-76) for the given operating temperature of the fuel cell (see appendix 1, page 291, for the detail of the required inputs). Specifically the least-squares method involves solving the following equations simultaneously to find the unknown parameters in BV equations:

$$\begin{aligned} \frac{\partial \sum_i (V_{cell,exp} - V_{cell,mod})_i^2}{\partial \alpha^o} &= 0 \\ \frac{\partial \sum_i (V_{cell,exp} - V_{cell,mod})_i^2}{\partial \alpha^H} &= 0 \\ \frac{\partial \sum_i (V_{cell,exp} - V_{cell,mod})_i^2}{\partial j_{sat}^{FC}} &= 0 \end{aligned} \quad (3-77)$$

where ‘*i*’ is the number of experimental points provided by the manufacturer or measured in the laboratory; and ‘exp’ and ‘mod’ stand for experimental and model respectively. This procedure is illustrated in figure 3-19 and figure 3-20.

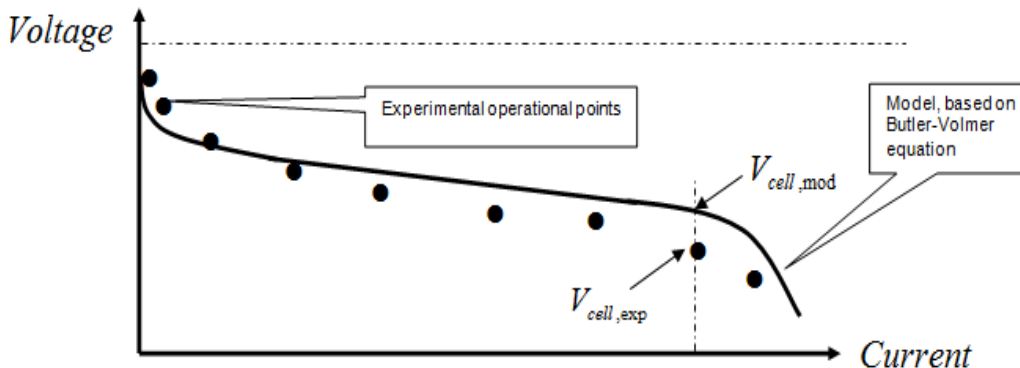


Figure 3-19. Least squares method used for curve fitting

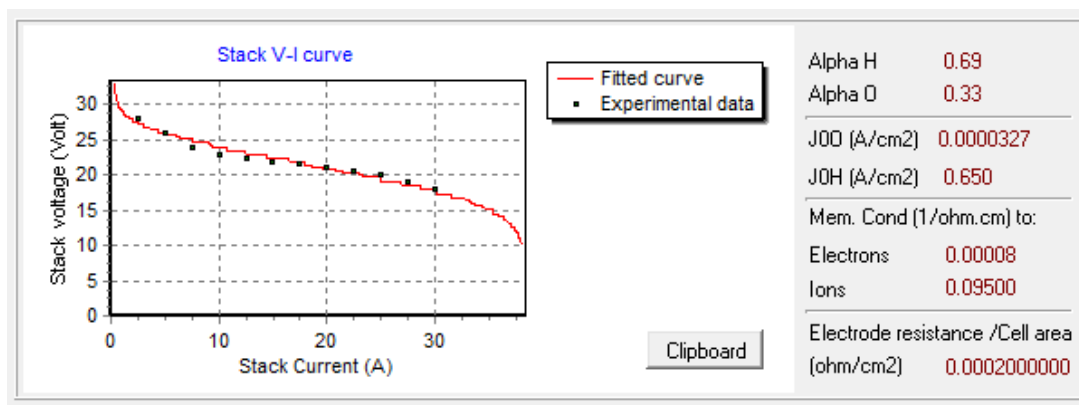


Figure 3-20. An example to show fuel cell polarisation curve fitting using the least squares method and Butler-Volmer equations; operating condition as given in table 3-3; saturation current density 0.6 A/cm²

2. Direct introduction of the key parameters, used in BV equations:

Alternatively the key parameters used in BV equations – the exchange current densities and charge transfer coefficients on the oxygen and hydrogen sides, the saturation current density, membrane conductivity, and the electrodes ohmic resistance - might be known or given (see more details in appendix 1, page 294). So putting these values into the model allows the polarisation curve to be generated directly. However, it is recommended to compare the results with the experimental curve to double-check the output, since these key parameters are influenced by cell’s operating condition and thus might change from one operating condition to another.

3.5.5 Fuel cell heat generation and CHP concept

As a consequence of the entropy change between products and reactants and the second law of thermodynamics, the efficiency of the fuel cell in converting the hydrogen energy into electricity is not 100%. Part of the hydrogen's energy content appears in the form of heat rather than electricity. For calculating this heat it is important to know whether the water produced is in vapour or liquid form, since part of the generated heat may be used for this vaporisation. As discussed earlier (section 3.5.3), the theoretical maximum energy available from the electrochemical reaction in a fuel cell is given by the change of enthalpy in the water-formation reaction in equation (3-38). When the product water is a liquid this enthalpy difference is 285.84 kJ/mol, but when it is in vapour form the magnitude of the enthalpy change is lower, and has to be found using the standard thermodynamic functions relating enthalpy to pressure and temperature for water vapour (see appendix 5). To find out whether the water produced is liquid or vapour, the partial pressure of water, given by equation (3-64), has to be compared with the saturation pressure of water at the cell operating temperature. The following empirical equation (Zhang *et al.* 2008) is used in the model for this purpose:

$$P_{sat,water} = \frac{602.724}{10^3} + \frac{438.484}{10^4}T + \frac{139.844}{10^5}T^2 + \frac{271.166}{10^7}T^3 + \frac{257.731}{10^9}T^4 + \frac{282.254}{10^{11}}T^5 \quad (3-78)$$

where temperature and pressure are in °C and kPa respectively. When the partial pressure of the water is higher than the saturated pressure at a particular water temperature, the water is in liquid form, while the water comes out in vapour form if the partial pressure is lower than this value.

The rate of heat generation by the fuel cell, Q_{total}^{\bullet} , is calculated by using the difference between the fully-efficient cell EMF for liquid water production (3-57) and the actual voltage of a single cell at a particular current. The energy content of the hydrogen reacted inside the fuel cell ideally has to be converted to electrical energy. Any inefficiency in this conversion appears in the form of heat, as shown in the following equation:

$$Q_{total}^{\bullet} = n.S.j_{cell} (EMF_{(100\% \text{ efficient cell.liquid water})} - V_{cell}) = n.S.j_{cell} (1.48 - V_{cell}) \quad (3-79)$$

Substituting V_{cell} using equation (3-65) gives:

$$Q_{total}^{\bullet} = n.S.j_{cell} \left\{ 1.48 - E + S.j_{cell} \cdot (R_e^O + R_e^H) + |\eta^O| + |\eta^H| + (|j_{cell}| + |j_{int}|)S.R_m^{H^+} \right\} \quad (3-80)$$

V_{cell} is the output voltage of a single cell with an effective area of S at the current density of j_{cell} . The voltage of the fuel cell, V_{cell} , is calculated using the BV equations .

If the water produced is in liquid form, no heat is absorbed by the water for evaporation. But if water vapour is produced, the part of the total heat generated by the fuel cell used for water evaporation is usually considerable and can be found using the following equation:

$$Q_{water\ evaporation}^{\bullet} = n.S.j_{cell} (1.48 - EMF_{100\% \text{ efficient cell, actual water condition}})$$

$$Q_{water\ evaporation}^{\bullet} = n.S.j_{cell} \left(1.48 + \frac{\Delta \bar{h}_f}{2F} \right) \quad (3-81)$$

Another part of the fuel cell heat is removed as sensible heat by the extra hydrogen and air (including its water content) in the exit stream of the fuel cell. This amount mainly depends on the air and hydrogen stoichiometry, although it is not more than a few percent of the total heat generated for the normal ranges of stoichiometries used. However, this form of heat removal can be considerable if higher stoichiometries of air are used for running the fuel cell. It will be shown later that this method of heat removal from the fuel cell is not recommended since it will result in dehydration of the membrane of the fuel cell. The amount of heat removed by the exit gas streams from the fuel cell is calculated by applying the definition of enthalpy in equation (3-56) and taking the water content of the air into account. The thermal capacity of these extra reactants (C_p) can be calculated by the following equation, by assuming the enthalpy to be only a function of temperature at low pressure:

$$C_p = \frac{\partial H}{\partial T} = \frac{\Delta H}{\Delta T} \quad (3-82)$$

Hence using the equation (3-56), the heat removed by these extra reactants ($C_p \Delta T$) for every mole of hydrogen (or half a mole of oxygen) reacted in the fuel cell is:

$$\frac{\text{the heat removed by the exit air and hydrogen stream}}{\text{a mole of hydrogen or half a mole of oxygen reacted}} = \frac{\Delta H_{\text{air and hydrogen stream}}}{\text{a mole of hydrogen or half a mole of oxygen reacted}} \quad (3-83)$$

where ΔH represents the increase in the total enthalpy of the extra reactants given by equation (3-56) (as well as the water content of the inlet air) for every mole of hydrogen (or every half a mole of oxygen) participated in the main reaction, shown by equation (3-38). To find out the total rate of heat removal through the exit air and hydrogen streams by these extra reactants, the rate of either hydrogen or oxygen moles reacted in the fuel cell has to be incorporated into equation (3-83). Hence, by using equation (3-45), discussed in section 3.5.2, we have:

$$\dot{Q}_{air\ and\ hydrogen\ stream} = \frac{nJ_{cell} / zF}{a\ mole\ of\ hydrogen\ or\ half\ a\ mole\ of\ oxygen} \Delta H_{air\ and\ hydrogen\ stream} \quad (3-84)$$

The rest of the heat generated by the fuel cell has to be removed from the stack by a proper cooling system; otherwise the stack temperature would keep rising and eventually exceed its desirable range of operation. It is this heat removed by the cooling system that has the potential to be utilised for a beneficial purpose such as hot water production or even space heating.

After taking into account the heat consumed for water evaporation and the heat removed by the exit streams of reactants, the heat removed by the cooling system is always considerably lower than the total heat generated by the fuel cell. The amount of heat available in practice from a fuel cell operating as a CHP system, and the multiple factors affecting this amount, will be discussed further in Chapter 4 and Chapter 5 by conducting a case study and an experimental investigation.

3.5.6 PEM fuel cell water management and relative humidity

While examining water management is not the main purpose of this fuel cell simulation model, a simple tool has been added to the code to check the water content/phase of the exit air to ensure that the fuel cell is neither dehydrated nor flooded.

The relative humidity is the ratio of partial pressure of water, P_w , to the saturation pressure of water, given by equation (3-78), at its temperature, P_{sat} :

$$\phi = \frac{P_w}{P_{sat}} \quad (3-85)$$

The simulation model is also flexible enough to consider the effect of the relative humidity of the inlet air on the operation of the fuel cell and its capacity to be used as a CHP unit in a solar-hydrogen system. The research done by Zhang, Tang *et al.* (2008) showed that the relative humidity of the inlet air has a negligibly-small effect on the open circuit voltage, but potentially a considerable effect on the fuel cell losses (figure 3-21). Zhang, Tang *et al.* (2008) also revealed that the membrane resistance, the charge transfer coefficients, and the exchange current density all increase if the relative humidity of the air increases (figure 3-22). Zhang, Tang *et al.* (2008) also introduced some empirical equations to show the dependency of these parameters on the relative humidity, ϕ , such as the following equation for the charge transfer coefficient :

$$\alpha = (0.001552 \phi + 0.000139) T \tag{3-86}$$

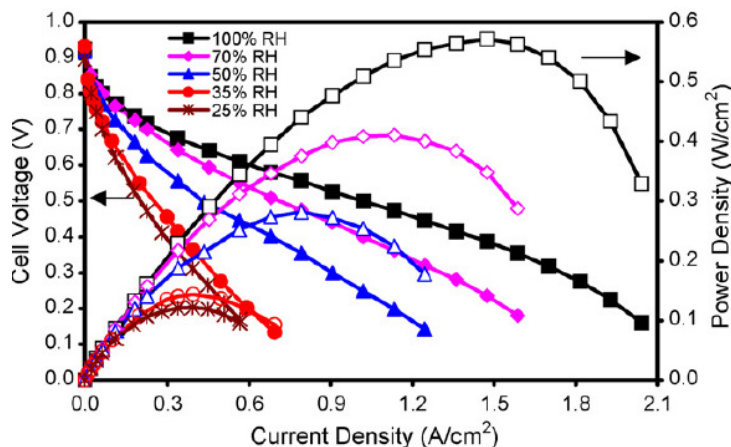


Figure 3-21. PEM fuel cell performance and relative humidity (Zhang *et al.* 2008) operating temperature 120 °C, 1 atm backpressure, MEA active area: 4.4cm²; hydrogen and air flow rates are 0.75 and 1 l/min, respectively.

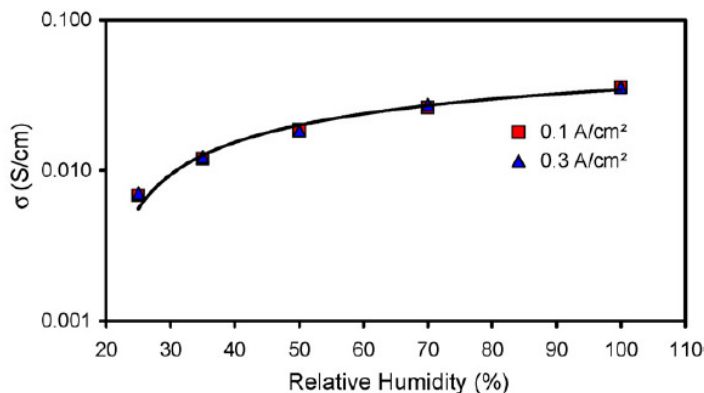


Figure 3-22. Membrane conductivity as a function of current density (Zhang *et al.* 2008) operating temperature 120 °C, 1 atm backpressure, Nafion 112 -based MEA with an active area of 4.4cm²; the thickness of the Nafion 112 membrane was adopted as 50 μm

The ideal relative humidity of the exit air is between 80% and 100%; relative humidity below this level is the sign of cell dehydration and above 100% (theoretically) means the membrane is flooded (Larminie and Dicks 2003). Parameters that have to be controlled to maintain humidity in this desirable range are the temperature, pressure, and stoichiometry of the inlet air, as well as the fuel cell operating temperature and the pressure of the exit air stream. However, in regulating the relative humidity of the exit air, it must be borne in mind that increasing this humidity by lowering the cell operating temperature will increase the fuel cell overpotentials; lowering the air stoichiometry by reducing the inlet air flow rate will reduce the reaction rate on the oxygen electrode (the cathode); and increasing the air pressure will mean more parasitic energy losses in rerunning the air compressor (Larminie and Dicks 2003). Also if too much air is fed into the fuel cell for cooling purposes it can lead to membrane dehydration.

The partial pressure of water vapour in the inlet air stream is found in terms of the relative humidity and temperature of this air as follows. If the total pressure of the moist inlet air is $P_{inlet,air}$, the pressure of just the dry air, P_a , in this mixture is:

$$P_a = P_{inlet,air} - P_w = P_{inlet,air} - \phi.P_{sat} \quad (3-87)$$

The humidity ratio (or specific humidity), ω , is defined as the ratio of mass of water in a particular sample of moist air, m_w , to the mass of just the dry air in the sample, m_a :

$$\omega = \frac{m_w}{m_a} \quad (3-88)$$

where the total mass of the moist air is $m_w + m_a$.

Given the molar mass of water is 18g and that of air 28.97 g, the humidity ratio for the inlet air to the fuel cell is:

$$\omega = \frac{m_w}{m_a} = \frac{18}{28.97} \cdot \frac{P_w}{P_a}$$

or:

$$m_w = 0.622 \frac{\phi.P_{sat}}{P_{inlet,air} - \phi.P_{sat}} m_a \quad (3-89)$$

The latter equation together with equation (3-50) is thus used in the model to find the water content of the exit stream. Equation (3-64) for the partial pressure of water in the exit stream can be modified as follows to take into account the relative humidity of the inlet air:

$$P_{H_2O} = \frac{(0.42 + \frac{P_w}{P_{inlet,air} - P_w})}{(1 + \frac{P_w}{P_{inlet,air} - P_w})\lambda_{air} + 0.21} P_{exit,air} \quad (3-90)$$

or:

$$P_{H_2O} = \frac{(0.42 + \frac{\phi \cdot P_{sat}}{P_{inlet,air} - \phi \cdot P_{sat}})}{(1 + \frac{\phi \cdot P_{sat}}{P_{inlet,air} - \phi \cdot P_{sat}})\lambda_{air} + 0.21} P_{exit,air} \quad (3-91)$$

The relative humidity of the air at the exit stream, which is best maintained between 80% and 100%, is then calculated in the model using:

$$\phi_{exit} = \frac{P_{H_2O}}{P_{sat}} \quad (3-92)$$

3.6 ELECTROLYSER MODELLING

The modified Butler-Volmer equations introduced by Doddathimmaiah and Andrews (2008) are used for electrolyser modelling as well as the fuel cell. Almost the same equations apply to both PEM fuel cell and electrolyser, except that the signs for the overpotentials change and hence different terms become predominant in the two cases (Doddathimmaiah and Andrews 2008):

$$j_{cell} - \frac{\sigma_m^{e-} \cdot V_{cell}}{L} = j_0^O \frac{\left[\exp\left(\frac{\eta^O \alpha^O 2F}{RT_{cell}}\right) - \exp\left(\frac{-(1-\alpha^O)2F\eta^O}{RT_{cell}}\right) \right]}{\left(1 + \frac{\exp\left(\frac{\eta^O \alpha^O 2F}{RT_{cell}}\right)}{\left(\frac{j_{sat}^E}{j_0^O}\right)} \right)} \quad (3-93)$$

$$j_{cell} - \frac{\sigma_m^{e-} \cdot V_{cell}}{L} = j_0^H \frac{\left[\exp\left(\frac{-\eta^H \alpha^H 2F}{RT_{cell}}\right) + \exp\left(\frac{(1-\alpha^H)2F\eta^H}{RT_{cell}}\right) \right]}{\left(1 + \frac{\exp\left(\frac{-\eta^H \alpha^H 2F}{RT_{cell}}\right)}{\left(\frac{j_{sat}^E}{j_0^H}\right)} \right)} \quad (3-94)$$

j_{sat}^E in equations (3-93) and (3-94) is the saturation exchange current density of the electrolyser. The other parameters used in these equations were already defined where equation (3-73) was introduced.

The equivalent electrical circuit for a PEM electrolyser that was introduced by Doddathimmaiah and Andrews (2008) is shown by figure 3-23.

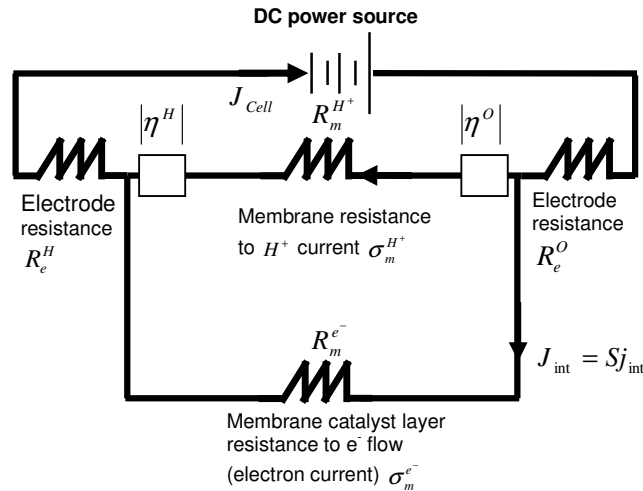


Figure 3-23. Equivalent circuit of an electrolyser used for applying the Butler-Volmer equations in electrolyser modelling (Doddathimmaiah and Andrews 2008)

Hence summing the potential changes and sources of electromotive force going round the circuit gives:

$$V_{cell} = E - S \cdot J_{cell} \cdot \gamma_e + |\eta^O| + |\eta^H| + \left(|j_{cell}| - \frac{\sigma_m^{e-} \cdot V_{cell}}{L} \right) \cdot \frac{L}{\sigma_m^{H+}} \quad (3-95)$$

This equation must be solved simultaneously with the modified Butler-Volmer equations, (3-93) and (3-94). The model does this using an iterative process similar to that used in the fuel cell model (Doddathimmaiah and Andrews 2008). The required inputs to the model are all introduced in appendix 1 (page 280) of the thesis.

3.7 SOLAR-HYDROGEN SYSTEM ANALYSIS AND SIZING

3.7.1 An overview of system sizing

Consider a typical stand-alone solar-hydrogen system (figure 2-1), where PV arrays supply the electrical demand fully or partly depending on the solar irradiance. Any surplus PV

power is fed into a PEM electrolyser to produce hydrogen that is stored in tanks. When the PV arrays are unable to meet the full demand, the stored hydrogen is used by a PEM fuel cell to supply the power deficit. The system simulation model developed here basically follows the same procedure to represent the operation of the solar-hydrogen system over time for durations up to a year.

Depending on the input format adopted for the final electricity demand and solar radiation profiles (half-hourly or hourly profile), a set of half hourly or hourly electrical outputs from the PV arrays is the main output of the PV sub-model. The difference between the PV output and demand determines the power surplus/deficit, and depends on the installed area of the PV array, which is thus a key parameter in system sizing. Another variable used for system sizing is the amount of hydrogen in the storage tank. This amount should always stay just above zero, that is, positive, throughout an annual period. In practice, of course, the minimum amount of hydrogen in the storage would need to be set above zero to provide a back-up in case of unforeseen events. This can be done by increasing the initial mass of hydrogen at the beginning of the year. Another cumulative parameter relevant to system sizing is the net annual hydrogen production – that is, the difference between the total annual hydrogen production and total hydrogen consumption – which for sustainable operation from year to year must be greater than or equal to zero. The area of the PV array is the main controlling parameter to satisfy both these conditions.

System sizing can be performed under a variety of constraints relating to the capacities of the hydrogen storage tank, the fuel cell, and the electrolyser. The capacity of the hydrogen tank may be left unconstrained in the model so the system uses all the available surplus power at all times to produce hydrogen and there is always enough room in the tank to store this hydrogen – this is termed the ‘unconstrained storage’ condition. Alternatively in the ‘constrained storage’ condition, the capacity of the hydrogen tank is limited to a certain preset value so that when the amount of hydrogen stored in the tank reaches this limit the electrolyser stops operating. Under constrained storage, the size of the PV array and electrolyser must be increased accordingly compared to unconstrained storage, since more of the final demand has to be met directly by the PV array and correspondingly less from stored hydrogen consumed in the fuel cell.

The minimum size of the fuel cell is the size that enables it to meet the peak demand all by itself if no power comes from the PV arrays. Hence, the minimum acceptable size of the fuel cell is set by the peak of the demand profile. However, a fuel cell larger than this minimum size can also be selected, which may be advantageous since the energy efficiency of a fuel cell increases as its current density falls. The term ‘oversized fuel cell’ will be used in this thesis, meaning any fuel cell size larger than this minimum size chosen for solar-hydrogen system analysis.

In the model the electrolyser is assumed to be large enough to accommodate the maximum power surplus from the PV array for hydrogen production purposes. So if the PV array size is changed, the size of the electrolyser is changed accordingly (Shabani and Andrews 2008). The electrolyser can also be constrained; this technique can be used in conjunction with the constrained hydrogen tank. More details of constrained electrolyser sizing technique has been provided by Ali and Andrews (2005); however, the condition will not be explored as a part of this thesis.

The effect of these various conditions on system sizing will be explored in depth from both a technical and economic viewpoints as a part of the case study presented in Chapter 4.

Once the system is sized it is possible to investigate the PV-to-load overall annual energy flow, the fuel cell and electrolyser lifetime, system economy, and fuel cell thermal/hydrogen waste recovery.

3.7.2 Solar-hydrogen system sizing for an unconstrained hydrogen storage

The following stepwise procedure is used in the model for sizing a solar-hydrogen system to meet a given demand at a particular location under the unconstrained hydrogen storage condition, with figure 3-24 summarising this procedure in a flowchart.

1. Read the electrical demand and solar irradiance profiles
2. Calculate the fuel cell minimum size requirement based on the peak of the demand
3. Choose a fuel cell size equal to, or larger than, its minimum size (either minimum fuel cell size or oversized fuel cell strategy can be followed)

4. Run the fuel cell model based on the chosen size of the fuel cell
5. Input a trial initial size for the PV array (number of modules)
6. Calculate the yearly output profile of the PV array
7. Calculate the power surplus/deficit yearly profile based on the PV output and the demand profile
8. Choose a trial electrolyser size and run the electrolyser sub-model
9. Input an initial mass of hydrogen in the hydrogen tank at the beginning of the year
10. Determine annual profile of the hydrogen variation in the tank by using the power deficit/surplus profile and the output of the electrolyser and fuel cell model
11. Check the net annual hydrogen level variation:
 - If it is greater than zero go to step 12
 - If it is less than zero go to step 18
 - If it is almost zero (within the specified error range) go to step 20
12. Remove one module from the PV array
13. Rerun the PV sub-model for the new size of the PV array
14. Using the new output of the model, calculate the new power surplus/deficit profile
15. Find the maximum available surplus power from the power surplus/deficit profile
16. Size the electrolyser to accommodate the maximum available power surplus and rerun the electrolyser sub-model
17. Go to step 10
18. Add one module to increase the size of the PV array
19. Go to step 13
20. Readjust the initial hydrogen mass to have the minimum point of the curve at almost zero (can be greater than zero, depending on the safety margin set for the minimum hydrogen in the tank); the sizing procedure is finished at this point.

Figure 3-25 presents an example of the annual profile of the hydrogen stored in an unconstrained hydrogen-tank system.

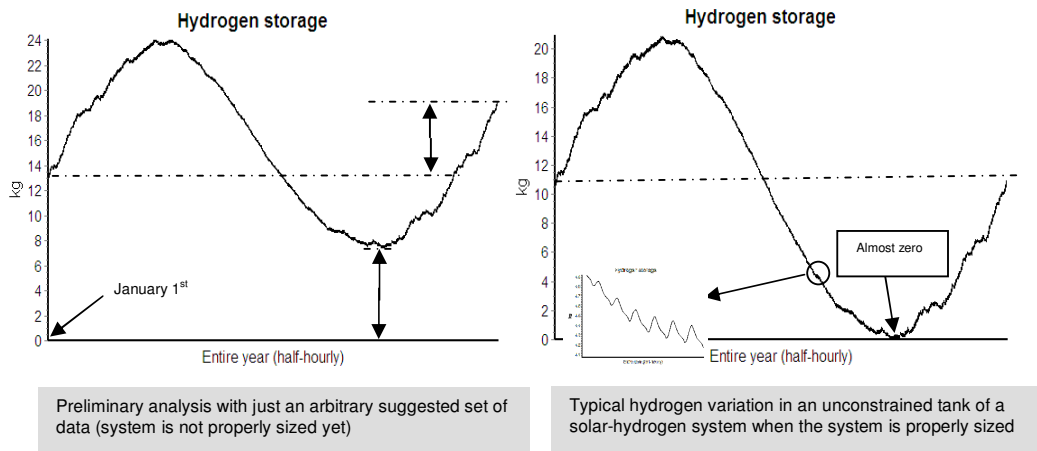


Figure 3-25. Typical annual variation of hydrogen stored in an unconstrained tank in a solar-hydrogen system

3.7.3 Solar-hydrogen system sizing for a constrained hydrogen storage

Under the constrained hydrogen storage condition, expressed as a maximum mass of hydrogen stored, the system sizing procedure is more complicated, as follows and explained in the flowchart in figure 3-26 and figure 3-27.

1. Read the electrical demand and solar irradiance profiles
2. Calculate the fuel cell minimum size requirement based on the peak of the demand
3. Choose a fuel cell size equal to or larger than its minimum size
4. Run the fuel cell model based on the chosen size of the fuel cell
5. Input a trial size for the PV array (number of modules)
6. Calculate the yearly output profile of the PV array
7. Calculate the power surplus/deficit yearly profile based on the PV output and the demand profile
8. Choose a trial electrolyser size and run the electrolyser sub-model
9. Use the constrained hydrogen mass as the initial mass of hydrogen in the hydrogen tank
10. Determine annual profile of the hydrogen variation in the tank by using the power deficit/surplus profile and the output of the electrolyser and fuel cell model (the

- electrolyser does not operate to generate hydrogen if the tank reaches its maximum constrained level)
11. Check the net yearly hydrogen level variation (it cannot be greater than zero, because of constrained tank used):
 - If it is less than zero go to step 21
 - If it is almost zero (considering a designated error) go to step 12
 12. Check the minimum hydrogen available in the tank throughout the year
 - If it is almost zero (considering an error) the system is already sized
 - If it is greater than zero go to step 13
 - If it is less than zero go to step 18
 13. Remove one module from the PV array
 14. Rerun the PV sub-model for the new size of the PV array
 15. Using the new output of the model, calculate the new power surplus/deficit profile
 16. Find the maximum available surplus power from the power surplus/deficit profile
 17. Size the electrolyser to accommodate the maximum available power surplus and rerun the electrolyser sub-model
 18. Go to step 10
 19. Add one module to increase the size of the PV array
 20. Go to step 14
 21. Add one module to increase the size of the PV array
 22. Rerun the PV sub-model for the new size of the PV array
 23. Using the new output of the model, calculate the new power surplus/deficit profile
 24. Find the maximum available surplus power from the power surplus/deficit profile
 25. Size the electrolyser to accommodate the maximum available power surplus and rerun the electrolyser sub-model
 26. Determine hydrogen yearly variation profile in the tank by using the power deficit/surplus profile and the output of the electrolyser and fuel cell model (the electrolyser does not operate to generate hydrogen if the tank reaches its maximum constrained level)
 27. Check the net yearly hydrogen level variation (it cannot be greater than zero, because of constrained tank used):
 - If it is almost zero go to step 28
 - If it is less than zero go to step 21

28. Check the minimum hydrogen available in the tank throughout the year
 - If it is almost zero (considering an error) the system is already sized
 - If it is less than zero go to step 19
 - If it is greater than zero go to step 29
29. Reduce the constrained size of the tank to: the initial constrained size minus the minimum hydrogen in the tank throughout the year

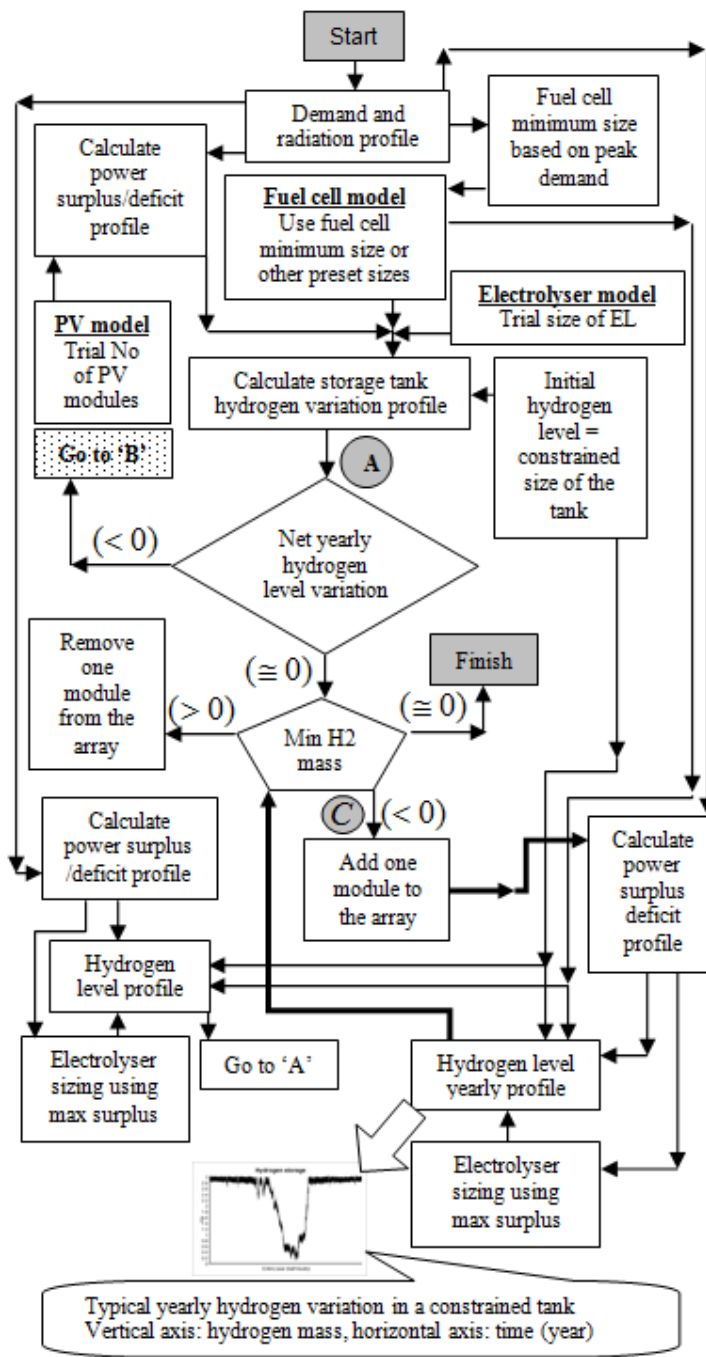


Figure 3-26. Solar-hydrogen system sizing procedure for constrained hydrogen tank

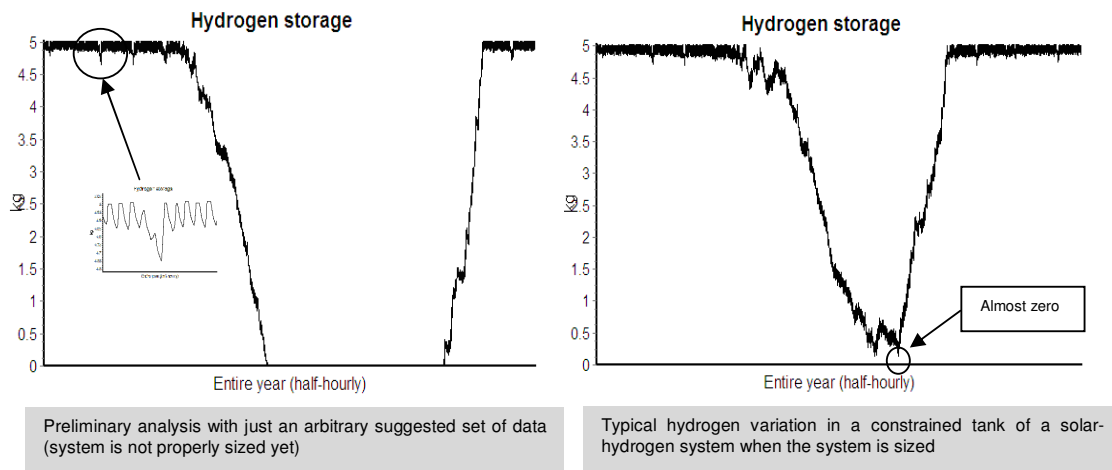


Figure 3-28. Typical annual variation of hydrogen level in a constrained tank in a solar-hydrogen system

3.8 MODELLING SYSTEM ECONOMICS

The economic analysis on the system is performed for an assessment period chosen by the user. The key economic criterion evaluated is the average unit cost of electricity produced over the assessment period, defined as the net present value (NPV) of all the costs over the period at a selected real discount rate, divided by the total electricity supplied over that period.

Based on the lifetime of the components, the replacement times of the components have to be determined; then based on the given assessment period and using the real discount rate (nominal rate minus the inflation rate) the NPV of the components at the time of their replacement are estimated. It is important to consider that the cost of a component at the time of replacement can be less than its cost when it is bought in the first place due to technological advancement or mass production. For simplicity it is assumed that the cost of the components will reach their predicted future cost linearly during a given period. At the end of the assessment period, the NPV of the residual value of the components are also calculated and taken off from the total cost of the system, before calculating the unit cost of the generated electricity. It is assumed that components like the fuel cell or electrolyser are replaced at the end of their lifetimes and the full cost of replacement is taken into account in calculating the unit cost of electricity. However, in practice it might be only membranes that are replaced, so that the estimates of unit cost of electricity may conservatively be high to this extent.

4 Use of model for a case study of a solar-hydrogen combined heat and power system

4.1 AN INTRODUCTION TO THE CASE STUDY

4.1.1 Location

The simulation model described in the previous chapter will now be applied to a case study of a stand-alone solar-hydrogen system used to supply a remote household in south-eastern Australia. The option of recovering heat and hydrogen from the fuel cell for use in domestic water heating will also be investigated.

4.1.2 Electrical demand profile

For the remote household examined it was assumed that the total daily demand for electricity is 5 kWh with a time profile shown by figure 4-1. Such a profile and the detail electrical equipment to be matched with were suggested by Ali (2007). This profile which is a conservative form of the load pattern used by Nelson *et al.* (2006) considers the fact that the electrical demand of a household normally has two peaks: the larger one around 8 am in the morning (0.3 kWh/h in this case) and the smaller one about 7 pm in the evening. Similar load profiles have been used by many others such as Peacock and Newborough (2007), LaMeres *et al.* (1999), and Al-Hamadi and S. A. Soliman (2006).

This electrical demand profile does not include any thermal equipment for heating and cooling purposes. The household was assumed to be passive solar designed to minimise its heating/cooling energy requirements while this minimum demand is supplied through renewables (e.g. biomass or solar-thermal equipment). This also justifies the assumption of using the same daily electrical demand profile throughout the year, as normally the difference between the demand profiles in summer and winter comes from the difference between the cooling/heating requirements of the household at different seasons of the year.

This daily load profile was used to populate a 365×48 matrix specifying the load to be met on half-hourly basis. In this case, the simplifying assumption of the same standard load profile applying for every day was made. However, the model allows any load profile to be used, with whatever seasonal, monthly, or daily variation is desired. The effect on the unit cost of electricity generated by the system of varying the shape and scale of this standard load profile will be investigated in the case study analysis.

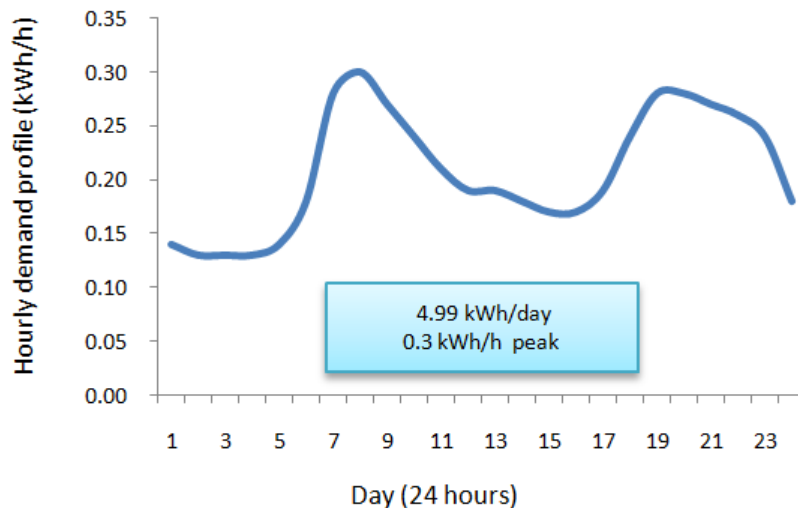


Figure 4-1. Demand profile used for the case study (Ali 2007)

4.1.3 Solar irradiance profile

The solar radiation profile for Melbourne, taken from the Australian Bureau of Metrology (BOM 2009), was used as the input to the model for this case study, which is broadly representative of the insolation prevailing in south-eastern Australia (figure 4-2). For half-hourly analysis forty eight values for solar irradiance are needed for every day. So for keeping everything in a traceable order, a matrix of dimension 1×17520 is provided in the model in which the horizontal rows are days and the vertical columns are the times, from zero to forty eight (half-hourly increment). It is also possible to input data on an hourly basis, and the program then changes these values into a half-hourly format simply by repeating the hourly value for each half hour.

Users can select whether to run the simulation using a sun-tracking array or a fixed array. The fixed array is assumed to be tilted to the horizontal plane at the local latitude angle. In such a case it is possible to give the solar radiation data at the local latitude angle directly.

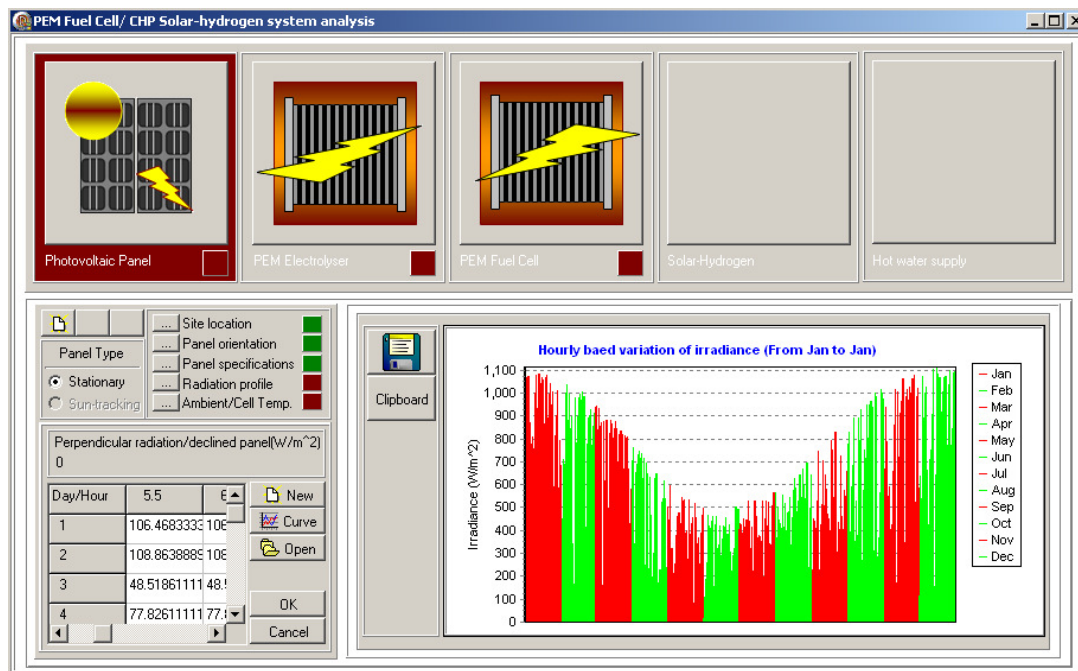


Figure 4-2. Irradiance on the surface tilted at local latitude of Melbourne (38.7°- South)

4.1.4 Wind speed and ambient temperature profiles

Wind speed and ambient temperature profiles are two key inputs to be used in the PV module sub-model as they are used to determine the PV cells temperature. The electrical output of the PV module is a function of the PV cells temperature as well as the solar irradiance. Two 365×48 matrices were provided in the model to store the half-hourly temperatures and wind speeds over a year for each run, which are provided as an input.

The average monthly values for wind speed from the Australian Bureau of Metrology (BOM 2009) (table 4-1) were fed into the program for the case study and all half-hourly wind speeds for each month were assumed to be equal to the monthly mean.

	Jan.	Feb.	Mar.	Apr.	May	Jun.	Jul.	Aug.	Sept.	Oct.	Nov.	Dec.
Wind speed (m/s)	2.7	2.6	2.3	2.3	2.7	2.4	3.2	3.1	3.1	3.0	3.0	3.0

Table 4-1. Monthly average wind velocity for Melbourne (BOM 2009)

Daily average minimum and maximum temperatures for each month are given as inputs to the program. A linear temperature variation (between the minimum and maximum

temperature) model is used to generate a half-hourly ambient temperature profile. A comparison between the results of this linear assumption and the available average statistical values showed the average differences of 5.6% and 3.9% for 9am and 3pm respectively (table 4-2).

Statistical values					Linear assumption	
	Min. Temperature (°C)	Max. Temperature (°C)	9am Average (statistical)	3pm Average (statistical)	9am Average	3pm Average
January	14.0	26.3	18.7	24.0	20.1	24.3
February	14.1	26.8	18.8	23.5	20.4	24.7
March	12.3	24.1	17.0	22.6	18.2	22.1
April	9.7	20.4	14.6	19.9	15.0	18.6
May	7.8	16.6	11.4	16.3	12.2	15.1
June	6.1	13.9	9.1	13.1	10.0	12.6
July	5.4	13.2	8.5	12.5	9.3	11.9
August	6.0	14.8	10.0	14.3	10.4	13.3
September	7.2	16.7	12.0	15.9	11.9	15.1
October	8.6	19.4	14.4	17.4	14.0	17.6
November	10.4	22.1	15.8	20.1	16.3	20.2
December	12.2	24.7	17.5	21.9	18.4	22.6
Average deviation from the statistical values					5.6%	3.9%

Table 4-2. Average daily minimum and maximum temperature for Bundoora (Victoria 3083, Australia), recorded at Latrobe University, and based on statistical information from 1979 to 2008 (BOM 2009).

4.2 SYSTEM COMPONENTS USED IN THE CASE STUDY

4.2.1 BP275 PV module and its performance

The PV module used in this case study is a BP275, as currently employed at the RMIT Renewable Energy Laboratory (REL) (figure 4-3). Each BP275 module comprises 36 single crystal silicon cells with overall dimensions of 119 cm × 53 cm × 3.8 cm and the specifications given in table 4-3 (Sandia 2009). The sizing procedure in the simulation model determines how many of these modules have to be put together to form the required PV array. The PV array is assumed to be fixed (non-tracking) and constantly facing north at a tilt angle of 37.8° equal to the local latitude of Melbourne.

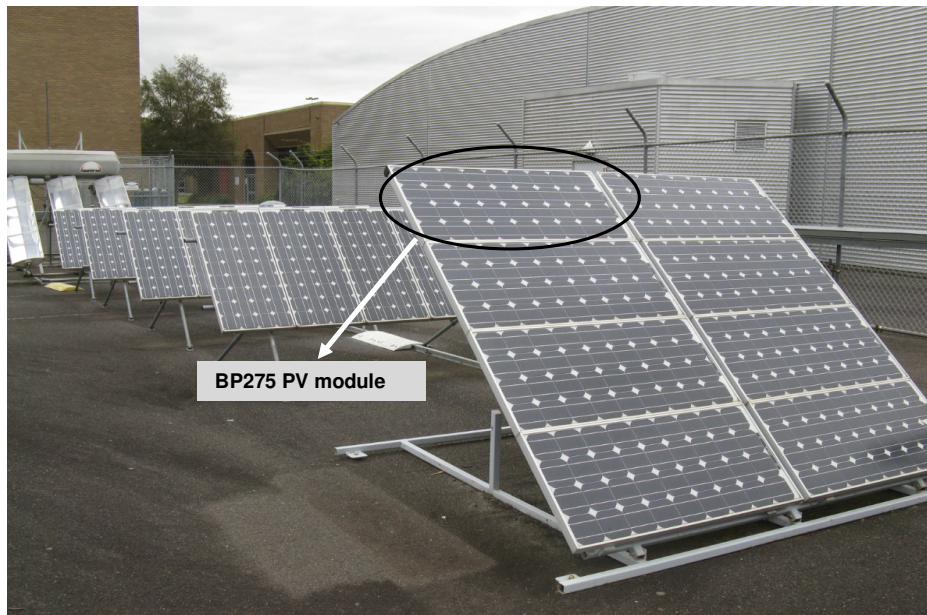


Figure 4-3. BP 275 modules at RMIT Renewable Energy Laboratory (REL), RMIT Bundoora East Campus

Material	Silicon
Module area	0.61 m ²
Material band gap energy \mathcal{E}_G	1.12 eV
Cell temperature at reference condition $T_{c,ref}$	25 °C
Solar irradiance at reference condition G_{ref}	1000 W/m ²
Short circuit current at reference condition $I_{SC,ref}$	4.75A
Open circuit voltage at reference condition $V_{OC,ref}$	21.4 V
Current of the maximum power point obtained at reference condition $I_{MP,ref}$	4.45 A
Voltage of the maximum power point obtained at reference condition $V_{MP,ref}$	17 V
Number of cells connected in series in a module NCS	36
Open circuit voltage temperature coefficient at reference condition μ_{VOC}	-(80±10) mV/°C
Short circuit current temperature coefficient at reference condition μ_{ISC}	(0.065±0.0115) %/ °C

Table 4-3. BP275 PV module technical specifications; the symbols used in this table were defined earlier in section 3.3

The outputs of a single BP275 PV module estimated by the model for this case study are shown in figure 4-4. The efficiency of the array varies according to changes in irradiance, and cell temperature. The cumulative annual output of the BP275 module is estimated to be 92.2 kWh for a total solar energy input of 924.5 kWh, resulting in an average energy efficiency of 9.97%.

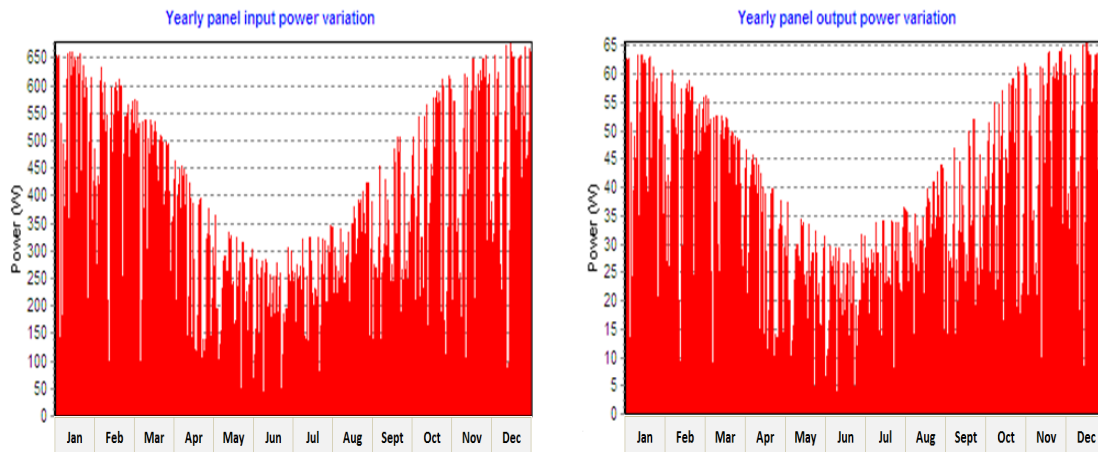


Figure 4-4. Power input and predicted output for a BP275 module (half-hourly) based on Melbourne irradiance, ambient temperature and wind speed profile

4.2.2 StaXX 7 electrolyser and its performance

The electrolyser characteristics used in the case study are based on a StaXX7 PEM electrolyser stack comprised of seven series-connected cells, with the average characteristics of a single cell obtained by normalising the stack performance (figure 4-5). This electrolyser with performance characteristics shown in figure 4-6 generates hydrogen at slightly above atmospheric pressure, which suits the RAPS application in the present case study.

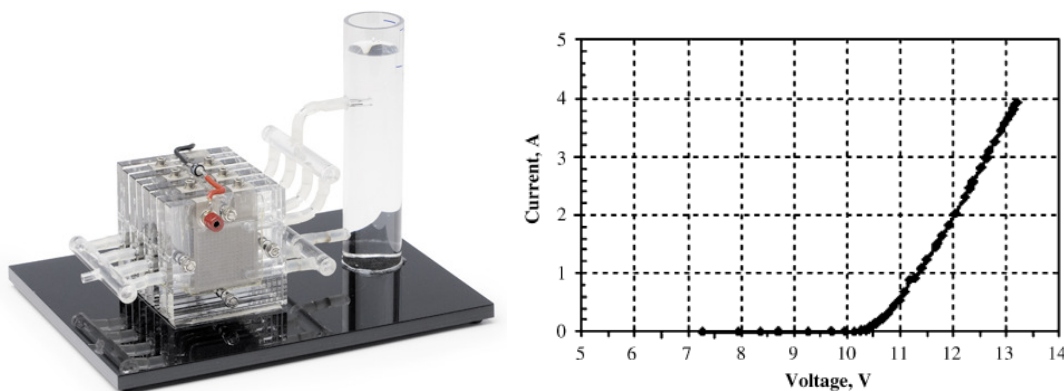


Figure 4-5. StaXX 7 PEM electrolyser (left) from Fuel cell store website (Fuelcellstore 2009)-typical polarisation (V-I) curve of a PEM electrolyser (right); the characteristics curve (right) is an experimental measurement done by Paul and Andrews (2008) on StaXX 7 PEM electrolyser stack

The electrolyser sizing is done based on the performance of a single cell of a StaXX7 electrolyser stack, by calculating the number of cells needed to make a new electrolyser stack for accommodating the surplus power over the load from the PV array.

Charge transfer coefficients of 0.35 for oxygen side, 0.71 for hydrogen side, exchange current density of 0.000006 A/cm^2 for oxygen and 0.23 A/cm^2 for hydrogen sides, and a saturation current density of 2 A/cm^2 were obtained for this electrolyser using the curve fitting procedure based on modified Butler-Volmer equations described in section 3.6. The P-I curve generated by the model (using the obtained above-mentioned key parameters) is compared with the experimental P-I curve in figure 4-6. This comparison showed a maximum deviation (power for a given current) of 4.4% from the experimental curve.

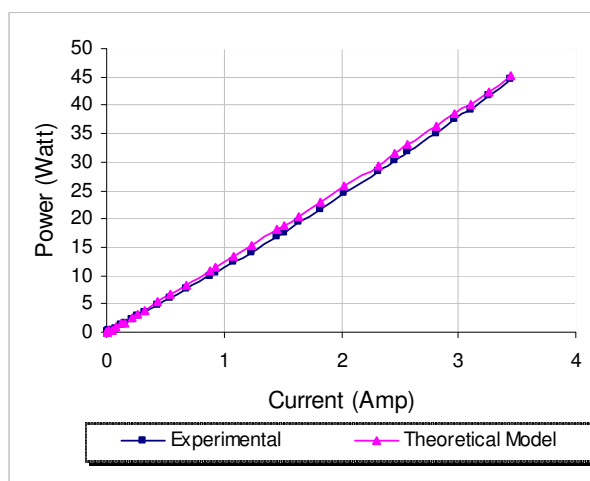


Figure 4-6. Comparing the theoretical (using Butler-Volmer equations) and experimental P-I curves of the 50W StaXX7 PEM electrolyser stack

4.2.3 500 W PEM fuel cell and its performance

A 500 W BCS PEM fuel cell (BCS 2009), as shown in figure 4-7 with a polarisation curve as in figure 4-8, is used as the basis for the fuel cell modelling in this case study. Similar to the procedure adopted with the electrolyser, the average performance of a single cell is found by dividing the output power of the stack at a given current by the number of series-connected cells. The model then determines the number of these individual cells that need to be connected together in series to construct a fuel cell stack capable of meeting the required demand.



Figure 4-7. 500 W PEM BCS fuel cell stack (BCS 2009)

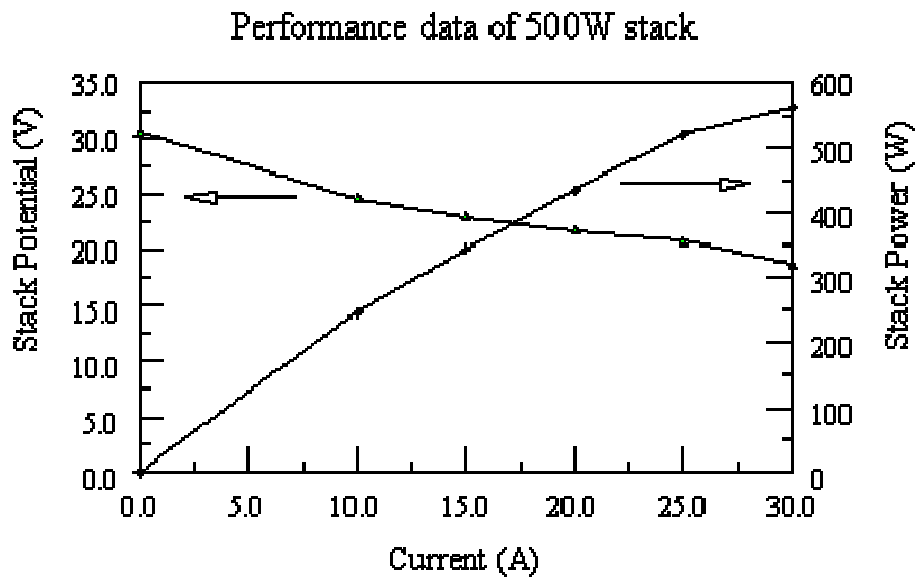


Figure 4-8. 500 W PEM BCS fuel cell polarisation curve (BCS 2009)

As explained in section 3.5.4, when the experimental polarisation curve of the fuel cell is available, the model employs a least squares method to find the theoretical curve based on modified Butler-Volmer equations that best fits the experimental performance curve. Subsequently the fuel cell is represented in the model by this fitted curve and its associated key parameters such as charge transfer coefficients, exchange current densities, and saturation current.

The application of this procedure to the 500-W PEM BSC fuel is shown in figure 4-9. The best-fit values were 0.6 A/cm^2 for saturation current density, 0.0000327 A/cm^2 and 0.650 A/cm^2 for the exchange current densities on the oxygen and hydrogen sides respectively, and 0.33 for the charge transfer coefficient on the oxygen and 0.69 on the hydrogen side. The fitted curve for the fuel cell showed a maximum deviation (voltage for a given current) of 3% from the experimental curve.

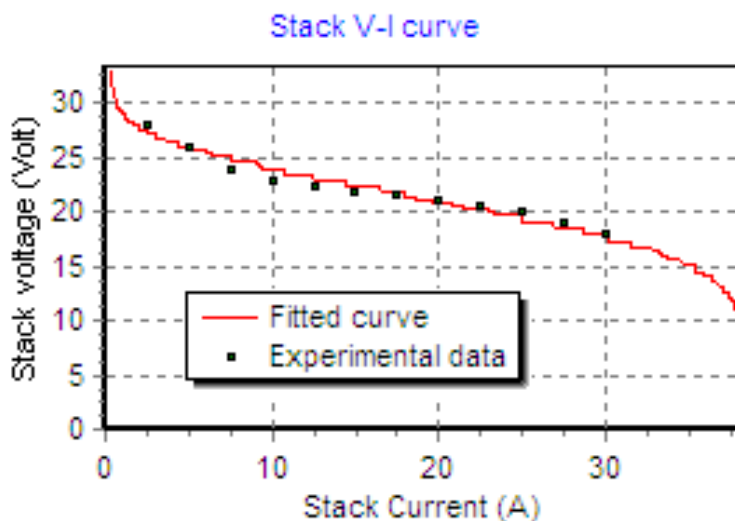


Figure 4-9. 500 PEM BCS theoretical polarisation curve fitted on the experimental curve using least-squares method and based on the Butler-Volmer equations

4.3 SYSTEM SIZING AND ECONOMY

4.3.1 Minimum size of fuel cell, unconstrained hydrogen storage

In the first scenario examined, the basic strategy for fuel cell sizing is employed in which the fuel cell capacity is set to its minimum possible value so that this component can just meet the peak demand by itself if no power comes from PV. In addition, the unconstrained storage condition is applied in which the hydrogen tank is sized to accommodate all the hydrogen produced by the electrolyser. The results for component sizing obtained by applying the model in this scenario are presented in figure 4-10 and table 4-4.

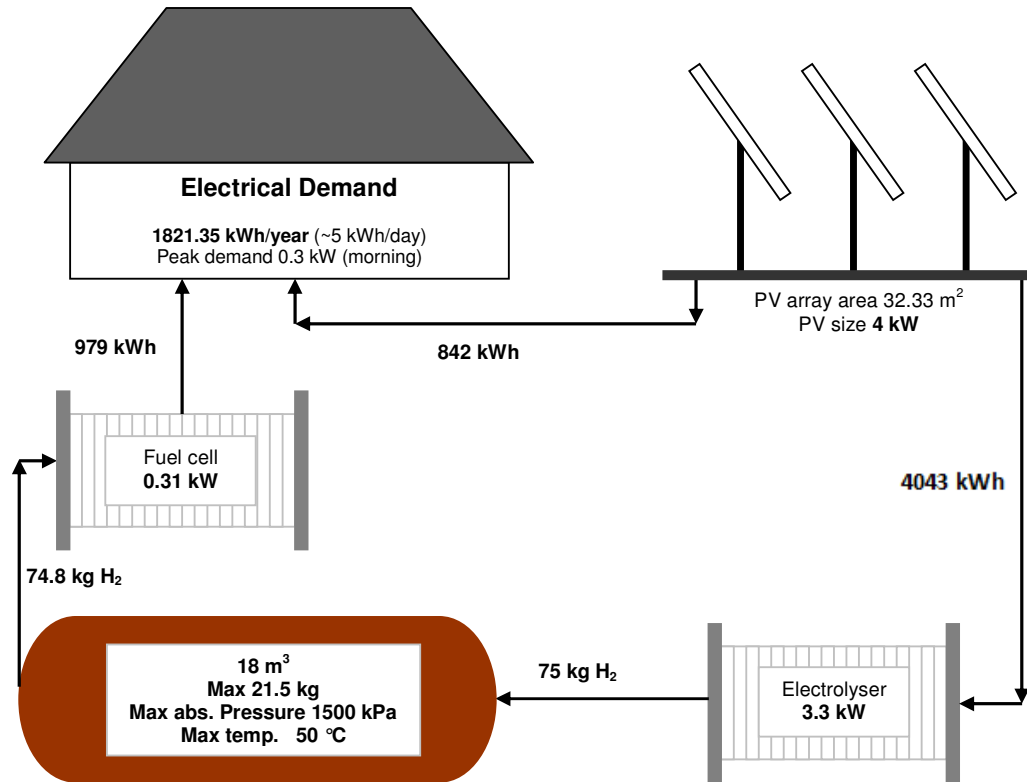


Figure 4-10. Solar-hydrogen system sizing results (for fuel cell minimum size and unconstrained tank)

Components		Size	Note
Load	Total demand	4.99 kWh/day or 1821.35 kWh/year (excluding heating and cooling load)	
	Peak	2 peaks: 0.3 kWh/h morning peak 0.28 kWh/h evening peak	
PV Array	Area	32.3 m ²	Equivalent to 53 modules of BP277 PV cells
	Power	4 kW	0.9 de-rating factor was applied
	Average annual efficiency	9.97%	
Electrolyser	Size	3.3 kW	Equivalent to 63 electrolyser stacks of SatXX 7
	Hours of operation per year	3549.5 h	A figure to estimate the lifetime of the electrolyser on yearly basis for doing economic analysis on the system
	Total annual hydrogen production	75 kg	
Hydrogen tank	Size	21.5 kg	<ul style="list-style-type: none"> Equivalent to 18 m³ Perfect gas law was applied Maximum ambient temperature was assumed to be 50 °C Relatively low pressure hydrogen storage: 1400 kPa-gauge (~1500 kPa-abs)
	Initial and final level of hydrogen	~11 kg	Based on assuming Jan 1 st as the first day of the year for sizing analysis

Fuel cell	Size	0.31 kW	18 cells-Based on singles cells of 500 W PEM BCS fuel cells (540 W maximum power)
	Annual electricity delivery	979 kWh	The additional electricity provided by the fuel cell in addition to the PV output to meet the demand
	Annual hydrogen consumption	74.9 kg	<ul style="list-style-type: none"> Based on hydrogen stoichiometry of 1.2 in the whole range of fuel cell operation. This will be more discussed based on the experimental data
	Hours of operation per year	5210.5 h	A figure to estimate the lifetime of the fuel cell on yearly basis for doing economic analysis on the system
	Annual hydrogen loss	18.7 kg	<ul style="list-style-type: none"> Equivalent to 737.7 kWh Based on 1.2 of hydrogen stoichiometry assumption
	Total annual heat generation	1214.9 kWh	It is higher than the yearly electricity generated by the fuel cell
	Estimated yearly cooling load	868 kWh	<p>The heat generated by the fuel cell:</p> <ul style="list-style-type: none"> is partly used inside the stack to evaporate the generated water is slightly removed by the excess reactants <p>It will be more discussed based on theoretical analysis and experimental results</p>
	Average annual electrical energy efficiency	33.2 %	<ul style="list-style-type: none"> Relatively low efficiency (high hydrogen loss assumed) Mainly operated close to the maximum power point of the fuel cell Minimum size of the fuel cell has been chosen to just meet the peak demand

Table 4-4. Solar-hydrogen system sizing results (for fuel cell minimum size and unconstrained tank)

The photovoltaic system is sized at 32.3 m², comprising 53 BP275 PV modules, rated at 4kW peak power, after applying a 90% de-rating factor to allow for the output tolerances provided by the manufacturer and losses through cabling. The PV array is found to generate electricity at an average annual efficiency of 9.97%. This value is slightly lower than that assumed by some other research studies such as 11.9% by Hedström *et al.* (2004) and 12% by Nelson *et al.* (2006) but is close to the 10% used by Ali and Andrews (2005) and Lagorse *et al.* (2008). By design, the PV system and electrolyser are about the same electrical capacity, while the fuel cell is much smaller.

The electrolyser is sized at 3.3 kW_e input and operates 3549.5 h/year, considerably less than the fuel cell at 5210.5 h/year. Hence it is expected that the electrolyser would be replaced less frequently than the fuel cell. The electrolyser produces 75 kg of hydrogen per year with as expected more during the summer than winter (figure 4-11).

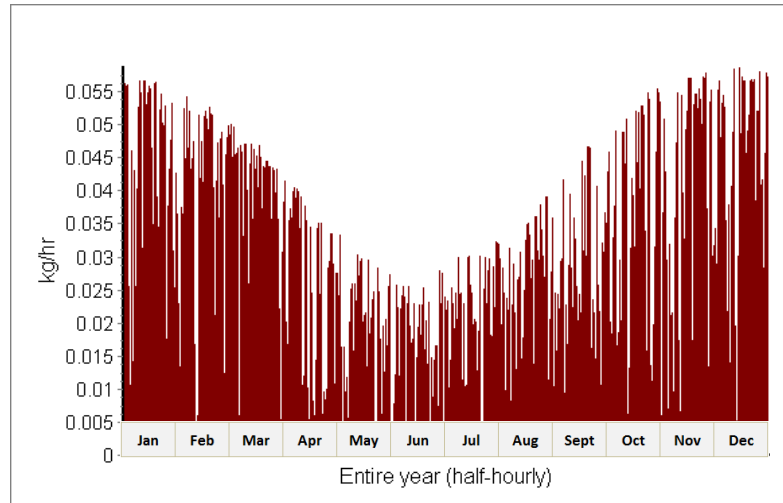


Figure 4-11. Case study: annual hydrogen production rate by the electrolyser; unconstrained tank and minimum fuel cell size

Out of the total annual electrical demand of the household, 1821 kWh/year, about 45% is supplied directly by the PV array with the rest coming from the fuel cell using the stored hydrogen. This is similar to the figure obtained by Santarelli and Macagno (2004) in their case study of a solar-hydrogen RAPS system in the Italian Alps (slightly above 50% supplied by the fuel cell). Allowing for a maximum hydrogen stoichiometry of 1.2 (suggested by the manufacturer of the fuel cell) results in considerable hydrogen wastage over the year, in fact slightly above 15% of the hydrogen gas input to the fuel cell. This PEM fuel, or an alternative, may be able to operate with a much lower hydrogen wastage rate in practice than that assumed for this case study (this will be investigated experimentally in the next chapter) and the overall energy efficiency and economics of the solar-hydrogen system would correspondingly be improved. Practical ways to reduce hydrogen wastage in the fuel cell is thus an area meriting further attention

The analysis showed that 1214.8 kWh of heat is generated by the fuel cell each year while supplying 979 kWh of electricity to meet the load. Some 28% of this heat is removed by the water produced in the fuel cell, and a further few percent taken away by the exit streams of unconsumed hydrogen and air. The remaining ~70% of the generated heat is supposed to be removed by the cooling system of the fuel cell, utilising either air or water cooling. This heat generation rate and its potential application will be further discussed later in this chapter.

The fuel cell operates for just over 5200 h/year. This figure can be used to estimate the replacement time of the fuel cell; for instance, if the expected operational lifetime of the fuel cell is 15 000 hours on average, it has to be replaced in nearly every 3 years.

The average energy efficiency of the fuel cell in this scenario is found from the modelling to be just above 33%, which is at the low end of its predicted efficiency range of just below 30% to above 50%, depending on the current drawn. This relatively low average efficiency is not unexpected, given the assumption of the relatively high hydrogen wastage rate (about 15%), and its operation close to its maximum power output for much of the time. The latter situation leads to operation at high current densities and hence low efficiency. This occurs largely because the minimum possible size of the fuel cell to handle the peak demand has been selected. In the research done by Lagorse *et al.* (2008) the average annual efficiency of 40% was used for the fuel cell for which just 3-5% hydrogen wastage was assumed. The round-trip energy efficiency for electricity into the electrolyser and out of the fuel cell is correspondingly low at 24%, although it is very close to the figure of 25% given by Shapiro, Duffy *et al.* (2005) from a theoretical and experimental investigation of a solar-hydrogen system of a similar kind.

The model estimates the required capacity of the hydrogen tank to be 21.5 kg of hydrogen. If a storage pressure of 1500 kPa at maximum 50 °C is assumed, the volume of the tank is 18 m³ (using the ideal gas law, which is a good approximation at this pressure). This storage capacity should be regarded as the minimum required since it does not allow for any emergency or contingency back-up capacity. Figure 4-12 shows how the mass of hydrogen stored varies over the year in this scenario. The hydrogen content of the tank at the beginning of the year (January, midsummer in Melbourne) is estimated to be slightly above 11 kg, rising to 21.5 kg at the end of March after the strong summer charging period. The charge then falls to its minimum value at the end of winter after a long period of lower solar radiation. The minimum charge is shown as zero here but in practice some reserve amount would need to be maintained. This reserve amount will ensure that hydrogen flow to the fuel cell can be maintained as the pressure in the storage falls, and that the system can cope with unexpectedly low irradiance periods. The mass of hydrogen stored then steadily increases again to its starting point, ready to start the next year at the same level of charge. Apart from this overall annual variation of hydrogen content in the storage tank,

there is a short-term daily variation as well because of periodic absence of sun during the night and short cloudy periods during some days (figure 4-13).

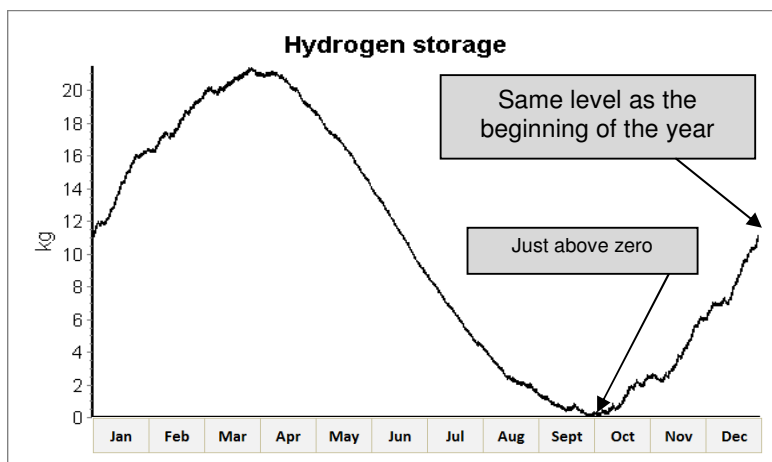


Figure 4-12. Case study: annual hydrogen level variation in the tank (half hourly basis); unconstrained tank and minimum fuel cell size

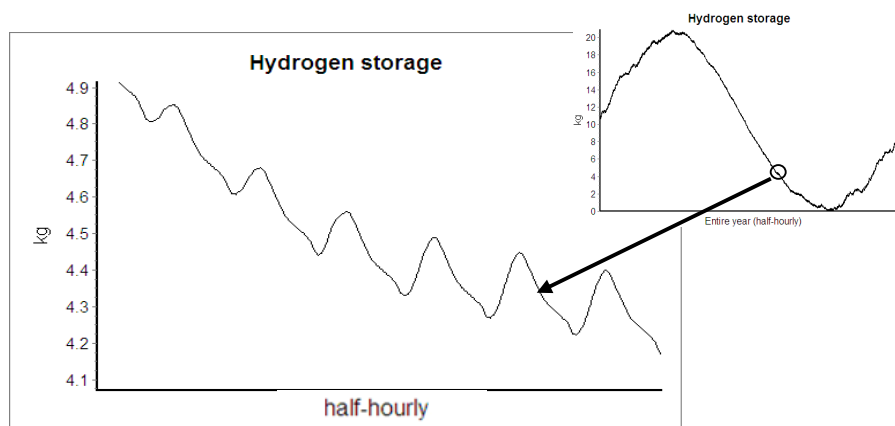


Figure 4-13. Case study: An example to show the short-term hydrogen variation (end of July); unconstrained tank and minimum fuel cell size

The unit cost and lifetime assumptions for components used in the economic analysis of the system are presented in table 4-5. The fuel cell and electrolyser are inherently of low maintenance cost and this cost is assumed negligible compared with the capital cost of these components. This assumption is further supported by the fact that the share of these components in the overall cost of the system is relatively low (figure 4-14). The annual operation and maintenance (O&M) cost of the PV array is reported as being between 0.5% and 2.4% of its initial cost (Koner *et al.* 2000). Based on this range, a value of 2%, that is 120 US\$/kW/y, has been used in the present case study. The balance of the system including items such as hydrogen/air lines piping (pipes, valves, regulators, safety

measures), the control system, hydrogen humidification and dehumidification, wiring, fuel cell cooling system, MPPT device (if needed), and assembling and commissioning, has been assumed to cost US\$6000, following Ali (2007).

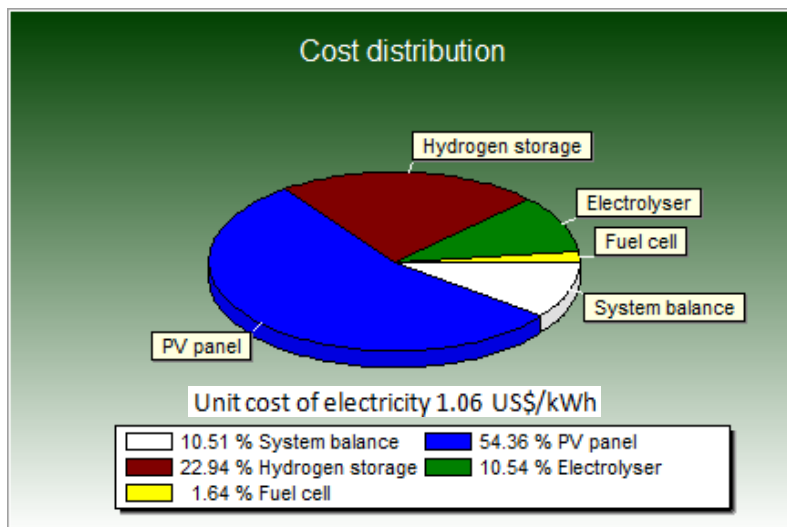


Figure 4-14. The detail of cost analysis on the solar-hydrogen system, with minimum size of the fuel cell and unconstrained tank

With this set of assumptions and using a real discount rate of 5%, the unit cost of electricity over the assessment period of 30 years (the longest lifetime component given in the table) comes out to be 1.06 US\$/kWh. This unit cost is slightly above 0.7 US\$/kWh obtained by Nelson *et al.* (2006), due most probably to differences in the model used, input assumptions, assessment period and real discount rate.

Component	Present cost	2015-2020 (Prediction)	Lifetime
PV module	5750 US\$/kW (Solardyne) Based on bp275 module	4500 US\$/kW Authors' estimation based on IEA report (IEA 2001)	30 years (Zoulias and Lymberopoulos 2007)
PEM electrolyser	1500 US\$/kW (Beccali <i>et al.</i> 2008)	500 US\$/kW (Beccali <i>et al.</i> 2008)	15000 h
PEM fuel cell	2000 US\$/kW (Beccali <i>et al.</i> 2008)	439 US\$/kW (Zoulias and Lymberopoulos 2007) (Lagorse <i>et al.</i> 2008)	15000 h (Zoulias and Lymberopoulos 2007)
Hydrogen storage tank	55 US\$/Nm ³ (Zoulias and Lymberopoulos 2007)	34.5 US\$/Nm ³ (Zoulias and Lymberopoulos 2007)	30 years (Greiner <i>et al.</i> 2007)
System's balance	US\$6000 (Ali 2007)	US\$6000	30 years

Table 4-5. Solar-hydrogen system components' costs and lifetimes

An analysis of the total unit cost obtained in this case study (figure 4-14) illustrates that the PV array is the most expensive part of the system, accounting for above 50% of the overall cost, followed by the storage tank (23%) and electrolyser (just over 10%). The fuel cell comprising less than 2% of the total is the cheapest component of the system, so variations in the assumed lifetime, capital and maintenance cost of this component have a negligible effect on the overall cost of the system.

4.3.2 Minimum size of fuel cell, constrained hydrogen storage

Figure 4-14 shows that in the unconstrained hydrogen storage condition the hydrogen tank is the second most expensive part of the system after the PV arrays. Hence a second condition has been investigated in which the capacity of the hydrogen tank is constrained to a smaller size than that found necessary in the unconstrained storage condition (that is, 21.5 kg) to see if this leads to any net reduction in the unit cost of power supplied. In the constrained storage condition, less hydrogen can be stored so the size of the PV array has to be enlarged instead to maintain continuous energy supply, and consequently a larger electrolyser has to be employed to accommodate the surplus power, as shown in figure 4-15 and figure 4-16. While the cost of the hydrogen storage is reduced, the PV array becomes more expensive (figure 4-17). Less available space for the hydrogen means less demand for the electrolyser to generate hydrogen, thus although this component is chosen to be larger, its capacity will not be fully used. A benefit here though is the reduced number of times the electrolyser has to be replaced over a given assessment period, due to the reduced number of hours this component has to operated (figure 4-16). The PV array is the most expensive part of the system, so the tradeoffs between increasing its size, decreasing the size of hydrogen tank, and the new size and operating condition for the electrolyser determine whether a constrained hydrogen tank results in a net unit cost of power reduction or not.

The results for the economic analysis of the solar-hydrogen system for a range of constrained storage values between 3 kg and 15 kg are presented in table 4-6. Clearly, under the assumptions made here, constraining the capacity of the hydrogen tank does not improve the economics of the system compared with an unconstrained tank. The cost increases due to the larger PV array and electrolyser offset cost saving from the lower

capacity storage, and longer lifetimes of the fuel cell and electrolyser. The cost analysis for the minimum size of fuel cell and hydrogen tank constrained to 3 kg is shown in figure 4-17.

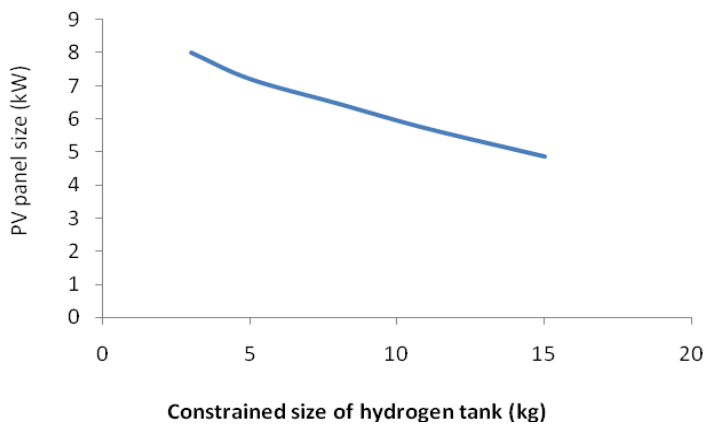


Figure 4-15. The effect of constrained size of hydrogen tank on the PV array size

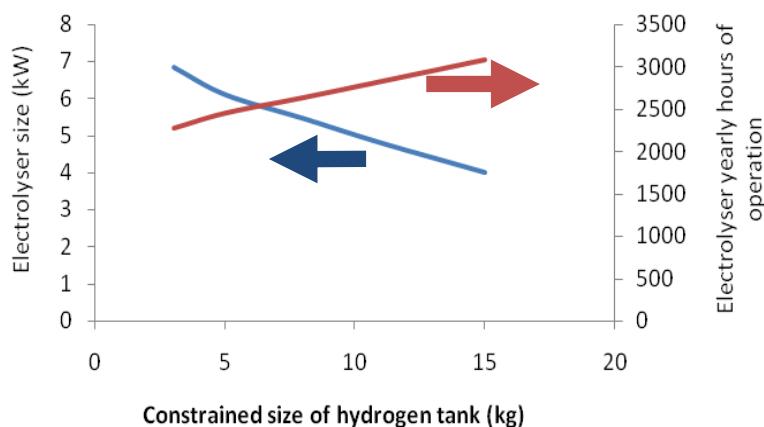


Figure 4-16. The effect of using constrained hydrogen tank on the electrolyser size and its total annual hours of operation

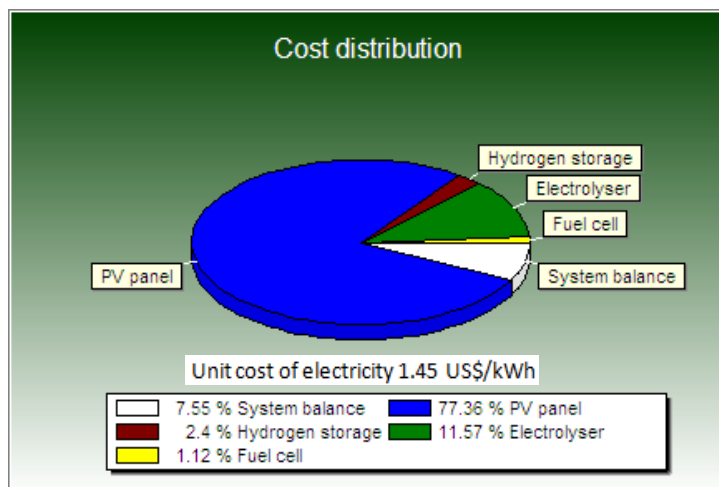


Figure 4-17. The detail of cost analysis of the solar-hydrogen system when the minimally-sized fuel cell (~0.3 kW) and a 3-kg constrained hydrogen tank are used

Constrained tank size (kg)		3	5	8	11	15
PV	Size (kW)	8	7.2	6.45	5.7	4.85
	BP275 Area (m ²)	65.27	58.56	52.46	46.36	39.65
PEM Electrolyser	Size (kW)	6.842	6.1	5.46	4.8	4
	Annual hours of operation	2280.5	2458	2638	2827	3080
	Annual hydrogen production (kg)	70.3	70.9	71.5	72.4	73
	Unused potential of hydrogen production (kg)	96	76.8	59.2	41.54	22
PEM Fuel Cell	Size (kW)	0.3	0.3	0.3	0.3	0.3
	Annual hours of operation	4859.5	4908	4958	5006.5	5076
	Annual electricity delivery (kWh)	924	931	939	948	960.9
	Annual hydrogen consumption (kg)	70.3	70.9	71.5	72.4	73
	Total annual heat generation (kWh)	1140.5	1149.5	1159.5	1170.5	1184
	Estimated annual cooling load (kWh)	814.2	820.5	827.7	835.5	845
	Average yearly efficiency (%)	33.2	33.3	33.3	33.3	33.3
Unit Cost of Electricity (US\$/kWh)		1.45	1.35	1.27	1.19	1.1

Table 4-6. The effect of the constrained size of hydrogen tank on the size and the performance of the other components and the unit cost of the electricity generated

Figure 4-18 shows how the hydrogen level in a 3-kg constrained hydrogen tank varies over a year. Such a pattern of hydrogen variation is similar to that of the state of charge in a battery bank if used in such a system as storage.

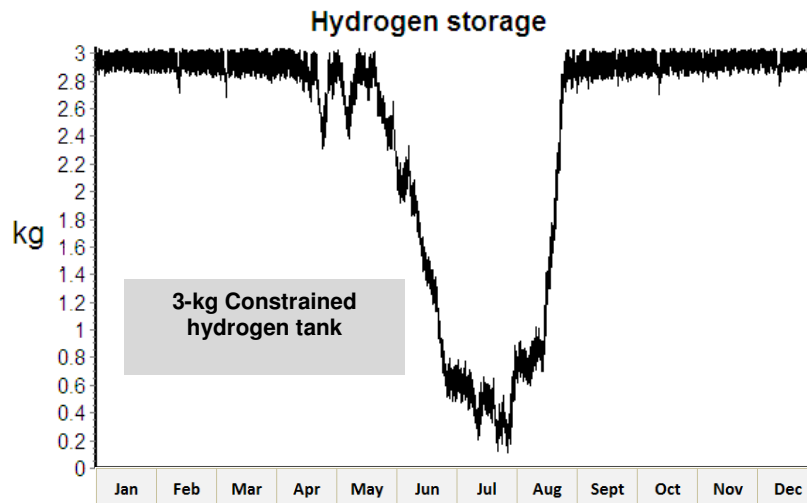


Figure 4-18. Case study: annual hydrogen level variation in a 3-kg constrained hydrogen tank

Table 4-6 also gives an indication of the underutilised capacity of the electrolyser to generate hydrogen due to the fact that the hydrogen tank size is constrained. When the tank

is already filled, any surplus power from the PV array (mainly in summer) cannot be used to generate hydrogen for storage (figure 4-19).

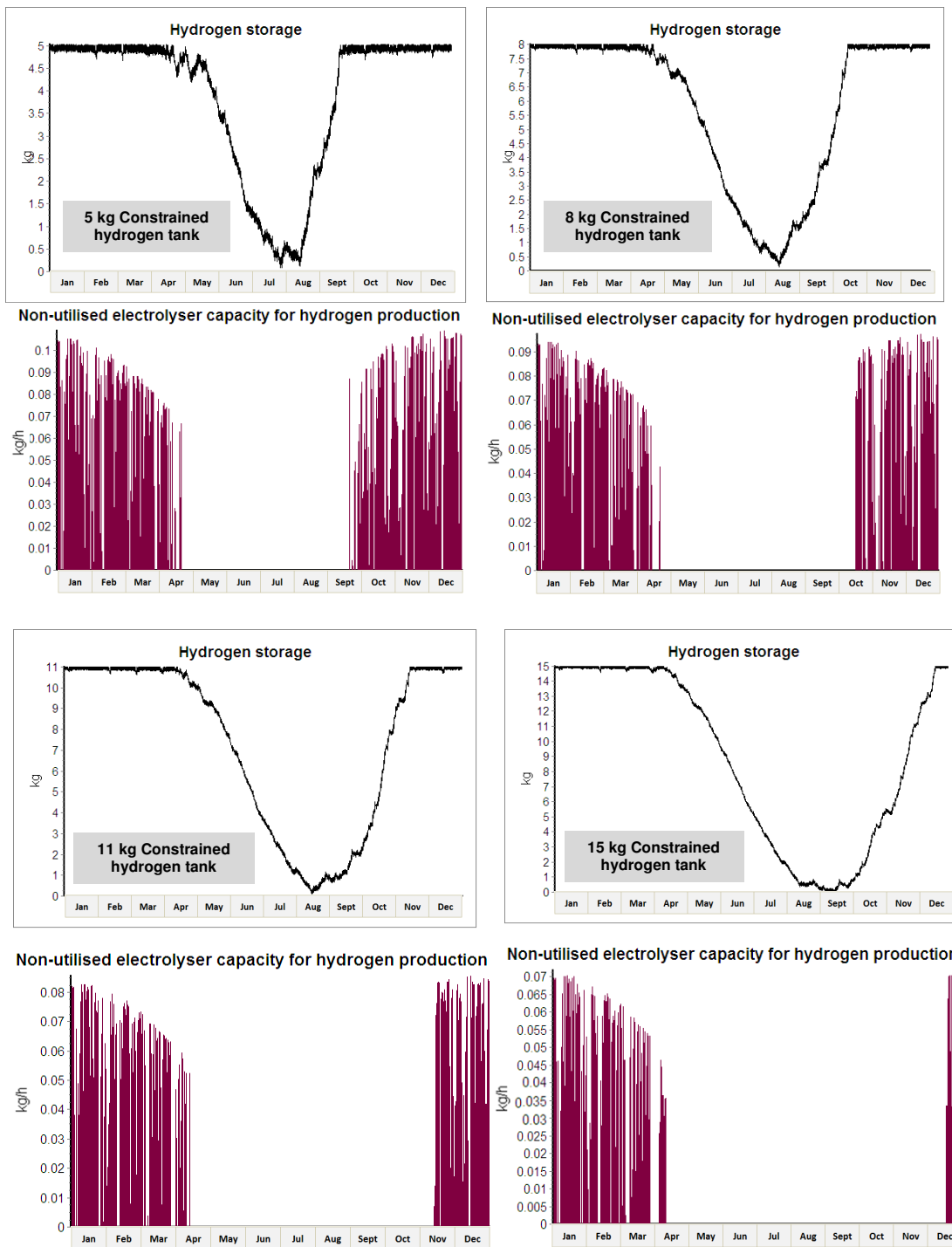


Figure 4-19. Case study: non-utilised capacity of electrolyser when using constrained hydrogen tank

4.3.3 System optimisation based on unit cost of electricity

4.3.3.1 Cost minimisation

The theoretical investigations using the model have shown that the unconstrained storage condition is preferable in the present case study from an economic point of view. Now the question addressed is whether the design and sizing done based on unconstrained storage can be further optimised to achieve further reductions in the unit cost of energy supplied.

4.3.3.2 Load management

Managing the load profile is the first thing to be considered as a possibility to reduce the cost of the system. In this regard two options are studied: the effect of the peak size of the electrical demand profile, and the effect of the overall scale of the system.

In a power generation system, the peak demand is always a determining factor in sizing the system. Hence the load profile given in figure 4-1 was varied by increasing the peak demand (0.3 kW) while keeping the total daily energy demand constant (~5 kWh/day). The amended load profiles fed into the model are shown in figure 4-20.

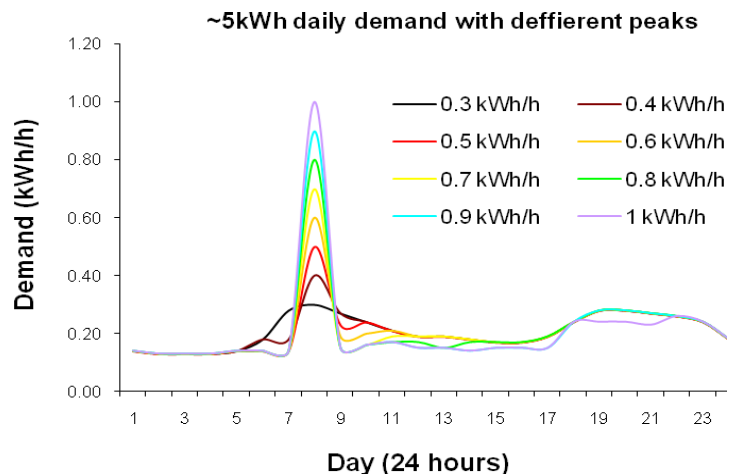


Figure 4-20. Changing the peak of the daily load profile while the total daily demand remains constant (Shabani *et. al.* 2009)

Figure 4-21 shows how these changes in peak demand of the household affect the size of the PV array, electrolyser, and hydrogen tank. The fuel cell size is set equal to the peak. The cost of the system over the assessment period of 30 years and real discount rate of 5%

follows the same pattern. As shown by figure 4-22, the present cost of the system is reduced by about 10% compared to the base case when a peak demand of 0.5 kW is used and the fuel cell size is increased accordingly; but increasing this peak to above 0.5 kWh/h led once again to an increase in the cost. This behaviour has a connection to the average annual efficiency of the fuel cells used to handle different peaks. Better fuel cell efficiency (figure 4-23) means simply less hydrogen consumption for a certain amount of electrical power supply. Hence the system needs a smaller PV array, electrolyser and storage tank, and has a lower total cost over a given assessment period. As shown in figure 4-23 this average annual energy efficiency initially increases rapidly by increasing the size of the peak (and the size of the fuel cell accordingly); however, after about 0.5 kW the rate of increasing this efficiency drops and the curve tends to show a saturation behaviour. Here is where the overall cost of the system starts increasing again.

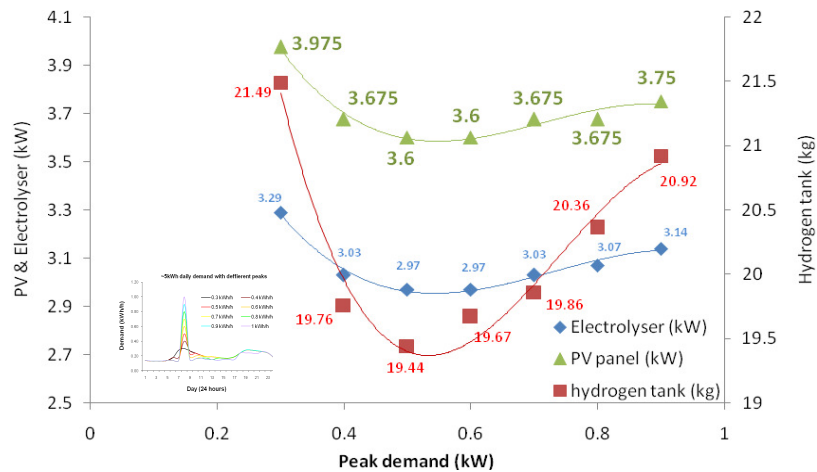


Figure 4-21. Case study: the effect of varying the peak demand on the size of the components

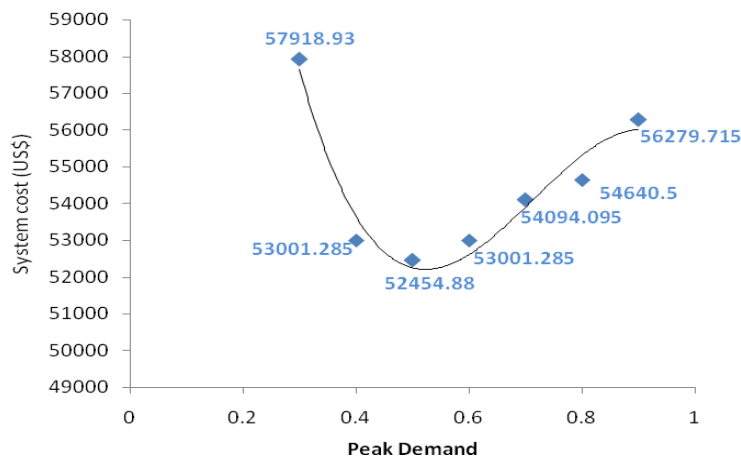


Figure 4-22. Case study: the effect of varying the peak demand on the overall cost of the system

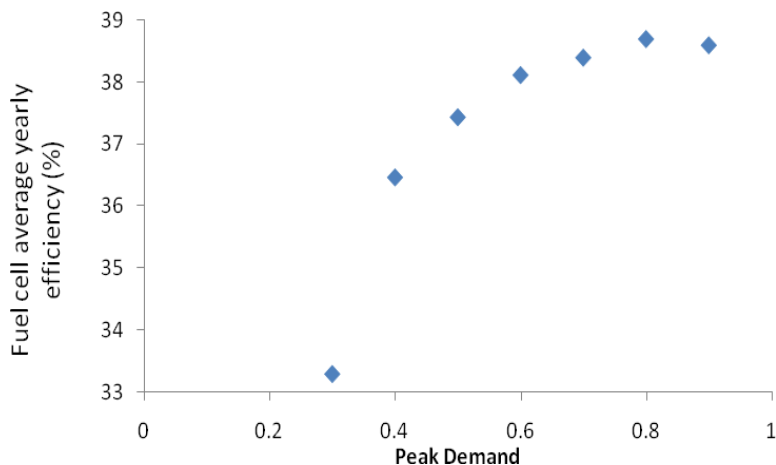


Figure 4-23. Case study: the effect of peak load on the average annual electrical energy efficiency of the fuel cell (based on minimum size of fuel cell required)

It is notable that in solar-hydrogen systems, unlike many other power supply systems, the peak of the demand is normally far smaller than the rated power of the main source of supply (PV arrays). Also the entire demand is not directly supplied by this main supplying component, since part is indirectly supplied through the hydrogen storage sub-system. Hence, the effects of this peak on the size and the cost of the system do not obey the general rule in which increasing the peak leads to increasing the size of the main power supplying component. The results of the simulation performed for the case study show that even completely removing the peak(s) by introducing a uniform demand (e.g. ~ 0.21 kWh/h for the entire day and night), while keeping the daily demand at 4.99 kWh/day, leads to a 16.2%, a 18.1%, and a 12.4% larger PV array, electrolyser, and hydrogen storage tank respectively compared to those obtained for the base case scenario (~ 5 kWh/day peaked at 0.3 kW). The size of the fuel cell is reduced to 0.21 kW to match with the new peak; however, the overall present cost of the system increases by over 13% as the result of increasing the size of the other components (figure 4-24). By applying this uniform load (no peak) the average annual efficiency of the new fuel cell (0.21 kW) drops from about 33% (for the base case scenario) to less than 28%. It means this fuel cell is less efficient in extracting electrical power out of hydrogen and hence more hydrogen has to be generated and stored (larger PV array, electrolyser, and storage tank are required) for supplying the same daily demand (~ 5 kWh/day). The effect of peak load on the economy of a solar-hydrogen system can alternatively be interpreted as just a fuel-cell sizing matter (Shabani *et. al.* 2009), which will be further discussed in the following section.

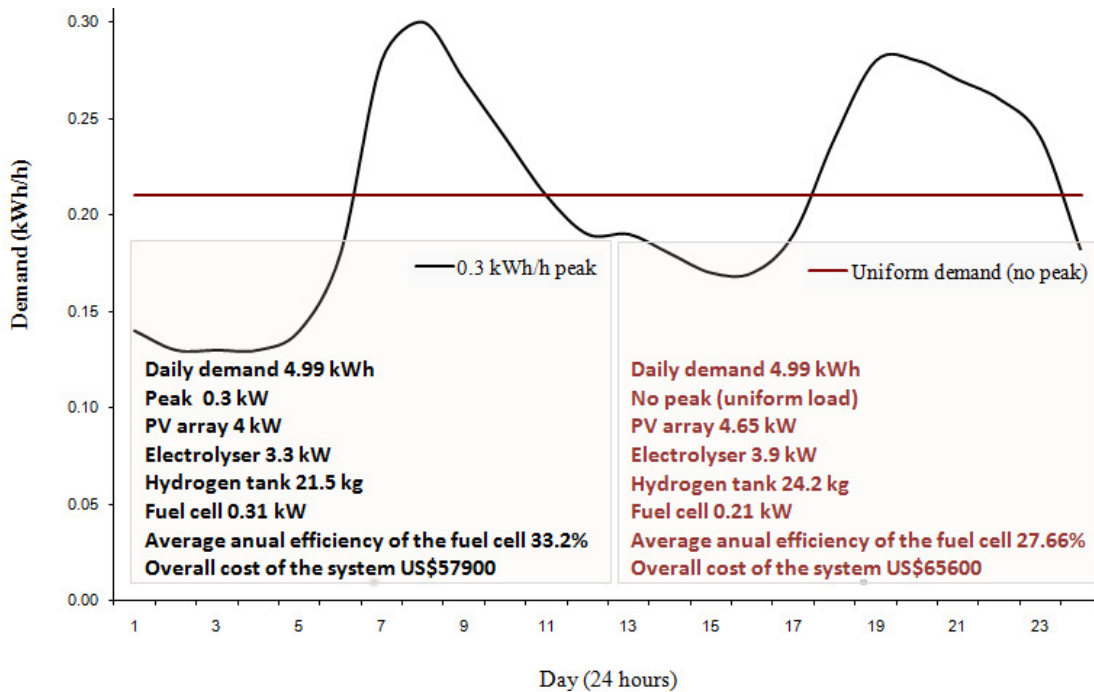


Figure 4-24. The effect of using uniform demand profile and avoiding the peak load (unconstrained tank and minimum fuel cell sizing strategy was applied)

If the entire daily load profile is scaled up by the same linear factor (figure 4-25), larger sizes of components are needed proportionately; that is why the simulation results show that the unit cost of the electricity does not change considerably. However, some cost components (for example, the ‘balance of the system’ cost given in table 4-5) might not increase much with overall system size, so this may lead to slightly less unit cost of electricity for larger loads in practice (Shabani *et. al.* 2009).

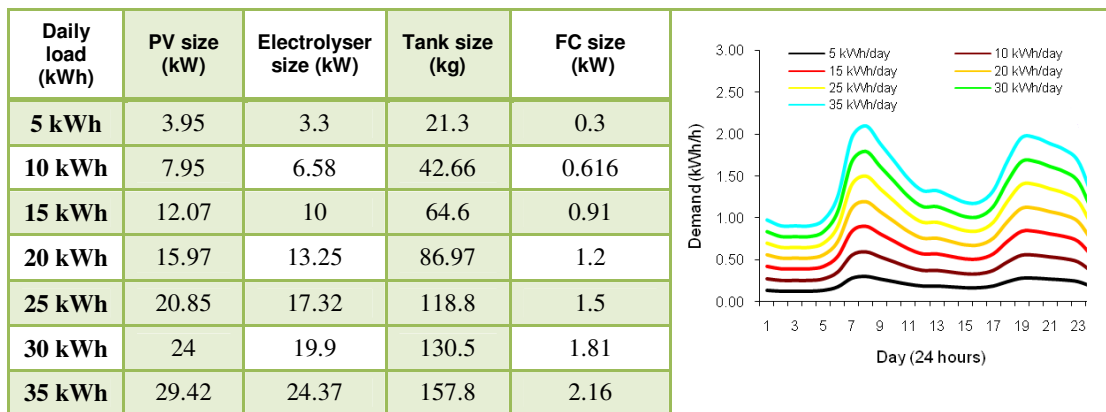


Figure 4-25. The effect of load profile scale on the system’s overall sizing and economy (Shabani *et. al.* 2009)

4.3.3.3 Oversized fuel cell condition

The effect of peak load on the economy of a solar-hydrogen system described in the previous section can alternatively be interpreted as just a fuel-cell sizing matter. The minimum required size of the fuel cell in a solar-hydrogen system is basically determined by the peak demand. However, choosing the fuel cell above this minimum size, for a particular daily load and a given peak, offers an opportunity to reduce the cost of the system, since the larger fuel cell operates at relatively lower average current densities and hence higher average efficiencies. Hence the other major components - PV array, electrolyser, and hydrogen storage - can be smaller since the fuel cell is now consuming hydrogen more efficiently. This effect has been investigated on an unconstrained tank design using the model by varying the fuel cell size above its minimum possible size, determined by the peak of the demand profile. Raising the fuel cell average annual efficiency (figure 4-26) leads to a smaller PV array size (figure 4-27). In turn, the smaller the PV the lower the surplus power, and this allows a smaller size of electrolyser to be employed and hence less hydrogen production and the need to smaller hydrogen tank (figure 4-28). These results open up another opportunity for minimising the cost of the system. By increasing the size of the fuel cell above its minimum value of 0.3 kW, the unit cost of electricity generated by the system over the assessment period of 30 years steadily falls until it reaches a minimum value when the size of the fuel cell is about 1 kW (figure 4-29). Further increases beyond this point leads to rising unit costs of electricity once again. The reduction in unit cost at the optimal point (from 1.06 US\$/kWh to 0.93 US\$/kWh) is over 12% lower than in the base case. The cost analysis for the economically optimum size of the fuel cell is shown in figure 4-29 (right), and can be compared with that for the minimum fuel cell size in figure 4-14. In the latter case, the fuel cell accounted for just 1.64% of the total system cost, but this rises to 6.2% for the economically optimal size of fuel cell. Meanwhile, the share of the total system cost of the PV array, the most expensive part of the system, falls from 54% for the minimum size of fuel cell, to 50% for the optimally-sized fuel cell. The effects of using an optimally-sized fuel cell on reducing the shares of total system cost of the hydrogen tank and electrolyser are less than for the PV array but the behaviour is still similar.

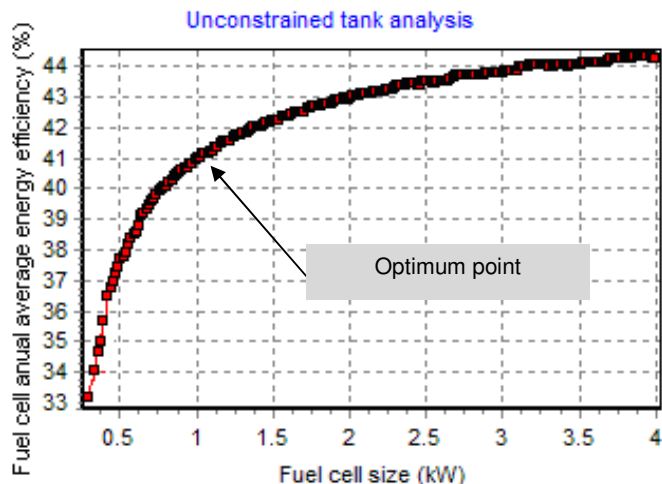


Figure 4-26. The effect of the fuel cell size on the average annual efficiency of this component when it is operated in the system of the case studied

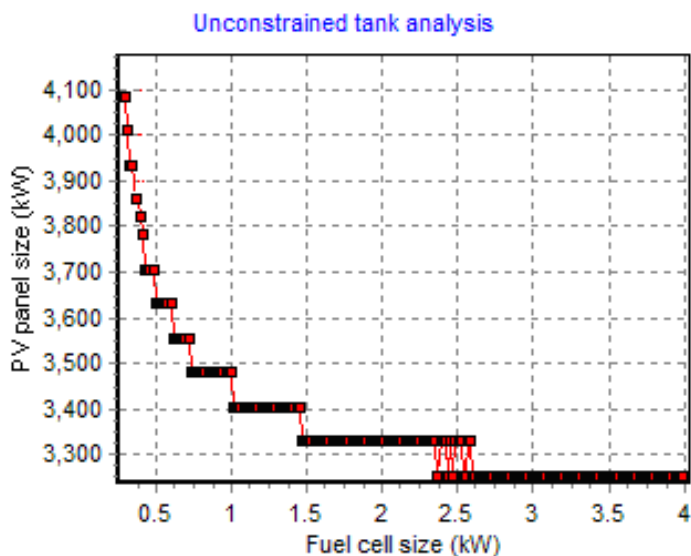


Figure 4-27. The effect of the fuel cell size on the size of the PV array

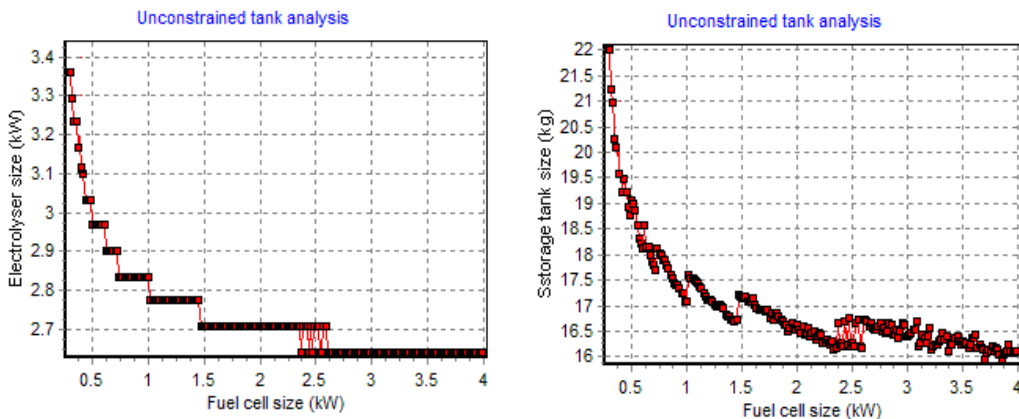


Figure 4-28. Left: The effect of fuel cell size on the size of the electrolyser; right: the effect of the fuel cell size on the size of the storage tank

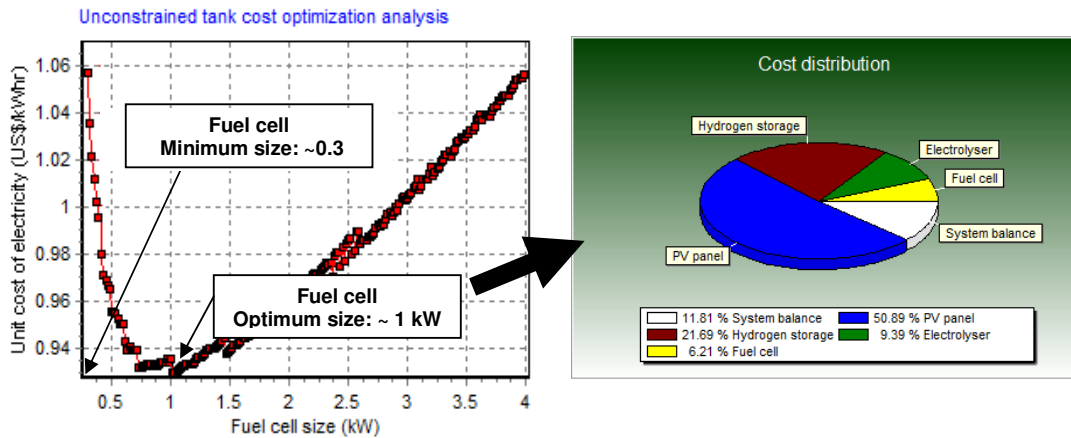


Figure 4-29. Left: The effect of the fuel cell size on the unit cost of the electricity (the idea of the fuel cell optimum size); right: The details of cost analysis on the solar-hydrogen system when the optimally-sized fuel cell, 1 kW, and unconstrained tank were used

The curves in figure 4-27 to figure 4-29, describing the effect of the fuel cell size on the size of the other components and the economy of the system, are not continuous because the size of the PV system, fuel cell and electrolyser could not be changed continuously in the model. For example, the size of the PV can be changed by just adding or removing whole modules (each 75 W) to the array.

Figure 4-30 and table 4-7 contain further details of the system specification when the optimally-sized fuel cell is employed. The round-trip electrical energy efficiency (the annual cumulative electrical output over the input) of the energy storage unit (the combination of the electrolyser, the storage tank, and the fuel cell) of the solar-hydrogen system is improved from 24% (for the base system) to just below 30% using the optimally-sized fuel cell.

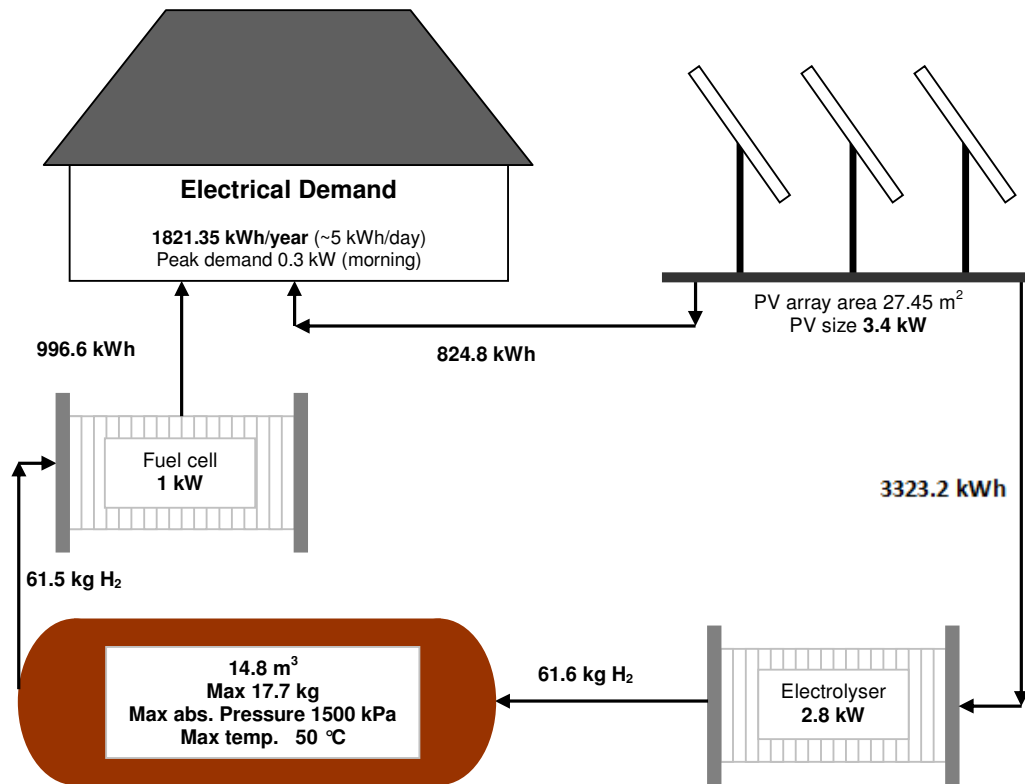


Figure 4-30. Solar-hydrogen system sizing results (for the optimally-sized fuel cell and unconstrained tank)

Components		Size	Note
Load	Total demand	4.99 kWh/day or 1821.35 kWh/year (excluding heating and cooling load)	
	Peak	2 peaks: 0.3 kWh/h morning peak 0.28 kWh/h evening peak	
PV Array	Area	27.5 m ²	Equivalent to 45 modules of BP277 PV cells
	Power	3.4 kW	0.9 of de-rating factor was applied
	Average annual efficiency	9.97%	
Electrolyser	Size	2.8 kW	Equivalent to 53 electrolyser stacks of SatXX 7
	Hours of operation per year	3455.5 h	A figure to estimate the lifetime of the electrolyser on yearly basis for doing economic analysis on the system
	Total annual hydrogen production	61.6 kg	
Hydrogen tank	Size	17.7 kg	<ul style="list-style-type: none"> Equivalent to 14.76 m³ Perfect gas law was applied Maximum ambient temperature was assumed to be 50 °C Relatively low pressure hydrogen storage: 1400 kPa-gauge (~1500 kPa-abs)
	Initial and final level of hydrogen	9 kg	Based on assuming Jan 1 st as the first day of the year for sizing analysis

<i>Fuel cell</i>	Size	1 kW	18 cells-Based on singles cells of 500 W PEM BCS fuel cells (540 W maximum power)
	Annual electricity delivery	996.6 kWh	The additional electricity provided by the fuel cell in addition to the PV output to meet the demand
	Annual hydrogen consumption	61.5 kg	<ul style="list-style-type: none"> Based on hydrogen stoichiometry of 1.2 in the whole range of fuel cell operation. This will be more discussed based on the experimental data
	Hours of operation per year	5304.5 h	A figure to estimate the lifetime of the fuel cell on yearly basis for doing economic analysis on the system
	annual hydrogen loss	15.4 kg	<ul style="list-style-type: none"> Equivalent to 607 kWh Based on 1.2 of hydrogen stoichiometry assumption
	Total annual heat generation	794.7 kWh	It is higher than the annual electricity generated by the fuel cell
	Estimated annual cooling load	512.4 kWh	The heat generated by the fuel cell: <ul style="list-style-type: none"> is partly used inside the stack to evaporate the generated water is slightly removed by the excess reactants It will be more discussed based on theoretical analysis and experimental results
	Average annual electrical energy efficiency	41.1 %	<ul style="list-style-type: none"> Relatively low efficiency Mainly operated close to the maximum power point of the fuel cell Minimum size of the fuel cell has been chosen to just meet the peak demand

Table 4-7. Solar-hydrogen system sizing results (for fuel cell optimum size and unconstrained tank)

4.3.3.4 Sensitivity analysis

Many input assumptions influence the results of this case study, so that changing these assumptions may lead to different results and conclusions, in particular for the average unit cost of electricity supplied. Three key categories of assumption are those relating to the financial assessment conditions and unit costs; component lifetimes; and fuel cell performance.

Key factors influencing the economic analysis are the assumed real discount rate and assessment period. The sensitivity of the estimated unit cost of electricity (with minimum fuel cell size and unconstrained tank) to varying these factors is shown in figure 4-31. Increasing the discount rate from 5% to 10% increases the unit cost of electricity by over three times, from 1.06 US\$/kWh to about 3.7 US\$/kWh. The longer the assessment period the lower the estimated unit cost of electricity becomes. The main reason for this reduction is the assumption that unit costs of the main components – PV modules, fuel cell,

electrolyser and storage tank – fall over time, due to technology development and higher volume production. As an example, increasing the assessment period from 10 years to 30 years leads to 56% reduction in the calculated unit cost of electricity, from 2.4 US\$/kWh to 1.06 US\$/kWh for a 5% real discount rate.

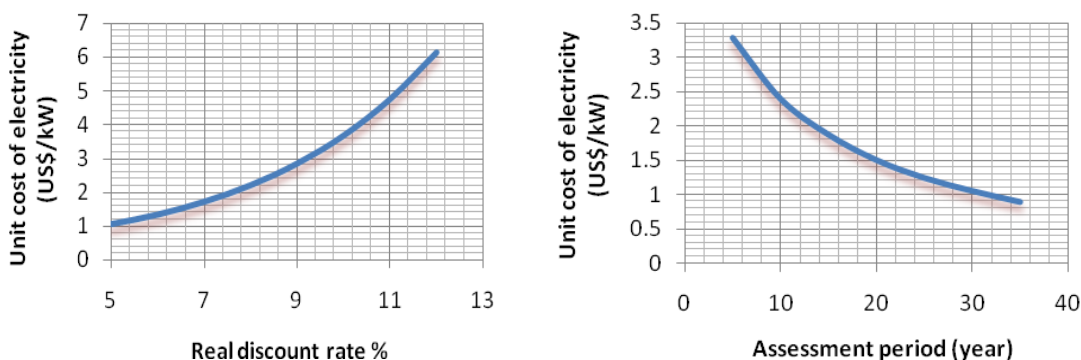


Figure 4-31. The effect of financial assumptions on the unit cost of electricity (left: the effect of discount rate in an assessment period of 30 years right: the effect of assessment period at the discount rate of 5%)

The variety of quoted assumptions that could be used for the cost of the components is another matter that has to be taken into account when performing any cost analysis on the solar-hydrogen system. The unit cost of a PEM fuel cell has been quoted between 3000-6000 €/kW by Zoulias and Lymberopoulos (2007) and ~6500 US\$/kW by Nelson *et al.* (2006). For the base case in the present case study, the unit cost of the fuel cell has been assumed to be 2000 US\$/kW with a predicted reduction to 439 US\$/kW within 5 to 10 years as quoted by Beccali *et al.* (2008). Nelson *et al.* (2006) used ~6500 US\$/kW for the electrolyser; however, 1500 US\$/kW for the unit cost of the electrolyser was used in the case study here, with a reduction to 500 US\$/kW within 10 years), as recommended by Beccali (2008).

As for the PV array, 6000-9000 US\$/kWh was used by Zoulias and Lymberopoulos (2007), 10200 US\$/kW by Beccali *et al.*(2008), and 6900 US\$/kW by Shaahid and Elhadidy (2008), compared to 5750 US\$/kW used in the present case study based on the real price quoted directly by the distributor (Solardyne 2008).

The sensitivity of the unit cost of electricity supplied in the case study to variations in the assumed unit costs of the PV array, electrolyser, hydrogen storage and fuel cell is illustrated in figure 4-32.

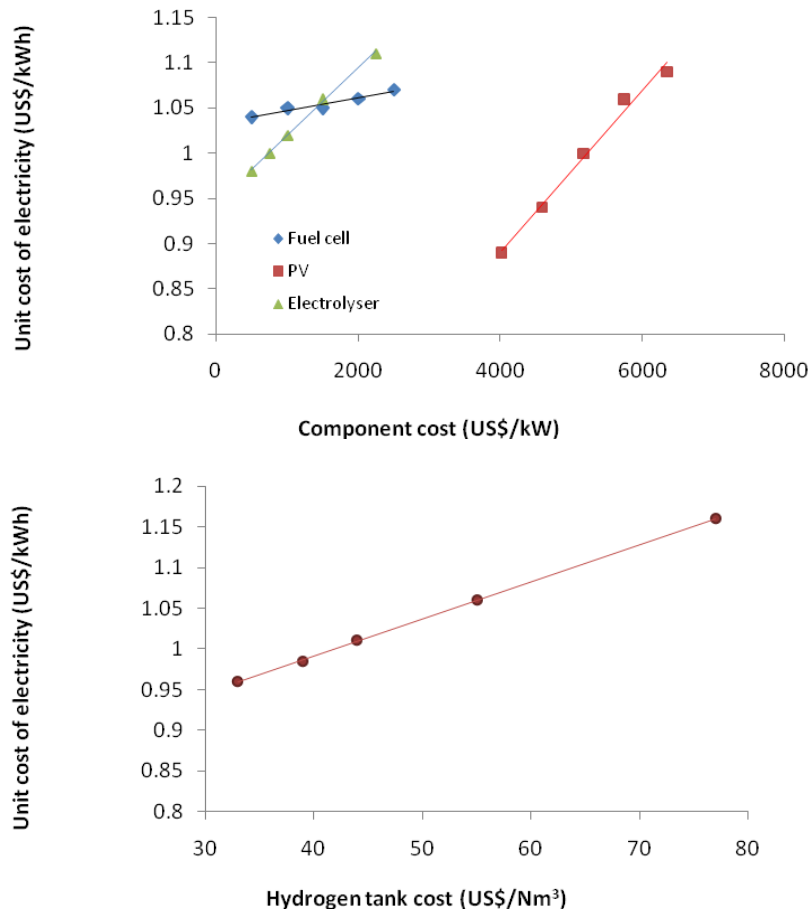


Figure 4-32. The effect of cost assumptions for the major components of the system on the unit cost of electricity generated; the future price and the maintenance costs are assumed to be varied proportionately; the cost of one component varies at a time and the costs of the others are based on table 4-5

The effect is linear but with a different slope in each case. For example, a 50% increase in the capital cost of the PV arrays leads to just over a 20% increase in the unit cost of electricity, while the same percentage increase in the hydrogen storage tank cost results in about a 10% increase in the electricity cost. A 50% increase in the electrolyser cost, however, lifts the unit cost of electricity by only 6%, and the same percentage increase for the fuel cell leads to only a 1% increase.

These results underline the fact that the cost assumptions for the PV array and storage tank in this case study are critical inputs, whereas variations in the assumed electrolyser and fuel cell costs have a much smaller influence.

The assumed lifetime of the components are other inputs for which sensitivity testing is warranted. For the hydrogen storage tank and PV module, most of the research studies done so far, assume a 25-30 year lifetime of these components (Greiner *et al.* 2007; Shaahid and Elhadidy 2008) consistent with the 30 years assumed in the base case here. The lifetime of the fuel cell has been assumed in the base case to be 15 000 hours, using the findings of Zoulias and Lymberopoulos (2007) where this lifetime was equivalent to 10 years operation. Nelson *et al.* (2006) reported a lifetime of 5 years for the fuel cell in their study without indicating the number of operational hours or saying if the fuel cell is operated at low, medium or high current densities. In the unconstrained storage and minimum fuel cell condition (see table 4-4) in the present case study, the fuel cell operates for just over 5000 hours per year, which is equivalent to just below a three year operational lifetime. The effects of lifetime assumptions (4000 hours to 18000 hours) for the fuel cell and electrolyser on the unit cost of electricity in the case study are presented in figure 4-33. Varying the fuel cell lifetime has a minimal impact on the electricity cost, as expected since the fuel cell just accounts for less than 2% of the cost of the system (figure 4-14). The effect of the lifetime assumption for the electrolyser is stronger at lower lifetimes (up to 12000 hours), but henceforth becomes much weaker.

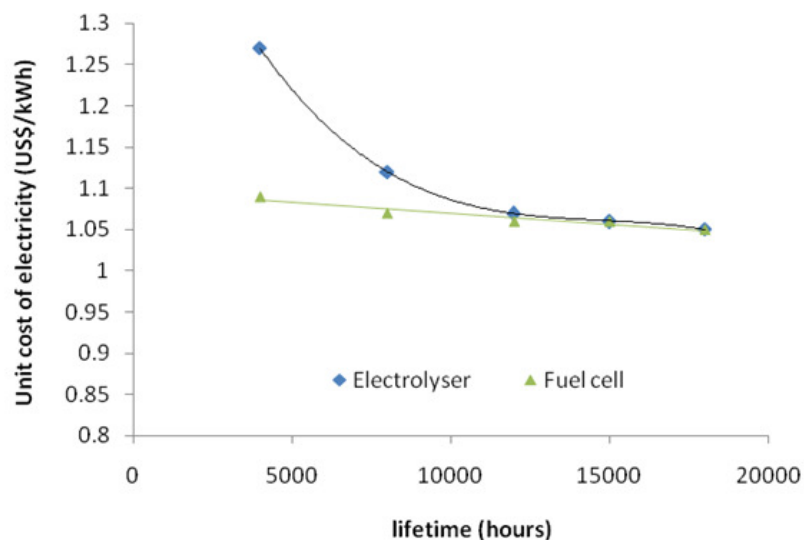


Figure 4-33. The effect of components' lifetime assumptions on the unit cost of electricity

Sensitivity analysis has also been conducted for variations in the assumed fuel cell performance in terms of both hydrogen utilisation coefficient and the overall characteristic performance curve (that is, voltage losses).

In the case study, a hydrogen stoichiometry of 1.2, that is, 20% excess hydrogen input, was assumed over the whole range of operating current densities. This assumption corresponds to a relatively low hydrogen utilisation coefficient (~85%), and is actually below the experimental value for this particular type of fuel cell, as will be discussed in the next chapter. The influence of lowering the hydrogen stoichiometry on component sizes and the unit cost of electricity for the unconstrained storage plus minimum fuel cell size scenario in the case study is shown in figure 4-34, figure 4-35, figure 4-36, and figure 4-37. Both size and cost increase almost linearly by increasing the hydrogen stoichiometry (decreasing the hydrogen utilisation coefficient). Decreasing the hydrogen stoichiometry from 1.2 to 1 can lead to about a 14% reduction in the unit cost of electricity. Similarly the unit cost of electricity for an optimal system which was found to be 0.93 US\$/kWh previously (figure 4-29) using a hydrogen stoichiometry of 1.2 can be reduced to about 0.8 US\$/kWh (14% improvement) when the hydrogen stoichiometry of 1 is applied.

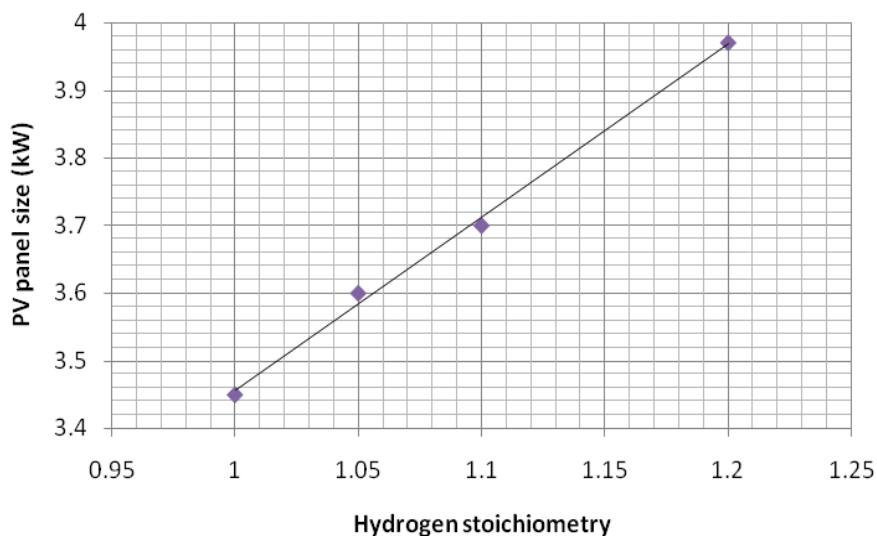


Figure 4-34. The effect of hydrogen stoichiometry on the PV array size in the case study (5 kWh daily demand peaked at 0.3 kW in south-eastern Australia)

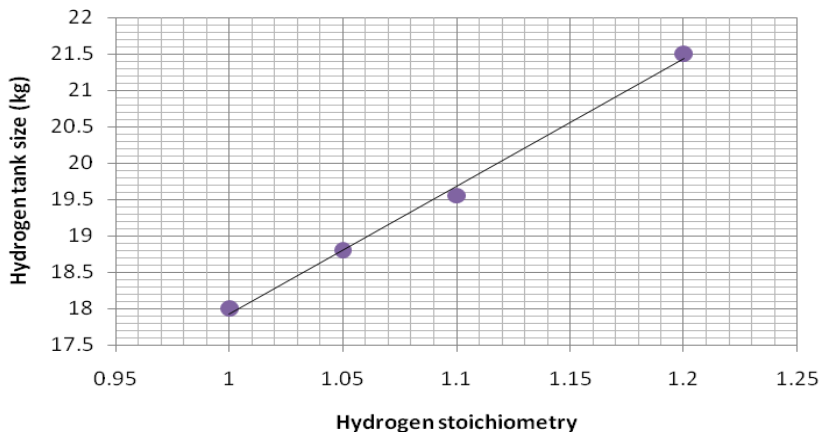


Figure 4-35. The effect of hydrogen stoichiometry on the hydrogen tank size in the case study (5 kWh daily demand peaked at 0.3 kW in south-eastern Australia)

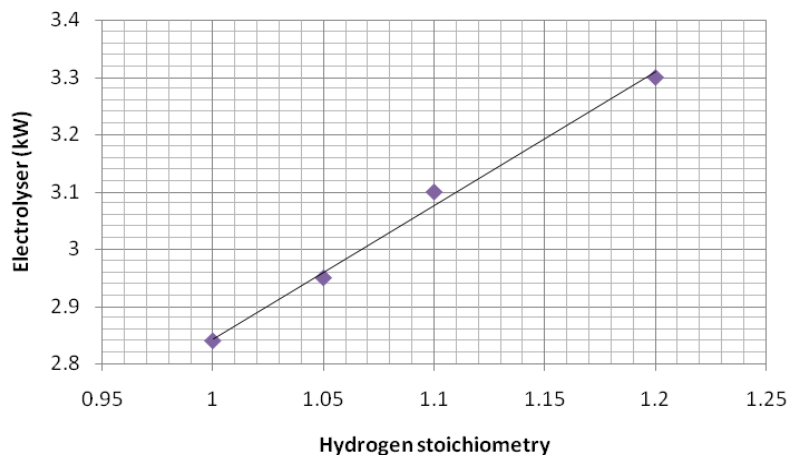


Figure 4-36. The effect of hydrogen stoichiometry on the electrolyser size in the case study (5 kWh daily demand peaked at 0.3 kW in south-eastern Australia)

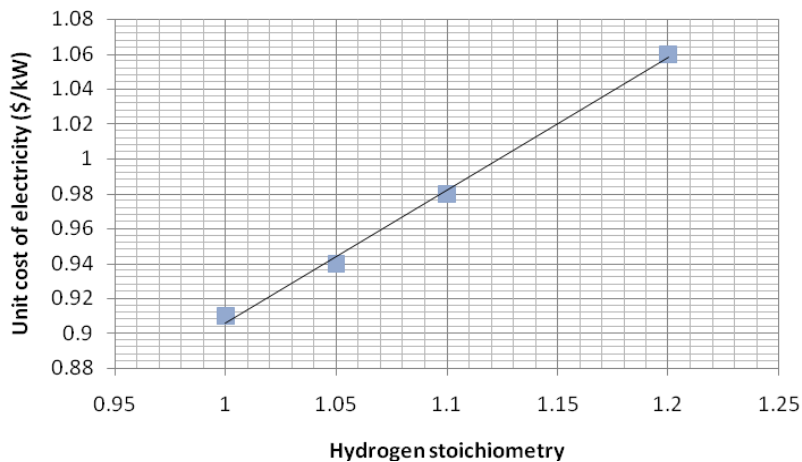


Figure 4-37. The effect of hydrogen stoichiometry on the unit cost of electricity generated by the solar-hydrogen system designed in the case study (5 kWh daily demand peaked at 0.3 kW in south-eastern Australia)

In regard to fuel cell performance, a 10% increase in voltage (that is, lower voltage losses) at each value of current (medium to high currents) as shown in figure 4-38 results in the reductions in component sizes and in the unit costs of electricity (table 4-8). For the system using an unconstrained hydrogen storage tank and an optimally-sized fuel cell, the unit cost cost of electricity falls by about 5% from 0.93 to 0.88 US\$/kWh.

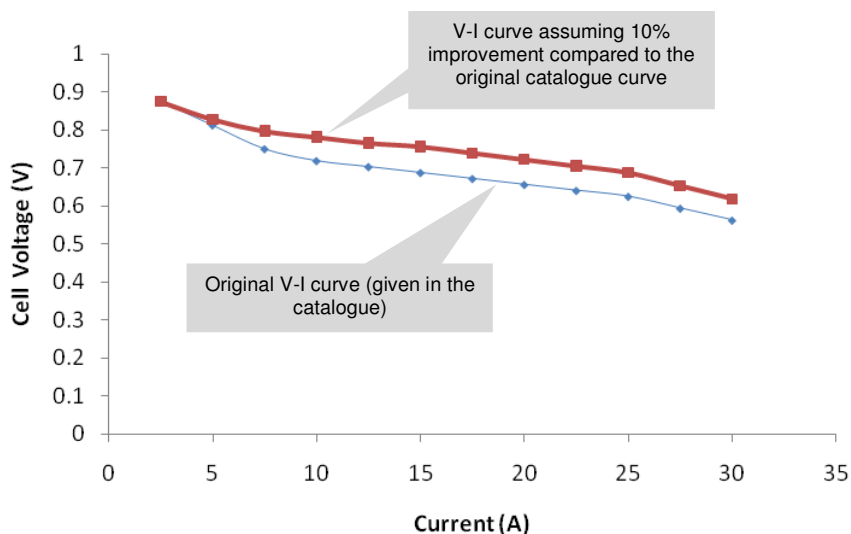


Figure 4-38. Improvement in the performance of a single cell of the 500W PEM fuel cell which was used for the case study

	Fuel cell performance	
	Normal performance	10% improvement
PV array size (kW)	4	3.7
Electrolyser size (kW)	3.3	3.1
Hydrogen tank size (kg)	21.5	20
Unit cost of electricity (US\$)	1.06	0.98
Minimum fuel cell size		
Unit cost of electricity (US\$)	0.93	0.88
Optimally-sized fuel cell		

Table 4-8. The effect of a 10% improvement in fuel cell performance on the system’s sizing and economics for an unconstrained tank analysis

4.4 SOLAR-HYDROGEN CHP SYSTEM

4.4.1 Potential for conversion to a CHP system

The theoretical investigation into the fuel cell used in this case study suggests that a considerable proportion of the hydrogen energy input is converted to heat rather than electricity. As shown by figure 4-39, obtained using the simulation program, at lower

current densities the heat generated by the stack is slightly less than its power generation. As the current density increases and the maximum power point is approached, the thermal losses rise and the stack generates power at lower efficiency. Here is where the idea of a combined heat and power (CHP) fuel-cell system originates (Shabani *et al.* 2010). As shown by figure 4-40 and figure 4-41, for the 500 W fuel cell (exactly 540 W) comprised of 32 cells, part of the generated heat (a few percent of the total heat) is removed from the stack by the extra air and hydrogen; another part is used for vaporising the product water (about 25% to 35% depending on the fuel cell operating point); and the rest is the fuel cell cooling load that has the potential to be used for a low-temperature heating application.

The typical Sankey diagram (energy flow diagram) of the PEM fuel cell used in this case study is similar to that shown by figure 4-42.

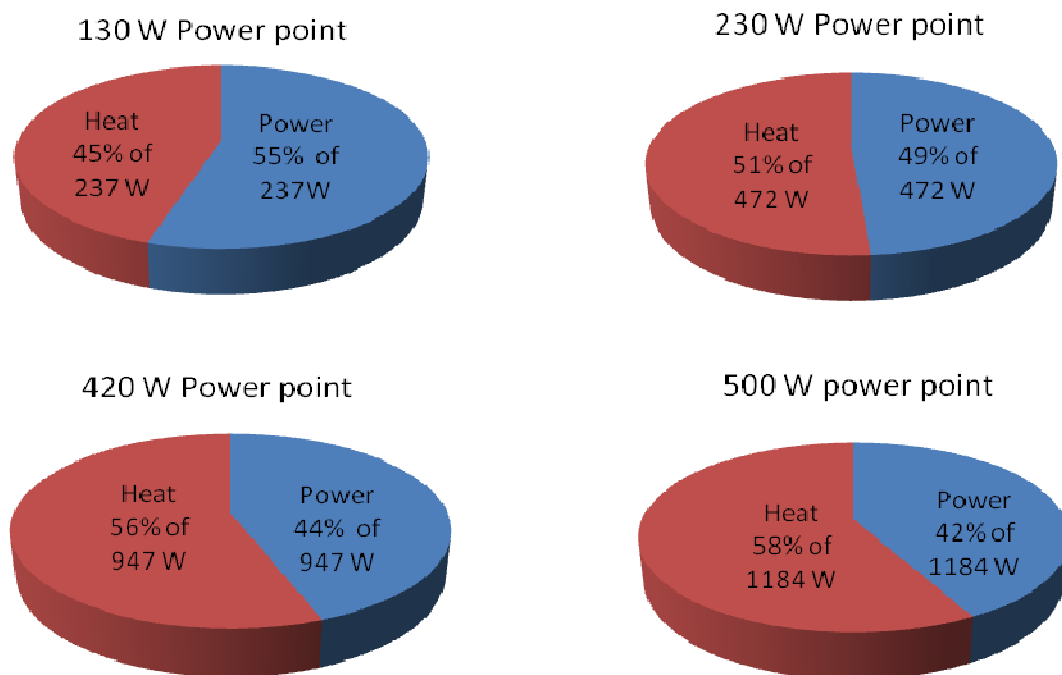


Figure 4-39. The results of the theoretical analysis to compare the heat and power generations of the 500 W PEM BCS fuel cell; operating condition: as shown in table 3-3, inlet air relative humidity 50%

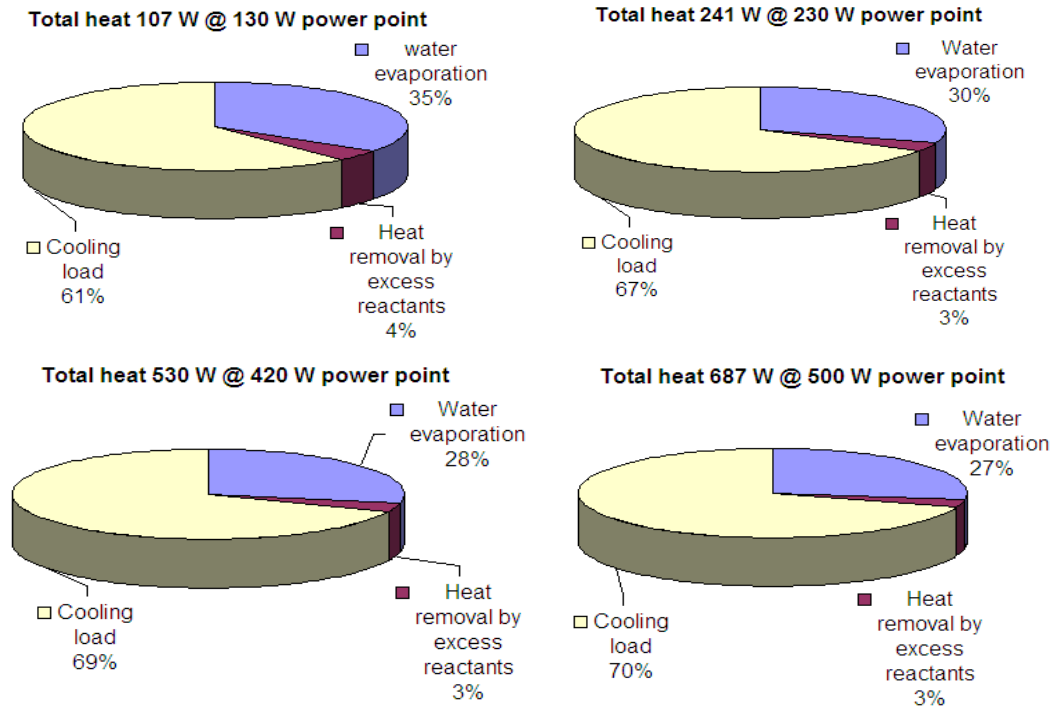


Figure 4-40. How the generated heat is removed from the 500 W (540 W) PEM BCS fuel cell; operating condition as shown by table 3-3

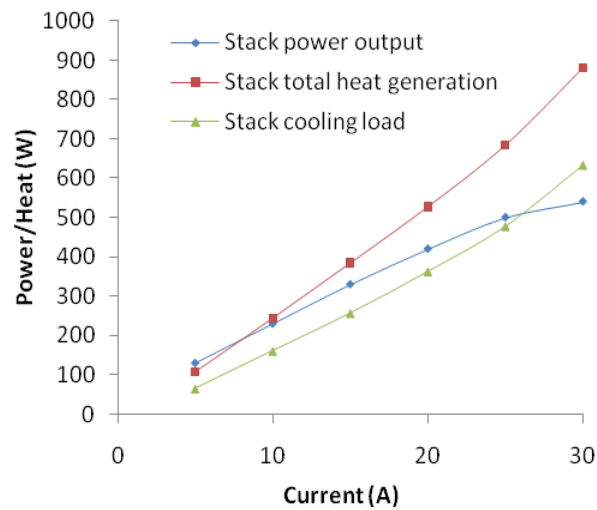


Figure 4-41. Theoretical investigation on the 500W (540 W maximum power) BCS PEM fuel cell stack, heat generation; operating condition as shown by table 3-3(Shabani *et al.* 2010)

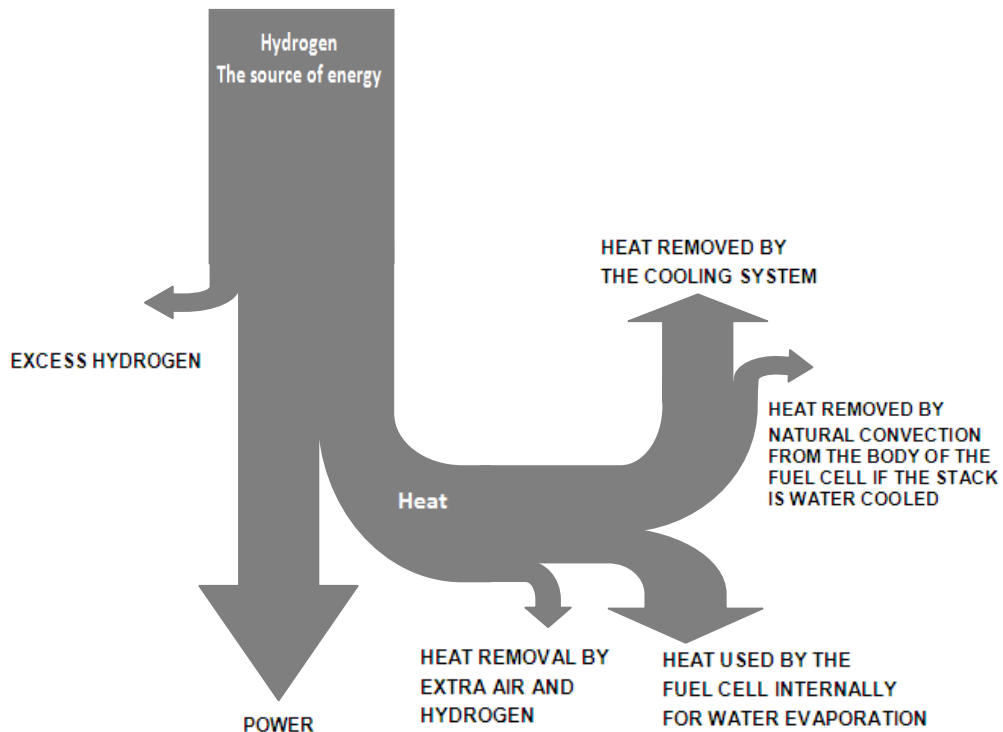


Figure 4-42. Typical Sankey diagram for a PEM fuel cell

The excess reactants and in particular the excess air (air stoichiometry) can play an important role in controlling the hydration of the cell's membrane. Low air stoichiometry can lead to flooding of the fuel cell membrane, while too much air can result in dehydration of the membrane. Just a few percent of the generated heat is removed by the extra reactants if the fuel cell is operated under the conditions recommended by the manufacturer. Increasing the air stoichiometry does have a cooling effect on the fuel cell and reduces the need for additional cooling, but the increase must be regulated to avoid dehydration of the membrane. The effect of increasing air stoichiometry on heat removal is illustrated for the 500-W PEM fuel cell used in this case study in figure 4-43 at one operating point (130 W). If the air stoichiometry is increased from 2 to 20, over 40% of the heat generated by the fuel cell could be removed by this excess stream of air. Table 4-9 provides a detailed analysis of the heat and power generation for this fuel cell over a range of power outputs and for air stoichiometries of 2 and 4.

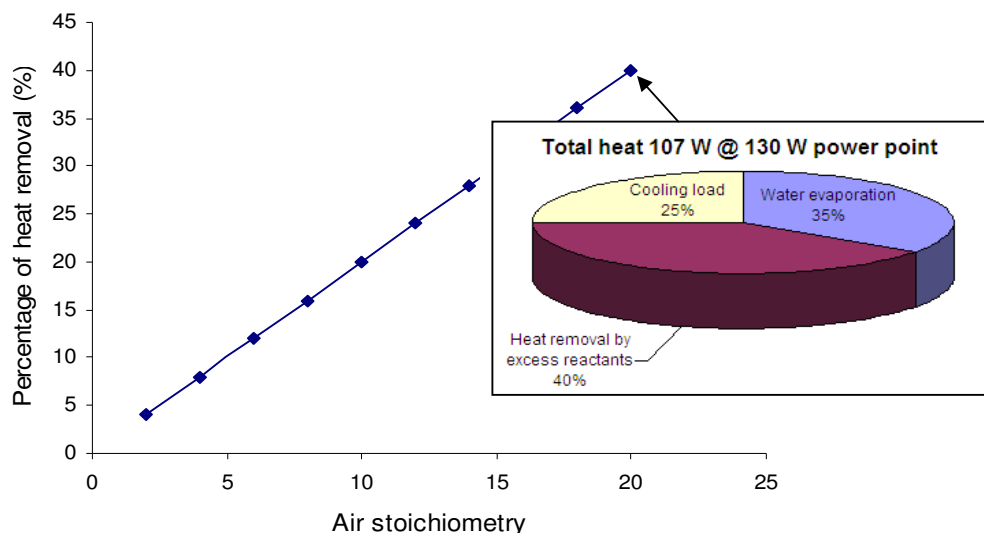


Figure 4-43. The effect of air stoichiometry on the heat removal from a 500 W BSC fuel cell at 130 W power point at operating condition shown in table 3-3

Operating point (W)	Air stoichiometry 2				Air stoichiometry 4		
	Total heat generation (W)	Water evaporation (W)	Extra Reactants Heat removal (W)	Cooling Load (W)	Water evaporation (W)	Extra Reactants Heat removal (W)	Cooling Load (W)
130	107	37.5	4	65.5	37.5	8.4	61.1
230	241	74	8	159	74	16	151
330	380	112	12	256	112	25	243
420	530	150	17	363	150	34	346
500	687	188	21	478	188	43	456
540	880	223	24	633	223	50	607

Table 4-9. 500 W BCS PEM fuel cell heat and power generation details for air stoichiometries of 2 and 4; water product has been assumed to be in vapour form

As demonstrated in figure 4-40 and table 4-9, a considerable amount of the heat generated is absorbed by the water produced. If the fuel cell is operated at low temperatures and/or the partial pressure of the produced water is increased (for example, by reducing the supply air flow rate), this water leaves the stack in liquid form, so that no heat is required for water evaporation and more heat has to be removed from the stack by the cooling system. This effect will be highlighted and discussed further in the next chapter.

4.4.2 Cumulative annual fuel cell cooling load

4.4.2.1 Cooling load with minimum fuel cell size

As discussed before (section 4.3.3.3), in a system with the minimum size of fuel cell, the cell operates for much of the time at relatively high current densities so that energy losses are higher and more heat is generated. Figure 4-44 shows the annual energy flows in the solar-hydrogen system in the case study with unconstrained storage and the minimum size of fuel cell. Out of the 1821.35 kWh of annual electrical demand (4.99 kWh/day), just 842.34 kWh is directly supplied by the PV arrays (~46%) and the rest (979 kWh) is indirectly supplied by the fuel cell, the end point of the hydrogen storage sub-system (electrolyser, hydrogen tank and fuel cell). The figure of 1214.9 kWh for the fuel cell heat generation is considerable, especially when compared with the PV or fuel cell shares in supplying the electrical demand: it is about 45% more than the PV output which is received by the load and 25% more than the fuel cell electrical output. Although just part of the heat generated is transferred to the cooling system (868 kWh/year), and hence potentially available for use in another application requiring heat, this cooling load is still of comparable magnitude to the PV and fuel cell outputs. Figure 4-44 also shows another waste stream of energy, namely hydrogen wastage, which will be discussed later. If a beneficial use can be found for all the heat extracted by the cooling system, the maximum overall annual energy efficiency of the fuel cell would be 63%, operating thus as a combined heat and power application, compared to only 33% on average, operating in just power production mode. The annual round-trip energy efficiency of the energy storage sub-system (the output power over the input power), including the electrolyser, storage tank, and fuel cell, is about 24% (figure 4-44). If the cooling load of the fuel (the collectable part of the fuel cell heat) is considered as another useful output of this component together with its electrical power, this round-trip energy efficiency can be improved to about 46%.

Figure 4-45 shows the half-hourly fuel cell heat, power, and cooling load throughout the year. This figure illustrates that the fuel cell heat generation is mostly higher than its power generation.

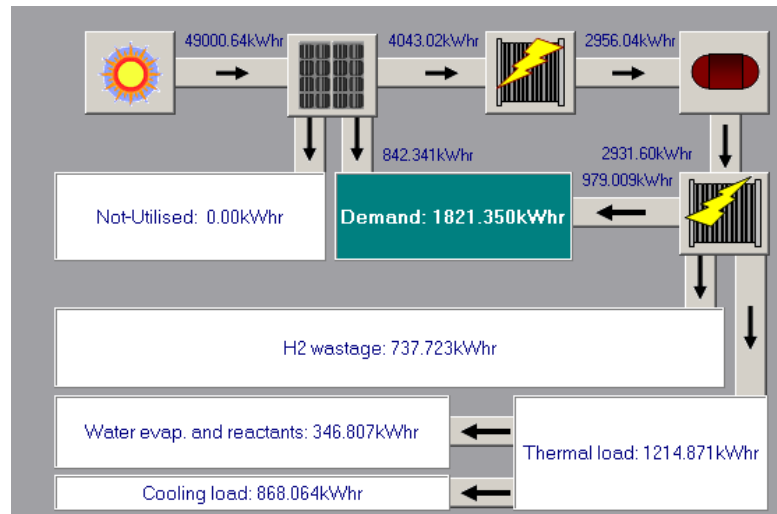


Figure 4-44. The cumulative annual energy flow of the solar-hydrogen system of the case study (fuel cell minimum size and unconstrained tank)

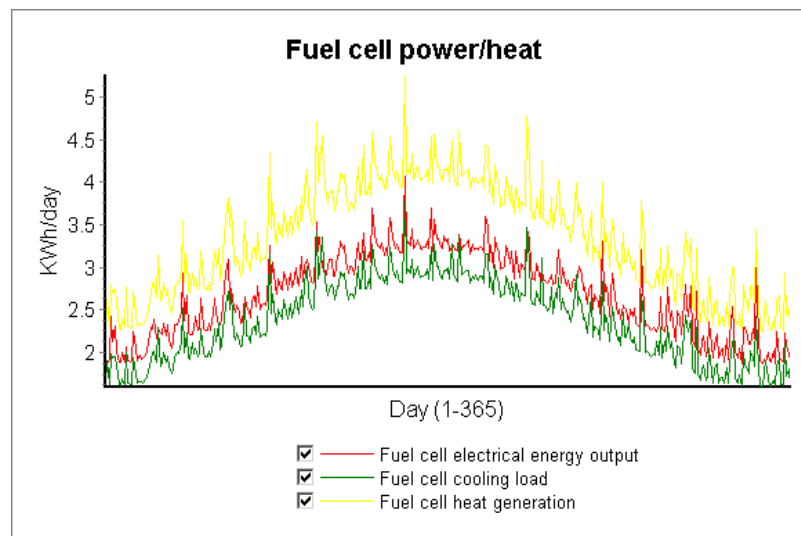


Figure 4-45. Daily variation of the fuel cell heat, cooling load, and power generation when it is operated in the solar-hydrogen system of the case study (fuel cell minimum size and unconstrained tank)

4.4.2.2 Cooling load with optimal fuel cell size

As a result of the relatively better average energy efficiency of the fuel cell when optimally rather than minimally sized (41% compared to 33%), the corresponding heat generation and cooling load are 35% and 41% lower than those obtained for the system in which the minimum size of the fuel cell was employed. The heat generation and cooling load of the fuel cell in such a system, the cumulative annual energy flows, and the daily heat, cooling

load and power output of the optimally-sized fuel cell are shown in figure 4-46 and figure 4-47. Similar to that estimated for the system with minimally-sized fuel cell, an overall annual CHP energy efficiency of 63% for the optimally-sized fuel cell is expected in this case. The annual round-trip energy efficiency of the energy storage sub-system is about 30% (figure 4-46). This efficiency can be improved to above 45% if the cooling load of the fuel cell (the collectable part of the fuel cell heat) is considered as another useful output of that together with its electrical power.

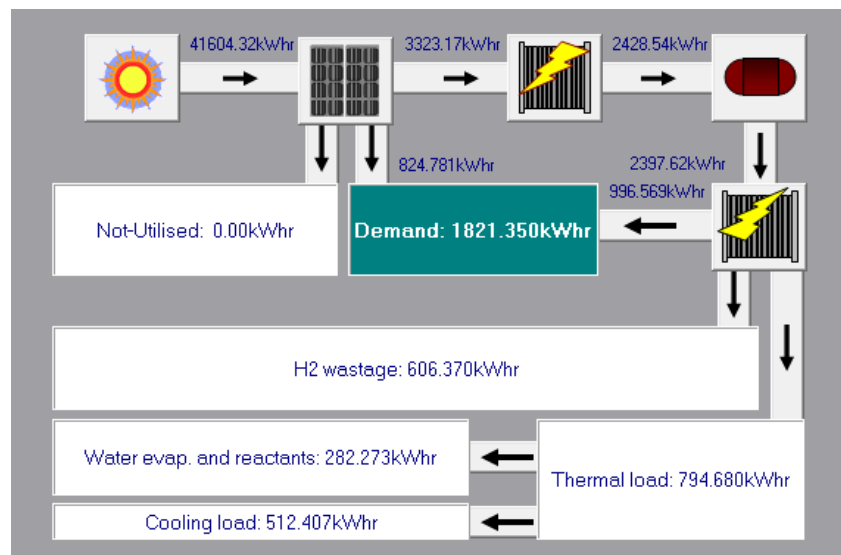


Figure 4-46. The cumulative annual energy flow of the solar-hydrogen system of the case study (optimally-sized fuel cell and unconstrained tank)

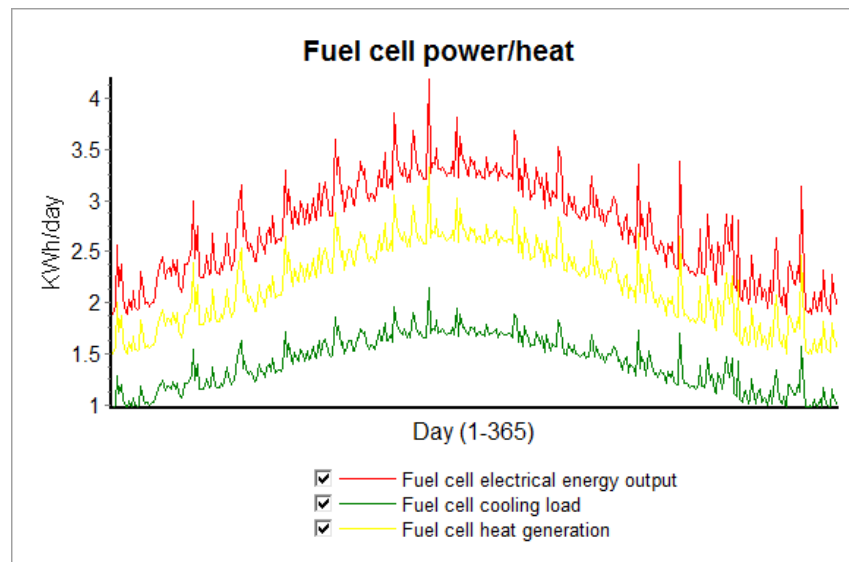


Figure 4-47. Daily variation of the fuel cell heat, cooling load, and power generation when it is operated in the solar-hydrogen system of the case study (optimally-sized fuel cell and unconstrained tank)

4.4.2.3 Cooling load: system with unconstrained/constrained tank

Adopting a constrained storage does not lead to a considerable difference in the heat and cooling load of the fuel cell compared to the unconstrained storage condition, as can be seen by comparing figure 4-48 and figure 4-49 for a 3-kg constrained hydrogen tank with the earlier figure 4-44 and figure 4-45.

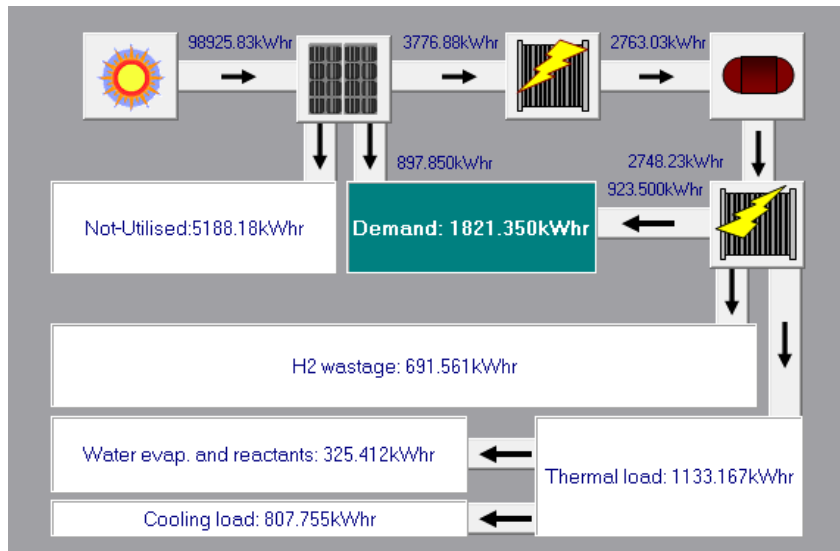


Figure 4-48. The cumulative annual energy flow of the solar-hydrogen system of the case study (fuel cell minimum size and a 3-kg constrained tank)

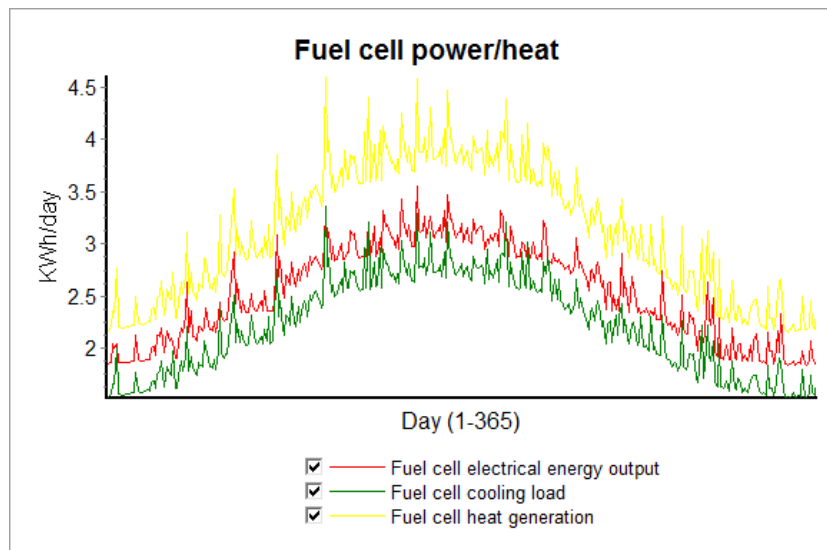


Figure 4-49. Daily variation of the fuel cell heat, cooling load, and power when it is operated in the solar-hydrogen system of the case study (fuel cell minimum size and a 3-kg constrained tank)

4.4.2.4 Cooling load and electrical load management in the solar-hydrogen system

With load management, and choosing the best electrical load profile as discussed earlier (section 4.3.3.2), the fuel cell operates at relatively higher energy efficiency in producing electricity and hence less heat is generated. The fuel cell overall annual energy efficiency in power-only mode is above 37% in this case (compared to 33% without load management). Figure 4-50 and figure 4-51 are the results of the investigation when load management is applied. The maximum overall annual energy efficiency in CHP mode is 63%, but relatively more of the total energy supplied is electricity as opposed to heat compared to the case with no load management.

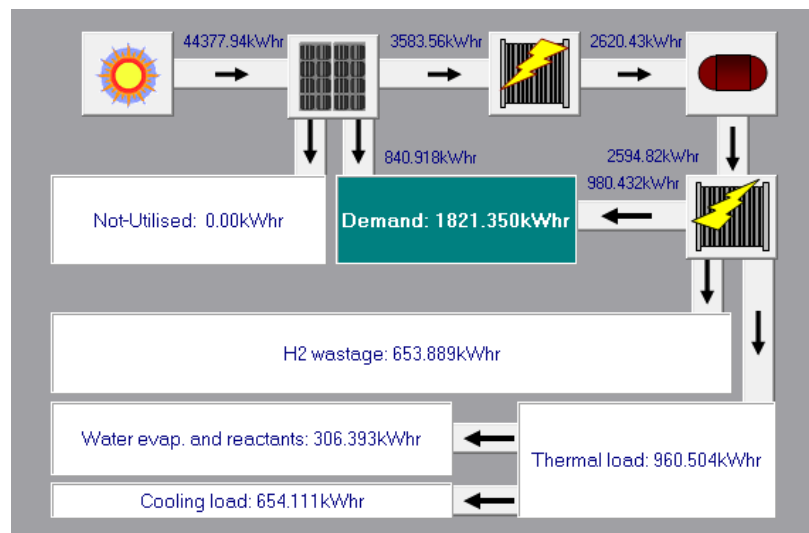


Figure 4-50. The cumulative annual energy flow of the solar-hydrogen system of the case study (fuel cell minimum size, unconstrained tank, and managed peak load)

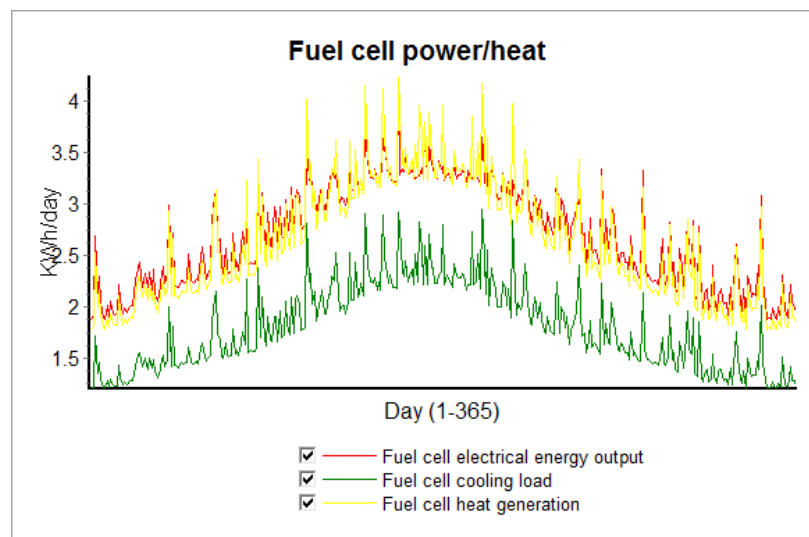


Figure 4-51. Fuel Daily variation of the fuel cell heat, cooling load, and power when it is operated in the solar-hydrogen system of the case study (cell minimum size, unconstrained tank, and managed peak load)

4.4.3 Using fuel cell heat and excess hydrogen for domestic hot water supply

4.4.3.1 System configuration

As discussed in section 2.4 the generated heat from the fuel cell is a useable grade of heat for a range of applications such as enhancing discharge of hydrogen from a solid-state metal hydride storage, space heating, and domestic hot water supply. A particularly attractive application for the heat provided by a solar-hydrogen CHP system is for domestic water heating, whether for a remote household or other remote facilities. This option has been investigated in detail in the present case study, assuming the heat recovered from the fuel cell is used to substitute for LPG used for water heating (figure 4-52).

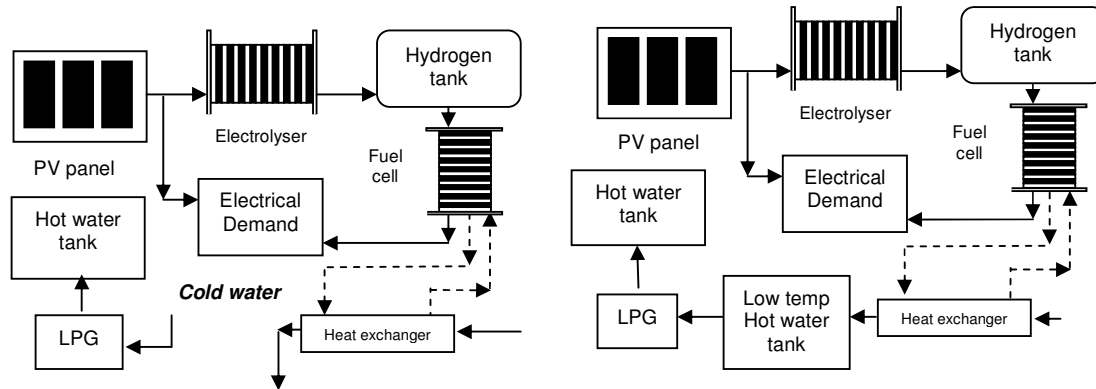


Figure 4-52. Suggested simplified configuration for a solar-hydrogen CHP system; **left:** no CHP application; **right:** fuel cell heat is used for boosting the hot water system (Shabani *et. al.* 2009)

4.4.3.2 Assumptions

The following assumptions have been made to enable a quantitative analysis to be conducted:

The main usage of hot water at home is typically for taking shower. According to the Australian Water Efficiency Labelling and Standards (WELS 2008), a water efficient showerhead uses as little as around 6 l/min of hot water, which is assumed to be 60% hot water @ 55 °C and 40% of cold tap water @ ~16 °C on average (~40 °C when mixed). Assuming around nine minutes of showering per day per person, the daily hot water consumption for a family of two comes to about 65 l/day of hot water @ 55 °C or 110 l/day @ ~40 °C. Adding other domestic hot water uses, e.g. for washing purposes, this

figure has been assumed conservatively to be 165 l/day @ ~40 °C or 100 l/day @ 55 °C. It is important to consider the fact that water and energy are supposed to be consumed conservatively in a remote household where such utilities are not easy to access and quite expensive.

The temperature of the cold water, to be warmed up to 55 °C, varies throughout the year. The average monthly cold water temperatures based on the 2008/2009 daily data recorded by the Australian Bureau of Meteorology (BOM 2009) for Melbourne as a typical place in southeast Australia were used for this purpose (table 4-10).

	Jan	Feb	Mar	April	May	June	July	Aug	Sept	Oct	Nov	Dec
Cold Water Temp (°C)	22.15	22.3	19.4	16.3	13.75	12.8	10.5	11	14.75	16.85	17.8	18.35

Table 4-10. Cold water monthly average temperature for Melbourne (BOM 2009)

An LPG hot water system with a typical 90% efficient burner has been assumed as the basic supply for the remote household hot water system for this case study. The cost of a 45-kg LPG bottle delivered to such a remote area in this case study is assumed to be US\$150.

It is also assumed that 70% of the fuel cell cooling load can be effectively used for boosting this hot water system due to this fact that the heat exchanger connected to the fuel cell is not 100% effective. If the heat exchanger is properly sized for the system, its effectiveness can be above 70%; however, still the conservative assumption of 70% was used for this analysis. This effectiveness can be changed as it is one of the inputs of the simulation program.

Recycling the excess hydrogen (collected from the exit hydrogen stream of the fuel cell) back to the hydrogen tank to be reused in the fuel cell is a possible option; however, a detail economic analysis is required to see if this solution for hydrogen waste recovery is economically viable or not. This option has not been considered to be investigated in this

case study and just for simplicity it is assumed that the excess hydrogen is collected and burned to boost the hot water system.

No additional cost was considered for the economic analysis of the solar-hydrogen CHP system compared to the basic power-only system, since the fuel cell is already a water-cooled one, and the cost of the cooling system has already been counted in the capital cost of the fuel cell system. Also the infrastructure for LPG hot water supply is already there and merely a little extra piping is needed to connect this system to the outlet of the existing water cooling system of the fuel cell.

4.4.3.3 Results

The results of the analysis of the solar-hydrogen CHP system as specified for this case study are presented in table 4-11. Without using fuel cell heat, the annual LPG consumption for supplying the total demand for hot water is 130 kg (that is, 6540 MJ) giving an annual cost of US\$433 (based on US\$150 per 45-kg LPG bottle delivered). Even if the yearly rate of increasing the cost of LPG is the same as the inflation rate, about US\$13 000 is needed for LPG supply to the hot water system over an assessment period of 30 years.

Under the minimum fuel cell condition in the present case study, the fuel cell cooling load can save almost a bottle of LPG (45 kg) at US\$150 per year or US\$4500 over the 30 years of assessment period (if the real cost of LPG remains constant). This is equivalent to about 8% of the total cost of the solar-hydrogen system when a 5% real discount rate is applied over this assessment period. It is to be noted that if a 4% annual increase in the real cost of LPG is considered, the saving out of the fuel cell heat recovery comes to just less than US\$8500 over 30 years of assessment period, which is equivalent to about 15% of the total cost of the system over this period.

For this particular fuel cell (FCS 6432 Model) the possibility of using hydrogen stoichiometry of either 1.1 or 1.2 are given by the manufacturer. Using the latter (1.2) implies considerable hydrogen wastage throughout the year as shown by table 4-4 and table 4-7 (15-20 kg). The theoretical calculation shows that if this excess hydrogen is

collected and just burned at 90% efficiency in a burner to supply further heat to the water heater, another 45-kg bottle of LPG can be saved. Hence taken together with the fuel cell cooling load, the total saving comes to US\$300 per year or US\$9000 over the 30 year assessment period, that is, equivalent to 16% of the overall cost of the solar-hydrogen system over the assumed assessment period (no annual rise in the real price of LPG is assumed). This figure increases to over 30% of the overall cost of the system if just a 4% annual increase in the real price of LPG is taken into consideration.

If an optimally-sized fuel cell is used (figure 4-29), the saving in LPG by using the fuel cell cooling load drops down to just 26 kg per year (figure 4-53), while the saving by consuming the excess hydrogen decreases by just 6 kg to 39 kg of LPG per year. This result is as expected since the optimum size of the fuel cell emits less heat and generates electricity more efficiently.

LPG demand for hot water supply (100 l/day @ 55 °C)		130 kg/year
Results for using minimum fuel cell size		
Saving on LPG when fuel cell heat recovery is applied		45 kg/year
Saving on LPG by burning the excess hydrogen collected from the exit stream (Hydrogen stoichiometry 1.2; burner efficiency 90%)		45 kg/year
Economic advantage of saving on LPG through fuel cell heat recovery over 30 years	0% annual rise in the real cost of LPG	US\$4500 (8% of the overall cost of the solar-hydrogen system)
	4% annual rise in the real cost of LPG	~US\$8500 (15% of the overall cost of the solar-hydrogen system)
Economic advantage of saving on LPG through fuel cell excess hydrogen recovery over 30 years	0% annual rise in the real cost of LPG	US\$4500 (8% of the overall cost of the solar-hydrogen system)
	4% annual rise for the real cost of LPG	~US\$8500 (15% of the overall cost of the solar-hydrogen system)
Results for using optimally-sized fuel cell		
Saving on LPG when fuel cell heat recovery is applied		26 kg/year
Saving on LPG by burning the excess hydrogen collected from the exit stream (Hydrogen stoichiometry 1.2; burner efficiency 90%)		39 kg/year
Economic advantage of saving on LPG through fuel cell heat recovery over 30 years	0% annual rise in the real cost of LPG	US\$2600 (5 % of the overall cost of the optimally-sized solar-hydrogen system)
	4% annual rise for the real cost of LPG	~US\$4900 (9.5% of the overall cost of the optimally-sized solar-hydrogen system)
Economic advantage of saving on LPG through fuel cell excess hydrogen recovery over 30 years	0% annual rise in the real cost of LPG	US\$3900 (7.5% of the overall cost of the optimally-sized solar-hydrogen system)
	4% annual rise for the real cost of LPG	~US\$7300 (14% of the overall cost of the optimally-sized solar-hydrogen system)

Table 4-11. The results of analysis on using fuel cell heat and excess hydrogen for domestic hot water supply

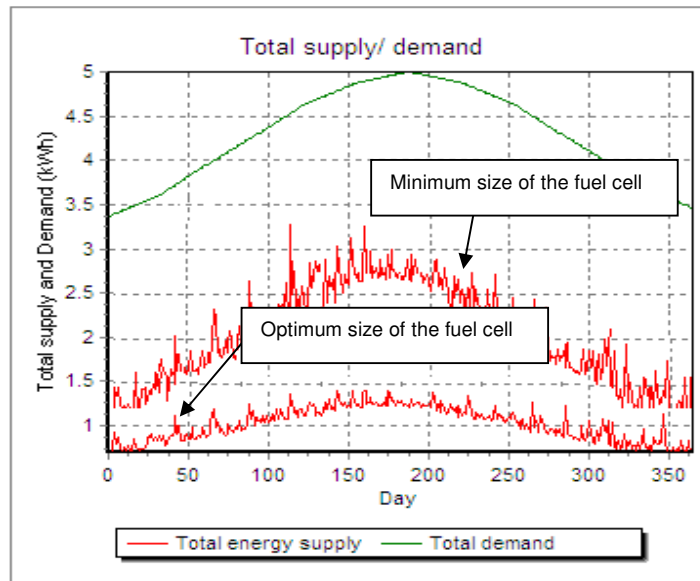


Figure 4-53. Fuel cell annual cooling load and energy demand for hot water supply, on daily basis

4.4.4 System optimisation based on overall economics of CHP system

Earlier in section (4.3.3.3) the system was optimised by minimising the unit cost of electricity produced through using an oversized fuel cell ($\sim 1 \text{ kW}_e$). By doing system optimisation based on the overall cost of the solar-hydrogen power supply system over 30 year assessment period, this cost was reduced from around US\$58000 (equivalent to 1.06 US\$/kWh) to about US\$51500 (equivalent to 0.93-0.94 US\$/kWh). This is noteworthy that the heat generated by the optimally-sized fuel cell is less than that generated by the fuel cell when chosen to be minimum size. Hence the opportunity of saving on LPG (used for hot water supply) in an optimal system is less than that system in which the fuel cell minimum size is used. Considering the benefit of using the fuel cell heat (in saving on LPG) and depending on the price of LPG and how it rises annually (the real value of LPG saved), the system optimisation was reconsidered. The overall present cost of the solar-hydrogen system minus the present cost of the total LPG saved over a given assessment period, the term that is named here Reduced Cost (RC), was used to assess the economics of the system for optimisation purpose. Based on this analysis, the optimally-sized fuel cell (the $\sim 1 \text{ kW}_e$ fuel cell previously obtained based on minimising the unit cost of electricity generated) does not necessarily lead to minimum RC for the solar-hydrogen system. As shown in figure 4-54 (obtained using RSHAP) the optimally-sized fuel cell ($\sim 1 \text{ kW}_e$), is

still better than the fuel cell minimum size (0.31 kW_e) economically based on the RC of the system if less than about 7.3% annual rise in the real price of LPG occurs. Otherwise (if the annual rise in the real price of LPG is above 7.3%) using fuel cell minimum size is the best option economically (figure 4-55). In fact, 7.3% is a high percentage of annual rise in the real price of LPG and is unlikely to be experienced in reality over a full 30-year assessment period.

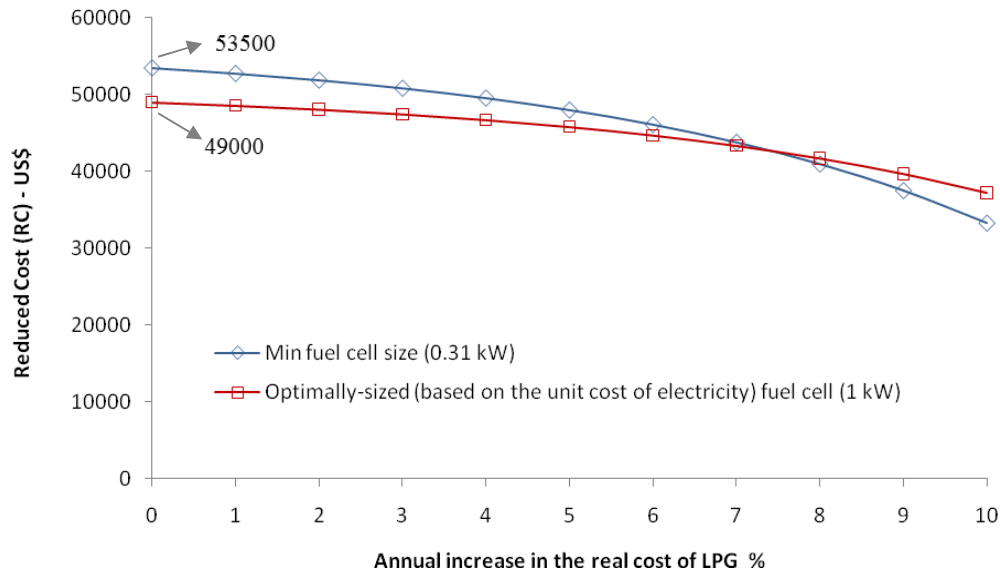


Figure 4-54. Economics of solar-hydrogen CHP system when using the fuel cell minimum size and optimally-sized fuel cell (based on power only application) and considering the value of fuel cell heat recovery

Further investigation (using RSHAP) has been done to size the system for achieving the best economic value when both heat (to boost the LPG hot water system) and power are extracted from the fuel cell. The results of this investigation (figure 4-55) shows that the already optimal system in power only application (see section 4.3.3.3) is still the best system economically in a CHP application (over an assessment period of 30 years and using 5% real discount rate) when the real price of LPG rises at less than 4% annually. For the annual LPG real price rises of above 8% the system in which the minimum fuel cell size was used is recommended. If the annual rise of LPG price is between 4% and 8%, the fuel cell size of 0.6 kW_e used in the solar-hydrogen system leads to just slightly and not much better economics ($\sim 0.1\text{-}1.8\%$) than the systems based on either the fuel cell minimum size or the 1-kW optimally-sized fuel cell (based on the unit cost of electricity). The maximum improvement of $\sim 1.8\%$ (when the 0.6 kW_e fuel cell is used) occurs when

the annual rise in the price of LPG is about 7.3%. The overall cost of the solar-hydrogen system in which this 0.6 kW_e fuel cell is used comes to US\$52450 (equivalent to ~0.96 US\$/kWh) and the saving on LPG is equivalent to US\$10300 over 30 year assessment period (7.3% annual rise in the price of LPG). Hence, the reduced cost of the system is US\$42150, which is about US\$800 (1.8%) less than that of the system in which either the optimally-sized or minimum size fuel cell is used. This maximum of 1.8% is negligible considering the possible sensitivities of the results to the assumptions made; hence, still using figure 4-54 for solar-hydrogen CHP optimisation is recommended.

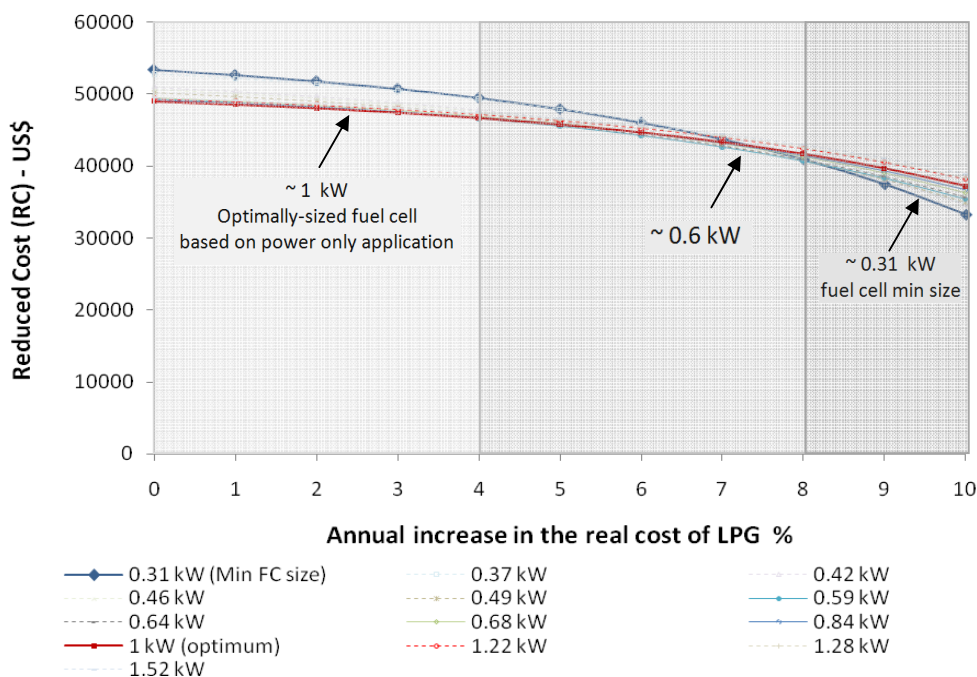


Figure 4-55. Economics of solar-hydrogen CHP system when using different sizes of fuel cells and considering the value of fuel cell heat recovery

4.5 CONCLUSION

A solar-hydrogen system with and without CHP for a remote household in south-eastern Australia with a total daily demand of 5 kWh peaked at 0.3 kW has been studied in detail using RSHAP. For the basic system without CHP, constraining the hydrogen tank to smaller sizes was not found to be effective in reducing the cost of the system. On the other hand, a greater than 12% reduction in the unit cost of electricity (and correspondingly the overall cost of the system) was achieved (from 1.06 US\$/kWh to 0.93-0.94 US\$/kWh) by

over sizing the fuel cell above the minimum capacity required (based on the peak of the electrical demand).

The possibilities of converting the basic solar-hydrogen system to a CHP system by recovering the heat generated by the fuel cell and the heat extracted from burning the excess hydrogen (from the exit hydrogen stream of the fuel cell) to be used for boosting a LPG hot water system have also been investigated. In this case, fuel cell heat recovery could increase the average annual energy efficiency of the fuel cell in the solar-hydrogen system from 33% in power only generation to about 63% in heat and power generation that is in CHP mode. When the fuel cell minimum size is used in the system, recovering this heat led to about 35% saving on LPG consumption (used for hot water supply) equivalent to about 15% of the overall cost of the system over an assessment period of 30 years when 4% annual increase in the real cost of LPG is assumed (8% if no annual rise for the real price of LPG is assumed). For the hydrogen stoichiometry of 1.2 assumed for this study the effect of excess hydrogen recovery (above 15 kg per year) to be burned in a 90% efficient burner was estimated almost the same as fuel cell heat recovery. Employing these two possibilities together can lead to a huge saving of about 70% on LPG normally used for hot water supply, which is equivalent to about 30% of the overall cost of the system (4% annual increase in the real cost of LPG was assumed). When the optimally-sized fuel cell was used in the system the saving figures on LPG were found 20% and 30% (50% together) for fuel cell heat and excess hydrogen recovery respectively.

Based on the results of this case study the fuel cell heat and hydrogen recovery are strongly recommended as effective tools to improve the economics of solar-hydrogen systems and increasing the round-trip efficiency of the storage sub-system (electrolyser, hydrogen tank, and fuel cell). For power only applications the system sizing optimisation proved very effective in enhancing the economics of the system and improving the round-trip efficiency of the hydrogen storage sub-system. When it comes to CHP application the economic viability of the optimal system compared to a system with minimum size of fuel cell depends on the annual rise in the cost of LPG. If the annual rise in the real price of LPG (delivered) is less than 7.3% the optimally-sized system (obtained based on minimising the cost of electricity generated) is more economic than a system with minimum size of fuel cell (for a CHP application). If the annual rise in the real price of LPG is less than 4% (the

most likely scenario) the optimally-sized system is the most economical option in CHP mode as well.

In this case study, the PV array is the most expensive part of the solar-hydrogen system; hence it has the first priority for further technological and cost improvement. The fuel cell is the cheapest component of the system. Although improvement in the cost of the fuel cell does not play a considerable role in reducing the overall cost of the system, any improvement in its electrical efficiency and hydrogen utilisation (technological improvement) can considerably enhance the economics of the solar-hydrogen system.

5 Experimental investigation into a fuel cell combined heat and power system

5.1 INTRODUCTION

Some of the research questions have already been partially answered using the theoretical investigation in the case study presented in the previous chapter. However, before giving more complete answers to these questions, the reliability of the results has to be tested using an experimental investigation. Based on the research questions posed in Chapter 1, the aims of the experimental part of this investigation on fuel cell CHP system are thus to:

- investigate how the fuel cell chosen in the case study performs compared to the performance predicted by the manufacturer,
- estimate the amount of heat that can be recovered through the fuel cell cooling system, and
- determine the factors that affect the performance of the fuel cell in both heat and power generation.

Running a fuel cell requires a very strict safety regimen to minimise the potential hazards associated with working with hydrogen. An appropriate safety set-up system has therefore been designed and implemented to support this experimental work.

5.2 EXPERIMENTAL SETUP

5.2.1 Overall system studied

The overall experimental setup is shown schematically in figure 5-1. A 500 W_e PEM fuel (similar to that used in the case study in Chapter 4), made by BCS Inc. and running on air/oxygen and hydrogen, has been employed. The fuel cell is water-cooled, which facilitates measuring the cooling load compared to an air-cooled cell. The hydrogen is supplied by a high pressure BOC hydrogen bottle (~13.7 MPa), regulated to about 50 kPa before the gas enters the fuel cell. Between the hydrogen bottle and the fuel cell, a number of safety measures have been implemented to minimise the risks associated with a hydrogen experiment and to conduct the experiment in a highly-safe environment.

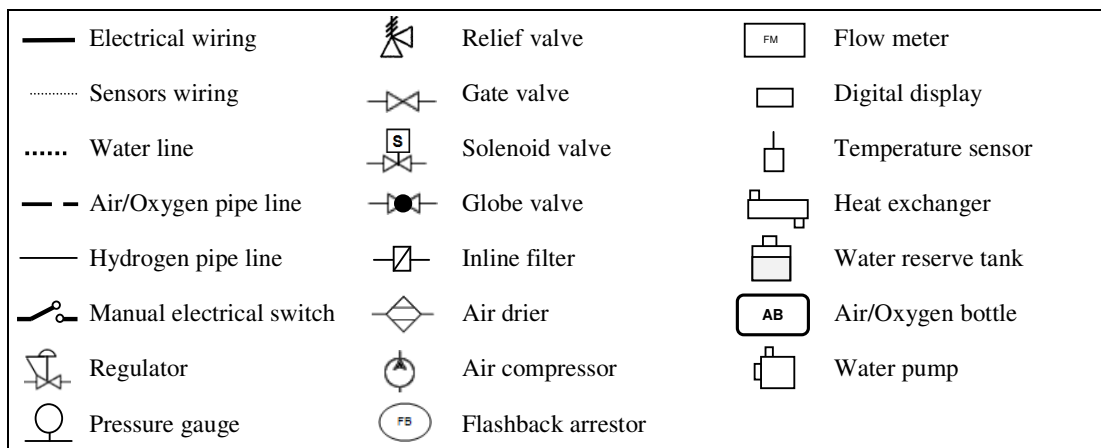
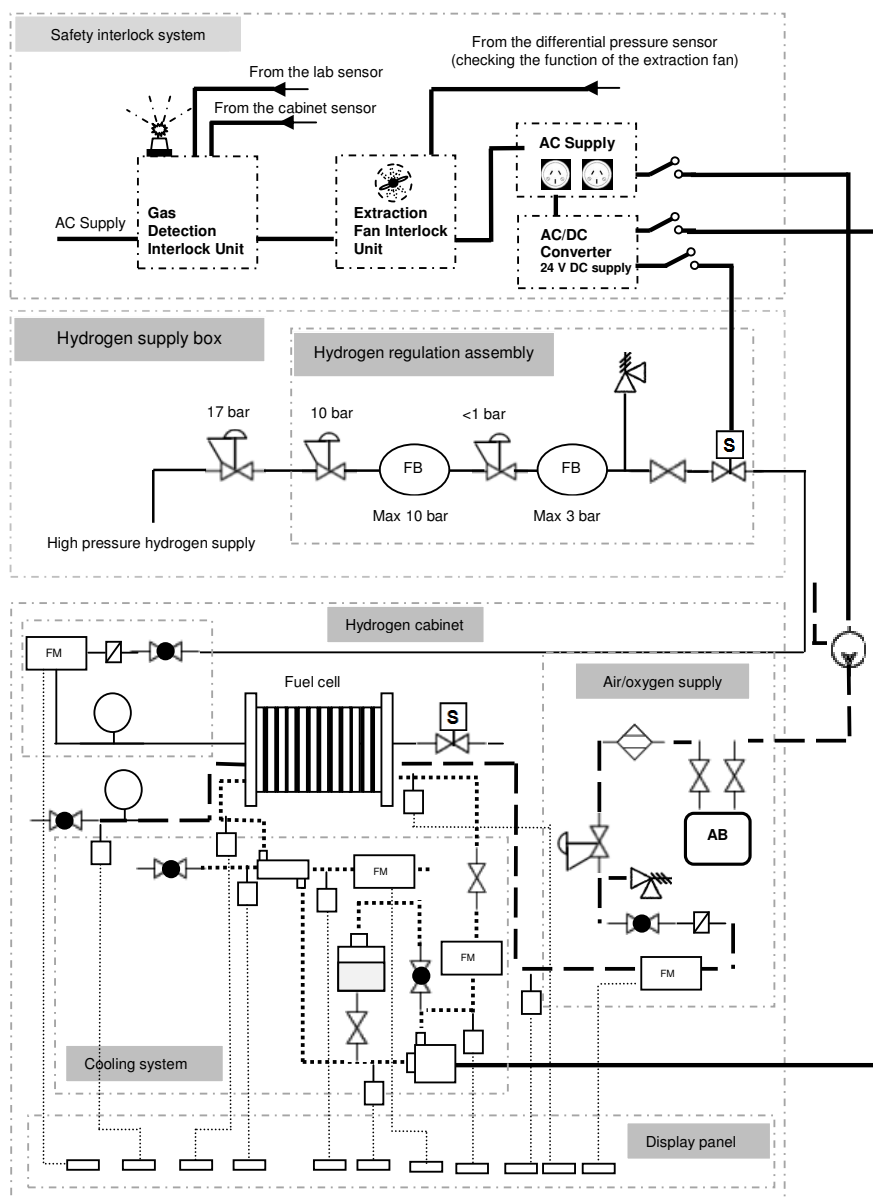


Figure 5-1. An overview of the experimental rig

5.2.2 Hydrogen supply line

5.2.2.1 Overall plan

An overview of the hydrogen supply line is shown in figure 5-2. Hydrogen is supplied from a high-pressure tank and then regulated to low pressure (about 50 kPa) for use in the 500-W fuel cell by passing through two regulators connected in series. A solenoid-operated valve is located at the outlet of the final regulator (after a manually-controlled valve), which is closed when no electrical signal is received by it. This valve is controlled by the safety interlock system and is allowed to be open only when the extraction fan in the hydrogen experimental cabinet containing the fuel cell rig is functioning correctly and no hydrogen is detected in the laboratory area and its manual switch is on. A manual valve is located between the solenoid valve and the last regulator to add the possibility of another control on the hydrogen supply line (manually) in series with the safety interlock system, so that if the safety system fails the line can still be controlled manually.

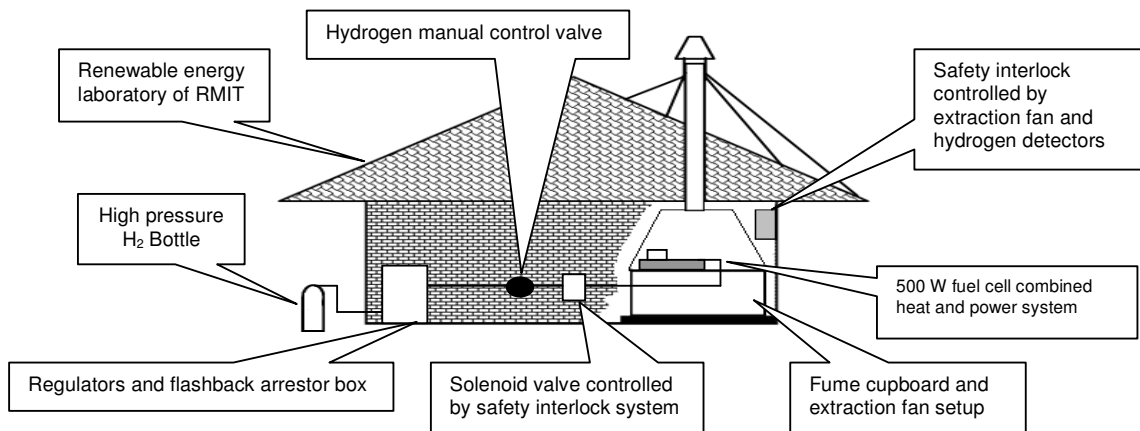


Figure 5-2. An overall view of the hydrogen line

5.2.2.2 Hydrogen bottle

A BOC high-pressure hydrogen bottle (13.7 MPa) supplies hydrogen at the purity of 99.5% to the fuel cell (figure 5-3).

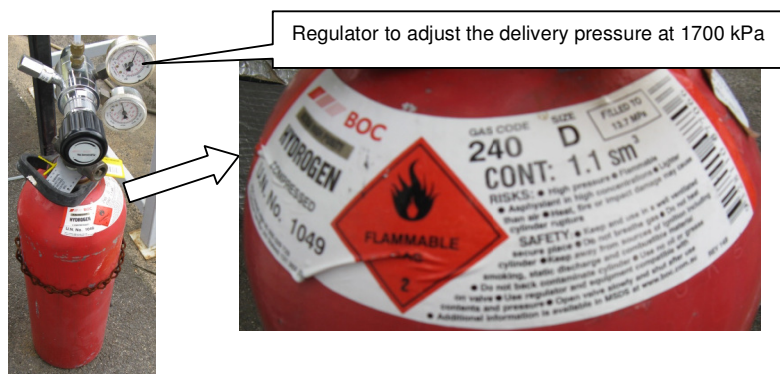


Figure 5-3. 13.7-MPa hydrogen bottle with a regulator preset to maximum output of 1700 kPa

5.2.2.3 Piping and fittings

The connectors, filter, tube, valve, and fittings used for hydrogen line are all Swagelok products (see appendix 7). These parts are mainly ¼” size (NPT thread) and depending on the situation, female, male, or pressure fittings have been used. On the high-pressure side of the hydrogen line only stainless steel parts have been used, and on the low pressure side (about 50 kPa) both brass and stainless steel have been connected to complete the line.

5.2.2.4 Safety setup

Hydrogen is highly flammable over a wide range of concentrations in air (4-75%) and explosive over the range of 15-59% of concentrations at standard atmospheric temperature (DOE 2001). As shown in figure 5-4, the flammability range of hydrogen is a function of temperature. The flammability range of hydrogen is much wider than methane (5.3-15%), propane (2.2-9.6%), methanol (6-36.5%), gasoline (1-7.6%), and diesel (0.6-5.5%) (DOE 2001). However, the auto-ignition temperature of hydrogen at 585 °C, which is the minimum temperature required to initiate self-sustained combustion in a fuel mixture in the absence of a source of ignition, is higher than other fuels (DOE 2001). Hydrogen can carry electrostatic charges (due to its poor electronic conductivity) when flowing through pipes. Releasing this charge in the presence of oxygen is very dangerous due to the low energy of ignition of hydrogen compared to other flammable gases (DOE 2001). Above all, hydrogen has a very low viscosity so the hydrogen line is always subject to the risk of leakage. Hydrogen gas leaks must be detected using gas-specific sensors since the gas is odourless and colourless. All these facts underline the need for a very careful and secure procedure for working with hydrogen during the experiments.

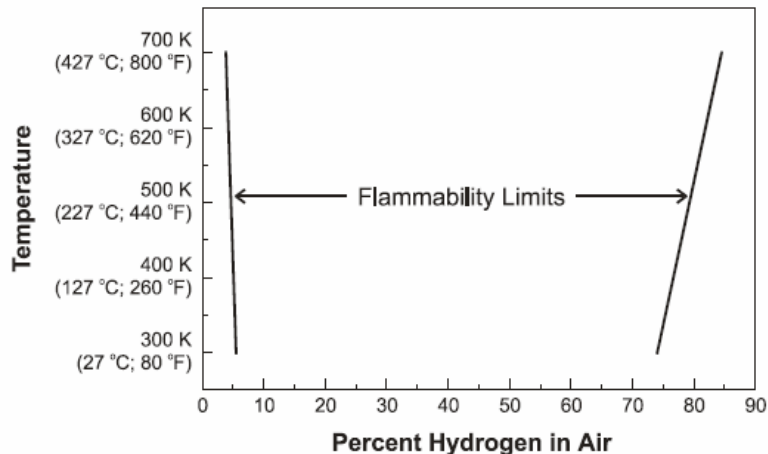


Figure 5-4. Hydrogen flammability level (DOE 2001)

With this requirement in mind, the following steps have been taken:

1. *A series arrangement of manual and solenoid valves, controlled by the safety interlock system to let hydrogen into the laboratory only when it is safe to do so.*

The high-pressure hydrogen is regulated down to about 50 kPa pressure for entry into the fuel cell by four valves in series: the bottle valve and three regulators. The resulting low-pressure hydrogen is controlled by another two valves in series: a manual flow-control valve and the solenoid valve (see appendix 7).

The safety interlock system, shown schematically in figure 5-5, ensures no electrical power is provided to the rig and its peripherals unless the extraction fan inside the hydrogen experimental cabinet is working and no hydrogen is detected by the hydrogen sensors around the laboratory and inside the cabinet. This system originally was designed for an earlier hydrogen experiment and its details can be found in (Paul 2009). This safety interlock system was modified for the present experiment by coupling it to the hydrogen storage safety system and also adding an additional logic circuit for providing AC power under a safe condition. This AC power, which is interlocked with the extraction fan and hydrogen sensors, then goes to an AC/DC converter to supply the DC electrical power to open the solenoid via another manual electrical switch. Hence even if all safety conditions are met for the solenoid valve controlling hydrogen input to the rig, the final step is manual operation of this switch to allow an experiment to commence. The solenoid valve (see appendix 7) is designed for use with neutral and aggressive gases and fluids, e.g.

compressed air, town and natural gas, water, hydraulic oil, vacuum and is suitable for hazardous areas. This valve has been installed outside the laboratory so that if there is any leakage from its connectors, the hydrogen readily disperses. Pressure fittings (tube adaptor and tube fittings) are used to connect the solenoid valve to the hydrogen line, which can easily be connected and disconnected with minimum risk of leakage.

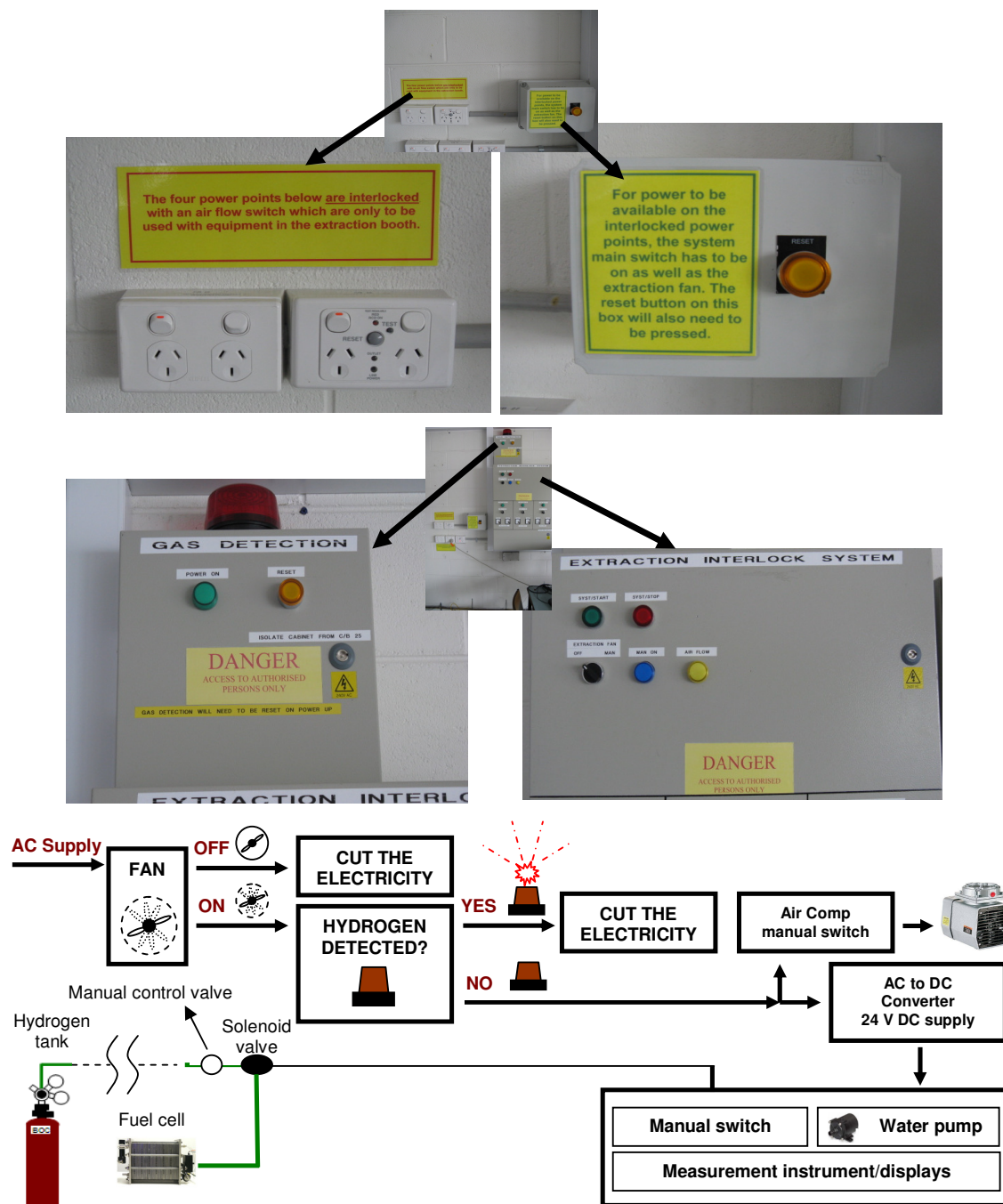


Figure 5-5. A schematic of the safety interlock system used for the experimental study on the 500 W PEM BCS fuel cell

2. A secured regulator and flashback arrestor setup

The regulators and flashback arrestor are installed in a secure enclosed cabinet that is lockable and was specially designed for this project, as schematically shown in figure 5-6. In addition to the regulator installed on top of the hydrogen tank, another two regulators are placed in the hydrogen line, all connected in series. The additional two regulators are placed in the lockable hydrogen storage unit accessible only to authorised people. The regulators are in series to make sure that nothing can go wrong with the delivery pressure of hydrogen to the fuel cell. Even if two regulators failed, the third one will still serve to provide the desirable delivery pressure. The first regulator, which is connected directly to the high-pressure tank, reduces the pressure to a maximum of 1700 kPa, then the second and third one, secured inside the cabinet, reduce the pressure further to 500 kPa and 50 kPa respectively. The second regulator (the first in the enclosure) is preset to deliver at 500 kPa irrespective of the inlet pressure (up to 30000 kPa). This limit is well above the hydrogen tank pressure and even if the tank regulator fails the inlet pressure is within the allowable limit. The third regulator (the second one in the cabinet) is adjustable, and was set to deliver hydrogen at about 50 kPa (gauge) after passing through the solenoid valve and manual control valve. Another safety measure was having two flashback arrestors in series in the hydrogen line. One flashback arrestor is right after the second regulator and can handle 1000 kPa of hydrogen pressure and the second one is installed after the third regulator with the maximum allowable pressure of 300 kPa.

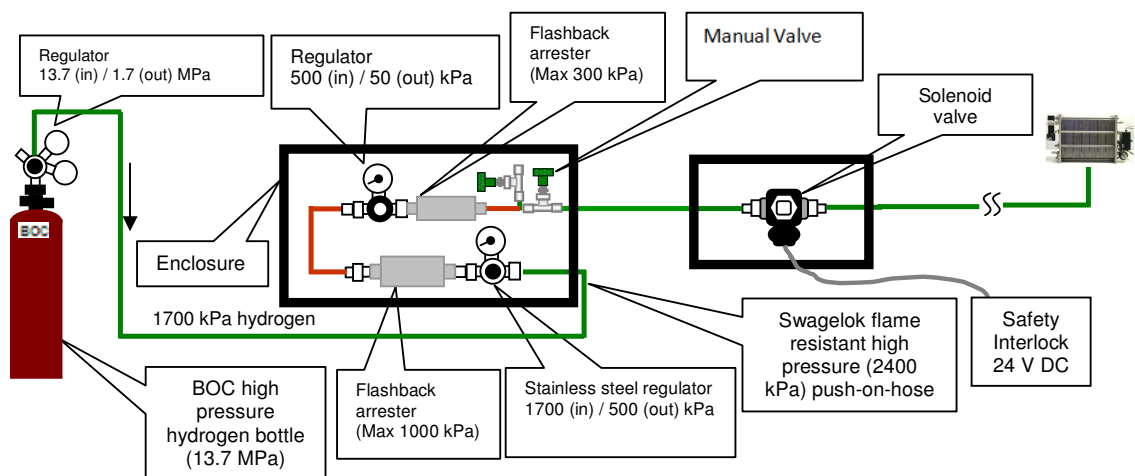


Figure 5-6. Regulator and flashback arrestor arrangement in the hydrogen storage unit

The hydrogen storage setup and the associated safety equipments (regulators, flashback arrestors, and solenoid valve) are shown in figure 5-7.

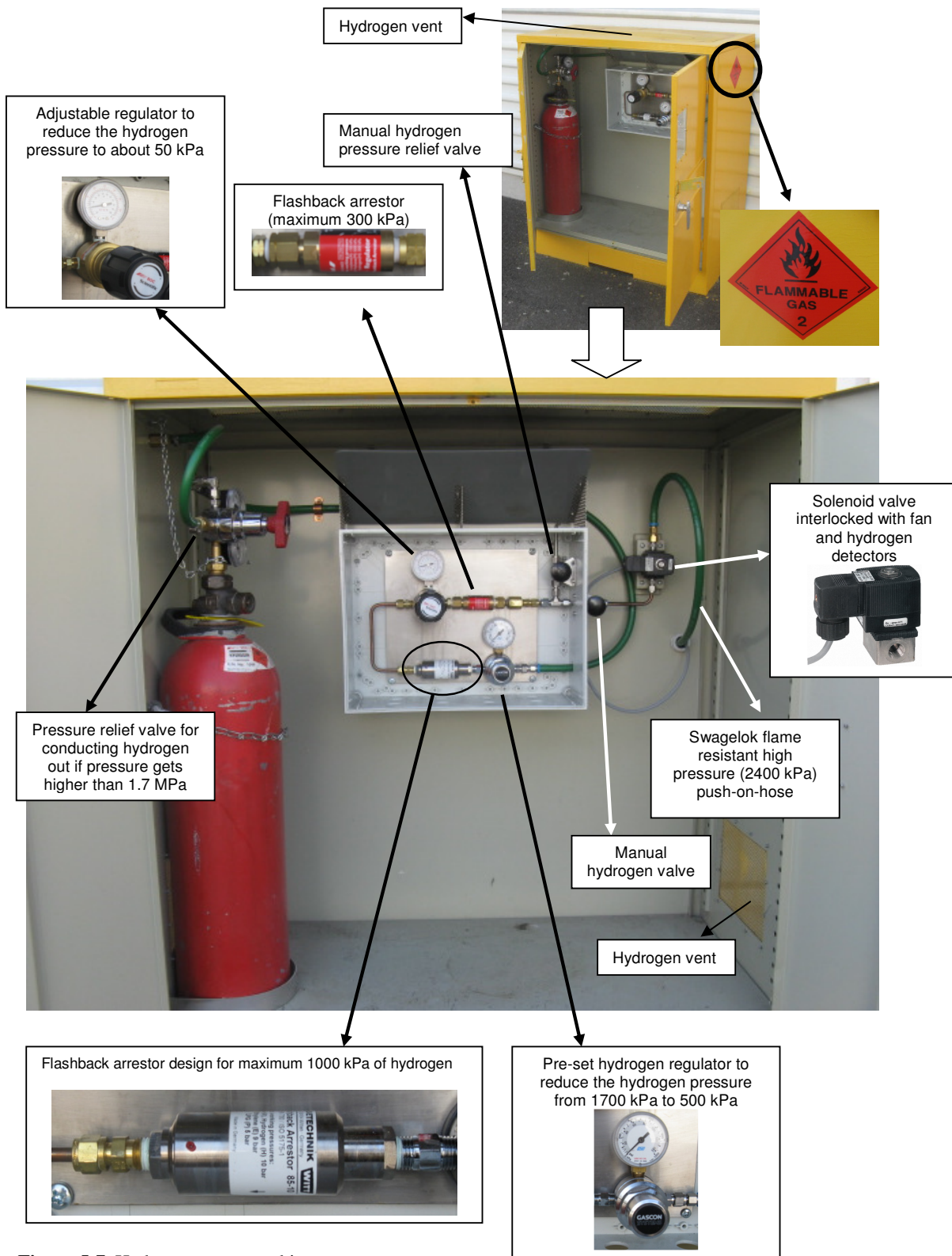


Figure 5-7. Hydrogen storage cabinet

3. Stainless steel fittings for high pressure side of the hydrogen line

As explained earlier the hydrogen pressure is reduced from 13.7 MPa to about 50 kPa before entering the fuel cell. The hydrogen line, from the 13.7-MPa point (hydrogen bottle) to 500-kPa point (after the second regulator), is equipped with stainless steel fittings, with brass fittings used thereafter since the pressure is relatively low (~50 kPa). At such low pressures even the standard equipments such as flashback arrester (300 kPa) and regulator are all made from brass materials.

4. Leak test

The entire hydrogen gas line was checked using special leak-detection soap and a handheld hydrogen detector (see appendix 7) to make sure that no hydrogen escaped from the joints and connectors. The hydrogen line between the high pressure tank and solenoid valve was put under pressure (while the solenoid valve was closed) for about a day to see if any pressure drop was observed thus indicating a leak.

5. Fume cupboard

The experimental setup was placed inside a fume cupboard made from polyvinyl chloride (PVC) shown in figure 5-8. This cabinet is mainly used for hydrogen-related experiments in Renewable Energy Laboratory (REL) at RMIT to make sure that any possible hydrogen leakage is confined to this cabinet. The fume cupboard has been designed and installed by Laboratory Systems Group (Australia) and was initially used for the PhD work done by Paul (2009). It is quite roomy with fairly generous size of 1700 mm (W) × 850 mm (D) × 1200 mm (H). This hydrogen cabinet is equipped with an externally located centrifugal extraction fan (minimum extraction flow rate of 660 l/min) powered by a three-phase motor inside the duct connected to the top of the fume cupboard. Also a hydrogen detector is placed inside the cabinet. No hydrogen detection and proper function of the fan are the preconditions for sending the electrical signal to the solenoid valve to open the hydrogen line. The hydrogen detector in the fume cupboard is supplemented by another hydrogen detector in the general laboratory area, which is integrated into the safety interlock system and works in parallel with the one inside the fume cupboard.

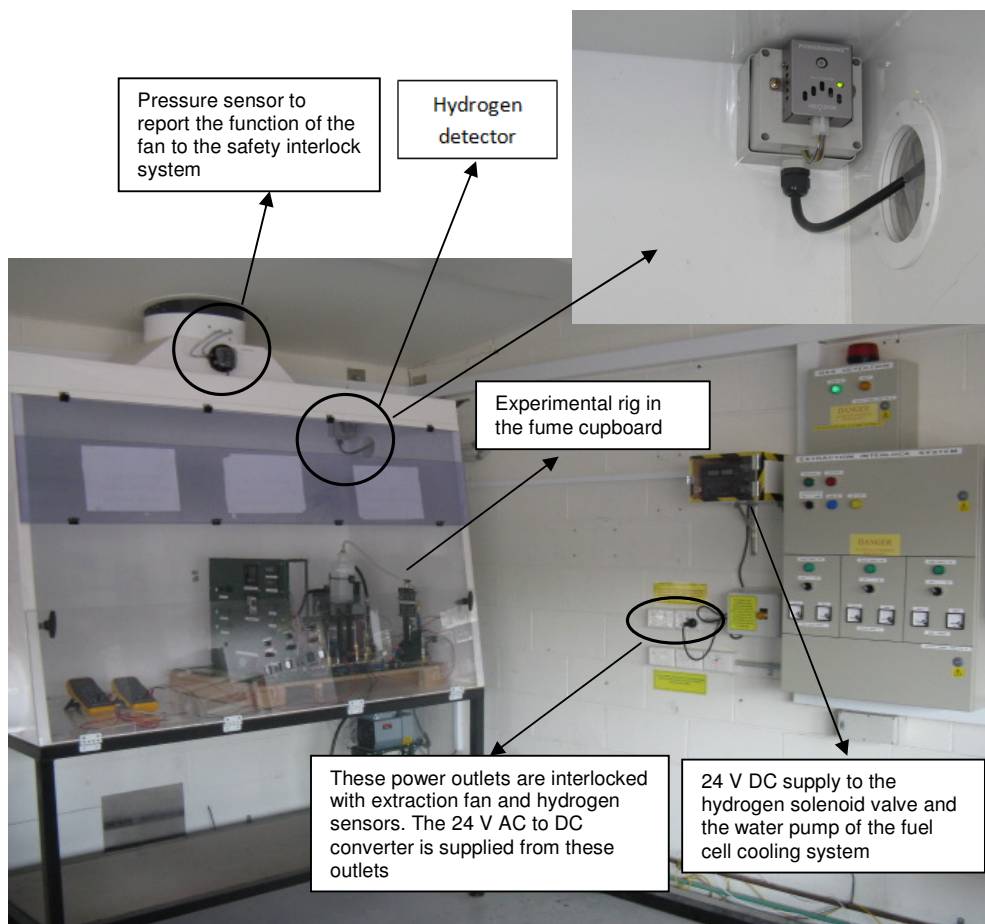


Figure 5-8. Fume cupboard for doing hydrogen-related experiments

5.2.2.5 Measuring instruments

The following measuring instruments were connected on the hydrogen line:

- Pressure gauge:* The pressures of the hydrogen just before entering the fuel cell, and its flow have to be monitored continuously. The pressure gauge has to be oil-free since penetrating of oil into the membrane through the hydrogen flow speeds up the membrane degradation and causes the fuel cell lifetime to decrease. The pressure gauge (appendix 7) is connected to the inlet side of the fuel cell. The fuel cell is operated mainly in dead-ended mode using a solenoid valve to switch periodically to open-ended operation. This valve is part of the fuel cell assembly provided by the manufacturer.

- Flow meter:* The flow meter and controller is a high-precision C100 model from Procon Instrument Technology (Sierra) which was specially calibrated for hydrogen for the range between 0-50 slpm (appendix 7). Figure 5-9 illustrates how it is connected to its neighbouring parts. The complete code for this mass flow meter and controller is C100-L-DD-13-OV1-SV1-D2-V1-S0-C0 and its specifications are described in table 5-1.

Smart -Trak Mass flow controller (C100-L-DD-13-OV1-SV1-D2-V1-S0-C0)	
Flow Range (L)	Flow from 0-10 sccm to 0-50 slpm
Pilot Module Display/Interface (DD)	Pilot module display / interface
Inlet / Outlet Fittings (13)	¼" FNPT (max 200 slpm)
Flow Body Elastomers (OV1)	Viton or equivalent standard
Valve Seat (SV1)	Viton standard
Input Power (Pv2) or (D2)	24 VDC, Linear (Standard)
Output Signal (V1)	4-20 mA and 0-5 VDC, linear
External Set Point Signal (S0)	Pilot module/ RS-232 (standard for DD, RD)
Electrical Connection (C0)	15 Pin mating connector with no cable (standard)
Calibrated gas	Hydrogen
Accuracy	± 1% full scale

Table 5-1. Code description for C100 mass flow controller used for the hydrogen line

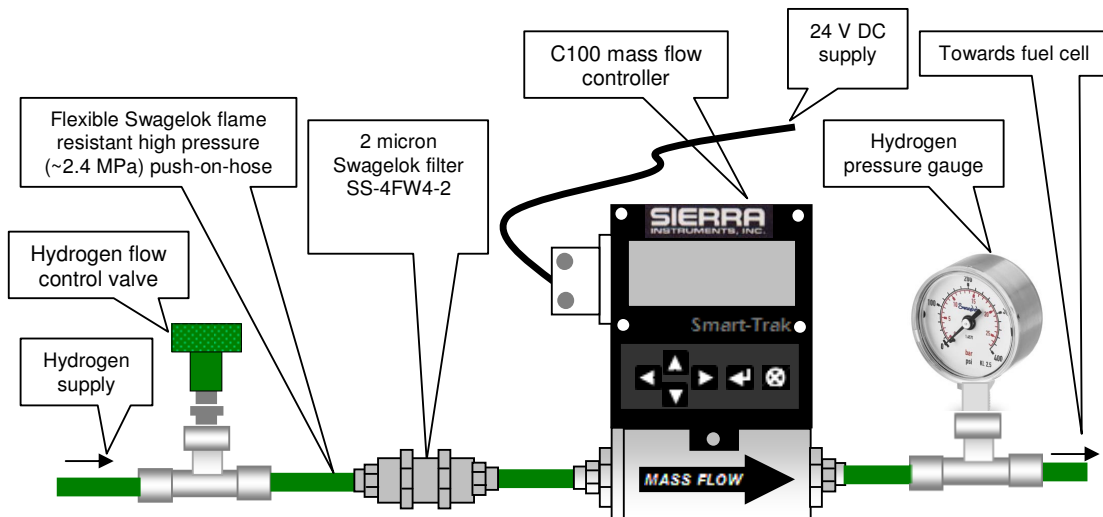


Figure 5-9. A schematic diagram showing how the mass flow meter and pressure gauge are installed in the hydrogen line

5.2.3 Air line

5.2.3.1 Overall plan

A schematic of the air supply line for the fuel cell is shown in figure 5-10. The line includes a diaphragm air compressor, a receiver (acting as a buffer), a regulator setting valve, a filter, a flow meter, and a pressure gauge.

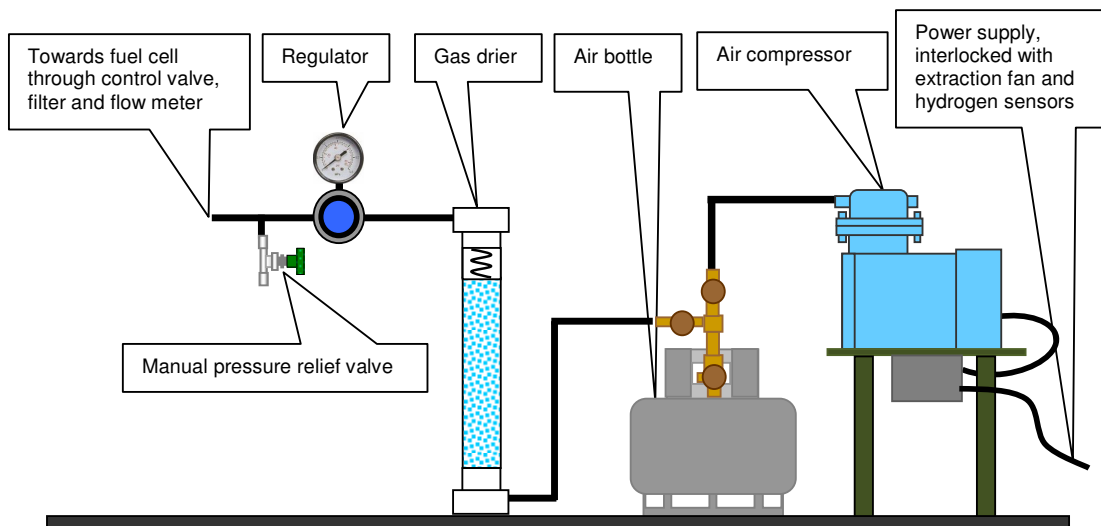


Figure 5-10. A schematic of the air supply line for the fuel cell

5.2.3.2 Air compressor

The compressed air used in the fuel cell is produced on site using an oil-free diaphragm air compressor (see appendix 7 for more details). A standard reciprocating air compressor is not recommended for fuel cell applications since the small amount of oil that may get into the compressed air can accelerate the degradation of the fuel cell membrane. The 1/3 hp (~250 W) air compressor used in the present apparatus is air-cooled, runs on 230 V AC (both 50 Hz and 60 Hz), and has a mass of about 6.6 kg. The air compressor is interlocked with the extraction fan and hydrogen detectors so that it cannot not receive any electrical power unless the extraction fan is in operation and no hydrogen is detected. The maximum pressure of this air compressor is just above 400 kPa (~60 psi); however, the fuel cell needs less than a 100 kPa of air gauge pressure when operating. The temperature of the air in-take by the compressor is recommended by the manufacturer to be between 5 °C and 38 °C.

5.2.3.3 Air bottle

Connecting the air compressor to the fuel cell directly is not practical since simultaneous control of air pressure and flow rate would then be very difficult or impossible. Moreover the outlet pressure of the air compressor is fluctuating whereas the fuel cell requires a smooth stream of air for efficient operation. Hence a gas cylinder is connected between the compressor and the fuel cell to even out the pressure fluctuations. The cylinder used for this purpose is a simple LPG cylinder as used for camping (figure 5-11), which is designed for operating at pressures up to 3000 kPa, but here the air compressor is only able to pressurise the air up to just above 400 kPa.

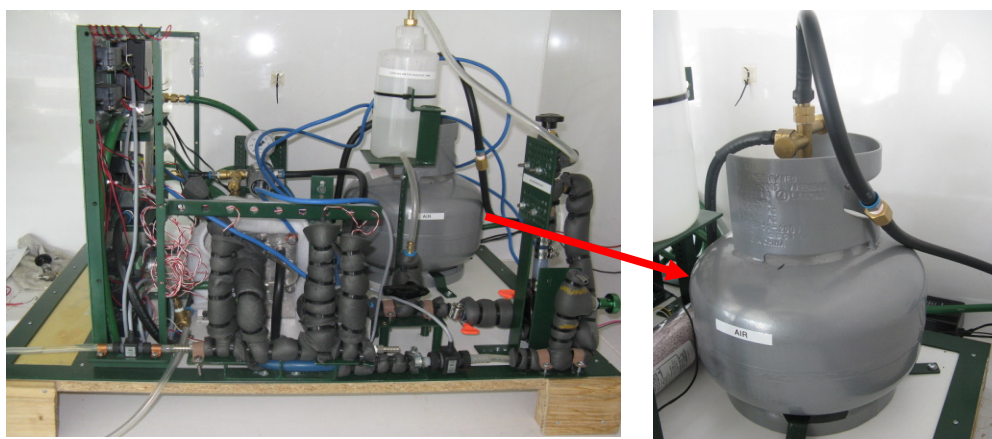


Figure 5-11. LPG camping gas cylinder used as a buffer between the air compressor and air regulator

5.2.3.4 Piping and connectors

The piping, connectors and other fittings on the air side, including push-on hose, a filter, valves, male and female connectors, and T-connectors are similar to the ones used in the hydrogen line.

5.2.3.5 Gas dryer

The compressed air coming from air compressor contains liquid water that could affect the performance of the fuel cell. To prevent these water droplets from entering the fuel cell, a gas drier (figure 5-12) is added right after the air bottle and before the regulators (figure 5-10). Thus the air entering the fuel cell is dry and cannot contribute to potential flooding of membranes inside the fuel cell stack.

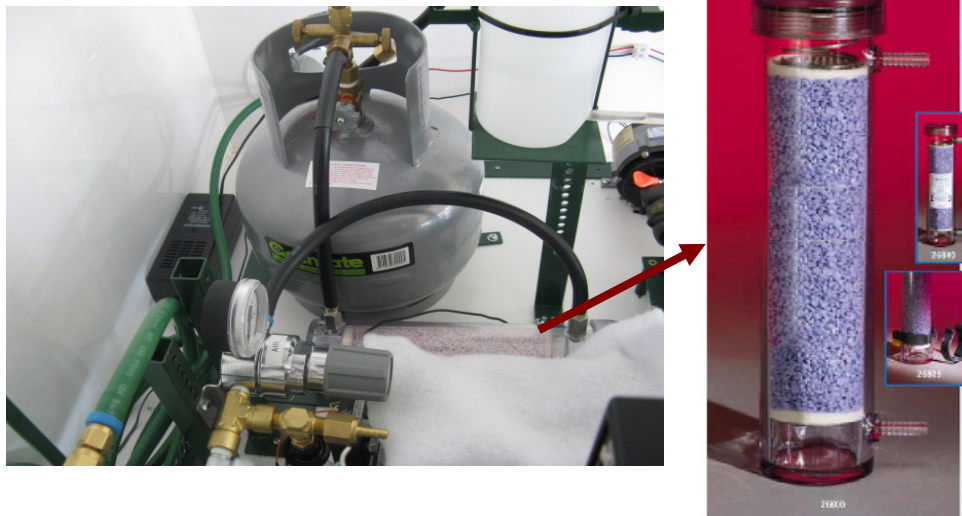


Figure 5-12. Gas dryer used for capturing the moisture in the air before it enters the fuel cell

5.2.3.6 Regulator, measurement, and monitoring instrument

The compressed air is regulated to the pressure required by the fuel cell (about 50 kPa when leaving the fuel cell). Between the regulator and fuel cell, a manual release valve is installed so that if the air pressure rose too high, the pressure in the air line can be released by opening this valve manually (figure 5-10). The regulator set-up is shown in figure 5-13.



Figure 5-13. The air regulator and release valve set-up, as part of 500 W fuel cell air supply line (see figure 5-10)

Similar to the hydrogen line, the air flow rate and pressure are monitored using a flow meter/controller and a pressure gauge (appendix 7). The flow pressure and rate are controlled using two valves located before and after the fuel cell in the air line. The main difference between hydrogen side and air side is that the pressure gauge in hydrogen line is located before the fuel cell but in the air side it is located after the fuel cell. Due to using mainly dead-ended operation on the hydrogen side of the fuel cell, monitoring the hydrogen pressure by putting the pressure gauge in the fuel cell exit port is not possible.

Figure 5-14 shows how the measurement instrument and control tools are placed in the air line. The flow meter (see appendix 7) is an 810C model purchased from Procon Instrument Technology (Sierra) and manufactured by McMillan Company set to show the flow rate in slpm and calibrated to be precise for the range of 0-50 slpm, based on a linear 4-20 mA or 0-5 VDC command signal. The flow meter works on the basis of temperature difference as the air is heated while passing through the flow meter. The higher the flow rate, the higher the temperature of the air which gets out from the flow meter.

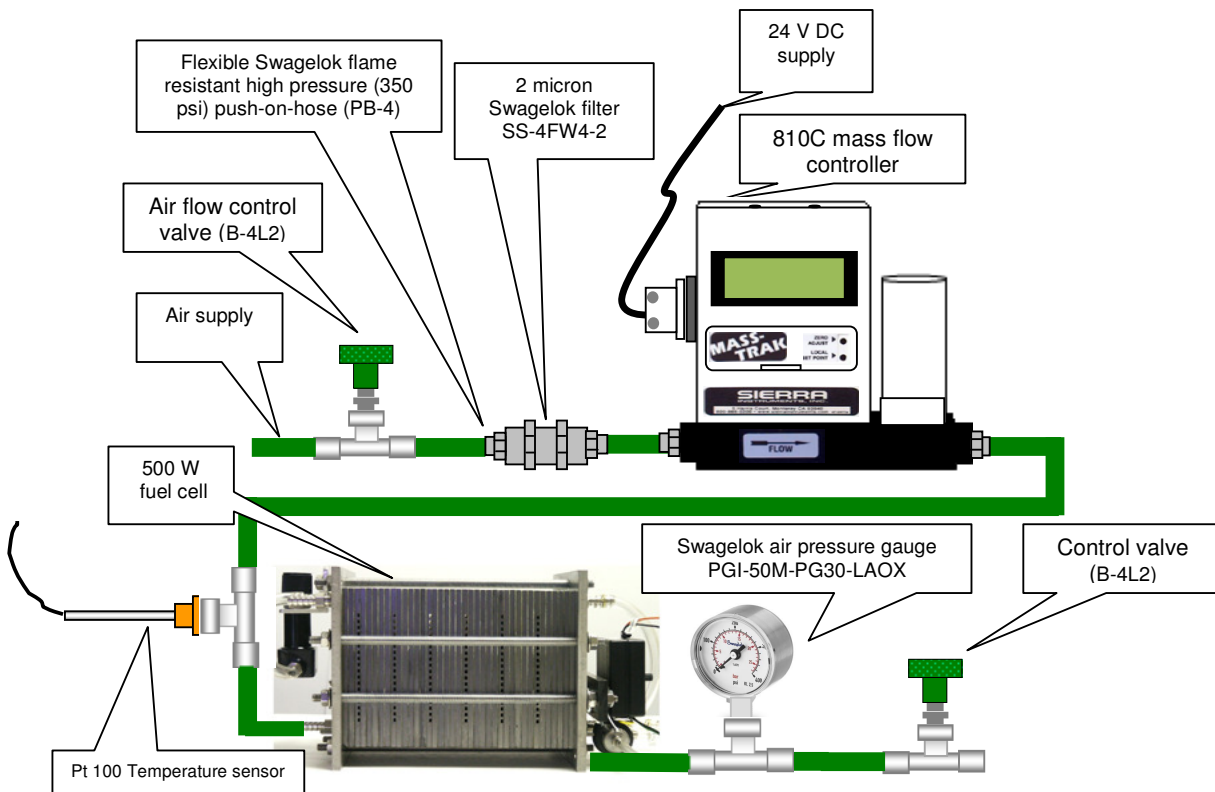


Figure 5-14. Schematic diagram of the mass flow meter and pressure gauge installed in the air side

5.2.4 Cooling system

5.2.4.1 Overall plan

The fuel cell can be cooled by air only when producing less than 200 W of electrical power and by water for larger power outputs. When air cooling is used, it needs to be started as soon as the fuel cell commences operation. Of course it is possible to use water cooling for the whole range of operation. To enable measurement and control of the generated heat, only water cooling system is used in this case study for the entire range of fuel cell operation from zero to maximum power. Water is circulated through the fuel cell water jackets to extract the generated heat to maintain the fuel cell operating temperature at a particular temperature.

The water cooling system, including the measurement instruments, is shown schematically in figure 5-15, and comprises the following parts:

1. Water pump (24 VDC & 3.2 Amps)
2. Miniature heat exchanger (specification to be described later)
3. Flow meters and display to measure the water flow rates on both cold and hot sides of the heat exchanger
4. Temperature sensors and displays
5. Water reserve tank to fill the water cooling system whenever required
6. Tubing, fittings, connectors, and flow control valves (all Swagelok)

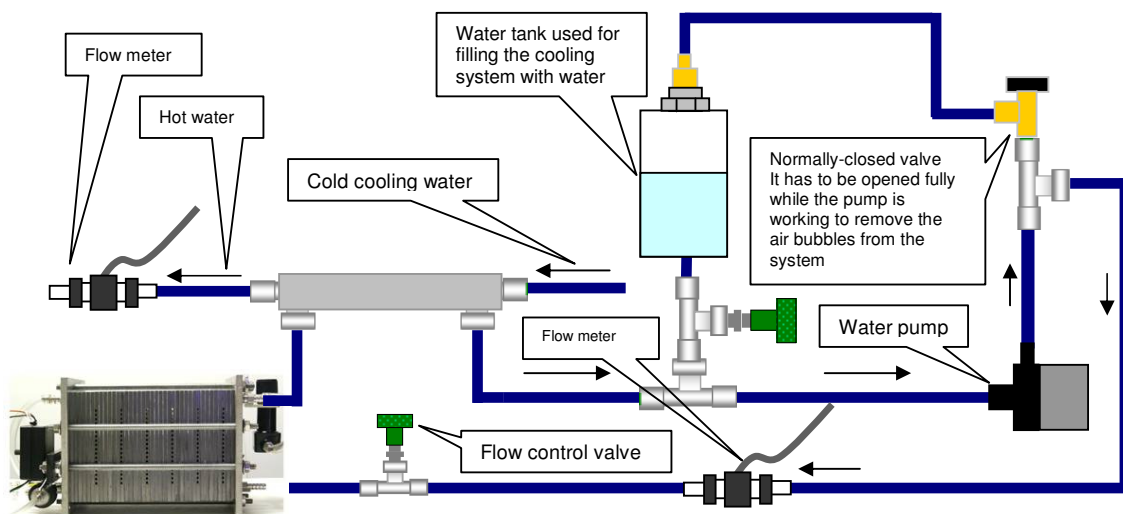


Figure 5-15. A schematic of the fuel cell cooling system

5.2.4.2 Water pump

The water pump injects water into the fuel cell water jackets. The pump was chosen from the Cole Parmer catalogue (catalogue number: 72008-30) and runs on 24 VDC at a maximum 3.2 A (appendix 7). The maximum head of this water pump is 10 m and the maximum flow rate is about 20 l/min. The temperature of the fluid running into the water pump is recommended by the manufacturer not to exceed 50 °C. As recommended by the fuel cell's operating manual, not more than 7 l/min of water pumping capacity is needed for the fuel cell cooling system. Thus the pump has been chosen to cope with the water path pressure drops while supplying this flow of water; however, the water flow rate needed during the experimental part was much less than this maximum flow of water. The pressure drop on the shell side of the heat exchanger is considerably less than on the tube side according to specifications on the manufacturer's website (Exergy 2009). Thus the cooling water passes through the shell rather than the tube to minimise the pressure drop and maintain sufficient water pressure to cope with other pressure drops in the circuit including the water jackets, pipes and connections, the water pump itself, and heat exchanger.

5.2.4.3 Heat exchanger

A miniature heat exchanger (figure 5-16), manufactured by Exergy LLC, specially designed for low-flow applications (Exergy 2009) was used in the fuel cell cooling system. To keep the shell of the heat exchanger and water jackets of the fuel cell clean, deionised water is used in the cooling system circuit. Also the heat exchanger is utilised in the counter-flow configuration, which is more effective than parallel flow in this application.

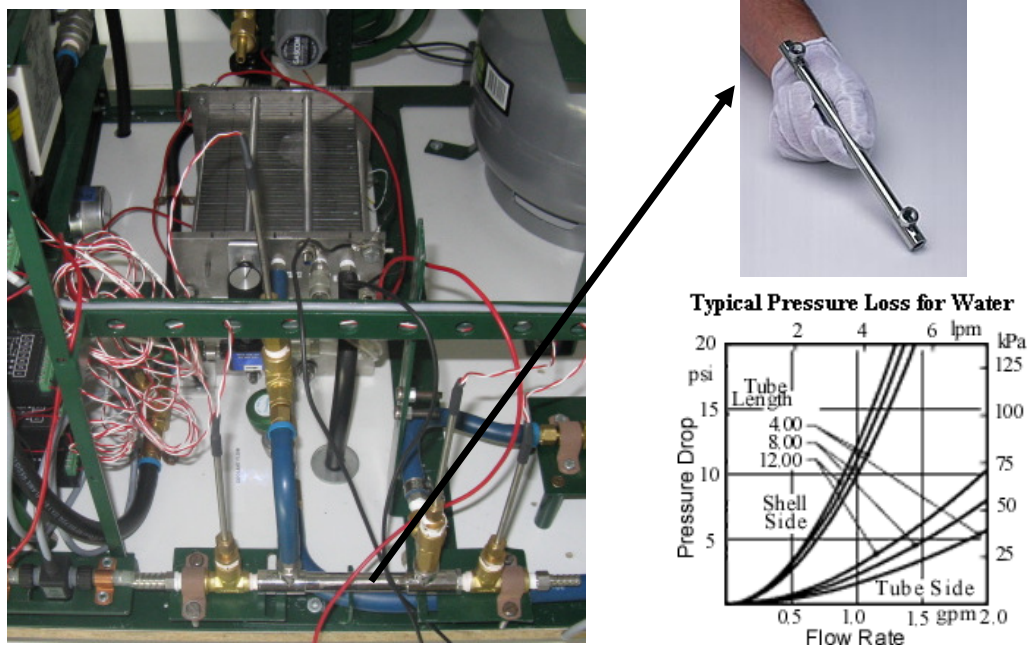


Figure 5-16. Exergy LLC miniature heat exchanger, model: 10 series 00268-2 (Exergy 2009)

The maximum operating limits of the heat exchanger provided by the manufacturer are given in table 5-2. However, in the present case the fuel cell operating conditions are such that it operates well away from these upper limits.

Maximum Operating Pressure for Non-Shock Service	Shell Side	6 900 kPa
	Tube Side	10 300 kPa
Maximum Pressure for Steam Service	860 kPa	
Maximum Operating Temperature	425 °C	
Maximum Average Temperature Difference (LMTD)	70 °C	

Table 5-2. Operating limitations of the heat exchanger, used in the fuel cell cooling system (Exergy 2009)

5.2.4.4 Measurement instrument

The main objective of the measurement instruments on the cooling system line is to measure the cooling load of the fuel cell. Hence two parameters have to be monitored and measured: the flow rates on both the cold and hot sides of the heat exchanger (two flow meters) and the temperatures at all inlets and outlets of the heat exchanger (four temperature probes).

The two flow meters (appendix 7) connected on the shell and tubes sides of the heat exchanger (figure 5-15) are both chosen from Cole Parmer list. The water circulated into the fuel cell passes through the shell side of the heat exchanger. According to the fuel cell manufacturer's manual the water flow rate required for the fuel cell cooling is less than 7 l/min; such a flow rate can be passed through the shell side of the heat exchanger. However, the tube side of the heat exchanger is not designed to allow more than about 2 l/min of water flow. That is why the flow meter connected to the tube side is smaller than that on the shell side. The full specifications of these two flow meters are provided in table 5-3. The smaller flow meter is used when only the exchanger is needed to be studied and the readings from this flow meter are not that critical for this experimental study.

Two McMillan model 220 displays (see the enlarged image in appendix 7) are connected to the flow meters to read the flow rates (figure 5-17). Both displays and flow meters run on a maximum 24 V DC.

	Tube side	Shell side
ColeParmer catalogue number	32250-02	32250-12
Calibration range	0.0 to 0.53 GPM	0.08 to 2.38 GPM
Temperature range	-40 °C and 85 °C	-40 °C and 85 °C
Power supply	24 VDC	24 VDC
Accuracy	1%	1%

Table 5-3. Specifications of the ColeParmer flow meters used in the fuel cell cooling system (ColeParmer 2009)

Four waterproof stainless steel Pt100 temperature probes, chosen from RS Australia list (appendix 7), are used to read the temperatures. The technical specifications of these temperature probes are shown in table 5-4. Two of these probes are placed right before and after the fuel cell and another two are installed before and after the tube side of the heat exchanger to read the fluid temperatures of these key points. The temperature indicators are also from the RS Australia list (RS stock No: 442-0694); they are compatible to the outlet signal of Pt100 probes and all run on DC power.

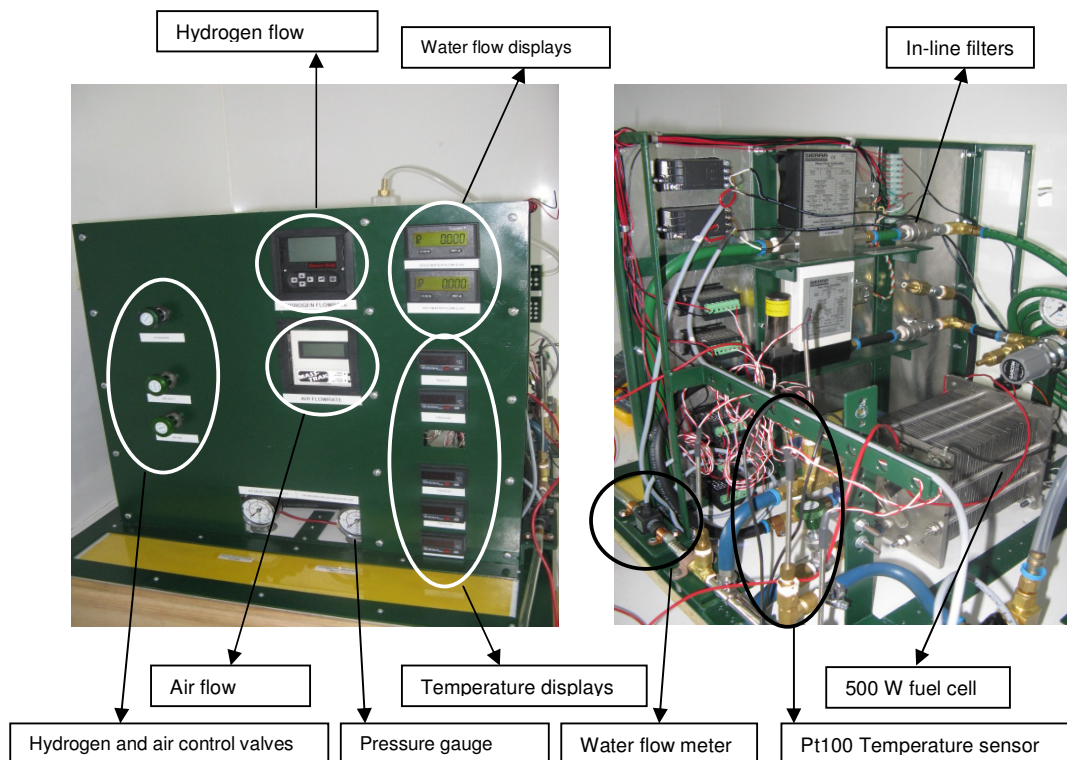


Figure 5-17. Temperature and water flow meters displays

RS stock number	2371663
Operating temperature range	-50-250 °C
Number of wires	2
Probe diameter	4 mm
Probe length	150 mm
Probe material	Platinum (Probe); Stainless Steel (Sheath)
Termination type	Lead
Connection	1/8" BSP (P) brass compression fitting (8 mm thread length)
Accuracy	$\pm(0.1 + 0.00167 \times T) \text{ } ^\circ\text{C}$

Table 5-4. Technical specifications of the Pt 100 temperature probe (RSAustralia 2009)

5.2.4.5 Reserve tank

The reserve tank is used for two purposes: filling the cooling system from coolant (deionised water) in the first place, and topping up the system if water is lost from it. Figure 5-18 shows the position of water reserve tank in the system. When the system is filled through this tank the valve located on top of the pump outlet has to be kept open so that the air of the system can be easily replaced with water. Some air bubbles still might

stay in the system, so while the water pump is running the trapped air can be released if this valve (located on top of the water pump outlet) is kept open for a while.

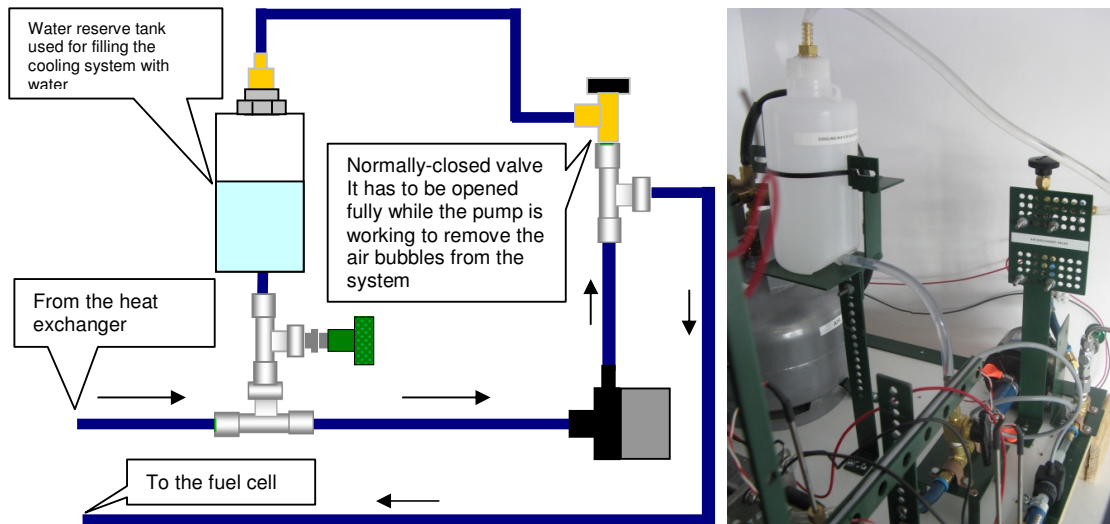


Figure 5-18. The water reserve tank to supply the fuel cell cooling system with water

5.2.4.6 Tubing, valves, and connectors

All the fittings, valves, flexible tubes, and connectors used for the cooling system are Swagelok products and except for the heat exchanger are all of ¼" sizes.

5.2.4.7 Insulation

The main purpose behind designing this experiment is measuring the fuel cell's potential of providing usable heat. So in practice if the fuel cell is used as a CHP unit, it must be designed to capture as much of the generated heat as possible. Hence as shown in figure 5-19 the cooling system including the pipes, connectors and heat exchanger were well insulated before conducting the experiment. Using this insulation layer to cover the fuel cell has also been recommended by Torchio, Santarelli *et al.* (2005) to minimise the convection heat transfer from the body of the fuel cell.

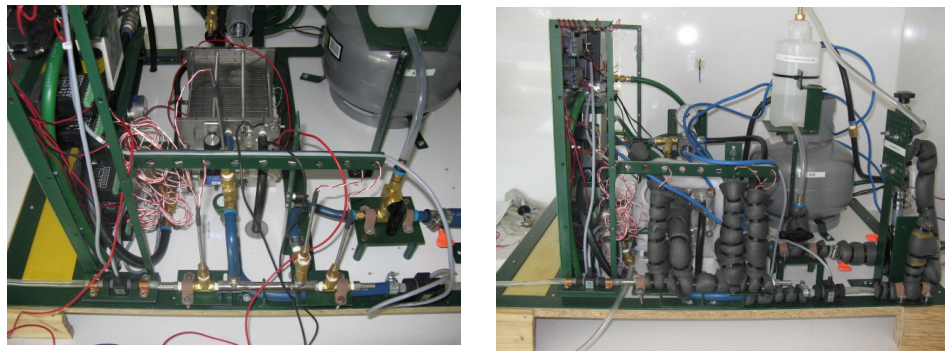


Figure 5-19. Fuel cell and its cooling system before and after insulation

5.2.5 Fuel cell

5.2.5.1 General introduction

The heart of the system is a 500 W PEM fuel cell (FCS 6432 Model), manufactured by BCS (maximum power is above 500 W), and all the components explained so far are just there to run and control it. The following information about this fuel cell is provided in the manufacturer's manual (BCS 2009).

This fuel cell is self-humidified and thus does not need any external humidification. The fuel cell stack comprises 32 cells (each of 64 cm² effective area) and six of these cells have air cooling ducts. The overall dimension of the stack is approximately 20 cm (L) × 14.5 cm (W) × 14.5 cm (H).

The stack comes with a hydrogen pressure controller, solenoid valve, and a control box (figure 5-20, figure 5-21, and figure 5-22). The hydrogen pressure controller keeps the hydrogen pressure delivered to the fuel cell at 20 kPa gauge approximately. The controller is rated at 1035 kPa gauge with air; however, the maximum inlet gauge pressure with hydrogen (into the controller) can be possibly 135-205 kPa. It is better to be conservative with the inlet pressure of hydrogen to the pressure controller and keep it between 35-70 kPa so that the pressure controller operates at a safe pressure, reasonably lower than its maximum allowable pressure (135-205 kPa). To set the controller, the pressure controller knob is to be turned clockwise completely, then 10 turns counter clockwise. The control box shown in figure 5-20 includes:

- On/Off switch
- Fan speed control knob
- Wires for fan
- Timer (purge interval) control knob
- Wires for solenoid valve

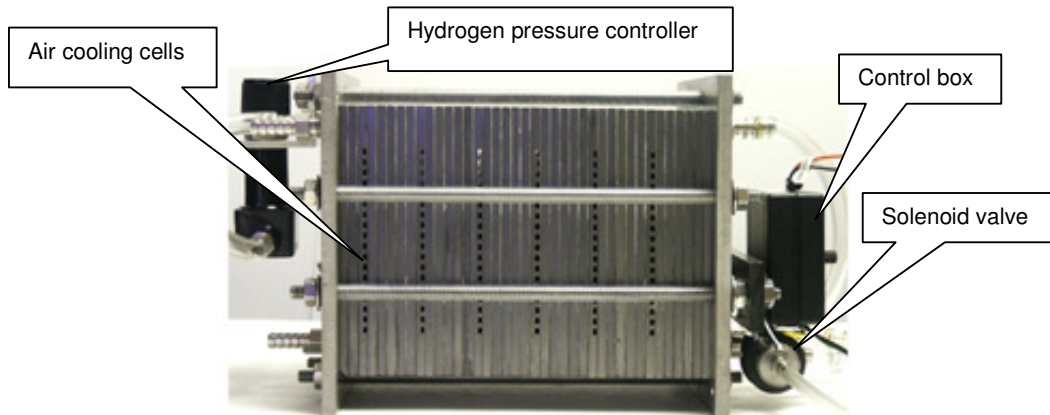


Figure 5-20. The 500 W PEM BCS fuel cell used in the experimental setup

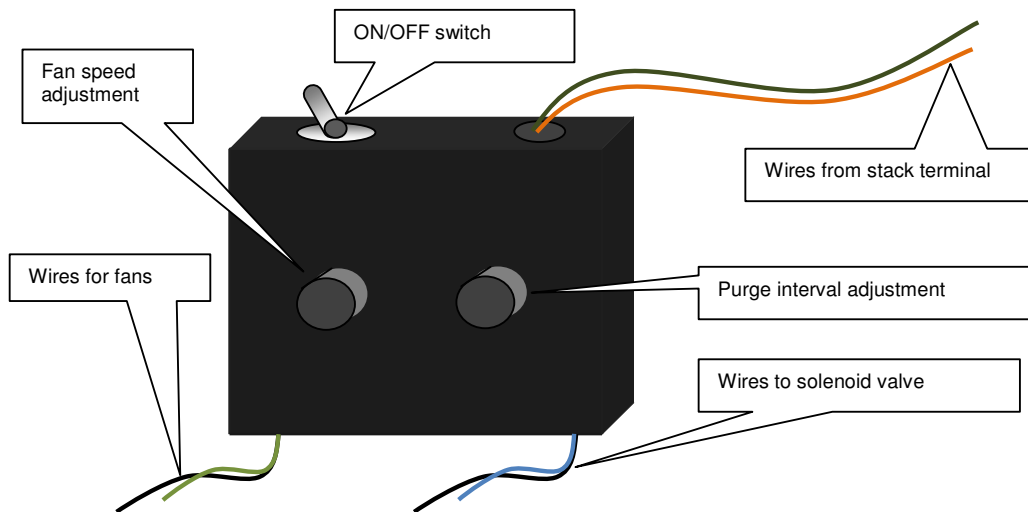


Figure 5-21. The fuel cell control box

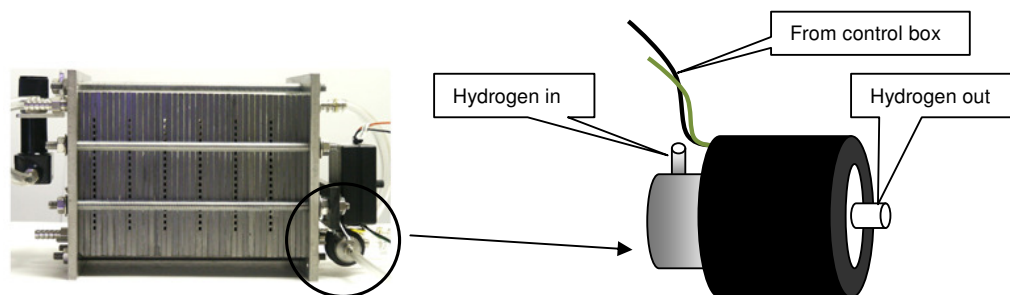


Figure 5-22. Solenoid valve for controlling the hydrogen purging

The solenoid valve (figure 5-22), is connected to the control box and controls the purge interval using a timer located in the box. The hydrogen is cyclically dead ended for a period of about 10 s and then opened for 0.3 s. The dead-end period can be varied, while the release time is fixed. The manufacturer's manual states that the inlet of the solenoid valve should be at the same level as the hydrogen outlet of the stack so that water is easily removed from the hydrogen channels. If the solenoid has rotated during shipping it needs to be returned to the horizontal position. The hydrogen exit tube also has to be checked to make sure that it is not bending upwards. The on/off switching of the solenoid valve should be audible; also the LED light becomes brighter during the on/off time of the solenoid valve.

5.2.5.2 *Manufacturer's polarisation curve*

The polarisation curve of the 500 W PEM BCS, predicted by the manufacturer for the recommended reactant pressures and flow rates, operating temperature and hydrogen dead-ended setting was shown earlier in figure 4-8.

5.2.5.3 *Air flow rates*

For continuous operation of the fuel cell stack, the air stoichiometry had to be maintained between 1.75 and 2.0. Table 5-5, shows the air flow rates recommended by the manufacturer at different currents and air stoichiometries.

Air Stoichiometry	Current (A)					
	5 A	10 A	15 A	20 A	25 A	30 A
	Air Flow Rate (slpm)					
1.5	4.2	8.4	12.6	16.8	21.0	25.2
1.75	4.9	9.8	14.7	19.6	24.5	29.4
2.0	5.6	11.2	16.7	22.3	27.8	33.4
2.5	7	13.9	20.9	27.8	34.8	42.1

Table 5-5. 500 W BCS fuel cell air flow rates (slpm) at different currents and air stoichiometries

5.2.6 Electronic load

A Kikusui PLZ1004W electronic load (appendix 7) was used for measuring the voltage and power variation of the fuel cell against current by varying the load connected to the fuel cell. The specifications of this electronic load are shown in table 5-6.

Kikusui PLZ1004W electronic load		
	Range	Error/Accuracy
Operating voltage (DC)	5V, 15V, 50V, and 150V	±0.1%
Maximum operating current	2 A, 20 A, 100 A, and 200 A	±0.2%
Power rating	10 W, 100 W, and 1000 W	±0.6%
External dimension	429.5 (W)×128 (H)×400 (D) mm	

Table 5-6. Specifications of the Kikusui electronic load

5.3 METHOD

5.3.1 An overview on the experimental plan and procedure

The main aim of the experimental part of this study was to measure the fuel cell heat recovery potential and compare the results with those obtained using the simulation program. It was also planned to investigate some of the controlling parameters to see how they may affect the fuel cell heat and power production. In this regard, the existing rig afforded the possibility of observing the effect of two of these key parameters: air stoichiometry and fuel cell operating temperature on the heat and power output of the fuel cell. These parameters then were investigated at six operating points of the 500 W PEM fuel cell: 5 A, 10 A, 15 A, 20 A, and 25 A.

The experimental part of this research was thus designed to test the reliability of the findings on heat recovery pattern obtained from the theoretical solar-hydrogen CHP system analysis. By using the actual measurements done on the performance of the fuel cell, some of the key assumptions and calculations about the fuel cell efficiency-related parameters, in particular the hydrogen utilisation coefficient, can also be reviewed and corrected if needed.

The following steps were followed to perform the experiment and collect the required data:

1. Check the hydrogen safety system to make sure that the safety equipments are all in function.
2. Check the hydrogen line for leakage using the handheld hydrogen leak detector (if required).
3. Connect the electronic load to the fuel cell.
4. Adjust the fuel cell controller to operate the hydrogen purging solenoid valve to that recommended by the manufacturer (see section 5.2.5.1).
5. Set the hydrogen pressure for gas entry in to the laboratory (when the solenoid valve is switched on) at 50 kPa.
6. Make sure all manual valves (both hydrogen and oxygen lines) on the rig are closed.
7. Switch all the measurement instruments and associated display panels on.
8. Let the air compressor runs for a few minutes before running the fuel cell so that enough air at about 400 kPa is stored in the air tank. Do not shut the air compressor while operating fuel cell; this ensures continuous air supply to the fuel cell at about 50 kPa for a required flow rate.
9. Adjust the air flow rate based on the air stoichiometry of 2 or 4 (see table 5-5).
10. Adjust the exit air pressure to about 30 kPa by using the two valves in the fuel cell air inlet and exit (have to be adjusted simultaneously).
11. Open the manual hydrogen valve (the valve right before the solenoid valve) located in the yellow cabinet (see figure 5-7). Note that the hydrogen solenoid valve (in the hydrogen storage cabinet) is still closed at this stage.
12. Switch on the hydrogen solenoid valve.
13. Open the hydrogen valve located on the rig.
14. Adjust the electronic load to operate the fuel cell at 5 A operating current. This load has to be continuously monitored and adjusted since it fluctuates a bit during the experiment.
15. Let the water pump run to circulate water into the fuel cell and shell side of the heat exchanger while keeping the tube side of the heat exchanger closed.
16. Keep operating the fuel cell until the exit water from the fuel cell goes a few degrees above the desirable operating temperature. For example, if intending to have the fuel cell operated at about 40 °C, let the fuel cell operates until the exit water temperature goes to about 43-44 °C. The fuel cell inlet water temperature is normally at about the same temperature while the tube side of the heat exchanger

- (normally connected to the tap water) is closed. This temperature is used as an indicator of the operating temperature of the fuel cell.
17. Open the tap water into the tube side of the heat exchanger.
 18. By adjusting the water flow rates at shell and/or tube side of the heat exchanger try to maintain the mean water temperature (between the inlet and exit of the fuel cell on the shell side of the heat exchanger) at about the fuel cell test temperature (e.g. 40 °C).
 19. Wait for a few minutes to make sure that the fuel cell is operating at a steady state condition.
 20. Start recording the data including fuel cell voltage, water flow rate into the fuel cell (on the shell side of the heat exchanger), hydrogen flow rate (consumption), and the water temperatures before and after the fuel cell.
 21. Repeat the reading maybe every 30 seconds or so for about 10 times so that the average of all these readings can be used for that particular operating point (e.g 5 A).
 22. Switch off the hydrogen solenoid valve and the water pump.
 23. Keep the air flow going for at least 5 minutes (do it at low pressure like just 10-15 kPa). This is to remove the water from the fuel cell and drying the membrane so that the fuel cell will become ready for the next run.
 24. Shut down the rest of the system (fan, air compressor).

The same procedure was followed at different fuel cell operating points (10 A, 15 A, 20 A, and 25 A), another two operating temperatures (50 °C and 60 °C), and air stoichiometries of 2 and 4.

To minimise the effect of human error and random measuring-instrument error, each operating point was monitored for a while and measured several times (10 times or more) to obtain an average figure about the extracted heat and power at that operating current. While it is questionable how many readings are needed to make reliable measurements, ten is a trusted number of readings suggested by many experts (Bell 2001), and used in this study. Figure 5-23 is an example of how this multi-measurement scheme was followed. The full tables of measurements are available in the appendix 2.

Current (A)	Voltage (V)	Fuel cell electrical power output (W)	Fuel cell inlet cooling water temperature (°C)	Fuel cell exit cooling water temperature (°C)	Cooling water flow rate through fuel cell (l/min)	Fuel cell cooling load (W)
10	20.63	206.3	48	50.5	1.426	248.36
10	20.42	204.2	47.3	49.8	1.429	248.88
10	20.84	208.4	47.5	50	1.421	247.49
10	20.67	206.7	47.2	49.8	1.433	259.56
10	20.46	204.6	47.5	50	1.432	249.41
10	20.85	208.5	47.7	50.2	1.428	248.71
10	20.73	207.3	47.5	50.1	1.423	257.75
10	20.79	207.9	47.9	50.4	1.429	248.88
10	20.86	208.6	47.6	50.2	1.428	258.66
10	20.82	208.2	47.6	50.1	1.438	250.45
10	20.98	209.8	47.9	50.3	1.434	239.76
10	21.01	210.1	48.2	50.7	1.436	250.10
10	20.69	206.9	48.3	50.9	1.42	257.21
10	20.77	207.7	48.7	51.2	1.418	246.97

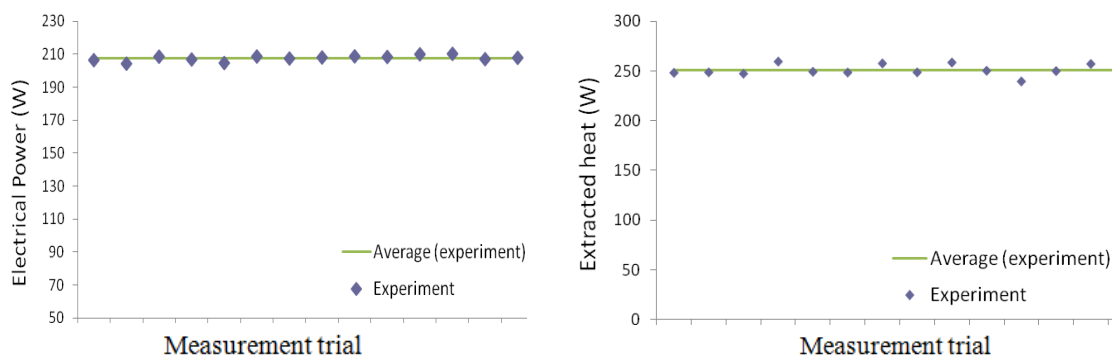


Figure 5-23. 500 W PEM fuel cell cooling load and power curves at 10 A operating point; operating temperature ~ 50 °C, exit air pressure 30 kPa, inlet hydrogen pressure 20-30 kPa, air stoichiometry 2

5.3.2 Restrictions imposed by the measurement instruments

- Fuel cell operating temperature:** The fuel cell is recommended to be operated at 60-65°C but the water pump that circulates the water into the fuel cell has a maximum operating temperature of 50 °C according to the manual provided by the supplier (ColeParmer 2009). However, crossing the water pump operating temperature limit, while still being conservative about it, the experiment has been conducted at 60 °C, at the lower limit of the operating temperature range (60-65 °C) recommended for the fuel cell by its manufacturer (BCS 2009).

- *Air supply line:* The sizes of the available air bottle and air compressor used for this experiment are such that up to 28 slpm could be supplied continuously for a reasonable time span in which the fuel cell reaches a steady state condition ready to be monitored for collecting data. That is why the following operating points have not been measured in this experiment:
 - 30 A at both air stoichiometry of 2 and 4 which need 33.4 slpm and 66.8 slpm of continuous air supplies respectively. The fuel cell heat and power at these points can be predicted by doing extrapolation on the relevant experimental curves if needed.
 - 25 A at air stoichiometry of 4, which requires a continuous air supply of 55.6 slpm.
 - 20 A at air stoichiometry of 4, which requires a continuous air supply of 44.6 slpm.
 - For the case of 15 A an air stoichiometry of slightly less than 4 was used regarding the maximum capacity of the air supply line (28 slpm).

5.3.3 Uncertainties associated with the experimental measurements

Error analysis is an essential part of an experimental study. This error, which is basically the difference between the measured parameter and its true value, leads to a quantification of the accuracy of the measurement, what is called uncertainly here. The precision of a measurement or in other word the associated uncertainly with a measured parameter is limited by the accuracy of the instrument used to measure it. This standard uncertainty which is usually called standard deviation of the mean is calculated using the following equation (Bell 2001):

$$u(x) = \pm \sqrt{\frac{\sum_{i=1}^n (x_i - \bar{x})^2}{n(n-1)}} \quad (5-1)$$

where u is standard deviation of the mean, n is the number is measurements, x is the measured value, and \bar{x} is the mean of x_i 's.

Sometimes the parameter, studied experimentally (Y), is not measured directly as it is a function of a number (N) of other experimentally-measured parameters (x_1, \dots, x_N). Thus the

errors involved in measuring each of these variables (x_i) appear in the experimentally-calculated Y .

$$Y = f(x_1, x_2, x_3, \dots, x_N) \quad (5-2)$$

In this experimental study the fuel cell output powers and hydrogen utilisation coefficients are measured and calculated through direct measurement of just one parameter for each of them; however, the fuel cell cooling load is calculated by measuring other parameters (two temperatures and one flow rate). The measurement of each of them comes with an error due to inaccuracies associated with the concerned measurement instruments. For an experimentally measured/calculated parameter similar to that shown by equation (5-2), the standard deviation associated with indirectly-measured parameter Y is known as combined uncertainty of this parameter and is shown by $u(Y)$. This combined uncertainty is connected to uncertainties associated with measuring each of x_i 's shown by $u(x_i)$, calculated using equation (5-1) or given by the manufacturer of the measurement instrument, and is found using the equation (5-3) (Bell 2001).

$$u(Y) = \pm \sqrt{\sum_{i=1}^N \left[\left(\frac{\partial f}{\partial x_i} \right)^2 \cdot u^2(x_i) \right]} \quad (5-3)$$

Applying equation (5-1) for a measured parameter such as voltage is possible as all the measured values are supposed to be the same. However, equation (5-1) cannot be applied for temperature or flow rate measurements in our case as these parameters are changing in nature and their variations are not because of human error or measurement instrument inaccuracy. The source of this variation is basically coming from the variation in the flow rate itself dictated by the oscillation of the input power to the water pump and needed manual adjustments due to the variation of the uncontrolled tap water flow rates (to keep the fuel cell operated at about a certain operating power). Hence to calculate the combined uncertainty for cooling loads calculated from flow rate and temperature measurements, the uncertainty of the measuring instruments provided by the manufacturers are applied in equation (5-3).

Some examples of how the uncertainties associated with experimentally measured and calculated power, fuel utilisation coefficient, and cooling load have been calculated in the present work are given in appendix 6.

5.4 EXPERIMENTAL RESULTS AND ANALYSIS

5.4.1 Polarisation curve

To make sure that the fuel cell was performing well and close to the manufacturer's specifications, the experimentally-measured performance curves of the fuel cell (V-I polarisation and power curves) were compared with the manufacturer's curves (figure 5-24). These curves were obtained by connecting a variable electronic load (Kikusui PLZ1004W electronic load) to the fuel cell and drawing different currents from the fuel cell: 5 A, 10 A, 15 A, 20 A, and 25 A. As mentioned earlier, for each operating current, the measurements were repeated about 10 times (as in figure 5-23), to check for the reproducibility of the data.

The experimental and manufacturer's polarisation curves are compared in figure 5-24. The two curves correspond very closely for medium to low currents (<20 A) with a maximum difference (voltage for a given current) of about 4%. However, the fuel cell in this experiment performs slightly less well than predicted by the manufacturer at higher currents. In this regard it can be noted that according to the simulation modelling in Chapter 4, an economically optimal fuel cell operates in the low to middle range of currents where the manufacturer's and experimental curves are closely matched. In addition, the fuel cell was operated in the experiment at about 60 °C; and it is expected that increasing the operating temperature to about 65 °C would further narrow the gap between the two curves (according to the fuel cell manual, the manufacturer's curves were obtained at operating temperatures between 60-65 °C). Other possible reasons for the gap between the two curves are as follows:

- At each measured operating point, every effort was made to keep the current constant, but in practice there were some fluctuations in the range of a few percent.
- The fuel cell was purchased in 2006 but had never been operated until the end of 2009. There might thus have been some deterioration in the membrane condition over time.
- Some tolerance is normally associated with manufacturer's specifications so that 100% conformity is not expected.

The precision of the instrument used for voltage measurement was $\pm 0.2\%$ (table 5-6). However, as given in figure 5-24, the average error associated with voltage reading is just

slightly above this maximum expected error ($\pm 0.2\%$). This is not unexpected for the following two reasons:

- There were current fluctuations in the range of a few percent when reading voltage data.
- The inherent error of $\pm 0.1\%$ associated with current measurement (table 5-6).

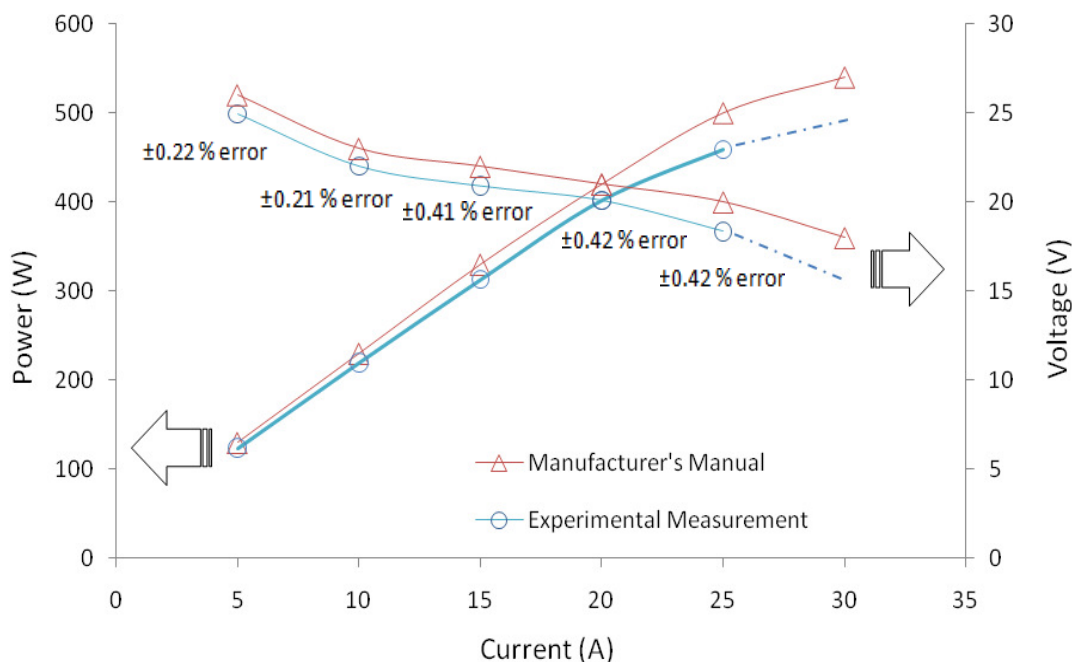


Figure 5-24. Experimental and manufacturer’s predicted polarisation and power curves for the 500 W BCS PEM fuel cell; operating temperature 60 °C; exit air pressure 30 kPa; air stoichiometry 2; inlet hydrogen pressure 20-30 kPa

5.4.2 Cooling load curve

For measuring the cooling load of the fuel cell, the temperatures of water in the cooling circuit before and after the fuel cell as well as the water flow rate were measured. Once again, the measurements of the cooling load were repeated around 10 times for each operating point at a given condition, to check for any departures from reproducibility due for example to, fluctuations in the cooling water (tap water) flow rate , any variations in the response of the measurement instruments, and possible human error. The flow rate of the tap water was found to fluctuate slightly and manual adjustments were made continuously

to minimise the variation. The effect of the remaining variation can be seen in the data taken and measured for the fuel cell cooling load (see the cooling load graphs in appendix 2).

Overall the fuel cell cooling load measurements showed less uniformity than the power measurements. The measured cooling loads were less than those predicted by the model up to about 22 A point and they tend to be greater than those estimated by the model thereafter. The maximum difference between the experimental curve and the one predicted by the model in figure 5-25 is 17% at 10 A operating current. This difference is still within the estimated range of error ($\pm 19.18\%$) calculated based on the error associated with the measurement instruments. Although the differences between the model and the experiment are within the estimated average error for the measured cooling loads, their magnitude reduces to 5-10% once the convection heat transfers from the body of the fuel cell (assumed zero by the model) and the new experimental polarisation curve of the fuel cell (figure 5-24) are taken into account. It is notable that no heat transfer from the fuel cell body was assumed by the model (an ideally-insulated stack); however, in practice a few percent of the cooling load is removed through convective heat transfer from the stack body. Similarly the average experimental errors, (when compared with the model) associated with the other operating currents, are mostly within the acceptable ranges of error shown in figure 5-25, next to these points. The details of the errors associated with every experimentally-measured point are presented in appendix 2.

For the cooling load measurements the errors are more dictated by the uncertainties associated with the temperature sensors than the water flow meter sensors. Hence, the errors associated with temperature sensors are more pronounced when the range of the water temperature variation between the inlet of the fuel cell and its outlet is relatively small (in the range of 2-3 °C). This situation is applicable to low current densities where the fuel cell heat generation is quite low.

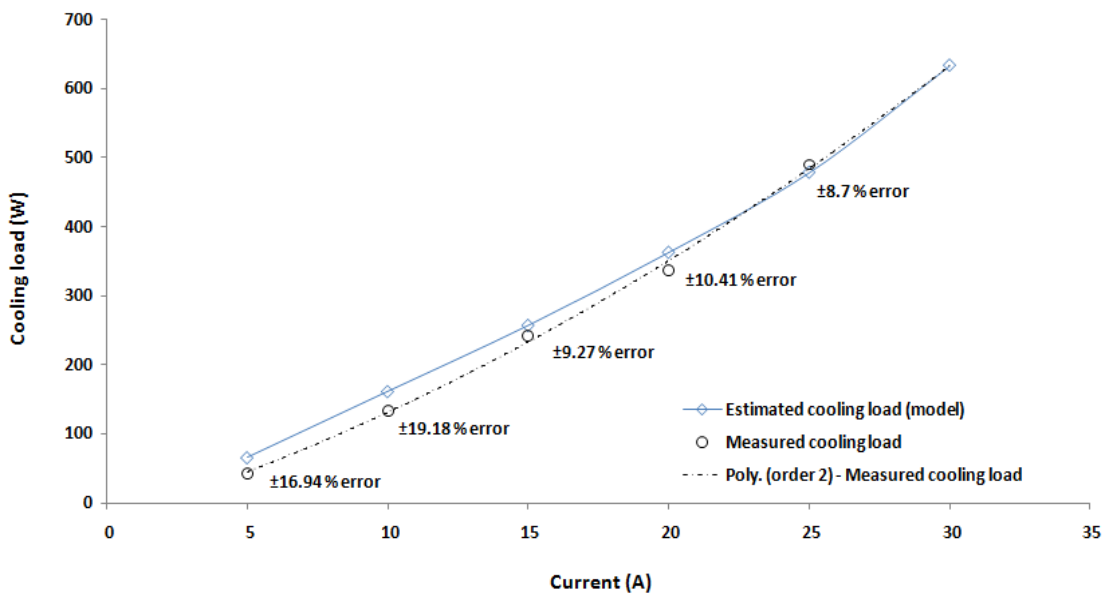


Figure 5-25. 500 W PEM BCS fuel cell cooling load curve; operating temperature 60 °C; exit air pressure 30 kPa; air stoichiometry 2; inlet hydrogen pressure 20-30 kPa

As predicted by the model (figure 4-41), the experimental results also show that the cooling load of the fuel cell is initially less than its power generation, but the situation is the reverse as the current approaches the maximum power point (figure 5-26). This result agrees with the experimental findings of Torchio, Santarelli *et al.* (2005) in which the thermal output of a PEM fuel cell was reported mostly less than its electrical output. A similar trend was reported by König, Weber *et al.* (2005) in their modelling and experimental analysis of a 2 kW_e PEM fuel cell CHP system.

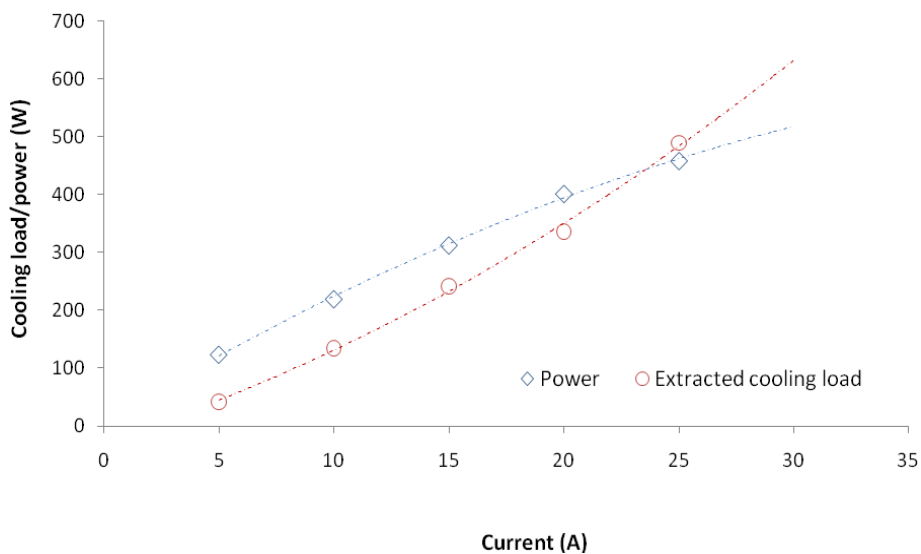


Figure 5-26. 500 W BCS PEM experimental power and cooling load curves; operating temperature 60 °C; exit air pressure 30 kPa; air stoichiometry 2; inlet hydrogen pressure 20-30 kPa

5.4.3 The effect of operating temperature and air stoichiometry on cooling load and power

The experimental setup allowed running the fuel cell when connected to different loads to study the effect of parameters such as air stoichiometry and fuel cell operating temperature on the output electrical power and the cooling load. The operating temperature was the first parameter influencing the electrical output of the fuel cell that was investigated experimentally. The theoretical analysis on this 500 W PEM BCS fuel cell demonstrated that the higher the operating temperature, the higher the cell voltage for a given current will be (figure 5-27). As shown by figure 5-27 produced using the simulation model, as the operating temperature of the cell increased from 40 °C to 80 °C, the voltage of the cell increased by just less than 4%. It is important to note that here it has been assumed that the fuel cell is neither flooded nor dehydrated while operated at the given temperatures. The experimental study on this fuel cell was conducted at three different operating temperatures: 40 °C, 50 °C, and 60 °C (figure 5-28). It can be seen that the gaps between the experimental polarisation curves at these three different temperatures are between 6-9% of the stack voltage for every 10 °C difference in the operating temperature. This change with temperature is considerably more than that predicted by the theoretical model (as shown in figure 5-27).

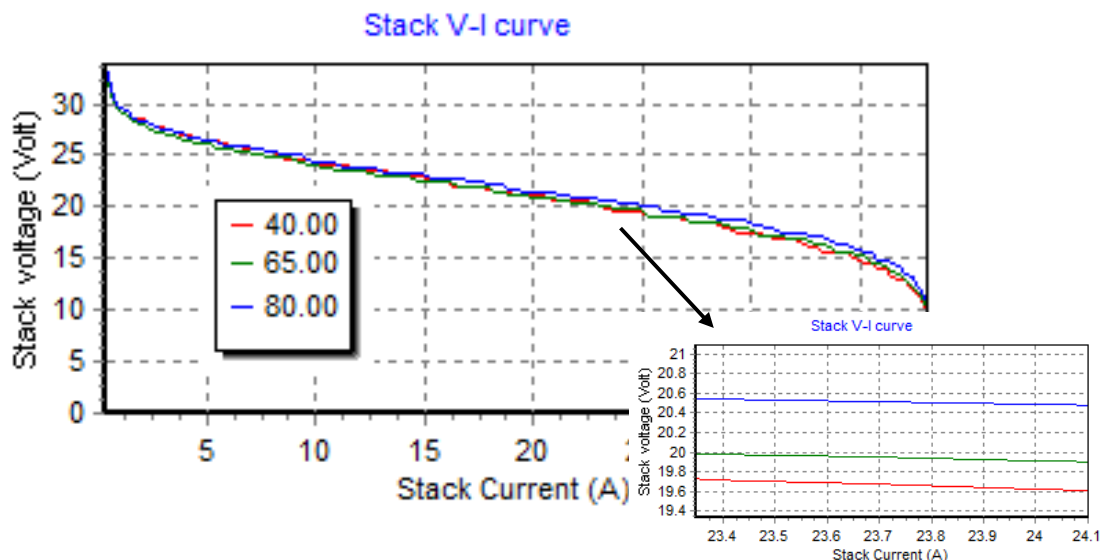


Figure 5-27. The effect of the operating temperature on the polarisation curve of the 500 W PEM BSC fuel cell predicted by the model; the relative humidity of the cell is controlled to be within its recommended range while changing the operating temperature

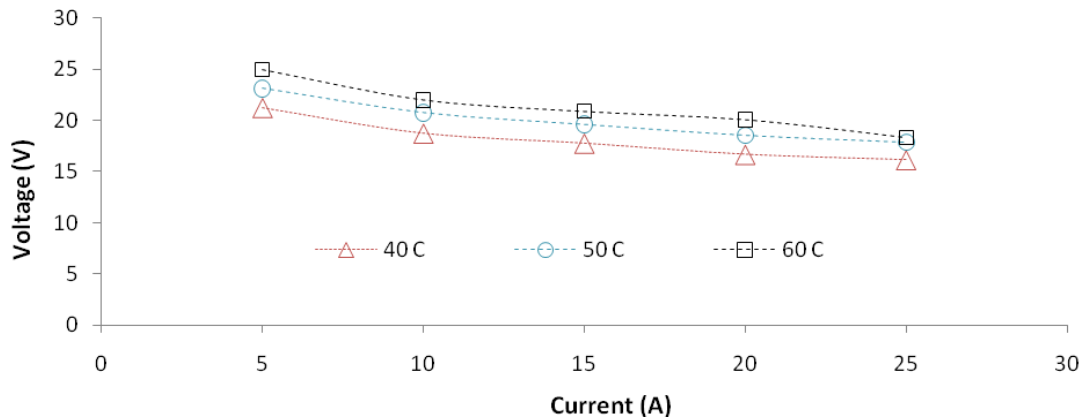


Figure 5-28. Experimental polarisation curves for the 500 W PEM BCS fuel cell at different fuel cell; operating temperatures; exit air pressure 30 kPa, air stoichiometry 2, and inlet hydrogen pressure 20-30 kPa

As shown by equation (3-62), the Gibbs free energy functions of the contributing elements in the fuel cell reaction equation, and hence the maximum reversible open circuit voltage (figure 3-13) of the fuel cell, are influenced by the operating temperature. Equations (3-74), (3-75), and (3-76) show that the membrane properties are also functions of this temperature.

The gap between the performance curves at different temperatures for an air stoichiometry of 2 arises not only because of the effect of operating temperature on the open circuit voltage and membrane properties (figure 5-28). The fact that the output power drops and cooling load increases with decreasing operating temperatures indicates another factor(s) involved. While operating the fuel cell at temperatures lower than recommended by the manufacturer, some water droplets were observed in the air exit stream. This observation was of help in finding out the reason for the considerable drop of the fuel cell performance at low operating temperatures.

This fuel cell is described as self-humidified by the manufacturer (BCS 2009) so that if it is operated at the proper air stoichiometry (1.75-2) and temperature (60-65 °C) it can maintain the exit air relative humidity level between 80-100% all the time to ensure the cell is neither flooded nor dehydrated. Water droplets in the air exit stream are the sign of the cell becoming wet or being flooded. Figure 5-29, one of the outputs of the model, shows clearly that increasing the air flow rate (air stoichiometry) while the cell temperature is

kept at 65 °C (recommended by the manufacturer) can lead to cell dehydration, while lowering the air stoichiometry specially at low operating temperature may cause the cell to be flooded. This figure also confirms that the air stoichiometry of about 2 and the operating temperature of about 65 °C suggested by the manufacturer are the best conditions to manage the fuel cell water level. The fuel cell tends to be flooded when operated at low operating temperatures (e.g. 40 °C) while low air stoichiometries (e.g. 2) are applied. At such operating conditions the performance of the fuel cell deteriorates due to the additional cell's internal resistance when the membrane becomes overly wet. The flooding is indicated by the increasing presence of water droplets in the exit air stream.

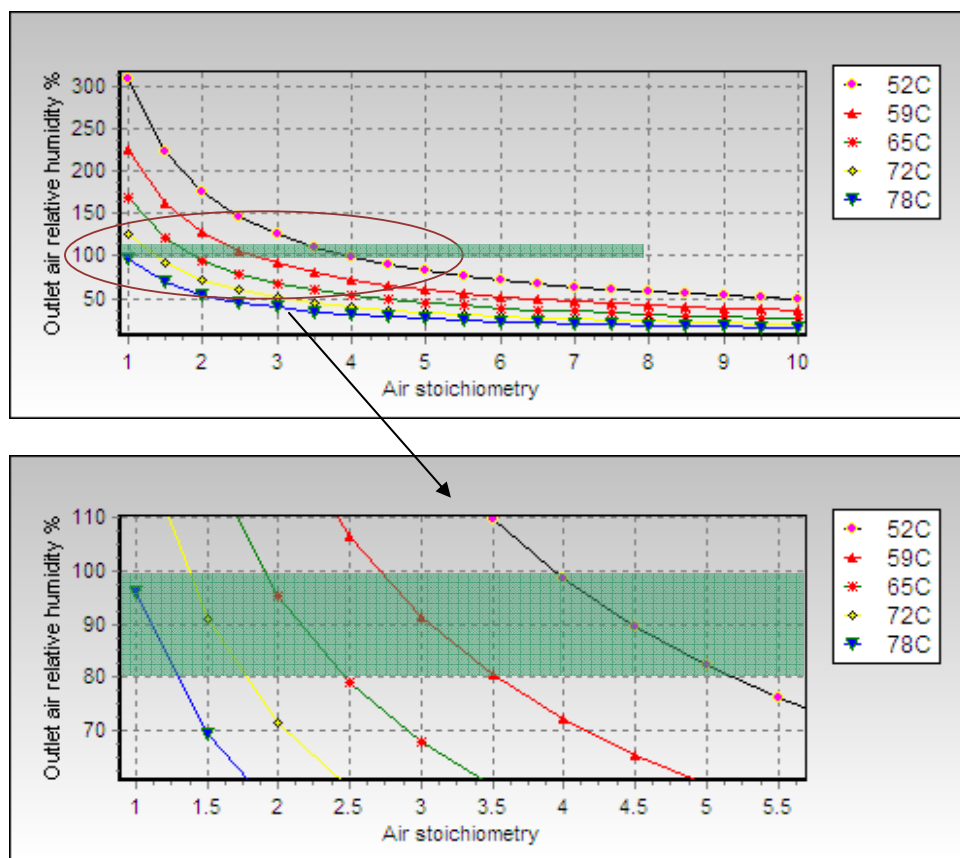


Figure 5-29. The effect of air stoichiometry and cell operating temperature on the exit air relative humidity for the 500 W BCS PEM fuel cell as predicted by the simulation model. (ambient temperature 30 °C; ambient pressures 100 kPa; inlet air relative humidity 50%; exit air pressure 30 kPa; and assuming about 15-20 kPa of pressure drop in the air channels)

To test this proposition, the fuel cell was also operated at a higher air stoichiometry by increasing it from 2 to 4, thus doubling the air flow rates used for obtaining the polarisation curves shown in figure 5-28. This increase in air stoichiometry led to an 8-12%

improvement in the performance of the fuel cell at 40 °C operating temperature and a 6-8% improvement at 50 °C. Removing some/all of the liquid water out from the fuel cell by this extra air flow appears to be the reason for this improvement in performance (figure 5-30).

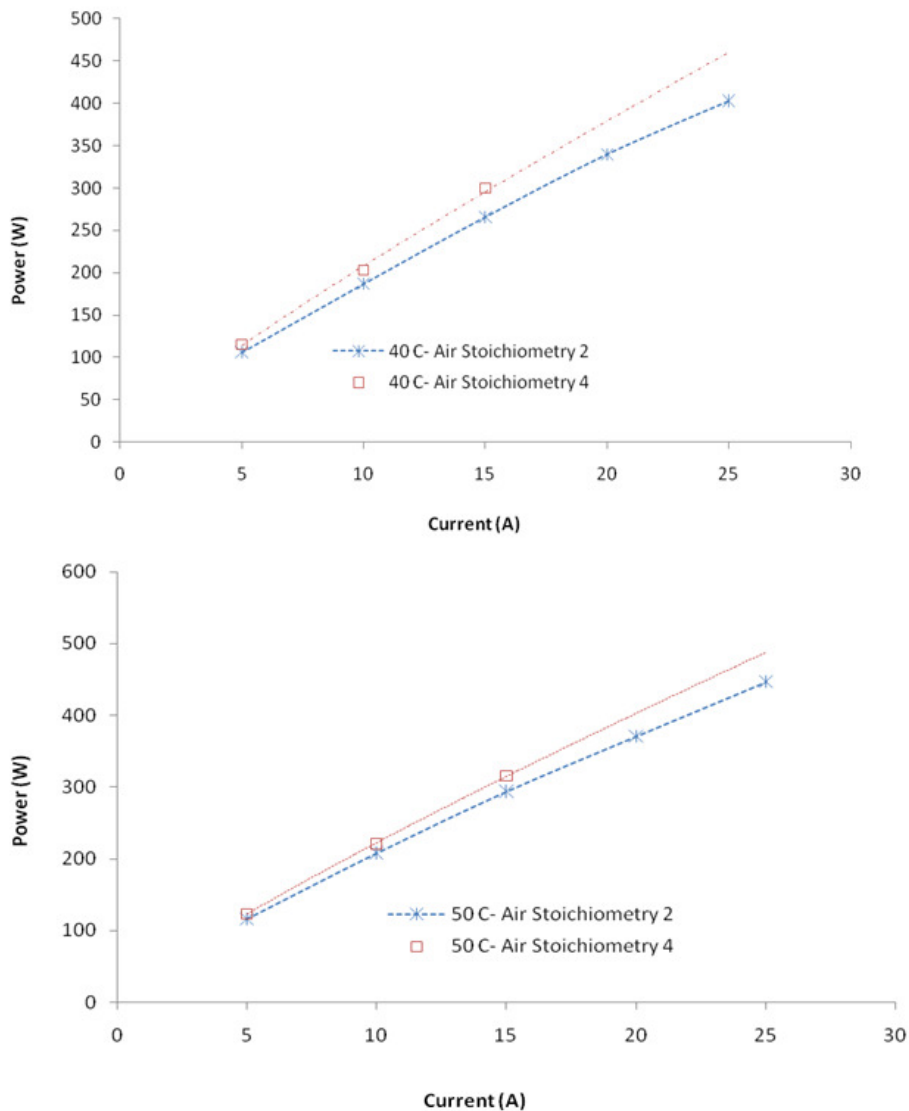


Figure 5-30. The effect of air stoichiometry on the performance of an already flooded 500 W fuel cell; operated at low temperatures; exit air pressure 30 kPa, and inlet hydrogen pressure 20-30 kPa

The graphs shown by figure 5-30 illustrate that the positive effect of increasing the air stoichiometry on the electrical performance of the fuel cell is more pronounced at higher current densities. In the experimental study performed by Torchio, Santarelli *et al.* (2005), a very similar conclusion about the effect of air stoichiometry on the performance of a 800 W PEM fuel cell was drawn.

In summary, the fuel cell operating temperature affects the performance of the stack in a number of ways:

- The effect on the Gibbs free energy function and hence the open circuit voltage of the fuel cell; the higher the temperature the less the open circuit voltage.
- The direct effect on the membrane properties and hence the fuel cell overpotential losses. The higher the temperature the less the overpotential losses.
- The indirect effect on the membrane property through changing the air relative humidity (figure 3-21 and figure 3-22). For example fully wet membranes show higher resistance against the hydrogen ionic flow than one that is partially wet; this leads to higher overpotentials for flooded cells

The experimentally-measured cooling load and that estimated by the simulation model are close when the fuel cell is properly operated at the recommended temperature (60 °C). However, at lower operating temperatures and lower air stoichiometry, the measured load is considerably more than that predicted by the theoretical model (figure 5-31). For example, as given in figure 5-31, the fuel cell cooling load obtained from the experiment for the 5 A operating point at 40 °C (30 kPa of exit air pressure and air stoichiometry of 2) is almost double the model's prediction at the recommended temperature (60 °C).

Formation of liquid water rather than water being left inside the fuel cell in vapour form is the likely explanation of the divergence under the latter conditions. As discussed earlier and shown in figure 4-40, a considerable part of the generated heat is absorbed by the product water for evaporation. At low operating temperature the water produced stays in the fuel cell in liquid form and hence the heat that is normally absorbed by this water during evaporation has to be removed from the fuel cell by the cooling system. As seen in figure 5-31 although the cooling load curves of the fuel cell at 40 °C and 50 °C are different, they are not far apart. However, on increasing the operating temperature to 60 °C the water produced is evaporated and in the process absorbs heat from the fuel cell, so that the cooling load of the fuel cell shows a considerable drop.

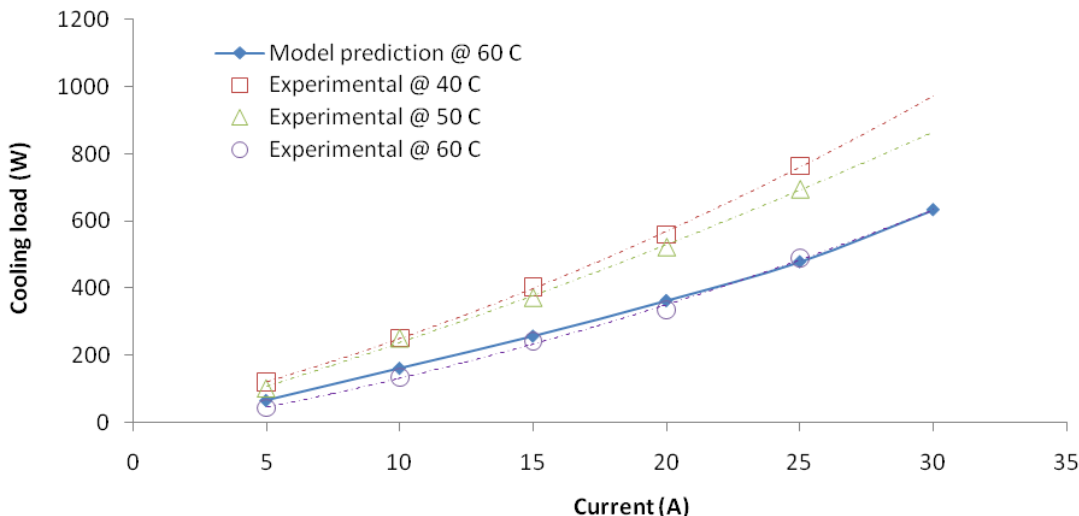


Figure 5-31. 500 W PEM BCS fuel cell measured cooling load at different operating temperatures compared with the cooling load curve predicted by the model at 60 °C; exit air pressure 30 kPa; air stoichiometry 2; inlet hydrogen pressure 20-30 kPa

Increasing the air stoichiometry can also increase the extent of water evaporation inside the fuel cell at a certain operating temperature. This effect was clearly observed when the fuel cell was operated at 50 °C and two different air stoichiometries, 2 and 4 (figure 5-32). It seems that at an air stoichiometry of 4 the conditions for strong water evaporation were present which is why the cooling load was considerably less than when the air stoichiometry of 2 was used. This difference also agrees with the figure of the heat used for water evaporation shown in table 4-9.

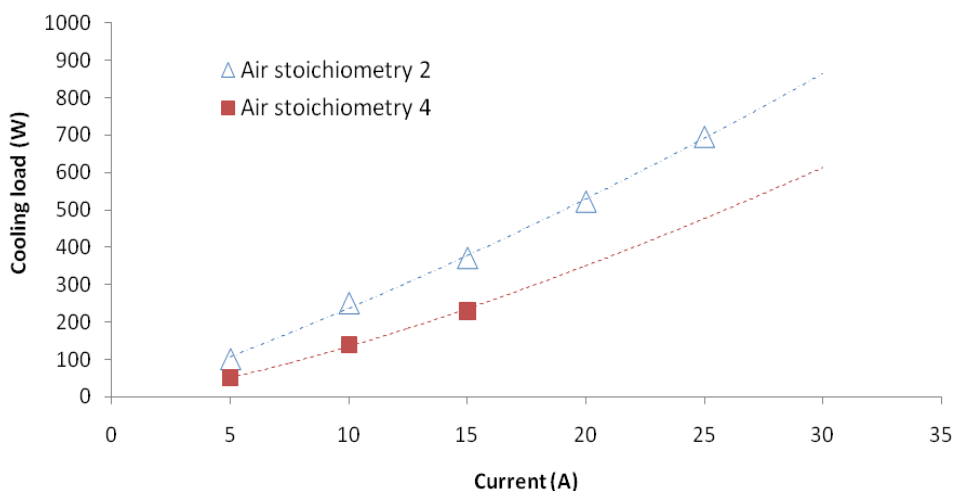


Figure 5-32. 500 W PEM BCS fuel cell cooling load; operating temperature 50 °C; air stoichiometries 2 and 4; exit air pressure 30 kPa; inlet hydrogen pressure 20-30 kPa

Here is another example of the effect of the rate of water evaporation on the performance of the fuel cell. According to the model, at the 5 A operating point (40 °C, 30 kPa of exit air pressure and air stoichiometry of 2), 35% of the total heat generated by the fuel cell (equivalent to 37.5 W) is consumed for evaporating the water produced. The average measured cooling load under these conditions was 119.8 W, much more than 65.8 W predicted by the model. The actual observation and also figure 5-29 both suggest that the water appears inside the stack in liquid and not in vapour phase. For the case of 5 A operating current, the difference between the measured cooling load and that predicted by the model is 54 W and part of this is obviously because of presence of the liquid water inside the fuel cell rather than water vapour. As mentioned above, 37.5 W of the generated heat that was supposed to be absorbed by the water product to be evaporated now has to be removed from the fuel cell by the coolant circulating inside the stack, as the water produced is not evaporated there anymore (low operating temperature of the fuel cell). Hence this 37.5 W is a part of this 54 W of difference. By taking this 37.5 W out from 54 W, the cooling load is still 16.5 W more than that predicted by the model. It is important to note that part of the heat is removed from the cell through natural convection from the fuel cell stack. Although by insulating the fuel cell body, attempt was made to minimise this heat loss, some loss would remain. This natural convection which is actually part of the cooling load has to be added to this difference (16.5 W) to make it more realistic. Based on a rough theoretical estimation this natural convection is at the order of about 10-20 W more or less. This in fact means that the cooling load difference between the model and the experiment has to be counted at about 25 W to 35 W. The measured power output at 5 A current and the given condition shows 106 W which is 24 W less than what is indicated in the manufacturer's manual. This difference, as discussed above, is due to the added internal resistance of the cell caused by cell flooding. Obviously this 24 W drop in the power output appears in the form of heat. Now the 25-35 W of difference between the experimental and theoretical cooling load is quite justifiable. It is to be noted here that the error of the experiment has also to be taken into account; particularly it will be shown that for the case of cooling load measurement and calculation this possible error is quite considerable (appendix 2). All this energy analysis for 5A operating point at the given condition is illustrated in the Sankey diagrams shown in figure 5-33. The fuel (hydrogen) utilisation coefficient which is connected to the excess hydrogen losses shown in these Sankey diagrams will be discussed later in this chapter. Similar data based on the average figures

of the experimental measurements are given for a few other operating loads and conditions of the fuel cell in table 5-7. The full measured data are available in appendix 2.

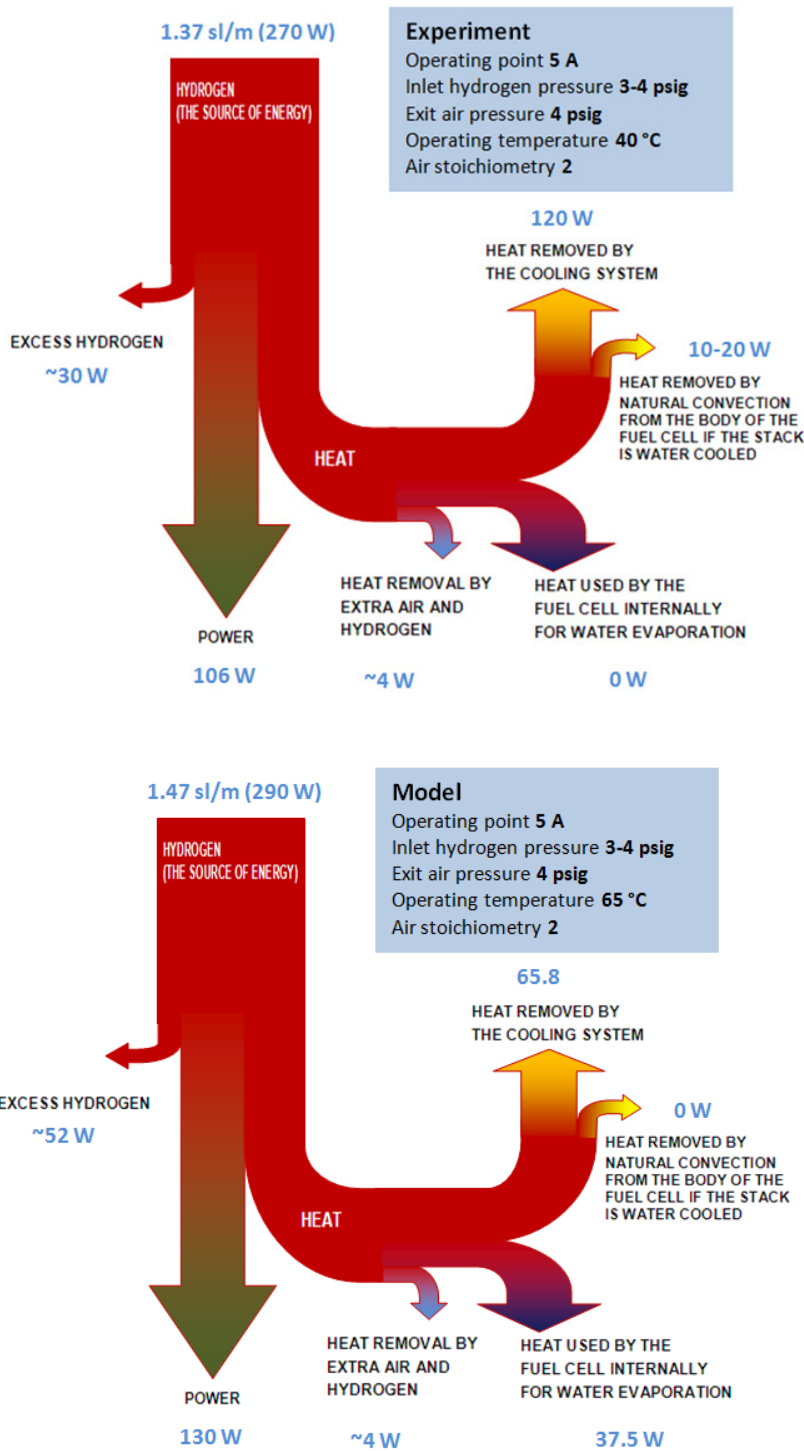


Figure 5-33. 500 W fuel cell Sankey diagram at 5A operating point, theoretical and experimental study

Operating point	Cooling load (W)						
	Experiment						Model
	40 °C		50 °C		60 °C		60-65 °C
	Air Stoich 2	Air Stoich 4	Air Stoich 2	Air Stoich 4	Air Stoich 2	Air Stoich 4	Air Stoich 2
5 A	120	102	101	51	42	38	65.8 W
10 A	253	227	252	140	134	125	161.6 W
15 A	406	379	364	232	242	208	257.4 W
20 A	560	N/A	559	N/A	336	N/A	363.2 W
25 A	764	N/A	696	N/A	490	N/A	478 W

Table 5-7. 500 W fuel cell: the average of the experimentally-measured cooling load at different operating points and conditions in compared with the model predictions; exit air pressure 30 kPa; inlet hydrogen pressure 20-30 kPa

5.4.4 Energy efficiency and fuel utilisation coefficient

Experimentally measured values for the fuel (hydrogen) utilisation coefficient and energy efficiency of the fuel cell can now be compared to the values used in the theoretical investigation of the small-scale solar-hydrogen system studied in Chapter 4.

Table 5-8 and table 5-9 show the experimental hydrogen utilisation coefficient of the 500-W PEM fuel cell at different operating loads and conditions. The figures shown by these tables are the averages obtained from number of measured data at each operating current and condition (the full history of these measurements is available in the appendix). Hydrogen utilisation coefficients are calculated using the experimentally-measured hydrogen consumption rates. The errors associated with these measured hydrogen consumption rates (see appendix 2) are consistently within the accuracy rate (1%) of the flow meter/controller used for this purpose (see table 5-1, and the technical specifications of C100 mass flow controller). Figure 5-34 shows the experimentally-calculated hydrogen utilisation coefficients at 60 °C operating temperature and air stoichiometries of 2 and 4 all on one graph. The following points can be deduced from table 5-8, table 5-9, and figure 5-34:

- The experimental hydrogen utilisation coefficient of the fuel cell (~90-98%) is much higher than the conservative figure of about 85% assumed in the theoretical analysis. Hence assuming an average hydrogen utilisation coefficient of 95% would be more realistic in the case study, although account may still need to be taken of some drop in the hydrogen utilisation coefficient as the fuel cell aged.

- At higher current densities, the hydrogen utilisation coefficient increases by a few percent.
- Supplying more air to the fuel cell (increasing the air stoichiometry) does not lead to a significant improvement in the hydrogen utilisation coefficient.

Operating temperature	Operating current				
	5 A	10 A	15 A	20 A	25 A
	Hydrogen utilisation coefficient (%)				
40 °C	89.5	91.6	96.3	98	98.1
50 °C	93.4	96.1	97.7	98	97.8
60 °C	94.1	95.4	96	97	97.5
Hydrogen consumption based on 100% utilisation (slpm)	1.22	2.44	3.67	4.89	6.12

Table 5-8. Average experimentally-measured values for the hydrogen utilisation coefficient for the 500 W BCS PEM fuel cell; exit air pressure 30 kPa; inlet hydrogen pressure 20-30 kPa; air stoichiometry 2

Operating temperature	Operating current				
	5 A	10 A	15 A	20 A	25 A
	Hydrogen utilisation coefficient (%)				
40 °C	91.8	92.8	97.9	N/A	N/A
50 °C	92.8	95.1	97	N/A	N/A
60 °C	95	95.6	97	N/A	N/A
Hydrogen consumption based on 100% utilisation (slpm)	1.22	2.44	3.67	4.89	6.12

Table 5-9. Average experimentally-measured values for the hydrogen utilisation coefficient for the 500 W BCS PEM fuel cell; exit air pressure 30 kPa; inlet hydrogen pressure 20-30 kPa; air stoichiometry 4

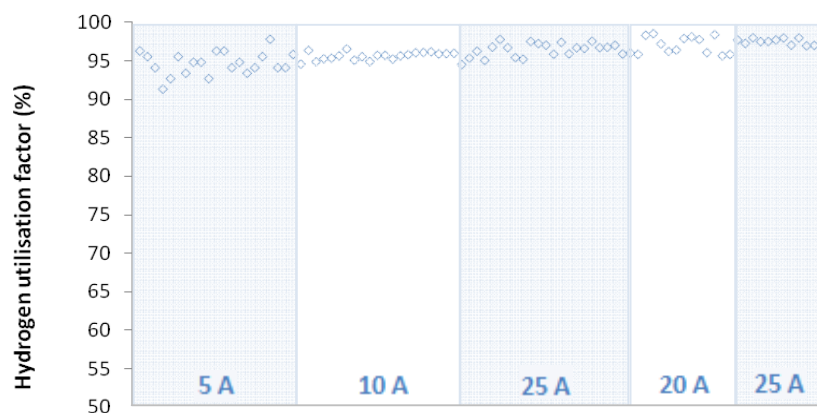


Figure 5-34. The measured hydrogen utilisation coefficient of 500-W BCS PEM fuel cell; operating temperature 60 °C; exit pressure 30 kPa; air stoichiometry 2 & 4; inlet hydrogen pressure 20-30 kPa

The experimental polarisation curve shows more overpotential and less electrical power output than the one provided by the manufacturer (figure 5-24). However, the measured energy efficiencies of the fuel cell at different operating currents (5 A to 25 A) are 7.5%-11.5% higher than those used in the model based on the manufacturer's polarisation curve

and a hydrogen utilisation coefficient of about 85% (figure 5-35). This is basically because of the higher hydrogen utilisation coefficient of this fuel cell obtained in practice.

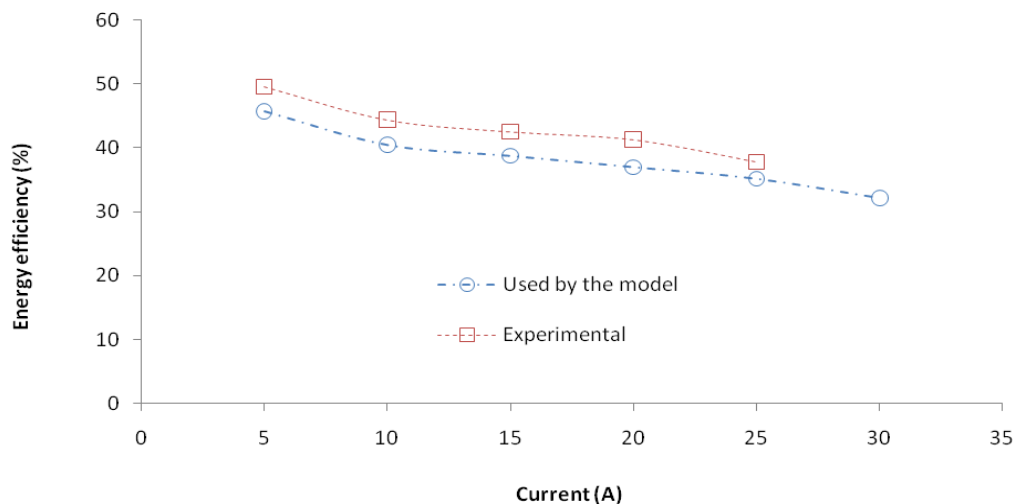


Figure 5-35. 500 W PEM BCS fuel cell energy efficiency; operating temperature 60 °C; exit air pressure 30 kPa; air stoichiometry 2; inlet hydrogen pressure 20-30 kPa

5.4.5 Solar-hydrogen CHP system overall energy efficiency

The overall energy efficiency of the system in both power and heat production - the CHP efficiency - was also calculated experimentally. The results show that this efficiency is about 72% on average (figure 5-36). This is a significant improvement compared to the efficiency of the fuel cell in power only generation shown in figure 5-35 (~35% to ~50%). Unlike the electrical energy efficiency of the fuel cell, the CHP efficiency is not inherently a function of fuel cell current density, provided that the hydrogen utilisation coefficient remains constant. However, in this experiment, the hydrogen utilisation coefficient increased a few percent at higher current densities and this is reflected in the CHP system energy efficiency at higher current densities. Although the predicted cooling load is very close to what was measured experimentally (figure 5-25), the average measured CHP efficiency of the fuel cell is about 10% more than that predicted by the model (63%). This is basically because of the better energy efficiency obtained for the fuel cell in practice compared to what used in the theoretical calculations (figure 5-35).

The experimental figure obtained here for the 500-W PEM fuel cell CHP system energy efficiency (~72%) agrees well with the 75% overall energy efficiency of a PEM fuel cell in

both heat and power generation measured experimentally by Hawkins, Joffe *et al.* (2005), and slightly less than the 80% figure obtained by Hawkes and Leach (2005) in another experimental study. The experimental CHP efficiency obtained here is also higher than the 50-60% CHP energy efficiency measured for a PEM fuel cell by Gigliucci, Petruzzi *et al.* (2004). Gigliucci, Petruzzi *et al.* (2004) also showed that CHP energy efficiency of the fuel cell can slightly improve by increasing the current density, similar to the result obtained in the present experimental study (figure 5-36).

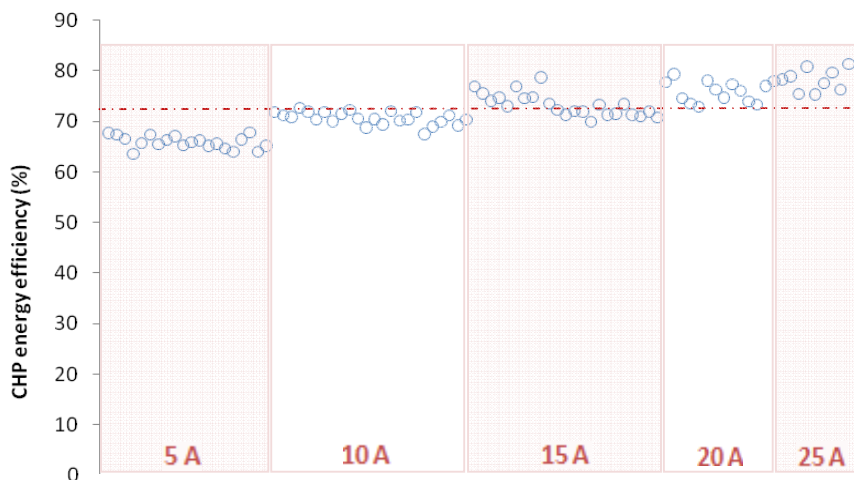


Figure 5-36. 500 W PEM BCS fuel cell CHP (overall) energy efficiency; operating temperature 60 °C; exit air pressure 30 kPa; air stoichiometry 2 and 4; inlet hydrogen pressure 20-30 kPa

The fuel cell CHP energy efficiency increases to about 90% on average when the fuel cell is operated at lower temperatures (e.g. 40-50 °C). The main reason is that at such temperatures the heat that is normally absorbed by the water product in evaporation is instead removed by the fuel cell cooling system. This situation adds to the available heat of the system. Having said that, a fuel cell is primarily sized based on its electrical output; hence operating the fuel cell at low temperatures is not desirable from the electrical efficiency point of view (figure 5-37). It is notable that the fuel cell is not stable for a continuous power output when operated at low temperature due to the membrane flooding problem.

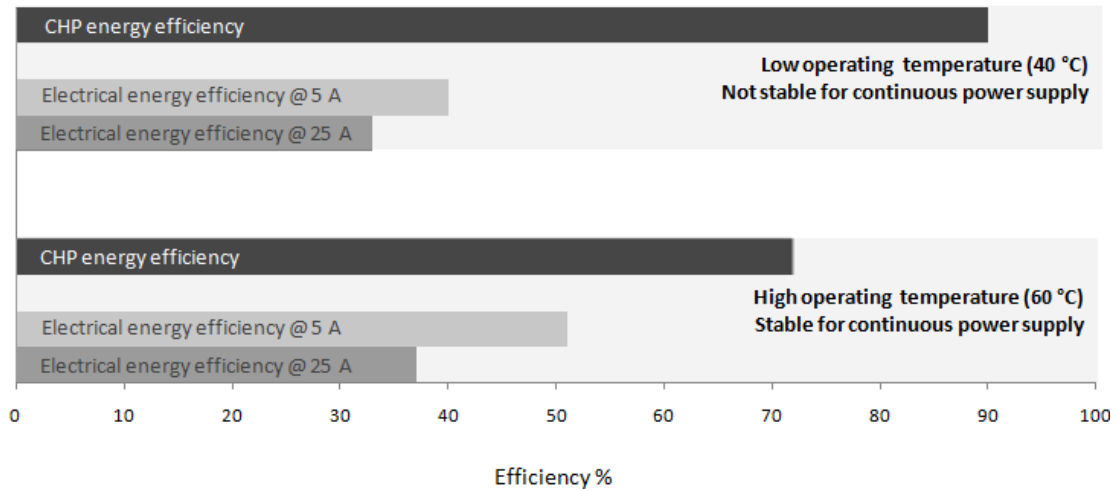


Figure 5-37. The fuel cell average electrical and CHP efficiencies at low and high operating temperatures; operating temperatures 40 °C and 60 °C; exit air pressure 30 kPa; air stoichiometry 2; inlet hydrogen pressure 20-30 kPa

5.4.6 Rerunning the model using the experiment fuel cell polarisation curve

The model was rerun using the fuel cell polarisation curve and hydrogen utilisation coefficient obtained experimentally. The charge transfer coefficients on the oxygen and hydrogen sides were calculated to be 0.3 and 0.7 respectively based on these experimental inputs. These two parameters were previously calculated to be at 0.35 and 0.71 when the manufacturer’s curve was used by the program. The size of the components for a basic design (minimum size of the fuel cell, ~0.3 kW, and unconstrained tank) were calculated slightly less than those calculated when the manufacturer’s polarisation curve and hydrogen utilisation coefficient of ~85% were used by the program (table 5-10).

	Experimental polarisation curve and hydrogen stoichiometry were used in the model	Manufacturer’s polarisation curve and hydrogen stoichiometry of 1.2 were used in the model
PV	3.7 kW	4 kW
Electrolyser	3 kW	3.3 kW
Hydrogen Tank	20 kg	21.5 kg

Table 5-10. Comparing the size of the components when the experimental and manufacturer’s polarisation curves and hydrogen utilisation coefficient s are used by the program

The average annual electrical energy efficiency of the fuel cell increased from 33% to above 38% in power only application and from 63% to 68% in a heat and power application. These improvements resulted in a cost of electricity of about 0.95 US\$/kWh,

about 10% better than the figure obtained using the manufacturer's data. This new unit cost of electricity (generated by the solar-hydrogen system) has the potential to be reduced to about 0.85 US\$/kWh when the system is optimised.

The gap between the newly-produced cooling load curve (by applying the experimental fuel cell polarisation curve into the model) and the experimental cooling load curve reduced by 2-7% points compared to that shown in figure 5-25. Recovering this heat led to about 33% saving on LPG consumption (used for hot water supply) equivalent to about 14% of the overall cost of the system over an assessment period of 30 years when 4% annual increase in the real cost of LPG is assumed. This saving figure is very close to what previously estimated by just using the results from the model (15%).

The experimentally-based annual hydrogen loss through the fuel cell (excess hydrogen fed into the fuel cell) was estimated 9.9 kg/year (for the case of using fuel cell minimum size). It was 48% less than that used previously in the model (18.7 kg/year). The effect of excess hydrogen recovery to be burned in a 90% efficient burner is estimated to be equivalent to about 20% saving on LPG normally used for hot water supply (or about 15% saving on LPG when an optimally-sized fuel cell is used). This saving on LPG consumption (used for hot water supply) is equivalent to about 8% of the overall cost of the system over an assessment period of 30 years when 4% annual increase in the real cost of LPG is assumed (minimum size of fuel cell is used).

5.5 CONCLUSIONS

The experimental study on the 500 W PEM BCS fuel cell described in this chapter has confirmed the central findings from the simulation modelling, mainly that:

- operating the fuel cell in CHP mode can nearly double the overall energy efficiency;
- utilising the heat recovered from the fuel cell in a solar-hydrogen CHP system for RAPS for domestic water heating can substantially enhance the overall economics of the system; and
- collecting the excess hydrogen from the hydrogen exit stream of the fuel cell can significantly contribute in improving the overall economics of the solar-hydrogen

system if burned for domestic water heating in a RAPS application. This improvement, through utilising the excess hydrogen, is almost half that achievable by recovering heat for supplying domestic hot water.

The experimentally-measured energy efficiency of the particular 500-W PEM fuel cell used in the present study in electrical power production varies from just above 50% down to about 35% depending on the magnitude of the electrical load being supplied (figure 5-35). The experimental results demonstrate that the overall energy efficiency of this fuel cell can be improved to an average of about 72% if the fuel cell is used for both heat and power production (figure 5-36). This figure is about 9% points higher than predicted earlier by the simulation model used in this study. This difference is mainly due to an overly conservative assumption made in the model (~85%) for the fuel cell hydrogen utilisation coefficient, whereas it was measured experimentally to be about 95% on average (figure 5-34). This higher hydrogen utilisation coefficient obtained in practice also led to slightly higher electrical energy efficiency for the fuel cell, 7.5-11.5% above that used in the model.

If the fuel cell characteristics in the model are amended to take account of this improved efficiency (that is, the new polarisation curve is used), the calculated unit cost of electricity in the case study (minimum fuel cell size) falls from 1.06 US\$/kWh to about 0.95 US\$/kWh, a reduction of more than 10%. The unit cost of electricity for the optimal system correspondingly reduces to 0.85 US\$/kWh.

The experimentally-measured cooling load of the fuel cell is very close to that predicted by the model at high currents, but at currents less than 20 A it is 7-17% lower than those predicted. This gap is reduced to 5-10% when the experimental polarisation curve and the convection heat transfer from the body of the fuel cell are considered by the model.

The experimental study found that the fuel cell CHP capability is strongly connected with its water management. In turn, water management is greatly affected by the operating temperature and air stoichiometry. Decreasing the fuel cell operating temperature can lead to the production of liquid water inside the fuel cell. This occurrence can add to the collectable cooling load of the fuel cell (figure 5-31), but at the expense of increasing the fuel cell overpotentials (figure 5-28) or decreasing the electrical energy efficiency, making

the fuel cell unstable in continuous uniform power generation, and hence worsening the economics of the overall solar-hydrogen system. When the fuel cell is operated at a lower temperature than it is designed to be operated at, increasing the air stoichiometry can partly reduce the negative effect of this low temperature operation on the performance of the fuel cell, by enhancing the electrical energy efficiency and suppressing its thermal output. These effects are more pronounced at high current densities.

The experimental results show that the overall energy efficiency of the system in CHP application does not depend on the electrical performance of the fuel cell (figure 5-36). By increasing the current density the electrical efficiency drops, but there is more usable heat available, so that the CHP efficiency stays almost constant. However, in most cases electrical energy output can be regarded as of higher value than the recovered heat. Another positive feature of a fuel cell CHP system is that as the fuel's electrical performance drops with age, there is more heat available for the heating application, thus partly offsetting the negative impact of aging.

6 Comparison of a solar-hydrogen CHP system with other alternatives

6.1 INTRODUCTION

A wide range of RAPS options, from non-renewable to renewable, are currently in use or under investigation. The preferred choice of RAPS system depends mainly on the nature of the load, feasibility of implementation, local environmental conditions, the degree of reliability required, and above all the cost (Akbarzadeh 1992). In this chapter, a number of the principal alternatives to solar-hydrogen RAPS systems (with and without CHP) are compared for the case study application discussed in Chapter 4 using both the system simulation model presented in this thesis, and the HOMER simulation model that has also been often used previously for system comparisons of this kind (Zoulias and Lymberopoulos 2007). The comparison is based on a triple bottom line (TBL) analysis, so that the competing systems can be compared with regard to their economic, environmental, and social performance. The particular alternative RAPS systems evaluated here are the following:

- 1- Diesel/petrol generator (with or without battery storage) (non-renewable)
- 2- Solar PV-battery-ICE generator (hybrid, non-renewable)
- 3- Solar-hydrogen-battery (hybrid, renewable).

The HOMER model is available via a free and extendable license (HOMER 2009). This software was originally developed by National Renewable Energy Laboratory in 1993 (NREL 2010). The strength of HOMER is its applicability to evaluate the economic and technical feasibility of a wide range of off-grid and grid-connected power systems and configurations (including hybrid systems) for remote, stand-alone, and distributed generation applications (NREL 2010). By contrast, RSHAP is specifically designed for analysing solar-hydrogen CHP systems and thus has the capability of analysing this particular system configuration in detail. The key advantages of RSHAP over HOMER for solar-hydrogen CHP system analysis are thus the following:

1. *Fuel cell and electrolyser modelling/analysis at the micro level.* RSHAP does system analysis by taking into account the effect of the key parameters (such as membrane electronic resistance, exchange current densities, and charge transfer coefficients) and the operating condition on the overall performance of a solar-hydrogen CHP system. By contrast, HOMER does not explicitly model these effects in the fuel cell and electrolyser. Hence some of the performance characteristics of these components (for example the annual average efficiencies) that are calculated by RSHAP as outputs have to be given to HOMER as estimated inputs to start the analysis.
2. *System sizing and optimisation.* RSHAP does system sizing and optimisation (under different sizing strategies) automatically, whereas with HOMER such an optimisation procedure must be conducted manually by the user, by giving different inputs for the sizes of the components and hence HOMER determines which combination gives the best result.

HOMER remains a very powerful tool for simulation and analysis of power supply systems, in particular the hybrid ones. The unique advantage of HOMER is its flexibility to model a wide range of systems, allowing a preliminary comparison to be made between them to identify preferred options. Hence HOMER is also used where appropriate in the present work. However, as mentioned HOMER is not a dedicated model for solar-hydrogen CHP systems analysis only; that is why some details considered by RSHAP are not investigated here using HOMER.

6.2 SYSTEM ARRANGEMENT, SIZING AND OPERATION

6.2.1 Solar-hydrogen system alone and with CHP

In Chapter 4 the possibility of employing a solar-hydrogen CHP system in a residential case in south-eastern Australia with a 5 kWh daily demand (peaked at 0.3 kW) was investigated using RSHAP. As shown in table 6-1, the system was sized to have a 4 kW PV array, a 3.3 kW electrolyser, a 21.5 kg hydrogen tank, and a 0.31 kW fuel cell (the minimum size of the fuel cell).

The case studied using RSHAP (Chapter 4) was also investigated using HOMER (figure 6-1) for comparison purposes (based on the minimum size of the fuel cell). Average annual energy efficiencies of 73% and 33% for the electrolyser and fuel cell respectively, obtained from the detail analysis performed using RSHAP, were fed to HOMER as inputs.

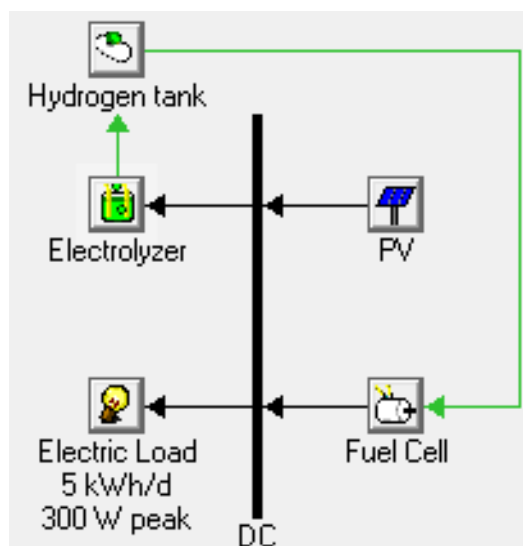


Figure 6-1. Solar-hydrogen system configuration studied using HOMER

The results of the HOMER analysis for component sizes obtained for this case study were a 4.5 kW PV array, 3.5 kW electrolyser, 18 kg hydrogen tank, and 0.31 kW fuel cell, and these values are reasonably similar to those found by RSHAP (table 6-1). It is notable that system sizing can be done using HOMER by trying different sizes for the components. The small differences between the sizes of component obtained using RSHAP and HOMER are likely to come from the different sub-models used for the main components in these two models (e.g. PV array, electrolyser, and fuel cell).

	PV array kW	Electrolyser kW	Hydrogen tank kg	Fuel cell kW
RSHAP	4.0	3.3	21.5	0.31
HOMER	4.5	3.5	18.0	0.31

Table 6-1. Solar-hydrogen system sizing by HOMER and RSHAP for the case study in Chapter 4 (5 kWh daily demand in south-eastern Australia)

Converting the system to a CHP unit does not affect the size of the main components given in table 6-1. The heat collected from the fuel cell boosts the hot water system and yields LPG saving, assuming the hot water system runs on LPG.

6.2.2 ICE generators

Generators running on fossil fuels, namely diesel or petrol are the traditional competitors for solar-hydrogen systems in RAPS applications. The time and costs involved in transporting these liquid fuels to remote areas are big disadvantages of diesel or petrol generators compared to solar-hydrogen systems (Ghosh *et al.* 2003). However, the relatively low initial capital cost of such generators systems is still a key factor encouraging their continued use for RAPS applications. Diesel fuel and petrol prices have been increasing and generators operated on these fuels need regular maintenance – e.g. oil and air filter changes, and overhauling – which can be expensive especially in remote areas. Fuel transportation is another issue with using these generators in remote areas. For the case studied in Chapter 4, in which the peak demand is 0.3 kW_e, a small generator in the order of half a kilowatt, e.g. Yamaha ET650 550 W, is sufficient. This option has been studied using HOMER (figure 6-2) and the results of this analysis will be further discussed in section 6.3.

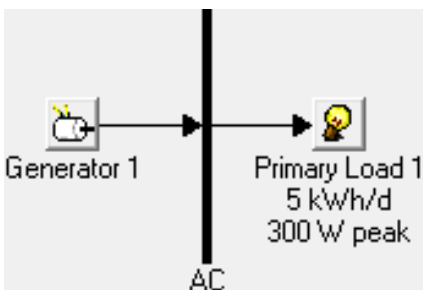


Figure 6-2. Petrol generator configuration for supplying the load simulated by HOMER

In practice the diesel/petrol generators usually supply a variable load, and their efficiency drops considerably when connected to small loads (compared to rated power) (Akbarzadeh 1992). A good solution to this problem is using battery storage in conjunction with a diesel/petrol generator. The presence of the battery in this system allows the ICE generator to operate more efficiently by having periods of constant charging rather than directly supplying the variable electrical load. This option has also been investigated using HOMER (figure 6-3). The battery chosen to be added to the petrol generator (Yamaha ET650 550 W) was a S4KS25P model. This battery costs about US\$1200 and has an allowable discharge depth of 40-50%, a capacity of 7.6 kWh (4 V, 1900 Ah), the round-trip efficiency of 80%, and a life span of 12 years (10 years of which is under warranty to provide the rated performance according to the HOMER database). HOMER suggested

using two of these S4KS25P batteries (15.2 kWh) in conjunction with the petrol generator to ensure that the batteries are always kept at above 50% of charge status (always above 65% of charge in this case).

The benefit of using a battery appears in the form of saving on fuel through operating the generator at a better average efficiency. Moreover, using batteries adds to the reliability of the system. With an ICE generator-battery system it is possible to oversize the generator while adding more batteries to feed some extra electrical energy to the batteries for storage to allow a few days of autonomous operation of the system. Hence, if in case the ICE generator is temporarily taken off the system or fails to operate for some reason, the battery can still meet the load while the generator is being repaired or replaced. For example if a string of five S4KS25P batteries is used for this case, rather than two, the system acquires the allowance of three days of autonomous operation just by receiving the electrical energy stored in the batteries.

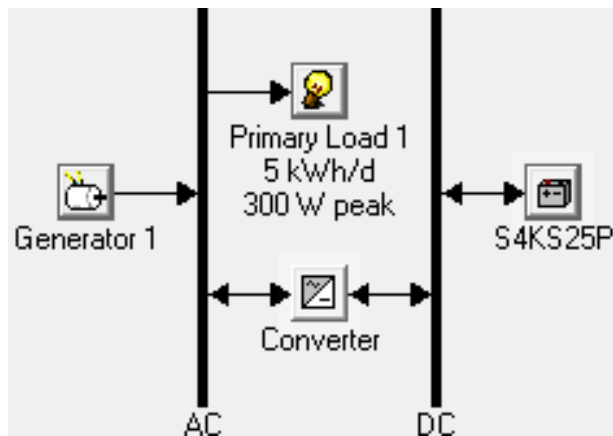


Figure 6-3. Petrol generators-battery system analysed by HOMER

The opportunity of heat recovery from the ICE generators is theoretically available; however, this option has not been considered as commercial generator systems have not been set up for this mode of operation in RAPS to date.

6.2.3 Solar PV-battery-ICE generator systems

Battery storage is still commonly used in conjunction with a solar-PV system. A solar PV-battery system for the case study presented in Chapter 4 has also been investigated using HOMER (figure 6-4). It has to be noted that normally when a solar-battery system is used

for RAPS, a back-up ICE generator also has to be added to the system to provide sufficient reliability and to ensure continuity of supply in heavily-cloudy periods. This reliability issue is more critical when the system is used in places like Melbourne with highly variable solar-radiation from summer to winter and unexpected cloudy periods (Richards and Conibeer 2007). However, for locations with a more uniform solar irradiance profile (e.g. Northern Australia) a solar PV-battery system with no back-up generator is feasible. The Yamaha ET650 550 W petrol generator (see the details in section 6.2.2) was used in this case as a back-up (supplying less than 15% of the annual load mostly for the winter time). By adding this generator to the system it is possible to avoid a large size of the PV array, which would usually be needed in solar PV-battery systems used in areas with highly variable seasonal solar irradiance (i.e., Melbourne).

Again S4KS25P batteries were employed and coupled with the PV arrays. Using a conservative assumption of 10-15 days of autonomy for the 5-kWh daily demand, and targeting a minimum state of charge for the batteries of about 80% (well above their allowable depth of discharge, 40-50% to prolong the lifetime of the batteries), 15 units of this type of battery (~US\$1200 each) were used to serve the purpose.

Figure 6-5 shows the hourly state of charge of the battery bank throughout the year as predicted by the HOMER modelling. The charge variation pattern is similar to that for the constrained hydrogen tank scenario in the solar-hydrogen system discussed in Chapter 4 (figure 4-18). According to the results obtained by HOMER such a solar PV-battery-ICE generator system needs a 2.1 kW PV array.

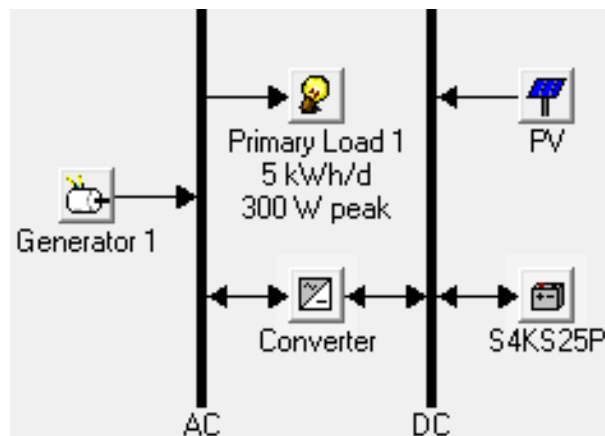


Figure 6-4. Solar PV-battery-ICE generator system analysed by HOMER

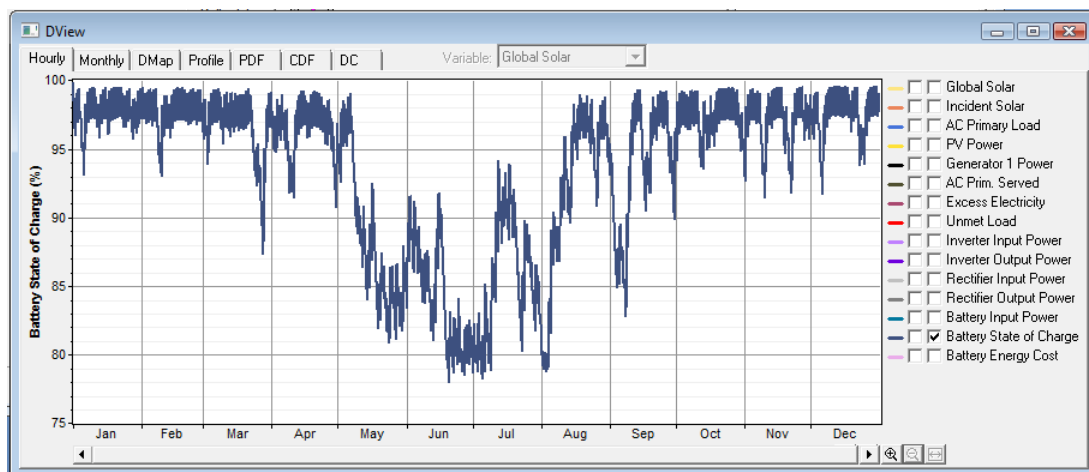


Figure 6-5. The battery hourly state of charge throughout the year for the solar PV-battery-ICE generator system for the case studied in Chapter 4

6.2.4 Solar- hydrogen-battery system

As stated earlier, although battery storage shows low round-trip energy efficiencies in long-term storage applications, it is an ideal option for short-term storage of electrical energy with a high round-trip efficiency of above 80% (Maclay *et al.* 2006). This suggests the possibility of using a solar-hydrogen system for RAPS with a combined hydrogen-battery storage or hybrid hydrogen energy storage system in which the battery is used as a short-term storage, e.g. night time, and hydrogen is used as the long-term storage, e.g. season to season. Such a system would be particularly suitable for areas with highly-variable yearly solar radiation such as Melbourne (Richards and Conibeer 2007). Lagorse, Simões *et al.* (2008) have also shown that such a hybrid system can be potentially cheaper than just using hydrogen for both long and short-term storage applications. This option has attracted many researchers, for example:

- solar-hydrogen system transient simulation using TRNSYS by Ulleberg and Mørner (1997);
- solar-hydrogen system demonstration in Mexico Torres *et al.* (1998); the study and demonstration of a technical feasibility of a stand-alone energy supply system, based on photovoltaic, battery, and hydrogen fuel cell system by Emonts *et al.* (2003); and
- hourly-based analysis done on a household located in a valley of the Alps in Italy by Santarelli and Macagno (2004) in which the battery system was used for short-term storage (up to three days and supplying slightly above 50% of the annual demand) and

the hydrogen (used in a fuel cell) as a long-term storage (supplying 20-25% of the total electrical demand), and the rest directly supplied by PVs.

A solar-hydrogen-battery system was therefore analysed for the case studied in Chapter 4 using HOMER (figure 6-6).

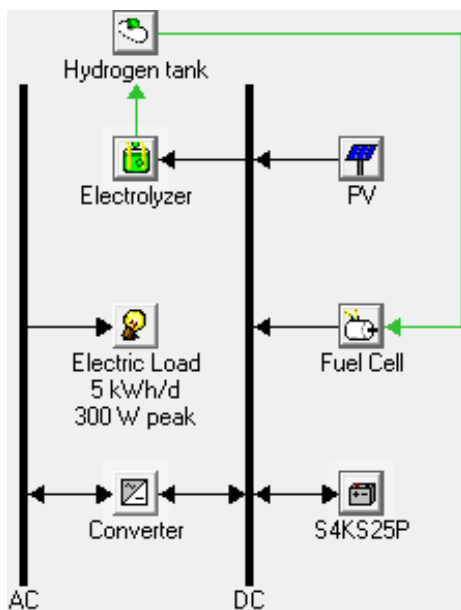


Figure 6-6. CHP solar-hydrogen-battery system analysed using HOMER

As shown in table 6-2, by adding the eight battery units (S4KS25P) to the solar-hydrogen system, the size of the PV array, electrolyser, and hydrogen tank can be reduced considerably. The minimum size of the fuel cell was chosen such that it can just meet the peak demand by itself if required. Again it is notable that in practice the size of the PV array has to be higher than 2.4 kW since the average 80% round-trip efficiency for batteries used in this analysis for Melbourne (with such a variable seasonal solar irradiance) might not be achievable, even with the presence of the long-term hydrogen storage solution.

System	PV array (kW)	Electrolyser (kW)	Hydrogen tank (kg)	Fuel cell (kW)	Battery Units (S4KS25P)
Solar-hydrogen	4.5	3.5	18	0.31	N/A
Solar-hydrogen-battery	2.4	1.6	9.5	0.31	8

Table 6-2. Comparing solar-hydrogen & solar-hydrogen-battery systems using HOMER for the case studied in Chapter 4

Figure 6-7 (the HOMER results) shows the annual charge status of the batteries in the system. The battery storage does not experience a long-term deep discharge in this system (as in the solar-battery system shown in figure 6-5), and the charge and discharge cycles for this case are quite uniform (except a short period during the winter at the beginning of August). The reason is simply that the batteries are supposed to serve as short-term storage by supplying mainly the night-time but not the seasonal storage requirement. This helps to prolong the lifetime of the battery system, which is actually a hidden benefit to the economics of the system, and ensure storing and delivering electrical energy (for batteries) at a high round-trip efficiency level for most of the year.

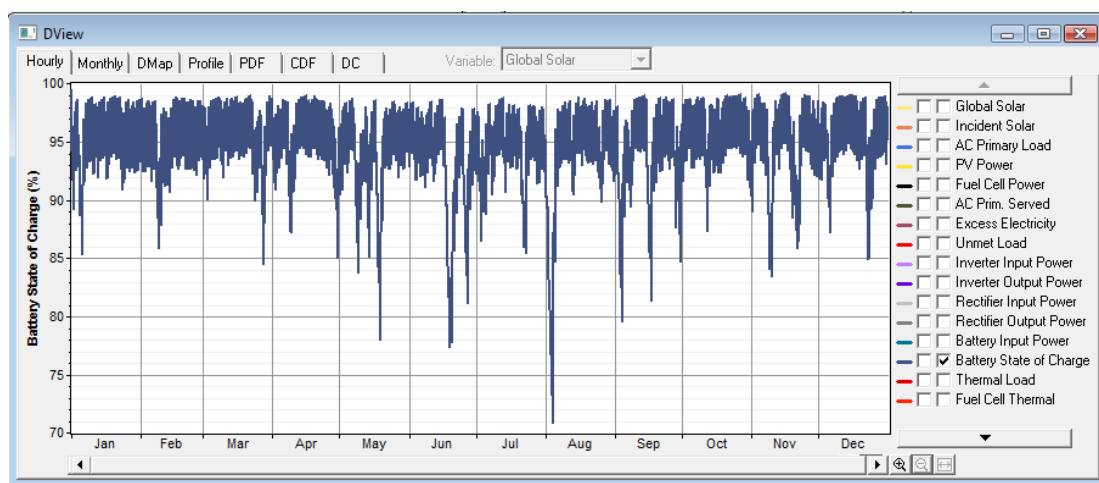


Figure 6-7. The battery bank charge status for the solar-hydrogen-battery system when it is sized for about 10 days of autonomous operation (case study chapter 4)

6.3 TRIPLE BOTTOM LINE COMPARISON

6.3.1 Economics

A solar-hydrogen system was sized and analysed again using HOMER for the case study in Chapter 4, as described in section 6.2.1. By using the same costs and lifetimes for components as in Chapter 4 (table 4-5), the unit cost of electricity is calculated as 1.17 US\$/kWh (total present cost ~US\$64 000), slightly more than the 1.06 US\$/kWh predicted earlier in Chapter 4 by RSHAP (total present cost ~US\$58 000). The difference in the results for the same system using RSHAP and HOMER, is no doubt a result of the different analytical approaches adopted by two models (section 6.1) that led to slightly different sizes for the components (table 6-1).

In the following economic comparison between the different RAPS options (listed in section 6.1) the results from HOMER are used to ensure consistency, except for the solar-hydrogen CHP system for which RSHAP is also used.

The first system discussed was a petrol generator system. The price of the Yamaha ET650 550 W generator used to meet the demand is around US\$500 (Macfarlane 2008). Assuming 20 000 hours of lifetime for a typical generator of this kind (Dalton *et al.* 2008) and considering the cost of the fuel delivered (1.6 US\$/l with 5% annual rise in the real price) and the associated maintenance cost, the cost of electricity generated by this petrol generator over an assessment period of 30 years is estimated to be about 2 US\$/kWh using HOMER (5% real discount rate used in the analysis). The average energy efficiency (output electricity per unit fuel energy input) of the generator was assumed to be 30% for this cost estimation (Ghosh *et al.* 2003). For highly-variable loads adding a battery storage to the system is recommended (Akbarzadeh 1992). Adding batteries to the system (section 6.2.2) costs about US\$2400; this adds about 10% to the overall cost of the system as well as the unit cost of electricity. Moreover, the assumption of 30% for the energy efficiency of the generator is more likely to be realistic if a battery is added to the system.

This unit cost of electricity for a petrol generator system (2 US\$/kWh) is almost double that obtained for the solar-hydrogen system sized using HOMER based on the minimum size of the fuel cell and over a 30 year assessment period (1.17 US\$/kWh). The analysis further shows that the solar-hydrogen system is competitive to the petrol generator studied provided the assessment period is 20 years if heat recovery is not considered, or 18 years or less, depending on the cost of LPG, if heat recovery is taken into consideration (figure 6-8).

These results completely agree with the findings from the research done by Ghosh *et al.* (2003), who compared a solar-hydrogen-battery system and diesel generator. The costs of the electrolyser (12,500 €/kW) and fuel cell (20,000 €/kW) used at that time were relatively high, for which the solar-hydrogen-battery system was not cost effective compared to the diesel generator. However, it was predicted that the system becomes competitive to the diesel generator when the target cost of 3000 €/kW is achieved for both fuel cell and electrolyser. It is notable that the costs of the electrolyser and fuel cell considered for the present analysis are even lower than this target cost mentioned in the research done by Ghosh, Emonts *et al.* (2003).

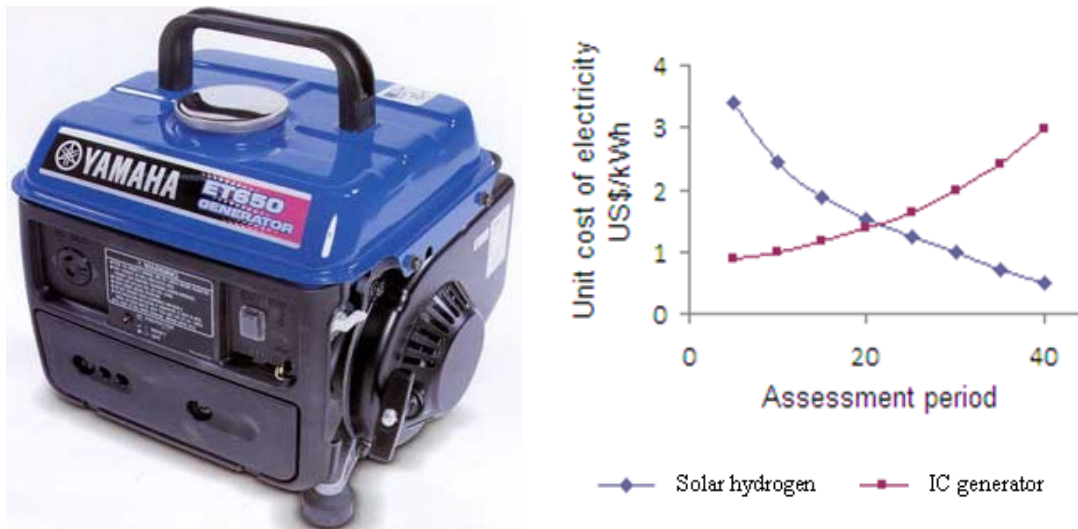


Figure 6-8. Left: Yamaha ET650 petrol generator (Macfarlane 2008); Right: The cost of the solar-hydrogen system Vs IC generator

The second system investigated was a solar PV-battery-ICE generator system (6.2.3). The unit cost of electricity for this system was estimated at above 3 US\$/kWh using HOMER, well above the cost of the electricity generated by the solar-hydrogen system (1.17 US\$/kWh). It is notable that the benefit of fuel cell heat recovery (CHP application) for the solar-hydrogen systems can also be considered. This benefit was estimated to be about US\$5000 using RSHAP in this case, equivalent to around 8% of the overall cost of the solar-hydrogen system (if no annual rise in the price of LPG saved is considered). Moreover, hydrogen-based energy storage systems are more reliable than battery-based systems due to unpredicted weather conditions and unexpected cloudy periods in south-eastern Australia (Richards and Conibeer 2007).

The unit cost of electricity for the solar-hydrogen-battery system obtained was slightly above 1 US\$/kWh. As given in table 6-2, by adding a string of eight S4KS25P battery units to the solar-hydrogen system (10 days of autonomous operation was used) the sizes of the PV array, electrolyser, and storage tank were reduced considerably compared to those obtained for the solar-hydrogen system with the minimum size of fuel cell (table 6-1). The breakdown of the cost over the assumed assessment period for this case (30 years) is shown in figure 6-9. This pie chart shows the battery storage sub-system is more expensive than the other components of the system. The battery bank in this system can potentially be

smaller if fewer days of autonomous operation are assumed for sizing the system; however, this is not recommended for the case of south east Australia due to unpredictable cloudy periods.

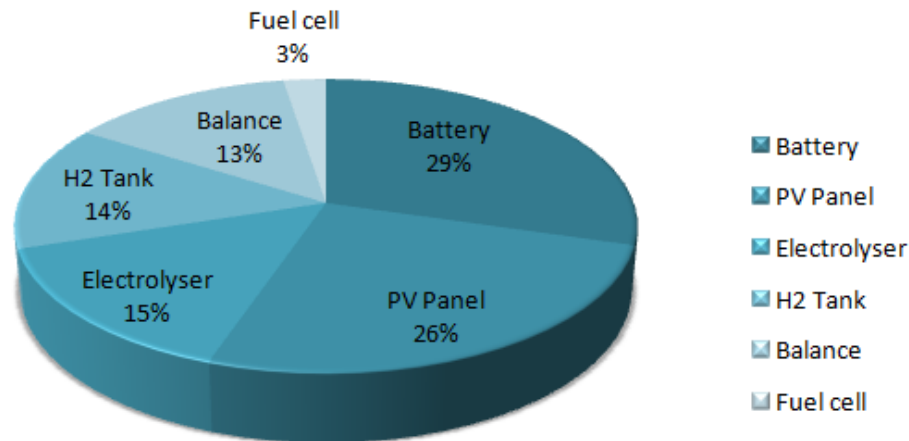


Figure 6-9. The breakdown of the total cost for a solar-hydrogen battery RAPS system used for the case study described in Chapter 4

These results suggest adding a battery storage system with a relatively low capacity to a solar-hydrogen system can lead to a more economical stand-alone RAPS system. The fuel cell in such a system lasts longer (more than 6 years) compared to the solar-hydrogen system analysed in Chapter 4 (less than 3 years) because the battery is mostly responsible for the short-duration demands supplied from the storage and this reduces the operating hours of the fuel cell. A solar-hydrogen-battery system still has the potential for fuel cell heat recovery, although to a lesser extent than in a solar-hydrogen system. The benefit of this heat recovery was estimated to be less than US\$2500 using RSHAP, equivalent to less than 4.5% of the overall cost of the system (if no annual rise in the price of LPG which is saved is considered). Table 6-3 summarises the economic comparison of the RAPS systems discussed in this section. It is noteworthy that the economic analyses on this case and all the considered RAPS alternative systems have been done assuming the existing performance and unit costs of key technologies such as PV modules, fuel cells, and electrolyzers. Undoubtedly these components are advancing technologically at a very fast pace. If the components of the solar-hydrogen system operate at higher efficiencies, and can be supplied at cheaper prices than those used for this case study, the competitiveness of the solar-hydrogen CHP system compared to the existing alternative RAPS systems will improve further relative to the results given here.

RAPS Alternative		Total present net cost of the system over 30 years (US\$) (The benefit ¹ of heat recovery was deducted from the total cost of the system where applicable)	Modelling tool used	Notes
Solar-hydrogen system	Without heat recovery	58 000-64 000	RSHAP/HOMER	<ul style="list-style-type: none"> Benefit of heat recovery rises to about US\$10 000 if 4% annual rise in real LPG price assume
	With heat recovery	~54 500-59 000	RSHAP/HOMER	
Petrol/Diesel generator	Without heat recovery	109 500	HOMER	<ul style="list-style-type: none"> Optimistic 30% energy efficiency used for the generator Cost of adding battery storage not been taken into account Recommended for relatively constant electrical loads
	With heat recovery	Some heat recovery possible from engine, but not considered here	N/A	
Solar PV-battery-ICE generator system	Without heat recovery	~170 000	HOMER	<ul style="list-style-type: none"> Back-up diesel generator needed in areas with highly variable solar irradiance Suitable for areas with relatively uniform solar irradiance profile (e.g. northern Australia)
	With heat recovery	Some heat recovery possible from engine, but not considered here	N/A	
Solar-hydrogen-battery system	Without heat recovery	55 000	HOMER	<ul style="list-style-type: none"> Optimistic 80% average round-trip efficiency for batteries assumed.
	With heat recovery	~52 500	RSHAP/HOMER	

Table 6-3. Comparing the RAPS alternatives from the techno-economics point of view (30 year assessment period) for the case study in Chapter 4

6.3.2 Environmental

If an average of 30% energy efficiency for a diesel/petrol generator is assumed (Ghosh *et al.* 2003), 0.25 kg (0.35 litre) of petrol or 0.27 kg (0.31 litre) of diesel fuel has to be

¹ This benefit comes from boosting the LPG hot water system and saving on LPG, when no annual rise in the real price of this fuel is assumed.

consumed by the generator to produce 1 kWh (3600 kJ) of electrical energy. In the case study introduced in Chapter 4 of this thesis, the conservative annual electrical demand of about 1821 kWh was assumed. Supplying such a demand needs 455 kg (0.675 kl) of petrol or 490 kg (0.565 kl) of diesel fuel per year. The emission (tonnes of CO₂-e) out of burning this amount of fuel can be estimated using the National Greenhouse Gas Accounts (NGA) factors provided by Australian Department of Climate Change (NGA 2009). According to the factors given by NGA, the emissions from liquid fuels when used in stationary power supply applications is calculated using the following equation (NGA 2009):

$$E_{ij} = Q_i \times EC_i \times EF_{ijoxec} \quad (6-1)$$

where E_{ij} is the emissions of gas type (j), (mainly carbon dioxide), from fuel type (i) (CO₂-e kg), Q_i is the quantity of type (i) (kl) combusted for stationary energy purposes, EC_i is the energy content factor of fuel type (i) (gigajoules per kl) for stationary, energy purposes (it is 34.2 GJ/kl for gasoline and 38.6 GJ/kl for diesel fuel), and EF_{ijoxec} is the emission factor for each gas type (j) (which includes the effect of an oxidation factor) for fuel type (i) (kilograms CO₂-e per gigajoule). It is 66.7 kg CO₂-e/GJ for gasoline and 69.2 kg CO₂-e/GJ for diesel fuel (NGA 2009).

Based on this equation 1540 kg CO₂-e/year for petrol and 1510 kg CO₂-e/year for diesel generators are estimated for this application. These emissions are completely avoided in the various solar-hydrogen system options, with or without batteries. This emission is also partly produced by the systems in which ICE generators are used as back-up. For example for the case of solar PV-battery system, discussed in section 6.2.3, the Yamaha ET650 petrol generator that was used to back-up the system mainly during the winter time was responsible to supply slightly less than 15% of the total annual load (~250 kWh), leading to above 200 kg CO₂-e/year.

This is not the only place that the amount of emission production is reduced. As investigated by this research the solar-hydrogen system can be potentially used for a remote area CHP application. If the amount of recovered heat is translated to saving on LPG consumed in a domestic hot water system, a further emission reduction of 140 kg CO₂-e/year is obtained.

When it comes to comparing the hydrogen energy storage systems (electrolyser, hydrogen storage tank, and fuel cell) with systems which include battery storage, the issue arises of end-of-life waste management of batteries. The disposal of batteries can potentially spread different toxic materials around, such as lead, cadmium, sodium, sulphur, bromine, etc. (Ro and Rahman 1998). Another obvious issue with batteries, in particular lead-acid batteries, is the volume of precious raw materials consumed in their manufacture. For example, lead acid batteries account for 88% of lead consumption in US (Genaidy *et al.* 2008), which is an issue from both raw material consumption and waste management points of view.

Pollution associated with manufacturing batteries is another matter to be considered here (Dahodwalla and Herat 2000), as well as with making the components of a solar-hydrogen system. A comprehensive life cycle analysis of all the options is necessary to compare them in terms of embodied emissions and other pollution issues. But such an analysis is beyond the scope of the present study, and the systems are compared here based on their in-operation emissions only. Table 6-4 is the summary of comparing the RAPS alternatives investigated in this chapter from the in-operating GHG production and environmental point of view:

RAPS Alternative	Total GHG emission (kg CO ₂ -e/year) (based on 5 kWh daily electrical demand throughout the year)	GHG reduction through heat recovery and saving on LPG (kg CO ₂ -e/year) (The hot water supply system runs on LPG)	Notes
Solar-hydrogen system	0	140	The most environmentally-friendly alternative
Petrol/Diesel generator	1510-1540	Applicable but not calculated	In practice the efficiency of the generator is less than 30% when connected to a variable load and hence more GHG emission is expected
Solar PV-battery-ICE generator system	~200	Applicable but not calculated	Less environmentally-friendly than solar-hydrogen systems due to the end-of-life waste emissions of the batteries
Solar-hydrogen-battery system	0	~50-70	Less environmentally-friendly than solar-hydrogen systems due to the end-of-life waste emissions of the batteries

Table 6-4. Comparing the RAPS alternatives from the environment point of view for the case study

6.3.3 Social

The potential of the solar-hydrogen system in avoiding the emissions associated with traditional systems, in which petrol/diesel generators or battery are used, can be counted as undeniable social benefits as well, for example, in terms of the contribution to avoiding catastrophic climate change that could have widespread adverse social impacts.

Despite the existing negative views about the hazard level associated with hydrogen, this fuel has been proven to be safer than liquid fossil fuels such as diesel and petrol fuels if handled properly and appropriate safety measures are taken (Dahoe and Molkov 2007; Edwards *et al.* 2008). Since the nature of hydrogen is different from the commonly-used fuels, its handling needs to be introduced to the public through well-established standards and educational programs (Dahoe and Molkov 2007) before its introduction to the energy market for general use by the public. These days, the lack of safety standards in this area is being dealt with in both national and international forums, such as: Canada's hydrogen safety program (MacIntyre *et al.* 2007); Spain's development of standards on hydrogen safety (Luis Aprea 2008); and efforts taken in the USA for developing national standards on hydrogen (Cairns 2010). These set the stage for the society gradually accept hydrogen as a safe alternative to the existing fossil fuels. These safety standards also help reduce the risks associated with hydrogen to an acceptably low level. It is very important to avoid accidents with hydrogen as this technology does not have yet a very established public position and any such accidents can create a negative perception that is very difficult to be reversed at a later stage (Schulte *et al.* 2004).

Exposure to solar-hydrogen systems must occur over a period of time before users can gain familiarity and accept this technology as part of their lives. It is quite expected that the general public are sceptical about a novel technology that has not been widely experienced and tried before. So such new hydrogen-based systems have to be well-introduced to the public with associated education and marketing programs to help establish their place in the market.

With respect to the recently-emerged public awareness about the issue of climate change and the rising price of fossil fuels, hydrogen has a great chance of being accepted by the public as a strong alternative to generators that run on non-renewable and emission-

intensive fuels. Reducing the cost of solar-hydrogen systems at the same time can definitely speed up this transition process. The present research will hopefully make a contribution to understanding and improving the economic competitiveness of solar-hydrogen RAPS systems, and hence improve their acceptability among potential users compared to the existing mostly fossil-fuel-based alternatives.

Another potential social benefit of introducing solar-hydrogen systems for RAPS is the economic development benefits in remote areas as they gain more reliable and cost-effective stand-alone energy supplies and though creating new jobs for local people in installing and maintaining such systems. These systems also have a very strong potential in rural areas in developing countries without grid power to provide both electricity and heat energy in a zero-emission and economically-competitive manner.

6.4 CONCLUSION

The nature of the load, local environmental condition, cost, and degree of reliability are the important factors to be considered when choosing a power supply system for a remote site. As part of this study, a number of RAPS alternatives including solar-hydrogen (CHP) systems, ICE-based generators (with or without battery back-up), solar PV-battery-ICE generator system, and solar-hydrogen-battery (CHP) have been investigated using HOMER and RSHAP (for the case studied in Chapter 4). This investigation on the case and power supply options introduced in chapter 4 and 6 revealed that solar-hydrogen CHP system is cheaper than diesel/petrol generators and solar PV-battery-ICE generator systems for areas with a highly variable seasonal solar irradiance profile such as south-eastern Australia with such a size (~ 5 kWh/day) and pattern of electrical demand profile. The investigation also showed that adding battery to the solar-hydrogen system can slightly improve the economic viability of the system.

From an environmental point of view, solar-hydrogen system can be the obvious choice due to generation of electricity at near zero-emission. Moreover, by employing the system as a CHP unit some more GHG emission can be avoided due to saving on conventional fossil fuels (e.g. LPG) normally used for remote area hot water supply. ICE-based generators are the worst options from the GHG emission view point and the alternatives

using battery are less environmentally-friendly than systems with hydrogen energy storage only (electrolyser, hydrogen storage tank, and fuel cell) due to the issue with their end-of-life toxic waste management.

Using solar-hydrogen systems can bring direct social advantages (particularly to remote areas) such as job creation and energy security and indirect advantages like contribution in building a healthier environment for the people around the world. However, these systems still needs improvement while being more introduced to the users so that people will get the chance of becoming friend with it to start enjoying the benefit.

Table 6-5 is the summary of TBL analysis on the RAPS alternatives investigated in this chapter. The results are mainly based on the remote residential case introduced and investigated for using solar-hydrogen system in Chapter 4.

RAPS Alternative	TBL Evaluation Summary		
	Economic	Environmental	Social
Solar-hydrogen	<ul style="list-style-type: none"> • Relatively high set-up cost • Recommended for areas with highly seasonal solar irradiance profile • The total cost is less than petrol/diesel generators and solar PV battery systems (with back-up ICE generator) <p>Additional benefits of CHP mode:</p> <ul style="list-style-type: none"> • at least an 8% reduction in the total present net cost of the system • Encourages users to choose these systems 	<ul style="list-style-type: none"> • Avoids above 1500 kg CO₂-e/year if replaced with diesel/petrol generators • Eliminates the problem with end-of-life waste management of batteries if replaced with systems using battery-based energy storage <p>Additional benefits of CHP mode:</p> <ul style="list-style-type: none"> • Offers the opportunity of avoiding about 140 kg CO₂-e/year through saving on LPG 	<ul style="list-style-type: none"> • Needs further introduction to be accepted by the users • Energy security (independency from fossil fuel supply) • Health improvement through reducing GHG emissions • Job creation for the local people living in remote areas

next page ...

... from the previous page

<p>Petrol/diesel generator</p>	<ul style="list-style-type: none"> • Low initial set-up cost • High running cost, including fuel and maintenance • Technically possible to collect the waste heat for purposes like hot water supply, but rarely done in practice in RAPS applications 	<ul style="list-style-type: none"> • At least above 1500 kg CO₂-e/year GHG production • The environmental issue with batteries may included if they are used in the system (for variable loads) • Heat recovery could lead to GHG emission reduction, but rarely implemented 	<ul style="list-style-type: none"> • Negative indirect effects on the societies due to its emissions • A mature technology and widely accepted by the users, particularly because of its low set-up cost
<p>Solar PV-battery-ICE generator</p>	<ul style="list-style-type: none"> • Relatively high set-up cost • The system is more expensive than the other alternatives here • Heat recovery from generator possible but rarely done 	<ul style="list-style-type: none"> • Production of above 200 kg CO₂-e/year • The issue with end-of-life waste handling of batteries • 	<ul style="list-style-type: none"> • Less popular than ICE-based generators due to its high set-up cost • Potential negative health impacts due to its hazardous end-of-life waste of batteries
<p>Solar-hydrogen-battery</p>	<ul style="list-style-type: none"> • Relatively high set-up cost • Adding batteries can lower the total cost of the solar-hydrogen CHP system by over 10% <p>Additional benefits of CHP mode:</p> <ul style="list-style-type: none"> • A 4-5% lowering of total costs compared to using the system in power-only mode 	<ul style="list-style-type: none"> • Avoiding above 1500 kg CO₂-e/year if replaced with diesel/petrol generators • The issue with end-of-life waste handling of batteries <p>Additional benefits of CHP mode:</p> <ul style="list-style-type: none"> • Offers the opportunity of avoiding above 50 kg CO₂-e/year through saving on LPG 	<ul style="list-style-type: none"> • Needs further introduction to be accepted by the users • Energy security (independency from fossil fuel supply) • Health improvement through reducing GHG emissions • Job creation for the local people living in remote areas

Table 6-5. Overview of TBL-based comparison of RAPS alternatives for the case study conducted

7 Conclusions and recommendations

7.1 RESPONSE TO THE RESEARCH QUESTIONS

7.1.1 Introduction

Both theoretical and experimental investigations performed in the course of this research project now allow responses to be given to the research questions posed at the beginning of this thesis in Chapter 1.

7.1.2 What are the main factors affecting the performance of solar-hydrogen CHP system?

The efficiency of the fuel cell is a determining factor for the overall efficiency of the solar-hydrogen system. This research focussed on the fuel cell to get this component performing at a higher efficiency to improve the overall performance of the system. By choosing a fuel cell larger than the minimum required size dictated by the peak of the demand in the case study of remote household in south-eastern Australia (Chapter 4), the average annual efficiency of this component, when operated in the solar-hydrogen system, was increased by up to 8% points. This improvement led to just above a 12% reduction in the unit cost of electricity generated by the system, and an improvement in the average annual round-trip electrical efficiency of the energy storage sub-system (electrolyser, hydrogen storage tank, and fuel cell) from 24% to just below 30%.

The experimental study and the results obtained from the model showed that when both heat and power are extracted from the fuel cell, the overall energy efficiency of this component can be doubled (to about 70%) compared to a power-only application. In the case of a PEM fuel cell, this heat is suitable for low-temperature heating applications such as domestic hot water supply. The option of using the recovered heat from the fuel cell was investigated by this research and the economic benefit of this heat recovery to be used for boosting an existing LPG hot water supply was quantified. The results will be summarised again in subsection 7.1.3.

Obviously, factors that affect the fuel cell heat generation also influence the overall performance of the solar-hydrogen CHP system. The fuel cell heat and water management are closely related. Particularly the amount of available heat for extraction is largely affected by how the water produced by the fuel cell is managed. This water can be formed inside the fuel cell either as a liquid, vapour, or a saturated mixture phase depending on the conditions (the operating temperature of the fuel cell and the partial pressure of the water produced). The energy source for evaporation of this water is the heat generated inside the fuel cell. If the water is evaporated, the available heat for extraction is reduced, since part is already used for water evaporation; and if the water remains in liquid form, more heat is available for extraction, but there is a considerable drop in the electrical performance of the fuel cell as the cell may become flooded.

The stoichiometry of the air fed into the fuel cell and the fuel cell operating temperature are the two key factors determining the saturation temperature of water at its partial pressure inside the fuel cell. The experimental setup allowed investigation of the effect of these two factors on the performance of the 500 W PEM BCS fuel cell used for the experimental part of this study.

Decreasing the operating temperature can lead to liquid water produced inside the fuel cell, and hence increases the heat available for collection by the cooling system. For example, it was found that the cooling load of the fuel cell was increased by 180% at a current of 5A, and by about 50% at 25 A when the operating temperature was reduced from 60 °C to 40 °C (figure 5-31).

As just mentioned, formation of liquid water inside the fuel cell (e.g. at low operating temperatures) is not a desirable situation from the power production point of view as at the same time it adds to the fuel cell overpotentials and reduces the electrical energy efficiency; moreover, the fuel cell may get flooded and operates at a very unstable condition for a continuous uniform power supply due to the accumulation of water in the fuel cell membrane (figure 5-28). When the fuel cell is operated at a low temperature compared to its designed operational temperature, increasing the air stoichiometry can partly reduce the negative effect of low temperature of operation on the performance of the fuel cell.

The experimental results showed the overall energy efficiency of the system in CHP application is almost independent of the electrical performance of the fuel cell as the current density is varied (figure 5-36). By increasing current density, the electrical efficiency drops but the CHP efficiency remains almost constant (its small variation is mainly due to the variation of hydrogen utilisation coefficient). This behaviour is simply due to conservation of energy: when the fuel cell operates at lower electrical efficiency more heat is generated and vice versa (figure 7-1). Clearly the primary purpose of the fuel cell in a solar-hydrogen system is electricity generation (see section 4.3.3.3), and its size is basically determined on the basis of electrical efficiency; heat comes as a by-product and is not a primary factor in system sizing.

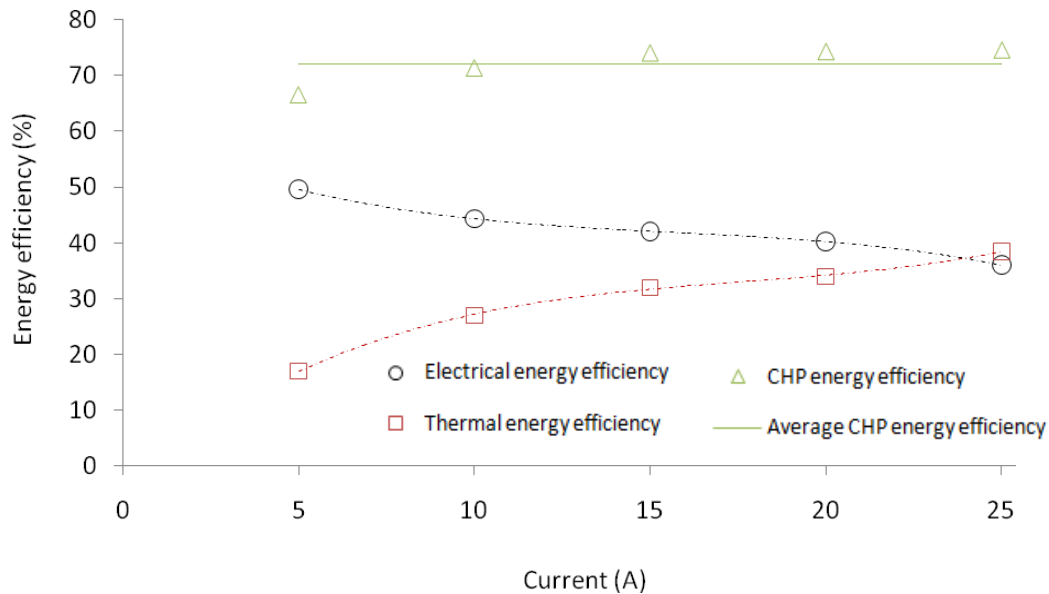


Figure 7-1. The experimentally-measured electrical, thermal (based on the cooling load extracted and not the total heat generated), and CHP energy efficiency of 500-W BCS PEM fuel cell; operating temperature 60 °C; exit air pressure 30 kPa; air stoichiometry 2; inlet hydrogen pressure 20-30 kPa

7.1.3 To what extent can the overall energy efficiency and hence economic viability of a solar-hydrogen system for remote applications be improved by utilising the waste heat from fuel cell operation for water or space heating?

Both theoretical and experimental investigations on the 500 W BCS PEM fuel cell used as the basis of the RAPS case study presented in Chapter 4 (figure 4-41) found that the heat generated by the fuel cell is almost equal to its electrical power generation at low current densities, and considerably more than its power generation rate at higher current densities.

The results showed that 60-70% of the heat produced by the PEM fuel cell can be collected by the fuel cell cooling system to boost an existing hot water system (figure 4-40). Correspondingly the overall average annual energy efficiency of the fuel cell was estimated by the model to be increased from 33% (or a few percent more according to the experimental polarisation curve of the fuel cell) in power only application to above 68% in combined heat and power production (the experimental fuel cell polarisation curve was fed into the model to obtain this). The experimental study also found an average CHP efficiency of about 72% for this fuel cell.

In this case study, the average annual round-trip energy efficiency of the hydrogen storage sub-system in a power only application was estimated using RSHAP, the solar-hydrogen system model developed in this research program, to be just above 24% for the basic system with the minimum size of the fuel cell, and about 30% when an economically-optimal fuel cell size was used. This round-trip energy efficiency in a CHP application was improved to about 45% for both systems with minimum size and optimally-sized fuel cells.

The net economic benefit of using the heat recovered from the fuel cell for domestic water heating in the content of the case study has been investigated (see section 4.4.3). It was assumed that the heat extracted from the fuel cell was utilised to reduce the amount of fuel used by an LPG water heating system. The use of this recovered heat yielded a 35% saving in annual LPG consumption. The economic benefit of this saving was equivalent to about 15% of the overall cost of the system over an assessment period of 30 years at a 5% real discount rate, when assuming a 4% annual rise in the real price of LPG, and equivalent to 8% of total system cost if no real price rise of LPG is assumed. Supplying 35% of the total annual energy demand for hot water supply system means the system could thus almost complement a conventional solar water heating system in such a location by providing the boosting energy (usually in the order of 40% of the total) normally obtained from gas or electricity. Hence the additional benefit of a zero greenhouse gas emission water heating system for RAPS applications would be provided, in which the fuel cell waste heat acts as the booster for a solar water heating system. The fuel cell in a solar-hydrogen system is usually operated when not enough solar radiation is received by the PV arrays. At this time the solar thermal collectors for hot water supply do not receive enough solar radiation input as well. Hence there is a perfect match between the boosting required by the solar water heater and fuel cell heat recovery.

Boosting a remote area hot water system is not the only envisaged potential application for the fuel cell heat. Other potential applications include space heating, cooling electronic equipment via an absorption chillier in remote telecommunications facilities, and use of the heat to stimulate hydrogen release from metal hydrides used for solid state storage of hydrogen.

7.1.4 What is the economically-optimal size of a solar-hydrogen CHP system for a remote household with given electrical and hot water demand?

The solar-hydrogen CHP system optimised using RSHAP for the case studied in this thesis (5 kWh daily demand peaked at 0.3 kW in south-eastern Australia) included a 3.4 kW PV array, a 2.8 kW PEM electrolyser, a 17.7 kg hydrogen tank, and a 1 kW PEM fuel cell. The PV array, the electrolyser, and the fuel cell operate at average annual energy efficiencies (based on HHV of hydrogen where applicable) of about 10%, 73%, and 41% respectively. This setting yields to generating electricity at a unit cost of about 0.94 US\$/kWh.

The fuel cell in a solar-hydrogen system is normally sized based on the peak point of the demand and this component has to be able to meet this peak if no other input is received from the PV array. For a load profile with a particular peak value the RSHAP modelling has shown that it is always possible to choose a fuel cell with a capacity larger than this peak in order to achieve a better overall fuel cell efficiency, and hence smaller sizes of other components and a lower system cost. Yet there is a definite limit as to how much the fuel cell size can be increased before its extra costs offset completely the savings in the rest of the system through its higher efficiency of operation. As shown by figure 4-26, the optimum size of the fuel cell (~1 kW) yielded about 8% point improvement (from 33% to 41%) in efficiency throughout the year compared to the fuel cell sized just for meeting the peak demand (0.31 kW). Using the optimally-sized fuel cell, which is above three times larger than its minimum size, for the case studied in Chapter 4, led to 15%, 15%, and 18% reductions in the size of the PV array, electrolyser, and hydrogen storage tank respectively compared to when the minimum size of the fuel cell was used (see figure 4-27 and figure 4-28). Such a situation led to a system 12% cheaper than the original system with the minimum size of fuel cell.

Furthermore, running the fuel cell at relatively low current densities helps increase its lifetime, leading to an additional system cost reduction; however, this potential benefit has not been taken into consideration in the economic analysis of the system for this case.

When using the optimally-sized fuel cell, the potential energy saving through heat and excess hydrogen recovery used for hot water supply reduces by about 19% points, and hence less LPG for hot water can be saved. In a CHP application, if the annual rise in the real price of LPG is less than 7.3%, the optimally-sized system still remains as an economically-preferable option for the CHP solar-hydrogen system compared to the system with the minimum size of fuel cell; however, if the annual rise is more than 7.3% (a highly-unlikely scenario), using the minimum size of the fuel cell is the preferable option economically.

As a part of effort for finding the best sizing strategy for the solar-hydrogen system in this case study, two conditions for the hydrogen tank were used in the analysis: constrained and unconstrained. The RSHAP modelling showed that constraining the hydrogen tank to smaller sizes leads to increasing the size of PV and hence the electrolyser. These two components are expensive, particularly the PV array (figure 4-14). Hence the overall cost of the system is increased under the constrained hydrogen tank condition due to the added cost to the PV array and electrolyser, despite the saving on the tank (table 4-6). For the case of a remote area, normally plenty of space is available for a large hydrogen storage tank.

7.1.5 How does a solar-hydrogen CHP system compare on a triple bottom line basis with conventional alternatives?

7.1.5.1 Economic benefits

Using an assessment period of 30 years, the cost of a petrol generator system (including O&M costs) for the case studied in Chapter 4 was estimated to be about US\$110 000 (using HOMER). This was considerably higher than the US\$52 500 - 54 500 estimated using RSHAP and HOMER for a solar-hydrogen CHP system for the same case. On the basis of the RSHAP analysis, the solar-hydrogen system remains economically competitive compared to the petrol generator (in this case a Yamaha ET650 550 W) provided the assessment period is more than 20 years (with no heat recovery). This can be reduced to 18

years if the economic benefit of fuel cell heat recovery is taken into account (no annual rise in the real price of LPG assumed). These minimum assessment periods are well within the lifetime of the solar-hydrogen system. The low initial capital cost of diesel/petrol generators is still an advantage over solar-hydrogen systems, although ICE generator-based power supply systems are on this analysis more expensive than solar-hydrogen systems in the longer term (e.g. 25-30 years).

Battery energy storage is an alternative to hydrogen-based storage system to be used in conjunction with PV arrays for electrical power supply. However, for areas like southeastern Australia with highly-variable seasonal solar irradiance profile, this storage system cannot provide sufficient reliability of supply throughout the year. An ICE generator is thus normally incorporated into a solar PV-battery system in such areas to provide the required continuity of supply particularly during winter time. According to the analysis done by HOMER, the cost of a solar PV battery-generator system (US\$170 000) is considerably higher than the solar-hydrogen system, even before taking the economic benefit of the fuel cell heat recovery into account.

The analysis using RSHAP and HOMER shows that adding a relatively low energy capacity battery bank to the solar-hydrogen system to handle the short-term storage requirements can slightly improve the economics of the solar-hydrogen system (by up to 10% in this case study). Solar-hydrogen-battery systems that offer both long-term and short-term storages are thus technically-sound RAPS alternatives for areas with highly-variable solar radiation from summer to winter such as Melbourne. In this system the battery is mostly responsible for the short-term storage (e.g. night time) and this partly removes the load from the fuel cell. Hence the fuel cell in such a system lasts longer than that used in a solar-hydrogen system (almost double the time in this case study in Chapter 4). The fuel cell heat recovery potential of the solar-hydrogen-battery system is reduced to less than half that in the straight solar-hydrogen system.

In a broader context, improving the economics of solar-hydrogen RAPS systems can help these and other sustainable hydrogen-based systems penetrate into national and international energy markets. Such systems can help reduce dependency of the global economy on fossil fuels and thereby improve the world's economic stability.

7.1.5.2 Environmental benefits

A diesel/petrol generator produces above 1500 kg CO₂-e/year to supply a 5 kWh daily demand throughout the year (Chapter 6). Solar-hydrogen systems are a near zero-emission power supply system and their introduction can eliminate the greenhouse gas emissions and other pollution normally associated with fossil-fuel-based systems. Hot water supply systems running on fossil fuels also contribute to CO₂ emissions, which can be partly avoided when fuel cell heat is recovered and used for hot water supply. While the emission reduction through fuel cell heat recovery is not considerable by itself (just less than 140 kg CO₂-e/year for the case studied in Chapter 4), this heat recovery is an advantage for the system's economy, which in turn promotes its market acceptance. A significant emission reduction is thus foreseeable if the system is widely deployed instead of traditional fossil-fuel-based power supply systems.

The GHG emission for solar PV-battery-ICE generator systems for the case study in south-eastern Australia (above 200 kg-CO₂-e/year) is considerably less than petrol/diesel generator systems, since the back-up generator supplies less than 15% of the demand. However, similar to any other systems with batteries, the end-of-life waste management of batteries is still an environmental concern. This problem can be avoided if hydrogen-based energy storage systems (electrolyser, hydrogen tank, and fuel cell) are replaced with battery-based storage systems.

7.1.5.3 Social benefits

Solar-hydrogen systems for stand-alone power supply, such as RAPS applications, can yield the following main potential social benefits:

- A contribution to the global effort to avoid climate change by providing a zero greenhouse gas emission solution for remote area and other stand-alone and back-up power supplies.
- Provision of a cost-effective, reliable, secure and low maintenance energy supply for remote and isolated communities that can help improve their quality of life and

economic independence, and for remote agricultural, industrial and mining facilities that can enhance their economic competitiveness.

- Opening up industry development and employment opportunities for Australian industry in manufacturing and installing the new solar-hydrogen CHP systems.

The social benefits of employing the solar-hydrogen system will not be achievable until they become widely accepted by potential users and the local communities. Currently, the high initial capital cost of such systems and the lack of proven commercially available units are barriers in the way of market take-up. The concept of using a solar-hydrogen system for both heat and power production (CHP) as investigated in the present thesis offers a promising opportunity for improving the system's economics and encourage market adoption by providing an integrated solution to both the electricity and the water heating requirements of remote applications.

There remains a lack of awareness in the community at large and by governments about the potentially-beneficial role of hydrogen as a storage solution allowing continuous supply from intermittent renewable energy sources. There is a lot of misunderstanding about the level of risks involved in using hydrogen as a fuel, and a lack of agreed safety standards. The benefits of hydrogen including its safety advantages compared to the conventionally-used fossil fuels must therefore be explained to the public and industry. Hydrogen safety standards are now being more developed and these will help create a more promising future for hydrogen in terms of acceptability by the public.

7.1.6 Which components of a solar-hydrogen CHP system require further research and development to enable such systems to compete with conventional alternatives?

The investigation here has identified and focussed on two opportunities to reduce the cost of solar-hydrogen systems:

- System optimisation
- Fuel cell hydrogen and heat waste recovery used for hot water supply

The system optimisation was done to minimise the overall net present cost of the system by oversizing the fuel cell (above the minimum size normally dictated by the peak of the demand). The optimally-sized fuel cell then showed an improvement in its average annual electrical energy efficiency from 33% to 41% when operated in a solar-hydrogen system. A 1 kW fuel cell yielded the minimum unit cost of electricity (~0.94 US\$/kWh) generated by the solar-hydrogen system, 12% less than that achieved in a system with minimum size of the fuel cell (dictated by the peak of the demand). The system optimisation led to an improvement in the round-trip electrical energy efficiency of the hydrogen storage sub-system (electrolyser, fuel cell, storage tank, and fuel cell) from 24% to about 30%. Although these figures are only applicable to the case study introduced in chapter 4 with its associated assumptions (e.g. load profile, economic assumptions and technical characteristics of the components), the overall optimisation methodology developed here (oversizing the size of the fuel cell) is valid to optimise any other systems of this kind.

This optimisation also indirectly indicates that improving the performance of the fuel cell through technological development can enhance the economic viability of the system (figure 4-37 and table 4-8). Technological advancement and research conducted in this area are promising more efficient fuel cells to be introduced to the market in the foreseeable future. Continued research and development to raise the energy efficiencies of the electrolyser, hydrogen storage and fuel cell all combined are critically important to raise the round-trip energy efficiency of the hydrogen energy storage sub-system

The possibility of recovering the waste heat and hydrogen from the fuel cell has also been investigated. The average annual round-trip energy efficiency of the energy storage sub-system (24% and 30% for the fuel cell minimum size and the optimally-sized fuel cell cases respectively in power only application) can be potentially increased to about 45% if the fuel cell heat recovery is utilised (this can be increased to 50-55% if hydrogen waste is recovered as well). The average energy efficiency of the fuel cell in power only application can also be increased to about 70% in CHP mode operation.

The heat recovered from the fuel cell was assumed to be utilised for boosting a remote areas LPG-based hot water system. This heat may also be utilised for other purposes, such as stimulating hydrogen extraction from metal hydride hydrogen storage system, heating up the water consumed by the electrolyser, or for space heating. Further investigations are

warranted into ways of utilising this heat effectively in improving the economics of the system in a range of RAPS applications.

The excess hydrogen was also assumed to be collected and burned to boost the hot water system. The other possible option is recycling this hydrogen back to the hydrogen tank to be reused in the fuel cell. However, the technical design and economics of this recycling process would need to be analysed to see if this option is practical and economically viable.

The feasibility of coupling the fuel cell cooling system with the hot water supply system and also collecting and burning the excess hydrogen to boost this hot water system are other potential areas for further investigation. Further R&D and a complete demonstration of this coupling in solar-hydrogen system (with and without utilising the excess hydrogen) can be a significant step towards commercialising the idea of solar-hydrogen CHP system.

An imperative requiring further work is to reduce the initial capital cost of a solar-hydrogen system. Although the total present net cost of the system for assessment periods in the range 20-30 years is better than that for mature systems such as petrol/diesel generators, the initial capital cost of solar-hydrogen systems is substantially higher. For example, the total present cost of the solar-hydrogen system studied in Chapter 4 and 6 of this thesis was about US\$60 000; a considerable part of it was the initial set-up cost. This is much higher than that needed to setup a ~0.5 kW petrol generator (the generator is only US\$500). As shown by figure 4-14 and figure 4-29, the PV array and the hydrogen tank were found to be the most expensive parts of the system. Using cheaper options for these two components would clearly assist in reducing this high initial capital cost. Entering into high-volume production for these components is another step towards lowering their costs and hence improving the economic attractiveness of the solar-hydrogen system as a RAPS system alternative. However, further research on these components to move them ahead technologically may also be necessary to achieve the required cost reductions.

Extending the lifetime of the electrolyser is another technical challenge requiring further research and development. Figure 4-33 shows increasing the lifetime of this component from 5000 hours to 15000 hours can lead to a 15% lowering of the unit cost of the electricity generated.

The simulation program RSHAP, created to model the solar-hydrogen CHP system can also be developed further to achieve more accurate estimations about the performance of the system under variety of inputs and operating conditions. The potential for improving this simulation model will be addressed in the recommendation section of this chapter.

7.2 CONCLUSIONS

The research for this PhD thesis focussed on computer modelling, design, optimisation, and evaluation of a stand-alone solar-hydrogen CHP system for supplying both electricity and heat for a remote application. The main challenge was to improve the overall economics of the system by harnessing the thermal load of the fuel cell to meet other heat demands (e.g. domestic hot water) that would otherwise require purchase of a fuel to supply.

As the first step towards achieving this aim, a general mathematical model to simulate the performance of a solar-hydrogen system for remote applications, both with and without operation in CHP mode, was developed. The model is able to perform both technical and economic analyses on the system, and is more comprehensive in terms of the scope of the parameters included than previous models. The novel model developed, named RSHAP (RMIT Solar-Hydrogen Analysis Program), comprises 20 000 plus lines of programming written in Pascal language, and is presented in a visual-based environment. The sub-models for the PV module, electrolyser, and fuel cell incorporate some of the most recently-developed theoretical frameworks. Importantly the program has the capability of optimising the system configuration, including sizing of all the components, to find the lowest unit cost of electricity. It also allows the user to perform a waste recovery analysis on the system with a focus on the fuel cell, normally the largest source of heat and hydrogen wastage in the system.

A remote household with a 5 kWh daily electrical demand peaked at 0.3 kW in south-eastern Australia was investigated as a case study using RSHAP. An array of BP275 PV modules, a fuel cell stack based on the performance of a single cell of a 500 W BCS PEM fuel cell, and an electrolyser stack based on the performance of a single cell of a 50 W StaXX7 electrolyser were used for this case study.

First, the basic scenario was analysed in which the fuel cell capacity was set to its minimum possible value (~0.3 kW) so that this component can just meet the peak demand by itself if no power comes from PV. In addition, the unconstrained storage condition was applied in which the hydrogen tank is sized to accommodate all the hydrogen produced by the electrolyser. The RSHAP modelling concluded that a 4 kW PV array, a 3.3 kW electrolyser, and a 21.5 kg hydrogen tank were needed to keep the system working continuously, and that the corresponding average cost of electricity supplied over an assessment period of 30 years would be 1.06 US\$/kWh.

Then different other sizing strategies, the possibility of system optimisation, and fuel cell heat and hydrogen waste recovery were investigated using this case study. Hydrogen tank and fuel cell sizes show flexibility for being varied by the designer while still providing the basic requirements for the system. The possibility of using a constrained hydrogen tank was studied, but the RSHAP modelling showed this option may not be a viable solution for reducing the cost of the system. Reducing the size of the tank from 21.5 kg (unconstrained tank) to a constrained size of 3 kg led to about 35% increase in the unit cost of the electricity (nonlinearly) generated by the system (minimum fuel cell size used). This is basically because a solar-hydrogen system with smaller hydrogen tank requires a larger PV array to keep providing continuous power supply throughout the year. In the example just provided, such a reduction in the size of hydrogen tank led to doubling the size of the PV array compared to that required for a system sized using an unconstrained tank.

The fuel cell of the system has to be able to handle the peak of the electrical demand all by itself if needed; thus the minimum required size of the fuel cell is normally determined by this peak. More than 50% of the total annual demand is provided through the fuel cell at an average efficiency of 33% and the rest is supplied directly by the PV arrays at an average annual efficiency of about 10%. The case study showed that by increasing the size of the fuel cell from 0.3 kW (minimum size to supply the peak) to about 1 kW the average annual electrical energy efficiency of this component improved by just more than 8% reaching just above 41%. Due to the better average efficiency of the 1-kW fuel cell, and less hydrogen consumption by this component, the size of the PV panel, and electrolyser can be reduced by about 15% each, and the hydrogen tank can be chosen 18% smaller than that used in the system with the minimum size of fuel cell. Adopting this strategy in sizing the system yielded a reduction in the unit cost of electricity produced to about 0.93-0.94 US\$/kWh,

12% lower than when the fuel cell is chosen just to meet the peak demand. The unit cost of electricity increased when the chosen fuel cell was larger than 1 kW, so the optimal size of the system was that in which a 1 kW fuel cell was used.

The sensitivity of these results to the basic assumptions used in the analysis was investigated. The two important factors in performing economic analysis on the system are the total cost of the individual components over an assumed assessment period and their lifetime. The cost of the fuel cell minimum size is just 1.64% of the total cost of the system and hence the effects of its lifetime and cost assumptions are quite negligible. For example a 50% increase in the initial cost of the fuel cell can only leave less than 1% increase in the overall cost of the system. The share of the fuel cell cost of the total cost of an optimal system is slightly more (6.2%); however, the sensitivity of the results to its cost and lifetime assumptions is still negligible. Although the results of the economic analysis on the system are almost independent of the assumptions made for the cost and lifetime of the fuel cell, the performance of this component has a critical role on the system's overall performance and hence the unit cost of electricity generated. For example the hydrogen utilisation coefficient of the fuel cell was assumed about 85% for doing the theoretical investigation using the model. But every 1% improvement in this assumption leads to around a 1% reduction in the overall cost of the system. A 10% lowering of the fuel cell overpotentials can yield up to a 7% reduction in the overall cost of the system.

The results of the cost analysis are very sensitive to the cost of the PV array as this component is the most expensive component in the system (above 50% of the overall cost of the system). A 50% increase in the initial cost of the PV array led to a 20% increase in the overall cost of the system (over 30 years and at a 5% real discount rate). The next most expensive part of the system after the PV array is the hydrogen storage tank (above 20% of the overall cost of the system). Increasing the cost of the storage tank by 50% gave a 10% increase in the overall cost of the system. The effect of the cost assumption for the electrolyser is less than those for the PV array and hydrogen tank. Increasing the cost of the electrolyser from 1500 US\$/kW to 2250 US\$/kW yielded a 6% increase in the overall cost of the system. The lifetime used for the electrolyser in this case study showed a considerable effect on the overall cost of the system. If the lifetime of 15000 h assumed for the electrolyser decreases to 5000 h, the unit cost of electricity can increase from 1.06 US\$/kWh to above 1.25 US\$/kWh.

The results obtained in the case study were also sensitive to the financial assumptions made. Doubling the real discount rate to 10% raises the unit cost of electricity to 3.7 US\$/kWh, more than three times the 1.06 US\$/kWh calculated by using a 5% discount rate (based on fuel cell minimum size). Alternatively, decreasing the assessment period to 10 years lifts the unit cost of electricity to 2.4 US\$/kWh.

The potential of the fuel cell for being used as a CHP unit in the context of the solar-hydrogen system was also investigated. Based on the RSHAP modelling results, the heat generated by the fuel cell at low current densities is almost equal to the electrical power output of the fuel cell. It gets even larger than its power output exponentially at higher current densities. Around 60-70% of this heat has to be removed by a properly designed cooling system. The rest is mostly used by the fuel cell internally to evaporate the water product; a few percent are removed from the fuel cell by the extra reactants. The case study revealed that, if the entire fuel cell cooling load is used for a beneficial application such as domestic water heating, the annual average energy efficiency of the fuel cell in both heat and power production in a CHP application can increase to about 70% for both systems with fuel cell minimum and optimum sizes. This heat recovery also led to an improvement in the round-trip efficiency of the system from about 24% in power only production to about 45% in both heat and electricity generation.

Then the possibility of using the fuel cell cooling load for boosting the hot water system of the remote household, which was assumed a LPG-based system for this case, was investigated. Utilisation of the fuel cell cooling load in this way led to a 35% reduction in the consumption of LPG for water heating. This saving is equivalent to 8% of the overall cost of the system over 30 years of assessment period if the price of LPG remains constant, and a 15% saving if the real cost of LPG rises at 4% per annum.

The excess hydrogen leaving the fuel cell stack without participating in any chemical reaction with oxygen is another waste stream of the fuel cell that can be prevented. The saving comes by collecting this hydrogen and burning it to boost the LPG hot water system is equivalent to another 8% of the overall cost of the system. This is based on the assumption of 85% hydrogen utilisation coefficient for the fuel cell. This hydrogen utilisation coefficient was measured ~90-98% experimentally which halves the obtained

figure of saving through collecting the hydrogen waste from 8% to about 4% of the overall cost of the system (when no annual rise in the price of LPG is assumed).

The RSHAP modelling investigations were followed by an experimental study on a 500 W PEM BCS fuel cell to investigate its potential of heat and power generation. The fuel cell showed efficiencies between ~35-50% over its polarisation curve (5-30 A currents) for just electricity generation (this is a few percent higher than that initially used in the model). By considering the fuel cell cooling load as another desirable output of this component, its efficiency in both heat and power generation (CHP) was measured in the range of 60-80% (the average of 72%). The CHP efficiency of the fuel cell was estimated to be 68% by the RSHAP when the experimental polarisation curve of the fuel cell was used by the model. A possible explanation for this 4% point difference is that a hydrogen utilisation coefficient of about 85% was assumed in the theoretical analysis, whereas it was measured experimentally to be on an average 95%.

Furthermore, if the new polarisation curve for the fuel cell obtained from the experiment is fed into the model, the unit cost of electricity that was previously estimated at 1.06 US\$/kWh is reduced to 0.95 US\$/kWh for a minimum size of the system used by the system; the unit cost of electricity can then be reduced to ~0.85 US\$/kWh for the optimal system. The cooling load of the fuel cell calculated experimentally is 7-17% less than that estimated by the model at currents less than 20 A. If the experimental polarisation curve of the fuel cell is fed into the model and the convection heat transfer from the body of the fuel cell is taken into account, this difference can be reduced to 5-10%. The experimental cooling load curve is in a much better agreement with the model at currents above 20 A. The differences between the experimental and theoretical results are mostly within the predicted range of uncertainties associated with the experimental measurement (see the tables of measurements in the appendix 2).

The fuel cell operating temperature and the air flow rate fed into the fuel cell (air stoichiometry) are two key factors affecting the performance of a fuel cell. The effects of these two factors on the heat and power outputs of the fuel cell were also investigated using the same experimental setup. The electrical output power of the fuel cell at 40 °C was measured to be up to 20% lower than that obtained at 60 °C while this difference was predicted to be about 5% by the model. The fuel cell water management-related output of

the model at operating temperature of 40 °C showed that the water product at such an operating condition appears in liquid form inside the fuel cell. This water can flood by the membrane and hence an extra resistance is added there. This could be the reason for such an unexpected performance drop. This possible explanation was confirmed by measuring the fuel cell cooling load. The measured cooling loads were considerably higher than the model estimates at operating temperatures in the range 60-65 °C. The reason was that at higher temperatures part of the heat liberated is absorbed by the water produced during its evaporation. However, at such a low operating temperature (e.g. 40 °C) water stays in liquid form, and then the heat normally absorbed by this water for evaporation has to be extracted from the fuel cell through the fuel cell cooling system. The amount of this heat is quite considerable as it is 30-40% of the total heat generated by the fuel cell. The poor performance of the fuel cell at low operating temperature can be partly resolved by increasing the air flow rate above the stoichiometric levels. This reduces the partial pressure of the water product and encourages evaporation at such lower temperatures. For example when the fuel cell was operated at 50 °C, by applying an air stoichiometry of 4 the power output of the fuel cell improved by 6-8% and the available cooling load dropped by 30-50%, depending on the operating point of the fuel cell, compared to performance at an air stoichiometry of 2.

A comprehensive error analysis was performed to assess the uncertainties associated with the results. The experimental errors for voltage and hydrogen consumption measurements were all within the accuracy range of the measurement instruments. As for the cooling load measurement, again the differences between the theory and the model were mostly within the estimated range of uncertainties calculated using the inherent inaccuracies of the thermometers and flow meters. The errors associated with a few of the measured cooling loads were slightly outside the estimated range of errors, although inaccuracies with the digital displays have not been taken into account.

The solar-hydrogen CHP system was evaluated from the triple bottom line (TBL) point of view (a 5 kWh daily demand in south-eastern Australia), and compared with its main competitors for RAPS applications (e.g. fossil-fuel-based generators, solar PV-battery systems, and solar-hydrogen-battery systems) in Chapter 6 using RSHAP and HOMER.

Economically speaking the solar-hydrogen system showed the potential of being competitive to diesel/petrol generators in assessment periods of about 20 years or more. This 20 year minimum period can be reduced to at least 18 years if the economic benefit of fuel cell heat recovery is also taken into account. Solar PV-battery systems for south-eastern Australia with a highly variable seasonal irradiance profile cannot be a feasible alternative as suggested by HOMER and a back-up generator has to be added to the system to ensure an uninterrupted supply throughout the year. The solar PV-battery-ICE generator system analysed, turned to be a relatively expensive alternative compared to the other systems for this case. The investigation on these alternatives also showed that adding a battery storage system to the solar-hydrogen CHP system to cover the short-term storage requirement can slightly improve the economics of the solar-hydrogen CHP system (in the order of 10%). In a solar-hydrogen-battery system the fuel cell operating hours is reduced since the load is partly supplied by the batteries and this adds to the lifetime of the fuel cell. The capacity of fuel cell heat recovery in solar-hydrogen system with battery storage is more 50% less than that in just the solar-hydrogen system.

From the environmental point of view in a small application such as in the case studied in this research (a 5 kWh/day in south-eastern Australia), greenhouse gas emissions of above 1500 kg CO₂-e per year can be avoided if a solar-hydrogen system replaces a petrol/diesel generator. Using heat recovered from the fuel cell for domestic water heating leads to a further emission reduction of about 140 kg CO₂-e/year. The GHG emission production of solar PV-battery-generator systems operated in south-eastern Australia for the same case (5kWh/day) is above 200 kg CO₂-e/year. This is considerably less than that generated by petrol/diesel generator systems for the same case since above 85% of the load is supplied by the PVs directly or indirectly (through the batteries) in solar PV-battery-generator systems in this case. By using solar-hydrogen system (with or without heat recovery) the problem with the end-of-life waste management of batteries, associated with systems using battery storage, can be completely avoided; also replacing the archaic fossil-fuel-based energy supply systems with emission-free systems such as solar-hydrogen CHP, first in RAPS markets and then more widely, can make a significant contribution to tackling the enormous challenge faced by the global community in avoiding catastrophic climate change.

The solar-hydrogen CHP systems can potentially bring lots of social benefits to remote communities in Australia and overseas. Energy security is one of the basic requirements for social stability. Solar-hydrogen CHP systems are flexible RAPS systems with a great potential of providing secure energy for such communities, whose lifestyles and economies are highly vulnerable to the expected rising costs of and supply interruptions to imported petroleum fuels. Installation, commissioning, and maintenance of such systems can also create new jobs for the local communities with significant economic multiplier effects in the local economies.

However, before all these potential economic and environmental benefits of solar-hydrogen systems can be realised, it is essential for users and the community generally to become better informed about hydrogen energy systems to make it a safe, sustainable and reliable source of energy to meet future energy needs. The government has a strong role to play in raising the public awareness on a large scale about the potential benefits of sustainable hydrogen energy, particularly through educational programs and by introducing appropriate safety standards and trainings.

7.3 RECOMMENDATIONS

On the basis of the theoretical and experimental investigations conducted in this research program, the following key recommendations are made:

- Further technological development and demonstrations of solar-hydrogen systems should be conducted to prepare the ground for the commercial deployment of these systems in suitable RAPS and other stand-alone applications. Priority areas for technological development include:
 - extending the lifetimes of PEM electrolyzers,
 - improving the electrical energy efficiency of PEM fuel cells used in RAPS systems,
 - developing solid-state hydrogen storage systems (metal hydride or others) with very high round-trip energy efficiencies for use in solar-hydrogen RAPS systems,
 - developing an overall control unit for a solar-hydrogen system that can regulate and optimise the performance of all the components (PV array, electrolyser, hydrogen

- storage, and fuel cell, including water management in the fuel cell and electrolyser) at all times, and
- incorporating a small-energy capacity battery bank into the system to meet peak demands and provide short-duration storage at high round-trip energy efficiency while hydrogen provides the required longer-duration storage.
- Fuel cell heat recovery should be integrated into a solar-hydrogen system whenever there is a suitable use for the low-temperature heat in order to increase the overall energy efficiency of the system and enhance its economic competitiveness:
- Potential uses for the recovered heat to be considered include domestic water heating, space heating, and supply of heat to metal hydride storages to increase discharge rates and amounts.
 - The body of the fuel cell should be well insulated, so that no heat is wasted through convection between the outer surfaces of the fuel cell and surrounding atmosphere, hence the maximum amount of heat generated by the fuel cell is transferred to the cooling system.
 - A complete demonstration in the field of a solar-hydrogen CHP system in an appropriate RAPS application requiring both electricity and heat should be conducted for extended periods (at least 1-3 years) to acquire the data and experience necessary to commercialise zero-emission cogeneration systems of this kind.
- Sizing of a solar-hydrogen system (with or without CHP) using the RSHAP or equivalent model and based on minimising the average unit cost of electricity produced over the system lifetime as introduced in this study, is recommended. The recommended procedure would thus include:
- increasing the size of the fuel cell above the minimum needed to meet the peak load until the economically optimal size is found that takes full advantage of the energy efficiency gains of operating the cell at less than its maximum power,
 - investigation of both unconstrained and constrained hydrogen storage tank capacities for the particular application being considered, and
 - allowing for some drop in the fuel cell hydrogen utilisation coefficient, and an additional contingency capacity in the hydrogen storage, so that the system is able to

maintain its continuous supply even after the performance of the fuel cell and other components falls slightly with age, and in the event of atypical patterns of solar radiation and demand in certain years.

- Full Life Cycle Analyses (LCA) should be conducted to compare solar-hydrogen systems with petrol/diesel generators, and solar PV-battery- ICE generator systems for RAPS applications in terms of cradle-to-grave greenhouse gas emissions and other environmental impacts.

The following additions and extensions of the RSHAP model developed in this study are recommended:

- Incorporation into the model of a more detailed and realistic model of the hydrogen storage sub-system, including compressed gas and metal hydride options allowing for round-trip efficiencies of less than 100%.
- Allowing for a more detailed breakdown of costs and lifetimes of all the components of the system to be input, including, for example, the costs of installation and commissioning, a control system, a MMPT (if needed), the cooling system, and a humidifier/dehumidifier.
- Extension of the model to represent the transient behaviour of the fuel cell when exposed to a variable load, or restarted after a period of being in operation, rather than assuming steady-state operation at all times.
- Adding the capability to the economic analysis program of taking into account government rebates or other financial incentives to encourage use of renewable sources of energy and to reduce the carbon footprint.
- Extending the model to cover the potentially-attractive combination of a solar-hydrogen system with a solar water heater to supply a remote household with both its electricity and domestic hot water needs with zero greenhouse gas emissions.

REFERENCES

- Abdallah, M. a. h., S. S. Asfour and T. N. Veziroglu (1999). "Solar-hydrogen energy system for Egypt." *International Journal of Hydrogen Energy* 24(6): 505–517.
- Agbossou, K., R. Chahine, J. Hamelin, F. Laurencelle, A. Anouar, J.-M. St-Arnaud and T. K. Bose (2001). "Renewable energy systems based on hydrogen for remote applications." *Journal of Power Sources* 96(1): 168-172.
- Ahluwalia, R. K., X. Wang, A. Rousseau and R. Kumar (2004). "Fuel economy of hydrogen fuel cell vehicles." *Journal of Power Sources* 130(1-2): 192-201.
- Akbarzadeh, A. A. (1992). *Fundamentals of remote area power supply systems*. Melbourne, Energy Victoria.
- Al-Hamadi, H. M. and S. A. Soliman (2006). "Long-term/mid-term electric load forecasting based on short-term correlation and annual growth." *Fuel and Energy (Electric Power Systems Research)* 47(2): 104-104.
- Ali, S. M. (2007). *Solar-hydrogen Systems for Remote Area Power Supply*. School of Aerospace Mechanical and Manufacturing Engineering. Melbourne, RMIT.
- Ali, S. M. and J. Andrews (2005). *Low-cost storage options for solar hydrogen systems for remote area power supply*. World Hydrogen Energy Conference, Lyon, France.
- Almogren, S. and T. N. T. N. Veziroglu (2004). "Solar-hydrogen energy system for Saudi Arabia." *International Journal of Hydrogen Energy* 29(11): 1181-1190.
- Arriaga, L. G., W. Martínez, U. Cano and H. Blud (2007). "Direct coupling of a solar-hydrogen system in Mexico." *International Journal of Hydrogen Energy* 32(13): 2247-2252.
- Aurora, P. H. (2003). *Modeling and control of a solar hydrogen fuel cell system for remote applications*. Massachusetts, Massachusetts Lowell.
- Barbir, F. (2005). "PEM electrolysis for production of hydrogen from renewable energy sources." *Solar Energy* 78(5): 661-669.

- Barreto, L., A. Makihiro and K. Riahi (2003). "The hydrogen economy in the 21st century: a sustainable development scenario." *International Journal of Hydrogen Energy* 28(3): 267-284.
- BCS. (2009). "Fuel cell, 500 W PEM fuel cell specification." <http://www.bcsfuelcells.com/>, viewed on March 2009.
- BCSE. (2009). "PV grid connect systems, (non-UPS), system design guideline, Technical document." Business Council for Sustainable Energy, <http://www.bcse.org.au>, viewed on March 2009.
- Beccali, M., S. Brunone, M. Cellura and V. Franzitta (2008). "Energy, economic and environmental analysis on RET-hydrogen systems in residential buildings." *Renewable Energy* 33(3): 366-382.
- Bell, S. (2001). *Measurement Good Practice Guide: A Beginner's Guide to Uncertainty of Measurement*, Centre for Basic, Thermal and Length Metrology National Physical Laboratory.
- Bilgen, E. (2001). "Solar hydrogen from photovoltaic-electrolyser systems." *Energy Conversion and Management* 42(9): 1047-1057.
- Bilgen, E. (2004). "Domestic hydrogen production using renewable energy." *Solar Energy Journal* 77(1): 47-55.
- BOM. (2009). "Climate statistics for Australian locations." Australian Bureau Of Meteorology, www.bom.gov.au, viewed on February 2009.
- Brunner, T. and O. Kircher (2008). Progress on cryogenic hydrogen vehicle storage. World Hydrogen Energy Conference, Brisbane, Australia.
- Cairns, J. (2010). "North American and international hydrogen/fuel cell standards." *International Journal of Hydrogen Energy* 35(7): 2767-2771.
- Cheng, X., J. Zhang, Y. Tang, C. Song, J. Shen, D. Song and J. Zhang (2007). "Hydrogen crossover in high-temperature PEM fuel cells." *Journal of Power Sources* 167(1): 25-31.

- Chenni, R., M. Makhlouf, T. Kerbache and A. Bouzid (2007). "A detailed modeling method for photovoltaic cells." *Energy* 32(9): 1724-1730.
- Clarke, R. E., S. Giddey, F. T. Ciacchi, S. P. S. Badwal, B. Paul and J. Andrews (2009). "Direct coupling of an electrolyser to a solar PV system for generating hydrogen." *International Journal of Hydrogen Energy* 34: 2531-2542.
- Colella, W. G. (2003). "Modeling results for the thermal management sub-system of a combined heat and power (CHP) fuel cell system (FCS)." *Journal of Power Sources* 118(1-2): 129-149.
- ColeParmer. (2009). Cole Parmer, www.coleparmer.com, viewed on Feb. 2009.
- Contreras, A., J. Carpio, M. Molero and T. N. Veziroglu (1999). "Solar-hydrogen:: an energy system for sustainable development in Spain." *International Journal of Hydrogen Energy* 24(11): 1041-1052.
- Coppo, M., N. P. Siegel and M. R. v. Spakovsky (2006). "On the influence of temperature on PEM fuel cell operation." *Journal of Power Sources* 159(1): 560-569.
- Cuoco, A., G. Sgalambro, M. Paolucci and L. D'Alessio (1995). "Is photovoltaic hydrogen in Italy competitive with traditional fossil fuels?" *Energy* 20(12): 1303-1309.
- Dahodwalla, H. and S. Herat (2000). "Cleaner production options for lead-acid battery manufacturing industry." *Journal of Cleaner Production* 8(2): 133-142.
- Dahoe, A. E. and V. V. Molkov (2007). "On the development of an International Curriculum on Hydrogen Safety Engineering and its implementation into educational programmes." *International Journal of Hydrogen Energy* 32(8): 1113-1120.
- Dalton, G. J., D. A. Lockington and T. E. Baldock (2008). "Feasibility analysis of stand-alone renewable energy supply options for a large hotel." *Renewable Energy* 33(7): 1475-1490.
- DEWHA. (2009). Australian Government, Department of the Environment, Water, Heritage and the Arts, <http://www.environment.gov.au/>, viewed on March 2009.

Doddathimmaiah, A. and J. Andrews (2009). "Theory, modeling, and performance measurement of unitised regenerative fuel cells." *International Journal of Hydrogen Energy* 34(19): 8157-8170.

Doddathimmaiah, A. K. (2008). *Unitised regenerative fuel cell in solar-hydrogen system for remote area power supply*. School of Aerospace Mechanical and Manufacturing Engineering, Melbourne, RMIT.

Doddathimmaiah, A. K. and J. Andrews (2008). *Modeling and performance measurement of unitised regenerative fuel cells*. World Hydrogen Energy Conference, Brisbane, Australia.

DOE. (2001). "Hydrogen Fuel Cell Engines and Related Technologies Technical report on Hydrogen Properties." *Energy Efficiency and Renewable Energy*, US Department of Energy, www.eere.energy.gov/, viewed on Feb. 2009.

DOE. (2007). *Carbone Dioxide Information Analysis Centre*, Oak Ridge National Laboratory, www.energy.gov, viewed on Oct. 2009.

DOE (2009). *Hydrogen storage sub-program overview*, US Department Of Energy.

Dunlop, J. (2004). "Renewable hydrogen technologies: A low-cost solar solution to the clean hydrogen problem." *Refocus* 5(1): 48-50.

Edwards, P. P., V. L. Kuznetsov, W. I. F. David and N. P. Brandon (2008). "Hydrogen and fuel cells: Towards a sustainable energy future." *Energy Policy* 36(12): 4356-4362.

EIA (2009). *Energy Information Administration*, <http://www.eia.doe.gov>, viewed Nov. 2009.

Exergy. (2009). *Exergy miniature heat exchangers*, <http://www.exergyllc.com/>, viewed on March 2009.

Ferguson, A. and V. Ismet Ugursal (2004). "Fuel cell modelling for building cogeneration applications." *Journal of Power Sources* 137(1): 30-42.

Florides, G. A. and P. Christodoulides (2009). "Global warming and carbon dioxide through sciences." *Environment International* 35(2): 390-401.

- Førde, T., J. Eriksen, A. G. Pettersen, P. J. S. Vie and Ø. Ulleberg (2009). "Thermal integration of a metal hydride storage unit and a PEM fuel cell stack." *International Journal of Hydrogen Energy* 34(16): 6730-6739.
- FuelCellsBulletin (2003). "Honda, Toyota expand California FCV fleets." *Fuel Cells Bulletin* 2003(11): 3-4.
- FuelCellsBulletin (2006). "Solar/hydrogen home nearing completion." *Fuel Cells Bulletin* 2006(10): 7-7.
- FuelCellsBulletin (2008). "GM, Chrysler unveil luxury concept FCVs." *Fuel Cells Bulletin* 2008(3): 2-2.
- Fuelcellstore. (2009). Fuel Cell Store, <http://fuelcellstore.com>, viewed on March 2009.
- Galli, S. and M. Stefanoni (1997). "Development of a solar-hydrogen cycle in Italy." *International Journal of Hydrogen Energy* 22(5): 453-458.
- Genaidy, A. M., R. Sequeira, T. Tolaymat, J. Kohler and M. Rinder (2008). "An exploratory study of lead recovery in lead-acid battery lifecycle in US market: An evidence-based approach." *Science of The Total Environment* 407(1): 7-22.
- Ghosh, P. C., B. Emonts, H. Janßen, J. Mergel and D. Stolten (2003). "Ten years of operational experience with a hydrogen-based renewable energy supply system." *Solar Energy* 75(6): 469-478.
- Ghosh, P. C., B. Emonts and D. Stolten (2003). "Comparison of hydrogen storage with diesel-generator system in a PV-WEC hybrid system." *Solar Energy* 75(3): 187-198.
- Gibbs, C. E. and M. C. F. Steel (1992). "European opportunities for fuel cell commercialisation." *Journal of Power Sources* 37(1-2): 35-43.
- Gibril, S. (2008). Solar Hydrogen Energy House for Libya. World Hydrogen Energy Conference, Brisbane, Australia.
- Gigliucci, G., L. Petruzzi, E. Cerelli, A. Garzisi and A. La Mendola (2004). "Demonstration of a residential CHP system based on PEM fuel cells." *Journal of Power*

Sources (selected papers presented at the Eighth Grove Fuel Cell Symposium) 131(1-2): 62-68.

Graf, C., A. Vath and N. Nicoloso (2006). "Modeling of the heat transfer in a portable PEFC system within MATLAB-Simulink." *Journal of Power Sources* (selected papers from the 88th Bunsenkolloquium - In honour of Prof. Dr. Jurgen Garche's 60th birthday) 155(1): 52-59.

Greencarcongress. (2009). "Toyota Plans Limited Consumer Sales of Hydrogen Fuel-Cell Vehicles by 2015 " www.greencarcongress.com, Green Car Congress Retrieved Dec., 2009.

Greiner, C. J., M. KorpAs and A. T. Holen (2007). "A Norwegian case study on the production of hydrogen from wind power." *International Journal of Hydrogen Energy* 32(10-11): 1500-1507.

Grigoriev, S. A., P. Millet, S. V. Korobtsev, V. I. Porembkiy, M. Pepic, C. Etievant, C. Puyenchet and V. N. Fateev (2009). "Hydrogen safety aspects related to high-pressure polymer electrolyte membrane water electrolysis." *International Journal of Hydrogen Energy* 34(14): 5986-5991.

Grigoriev, S. A., V. I. Porembsky and V. N. Fateev (2006). "Pure hydrogen production by PEM electrolysis for hydrogen energy." *International Journal of Hydrogen Energy* 31(2): 171-175.

Harrison, K. W. (2006). Design, integration and control of proton exchange membrane electrolyser for wind based renewable energy applications. United States, North Dakota, The University of North Dakota.

Hawkes, A. and M. Leach (2005). "Solid oxide fuel cell systems for residential micro-combined heat and power in the UK: Key economic drivers." *Journal of Power Sources* 149: 72-83.

Hawkins, S., D. Joffe and N. Hughes. (2005). "Hydrogen fuel cells for stationary power: Technological characterisation and market assessment " UKSHEC Social Science, <http://www.psi.org.uk/ukshec/>, viewed on Dec. 2009.

- Hedström, L., C. Wallmark, P. Alvfors, M. Rissanen, B. Stridh and J. Ekman (2004). "Description and modeling of the solar-hydrogen-biogas-fuel cell system in GlashusEtt." *Journal of Power Sources* 131(1-2): 340-350.
- Heffel, J. W. (2003). "NOx emission reduction in a hydrogen fueled internal combustion engine at 3000 rpm using exhaust gas recirculation." *International Journal of Hydrogen Energy* 28(11): 1285-1292.
- Hoffmann, P. (2001). *Tomorrow's energy: hydrogen, fuel cells, and the prospects for a cleaner planet*, The MIT Press, Cambridge, Massachusetts, London, England.
- Hollenberg, J. W., E. N. Chen, K. Lakeram and D. Modroukas (1995). "Development of a photovoltaic energy conversion system with hydrogen energy storage." *International Journal of Hydrogen Energy* 20(3): 239-243.
- HOMER. (2009). HOMER Energy, www.homerenergy.com, viewed on Dec. 2009.
- IEA. (2001). "World Energy Outlook." International Energy Agency, www.iea.org, viewed on Dec. 2009.
- IEA (2009) "CO2 emissions from fuel combustion." International Energy Agency, www.iea.org, viewed on Dec. 2009.
- IEA. (2009). "Key world energy statistics." International Energy Agency, www.iea.org, viewed on Dec. 2009.
- IPCC. (2007). "IPCC Fourth Assessment Report, Climate Change 2007 (AR4)." Intergovernmental Panel on Climate Change, www.IPCC.ch, viewed on Nov. 2009.
- Jalalzadeh-Azar, A. A. (2004). *Investigating Methods of Heat Recovery from Low-Temperature PEM Fuel Cells in CHP Applications*
ASME International Mechanical Engineering Congress and Exhibition. Anaheim, California, USA, November 13-19: pp 533-542.
- Jiang, Z., R. A. Dougal, S. Liu, S. A. Gadre, A. D. Ebner and J. A. Ritter (2005). "Simulation of a thermally coupled metal-hydride hydrogen storage and fuel cell system." *Journal of Power Sources* 142(1-2): 92-102.

- Kazim, A. and T. N. Veziroglu (2001). "Utilization of solar-hydrogen energy in the UAE to maintain its share in the world energy market for the 21st century." *Renewable Energy* 24(2): 259-274.
- Klucher, T. M. (1979). "Evaluation of models to predict insolation on tilted surfaces." *Solar Energy* 23(2): 111-114.
- Koner, P. K., V. Dutta and K. L. Chopra (2000). "A comparative life cycle energy cost analysis of photovoltaic and fuel generator for load shedding application." *Solar Energy Materials and Solar Cells* 60(4): 309-322.
- König, P., A. Weber, N. Lewald, T. Aicher, L. Jörissen, E. Ivers-Tiffée, R. Szolak, M. Brendel and J. Kaczerowski (2005). "Testing and model-aided analysis of a 2 kWe PEMFC CHP-system." *Journal of Power Sources* 145(2): 327-335.
- Lagorse, J., M. G. Simões, A. Miraoui and P. Costerg (2008). "Energy cost analysis of a solar-hydrogen hybrid energy system for stand-alone applications." *International Journal of Hydrogen Energy* 33(12): 2871-2879.
- LaMeres, B. J., M. H. Nehrir and V. Gerez (1999). "Controlling the average residential electric water heater power demand using fuzzy logic." *Electric Power Systems Research* 52(3): 267-271.
- Larminie, J. and A. Dicks (2003). *Fuel cell explained*, 2nd edition, John Wiley & Sons.
- Levene, J. I., M. K. Mann, R. M. Margolis and A. Milbrandt (2007). "An analysis of hydrogen production from renewable electricity sources." *Solar Energy* 81(6): 773-780.
- Lior, N. (2008). "Energy resources and use: The present situation and possible paths to the future." *Energy* 33(6): 842-857.
- Liu, Z., Z. Qiu, Y. Luo, Z. Mao and C. Wang (2009). "Operation of first solar-hydrogen system in China." *International Journal of Hydrogen Energy* 35(7): 2762-2766.
- Lowe, D. and C. R. Lloyd (2001). "Renewable energy systems for remote areas in Australia." *Renewable Energy* 22(1-3): 369-378.

- Luis Aprea, J. (2008). "New standard on safety for hydrogen systems in Spain: Keys for understanding and use." *International Journal of Hydrogen Energy* 33(13): 3526-3530.
- Macfarlane. (2008). www.macgen.com, viewed on Dec. 2008.
- MacIntyre, I., A. V. Tchouvelev, D. R. Hay, J. Wong, J. Grant and P. Benard (2007). "Canadian hydrogen safety program." *International Journal of Hydrogen Energy* 32(13): 2134-2143.
- Maclay, J. D., J. Brouwer and G. Scott Samuelsen (2006). "Dynamic analyses of regenerative fuel cell power for potential use in renewable residential applications." *International Journal of Hydrogen Energy* 31(8): 994-1009.
- Marangio, F., M. Santarelli and M. Cali (2009). "Theoretical model and experimental analysis of a high pressure PEM water electrolyser for hydrogen production." *International Journal of Hydrogen Energy* 34(3): 1143-1158.
- Marbán, G. and T. Valdés-Solís (2007). "Towards the hydrogen economy?" *International Journal of Hydrogen Energy* 32(12): 1625-1637.
- Martínez Chaparro, A., J. Soler, M. José Escudero and L. Daza (2003). "Testing an isolated system powered by solar energy and PEM fuel cell with hydrogen generation." *Fuel Cells Bulletin* 2003(11): 10-12.
- McMillan. (2009). McMillan Company, www.mcmflow.com, viewed on Jan. 2009.
- Miland, H. and Ø. Ulleberg (2008). "Testing of a small-scale stand-alone power system based on solar energy and hydrogen." *Solar Energy In Press, Uncorrected Proof*.
- Moriarty, P. and D. Honnery (2007). "Intermittent renewable energy: The only future source of hydrogen?" *International Journal of Hydrogen Energy* 32(12): 1616-1624.
- Nelson, D. B., M. H. Nehrir and C. Wang (2006). "Unit sizing and cost analysis of stand-alone hybrid wind/PV/fuel cell power generation systems." *Renewable Energy* 31(10): 1641-1656.
- Nexergy (2010). Battery custom designer, www.nexergy.com/battery-density.htm, viewed on July 2009

- NGA (2009). National Greenhouse Account Factors, Australian Government, Department of Climate Change.
- Nowotny, J., C. C. Sorrell, L. R. Sheppard and T. Bak (2005). "Solar-hydrogen: Environmentally safe fuel for the future." *International Journal of Hydrogen Energy* 30(5): 521-544.
- NREL. (2010). "National Renewable Energy Lab, HOMER software." <https://analysis.nrel.gov/homer/>, viewed on May 2010.
- ORER. (2009). Office of the Renewable Energy Regulator, www.orer.gov.au, viewed on March 2009.
- Packer, J. (1992). "Commercialisation of fuel cells for combined heat and power (CHP) application." *Journal of Power Sources* 37(1-2): 101-109.
- Pahomov, V. and V. Fateev (1990). Electrolysis of water with solid polymer electrolyte. (Preprint, in Russian), RRC "Kurchatov Institute".
- Paul, B. (2009). Direct-coupling of the photovoltaic array and PEM electrolyser in solar-hydrogen system for remote area power supply. School of Aerospace, Mechanical and Manufacturing Engineering. Melbourne, RMIT.
- Paul, B. and J. Andrews (2008). "Optimal coupling of PV arrays to PEM electrolysers in solar-hydrogen systems for remote area power supply." *International Journal of Hydrogen Energy* 33(2): 490-498.
- Peacock, A. D. and M. Newborough (2007). "Controlling micro-CHP systems to modulate electrical load profiles." *Energy* 32(7): 1093-1103.
- Quaschnig, V. (2005). *Understanding renewable energy systems*. London.
- Richards, B. S. and G. J. Conibeer (2007). "A comparison of hydrogen storage technologies for solar-powered stand-alone power supplies: A photovoltaic system sizing approach." *International Journal of Hydrogen Energy* 32(14): 2712-2718.
- Ro, K. and S. Rahman (1998). "Battery or fuel cell support for an autonomous photovoltaic power system." *Renewable Energy* 13(2): 203-213.

- RSAustralia. (2009). <http://australia.rs-online.com/web>, viewed on March 2009.
- Ryan O'Hayre, Suk-Won Cha, Whitney Colella and Fritz B. Prinz (2008). Fuel Cell Fundamentals, 2nd Edition, John Wiley & Sons.
- Rzayeva, M. P., O. M. Salamov and M. K. Kerimov (2001). "Modeling to get hydrogen and oxygen by solar water electrolysis." *International Journal of Hydrogen Energy* 26(3): 195-201.
- Saddler, H., M. Diesendorf and R. Denniss (2007). "Clean energy scenarios for Australia." *Energy Policy* 35(2): 1245-1256.
- Sakintuna, B., F. Lamari-Darkrim and M. Hirscher (2007). "Metal hydride materials for solid hydrogen storage: A review." *International Journal of Hydrogen Energy* 32(9): 1121-1140.
- Sammes, N. and H. F. Coors (2006). Fuel cell technology, Springer.
- Sandia. (2009). "National Laboratories, database of photovoltaic module performance parameters."
- Santarelli, M. and S. Macagno (2004). "Hydrogen as an energy carrier in stand-alone applications based on PV and PV-micro-hydro systems." *Energy* 29(8): 1159-1182.
- Santos, S. F. and J. Huot (2009). "Hydrogen storage in $\text{TiCr}_{1.2}(\text{FeV})_x$ BCC solid solutions." *Journal of Alloys and Compounds* 472(1-2): 247-251.
- Schoots, K., F. Ferioli, G. J. Kramer and B. C. C. van der Zwaan (2008). "Learning curves for hydrogen production technology: An assessment of observed cost reductions." *International Journal of Hydrogen Energy* 33(11): 2630-2645.
- Schulte, I., D. Hart and R. van der Vorst (2004). "Issues affecting the acceptance of hydrogen fuel." *International Journal of Hydrogen Energy* 29(7): 677-685.
- Shaahid, S. M. and M. A. Elhadidy (2008). "Economic analysis of hybrid photovoltaic-diesel-battery power systems for residential loads in hot regions--A step to clean future." *Renewable and Sustainable Energy Reviews* 12(2): 488-503.

Shabani, B. and J. Andrews (2008). Modeling of a solar-hydrogen combined heat and power system for remote power supply. World Hydrogen Energy Conference, Brisbane, Australia.

Shabani, B., J. Andrews and S. Watkins (2010). "Energy and cost analysis of a solar-hydrogen combined heat and power system for remote power supply using a computer simulation." *International Solar Energy Journal* 84(1): 144-155.

Shafiee, S. and E. Topal (2009). "When will fossil fuel reserves be diminished?" *Energy Policy* 37(1): 181-189.

Shamardina, O., A. Chertovich, A. A. Kulikovskiy and A. R. Khokhlov (2009). "A simple model of a high temperature PEM fuel cell." *International Journal of Hydrogen Energy* In Press, Corrected Proof.

Shapiro, D., J. Duffy, M. Kimble and M. Pien (2005). "Solar-powered regenerative PEM electrolyser/fuel cell system." *Solar Energy* 79(5): 544-550.

Solardyne. (2008). www.solardyne.com, viewed on Dec. 2008.

Solmecke, H., O. Just and D. Hackstein (2000). "Comparison of solar hydrogen storage systems with and without power-electronic DC-DC-converters." *Renewable Energy* 19(1-2): 333-338.

Sonntag, R. E., C. Borgnakke and G. J. V. Wylen (2003). *Fundamentals of Thermodynamics*. England, John Wiley & Sons Ltd.

Swagelok (2008). <http://www.swagelok.com.au/>, viewed on March 2009.

Tani, T., N. Sekiguchi, M. Sakai and D. Ohta (2000). "Optimization of Solar Hydrogen Systems Based on Hydrogen Production Cost." *Solar Energy* 68(2): 143-149.

Torchio, M. F., M. G. Santarelli and A. Nicali (2005). "Experimental analysis of the CHP performance of a PEMFC stack by a 24 factorial design." *Journal of Power Sources* 149: 33-43.

- Torres, L. A., F. J. Rodríguez and P. J. Sebastian (1998). "Simulation of a solar-hydrogen-fuel cell system: results for different locations in Mexico." *International Journal of Hydrogen Energy* 23(11): 1005-1009.
- Townsend, T. U. (1989). A method for estimating the long-term performance of direct-coupled photovoltaic systems. Solar Energy Laboratory, University of Wisconsin, Madison.
- Tzimas, E., C. Filiou, S. D. Perves and J. B. Veyret (2003). Hydrogen storage: state of art and future perspective. Petten, Netherlands, European Commission, Directorate general Joint Research Centre (DG JRC) Institute of Energy.
- Ulleberg, Ø. and S. O. Mørner (1997). "TRNSYS simulation models for solar-hydrogen systems." *Solar Energy* 59(4-6): 271-279.
- Uzunoglu, M., O. C. Onar and M. S. Alam (2009). "Modeling, control and simulation of a PV/FC/UC based hybrid power generation system for stand-alone applications." *Renewable Energy* 34(3): 509-520.
- Vanhanen, J. P., P. D. Lund and M. T. Hagström (1996). "Feasibility study of a metal hydride hydrogen store for a self-sufficient solar hydrogen energy system." *International Journal of Hydrogen Energy* 21(3): 213-221.
- Varkaraki, E., N. Lymberopoulos and A. Zachariou (2003). "Hydrogen based emergency back-up system for telecommunication applications." *Journal of Power Sources* 118(1-2): 14-22.
- Verhelst, S. and T. Wallner (2009). "Hydrogen-fueled internal combustion engines." *Progress in Energy and Combustion Science* 35(6): 490-527.
- Veziroglu, T. N. and S. Sahin (2008). "21st Century's energy: Hydrogen energy system." *Energy Conversion and Management* 49(7): 1820-1831.
- Wallmark, C. and P. Alvfors (2002). "Design of stationary PEFC system configurations to meet heat and power demands." *Journal of Power Sources* 106(1-2): 83-92.
- WELS. (2008). Australian Government, Water Efficiency Labeling and Standards Scheme, www.waterrating.gov.au, viewed on June 2009.

White, C. M., R. R. Steeper and A. E. Lutz (2006). "The hydrogen-fueled internal combustion engine: a technical review." *International Journal of Hydrogen Energy* 31(10): 1292-1305.

Zhang, J., Y. Tang, C. Song, Z. Xia, H. Li, H. Wang and J. Zhang (2008). "PEM fuel cell relative humidity (RH) and its effect on performance at high temperatures." *Electrochimica Acta* 53(16): 5315-5321.

Zhang, J., Z. Xie, J. Zhang, Y. Tang, C. Song, T. Navessin, Z. Shi, D. Song, H. Wang, D. P. Wilkinson, Z.-S. Liu and S. Holdcroft (2006). "High temperature PEM fuel cells." *Journal of Power Sources* (Special issue including selected papers presented at the International Workshop on Molten Carbonate Fuel Cells and Related Science and Technology 2005 together with regular papers) 160(2): 872-891.

Zhang, Y., M. Ouyang, Q. Lu, J. Luo and X. Li (2004). "A model predicting performance of proton exchange membrane fuel cell stack thermal systems." *Applied Thermal Engineering* 24(4): 501-513.

Zoulias, E. I., R. Glockner, N. Lymberopoulos, T. Tsoutsos, I. Vosseler, O. Gavalda, H. J. Mydske and P. Taylor (2006). "Integration of hydrogen energy technologies in stand-alone power systems analysis of the current potential for applications." *Renewable and Sustainable Energy Reviews* 10(5): 432-462.

Zoulias, E. I. and N. Lymberopoulos (2007). "Techno-economic analysis of the integration of hydrogen energy technologies in renewable energy-based stand-alone power systems." *Renewable Energy* 32(4): 680-696.

Züttel, A. (2003). "Materials for hydrogen storage." *Materials Today* 6(9): 24-33.

APPENDICES

Appendix 1: The RSHAP user manual

The opening page of RSHAP

The main page of RSHAP includes five large buttons (Figure A- 1): *Photovoltaic Panel*, *PEM Electrolyser*, *PEM Fuel Cell*, *Solar-Hydrogen*, and *Hot Water Supply*. Initially the *Solar-Hydrogen* and *Hot Water supply* buttons are inactive. Once the PV array, PEM electrolyser and PEM fuel cell are introduced mathematically to RSHAP the *Solar-Hydrogen* button gets activated to start the system analysis. The small red panels located on the bottom right of these buttons become green when the associated elements are mathematically introduced to the model. After doing solar-hydrogen system analysis it is possible to have the *Hot Water Supply* button activated as well. Any of these main parts of the simulation code have their own features and functions which are introduced here.

There is no specific order for analysing PV array, electrolyser and fuel cell and they can be analysed in any order. Following the order of the buttons, the details of PV array analysis will be explained first.

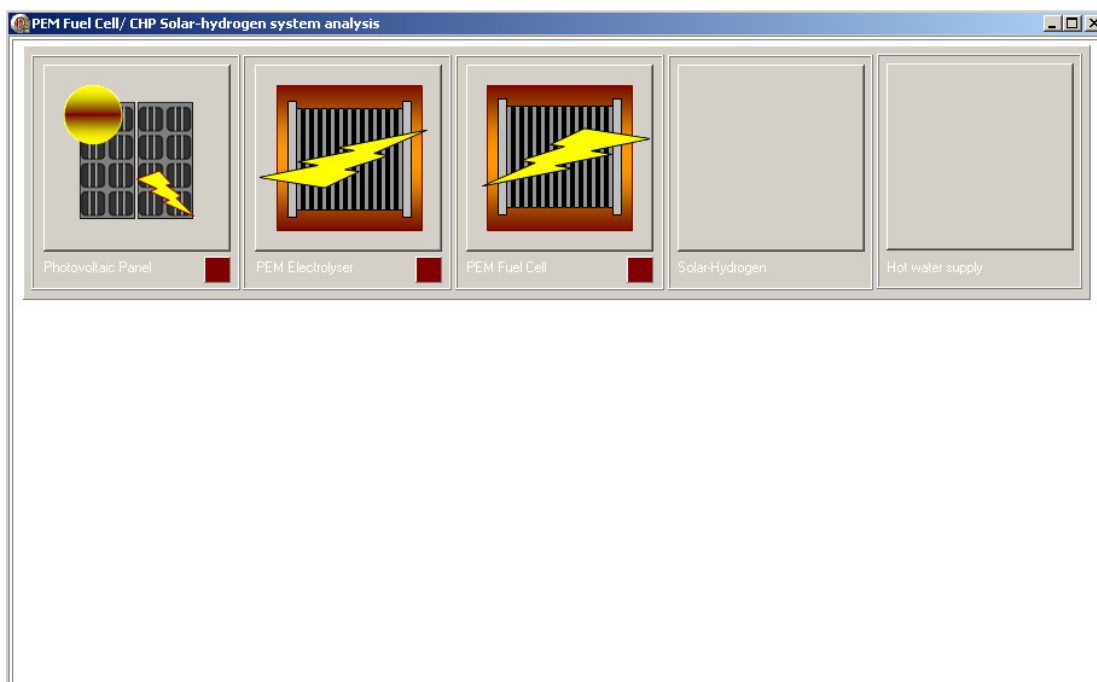


Figure A- 1. The simulation code opening panel

Photovoltaic Panel

By clicking on *Photovoltaic Panel* button the page shown in Figure A- 2 opens. Here the user can choose between ‘*Yearly Analysis*’ and ‘*Single Point Analysis*’.

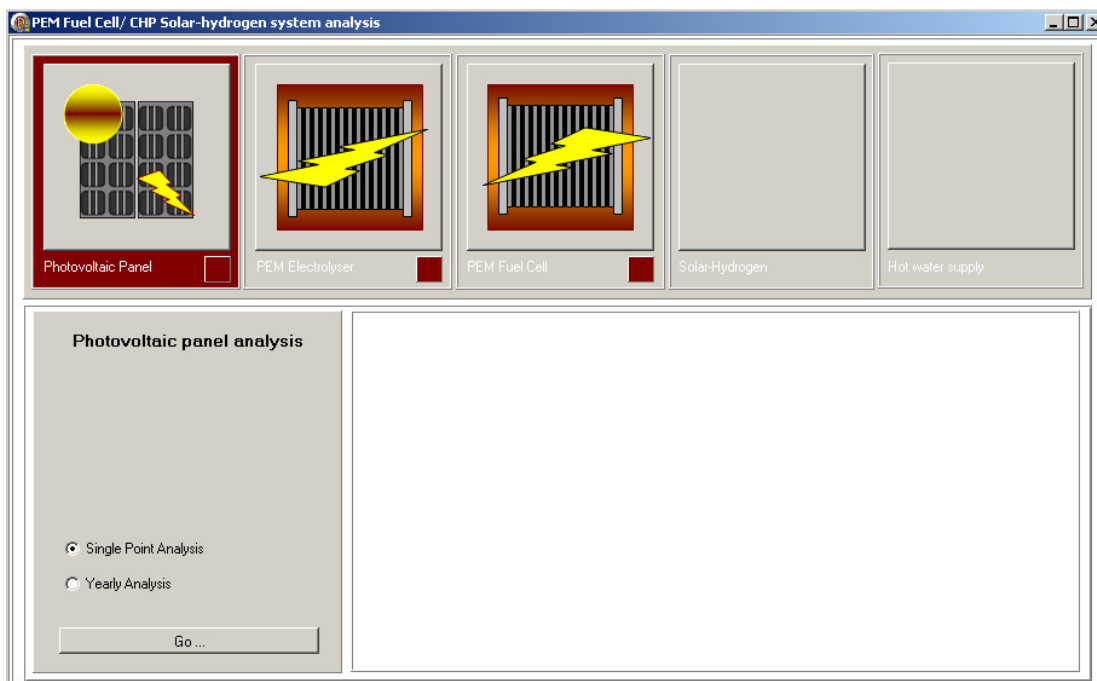


Figure A- 2. Photovoltaic array analysis modes

Single Point Analysis mode allows analysis on a particular date and time; however, the *Yearly Analysis* makes it possible to do the analysis over the entire year on a half-hourly or hourly basis. For doing the solar-hydrogen system analysis the ‘*Yearly Analysis*’ has to be selected.

In *Single Point Analysis* mode, as shown in Figure A- 3, the input data are taken in four groups. Once all these are completely filled the small red squares in front of them turn green to show that the program is ready to start the analysis. Pressing the ‘*Start Analysis*’ button before receiving the green light for all the input data groups will result in a message appearing on the screen to let the operator know that necessary data are missing and the program cannot resume the analysis. By choosing any group, the associated data entry panel opens to receive the data and the rest of the buttons for the other groups become inactive while this panel is open.

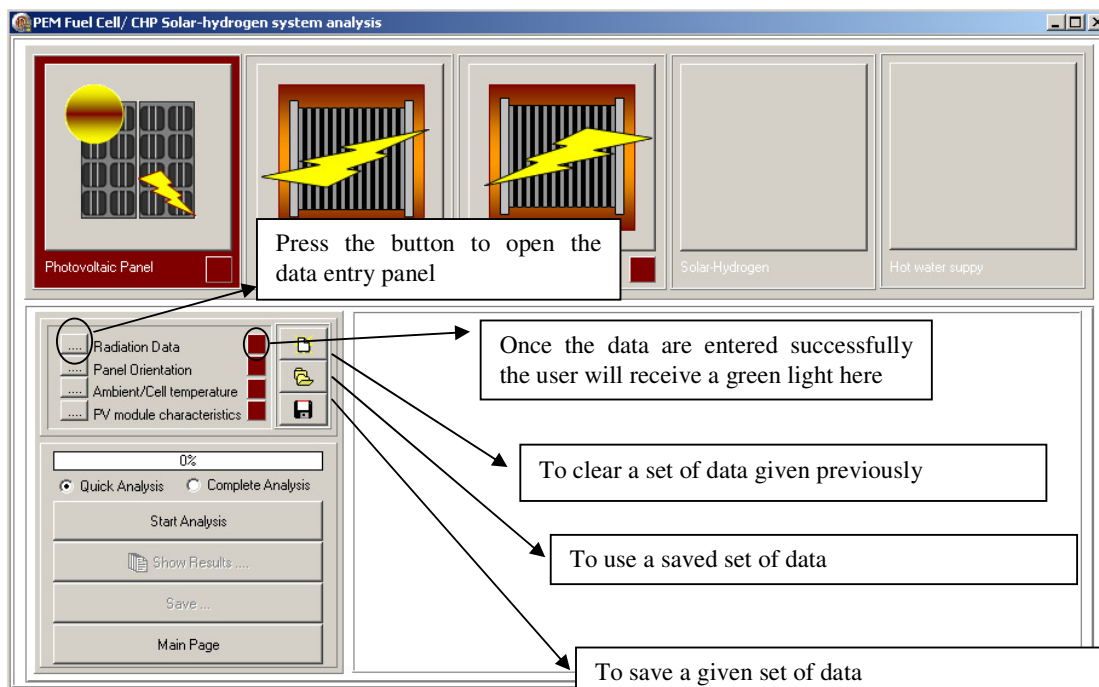


Figure A- 3. The PV array ‘Single Point Analysis’ mode

These input data groups are:

1. Radiation data

The following parameters are asked to be filled in this panel (Figure A- 4):

- *Direct radiation on the horizontal surface.*
- *The local latitude angle of the PV array’s location:* The program allows for the user’s choice of north hemisphere or south hemisphere (negative values for local latitude are not accepted by the program).
- *Date and time:* The time that is used here is the solar time; so the local conventional time has to be converted to the solar time before feeding it into the program.

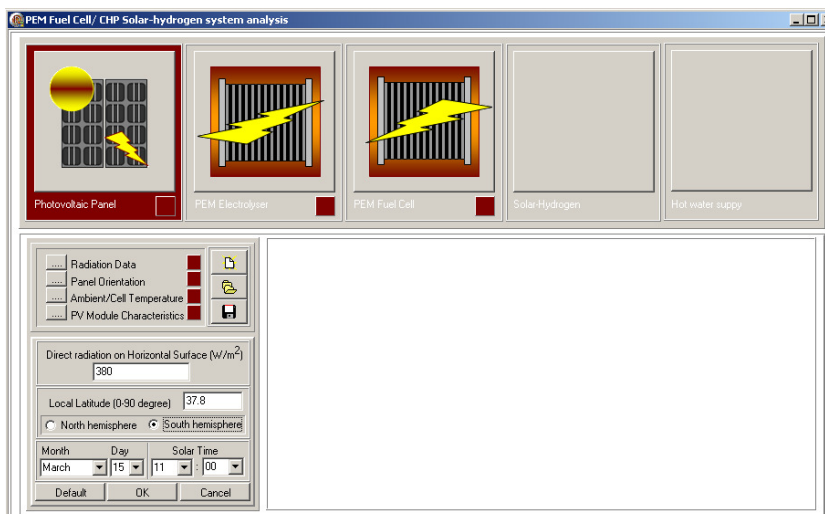


Figure A- 4. ‘Radiation Data’ panel

By pressing the ‘OK’ button, the user can introduce the data to the program and after accepting the given values by the program, the data entry panel closes and the small red box in front of the ‘Radiation Data’ button turns green. If the input data are inappropriate (like the direct radiation shown in Figure A- 5) the panels remains open waiting to receive an appropriate set of data and the improper value(s) is (are) marked in yellow. If the ‘Cancel’ button is pushed the panel will disappear and the previously-accepted data will be used (if there are any), or the blank data entry form will appear if nothing has been accepted previously.

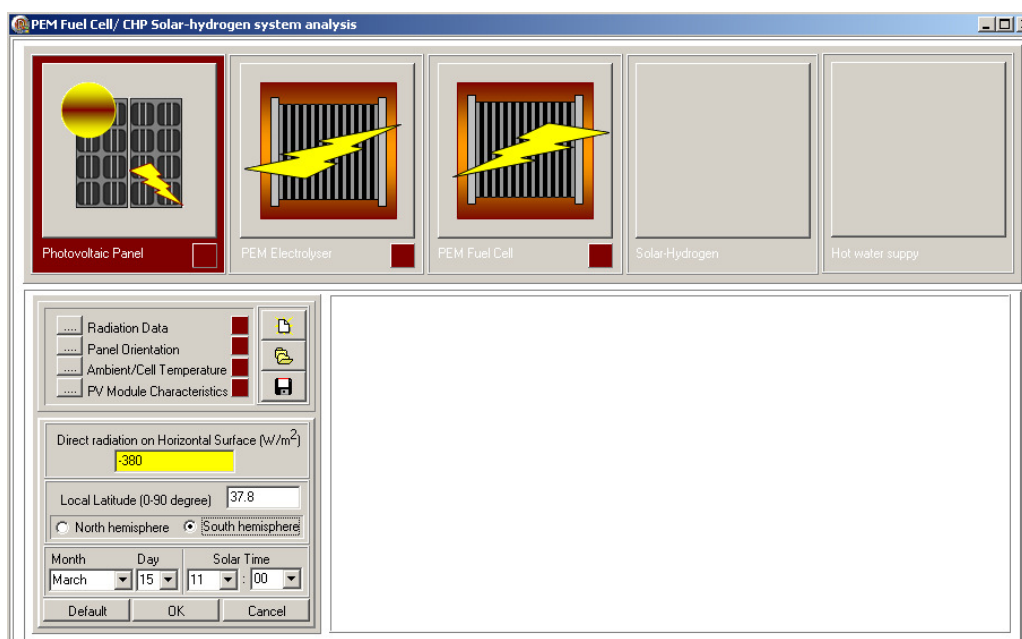


Figure A- 5. An example to show how the program rejects an unacceptable input

2. Array Orientation

As shown in Figure A- 6, the following data are required:

- *The direction that the array is faced to:* If the array is located in the northern hemisphere the option for south facing panels are activated and the ones for north facing array are off; the situation is the reverse if the PV array is located in the southern hemisphere.
- *Array deviation from N-S line:* If the user select north or south, this field is considered zero by the program automatically and becomes inactive so that the user cannot change it to another value. Once the user chooses eastern or western directions (e.g. north east) this field becomes clear and activated, waiting for an angle to be input to show the deviation from N-S line.
- *Plane slope:* The user can enter the PV array slope with respect to the horizontal surface.

Again inappropriate data are notified by marking them in yellow. After completing the data entry the user needs to press ‘OK’ and then if there is no problem with the entered data a green approval light is given to show the data are accepted. By pressing the ‘Cancel’ button the previously-accepted set of data are considered by the program automatically.

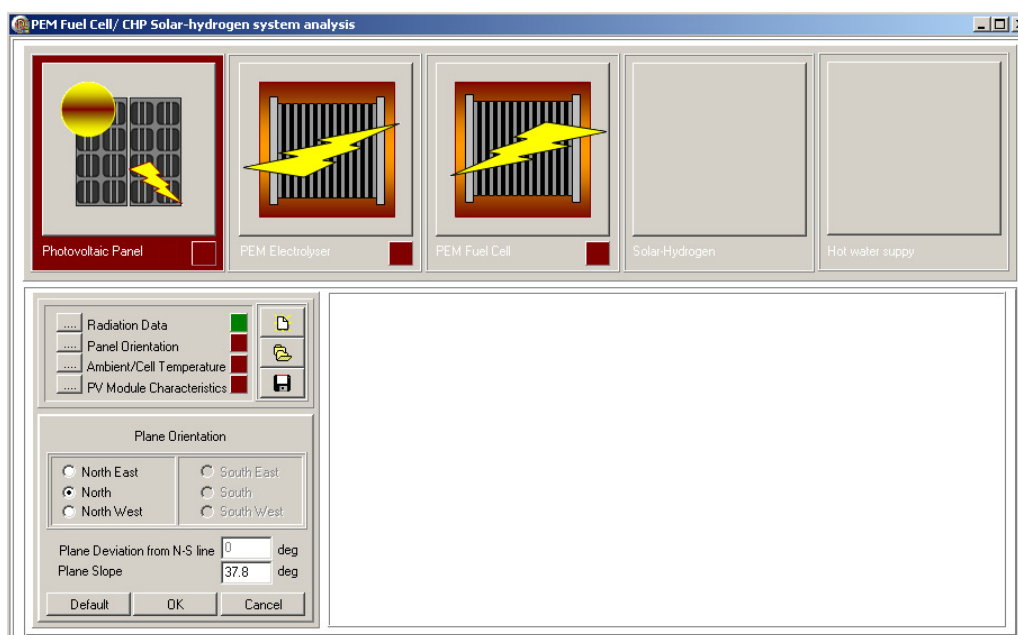


Figure A- 6. Entering the PV array orientation data

3. Ambient/Cell temperature

To introduce the cell temperature the user is provided with two choices:

- *Experimental formula for cell temperature:* ambient temperature, wind velocity and the solar irradiance are the inputs to be used in this part. The irradiance is calculated by the program separately and the other two parameters (Figure A- 7) are to be entered by the user.

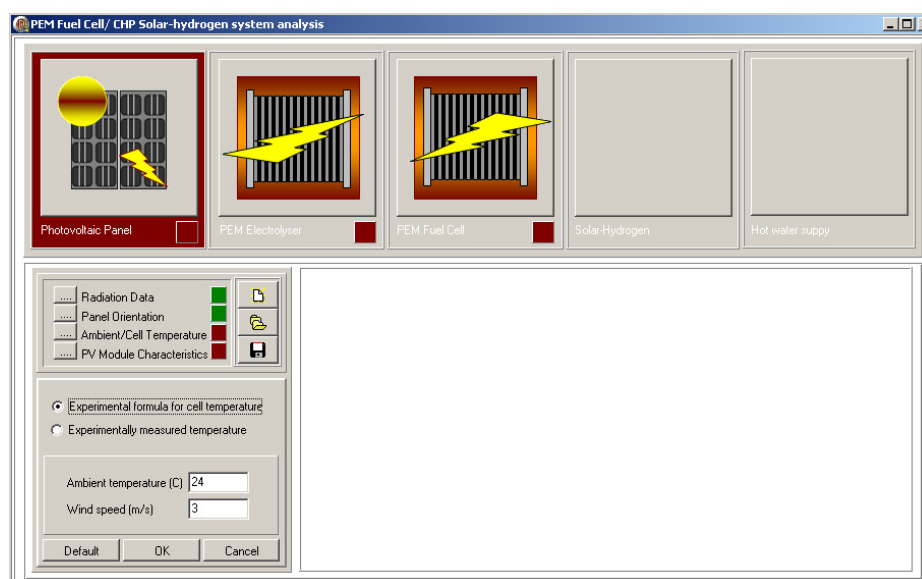


Figure A- 7. Calculating the cell temperature using an empirical formula

- Experimentally-measured temperature: Here the user can introduce the cell temperature directly from an actual measurement (Figure A- 8).

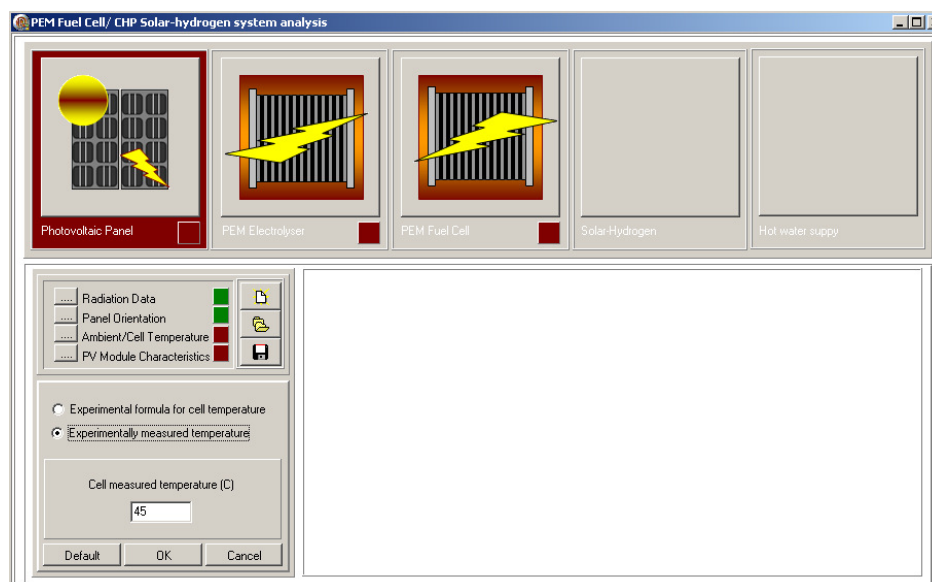




Figure A- 8. Entering the cell temperature which comes directly from an actual measurement

4. The PV module characteristics

The following PV module characteristics are to be entered to RSHAP:

- **NSC:** Number of series cells. A PV module comprises a number of cells which are connected in series
- **NP:** Number of parallel modules in one string. Basically it is possible to connect the PV modules in any parallel-series configuration. NP is the number of parallel strings of the PV modules in the PV array, analysed by RSHAP
- **NS:** Number of series modules in one string
- **Area:** The area of a single module (note that this is not the total area of the array)

- **Reference Condition:** The following parameters at standard test condition (STC) are to be entered. The STC is considered 25 °C cell temperature and 1000 W/m² of irradiance by default; however, any new values can be entered for these two parameters.
 - **T:** Reference temperature (the temperature at standard test condition)
 - **G:** The irradiance at standard test condition
 - **Imp:** The current at maximum power point (STC)
 - **Vmp:** The voltage at maximum power point (STC)
 - **Isc:** Short circuit current at STC
 - **Voc:** Open circuit voltage at STC
 - μ_{isc} : Short circuit current temperature coefficient
 - μ_{voc} : Open circuit voltage temperature coefficient. This is expected to be negative and if it is chosen inappropriately the iteration diverges. A procedure here has been added to the program so that it sends a warning message to the user when this parameter is chosen inappropriately. The message also contains a suggestion to modify the given value (Figure A- 9).
- **Material:** Here the band gap of two materials, Si and GaGs which are usually used in PV cells are provided; however, by selecting 'other' it is possible to enter a user-defined band gap in this field for a new material.

The open () and save () buttons are also specially designed for this part so that the user can recall an already-saved technical specifications of a PV array.

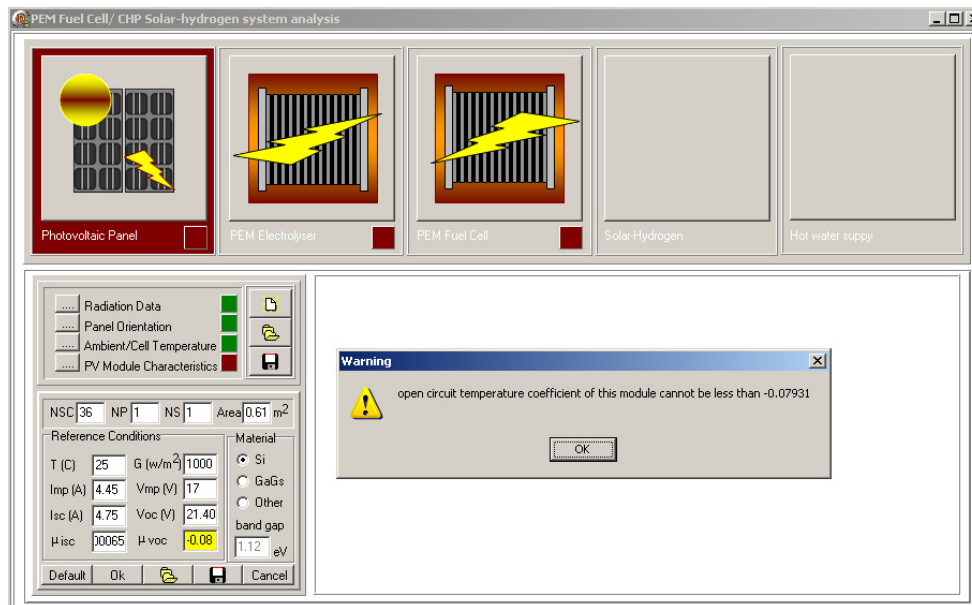


Figure A- 9. Entering the PV module specifications

Start Analysis

After completing the input data, the program is ready to perform analysis on the PV array to estimate its performance. As shown in Figure A- 10 the user is provided with two analysis option here: '*Quick Analysis*' and '*Complete Analysis*'. In quick analysis mode less points are used by the program so the saturation behaviour of the curve when getting close to short circuit current is shown with less accuracy; however, by choosing '*Complete Analysis*' the curve is drawn with more accuracy in this area. Both modes have the same level of accuracy in finding the maximum power point of the PV array characteristic curve. '*Show Results*' and '*Save*' buttons are not yet activated and once the user clicks on '*Start Analysis*' and the analysis is complete these buttons become activated. The results can be saved using the '*Save*' button.

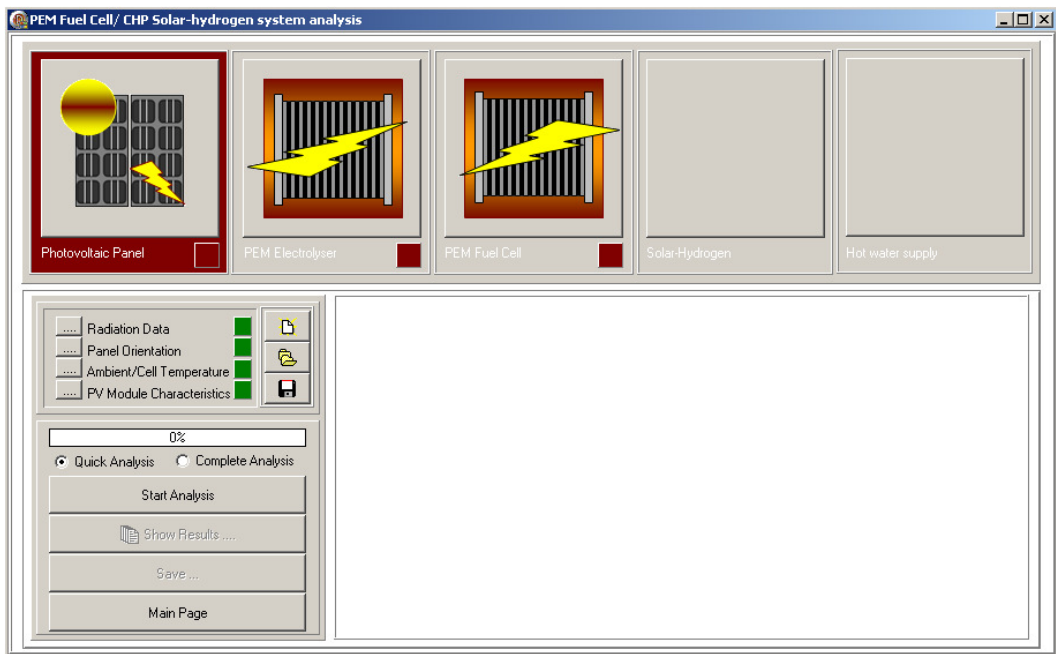


Figure A- 10. Starting the PV array analysis

Show Results

Once the analysis is finished the ‘*Show Results*’ button gets activated and by pressing this button it is possible to see the analysis results, organised in four groups (Figure A- 11).

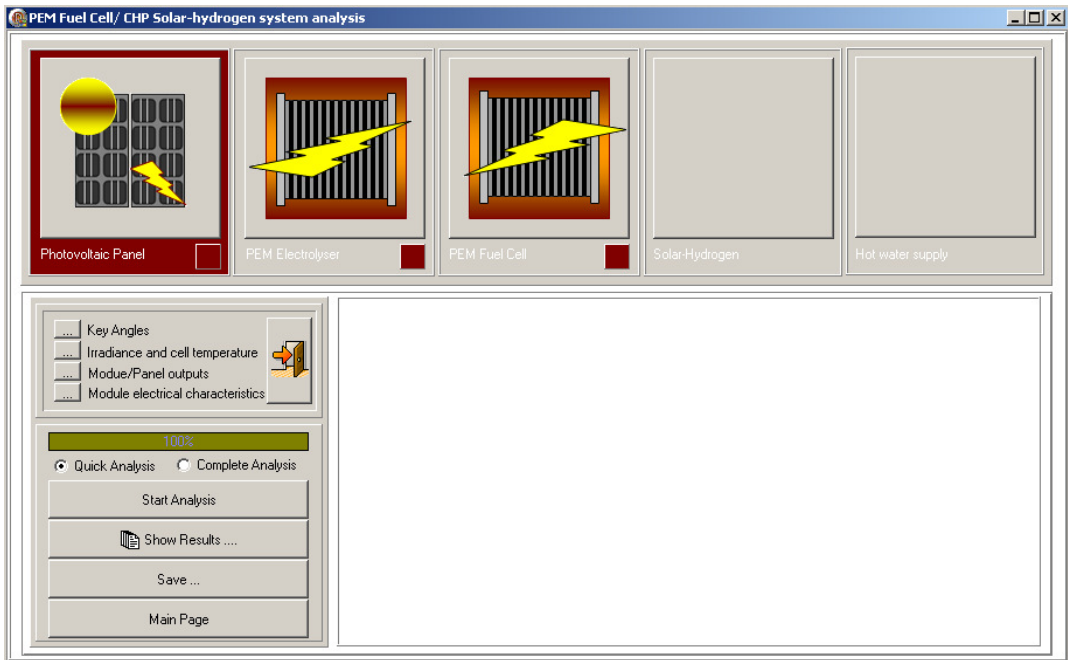


Figure A- 11. ‘Show Results’ button to see the PV module analysis results

1- *Key Angles (Figure A- 12)*: by clicking on this button declination, solar altitude and azimuth angles are displayed. Moreover, the code suggests the best angle and orientation for the PV array to receive the sun rays.

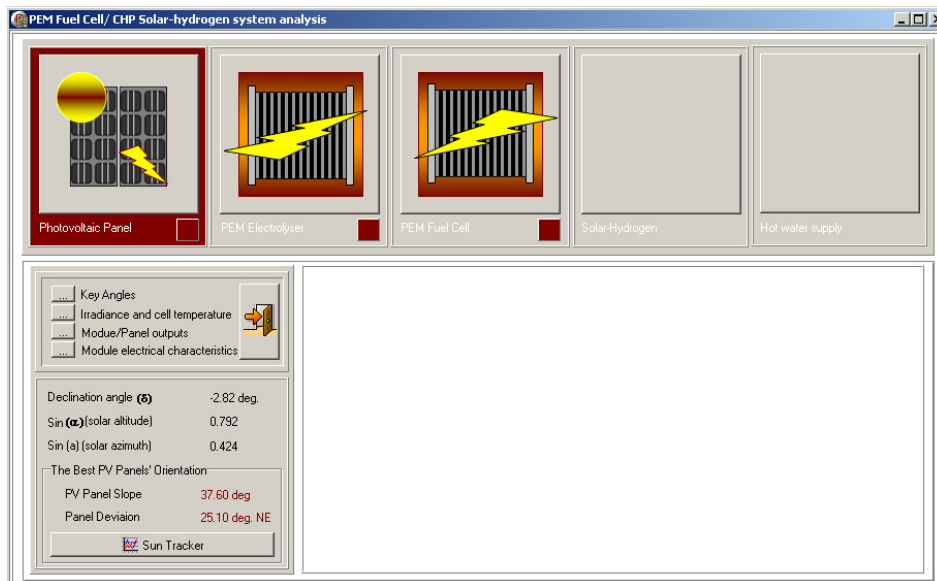


Figure A- 12. Key solar angles

‘*Sun Tracker*’, the button shown in Figure A- 13, is for displaying the daily variations of array slope and azimuth angles when it tracks the sun for the selected date.

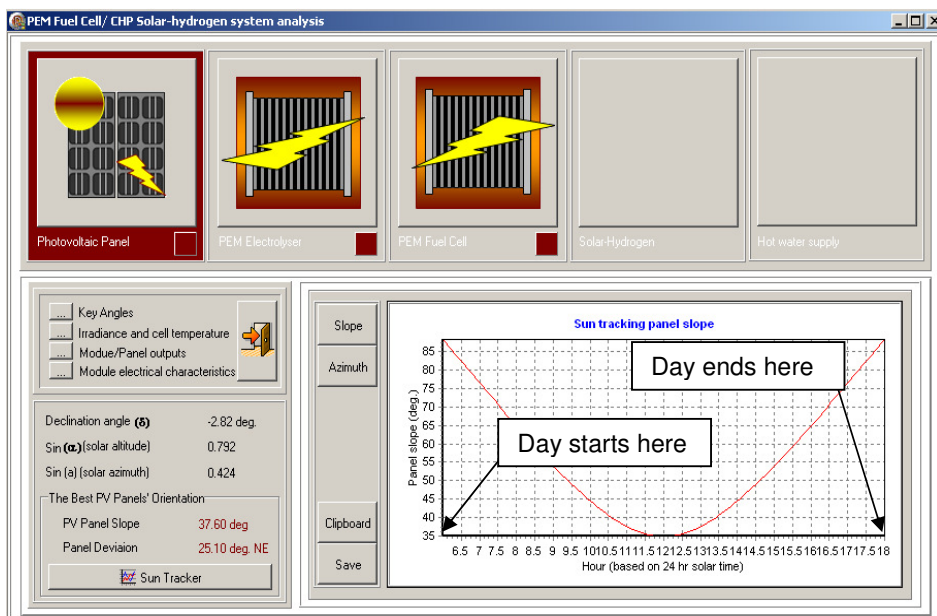


Figure A- 13. The PV array analysis while it is tracking the sun

Irradiance and cell temperature (Figure A- 14): here the horizontal irradiance, the perpendicular and the direct irradiance to the array are entered to RSHAP. Moreover, the user can see the estimated PV cell temperature in this section.

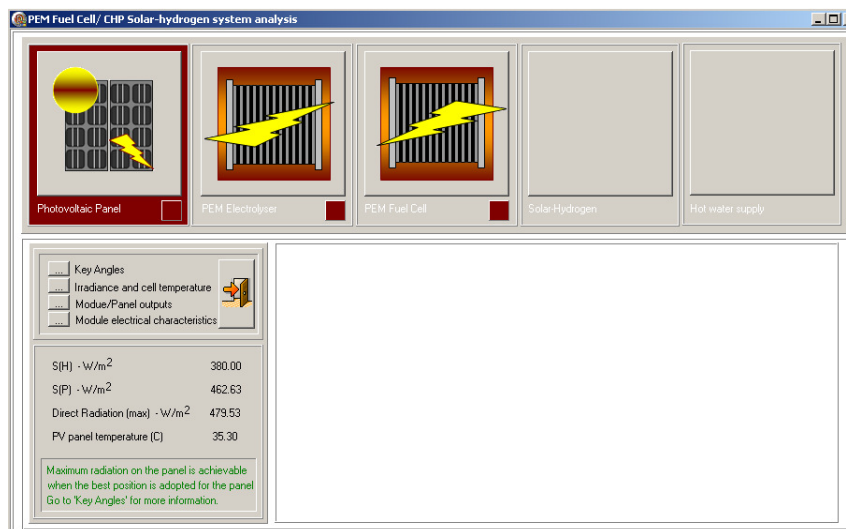


Figure A- 14. Irradiance and cell temperature

2- *Module/Array outputs*: By clicking on this button the user can see the following parameters for both the PV module and the defined PV array (Figure A- 15).

- SC current (A): short circuit current (A)
- OC voltage (V): open circuit voltage (V)
- Max P (W): maximum power (W)
- MPP voltage (V): the voltage at maximum power point (V)
- MPP current (A): the current at maximum power point (A)
- Maximum efficiency (%): the maximum efficiency of the module/array which happens at the maximum power point.

Also using a button located at the bottom left of the panel (Figure A- 16) it is possible to see the performance curves of the PV array including the I-V, P-V and eff-V curves. Again here the possibilities of saving these graphs or importing them to the clipboard are provided. Two more buttons have been designed here to follow the effect of temperature and irradiance on the array's performance (Figure A- 17).

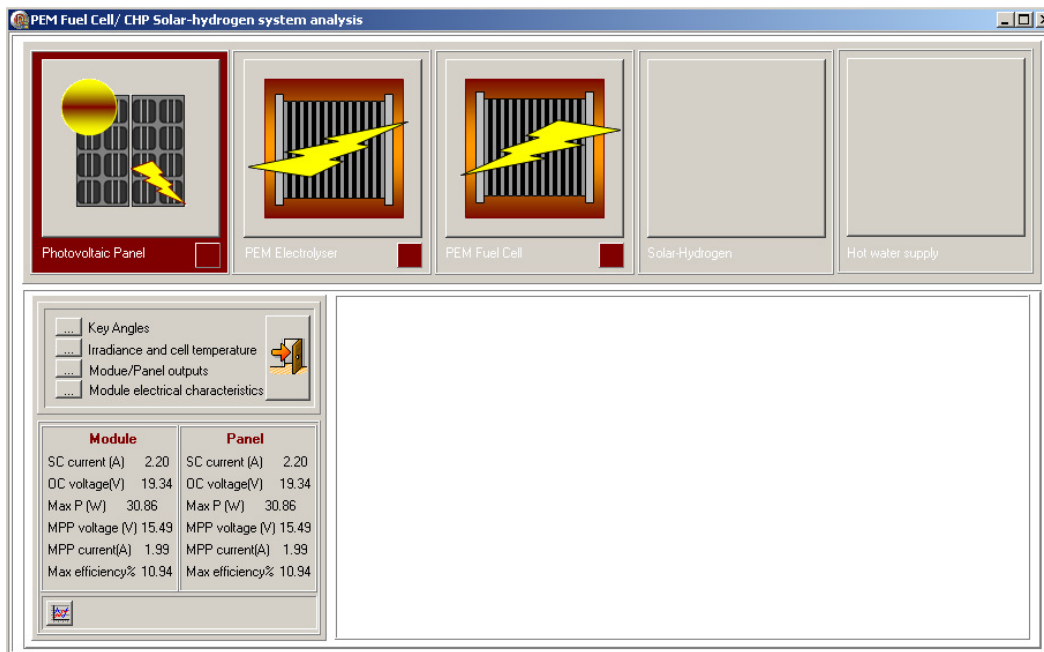


Figure A- 15. Module/Array outputs

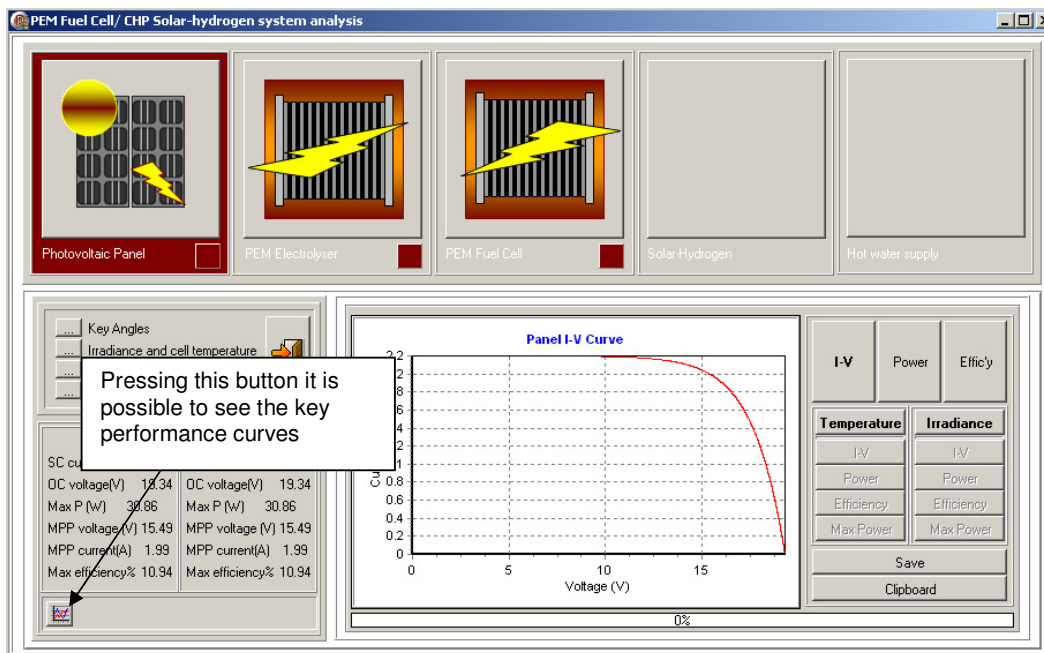


Figure A- 16. The button used to show the performance curves of the PV array

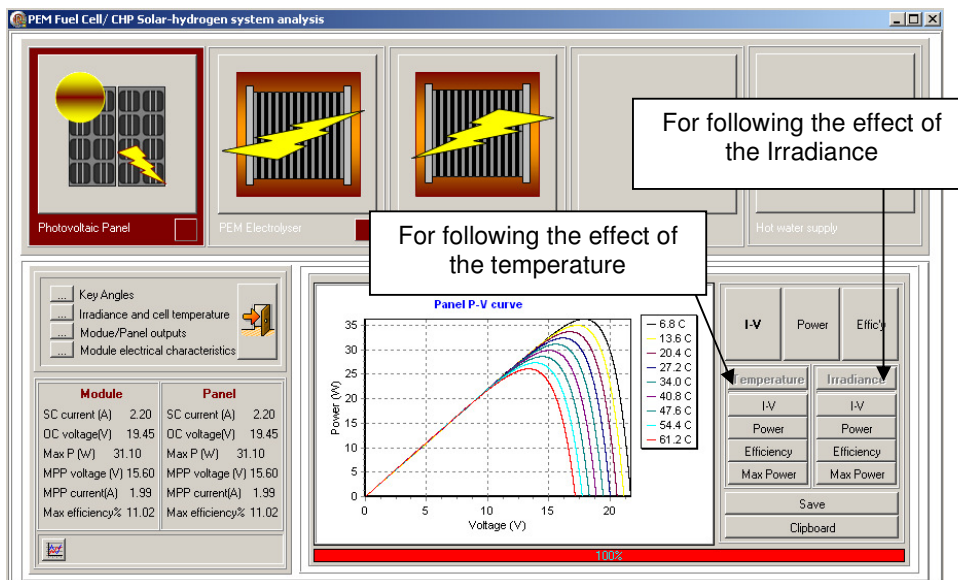


Figure A- 17. The effect of temperature and irradiance on the performance of the PV array

3- *Module electrical characteristics*: Here the electrical characteristics of the module such as diode current, series resistance, shape factor, etc are displayed.

Yearly Analysis

To do solar-hydrogen system analysis on a yearly basis this mode of analysis has to be selected and completed by the user. As shown in Figure A- 18 the inputs are taken in five separate groups, similar to that explained for the ‘*Single Point*’ analysis mode.

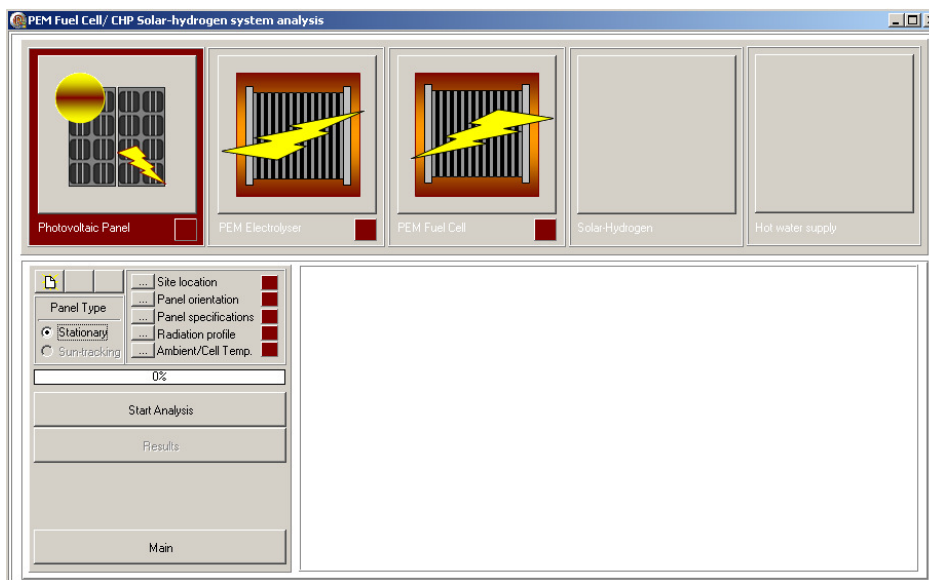


Figure A- 18. The PV array ‘Yearly Analysis’ mode

Input data

The data for running this part of the program are asked in the following groups:

1. *Site location*: here the user has to enter the local latitude of the site (Figure A- 19). By pressing the ‘OK’ button the validity of the entered data are checked by the program. By pressing the ‘Cancel’ button the user can close the PV array data entry panel without accepting the new set of data and the previous set of accepted data are considered by the program.

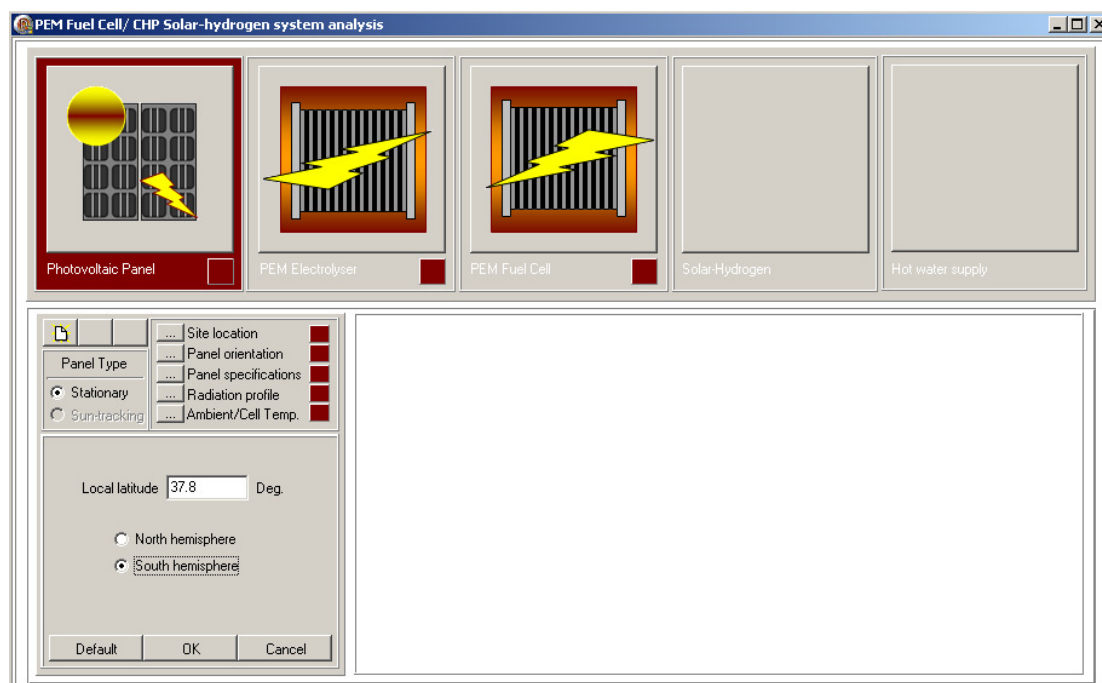


Figure A- 19. Input data, site location

2. *PV panel orientation*: the user has to specify the array deviation from the N-S direction, if there is any, as well as the slope of the array (Figure A- 20). The detail of the data entry in this section is similar to that described earlier in ‘*Single Point Analysis*’ part. Usually fixed arrays are tilted at the local latitude of the place, so for the convenience of the user this option has been provided and automatically selected as default. It is possible for the user to do the analysis at another slope angle. By choosing this option a new edit box appears on the panel where the user can introduce this new slope angle. It is notable that the global solar radiation data are typically available for the horizontal surface and the one tilted at a local latitude angle. If the option of ‘*local latitude angle*’ is chosen, the program

will consider the given irradiance profile for the local latitude angle; however, if ‘*other angle*’ is chosen the irradiance profile taken by the program is considered to be the one received by a horizontal surface. If the only available solar radiation profile is the horizontal one and the user wants to analyse the array when tilted at a local latitude angle, ‘*other angle*’ option has to be selected and then the local latitude has to be used by the code. By choosing the ‘*local latitude angle*’ option the program considers the given horizontal irradiance profile as the one received by a surface tilted at the local latitude angle and this leads to a completely wrong set of results.

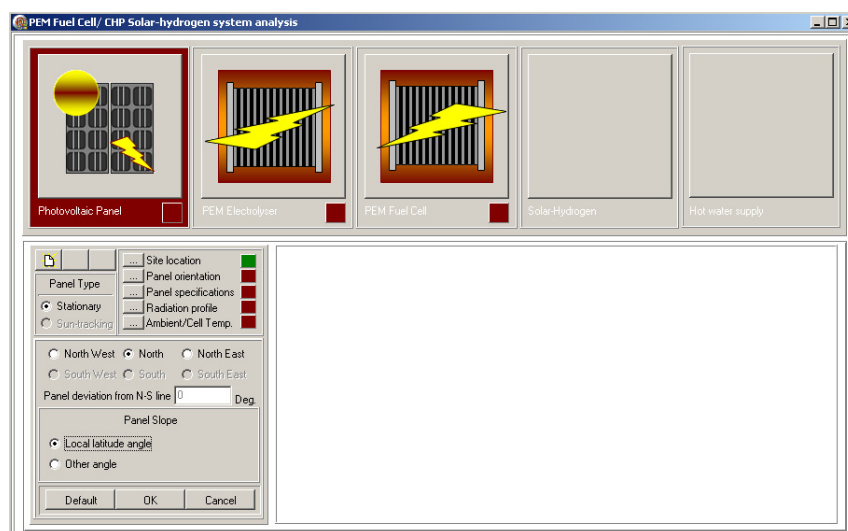


Figure A- 20. Input data, array orientation

3. *Array specification*: this is similar to the one in ‘*Single Point Analysis*’ and the explanations given earlier are applicable for this part as well.

4. *Radiation profile*: the radiation profile is loaded in using a text file (e.g. notepad file) which is to be saved in advanced to be used for this purpose. The user has to save the half-hourly or hourly irradiance data which is given for the entire year in such a text file format, given in separate lines starting from line 1. Basically this text file is expected to be 17520 lines if half-hourly profile is used (17520 half hours for the entire year) and 8760 lines if hourly profile is used. The ‘*Open*’ button showed in Figure A- 21 is used for uploading this file into the program. The buttons, named ‘*Curve*’ and ‘*OK*’ are not activated until the solar irradiance profile are introduced. By pressing ‘*OK*’ button the given irradiance profile is confirmed. By pushing the ‘*Curve*’ button, the user can see the introduced irradiance profile in a chart which appears on the right bottom of the program panel (Figure A- 21). It

is possible to save this chart as a bitmap file or to import it as an image into the clipboard. The ‘New’ button is used for clearing the given data and by pressing the ‘Cancel’ button the panel solar irradiance entering data panel is closed and the previous set of given data for the solar irradiance (if any has been introduced previously) is automatically used by the program.

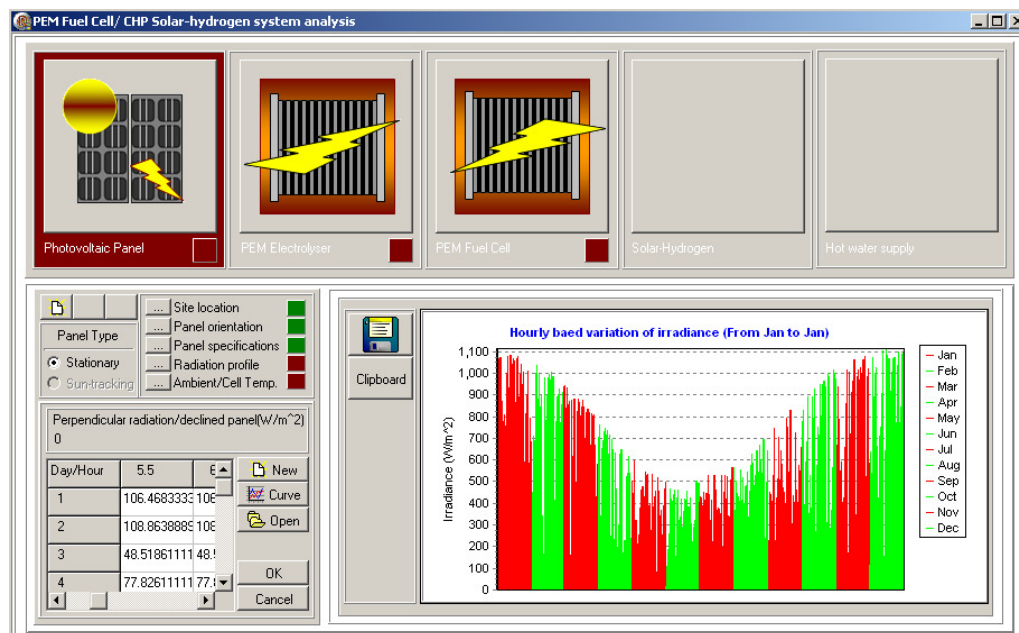


Figure A- 21. Input data, radiation profile

5. *Ambient/Cell Temp.*: the ambient condition including the ambient temperature and wind speed profile are introduced to the program here and this information is used to calculate the cell temperature profile. By clicking on this button a new panel opens, as shown in Figure A- 22, and the user can see four buttons: ‘Ambient temp.’, ‘Wind speed’, ‘OK’, and ‘Cancel’.

The ‘OK’ button is not initially activated and once the temperature and wind speed profiles are introduced, and they are recognised by the program, this button becomes activated so that the user can finalise the given data by pressing this button. The ‘Cancel’ button also has a similar function as explained in previous steps.

By clicking on the ‘Ambient temp.’ button the panel shown in Figure A- 23 appears. The user needs to load the temperature data there. The program takes the average monthly minimum and maximum temperatures. The user has to prepare this information beforehand

in a text file (e.g. a notepad file) as shown in Figure A- 24. Before loading the temperature data file, all the other buttons in this panel are deactivated. Once the temperature data file is loaded they get activated and it is possible to see the complete temperature profile data in a separate table ,or to see the graph of the average values variation for both maximum and minimum temperatures.

The program estimates the half-hourly temperature profile by applying a linear function to the daily temperature variation between the maximum and minimum temperatures given to the program (see section 4.1.4 for more details).

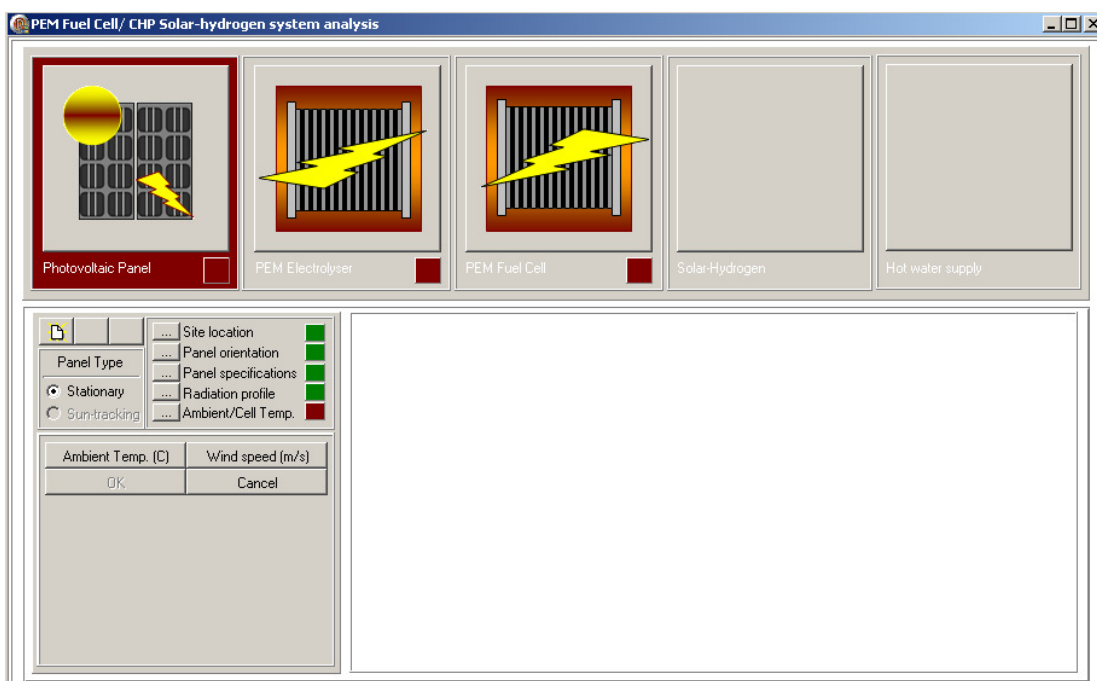


Figure A- 22. Input data, Ambient/Cell Temp.

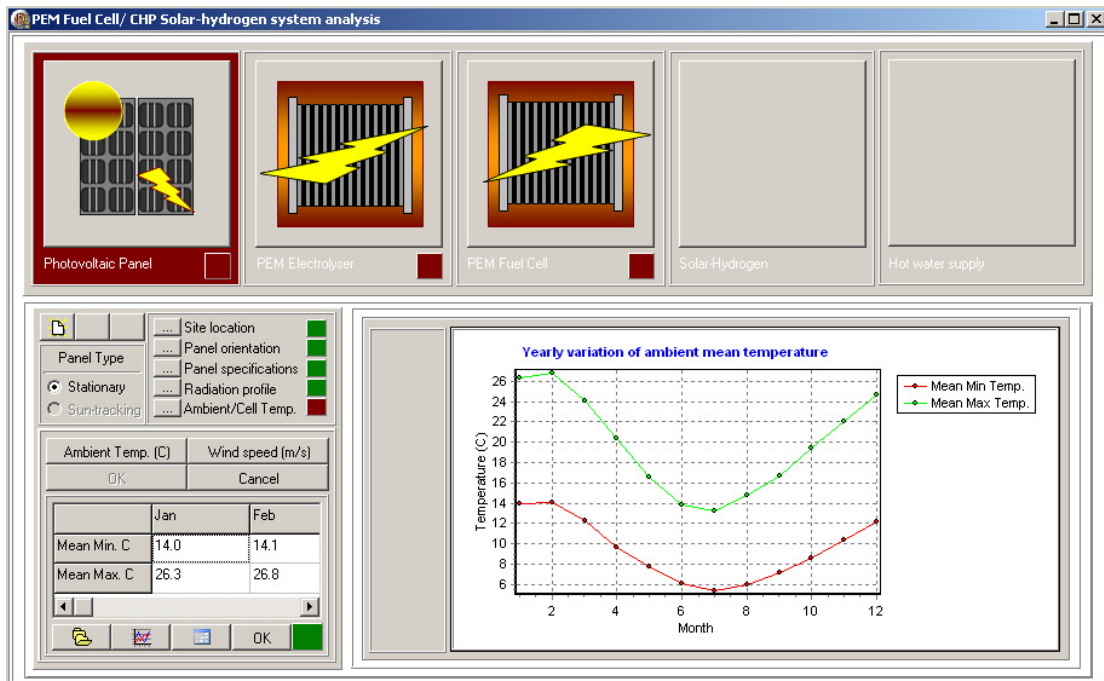


Figure A- 23. Input data, ambient temperature profile

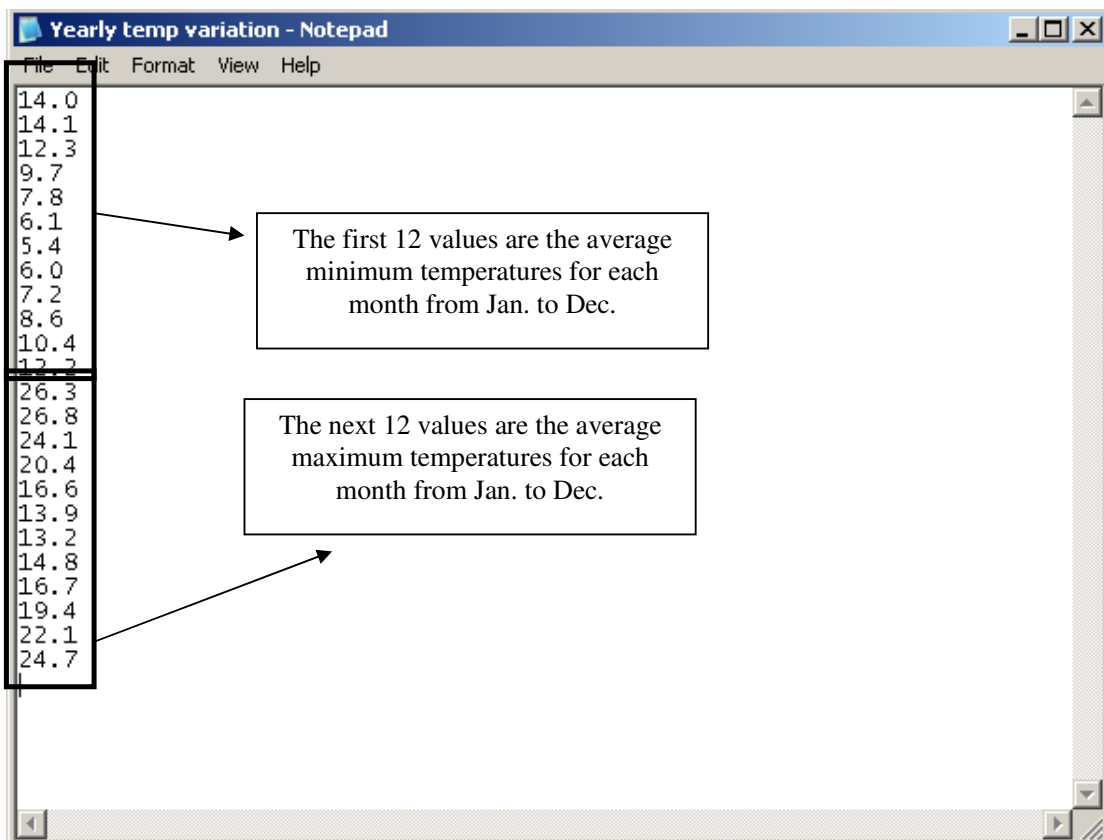


Figure A- 24. The right format for arranging a compatible temperature data file to be loaded into the program.

Clicking on the ‘OK’ button is not enough to get a green light of approval for this group of data. The wind speed profile has also to be introduced to receive this green light.

By clicking on the ‘Wind Speed’ button, the page shown in Figure A- 25 is opened in which the user can upload another text file for the wind speed profile. An average monthly wind speed profile is what is required by the program. A linear assumption is used to create a daily wind speed profile (see section 4.1.4 for more details) and then the wind speed profile is assumed constant for each day for creating an hourly or a half-hourly wind speed profile. The text file to be loaded here includes twelve lines (with twelve values together); the first value (first line) is for January and the last one represents the average wind speed in December.

After clicking on the ‘OK’ button for wind speed (Figure A- 25), the user has to click on another ‘OK’ button to confirm all the temperature and wind speed profiles, then the green light is given to this group of data. Now by clicking on the ‘Start Analysis’ button the program starts analysing the half-hourly or hourly output of the PV array and a progress gauge shows the progress status of this analysis. Other buttons in this page are: ‘Results’ (not activated until the analysis is finished) and ‘Main’ button, used to go back to the main page where the user can choose between analysis modes.

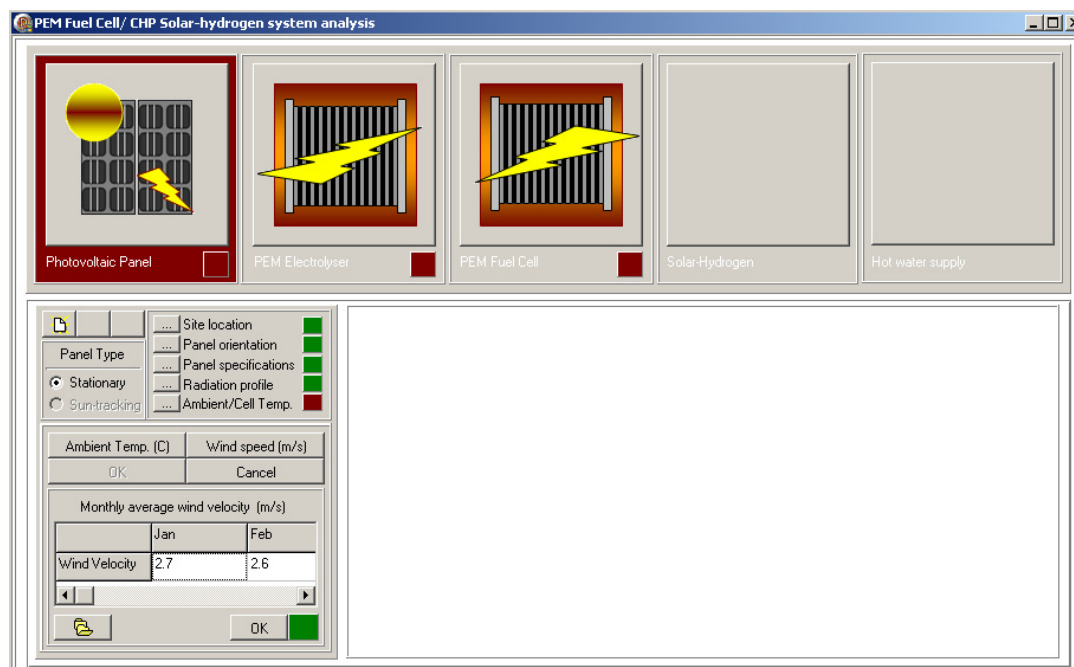


Figure A- 25. Input data, the wind speed profile

Analysis results

By clicking on the ‘Results’ button the page shown in Figure A- 26 is displayed where the user can see the PV array yearly and daily outputs.

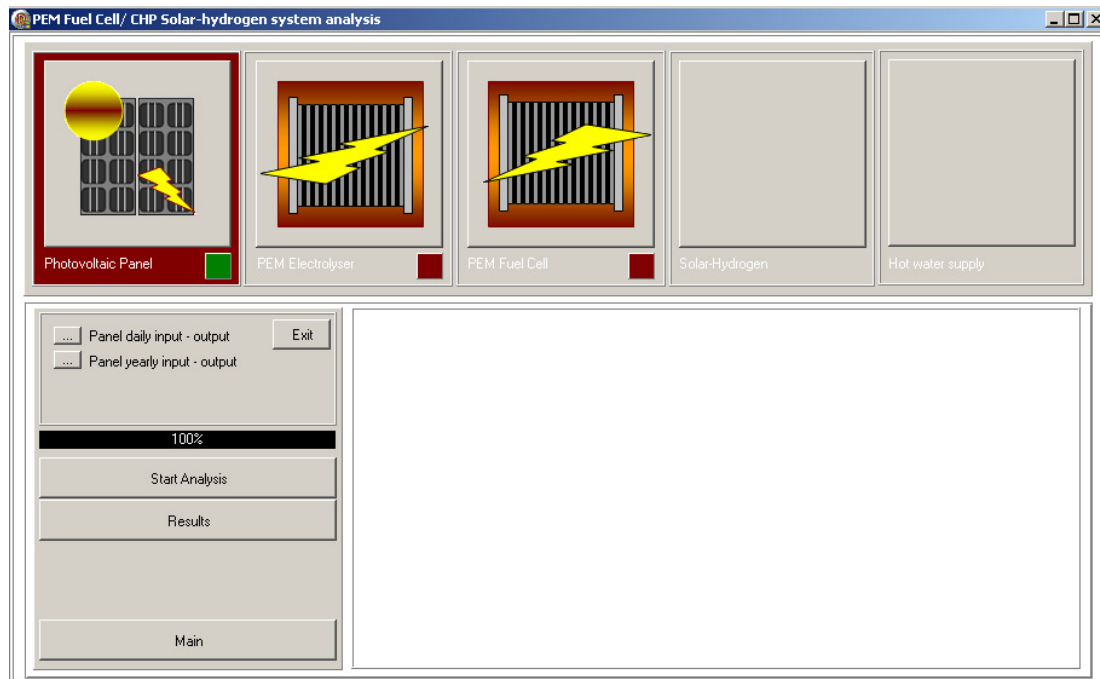


Figure A- 26. Results button, press to see the PV array yearly analysis results

By choosing the ‘Panel daily input-output’ the user can see the input to and output of the PV array in a particular selected date selected (Figure A- 27). The program does not accept negative values for date as input in this part and such wrong input data are highlighted in yellow. After choosing date and pressing ‘OK’ the results for the chosen date appear and also a small button is activated for showing the graphs of input and output of the array. The button for importing an image of the graph to the clipboard is also designed on the top left of the graph as shown in Figure A- 27.

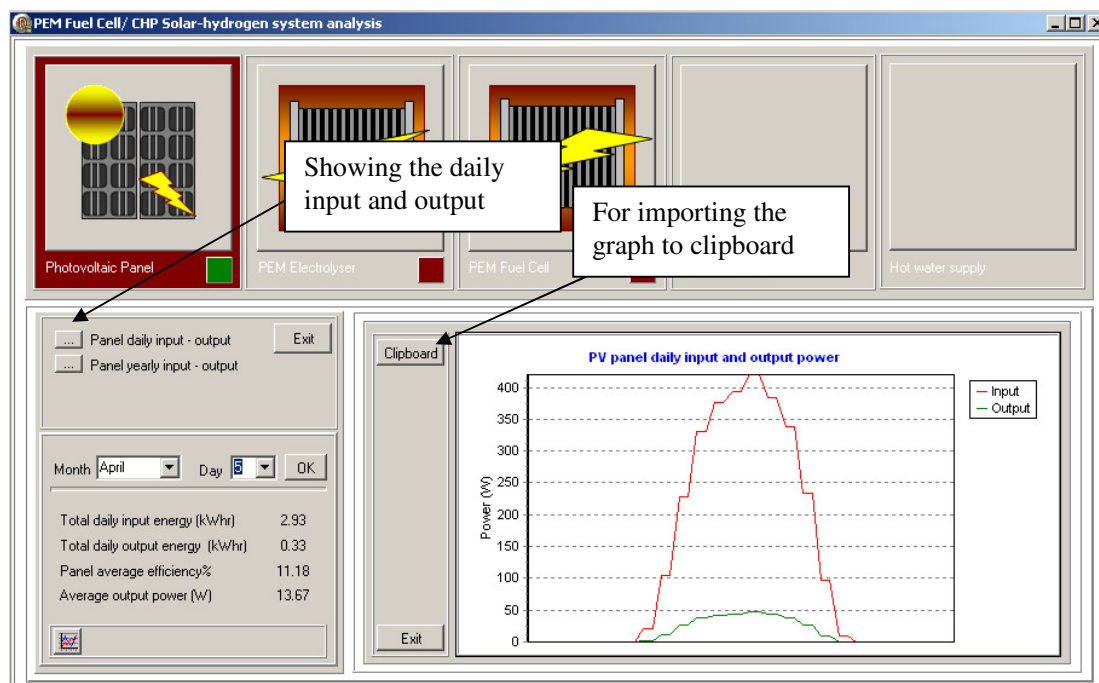


Figure A- 27. Results, daily input and output

PEM electrolyser

The second large button on top of the main page is for the PEM electrolyser analysis. By clicking on this button the panel shown in Figure A- 28 becomes visible. The program is able to recognise the electrolyser using the Butler-Volmer equations. Before the program asks for the key parameters used in the Butler-Volmer equations the following information are needed by the program:

1. The membrane effective area (cm^2): this is the effective area of a single cell and the user is not expected to enter the membrane effective area of the whole stack.
2. The membrane thickness (cm)
3. The number of series cells in the stack: the electrolyser is not supposed to be properly sized at this stage, just a trial electrolyser stack size (the number of series cells) is given here, and then an appropriate size for the electrolyser stack will be calculated when the solar-hydrogen system is analysed by the program.
4. The electrolyser operating temperature ($^{\circ}\text{C}$)
5. The electrolyser maximum permissible current (A), provided by the manufacturer.
6. The cell's maximum permissible voltage (V), provided by the manufacturer.

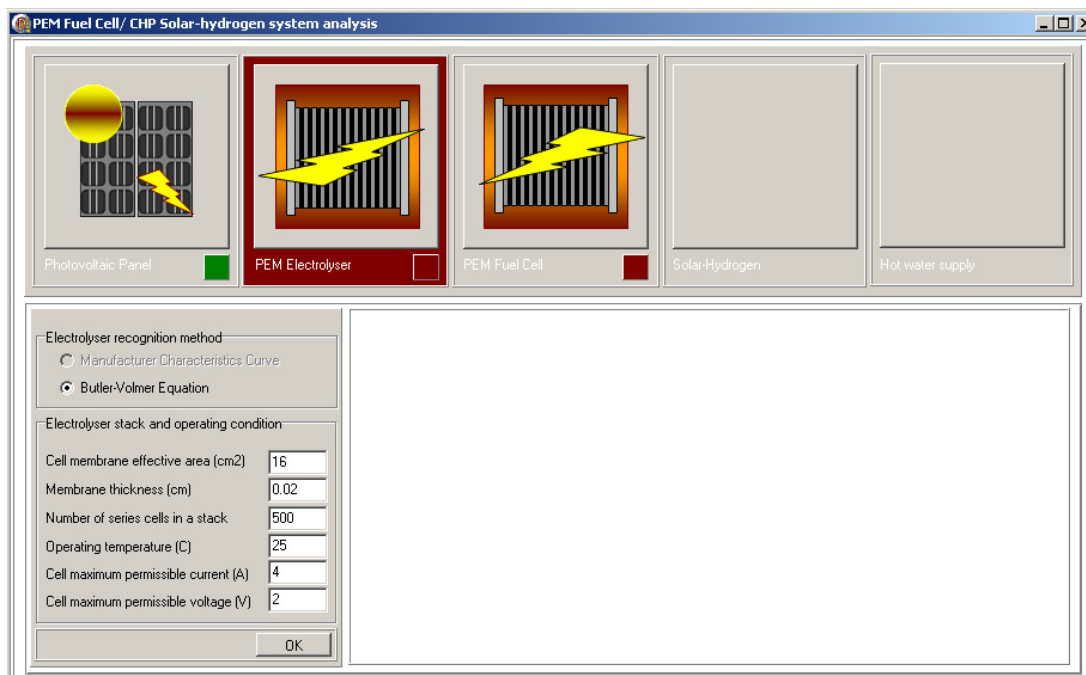


Figure A- 28. Electrolyser input data, electrolyser size and operating condition

By pressing the ‘OK’ button, if the input data are appropriate, another panel will be opened asking for the key parameters used in the Butler-Volmer equations (Figure A- 29). Using the default button located on the left bottom of this panel the code suggests some values for these key parameters; however, the user can change these values if needed. The user has to be experienced in choosing a proper set of data otherwise the iteration process used by the program to solve the Butler-Volmer equations may diverge. By clicking on the ‘Exit’ button this page is closed and the user is directed back to the previous page. By pressing the ‘Start Analysis’ button the user can see the I-V and the P-I performance curves in a few seconds. After the progress gauge shows the completion of the analysis a green light is given to let the user know that the electrolyser is recognised by the program.

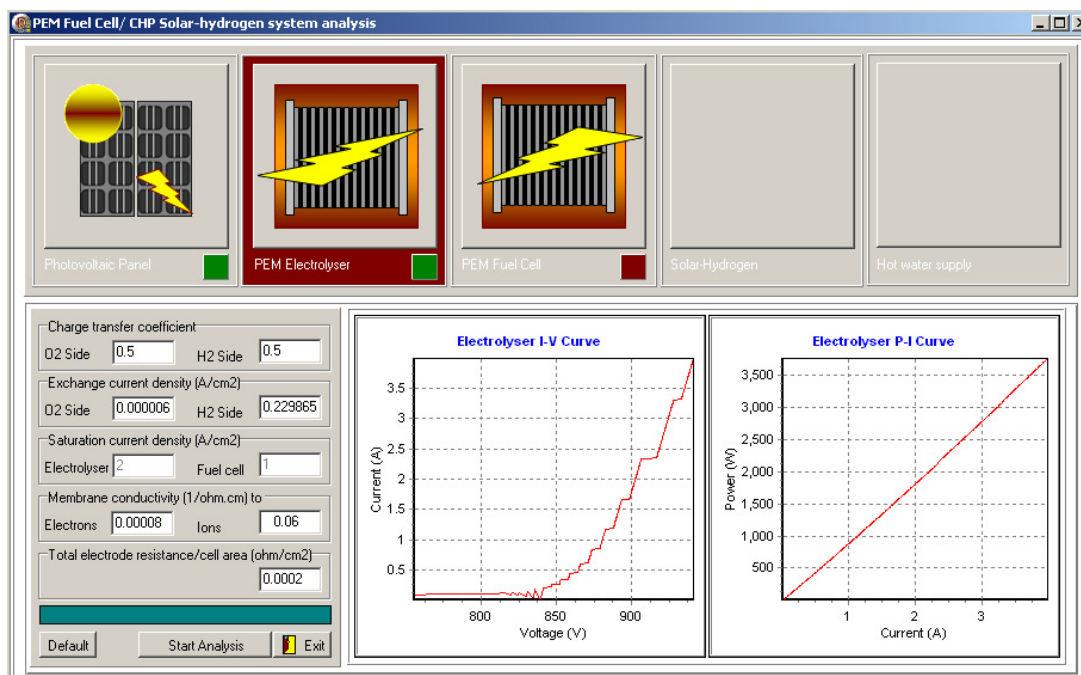


Figure A- 29. Electrolyser analysis mode

PEM Fuel Cell

Fuel cell analysis is done comprehensively using RSHAP since one of the main purposes of developing this program was particularly looking at the waste recovery analysis of this element to investigate the possibility of converting the fuel cell to an efficient combined heat and power supply unit. By clicking on the fuel cell analysis button two options are provided on the main page (Figure A- 30):

1. Single point analysis
2. Stack characteristic curve recognition

The user has to choose between these two analysis modes and then press the ‘Go’ button to continue with the selected mode.

Single point analysis

This part is for analysing a single operating point of a fuel cell. Inputs are taken and outputs are provided in different groups. As previously explained in PV array analysis mode, the small red and green panels have the same application for showing whether the required data are properly provided or not. Once all the necessary input data are given to

the program, all these red panels turn green and the ‘*Start analysis*’ button becomes enabled. Some of the data used for ‘*Single point analysis*’ are carried over to the ‘*stack characteristic curve recognition*’ part, so that they will be used there as well if needed. Figure A- 31 shows how this page looks.

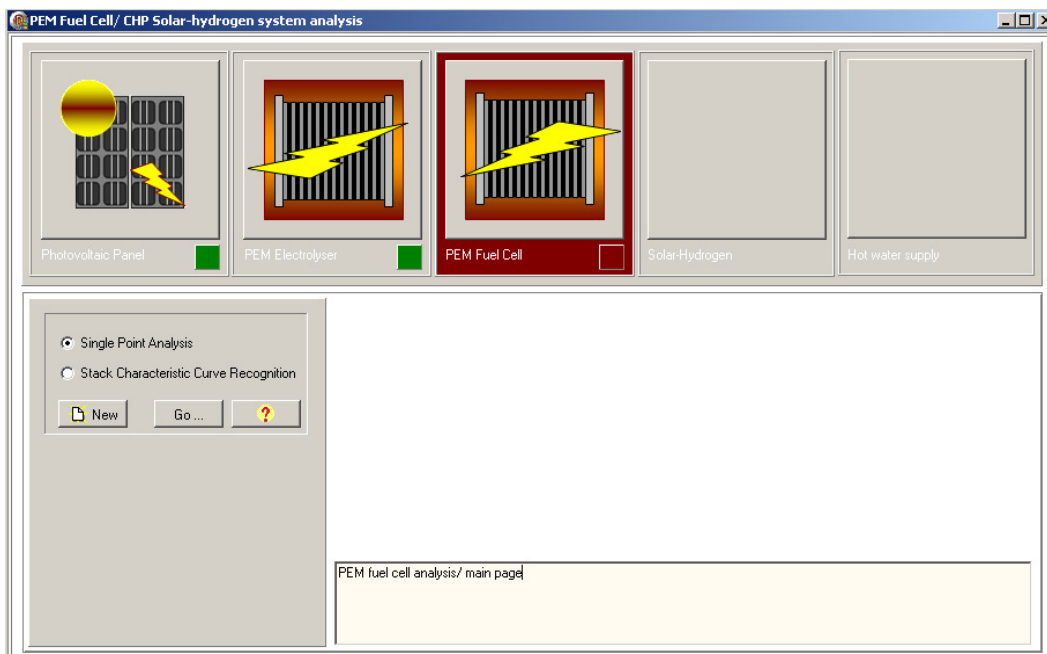


Figure A- 30. Fuel cell analysis main page

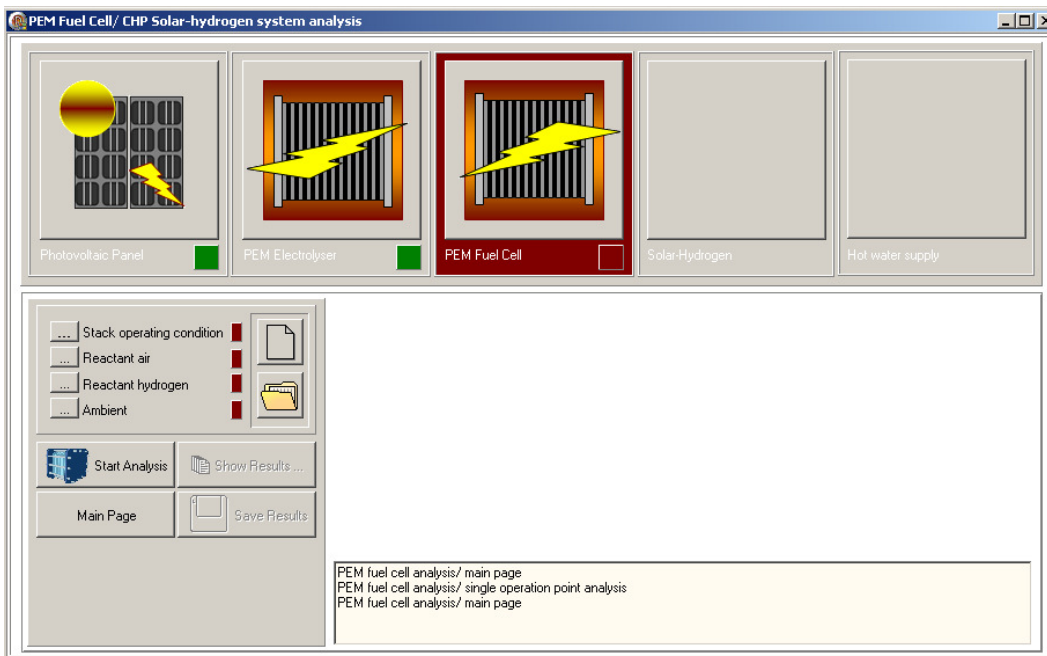


Figure A- 31. Fuel cell analysis, ‘*Single Point Analysis*’ mode

Input data

The input data are taken in four groups:

1. *Stack operating condition* (Figure A- 32): this part includes stack current and voltage or power, number of cells in the stack, and the fuel cell operating temperature.

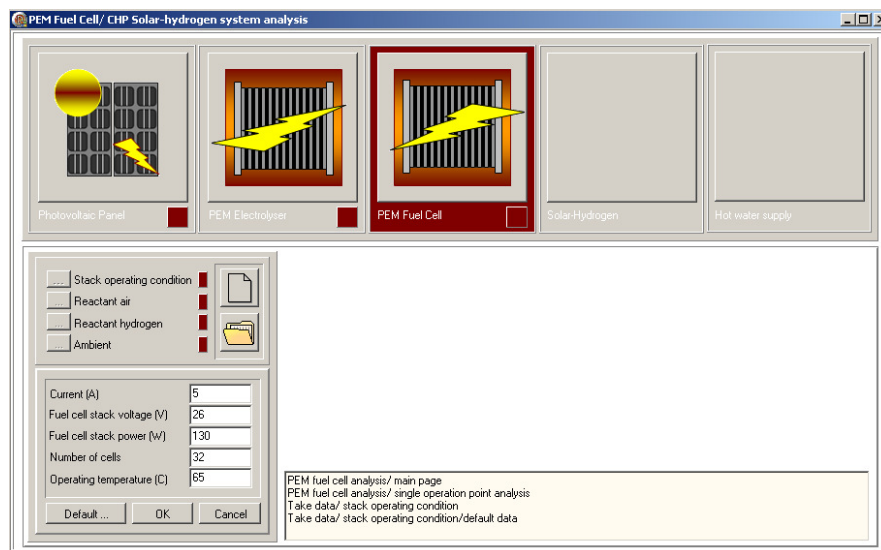


Figure A- 32. Entering the fuel cell stack operating data

2. *Air* (Figure A- 33): air stoichiometry, inlet and exit air pressures, and the inlet air relative humidity are taken here.

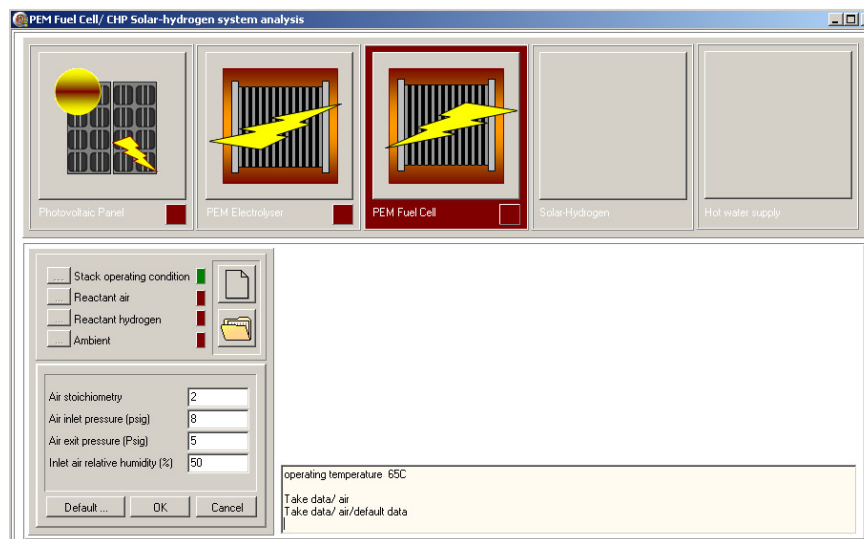


Figure A- 33. Entering the data related to the air side of the fuel cell

3. *Hydrogen* (Figure A- 34): The data needed for the hydrogen side data (similar to the air side) are entered here. Also the actual hydrogen consumption, measured or given by the manufacturer’s manual, is taken here for calculating the hydrogen utilisation coefficient of the fuel cell at the particular operating point of the fuel cell. This field can be left blank and then the program uses its own default value for the Faraday efficiency in calculating the hydrogen utilisation coefficient.

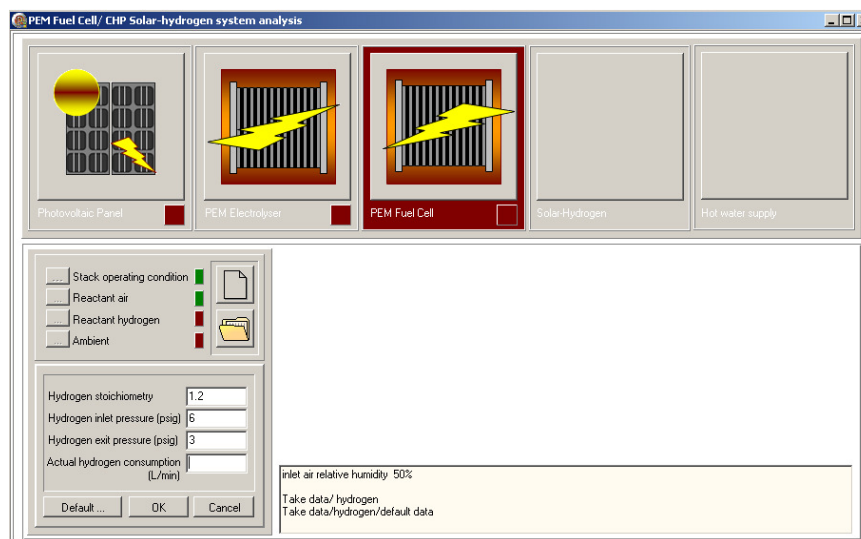


Figure A- 34. Hydrogen reactant specifications

4. *Ambient* (Figure A- 35): the ambient pressure and temperature are asked to be filled in this section.

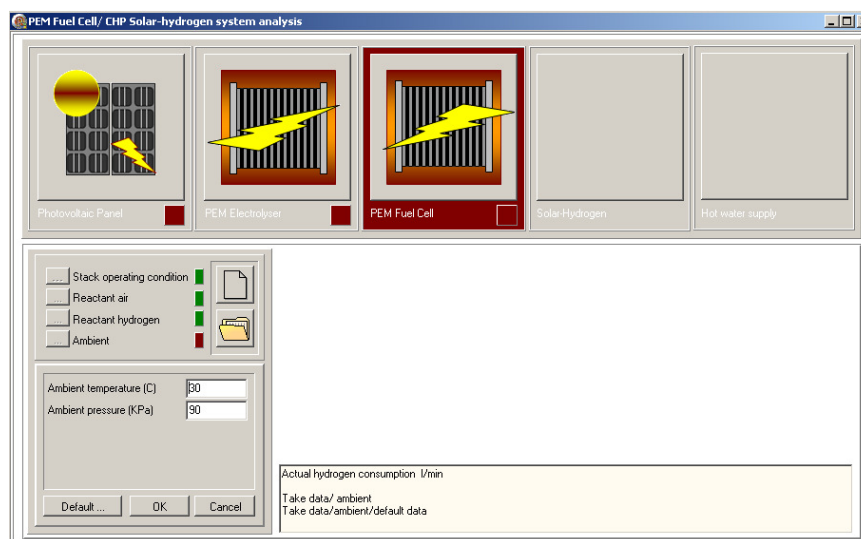


Figure A- 35. Ambient condition, used for the fuel cell analysis

Now the ‘*Start Analysis*’ button shown in Figure A- 36 is ready to be pressed; by pushing this button (if all the necessary input data are introduced in the previous step) the simulation program will analyse the fuel cell and then the ‘*show Results*’ button becomes enabled to see the fuel cell performance characteristics. By pressing this button the results can be reviewed in four groups. Next to each of these groups (on the left), there are buttons that the user can click on to see the details.

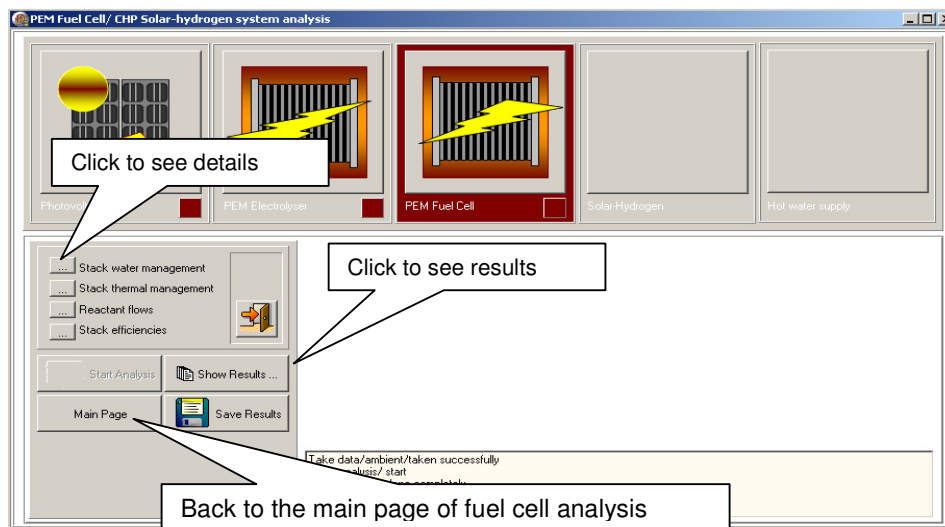


Figure A- 36. The results of the Fuel cell analysis provided in four categories

These outputs of the fuel cell analysis in ‘*single point analysis*’ mode are:


Stack water management

As shown by Figure A- 37 the following results/information, related to the water management of the fuel cell are provided in this section:

- The water content of the inlet air
- The fuel cell water production rate
- The phase of the water content of the air exit stream (liquid or steam)
- The total water content in the exit air stream and the exit air relative humidity

The air relative humidity is used to judge whether the cell is flooded, dehydrated (less than 80%), or is operated at a suitable level of water content (if the relative humidity of the exit air is between 80% and 100%).

The user can also see the effect of the air stoichiometry and the cell operating temperature on the outlet air relative humidity by using the ‘*graph*’ button shown in Figure A- 37. By using the ‘*Save*’ button it is possible to save this graph as a bitmap file and using the ‘*Clipboard*’ button an image of the graph can be imported to the clipboard.

To go to the other result group, the current panel has to be closed first by pressing on the ‘*exit*’ button () shown in Figure A- 37.

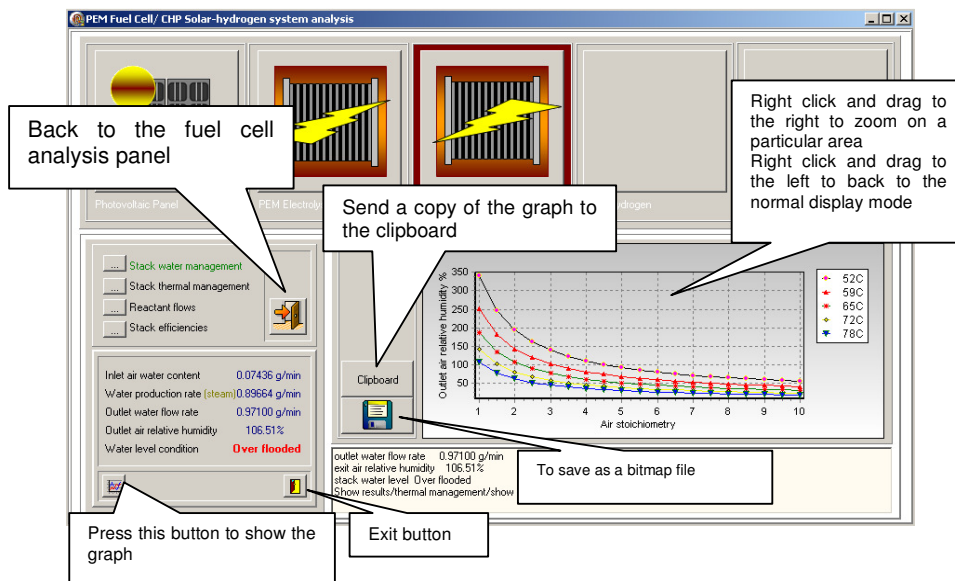


Figure A- 37. The fuel cell water management results

Thermal management

The followings are shown in this section:

- Stack total heat generation rate
- Hydrogen heat transfer, the heat which is transferred out from the stack by the excess hydrogen
- Dry air heat transfer, the heat which is removed by just the extra air that leaves the fuel cell stack. Here the water content of the air is not taken into account and just the dry air temperature difference between inlet and outlet is considered for heat transfer calculation
- Wet air heat transfer: The heat removed out from the cell by the inlet air water content
- Produced water latent heat: The water product if it appears in vapour form

- Fuel cell cooling load
- *Graphs*: Two graphs are provided here (Figure A- 38) to observe the fuel cell heat and power production situation and the fuel cell heat removal status.

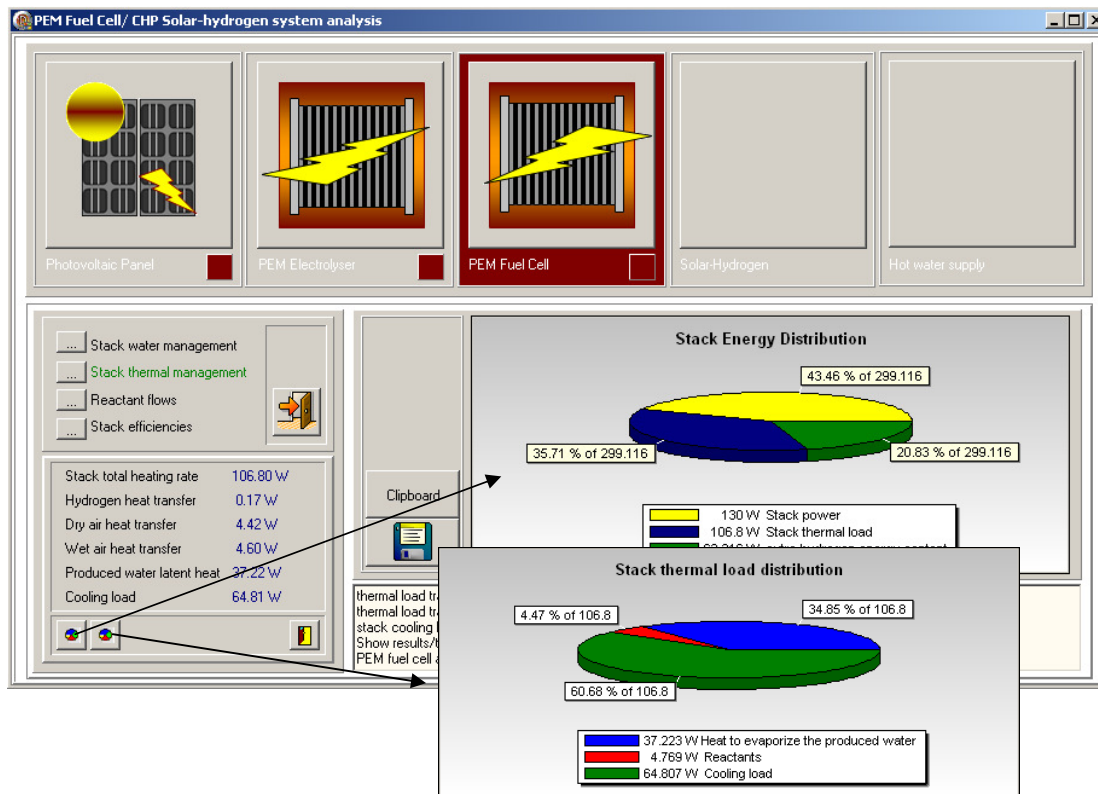


Figure A- 38. The fuel cell analysis results: thermal management

1. Hydrogen and air flow (Figure A- 39)

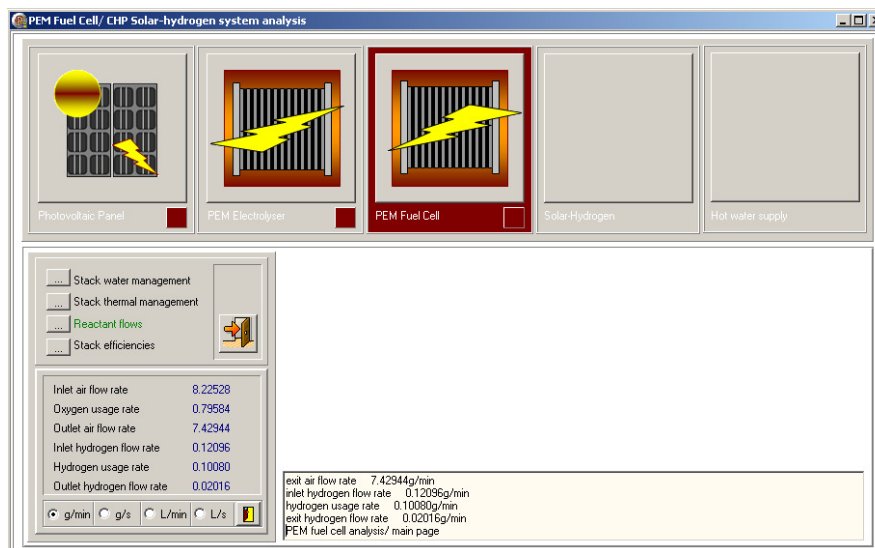


Figure A- 39. The air and hydrogen inlet/exit/consumption flow rates

2. *Stack efficiencies* (Figure A- 40), including the energy efficiency, the Faraday efficiency, the hydrogen utilisation coefficient, the maximum theoretical reversible energy efficiency, and the reversible open circuit voltage are the outputs shown on this panel.

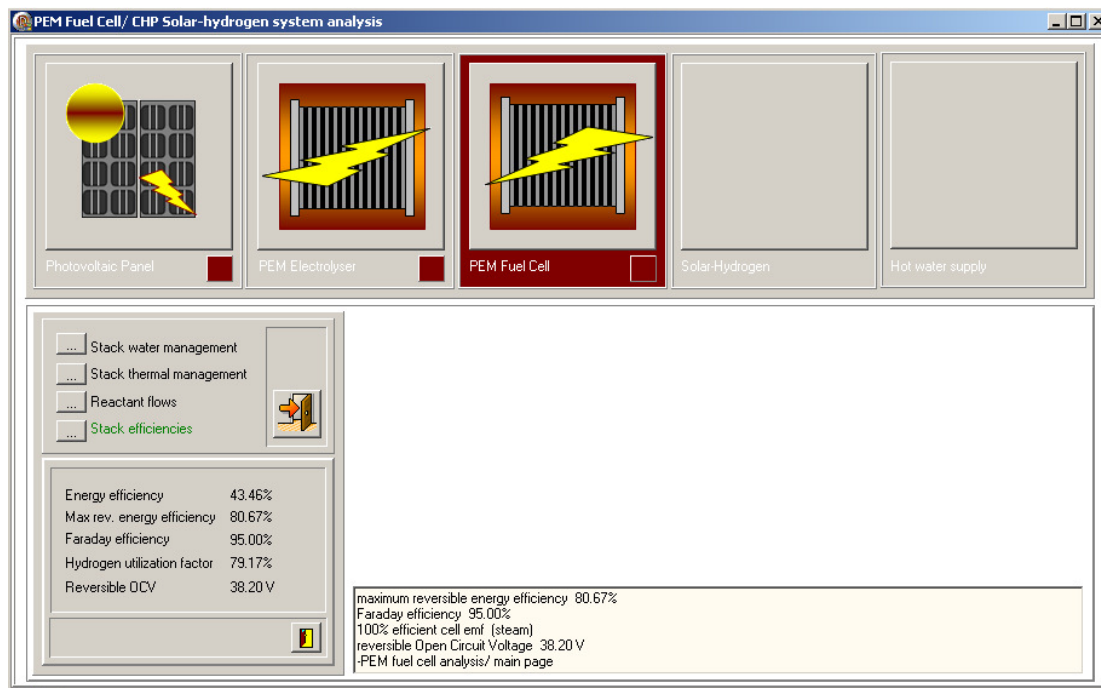


Figure A- 40. Fuel cell analysis results: Efficiencies

Stack Characteristic Curve Recognition

By clicking on the 'main page' button and then choosing the appropriate radio-button and clicking on the 'Go' button (Figure A- 41) the program gets into this mode of the fuel cell analysis. If 'single point analysis' is done before, the key data are automatically carried over to this part of the program and then the user can either edit them before using them again, or use them as they are.

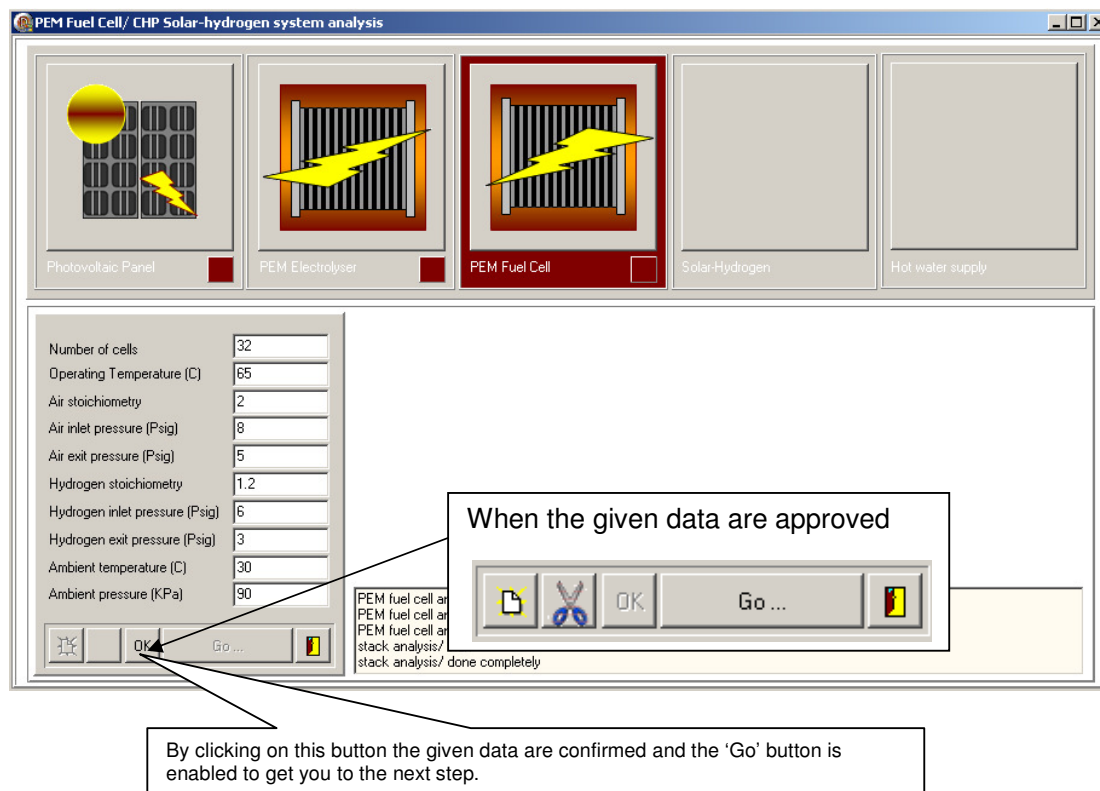


Figure A- 41. Start page for Stack Characteristic Curve Recognition

By clicking on the ‘Go’ button (Figure A- 41) and going to the next panel, two groups of questions are asked (figure a- 42):

1. *Fuel cell identification strategy:* A model based on Butler-Volmer equations is used for introducing a fuel cell polarisation curve to the model. These equations can be obtained in two different ways:
 - Direct introduction of the fuel cell key parameters (Figure A- 48) to solve the Butler-Volmer equations.
 - Introducing the experimental polarisation curve of the fuel cell; then by fitting a curve on this experimental curve based on the Butler-Volmer equations (using the least squares method) the key parameters in these equation are determined.
2. The geometry/dimension of a single cell of the fuel cell stack including the cell effective area and the cell thickness.

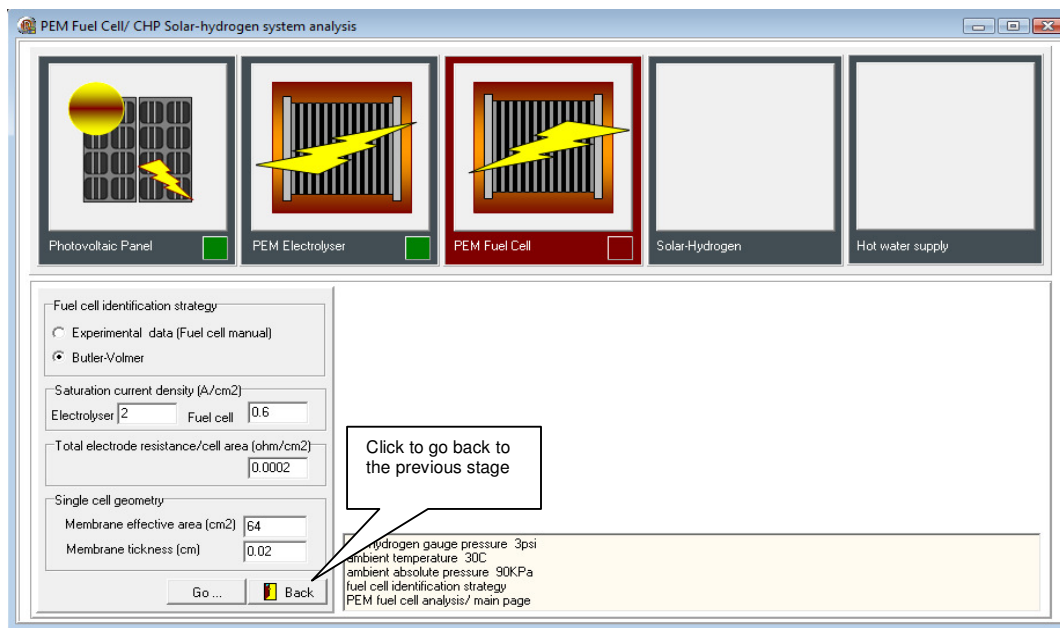


Figure A- 42. Fuel cell identification strategy

Experimental data used for fuel cell identification

The first option is using the ‘*Experimental data*’. The experimental data are basically the polarisation (I-V) curve of the fuel cell that can be either obtained by the user experimentally or be taken from the fuel cell manual provided by the manufacturer. After choosing this option and filling in the required fields (Figure A- 42) by clicking on the ‘GO’ button, the page (Figure A- 43) appears on the screen. Now the user can enter the experimental data for the fuel cell polarisation curve.

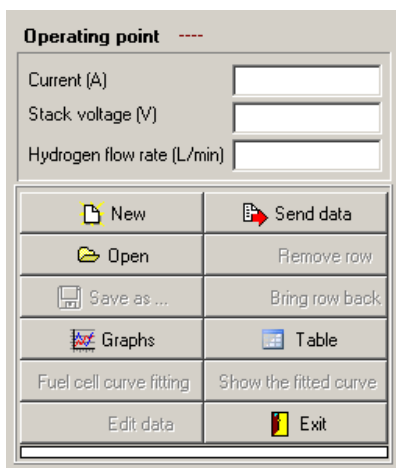

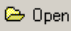
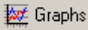
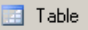


Figure A- 43. Introducing the experimental fuel cell polarisation curve

Current, voltage, and hydrogen consumption rate are to be entered for any operating point to be used. Then by clicking on ‘Send data’ button (Figure A- 43) these data are recorded by the program and a number is given to the introduced operating point. The hydrogen flow rate which is normally used by the program to estimate the fuel cell Faraday efficiency can be left blank if no information is available for it. The default value of 95% Faraday efficiency is used. Voltage and current are to be entered as they are essential data in this part. Using the ‘New’ button () it is possible to clear a set of experimental data, already introduced to the program. The data can be saved by using ‘Save as’ button (if at least one point is given) and can be called later using the ‘Open’ button ().

Using graph () and table () buttons (activated when at least one set of data is provided for an operating point) it is possible to see the given data and the calculated results in the graphical format as well as a table (Figure A- 44 and Figure A- 45). By clicking on ‘Graphs’ button it is possible to see seven different graphs which show the fuel cell performance situation.

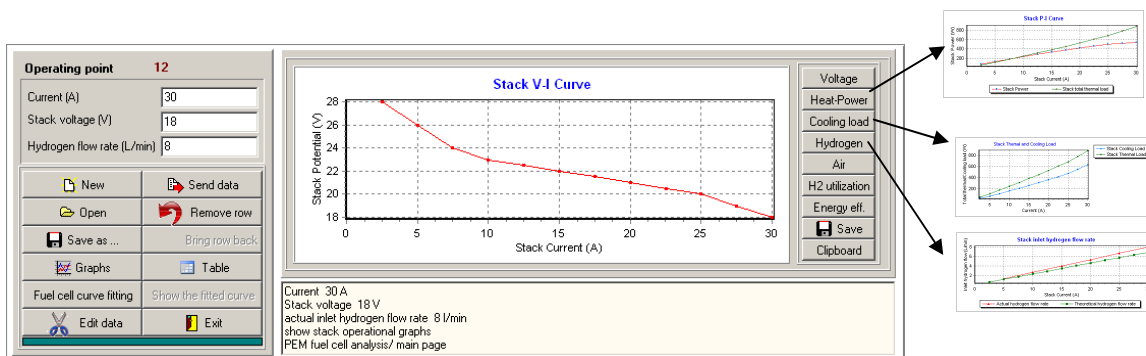


Figure A- 44. Fuel cell graphs

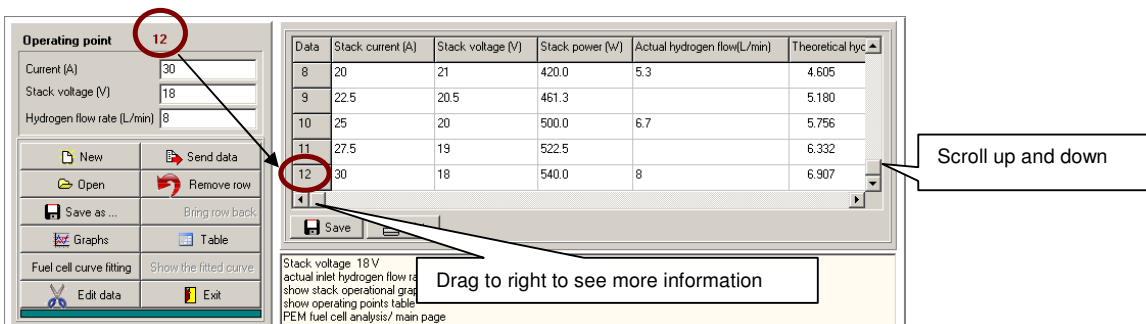


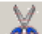


Figure A- 45. Fuel cell operating data provided in the table

The given data can be edited in two different ways:

- Removing the last given point using the 'Remove row' button ( Remove row); If user wants to bring the removed data back, the 'Bring row back' button ( Bring row back) is the right button to be used.
- Editing a particular row in the table of data directly. For this purpose the 'Edit data' button ( Edit data) is used. By clicking on this button the panel shown by Figure A- 46 is opened. The instruction on how to edit the already-provided data is given in this figure. Once the data are edited the tables and graphs are changed accordingly.

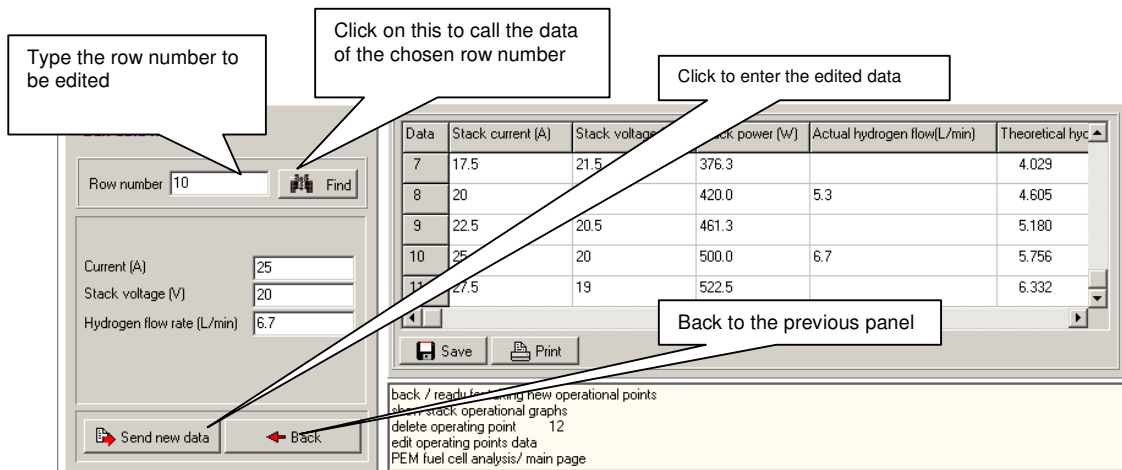


Figure A- 46. Editing the given data

Now by clicking on the 'Fuel cell curve fitting' button (Figure A- 47) the best curve is fitted on the given experimental polarisation curve using the Butler-Volmer equations and the suggested key parameters of these equations appear on the right hand side of the panel (Figure A- 47).

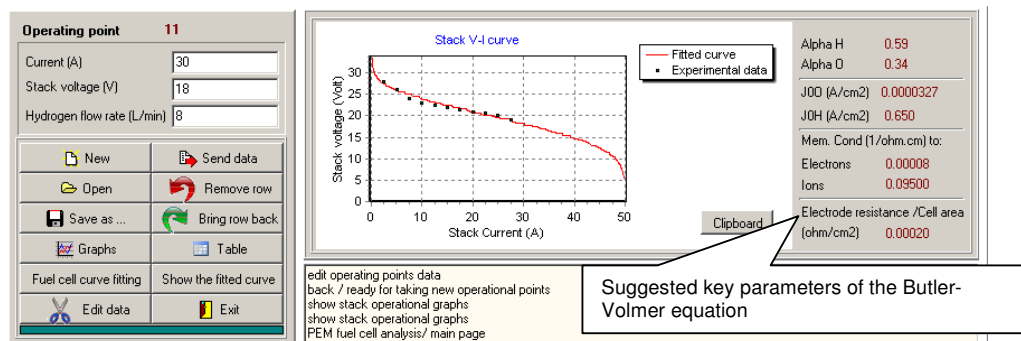


Figure A- 47. Curve fitting on the fuel cell experimental polarisation curve based on Butler-Volmer equations and using the least squares method

Fuel cell identification using Butler-Volmer equations directly

This option is used when the key parameters of the Butler-Volmer equations are known. By choosing this option and clicking on the 'Go' button the simulation goes to the next stage asking for these parameters (Figure A- 48). Once these parameters are entered the user can click on the 'Analyse' button to start analysis and finding the polarisation curve and the other performance curves of the fuel cell.

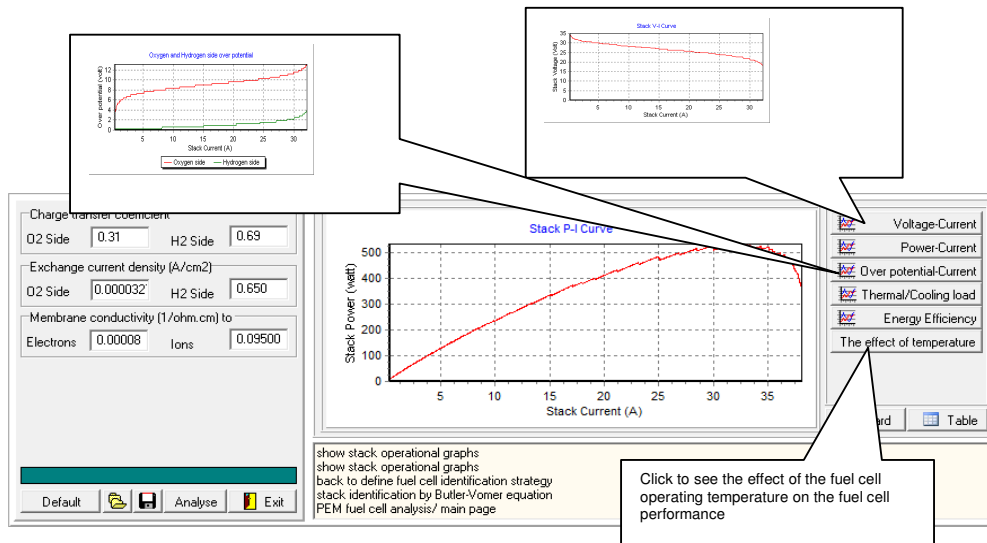


Figure A- 48. Fuel cell performance curve identification by direct use of the Butler-Volmer equations

Solar-hydrogen system analysis

When the PV module, the electrolyser, and the fuel cell are analysed by the program, they all receive green lights of recognition (Figure A- 49) and the 'Solar-hydrogen' button is ready to be used.

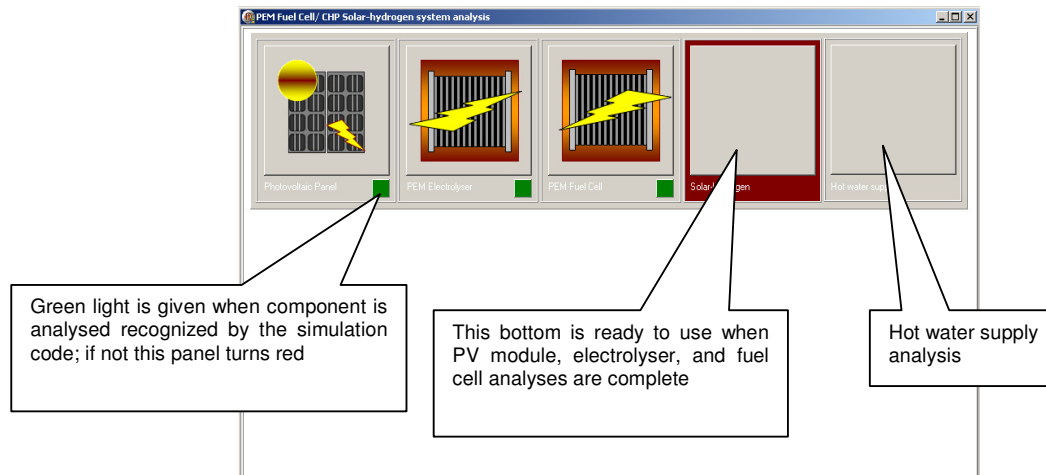


Figure A- 49. Solar-hydrogen system analysis

By clicking on ‘Solar-hydrogen’ analysis button the panel shown in Figure A- 50 appears.

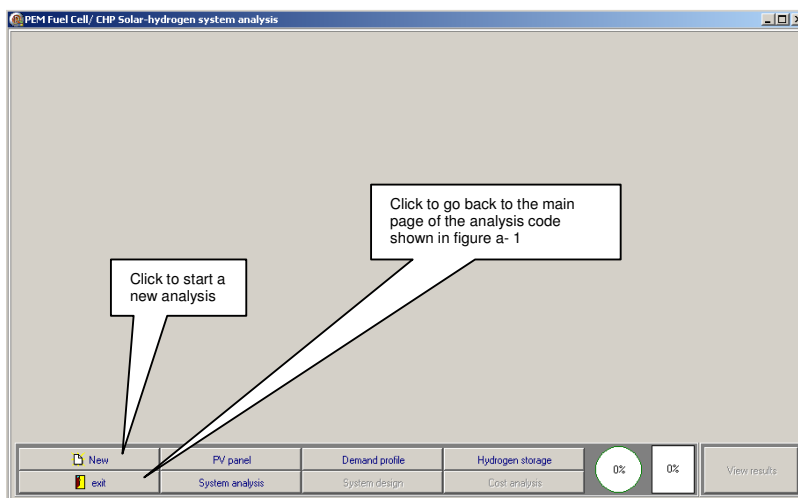


Figure A- 50. The main panel of solar-hydrogen system analysis

Following is the guide to start the solar-hydrogen system analysis:

- **PV:** The PV module is already analysed in the previous stage and based on this analysis the performance of a single module is recognised by the program. Here the user suggests a trial number of PV modules (Figure A- 51). The iteration process to size the system is started using this trial value.

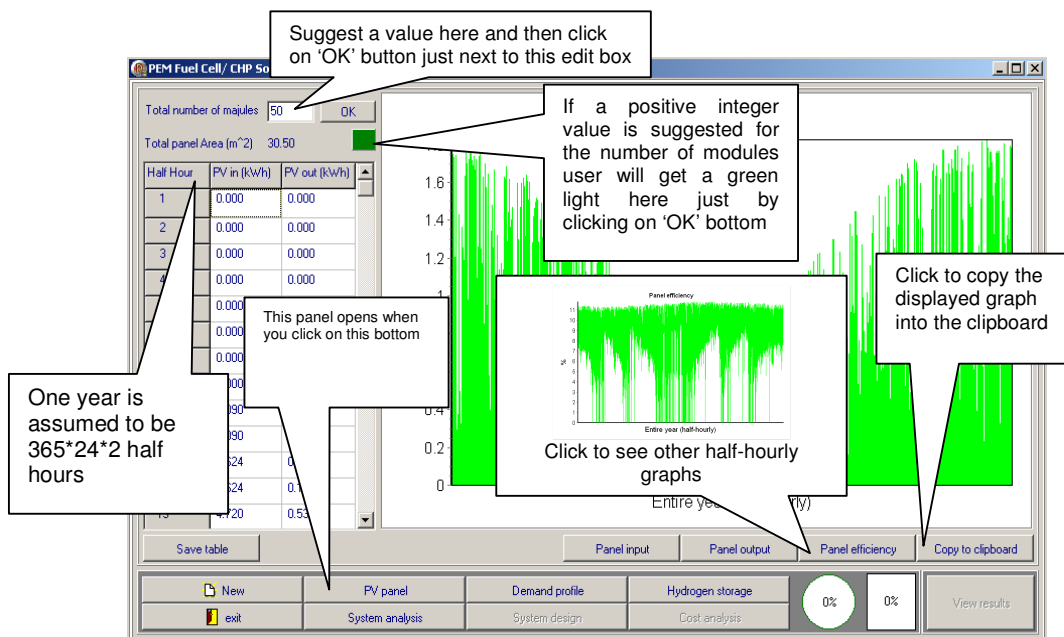


Figure A- 51. Initial suggestion for PV panel size for doing solar-hydrogen system analysis

- **Demand profile:** The electrical demand profile can be taken in three different formats:

1. Half-hourly profile on identical daily basis: The program receives the demand profile for a typical day and uses the same profile for the other days of the year.
2. Half-hourly on yearly basis: it is a single column of data including 17520 rows to cover the whole year and the daily profiles are not identical anymore.
3. Hourly profile on yearly basis: it is a single column of data, including 8760 rows to cover the whole year.

Figure A- 52 shows the panel in which the input data of the demand profile is uploaded (half-hourly basis data). The demand profile has to be prepared in a text format starting from midnight (Jan 1 if it is on yearly basis) and adding the half-hourly demand data line by line. Then using the ‘*Call a demand profile*’ button this text file is uploaded to the program. By calling this file, a graph to show an overview of the demand profile appears on the screen.

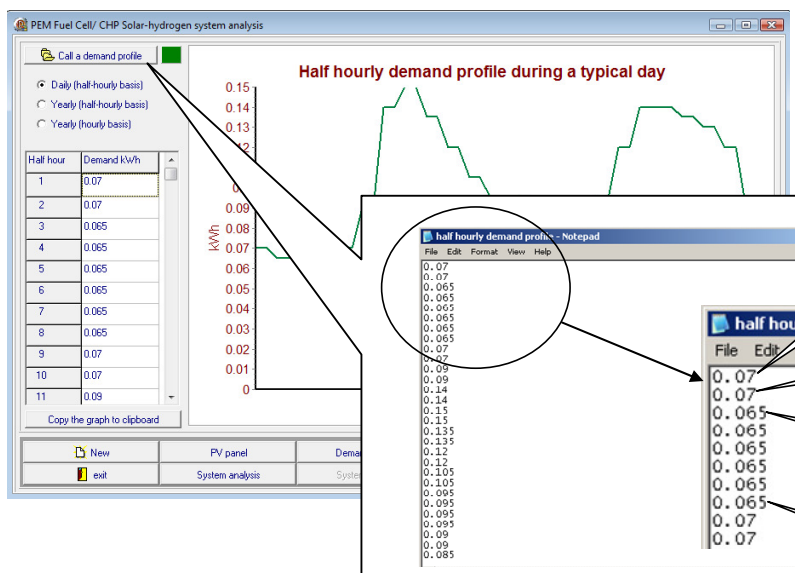


Figure A- 52. Calling the demand profile file

- **Hydrogen storage tank:** here is where the user can define the system sizing strategy (constrained /unconstrained). Also an initial trial value for the hydrogen mass in the storage at the beginning of the year (Jan. 1) has to be suggested to start the analysis. Later when the system is sized this initial hydrogen mass is corrected. If constrained tank is chosen for performing the analysis, the maximum allowable hydrogen mass inside the tank is asked to be entered. In case of doing constrained tank analysis, if the

given initial hydrogen mass does not match the maximum allowable hydrogen mass, the program fixes the problem automatically by choosing a proper value for the initial hydrogen mass. Figure A- 53 shows the page where the required information, in relation to the hydrogen storage tank, is asked to be filled.

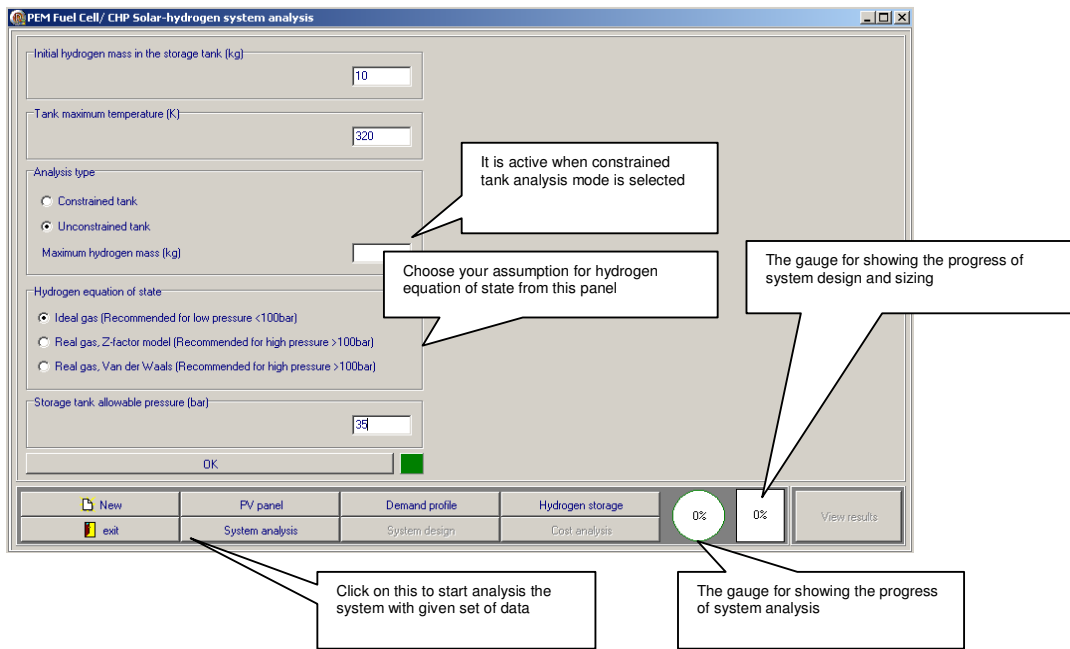


Figure A- 53. Hydrogen storage tank definition for solar-hydrogen system analysis

When the required data for the PV panel, the demand profile, and the hydrogen storage are provided to the simulation code, the analysis can be started by clicking on ‘*System analysis*’ button (Figure A- 53). The system then will be analysed using the given set of data including the trial number of PV modules and the initial hydrogen content of the storage tank. This set is not necessarily a technically-accepted set for the solar-hydrogen system from the design point of view as the system is not properly sized yet. It is just analysed with a given set of trial sizes for PV, hydrogen storage, electrolyser, and fuel cell. After performing this initial analysis on the system another button named ‘*System design*’ (next to the ‘*system analysis*’ button) gets enabled. By clicking on this button the program starts the systematic changing of the variables (see section 3.7 for more details), to size the system. To minimise the time which is taken by the program to size the system it is better to revise the initial given data by looking at the storage tank yearly hydrogen variation obtained from the system analysis and repeating the system analysis before clicking on the ‘*System design*’ button. This can be done by changing the size of the PV array (changing the number of modules) and/or the initial hydrogen mass in the tank to minimise ‘A’ and/or

‘B’, shown in Figure A- 54. Going through this step is not necessary; however, it is recommended to reduce the time to complete sizing the system.

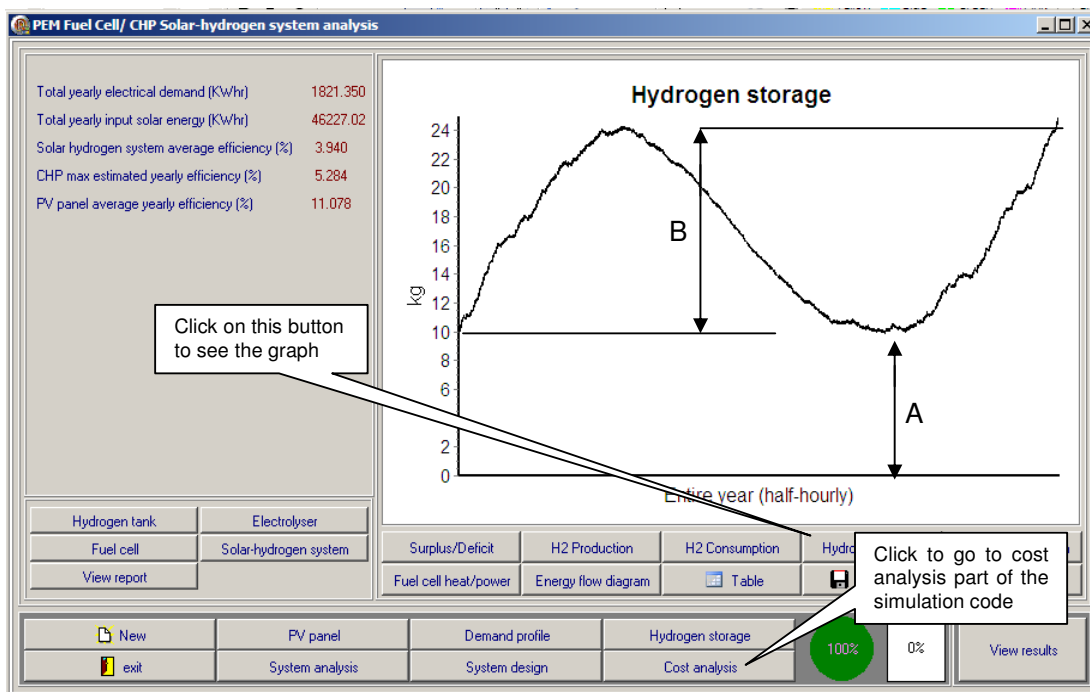


Figure A- 54. The system is sized when ‘A’ and ‘B’ are equal to zero

When the system analysis/design is complete the ‘View results’ button, located on the left bottom of the panel (Figure A- 54), becomes activated and the results are shown on the screen. The results include graphs and tables showing the size of the solar-hydrogen (components) and the performance of the system and the individual components. The graphs, tables, and diagram shown in the results section represent the performance of the system and include:

- Yearly power surplus/deficit diagram, on half-hourly or hourly basis (Figure A- 55).

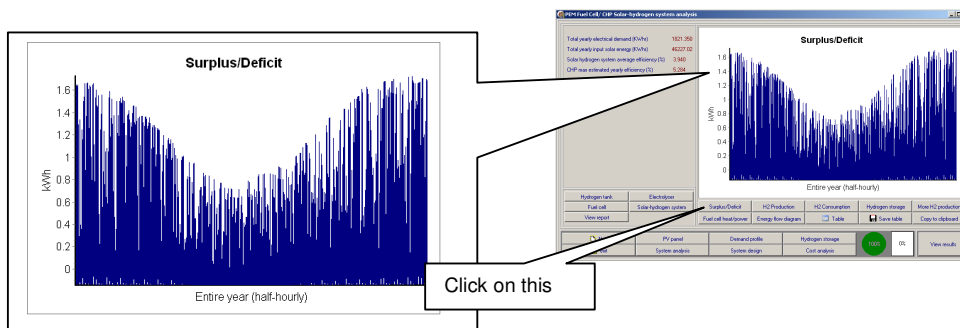


Figure A- 55. The power surplus/deficit graph for the entire year

- Hydrogen production rate on half-hourly or hourly basis (Figure A- 56).

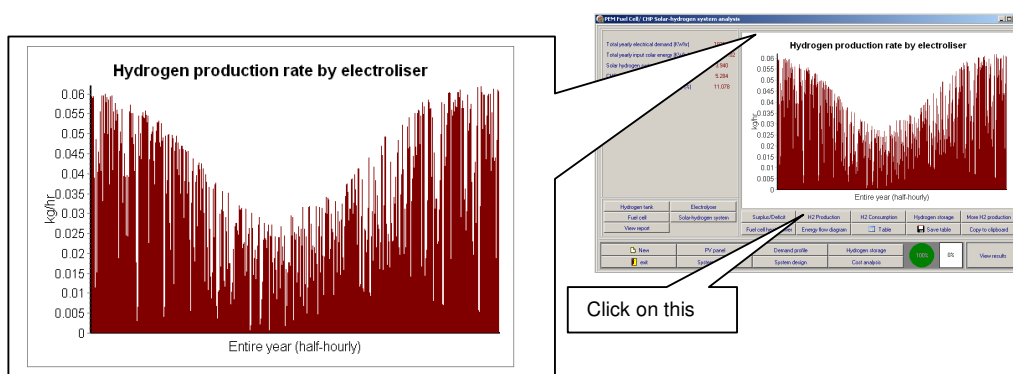


Figure A- 56. The graph showing the hydrogen production rate on hourly or half-hourly basis

- Hydrogen consumption (Figure A- 57)

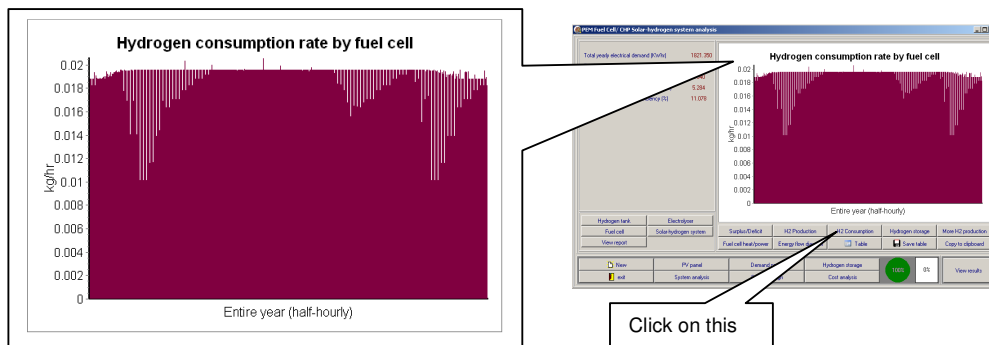


Figure A- 57. Hydrogen consumption

- Hydrogen storage (Figure A- 54).
- Potential hydrogen production shown by pressing the ‘More H2 production’ button. This is the capacity of the electrolyser which is not utilised when the hydrogen tank is constrained; in such a condition part of the PV surplus may not be directed to the electrolyser for hydrogen production purposes, since there is no more room in the hydrogen tank to accommodate this hydrogen. This graph shows the extra capacity of the electrolyser hydrogen production if this surplus power is also utilised by this component. If the unconstrained tank analysis mode is selected, this graph shows noting since the electrolyser capacity is fully used already and the entire surplus power is utilised by the electrolyser for hydrogen production (Figure A- 58).

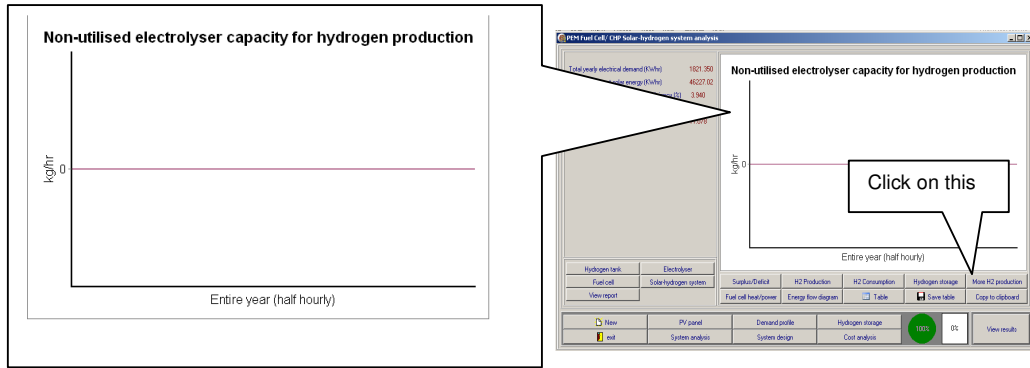


Figure A- 58. Extra capacity of the electrolyser in hydrogen production (in this graph this extra capacity is zero as it is for a system with an unconstrained tank)

- The fuel cell heat and power generation status (Figure A- 59)

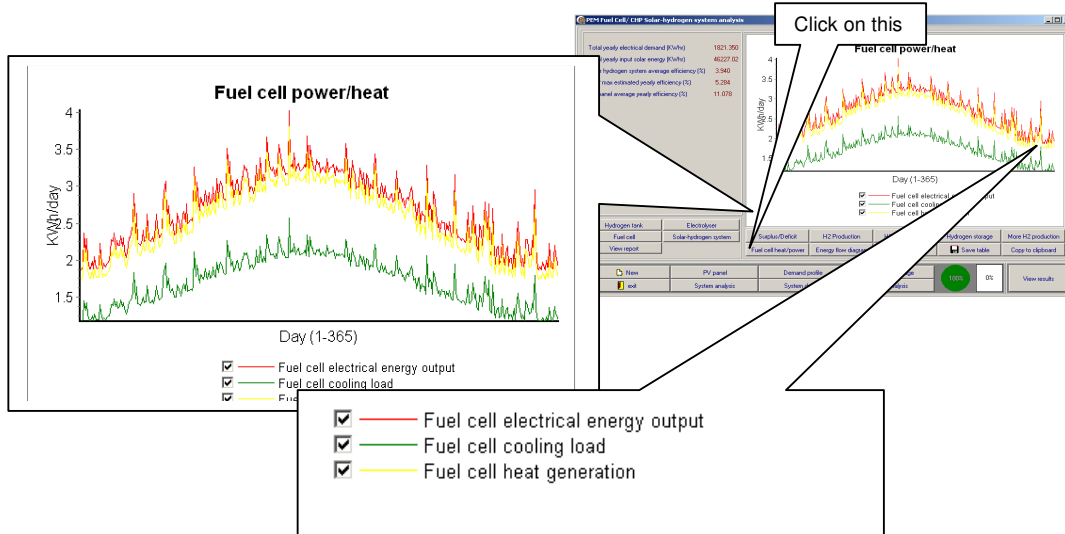


Figure A- 59. The fuel cell yearly heat and power generation profile (on daily basis)

- Energy flow diagram (Figure A- 60). This is a kind of Sankey diagram and shows how the solar energy flows through solar-hydrogen system to meet the demand.

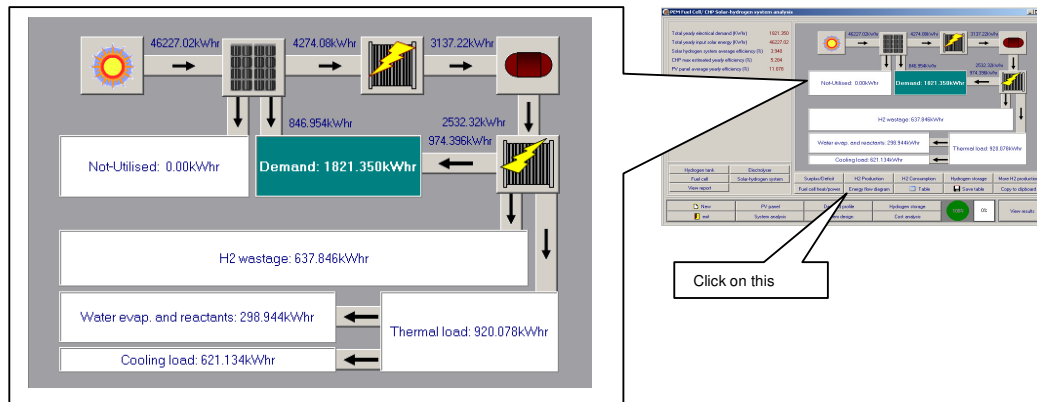


Figure A- 60. Energy flow diagram of solar-hydrogen system

- Table of half-hourly results (Figure A- 61)

Time Interval	Sur./Def. (KWhr)	H2 Prod. (kg/hr)
1	-0.070000	0
2	-0.070000	0
3	-0.065000	0
4	-0.065000	0
5	-0.065000	0
6	-0.065000	0
7	-0.065000	0
8	-0.065000	0
9	-0.063007	0
10		
11		
12	0.082654	0.003364
13	0.394230	0.015072
14	0.391138	0.014937

Figure A- 61. Table of half-hourly results

As shown in Figure A- 63 the performance data of the components (yearly basis) are provided in four groups: hydrogen tank, electrolyser, fuel cell, and solar-hydrogen system. After doing the system design analysis the suggested size of the PV panel can be seen by clicking on the ‘PV panel’ button (Figure A- 61).

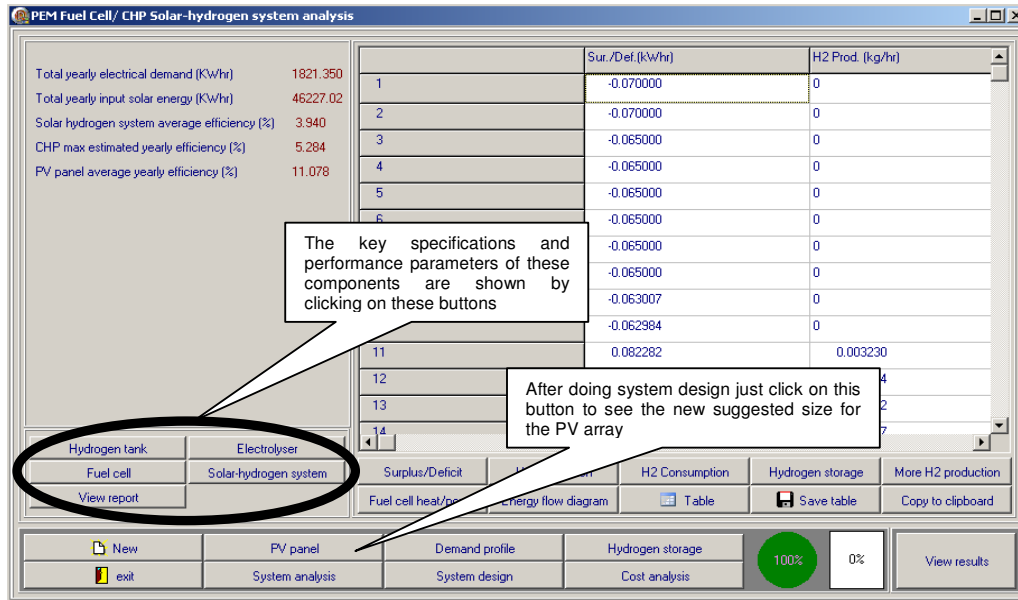


Figure A- 62. The yearly performance of the solar-hydrogen system and its components

- Hydrogen tank:

By clicking on 'Hydrogen tank' button the key performance characteristics of the hydrogen storage tank are provided (Figure A- 63).

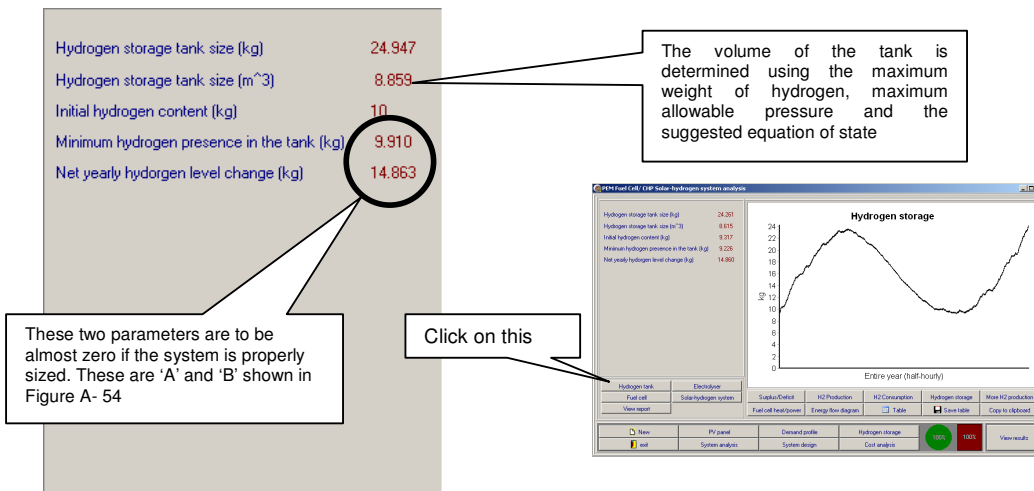


Figure A- 63. Hydrogen tank yearly performance results

- Electrolyser:

By clicking on the electrolyser button (Figure A- 64) the size and the performance details of the electrolyser appear in the panel shown by Figure A- 64.

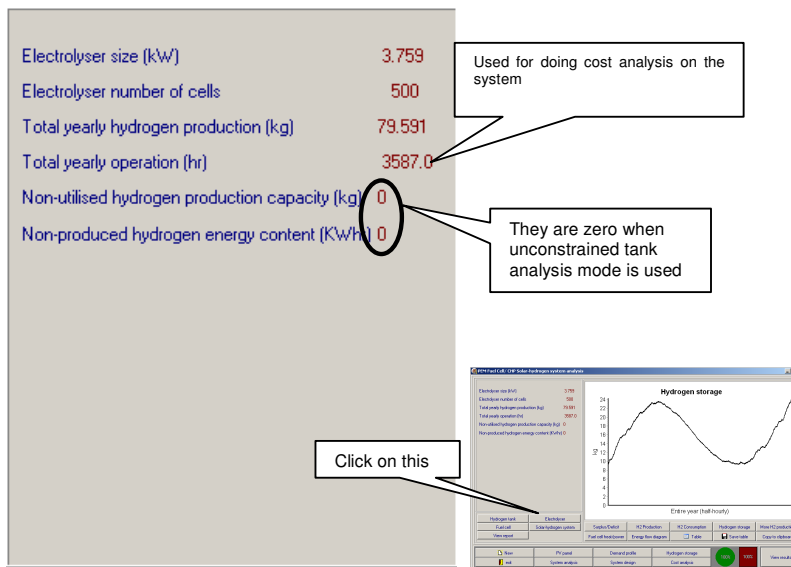


Figure A- 64. Yearly performance results for the electrolyser

- Fuel cell:

This program has got a special emphasis on the fuel cell operation and its heat generation; that is why more comprehensive data is provided in this part of the results section (Figure A- 65).

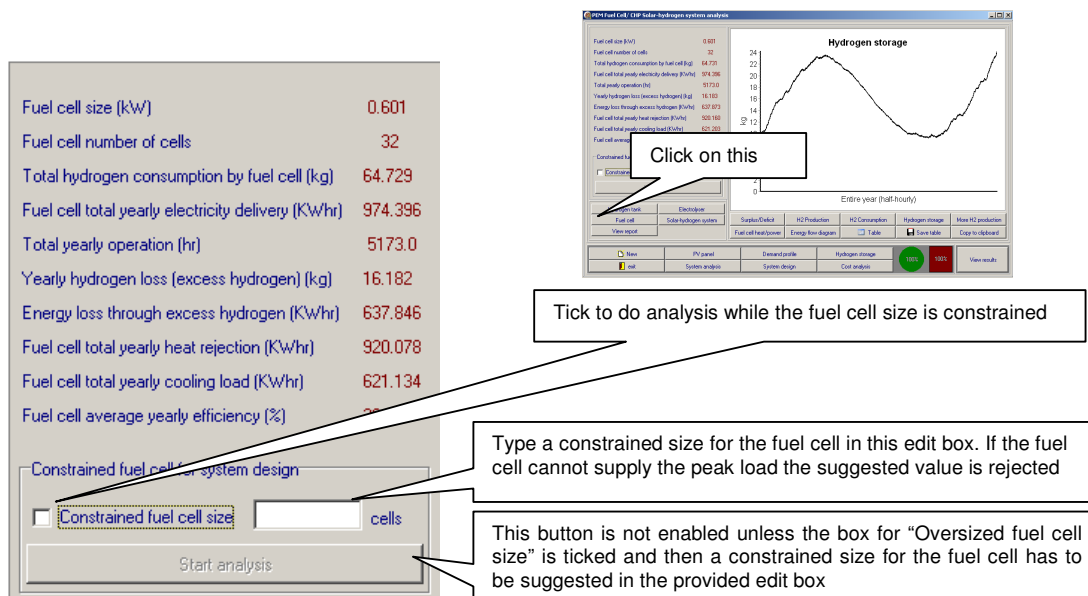


Figure A- 65. Fuel cell performance parameters

A check box named: 'Constrained fuel cell size' is provided in the fuel cell results panel which gives the user the possibility of sizing the system while the fuel cell is

constrained to be oversized (larger than its minimum requirement determined by the peak of the demand profile).

- Solar-hydrogen system (Figure A- 66):

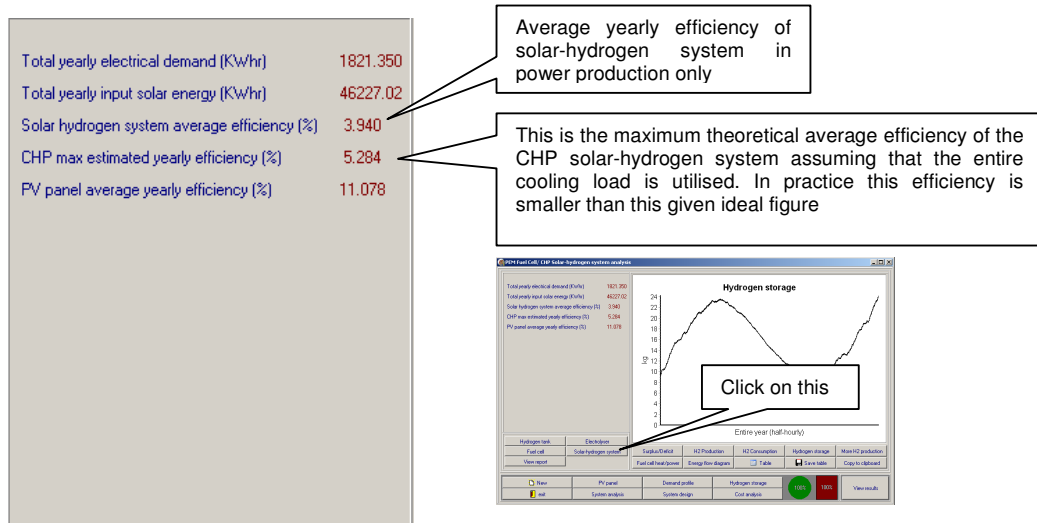


Figure A- 66. Solar-hydrogen system performance results

Cost analysis

The cost analysis can be performed when the solar-hydrogen system analysis is completed. The 'Cost Analysis' button shown in Figure A- 54 is to be clicked and then the page shown in Figure A- 67 is opened.

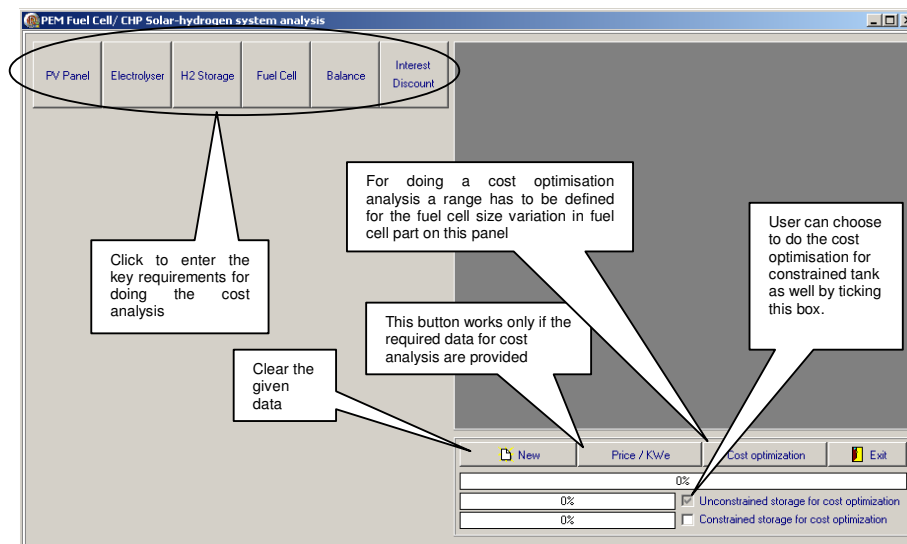


Figure A- 67. The cost analysis panel

The user has to enter the following required data to start the cost analysis:

- Financial assumptions:
 - By clicking on ‘*Interest Discount*’ button (Figure A- 68) the following information are asked to be provided:
 1. Nominal interest rate
 2. Inflation rate
 3. Assessment period
 4. The cost information of a competing technology

Figure A- 68. The panel for entering the key parameters to do economic analysis on the solar-hydrogen system

- PV panel:
 - By clicking on ‘*PV panel*’ button (Figure A- 68) the panel shown in Figure A- 69 is opened. The ‘*time-value*’ button for showing the graph of present value variation of the component is not active unless the fields in the ‘*Interest Discount*’ section are filled.

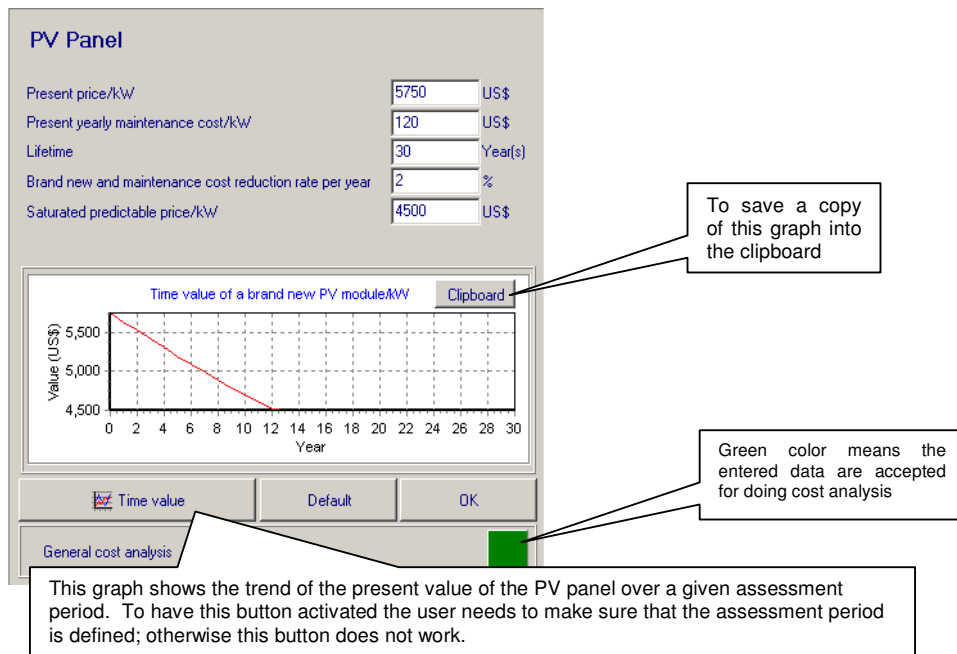


Figure A- 69. The page for entering the cost data of the PV array

- Electrolyser:

Similar set of cost data to those used for the PV module, have to be provided for the electrolyser as well (Figure A- 70).

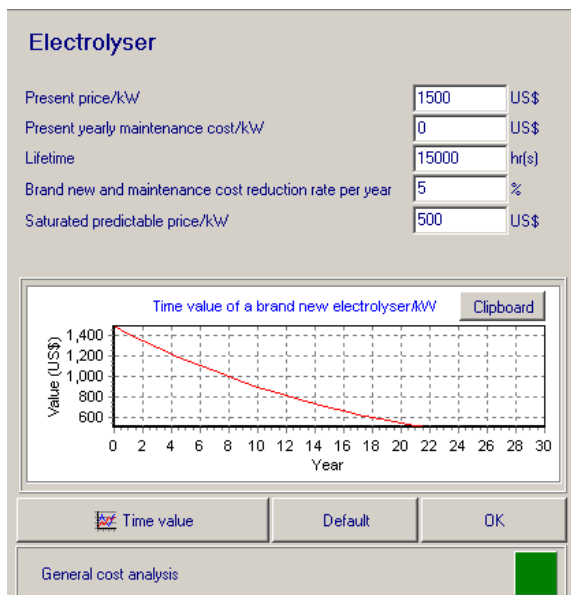


Figure A- 70. The panel for entering the cost data of the electrolyser

- H₂ Storage (Figure A- 71):

It is very similar to the PV panel and the electrolyser. Two extra fields are provided to take the range of variation for the size of the hydrogen tank. These fields are required to be filled for performing system optimisation.

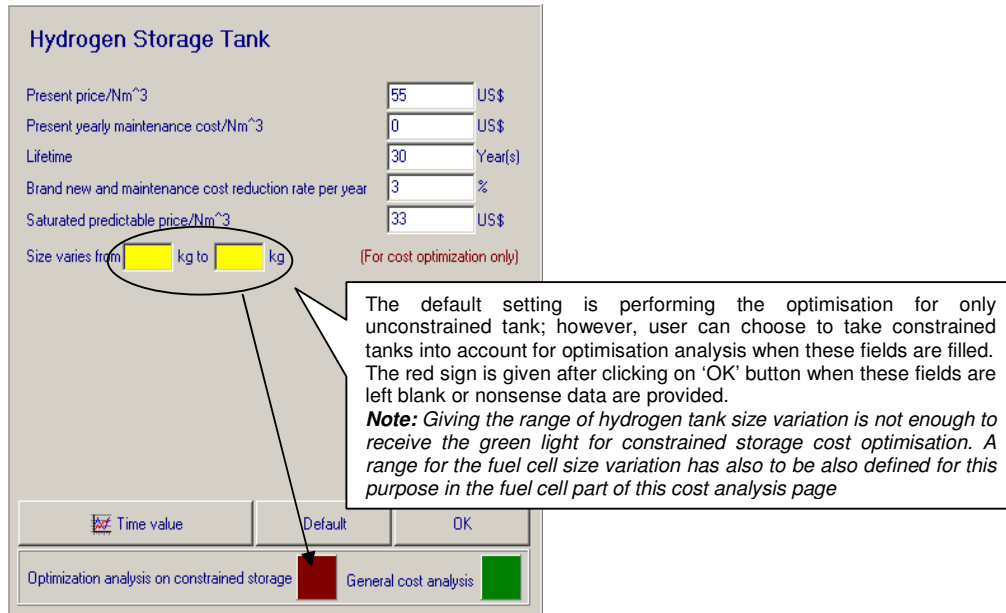


Figure A- 71. The panel for entering the cost data of the hydrogen storage tank

- Fuel cell (Figure A- 72):

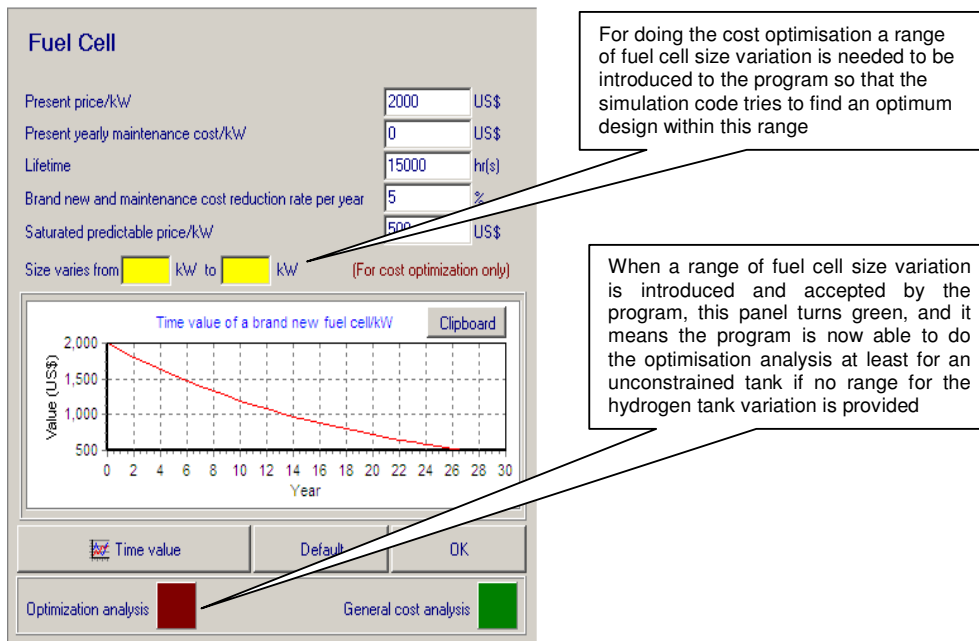


Figure A- 72. The panel for entering the cost data of the fuel cell

- Balance (Figure A- 73):

This is the cost of accessories like piping, compressor, water pump, heat exchanger, dehumidification and humidification, controlling devices, and etc, plus the installation cost.

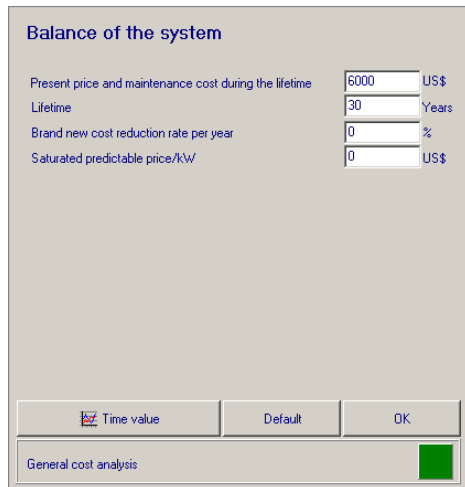


Figure A- 73. The balance cost of the system

After entering the required input data, the simulation code is ready to run the cost analysis. The unit cost of the electricity produced is a key economic index that can be seen by clicking on 'Price/KW_e' button shown in Figure A- 74.

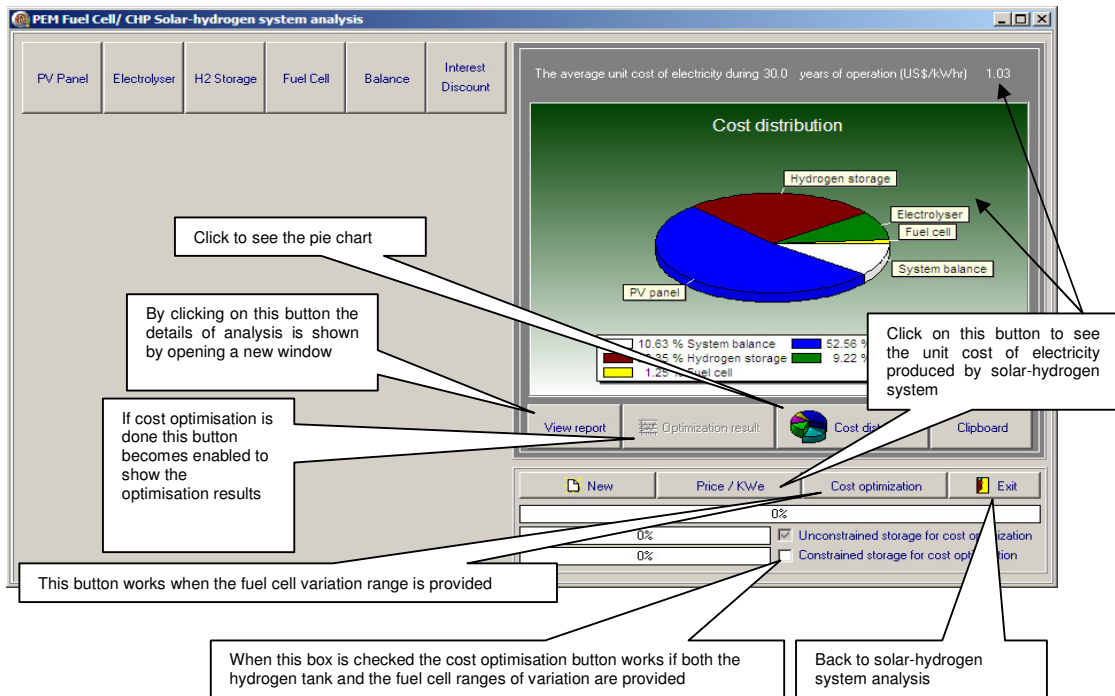


Figure A- 74. The unit cost of the electricity generated by the solar-hydrogen system

Hot water supply analysis

After finishing the solar-hydrogen system analysis, the ‘Hot water supply’ analysis mode becomes accessible (Figure A- 1). This part gives the user the possibility of investigating the potential of the fuel cell heat recovery and utilising this heat for hot water supply. By clicking on ‘Hot water supply’ button the panel shown in Figure A- 75, appears. The user can enter the daily hot water demand and the desirable temperature to analyse the hot water system. The average temperatures of the tap cold water for each month are the other key inputs into the program. Also some heat losses (e.g. piping and heat exchanger) are to be considered.

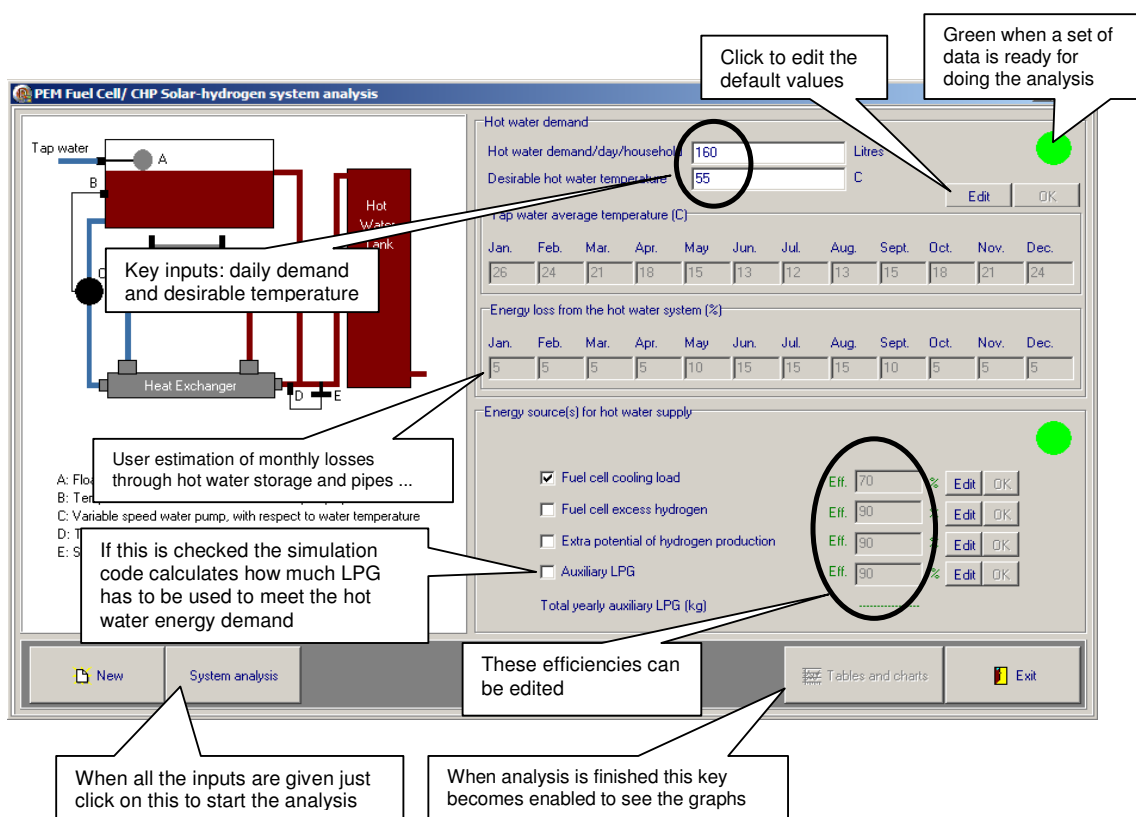


Figure A- 75. Hot water supply analysis mode

As shown in Figure A- 75 the energy sources for supplying the daily hot water demand are ticked by the user (e.g. fuel cell heat, LPG gas, etc) as another key input to perform the analysis in this section. After completion of the analysis, the user can see the results in the form of graphs and a table by clicking on the ‘Tables and charts’ button shown in Figure A- 76 where an example of this form of output is provided.

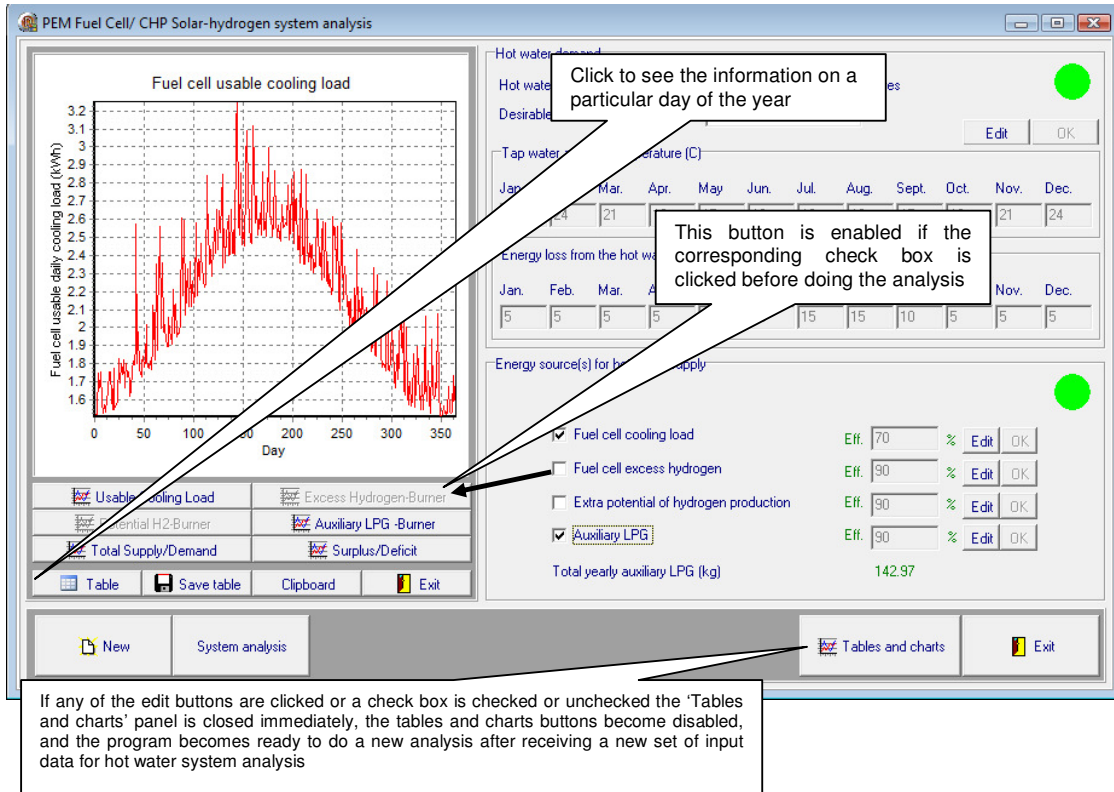


Figure A- 76. The results of the hot water supply analysis

Appendix 2: Experimental measurements, 500 W BCS PEM fuel cell

5 A/130 W operating point/ Power measurement

- Operating temperature 40 °C, exit air 30 kPa, air stoichiometry 2, inlet hydrogen ~20-30 kPa
- Theoretical hydrogen consumption if fuel cell hydrogen utilisation coefficient is 100% ideally: 1.223 slpm
- Assumed hydrogen consumption rate for the theoretical calculations: 1.468 slpm (based on 20% extra hydrogen fed into the fuel cell)
- Expected power (manufacturer manual): 130 W
- Maximum uncertainty associated with the measurement instrument for voltage readings when the error for current adjustment (5A) is taken into account: 0.6%
- Maximum uncertainty associated with hydrogen flow meter: 1%
- Energy efficiency assumed for the theoretical calculation: 45.7%
- Hydrogen utilisation coefficient assumed in the theoretical calculations: ~85%

Voltage (V)	% of uncertainty for the voltage measurement	Power output (W)	Hydrogen consumption (slpm)	% of uncertainty for the hydrogen consumption measurement	Hydrogen utilisation coefficient (%)	Electrical energy efficiency (%)
21.32	±0.30	106.6	1.37	±0.51	89.27	40.18
21.2	±0.30	106	1.33	±0.53	91.95	41.16
21.33	±0.30	106.65	1.39	±0.50	87.98	39.62
21.11	±0.30	105.55	1.38	±0.51	88.62	39.50
21.43	±0.30	107.15	1.35	±0.52	90.59	41
21	±0.30	105	1.37	±0.51	89.27	39.58
20.93	±0.30	104.65	1.374	±0.51	89.01	39.33
21.12	±0.30	105.6	1.388	±0.50	88.11	39.29
21.48	±0.29	107.4	1.34	±0.52	91.26	41.39

Table A- 1. 500 W BSC PEM fuel cell power and hydrogen consumption measurement at 5 A; Operating temperature ~40 °C, exit air 30 kPa, air stoichiometry 2, inlet hydrogen ~20-30 kPa

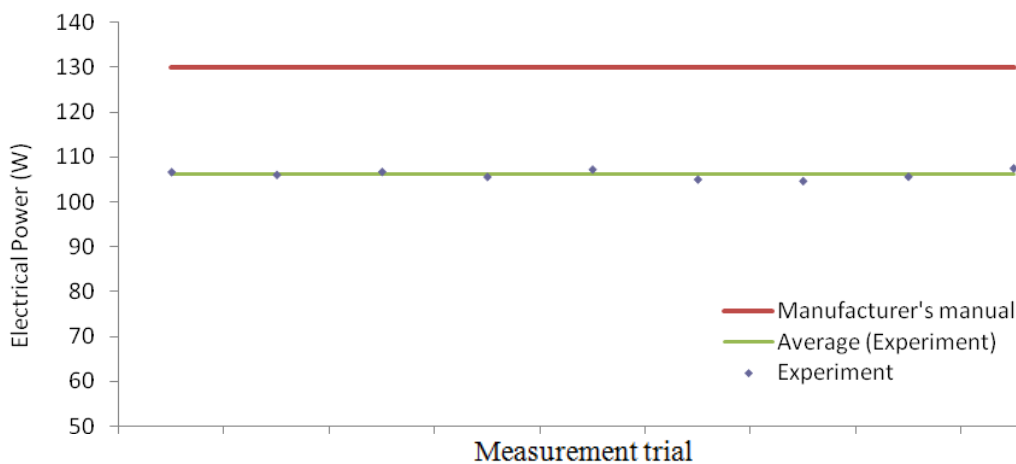


Figure A- 77. 500 W BSC PEM fuel cell power measurements at 5 A; Operating temperature ~40 °C, exit air 30 kPa, air stoichiometry 2, inlet hydrogen ~20-30 kPa

5 A/130 W operating point/ Cooling load measurement

- Operating temperature 40 °C, exit air 30 kPa, air stoichiometry 2, inlet hydrogen ~20-30 kPa
- Theoretically estimated cooling load at the ideal operating condition recommended by the manufacturer: 65.8 W

Note:

- The estimated cooling load at the experimental operating condition (the following table) is found by considering: fuel cell heat used for water evaporation, heat removal by the extra reactants, the convection heat transfer from the body of the fuel cell, and the power drop compared to the ideal condition

Fuel cell inlet water temperature (°C)	Fuel cell exit water temperature (°C)	Water flow rate (litre/min)	Measured cooling load (W)	Estimated cooling load (W)	Experimental error (%)	Estimated uncertainty (%)	CHP energy efficiency (%)
39.8	41.5	0.96	113.7	111.7	1.76	±13.98	83.05
39.3	41.2	0.915	121.12	112.3	7.28	±12.47	88.19
39	40.9	0.918	121.51	111.65	8.12	±12.43	84.78
38.5	40.3	0.924	115.87	112.75	2.69	±13.05	82.87
38.5	40.4	0.914	120.98	111.15	8.13	±12.37	87.28
38.6	40.5	0.926	122.57	113.3	7.56	±12.38	85.79
38.9	40.7	0.927	116.25	113.65	2.23	±13.10	83.03
39	40.9	0.953	126.15	112.7	6.74	±12.43	84.26
38.8	40.6	0.916	114.87	110.9	3.45	±13.09	85.67

Table A- 2. 500 W BSC PEM fuel cell cooling load measurements at 5 A; Operating temperature ~40 °C, exit air 30 kPa, air stoichiometry 2, inlet hydrogen ~20-30 kPa

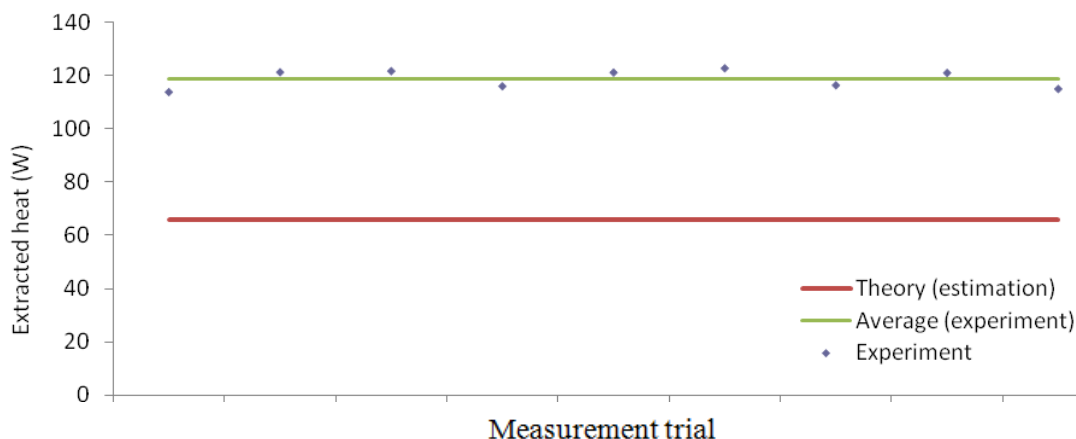


Figure A- 78. 500 W BSC PEM fuel cell cooling load measurements at 5 A; Operating temperature ~40 °C, exit air 30 kPa, air stoichiometry 2, inlet hydrogen ~20-30 kPa

5 A/130 W operating point/ Power measurement

- Operating temperature 40 °C, exit air 30 kPa, air stoichiometry 4, inlet hydrogen ~20-30 kPa
- Theoretical hydrogen consumption if fuel cell hydrogen utilisation coefficient is 100% ideally: 1.223 slpm
- Assumed hydrogen consumption rate for the theoretical calculations: 1.468 slpm (based on 20% extra hydrogen fed into the fuel cell)
- Expected power (manufacturer manual): 130 W
- Maximum uncertainty associated with the measurement instrument for voltage readings when the error for current adjustment (5A) is taken into account: 0.6%
- Maximum uncertainty associated with hydrogen flow meter: 1%
- Energy efficiency assumed for the theoretical calculation:45.7%
- Hydrogen utilisation coefficient assumed in the theoretical calculations: ~85%

Voltage (V)	% of uncertainty for the voltage measurement	Power output (W)	Hydrogen consumption (slpm)	% of uncertainty for the hydrogen consumption measurement	Hydrogen utilisation coefficient (%)	Electrical energy efficiency (%)
22.68	±0.30	113.4	1.32	±0.32	92.65	44.36
23.05	±0.29	115.25	1.33	±0.32	91.95	44.75
23.13	±0.29	115.65	1.35	±0.31	90.59	44.24
23.22	±0.29	116.1	1.32	±0.32	92.65	45.42
23.11	±0.29	115.55	1.354	±0.31	90.32	44.07
22.98	±0.29	114.9	1.335	±0.31	91.61	44.45
23.16	±0.29	115.8	1.32	±0.32	92.65	45.30
23.28	±0.29	116.4	1.336	±0.31	91.54	44.99
22.74	±0.30	113.7	1.33	±0.32	91.95	44.15

Table A- 3. 500 W BSC PEM fuel cell power and hydrogen consumption measurement at 5 A; Operating temperature ~40 °C, exit air 30 kPa, air stoichiometry 4, inlet hydrogen ~20-30 kPa

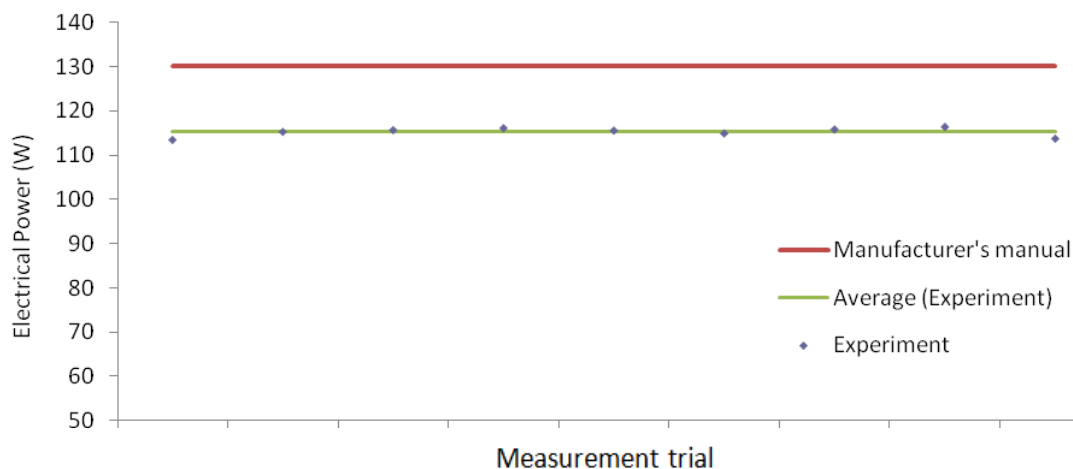


Figure A- 79. 500 W BSC PEM fuel cell power measurements at 5 A; Operating temperature ~40 °C, exit air 30 kPa, air stoichiometry 4, inlet hydrogen ~20-30 kPa

5 A/130 W operating point/ Cooling load measurement

- Operating temperature 40 °C, exit air 30 kPa, air stoichiometry 4, inlet hydrogen ~20-30 kPa
- Theoretically estimated cooling load at the ideal operating condition recommended by the manufacturer: 65.8 W

Note:

- The estimated cooling load at the experimental operating condition (the following table) is found by considering: fuel cell heat used for water evaporation, heat removal by the extra reactants, the convection heat transfer from the body of the fuel cell, and the power drop compared to the ideal condition

Fuel cell inlet water temperature (°C)	Fuel cell exit water temperature (°C)	Water flow rate (litre/min)	Measured cooling load (W)	Estimated cooling load (W)	Experimental error (%)	Estimated uncertainty (%)	CHP energy efficiency (%)
40.8	42.5	0.874	103.51	100.5	2.91	±14.12	84.87
40.4	42.3	0.801	106.02	98.65	6.96	±12.61	85.93
40	41.8	0.821	102.95	98.25	4.57	±13.24	83.63
39.9	41.7	0.813	101.95	97.8	4.07	±13.23	85.32
39.8	41.5	0.824	97.58	98.35	-0.78	±13.98	81.30
39.6	41.3	0.874	103.51	99	4.36	±13.96	84.50
39.5	41.2	0.846	100.19	98.1	2.09	±13.94	84.51
39.4	41.1	0.857	101.49	97.5	3.94	±13.93	84.23
39.5	41.2	0.839	99.36	100.2	-0.84	±13.94	82.74

Table A- 4. 500 W BSC PEM fuel cell cooling load measurements at 5 A; Operating temperature ~40 °C, exit air 30 kPa, air stoichiometry 4, inlet hydrogen ~20-30 kPa

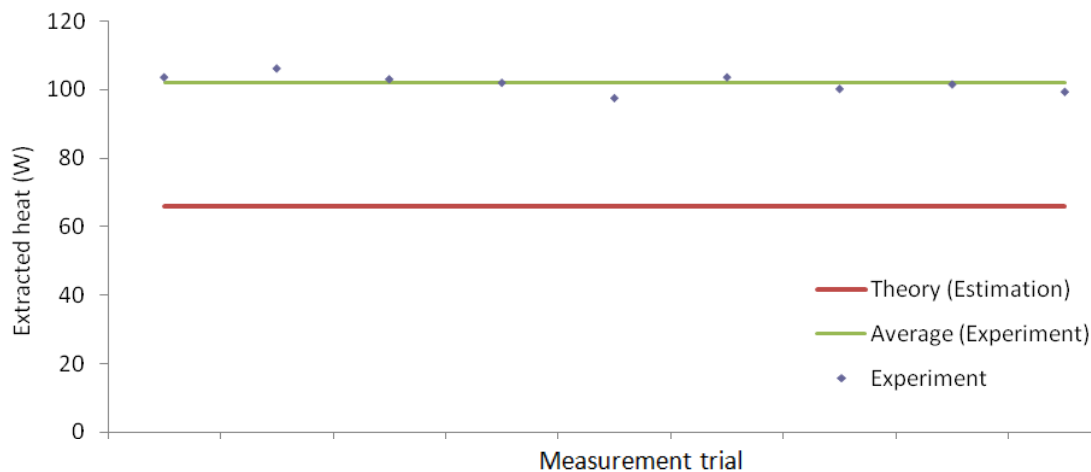


Figure A- 80. 500 W BSC PEM fuel cell cooling load measurement at 5 A; Operating temperature ~40 °C, exit air 30 kPa, air stoichiometry 4, inlet hydrogen ~20-30 kPa

5 A/130 W operating point/ Power measurement

- Operating temperature 50 °C, exit air 30 kPa, air stoichiometry 2, inlet hydrogen ~20-30 kPa
- Theoretical hydrogen consumption if fuel cell hydrogen utilisation coefficient is 100% ideally: 1.223 slpm
- Assumed hydrogen consumption rate for the theoretical calculations: 1.468 slpm (based on 20% extra hydrogen fed into the fuel cell)
- Expected power (manufacturer manual): 130 W
- Maximum uncertainty associated with the measurement instrument for voltage readings when the error for current adjustment (5A) is taken into account: 0.6%
- Maximum uncertainty associated with hydrogen flow meter: 1%
- Energy efficiency assumed for the theoretical calculation:45.7%
- Hydrogen utilisation coefficient assumed in the theoretical calculations: ~85%

Voltage (V)	% of uncertainty for the voltage measurement	Power output (W)	Hydrogen consumption (slpm)	% of uncertainty for the hydrogen consumption measurement	Hydrogen utilisation coefficient (%)	Electrical energy efficiency (%)
23.15	±0.24	115.75	1.34	±0.46	91.27	44.61
23.24	±0.23	116.2	1.32	±0.47	92.65	45.46
23.12	±0.24	115.6	1.28	±0.48	95.55	46.64
22.97	±0.24	114.85	1.29	±0.48	94.81	45.98
23.16	±0.24	115.8	1.31	±0.47	93.36	45.65
22.96	±0.24	114.8	1.34	±0.46	91.27	44.25
23.1	±0.24	115.5	1.336	±0.46	91.54	44.65
23.21	±0.23	116.05	1.321	±0.47	92.58	45.37
23.34	±0.23	116.7	1.287	±0.48	95.03	46.83
23.41	±0.23	117.05	1.298	±0.48	94.22	46.57
23.14	±0.24	115.7	1.29	±0.48	94.81	46.32
22.69	±0.24	113.45	1.312	±0.47	93.22	44.66

Table A- 5. 500 W BSC PEM fuel cell power and hydrogen consumption measurement at 5 A; Operating temperature ~50 °C, exit air 30 kPa, air stoichiometry 2, inlet hydrogen ~20-30 kPa

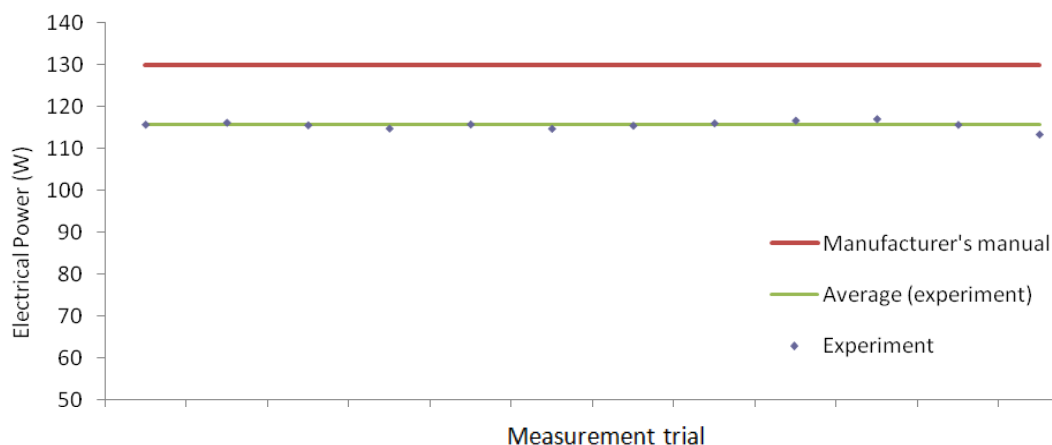


Figure A- 81. 500 W BSC PEM fuel cell power measurements at 5 A; Operating temperature ~50 °C, exit air 30 kPa, air stoichiometry 2, inlet hydrogen ~20-30 kPa

5 A/130 W operating point/ Cooling load measurement

- Operating temperature 50 °C, exit air 30 kPa, air stoichiometry 2, inlet hydrogen ~20-30 kPa
- Theoretically estimated cooling load at the ideal operating condition recommended by the manufacturer: 65.8 W

Note:

- The estimated cooling load at the experimental operating condition (the following table) is found by considering: fuel cell heat used for water evaporation, heat removal by the extra reactants, the convection heat transfer from the body of the fuel cell, and the power drop compared to the ideal condition

Fuel cell inlet water temperature (°C)	Fuel cell exit water temperature (°C)	Water flow rate (litre/min)	Measured cooling load (W)	Estimated cooling load (W)	Experimental error (%)	Estimated uncertainty (%)	CHP energy efficiency (%)
48.9	50.3	0.994	96.95	92.55	4.54	±18.48	83.42
49	50.4	0.986	96.17	92.1	4.23	±18.50	84.86
48.7	50.3	0.98	109.24	92.7	15.14	±16.16	87.27
48.5	50	0.982	102.62	93.45	8.93	±17.20	86.29
48.4	49.9	0.988	103.25	92.5	10.41	±17.18	85.35
48.5	50	0.973	101.68	93.5	8.04	±17.20	83.05
48.7	50.1	0.997	97.24	92.8	4.57	±18.44	83.57
48.8	50.3	0.956	99.90	92.25	7.66	±17.24	84.74
48.5	50	0.993	103.77	91.6	11.73	±17.20	87.24
48.7	50.1	0.99	96.56	91.25	5.50	±18.44	86.64
48.8	50.2	0.983	95.88	92.6	3.42	±18.46	86.63
48.9	50.2	1.159	104.97	94.85	9.64	±19.89	84.29

Table A- 6. 500 W BSC PEM fuel cell cooling load measurements at 5 A; Operating temperature ~50 °C, exit air 30 kPa, air stoichiometry 2, inlet hydrogen ~20-30 kPa

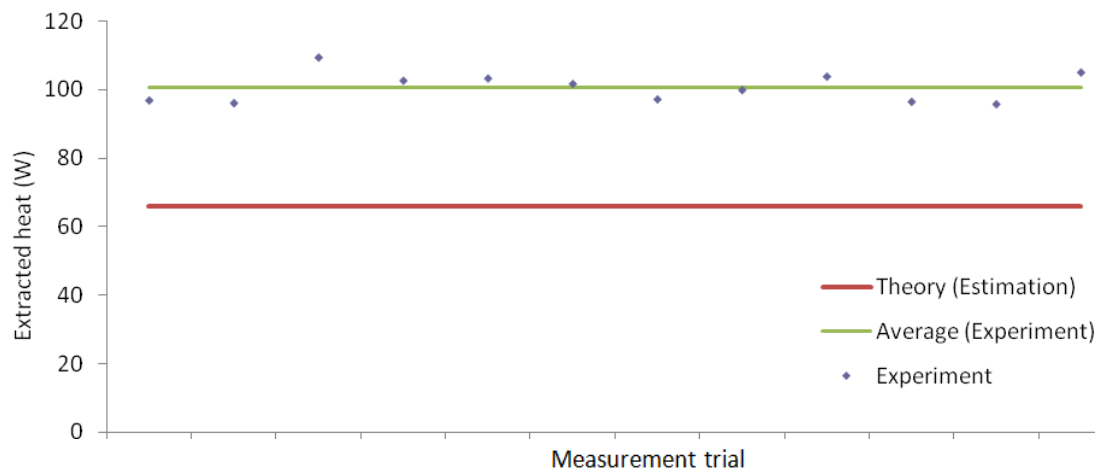


Figure A- 82. 500 W BSC PEM fuel cell cooling load measurements at 5 A; Operating temperature ~50 °C, exit air 30 kPa, air stoichiometry 2, inlet hydrogen ~20-30 kPa

5 A/130 W operating point/ Power measurement

- Operating temperature 50 °C, exit air 30 kPa, air stoichiometry 4, inlet hydrogen ~20-30 kPa
- Theoretical hydrogen consumption if fuel cell hydrogen utilisation coefficient is 100% ideally: 1.223 slpm
- Assumed hydrogen consumption rate for the theoretical calculations: 1.468 slpm (based on 20% extra hydrogen fed into the fuel cell)
- Expected power (manufacturer manual): 130 W
- Maximum uncertainty associated with the measurement instrument for voltage readings when the error for current adjustment (5A) is taken into account: 0.6%
- Maximum uncertainty associated with hydrogen flow meter: 1%
- Energy efficiency assumed for the theoretical calculation:45.7%
- Hydrogen utilisation coefficient assumed in the theoretical calculations: ~85%

Voltage (V)	% of uncertainty for the voltage measurement	Power output (W)	Hydrogen consumption (slpm)	% of uncertainty for the hydrogen consumption measurement	Hydrogen utilisation coefficient (%)	Electrical energy efficiency (%)
24.65	±0.12	123.25	1.33	±0.25	91.95	47.86
24.68	±0.12	123.4	1.31	±0.25	93.36	48.65
24.46	±0.13	122.3	1.325	±0.25	92.30	47.67
24.57	±0.13	122.85	1.336	±0.25	91.54	47.49
24.63	±0.12	123.15	1.321	±0.25	92.58	48.15
24.71	±0.12	123.55	1.314	±0.25	93.07	48.56
24.82	±0.12	124.1	1.31	±0.25	93.36	48.93
24.66	±0.12	123.3	1.32	±0.25	92.65	48.24
24.73	±0.12	123.65	1.3	±0.26	94.08	49.12
24.71	±0.12	123.55	1.316	±0.25	92.93	48.49

Table A- 7. 500 W BSC PEM fuel cell power and hydrogen consumption measurement at 5 A; Operating temperature ~50 °C, exit air 30 kPa, air stoichiometry 4, inlet hydrogen ~20-30 kPa

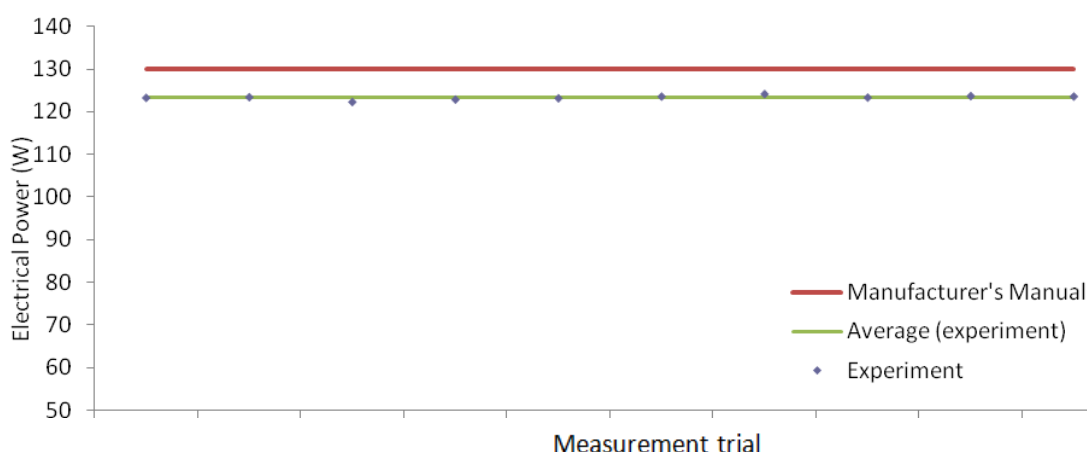


Figure A- 83. 500 W BSC PEM fuel cell power measurements at 5 A; Operating temperature ~50 °C, exit air 30 kPa, air stoichiometry 4, inlet hydrogen ~20-30 kPa

5 A/130 W operating point/ Cooling load measurement

- Operating temperature 50 °C, exit air 30 kPa, air stoichiometry 4, inlet hydrogen ~20-30 kPa
- Theoretically estimated cooling load at the ideal operating condition recommended by the manufacturer: 65.8 W

Note:

- The estimated cooling load at the experimental operating condition (the following table) is found by considering: fuel cell heat used for water evaporation, heat removal by the extra reactants, the convection heat transfer from the body of the fuel cell, and the power drop compared to the ideal condition

Fuel cell inlet water temperature (°C)	Fuel cell exit water temperature (°C)	Water flow rate (litre/min)	Measured cooling load (W)	Estimated cooling load (W)	Experimental error (%)	Estimated uncertainty (%)	CHP energy efficiency (%)
50.2	51.3	0.645	49.43	43.15	12.70	±23.75	67.06
50	51.1	0.645	49.43	43	13.01	±23.71	68.14
49	50.3	0.606	54.88	44.1	19.65	±19.90	69.06
48.9	50.5	0.459	51.16	43.55	14.88	±16.19	67.27
48.4	49.8	0.491	47.89	43.25	9.69	±18.39	66.87
48.3	49.9	0.503	56.07	42.85	23.57	±16.10	70.60
48.3	49.7	0.511	49.84	42.3	15.13	±18.38	68.58
48.4	50	0.473	52.72	43.1	18.25	±16.12	68.87
48.5	49.9	0.498	48.57	42.75	11.99	±18.41	68.42
48.4	49.9	0.467	48.80	42.85	12.20	±17.18	67.64

Table A- 8. 500 W BSC PEM fuel cell cooling load measurements at 5 A; Operating temperature ~50 °C, exit air 30 kPa, air stoichiometry 4, inlet hydrogen ~20-30 kPa

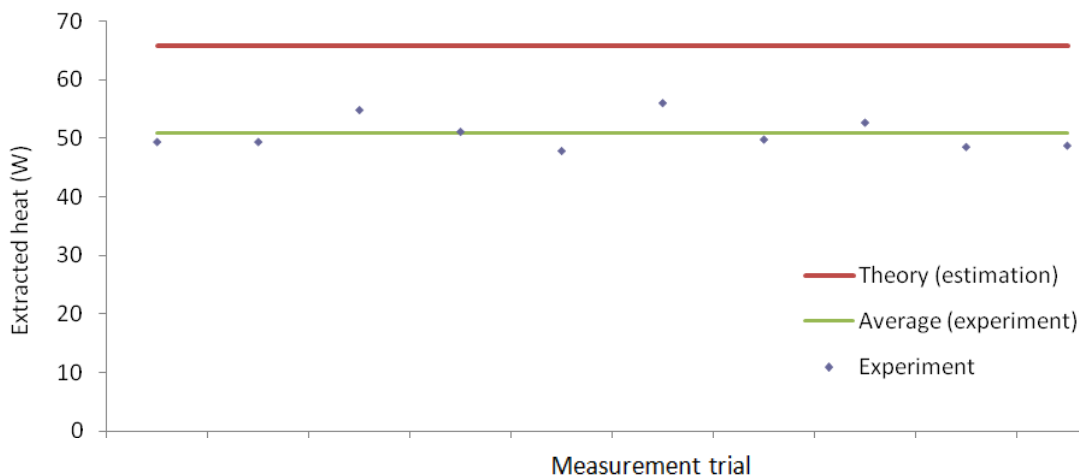


Figure A- 84. 500 W BSC PEM fuel cell cooling load measurements at 5 A; Operating temperature ~50 °C, exit air 30 kPa, air stoichiometry 4, inlet hydrogen ~20-30 kPa

5 A/130 W operating point/ Power measurement

- Operating temperature 60 °C, exit air 30 kPa, air stoichiometry 2, inlet hydrogen ~20-30 kPa
- Theoretical hydrogen consumption if fuel cell hydrogen utilisation coefficient is 100% ideally: 1.223 slpm
- Assumed hydrogen consumption rate for the theoretical calculations: 1.468 slpm (based on 20% extra hydrogen fed into the fuel cell)
- Expected power (manufacturer manual): 130 W
- Maximum uncertainty associated with the measurement instrument for voltage readings when the error for current adjustment (5A) is taken into account: 0.6%
- Maximum uncertainty associated with hydrogen flow meter: 1%
- Energy efficiency assumed for the theoretical calculation:45.7%
- Hydrogen utilisation coefficient assumed in the theoretical calculations: ~85%

Voltage (V)	% of uncertainty for the voltage measurement	Power output (W)	Hydrogen consumption (slpm)	% of uncertainty for the hydrogen consumption measurement	Hydrogen utilisation coefficient (%)	Electrical energy efficiency (%)
24.89	±0.22	124.45	1.27	±0.55	96.30	50.61
25.03	±0.22	125.15	1.28	±0.55	95.55	50.50
25.1	±0.22	125.5	1.3	±0.54	94.08	49.86
24.61	±0.22	123.05	1.34	±0.52	91.27	47.43
25.16	±0.22	125.8	1.32	±0.53	92.65	49.22
25	±0.22	125	1.28	±0.55	95.55	50.44
24.84	±0.22	124.2	1.31	±0.53	93.36	48.97
24.75	±0.22	123.75	1.29	±0.54	94.81	49.55
25.09	±0.22	125.45	1.29	±0.54	94.81	50.23
24.97	±0.22	124.85	1.32	±0.53	92.65	48.85

Table A- 9. 500 W BSC PEM fuel cell power and hydrogen consumption measurement at 5 A; Operating temperature ~60 °C, exit air 30 kPa, air stoichiometry 2, inlet hydrogen ~20-30 kPa

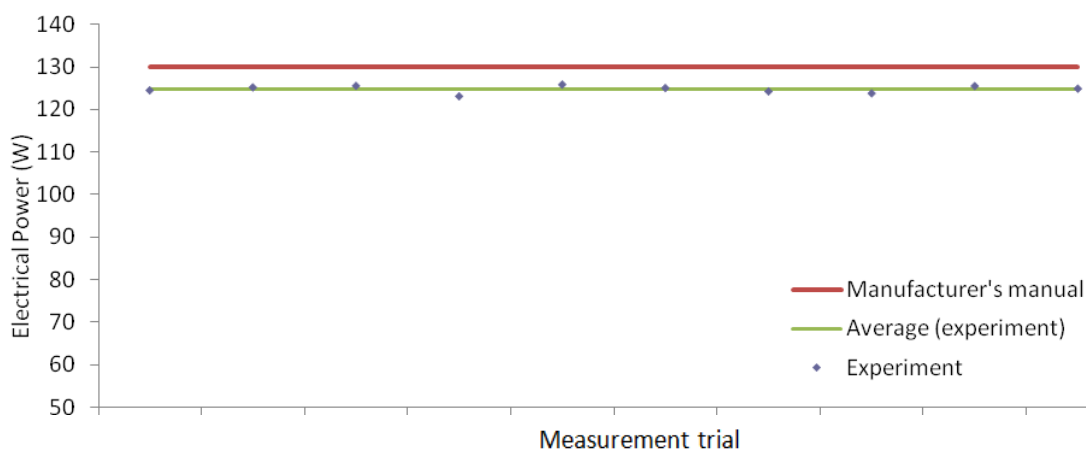


Figure A- 85. 500 W BSC PEM fuel cell power measurements at 5 A; Operating temperature ~60 °C, exit air 30 kPa, air stoichiometry 2, inlet hydrogen ~20-30 kPa

5 A/130 W operating point/ Cooling load measurement

- Operating temperature 60 °C, exit air 30 kPa, air stoichiometry 2, inlet hydrogen ~20-30 kPa
- Theoretically estimated cooling load at the ideal operating condition recommended by the manufacturer: 65.8 W

Note:

- The estimated cooling load at the experimental operating condition (the following table) is found by considering: fuel cell heat used for water evaporation, heat removal by the extra reactants, the convection heat transfer from the body of the fuel cell, and the power drop compared to the ideal condition

Fuel cell inlet water temperature (°C)	Fuel cell exit water temperature (°C)	Water flow rate (litre/min)	Measured cooling load (W)	Estimated cooling load (W)	Experimental error (%)	Estimated uncertainty (%)	CHP energy efficiency (%)
59.3	61.2	0.328	43.42	36.35	16.28	±14.95	67.69
59.2	61	0.308	38.62	35.65	7.70	±15.76	67.44
59.4	60.8	0.399	38.92	35.3	9.29	±20.25	66.54
59.4	61.1	0.343	40.62	37.75	7.07	±16.70	63.61
59.5	61.1	0.367	40.91	35	14.44	±17.75	65.65
59.2	60.9	0.302	35.77	35.8	-0.09	±16.68	67.38
59.3	60.9	0.389	43.36	36.6	15.59	±17.72	65.52
59.4	60.9	0.416	43.47	37.05	14.77	±18.91	66.36
59.2	61	0.384	48.15	35.35	26.59	±15.76	67.04
59.1	61	0.353	46.73	35.95	23.06	±14.93	65.28

Table A- 10. 500 W BSC PEM fuel cell cooling load measurements at 5 A; Operating temperature ~60 °C, exit air 30 kPa, air stoichiometry 2, inlet hydrogen ~20-30 kPa

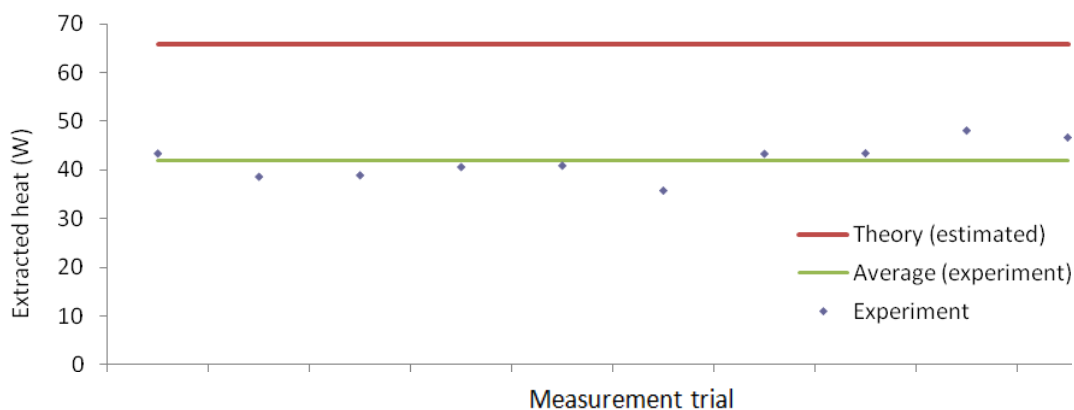


Figure A- 86. 500 W BSC PEM fuel cell cooling load measurements at 5 A; Operating temperature ~60 °C, exit air 30 kPa, air stoichiometry 2, inlet hydrogen ~20-30 kPa

5 A/130 W operating point/ Power measurement

- Operating temperature 60 °C, exit air 30 kPa, air stoichiometry 4, inlet hydrogen ~20-30 kPa
- Theoretical hydrogen consumption if fuel cell hydrogen utilisation coefficient is 100% ideally: 1.223 slpm
- Assumed hydrogen consumption rate for the theoretical calculations: 1.468 slpm (based on 20% extra hydrogen fed into the fuel cell)
- Expected power (manufacturer manual): 130 W
- Maximum uncertainty associated with the measurement instrument for voltage readings when the error for current adjustment (5A) is taken into account: 0.6%
- Maximum uncertainty associated with hydrogen flow meter: 1%
- Energy efficiency assumed for the theoretical calculation:45.7%
- Hydrogen utilisation coefficient assumed in the theoretical calculations: ~85%

Voltage (V)	% of uncertainty for the voltage measurement	Power output (W)	Hydrogen consumption (slpm)	% of uncertainty for the hydrogen consumption measurement	Hydrogen utilisation coefficient (%)	Electrical energy efficiency (%)
24.77	0.28	123.85	1.27	0.47	96.30	50.37
24.97	0.22	124.85	1.27	0.47	96.30	50.77
25.17	0.22	125.85	1.3	0.46	94.08	50.00
25.13	0.22	125.65	1.29	0.46	94.81	50.31
25.19	0.22	125.95	1.31	0.46	93.36	49.66
24.59	0.22	122.95	1.3	0.46	94.08	48.85
25.29	0.22	126.45	1.28	0.47	95.55	51.02
25.23	0.22	126.15	1.25	0.48	97.84	52.12
24.58	0.22	122.9	1.3	0.46	94.08	48.83
25.18	0.22	125.9	1.3	0.46	94.08	50.02

Table A- 11. 500 W BSC PEM fuel cell power and hydrogen consumption measurement at 5 A; Operating temperature ~60 °C, exit air 30 kPa, air stoichiometry 4, inlet hydrogen ~20-30 kPa

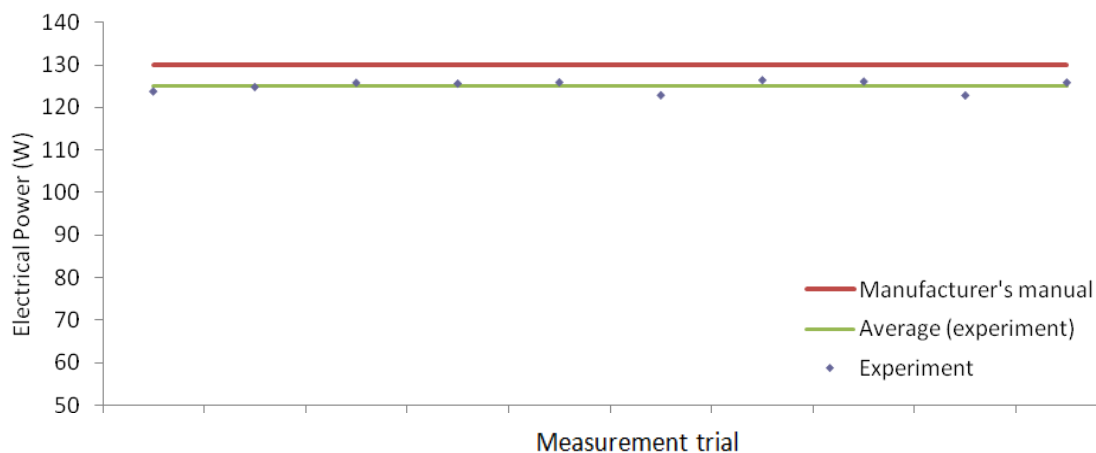


Figure A- 87. 500 W BSC PEM fuel cell power measurements at 5 A; Operating temperature ~60 °C, exit air 30 kPa, air stoichiometry 4, inlet hydrogen ~20-30 kPa

5 A/130 W operating point/ Cooling load measurement

- Operating temperature 60 °C, exit air 30 kPa, air stoichiometry 4, inlet hydrogen ~20-30 kPa
- Theoretically estimated cooling load at the ideal operating condition recommended by the manufacturer: 65.8 W

Note:

- The estimated cooling load at the experimental operating condition (the following table) is found by considering: fuel cell heat used for water evaporation, heat removal by the extra reactants, the convection heat transfer from the body of the fuel cell, and the power drop compared to the ideal condition

Fuel cell inlet water temperature (°C)	Fuel cell exit water temperature (°C)	Water flow rate (litre/min)	Measured cooling load (W)	Estimated cooling load (W)	Experimental error (%)	Estimated uncertainty (%)	CHP energy efficiency (%)
59.6	61.1	0.358	37.41	11.92	32.95	18.94	65.86
59.4	61.2	0.323	40.50	21.12	31.95	15.79	66.27
59.3	60.9	0.355	39.57	21.79	30.95	17.72	65.14
59.5	60.9	0.353	34.43	9.52	31.15	20.26	65.56
59.6	61	0.397	38.72	20.33	30.85	20.28	64.68
59.5	61.1	0.352	39.24	13.73	33.85	17.75	63.98
59.4	61	0.376	41.91	27.59	30.35	17.74	66.40
59.5	61.1	0.331	36.90	16.93	30.65	17.75	67.86
59.4	60.9	0.359	37.52	9.64	33.9	18.91	63.96
59.6	61	0.357	34.82	11.26	30.9	20.28	65.16

Table A- 12. 500 W BSC PEM fuel cell cooling load measurements at 5 A; Operating temperature ~60 °C, exit air 30 kPa, air stoichiometry 4, inlet hydrogen ~20-30 kPa

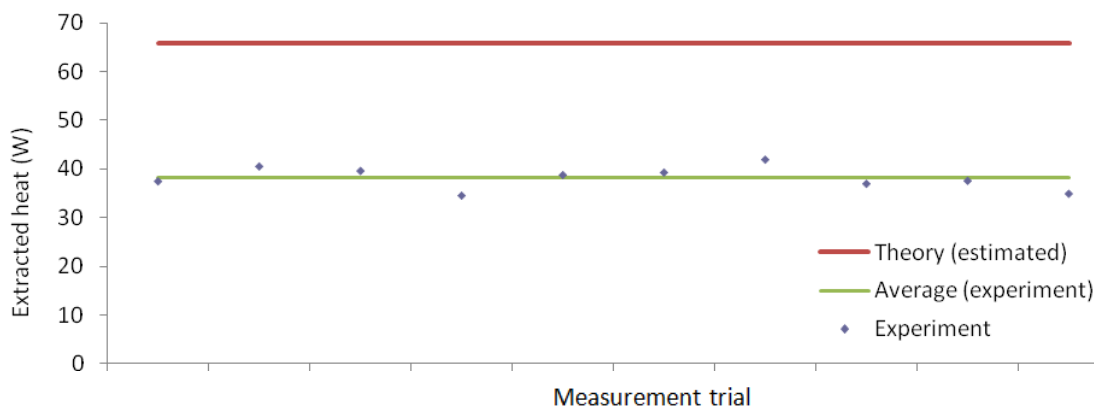


Figure A- 88. 500 W BSC PEM fuel cell cooling load measurements at 5 A; Operating temperature ~60 °C, exit air 30 kPa, air stoichiometry 4, inlet hydrogen ~20-30 kPa

10 A/230 W operating point/ Power measurement

- Operating temperature 40 °C, exit air 30 kPa, air stoichiometry 2, inlet hydrogen ~20-30 kPa
- Theoretical hydrogen consumption if fuel cell hydrogen utilisation coefficient is 100% ideally: 2.44 slpm
- Assumed hydrogen consumption rate for the theoretical calculations: 2.93 slpm (based on 20% extra hydrogen fed into the fuel cell)
- Expected power (manufacturer manual): 230 W
- Maximum uncertainty associated with the measurement instrument for voltage readings when the error for current adjustment (10A) is taken into account: 0.6%
- Maximum uncertainty associated with hydrogen flow meter: 1%
- Energy efficiency assumed for the theoretical calculation:40.44%
- Hydrogen utilisation coefficient assumed in the theoretical calculations: ~85%

Voltage (V)	% of uncertainty for the voltage measurement	Power output (W)	Hydrogen consumption (slpm)	% of uncertainty for the hydrogen consumption measurement	Hydrogen utilisation coefficient (%)	Electrical energy efficiency (%)
18.89	±0.33	188.9	2.65	±0.24	92.08	36.73
18.97	±0.33	189.7	2.68	±0.24	91.04	36.47
18.59	±0.34	185.9	2.67	±0.24	91.39	35.87
18.37	±0.34	183.7	2.69	±0.24	90.71	35.18
18.91	±0.33	189.1	2.62	±0.25	93.13	37.19
18.49	±0.34	184.9	2.65	±0.24	92.08	35.95
18.61	±0.34	186.1	2.66	±0.24	91.73	36.04
18.78	±0.33	187.8	2.64	±0.25	92.42	36.65
18.52	±0.34	185.2	2.67	±0.24	91.39	35.74
18.9	±0.33	189	2.69	±0.24	90.71	36.20
18.88	±0.33	188.8	2.67	±0.24	91.39	36.43

Table A- 13. 500 W BSC PEM fuel cell power and hydrogen consumption measurement at 10 A; Operating temperature ~40 °C, exit air 30 kPa, air stoichiometry 2, inlet hydrogen ~20-30 kPa

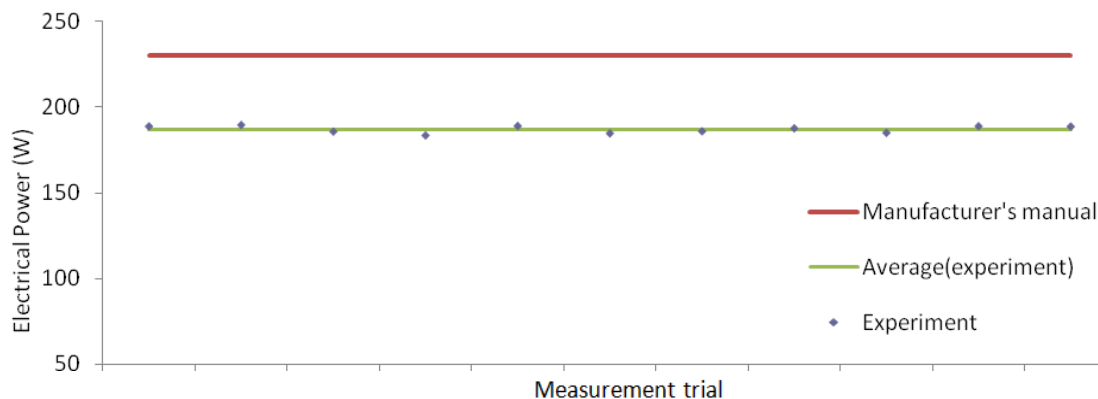


Figure A- 89. 500 W BSC PEM fuel cell power measurements at 10 A; Operating temperature ~40 °C, exit air 30 kPa, air stoichiometry 2, inlet hydrogen ~20-30 kPa

10 A/230 W operating point/ Cooling load measurement

- Operating temperature 40 °C, exit air 30 kPa, air stoichiometry 2, inlet hydrogen ~20-30 kPa
- Theoretically estimated cooling load at the ideal operating condition recommended by the manufacturer: 161.59 W

Note:

- The estimated cooling load at the experimental operating condition (the following table) is found by considering: fuel cell heat used for water evaporation, heat removal by the extra reactants, the convection heat transfer from the body of the fuel cell, and the power drop compared to the ideal condition

Fuel cell inlet water temperature (°C)	Fuel cell exit water temperature (°C)	Water flow rate (litre/min)	Measured cooling load (W)	Estimated cooling load (W)	Experimental error (%)	Estimated uncertainty (%)	CHP energy efficiency (%)
37.2	39.4	1.623	248.75	261.69	-5.20	±10.58	85.09
37.3	39.5	1.638	251.05	260.89	-3.92	±10.59	84.73
37.5	39.8	1.628	260.86	264.69	-1.47	±10.16	86.21
37.4	39.6	1.647	252.43	266.89	-5.73	±10.60	83.53
37.6	39.7	1.657	242.42	261.49	-7.87	±11.12	84.85
37.5	39.8	1.629	261.02	265.69	-1.79	±10.16	86.69
37.6	39.8	1.636	250.74	264.49	-5.48	±10.62	84.61
37.7	39.9	1.638	251.05	262.79	-4.68	±10.63	85.64
37.9	40	1.632	238.76	265.39	-11.15	±11.15	81.81
38	40.3	1.614	258.62	261.59	-1.15	±10.21	85.73
38.2	40.4	1.634	250.44	261.79	-4.53	10.68	84.76

Table A- 14. 500 W BSC PEM fuel cell cooling load measurements at 10 A; Operating temperature ~40 °C, exit air 30 kPa, air stoichiometry 2, inlet hydrogen ~20-30 kPa

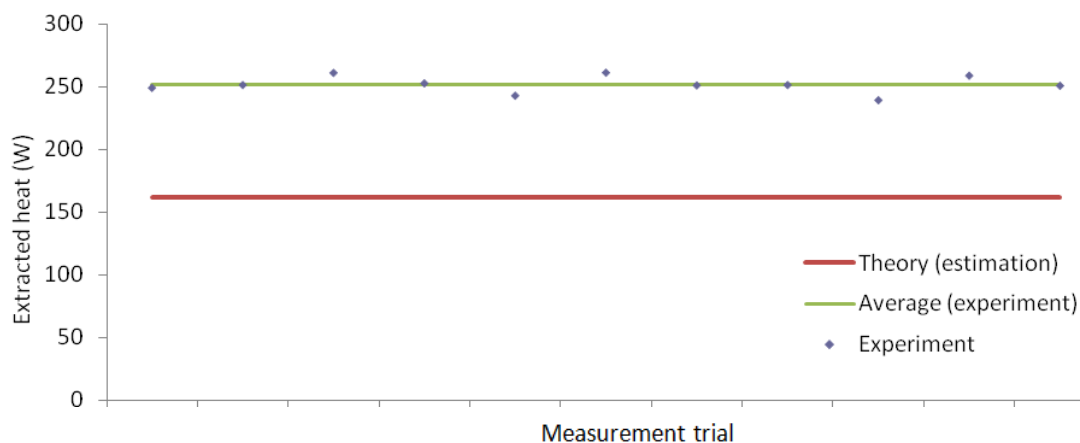


Figure A- 90. 500 W BSC PEM fuel cell cooling load measurements at 10 A; Operating temperature ~40 °C, exit air 30 kPa, air stoichiometry 2, inlet hydrogen ~20-30 kPa

10 A/230 W operating point/ Power measurement

- Operating temperature 40 °C, exit air 30 kPa, air stoichiometry 4, inlet hydrogen ~20-30 kPa
- Theoretical hydrogen consumption if fuel cell hydrogen utilisation coefficient is 100% ideally: 2.44 slpm
- Assumed hydrogen consumption rate for the theoretical calculations: 2.93 slpm (based on 20% extra hydrogen fed into the fuel cell)
- Expected power (manufacturer manual): 230 W
- Maximum uncertainty associated with the measurement instrument for voltage readings when the error for current adjustment error (10 A) is taken into account: 0.6%
- Maximum uncertainty associated with hydrogen flow meter: 1%
- Energy efficiency assumed for the theoretical calculation:40.44%
- Hydrogen utilisation coefficient assumed in the theoretical calculations: ~85%

Voltage (V)	% of uncertainty for the voltage measurement	Power output (W)	Hydrogen consumption (slpm)	% of uncertainty for the hydrogen consumption measurement	Hydrogen utilisation coefficient (%)	Electrical energy efficiency (%)
20.56	±0.28	205.6	2.65	±0.36	92.08	39.97
20.12	±0.29	201.2	2.66	±0.35	91.73	38.97
20.08	±0.29	200.8	2.67	±0.35	91.39	38.75
20.27	±0.29	202.7	2.63	±0.36	92.78	39.71
20.51	±0.29	205.1	2.59	±0.36	94.21	40.80
20.2	±0.29	202	2.58	±0.37	94.57	40.34
20.47	±0.29	204.7	2.65	±0.36	92.08	39.80
20.22	±0.29	202.2	2.62	±0.36	93.13	39.76
20.05	±0.29	200.5	2.61	±0.36	93.49	39.58
20.39	±0.29	203.9	2.64	±0.36	92.42	39.79

Table A- 15. 500 W BSC PEM fuel cell power and hydrogen consumption measurement at 10 A; Operating temperature ~40 °C, exit air 30 kPa, air stoichiometry 4, inlet hydrogen ~20-30 kPa

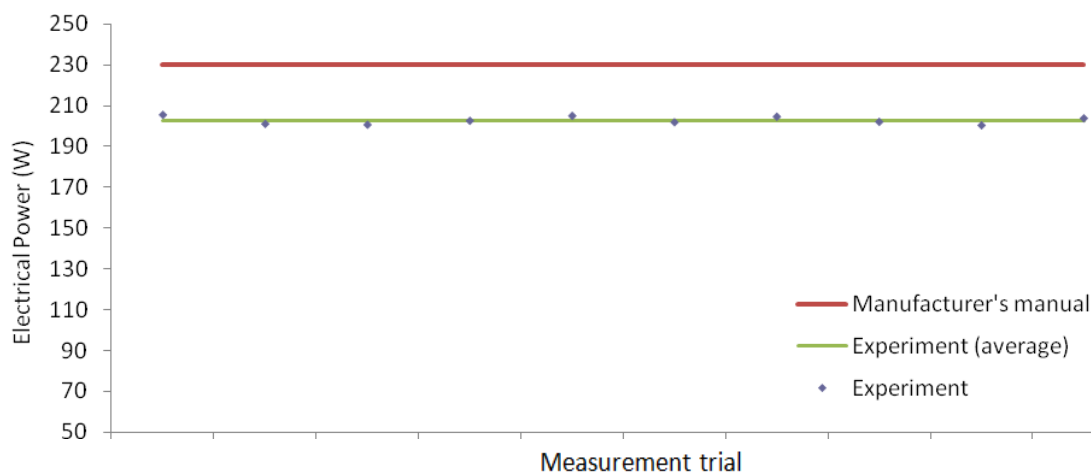


Figure A- 91. 500 W BSC PEM fuel cell power measurements at 10 A; Operating temperature ~40 °C, exit air 30 kPa, air stoichiometry 4, inlet hydrogen ~20-30 kPa

10 A/230 W operating point/ Cooling load measurement

- Operating temperature 40 °C, exit air 30 kPa, air stoichiometry 4, inlet hydrogen ~20-30 kPa
- Theoretically estimated cooling load at the ideal operating condition recommended by the manufacturer: 161.59 W

Note:

- The estimated cooling load at the experimental operating condition (the following table) is found by considering: fuel cell heat used for water evaporation, heat removal by the extra reactants, the convection heat transfer from the body of the fuel cell, and the power drop compared to the ideal condition

Fuel cell inlet water temperature (°C)	Fuel cell exit water temperature (°C)	Water flow rate (litre/min)	Measured Cooling load (W)	Estimated cooling load (W)	Experimental error (%)	Estimated uncertainty (%)	CHP energy efficiency (%)
39.3	41.4	1.522	222.67	236.99	-6.43	±11.31	83.26
39.4	41.5	1.509	220.77	241.39	-9.34	±11.32	81.73
38.9	41	1.537	224.86	241.79	-7.53	±11.26	82.14
38.5	40.6	1.512	221.21	239.89	-8.45	±11.22	83.04
38.7	40.8	1.569	229.54	237.49	-3.46	±11.24	86.46
38.8	40.9	1.542	225.59	240.59	-6.65	±11.25	85.39
38.5	40.7	1.534	235.11	237.89	-1.18	±10.72	85.51
38.6	40.8	1.506	230.82	240.39	-4.15	±10.73	85.15
38.4	40.5	1.542	225.59	242.09	-7.31	±11.21	84.11
38.2	40.3	1.538	225.01	238.69	-6.08	±11.18	83.70

Table A- 16. 500 W BSC PEM fuel cell cooling load measurements at 10 A; Operating temperature ~40 °C, exit air 30 kPa, air stoichiometry 4, inlet hydrogen ~20-30 kPa

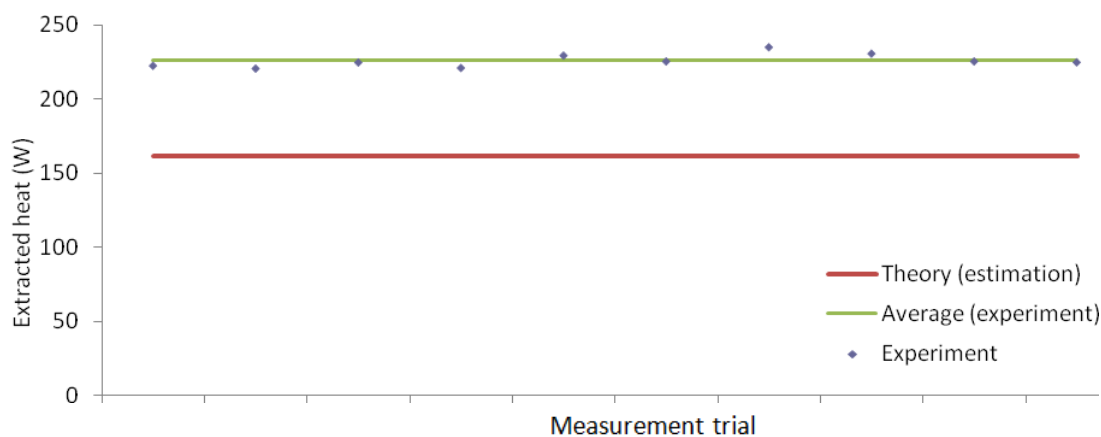


Figure A- 92. 500 W BSC PEM fuel cell cooling load measurements at 10 A; Operating temperature ~40 °C, exit air 30 kPa, air stoichiometry 4, inlet hydrogen ~20-30 kPa

10 A/230 W operating point/ Power measurement

- Operating temperature 50 °C, exit air 30 kPa, air stoichiometry 2, inlet hydrogen ~20-30 kPa
- Theoretical hydrogen consumption if fuel cell hydrogen utilisation coefficient is 100% ideally: 2.44 slpm
- Assumed hydrogen consumption rate for the theoretical calculations: 2.93 slpm (based on 20% extra hydrogen fed into the fuel cell)
- Expected power (manufacturer manual): 230 W
- Maximum uncertainty associated with the measurement instrument for voltage readings when the error for current adjustment (10 A) is taken into account: 0.6%
- Maximum uncertainty associated with hydrogen flow meter: 1%
- Energy efficiency assumed for the theoretical calculation:40.44%
- Hydrogen utilisation coefficient assumed in the theoretical calculations: ~85%

Voltage (V)	% of uncertainty for the voltage measurement	Power output (W)	Hydrogen consumption (slpm)	% of uncertainty for the hydrogen consumption measurement	Hydrogen utilisation coefficient (%)	Electrical energy efficiency (%)
20.63	±0.22	206.3	2.54	±0.22	97.02	42.26
20.42	±0.22	204.2	2.527	±0.22	96.56	41.63
20.84	±0.22	208.4	2.564	±0.21	95.16	41.88
20.67	±0.22	206.7	2.54	±0.21	96.06	41.93
20.46	±0.22	204.6	2.512	±0.22	97.13	41.96
20.85	±0.22	208.5	2.54	±0.21	95.31	41.96
20.73	±0.22	207.3	2.55	±0.21	95.69	41.88
20.79	±0.22	207.9	2.57	±0.21	94.94	41.68
20.86	±0.22	208.6	2.52	±0.22	96.83	42.65
20.82	±0.22	208.2	2.53	±0.22	97.21	42.74
20.98	±0.22	209.8	2.54	±0.21	96.06	42.55
21.01	±0.22	210.1	2.54	±0.21	95.20	42.23
20.69	±0.22	206.9	2.534	±0.22	96.29	42.07
20.77	±0.22	207.7	2.538	±0.21	96.14	42.16

Table A- 17. 500 W BSC PEM fuel cell power and hydrogen consumption measurement at 10 A; Operating temperature ~50 °C, exit air 30 kPa, air stoichiometry 2, inlet hydrogen ~20-30 kPa

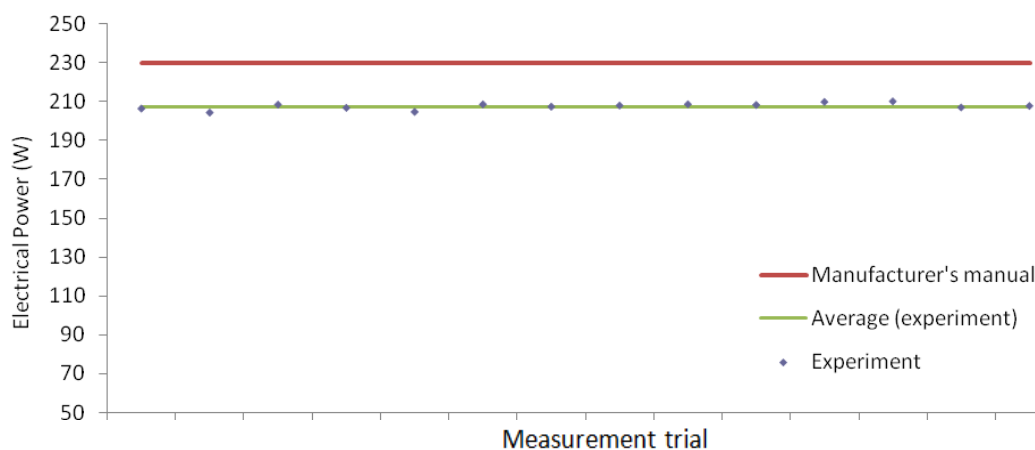


Figure A- 93. 500 W BSC PEM fuel cell power measurements at 10 A; Operating temperature ~50 °C, exit air 30 kPa, air stoichiometry 2, inlet hydrogen ~20-30 kPa

10 A/230 W operating point/ Cooling load measurement

- Operating temperature 50 °C, exit air 30 kPa, air stoichiometry 2, inlet hydrogen ~20-30 kPa
- Theoretically estimated cooling load at the ideal operating condition recommended by the manufacturer: 161.59 W

Note:

- The estimated cooling load at the experimental operating condition (the following table) is found by considering: fuel cell heat used for water evaporation, heat removal by the extra reactants, the convection heat transfer from the body of the fuel cell, and the power drop compared to the ideal condition

Fuel cell inlet water temperature (°C)	Fuel cell exit water temperature (°C)	Water flow rate (litre/min)	Measured cooling load (W)	Estimated cooling load (W)	Experimental error (%)	Estimated uncertainty (%)	CHP energy efficiency (%)
48	50.5	1.426	248.36	234.29	5.67	±10.35	93.14
47.3	49.8	1.429	248.88	236.39	5.02	±10.28	92.37
47.5	50	1.421	247.49	232.19	6.18	±10.30	91.61
47.2	49.8	1.433	259.56	233.89	9.89	±9.89	94.58
47.5	50	1.432	249.41	235.99	5.38	±10.30	93.12
47.7	50.2	1.428	248.71	232.09	6.68	±10.32	92.01
47.5	50.1	1.423	257.75	233.29	9.49	±9.91	93.96
47.9	50.4	1.429	248.88	232.69	6.51	±10.34	91.57
47.6	50.2	1.428	258.66	231.99	10.31	±9.92	95.53
47.6	50.1	1.438	250.45	232.39	7.21	±10.31	94.14
47.9	50.3	1.434	239.76	230.79	3.74	±10.76	91.19
48.2	50.7	1.436	250.10	230.49	7.84	±10.37	92.51
48.3	50.9	1.42	257.21	233.69	9.14	±9.99	94.36
48.7	51.2	1.418	246.97	232.89	5.70	±10.41	92.30

Table A- 18. 500 W BCS PEM fuel cell cooling load measurements at 10 A; Operating temperature ~50 °C, exit air 30 kPa, air stoichiometry 2, inlet hydrogen ~20-30 kPa

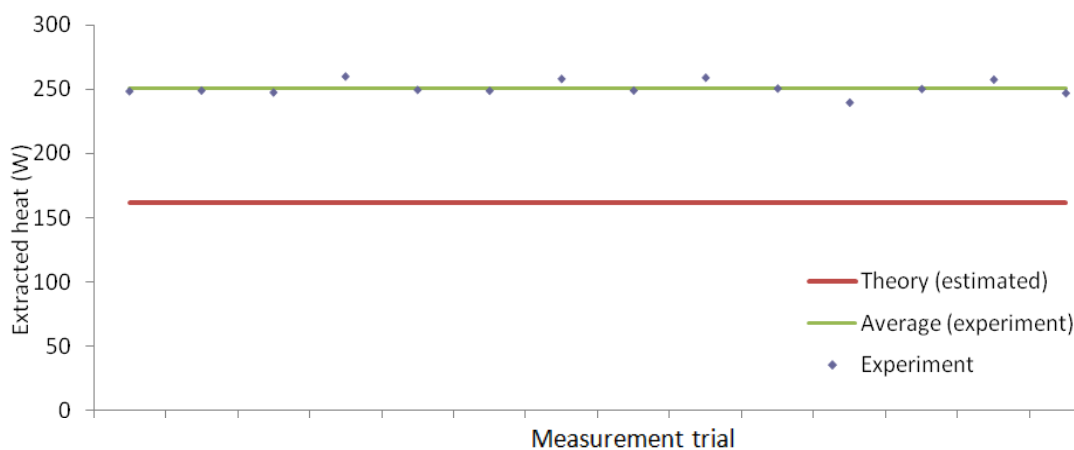


Figure A- 94. 500 W BCS PEM fuel cell cooling load measurements at 10 A; Operating temperature ~50 °C, exit air 30 kPa, air stoichiometry 2, inlet hydrogen ~20-30 kPa

10 A/230 W operating point/ Power measurement

- Operating temperature 50 °C, exit air 30 kPa, air stoichiometry 4, inlet hydrogen ~20-30 kPa
- Theoretical hydrogen consumption if fuel cell hydrogen utilisation coefficient is 100% ideally: 2.44 slpm
- Assumed hydrogen consumption rate for the theoretical calculations: 2.93 slpm (based on 20% extra hydrogen fed into the fuel cell)
- Expected power (manufacturer manual): 230 W
- Maximum uncertainty associated with the measurement instrument for voltage readings when the error for current adjustment (10 A) is taken into account: 0.6%
- Maximum uncertainty associated with hydrogen flow meter: 1%
- Energy efficiency assumed for the theoretical calculation:40.44%
- Hydrogen utilisation coefficient assumed in the theoretical calculations: ~85%

Voltage (V)	% of uncertainty for the voltage measurement	Power output (W)	Hydrogen consumption (slpm)	% of uncertainty for the hydrogen consumption measurement	Hydrogen utilisation coefficient (%)	Electrical energy efficiency (%)
22.3	±0.26	223	2.584	±0.23	94.43	44.46
22.05	±0.27	220.5	2.554	±0.23	95.54	44.48
22.44	±0.26	224.4	2.59	±0.23	94.21	44.64
22.09	±0.27	220.9	2.55	±0.23	95.69	44.63
22.16	±0.26	221.6	2.539	±0.23	96.10	44.97
21.81	±0.27	218.1	2.545	±0.23	95.87	44.15
22.08	±0.27	220.8	2.579	±0.23	94.61	44.11
22.47	±0.26	224.7	2.58	±0.23	94.57	44.87
22.1	±0.26	221	2.581	±0.23	94.54	44.11
21.79	±0.27	217.9	2.575	±0.23	94.76	43.60
22.12	±0.26	221.2	2.59	±0.23	94.21	44.00
22.07	±0.27	220.7	2.529	±0.23	96.48	44.96
22.38	0.26	223.8	2.546	±0.23	95.84	45.29

Table A- 19. 500 W BSC PEM fuel cell power and hydrogen consumption measurement at 10 A; Operating temperature ~50 °C, exit air 30 kPa, air stoichiometry 4, inlet hydrogen ~20-30 kPa

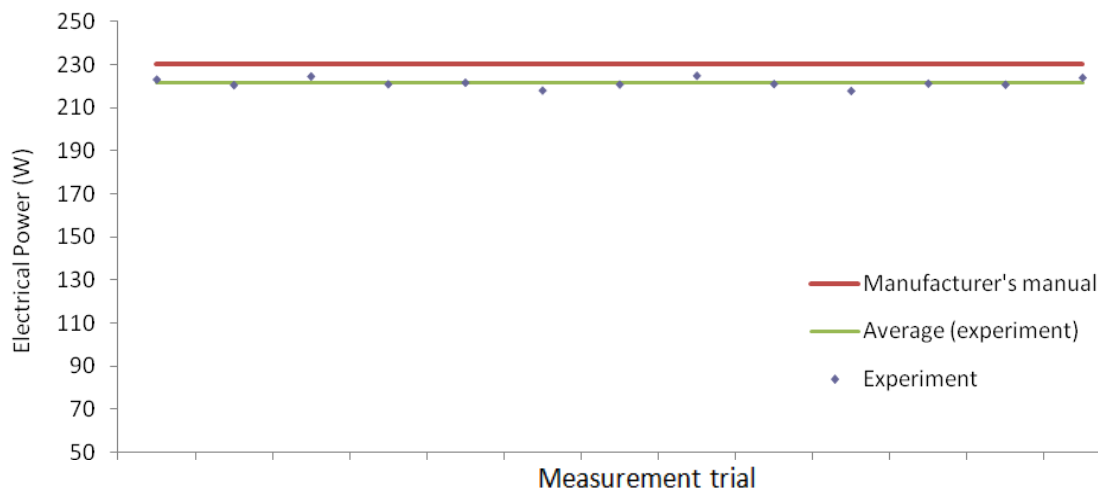


Figure A- 95. 500 W BSC PEM fuel cell power measurements at 10 A; Operating temperature ~50 °C, exit air 30 kPa, air stoichiometry 4, inlet hydrogen ~20-30 kPa

10 A/230 W operating point/ Cooling load measurement

- Operating temperature 50 °C, exit air 30 kPa, air stoichiometry 4, inlet hydrogen ~20-30 kPa
- Theoretically estimated cooling load at the ideal operating condition recommended by the manufacturer: 161.59 W

Note:

- The estimated cooling load at the experimental operating condition (the following table) is found by considering: fuel cell heat used for water evaporation, heat removal by the extra reactants, the convection heat transfer from the body of the fuel cell, and the power drop compared to the ideal condition

Fuel cell inlet water temperature (°C)	Fuel cell exit water temperature (°C)	Water flow rate (litre/min)	Measured Cooling load (W)	Estimated cooling load (W)	Experimental error (%)	Estimated uncertainty (%)	CHP energy efficiency (%)
47.7	50.3	0.721	130.60	135.59	-3.82	±9.23	70.50
47.5	50.3	0.709	138.30	138.09	0.15	±8.66	72.38
47.6	50.2	0.741	134.22	134.19	0.02	±9.01	71.34
47.5	51	0.569	138.74	137.69	0.76	±15.49	72.66
47.7	50.9	0.587	130.86	136.99	-4.68	±16.91	71.52
47.3	50.6	0.581	133.57	140.49	-5.18	±16.31	71.19
47.4	50.4	0.633	132.30	137.79	-4.15	±17.87	70.54
47.4	50.5	0.648	139.95	133.89	4.33	±17.33	72.82
47.5	50.2	0.762	143.33	137.59	4.01	±19.78	72.73
47.3	50.2	0.738	149.10	140.69	5.64	±18.42	73.43
47.1	50.5	0.606	143.54	137.39	4.29	±15.80	72.55
47.2	50.6	0.614	145.44	137.89	5.19	±15.83	74.59
47.3	50.7	0.589	139.51	134.79	3.39	±15.85	73.52

Table A- 20. 500 W BCS PEM fuel cell cooling load measurements at 10 A; Operating temperature ~50 °C, exit air 30 kPa, air stoichiometry 4, inlet hydrogen ~20-30 kPa

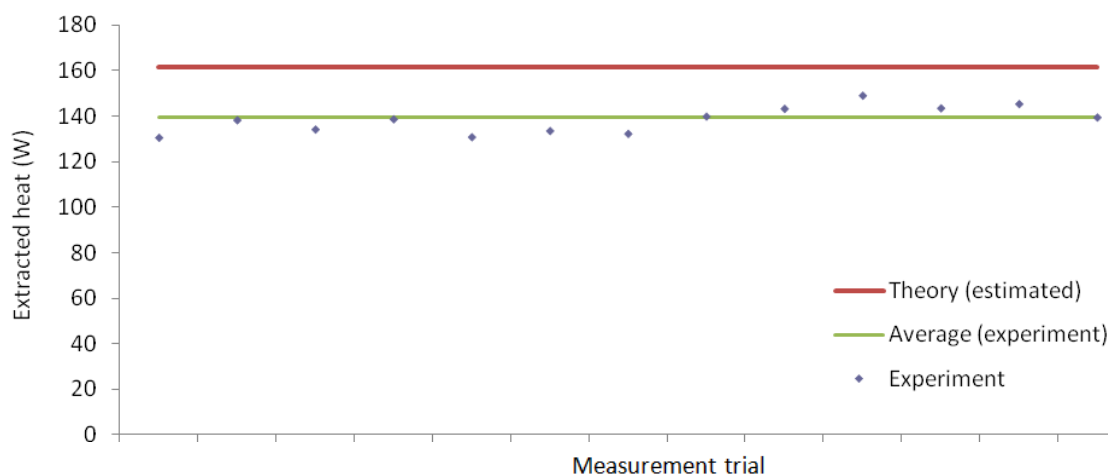


Figure A- 96. 500 W BCS PEM fuel cell cooling load measurements at 10 A; Operating temperature ~50 °C, exit air 30 kPa, air stoichiometry 4, inlet hydrogen ~20-30 kPa

10 A/230 W operating point/ Power measurement

- Operating temperature 60 °C, exit air 30 kPa, air stoichiometry 2, inlet hydrogen ~20-30 kPa
- Theoretical hydrogen consumption if fuel cell hydrogen utilisation coefficient is 100% ideally: 2.44 slpm
- Assumed hydrogen consumption rate for the theoretical calculations: 2.93 slpm (based on 20% extra hydrogen fed into the fuel cell)
- Expected power (manufacturer manual): 230 W
- Maximum uncertainty associated with the measurement instrument for voltage readings when the error for current adjustment (10 A) is taken into account: 0.6%
- Maximum uncertainty associated with hydrogen flow meter: 1%
- Energy efficiency assumed for the theoretical calculation:40.44%
- Hydrogen utilisation coefficient assumed in the theoretical calculations: ~85%

Voltage (V)	% of uncertainty for the voltage measurement	Power output (W)	Hydrogen consumption (slpm)	% of uncertainty for the hydrogen consumption measurement	Hydrogen utilisation coefficient (%)	Electrical energy efficiency (%)
22.27	±0.21	222.7	2.58	±0.29	94.57	44.47
21.82	±0.21	218.2	2.532	±0.30	96.37	44.40
22.18	±0.21	221.8	2.572	±0.29	94.87	44.43
22.07	±0.21	220.7	2.561	±0.29	95.28	44.40
22	±0.21	220	2.559	±0.29	95.35	44.29
21.94	±0.21	219.4	2.551	±0.29	95.65	44.31
21.9	±0.21	219	2.527	±0.30	96.56	44.65
22.03	±0.21	220.3	2.566	±0.29	95.09	44.23
22.13	±0.21	221.3	2.554	±0.29	95.54	44.64
21.79	±0.21	217.9	2.571	±0.29	94.90	43.66
21.88	±0.21	218.8	2.549	±0.29	95.72	44.22

Table A- 21. 500 W BSC PEM fuel cell power and hydrogen consumption measurement at 10 A; Operating temperature ~60 °C, exit air 30 kPa, air stoichiometry 2, inlet hydrogen ~20-30 kPa

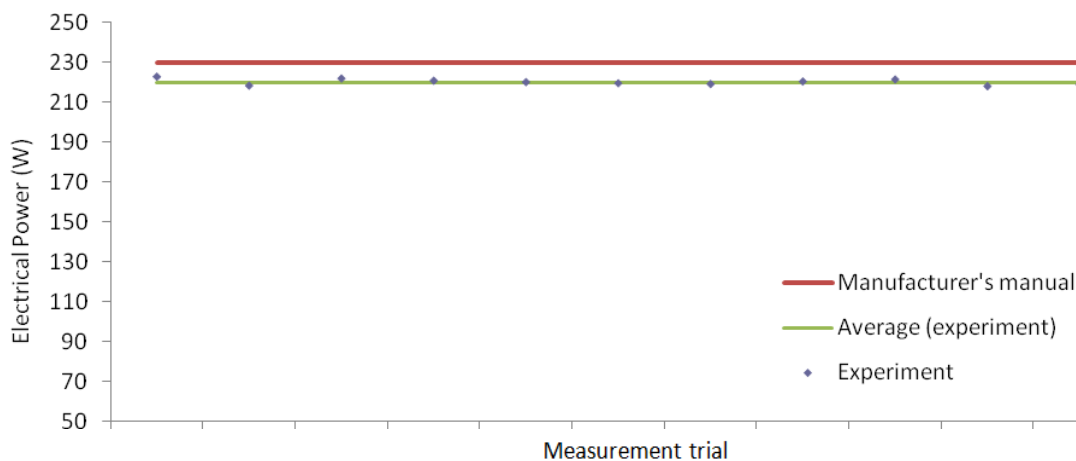


Figure A- 97. 500 W BSC PEM fuel cell power measurements at 10 A; Operating temperature ~60 °C, exit air 30 kPa, air stoichiometry 2, inlet hydrogen ~20-30 kPa

10 A/230 W operating point/ Cooling load measurement

- Operating temperature 60 °C, exit air 30 kPa, air stoichiometry 2, inlet hydrogen ~20-30 kPa
- Theoretically estimated cooling load at the ideal operating condition recommended by the manufacturer: 161.59 W

Note:

- The estimated cooling load at the experimental operating condition (the following table) is found by considering: fuel cell heat used for water evaporation, heat removal by the extra reactants, the convection heat transfer from the body of the fuel cell, and the power drop compared to the ideal condition

Fuel cell inlet water temperature (°C)	Fuel cell exit water temperature (°C)	Water flow rate (litre/min)	Measured cooling load (W)	Estimated cooling load (W)	Experimental error (%)	Estimated uncertainty (%)	CHP energy efficiency (%)
58.8	60.3	1.314	137.31	133.89	2.49	±18.81	71.89
58.7	60.2	1.261	131.77	138.39	-5.02	±18.80	71.21
58.9	60.3	1.355	132.16	134.79	-1.99	±20.16	70.90
58.7	60.2	1.344	140.45	135.89	3.25	±18.80	72.65
58.6	60.1	1.316	137.52	136.59	0.68	±18.78	71.98
58.8	60.2	1.324	129.13	137.19	-6.24	±20.14	70.39
58.7	60.2	1.279	133.66	137.59	-2.94	±18.80	71.90
58.6	60	1.319	128.65	136.29	-5.94	±20.11	70.06
58.7	60.2	1.276	133.34	135.29	-1.46	±18.80	71.54
58.8	60.4	1.283	143.01	138.69	3.02	±17.65	72.32
58.9	60.3	1.339	130.60	137.79	-5.51	±20.16	70.62

Table A- 22. 500 W BSC PEM fuel cell cooling load measurements at 10 A; Operating temperature ~60 °C, exit air 30 kPa, air stoichiometry 2, inlet hydrogen ~20-30 kPa

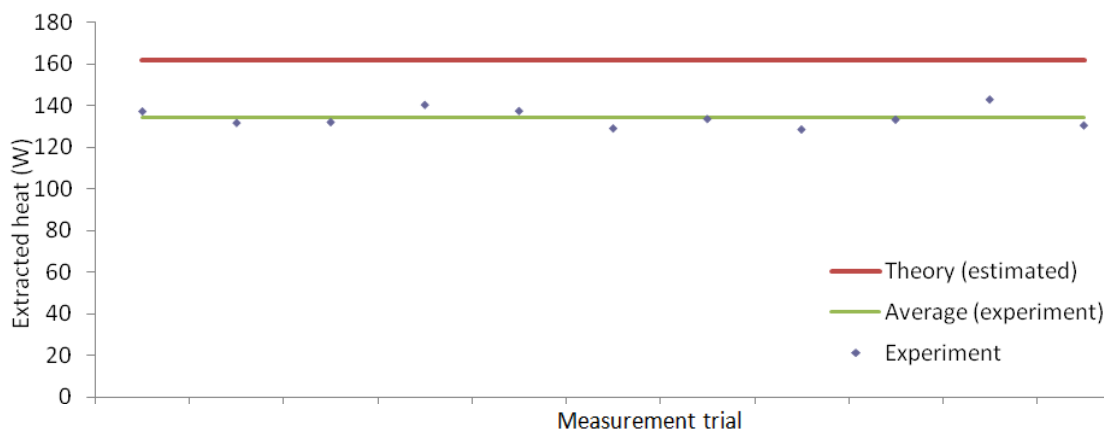


Figure A- 98. 500 W BSC PEM fuel cell cooling load measurements at 10 A; Operating temperature ~60 °C, exit air 30 kPa, air stoichiometry 2, inlet hydrogen ~20-30 kPa

10 A/230 W operating point/ Power measurement

- Operating temperature 60 °C, exit air 30 kPa, air stoichiometry 4, inlet hydrogen ~20-30 kPa
- Theoretical hydrogen consumption if fuel cell hydrogen utilisation coefficient is 100% ideally: 2.44 slpm
- Assumed hydrogen consumption rate for the theoretical calculations: 2.93 slpm (based on 20% extra hydrogen fed into the fuel cell)
- Expected power (manufacturer manual): 230 W
- Maximum uncertainty associated with the measurement instrument for voltage readings when the error for current adjustment (10 A) is taken into account: 0.6%
- Maximum uncertainty associated with hydrogen flow meter: 1%
- Energy efficiency assumed for the theoretical calculation:40.44%
- Hydrogen utilisation coefficient assumed in the theoretical calculations: ~85%

Voltage (V)	% of uncertainty for the voltage measurement	Power output (W)	Hydrogen consumption (slpm)	% of uncertainty for the hydrogen consumption measurement	Hydrogen utilisation coefficient (%)	Electrical energy efficiency (%)
22.45	±0.19	224.5	2.59	±0.23	94.21	44.66
22.29	±0.19	222.9	2.541	±0.23	96.03	45.19
22.18	±0.19	221.8	2.549	±0.23	95.72	44.83
22.5	±0.19	225	2.562	±0.23	95.24	45.25
22.01	±0.19	220.1	2.551	±0.23	95.65	44.45
22.27	±0.19	222.7	2.547	±0.23	95.80	45.05
22.28	±0.19	222.8	2.54	±0.23	96.06	45.35
22.41	±0.19	224.1	2.539	±0.23	96.10	44.99
22.03	±0.19	220.3	2.537	±0.23	96.18	44.74
22.14	±0.19	221.4	2.544	±0.23	95.91	44.84
22.16	±0.19	221.6	2.543	±0.23	95.95	44.90
22.36	±0.19	223.6	2.542	±0.23	95.99	45.16
22.17	±0.19	221.7	2.582	±0.23	94.50	44.72

Table A- 23. 500 W BSC PEM fuel cell power and hydrogen consumption measurement at 10 A; Operating temperature ~60 °C, exit air 30 kPa, air stoichiometry 4, inlet hydrogen ~20-30 kPa

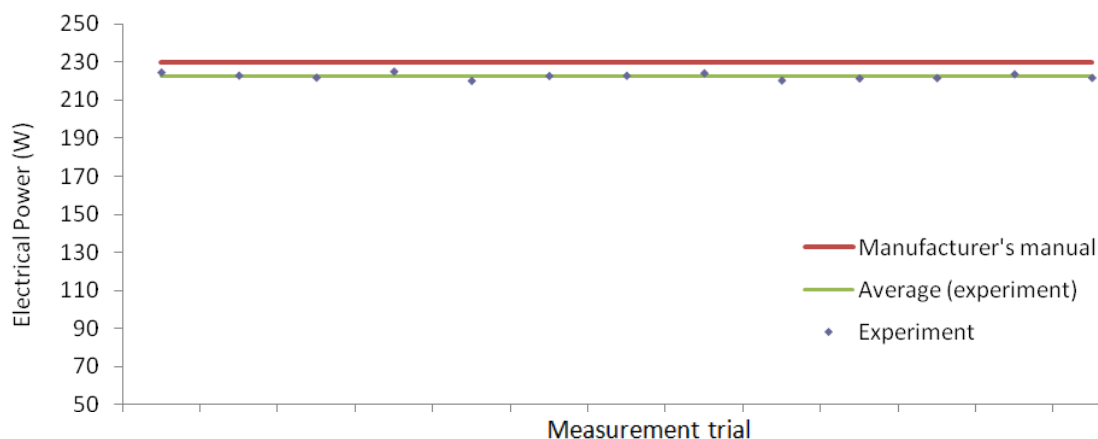


Figure A- 99. 500 W BSC PEM fuel cell power measurements at 10 A; Operating temperature ~60 °C, exit air 30 kPa, air stoichiometry 4, inlet hydrogen ~20-30 kPa

10 A/230 W operating point/ Cooling load measurement

- Operating temperature 60 °C, exit air 30 kPa, air stoichiometry 4, inlet hydrogen ~20-30 kPa
- Theoretically estimated cooling load at the ideal operating condition recommended by the manufacturer: 161.59 W

Note:

- The estimated cooling load at the experimental operating condition (the following table) is found by considering: fuel cell heat used for water evaporation, heat removal by the extra reactants, the convection heat transfer from the body of the fuel cell, and the power drop compared to the ideal condition

Fuel cell inlet water temperature (°C)	Fuel cell exit water temperature (°C)	Water flow rate (litre/min)	Measured cooling load (W)	Estimated cooling load (W)	Experimental error (%)	Estimated uncertainty (%)	CHP energy efficiency (%)
58.6	60.8	0.791	121.23	124.09	-2.36	±12.30	68.77
58.4	60.7	0.779	124.82	125.69	-8.71	±11.77	70.50
58.3	60.7	0.728	121.72	126.79	-12.38	±11.78	69.43
58.4	60.8	0.796	133.09	123.59	-0.37	±26.66	72.01
58.2	60.7	0.729	126.97	128.49	-9.08	±25.56	70.09
58.4	60.8	0.747	124.90	125.89	-8.80	±26.66	70.31
58.5	60.8	0.814	130.43	125.79	-3.50	±27.82	71.90
58.6	60.8	0.732	112.19	124.49	-22.01	±29.09	67.51
58.6	60.9	0.745	119.37	128.29	-15.85	±27.87	68.98
58.6	61	0.741	123.90	127.19	-10.73	±26.75	69.93
58.6	61.2	0.718	130.05	126.99	-5.33	±24.77	71.24
58.7	61.1	0.711	118.88	124.99	-14.23	±26.79	69.16
58.5	61	0.729	126.97	126.89	-5.92	±25.68	70.32

Table A- 24. 500 W BSC PEM fuel cell cooling load measurements at 10 A; Operating temperature ~60 °C, exit air 30 kPa, air stoichiometry 4, inlet hydrogen ~20-30 kPa

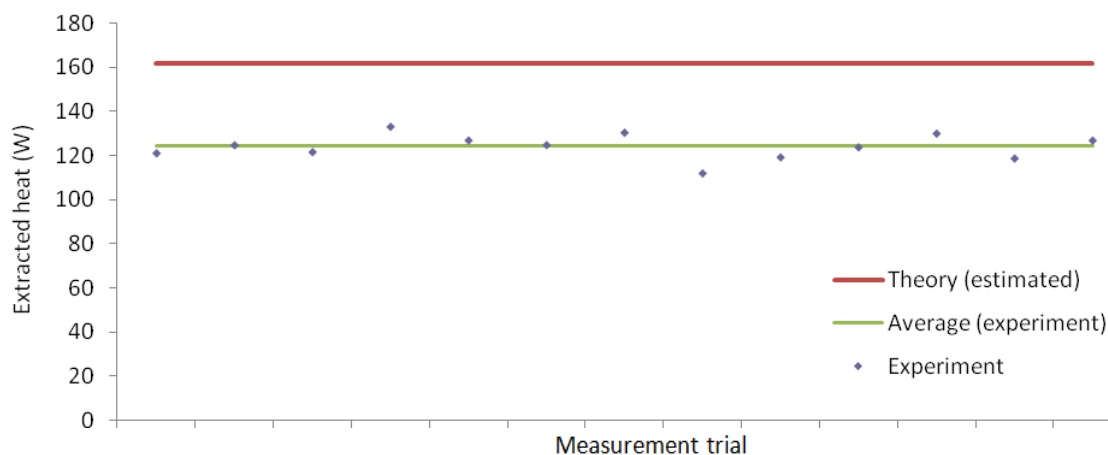


Figure A- 100. 500 W BSC PEM fuel cell cooling load measurements at 10 A; Operating temperature ~60 °C, exit air 30 kPa, air stoichiometry 4, inlet hydrogen ~20-30 kPa

15 A/330 W operating point/ Power measurement

- Operating temperature 40 °C, exit air 30 kPa, air stoichiometry 2, inlet hydrogen ~20-30 kPa
- Theoretical hydrogen consumption if fuel cell hydrogen utilisation coefficient is 100% ideally: 3.67 slpm
- Assumed hydrogen consumption rate for the theoretical calculations: 4.4 slpm (based on 20% extra hydrogen fed into the fuel cell)
- Expected power (manufacturer manual): 330 W
- Maximum uncertainty associated with the measurement instrument for voltage readings when the error for current adjustment (15 A) is taken into account: 0.6%
- Maximum uncertainty associated with hydrogen flow meter: 1%
- Energy efficiency assumed for the theoretical calculation: 38.74%
- Hydrogen utilisation coefficient assumed in the theoretical calculations: ~85%

Voltage (V)	% of uncertainty for the voltage measurement	Power output (W)	Hydrogen consumption (slpm)	% of uncertainty for the hydrogen consumption measurement	Hydrogen utilisation coefficient (%)	Electrical energy efficiency (%)
17.89	±0.24	268.35	3.849	±0.22	95.35	36.02
17.51	±0.24	262.65	3.826	±0.22	95.92	35.46
17.58	±0.24	263.7	3.782	±0.23	97.04	36.02
17.66	±0.24	264.9	3.777	±0.23	97.17	36.23
17.54	±0.24	263.1	3.836	±0.22	95.67	35.43
17.62	±0.24	264.3	3.838	±0.22	95.62	35.58
17.77	±0.24	266.55	3.767	±0.23	97.43	36.55
17.84	±0.24	267.6	3.841	±0.22	95.55	35.99
17.98	±0.23	269.7	3.788	±0.23	96.88	36.78
17.84	±0.24	267.6	3.851	±0.22	95.30	35.90
17.92	±0.24	268.8	3.842	±0.22	95.52	36.14
17.78	±0.24	266.7	3.835	±0.22	95.70	35.93
17.81	±0.24	267.15	3.849	±0.22	95.35	35.86

Table A- 25. 500 W BSC PEM fuel cell power and hydrogen consumption measurement at 10 A; Operating temperature ~40 °C, exit air 30 kPa, air stoichiometry 2, inlet hydrogen ~20-30 kPa

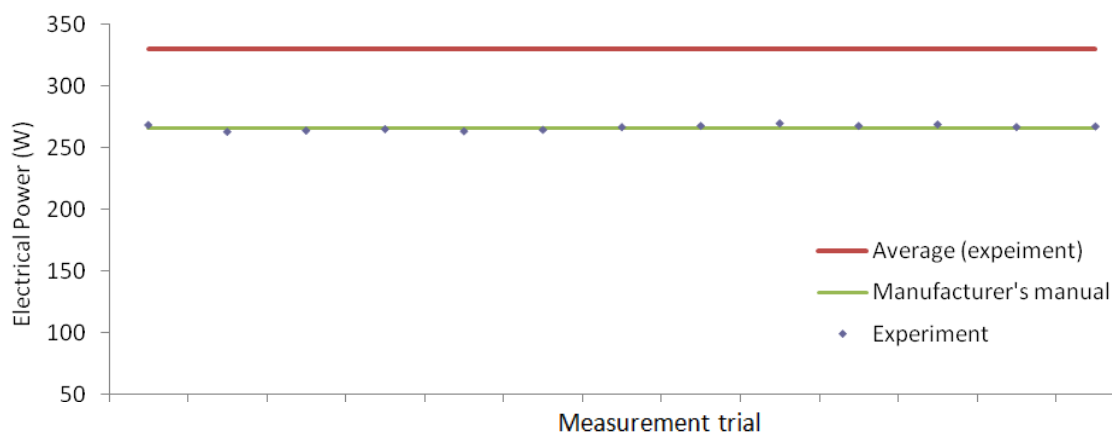


Figure A- 101. 500 W BSC PEM fuel cell power measurements at 15 A; Operating temperature ~40 °C, exit air 30 kPa, air stoichiometry 2, inlet hydrogen ~20-30 kPa

15 A/330 W operating point/ Cooling load measurement

- Operating temperature 40 °C, exit air 30 kPa, air stoichiometry 2, inlet hydrogen ~20-30 kPa
- Theoretically estimated cooling load at the ideal operating condition recommended by the manufacturer: 257.39 W

Note:

- The estimated cooling load at the experimental operating condition (the following table) is found by considering: fuel cell heat used for water evaporation, heat removal by the extra reactants, the convection heat transfer from the body of the fuel cell, and the power drop compared to the ideal condition

Fuel cell inlet water temperature (°C)	Fuel cell exit water temperature (°C)	Water flow rate (litre/min)	Measured cooling load (W)	Estimated cooling load (W)	Experimental error (%)	Estimated uncertainty (%)	CHP energy efficiency (%)
35.2	40.8	1.011	394.42	416.04	-5.48	±4.24	88.96
35.1	41.1	1.028	429.70	421.74	1.85	±3.98	93.49
35.8	41.5	1.055	418.94	420.69	-0.42	±4.20	93.25
35.4	41.2	1.005	406.09	419.49	-3.30	±4.12	91.78
35.1	41	0.987	405.69	421.29	-3.85	±4.04	90.07
35.2	41.2	1.002	418.84	420.09	-0.30	±3.99	91.95
34.8	40.9	0.887	376.95	417.84	-10.85	±3.91	88.25
34.8	40.8	0.986	412.15	416.79	-1.13	±3.97	91.43
34.7	40.9	0.933	402.99	414.69	-2.90	±3.85	91.74
35.1	41.3	0.911	393.49	416.79	-5.92	±3.87	88.69
35	40.5	1.013	388.15	415.59	-7.07	±4.31	88.34
35	40.5	1.038	397.73	417.69	-5.02	±4.31	89.50
34.7	40.4	1.037	411.79	417.24	-1.32	±4.16	91.13

Table A- 26. 500 W BSC PEM fuel cell cooling load measurements at 15 A; Operating temperature ~40 °C, exit air 30 kPa, air stoichiometry 2, inlet hydrogen ~20-30 kPa

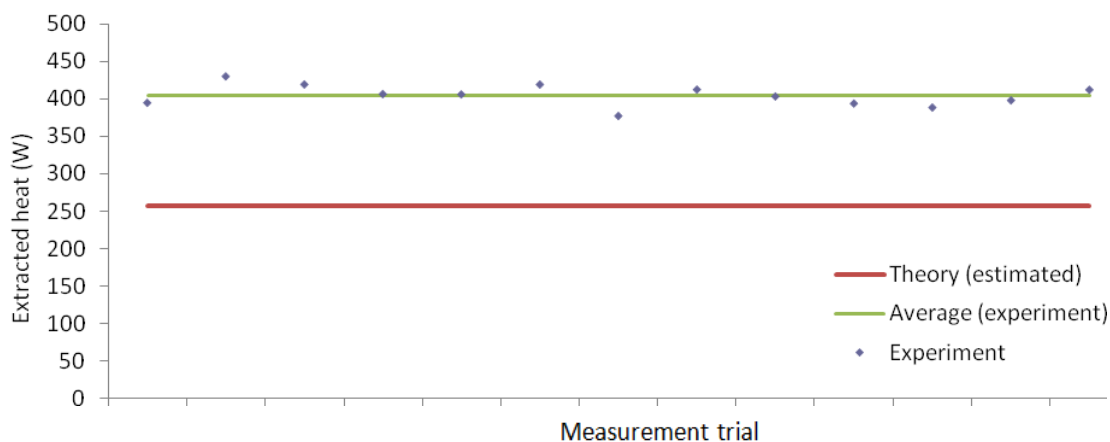


Figure A- 102. 500 W BSC PEM fuel cell cooling load measurements at 15 A; Operating temperature ~40 °C, exit air 30 kPa, air stoichiometry 2, inlet hydrogen ~20-30 kPa

15 A/330 W operating point/ Power measurement

- Operating temperature 40 °C, exit air 30 kPa, air stoichiometry 4, inlet hydrogen ~20-30 kPa
- Theoretical hydrogen consumption if fuel cell hydrogen utilisation coefficient is 100% ideally: 3.67 slpm
- Assumed hydrogen consumption rate for the theoretical calculations: 4.4 slpm (based on 20% extra hydrogen fed into the fuel cell)
- Expected power (manufacturer manual): 330 W
- Maximum uncertainty associated with the measurement instrument for voltage readings when the error for Current adjustment (15 A) is taken into account: 0.6%
- Maximum uncertainty associated with hydrogen flow meter: 1%
- Energy efficiency assumed for the theoretical calculation:38.74%
- Hydrogen utilisation coefficient assumed in the theoretical calculations: ~85%

Voltage (V)	% of uncertainty for the voltage measurement	Power output (W)	Hydrogen consumption (slpm)	% of uncertainty for the hydrogen consumption measurement	Hydrogen utilisation coefficient (%)	Electrical energy efficiency (%)
19.94	±0.30	299.1	3.691	±0.26	99.43	41.86
19.53	±0.31	292.95	3.761	±0.26	97.58	40.24
19.58	±0.31	293.7	3.768	±0.26	97.40	40.27
19.7	±0.30	295.5	3.754	±0.26	97.76	40.67
19.79	±0.30	296.85	3.782	±0.26	97.04	40.55
19.43	±0.31	291.45	3.76	±0.26	97.61	40.04
19.67	±0.30	295.05	3.693	±0.26	99.38	41.27
19.88	±0.30	298.2	3.748	±0.26	97.92	41.10
19.59	±0.31	293.85	3.766	±0.26	97.45	40.31
20.01	±0.30	300.15	3.753	±0.26	97.79	41.32

Table A- 27. 500 W BSC PEM fuel cell power and hydrogen consumption measurement at 15 A; Operating temperature ~40 °C, exit air 30 kPa, air stoichiometry 4, inlet hydrogen ~20-30 kPa

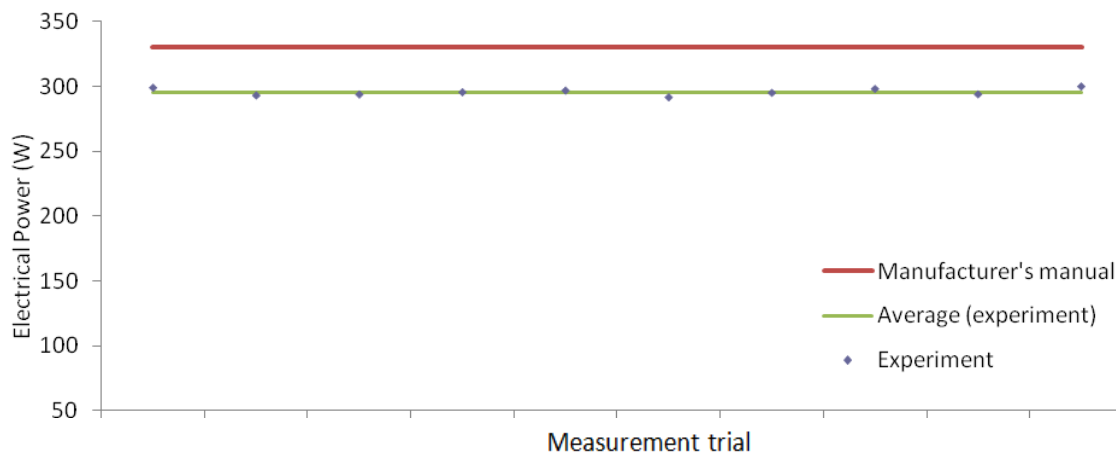


Figure A- 103. 500 W BSC PEM fuel cell power measurements at 15 A; Operating temperature ~40 °C, exit air 30 kPa, air stoichiometry 4, inlet hydrogen ~20-30 kPa

15 A/330 W operating point/ Cooling load measurement

- Operating temperature 40 °C, exit air 30 kPa, air stoichiometry 4, inlet hydrogen ~20-30 kPa
- Theoretically estimated cooling load at the ideal operating condition recommended by the manufacturer: 257.39 W

Note:

- The estimated cooling load at the experimental operating condition (the following table) is found by considering: fuel cell heat used for water evaporation, heat removal by the extra reactants, the convection heat transfer from the body of the fuel cell, and the power drop compared to the ideal condition

Fuel cell inlet water temperature (°C)	Fuel cell exit water temperature (°C)	Water flow rate (litre/min)	Measured cooling load (W)	Estimated cooling load (W)	Experimental error (%)	Estimated uncertainty (%)	CHP energy efficiency (%)
36.5	40.3	1.386	369.30	372.29	-1.46	±6.18	93.22
36.8	40.2	1.498	365.26	378.44	-6.66	±6.90	88.98
36.9	40.5	1.569	382.57	377.69	4.02	±6.54	94.22
36.9	40.3	1.591	365.77	375.89	0.26	±6.91	92.53
36.8	40.5	1.562	380.87	374.54	6.98	±6.36	95.55
36.8	40.4	1.517	380.46	379.94	0.14	±6.53	92.32
36.8	40.5	1.524	392.84	376.34	4.20	±6.36	96.23
36.6	40.1	1.534	374.04	373.19	0.23	±6.70	92.66
36.7	40.1	1.548	377.45	377.54	-2.96	±6.89	90.61
36.9	40.5	1.522	381.72	371.24	2.74	±6.54	93.86

Table A- 28. 500 W BSC PEM fuel cell cooling load measurements at 15 A; Operating temperature ~40 °C, exit air 30 kPa, air stoichiometry 4, inlet hydrogen ~20-30 kPa

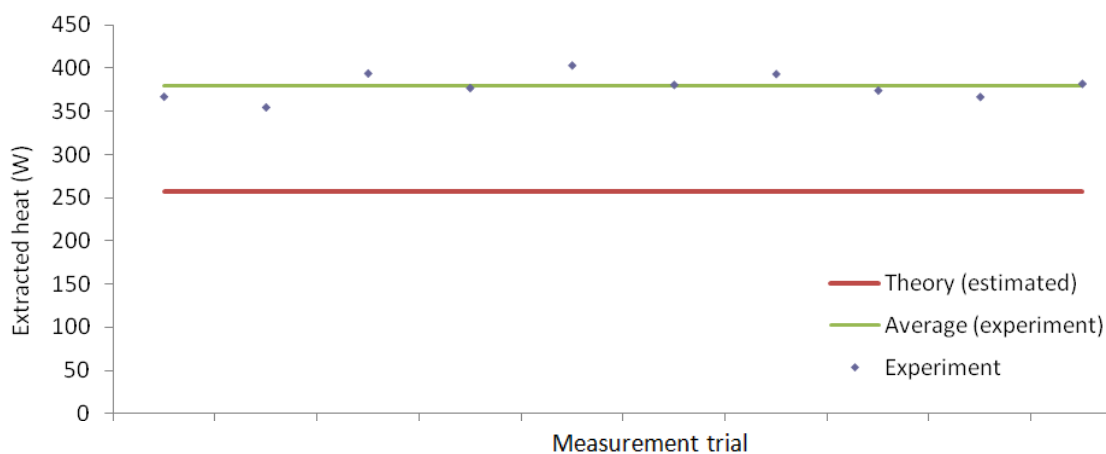


Figure A- 104. 500 W BSC PEM fuel cell cooling load measurements at 15 A; Operating temperature ~40 °C, exit air 30 kPa, air stoichiometry 4, inlet hydrogen ~20-30 kPa

15 A/330 W operating point/ Power measurement

- Operating temperature 50 °C, exit air 30 kPa, air stoichiometry 2, inlet hydrogen ~20-30 kPa
- Theoretical hydrogen consumption if fuel cell hydrogen utilisation coefficient is 100% ideally: 3.67 slpm
- Assumed hydrogen consumption rate for the theoretical calculations: 4.4 slpm (based on 20% extra hydrogen fed into the fuel cell)
- Expected power (manufacturer manual): 330 W
- Maximum uncertainty associated with the measurement instrument for voltage readings when the error for Current adjustment (15 A) is taken into account: 0.6%
- Maximum uncertainty associated with hydrogen flow meter: 1%
- Energy efficiency assumed for the theoretical calculation: 38.74%
- Hydrogen utilisation coefficient assumed in the theoretical calculations: ~85%

Voltage (V)	% of uncertainty for the voltage measurement	Power output (W)	Hydrogen consumption (slpm)	% of uncertainty for the hydrogen consumption measurement	Hydrogen utilisation coefficient (%)	Electrical energy efficiency (%)
19.97	±0.30	299.55	3.79	±0.22	96.83	40.83
19.46	±0.31	291.9	3.712	±0.22	98.87	40.62
19.49	±0.31	292.35	3.755	±0.22	97.74	40.22
19.66	±0.31	294.9	3.743	±0.22	98.05	40.70
19.39	±0.31	290.85	3.759	±0.22	97.63	39.97
19.85	±0.30	297.75	3.774	±0.22	97.24	40.76
19.48	±0.31	292.2	3.77	±0.22	97.35	40.04
19.44	±0.31	291.6	3.729	±0.22	98.42	40.40
19.58	±0.31	293.7	3.742	±0.22	98.08	40.55
19.69	±0.31	295.35	3.792	±0.22	96.78	40.24

Table A- 29. 500 W BSC PEM fuel cell power and hydrogen consumption measurement at 15 A; Operating temperature ~50 °C, exit air 30 kPa, air stoichiometry 2, inlet hydrogen ~20-30 kPa

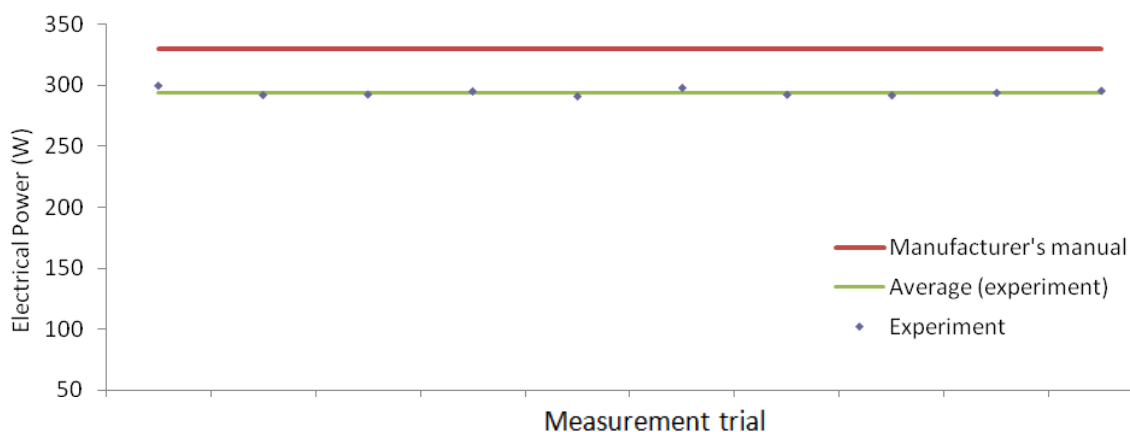


Figure A- 105. 500 W BSC PEM fuel cell power measurements at 15 A; Operating temperature ~50 °C, exit air 30 kPa, air stoichiometry 2, inlet hydrogen ~20-30 kPa

15 A/330 W operating point/ Cooling load measurement

- Operating temperature 50 °C, exit air 30 kPa, air stoichiometry 2, inlet hydrogen ~20-30 kPa
- Theoretically estimated cooling load at the ideal operating condition recommended by the manufacturer: 257.39 W

Note:

- The estimated cooling load at the experimental operating condition (the following table) is found by considering: fuel cell heat used for water evaporation, heat removal by the extra reactants, the convection heat transfer from the body of the fuel cell, and the power drop compared to the ideal condition

Fuel cell inlet water temperature (°C)	Fuel cell exit water temperature (°C)	Water flow rate (litre/min)	Measured cooling load (W)	Estimated cooling load (W)	Experimental error (%)	Estimated uncertainty (%)	CHP energy efficiency (%)
47.3	52.1	1.112	371.85	374.84	-0.80	±5.48	91.52
47.6	52.2	1.136	364.05	382.49	-5.07	±5.72	91.29
47.7	52.1	1.123	344.24	382.04	-10.98	±5.97	87.58
47.5	52.4	1.122	383.01	379.49	0.92	±5.38	93.57
47.3	52.3	1.145	398.84	383.54	3.84	±5.27	94.79
47.5	52	1.158	363.03	376.64	-3.75	±5.84	90.45
47.4	52.2	1.114	372.52	382.19	-2.60	±5.48	91.09
47.6	52.4	1.098	367.17	382.79	-4.25	±5.49	91.27
47.7	52.4	1.198	392.27	380.69	2.95	±5.61	94.70
47.6	52.1	1.149	360.21	379.04	-5.23	±5.84	89.31

Table A- 30. 500 W BSC PEM fuel cell cooling load measurements at 15 A; Operating temperature ~50 °C, exit air 30 kPa, air stoichiometry 2, inlet hydrogen ~20-30 kPa

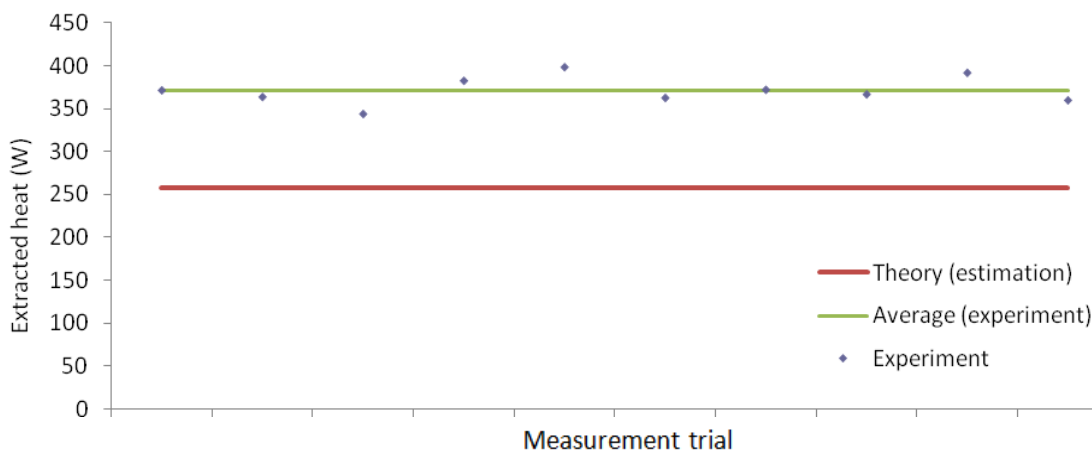


Figure A- 106. 500 W BSC PEM fuel cell cooling load measurements at 15 A; Operating temperature ~50 °C, exit air 30 kPa, air stoichiometry 2, inlet hydrogen ~20-30 kPa

15 A/330 W operating point/ Power measurement

- Operating temperature 50 °C, exit air 30 kPa, air stoichiometry 4, inlet hydrogen ~20-30 kPa
- Theoretical hydrogen consumption if fuel cell hydrogen utilisation coefficient is 100% ideally: 3.67 slpm
- Assumed hydrogen consumption rate for the theoretical calculations: 4.4 slpm (based on 20% extra hydrogen fed into the fuel cell)
- Expected power (manufacturer manual): 330 W
- Maximum uncertainty associated with the measurement instrument for voltage readings when the error for Current adjustment (15 A) is taken into account: 0.6%
- Maximum uncertainty associated with hydrogen flow meter: 1%
- Energy efficiency assumed for the theoretical calculation:38.74%
- Hydrogen utilisation coefficient assumed in the theoretical calculations: ~85%

Voltage (V)	% of uncertainty for the voltage measurement	Power output (W)	Hydrogen consumption (slpm)	% of uncertainty for the hydrogen consumption measurement	Hydrogen utilisation coefficient (%)	Electrical energy efficiency (%)
21.47	±0.28	322.05	3.761	±0.22	97.58	76.94
20.96	±0.29	314.4	3.713	±0.23	98.84	75.50
21.08	±0.28	316.2	3.757	±0.22	97.68	74.68
21.05	±0.28	315.75	3.727	±0.23	98.47	73.89
21.41	±0.28	321.15	3.781	±0.22	97.06	76.17
20.88	±0.29	313.2	3.781	±0.22	97.06	76.24
21.25	±0.28	318.75	3.779	±0.22	97.12	73.41
20.82	±0.29	312.3	3.799	±0.22	96.60	72.31
20.91	±0.29	313.65	3.794	±0.22	96.73	76.68
20.79	±0.29	311.85	3.792	±0.22	96.78	73.94
21.19	±0.28	317.85	3.785	±0.22	96.96	74.57
20.97	±0.29	314.55	3.711	±0.23	98.90	75.21
21.17	±0.28	317.55	3.764	±0.22	97.50	75.44

Table A- 31. 500 W BSC PEM fuel cell power and hydrogen consumption measurement at 15 A; Operating temperature ~50 °C, exit air 30 kPa, air stoichiometry 4, inlet hydrogen ~20-30 kPa

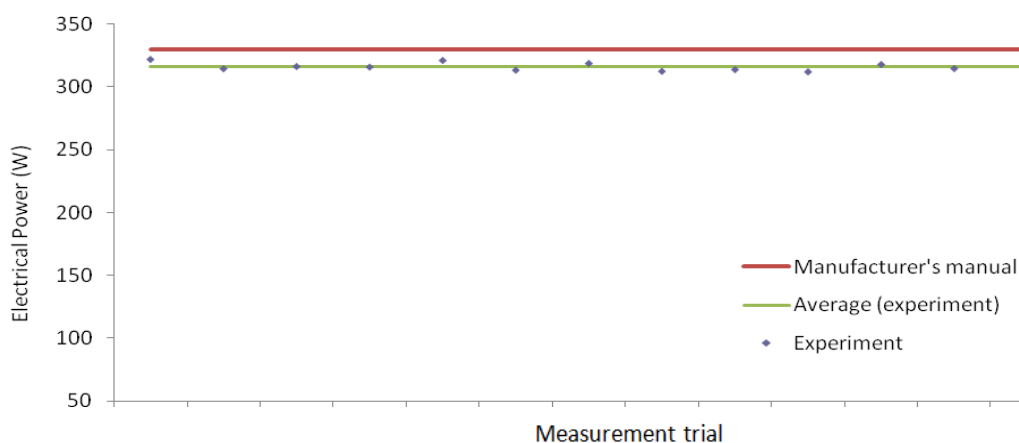


Figure A- 107. 500 W BSC PEM fuel cell power measurements at 15 A; Operating temperature ~50 °C, exit air 30 kPa, air stoichiometry 4, inlet hydrogen ~20-30 kPa

15 A/330 W operating point/ Cooling load measurement

- Operating temperature 50 °C, exit air 30 kPa, air stoichiometry 4, inlet hydrogen ~20-30 kPa
- Theoretically estimated cooling load at the ideal operating condition recommended by the manufacturer: 257.39 W

Note:

- The estimated cooling load at the experimental operating condition (the following table) is found by considering: fuel cell heat used for water evaporation, heat removal by the extra reactants, the convection heat transfer from the body of the fuel cell, and the power drop compared to the ideal condition

Fuel cell inlet water temperature (°C)	Fuel cell exit water temperature (°C)	Water flow rate (litre/min)	Measured cooling load (W)	Estimated cooling load (W)	Experimental error (%)	Estimated uncertainty (%)	CHP energy efficiency (%)
47.9	51.3	1.005	238.05	227.34	4.50	±7.66	76.94
48.2	51.2	1.092	228.23	234.99	-2.96	±8.68	75.50
48.2	51.5	0.987	226.91	233.19	-2.77	±7.91	74.68
48.3	51.1	1.114	217.30	233.64	-7.52	±9.29	73.89
48.4	51.7	1.028	236.34	228.24	3.43	±7.92	76.17
48	51.5	1.004	244.81	236.19	3.52	±7.46	76.24
47.9	50.7	1.119	218.28	230.64	-5.66	±9.26	73.41
48.3	51.1	1.125	219.45	237.09	-8.04	±8.98	72.31
48.5	51.7	1.119	249.46	235.74	-4.45	±9.27	76.68
48.4	51.5	1.069	230.87	237.54	-2.34	±9.60	73.94
48.3	51.2	1.131	228.50	231.54	-1.33	±9.29	74.57
48.1	50.9	1.157	225.69	234.84	5.86	±8.17	75.21
48	50.7	1.234	232.12	231.84	-0.42	±8.42	75.44

Table A- 32. 500 W BCS PEM fuel cell cooling load measurements at 15 A; Operating temperature ~50 °C, exit air 30 kPa, air stoichiometry 4, inlet hydrogen ~20-30 kPa

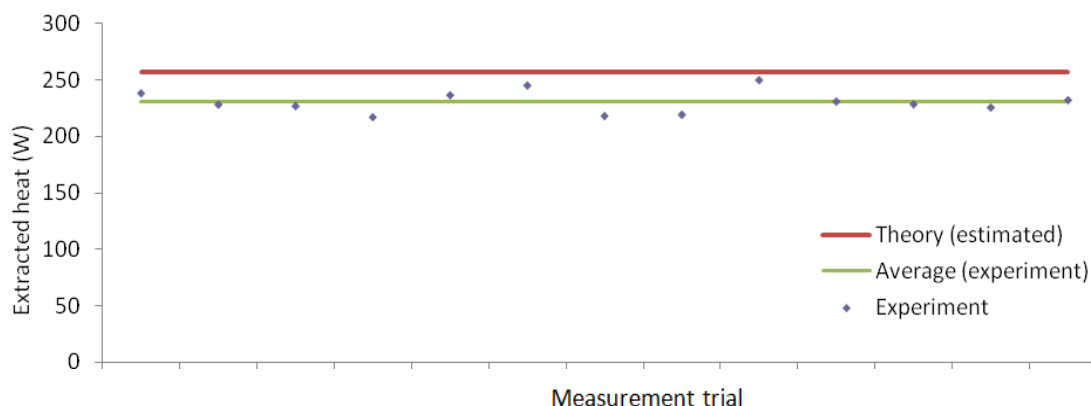


Figure A- 108. 500 W BCS PEM fuel cell cooling load measurements at 15 A; Operating temperature ~50 °C, exit air 30 kPa, air stoichiometry 4, inlet hydrogen ~20-30 kPa

15 A/330 W operating point/ Power measurement

- Operating temperature 60 °C, exit air 30 kPa, air stoichiometry 2, inlet hydrogen ~20-30 kPa
- Theoretical hydrogen consumption if fuel cell hydrogen utilisation coefficient is 100% ideally: 3.67 slpm
- Assumed hydrogen consumption rate for the theoretical calculations: 4.4 slpm (based on 20% extra hydrogen fed into the fuel cell)
- Expected power (manufacturer manual): 330 W
- Maximum uncertainty associated with the measurement instrument for voltage readings when the error for Current adjustment (15 A) is taken into account: 0.6%
- Maximum uncertainty associated with hydrogen flow meter: 1%
- Energy efficiency assumed for the theoretical calculation:38.74%
- Hydrogen utilisation coefficient assumed in the theoretical calculations: ~85%

Voltage (V)	% of uncertainty for the voltage measurement	Power output (W)	Hydrogen consumption (slpm)	% of uncertainty for the hydrogen consumption measurement	Hydrogen utilisation coefficient (%)	Electrical energy efficiency (%)
20.59	±0.41	308.85	3.849	±0.34	95.35	41.45
20.91	±0.40	313.65	3.812	±0.34	96.27	42.51
20.74	±0.41	311.1	3.861	±0.34	95.05	41.63
20.98	±0.40	314.7	3.791	±0.34	96.81	42.89
21.19	±0.40	317.85	3.752	±0.35	97.81	43.76
20.82	±0.41	312.3	3.794	±0.34	96.73	42.52
20.4	±0.41	306	3.846	±0.34	95.42	41.10
21.17	±0.40	317.55	3.855	±0.34	95.20	42.56
21.21	±0.40	318.15	3.762	±0.34	97.55	43.69
20.83	±0.40	312.45	3.773	±0.34	97.27	42.78

Table A- 33. 500 W BSC PEM fuel cell power and hydrogen consumption measurement at 15 A; Operating temperature ~60 °C, exit air 30 kPa, air stoichiometry 2, inlet hydrogen ~20-30 kPa

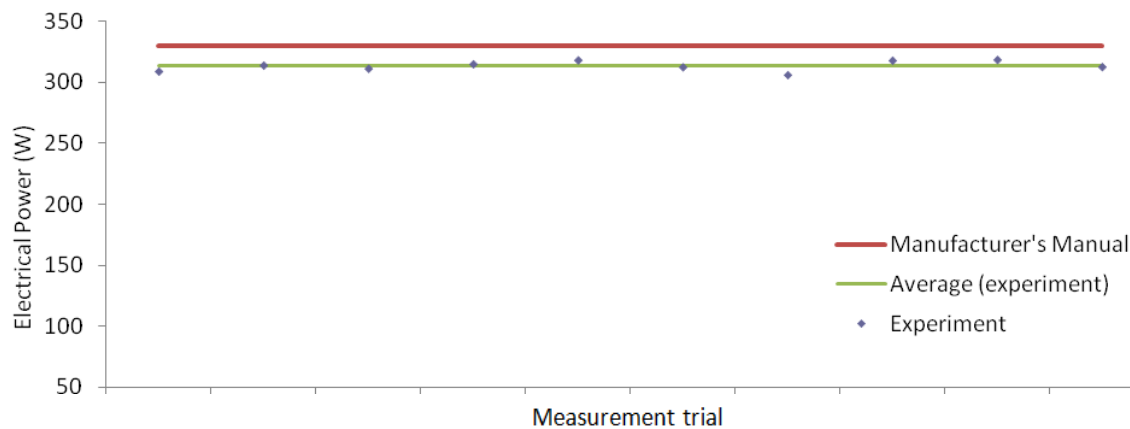


Figure A- 109. 500 W BSC PEM fuel cell power measurements at 15 A; Operating temperature ~60 °C, exit air 30 kPa, air stoichiometry 2, inlet hydrogen ~20-30 kPa

15 A/330 W operating point/ Cooling load measurement

- Operating temperature 60 °C, exit air 30 kPa, air stoichiometry 2, inlet hydrogen ~20-30 kPa
- Theoretically estimated cooling load at the ideal operating condition recommended by the manufacturer: 257.39 W

Note:

- The estimated cooling load at the experimental operating condition (the following table) is found by considering: fuel cell heat used for water evaporation, heat removal by the extra reactants, the convection heat transfer from the body of the fuel cell, and the power drop compared to the ideal condition

Fuel cell inlet water temperature (°C)	Fuel cell exit water temperature (°C)	Water flow rate (litre/min)	Measured cooling load (W)	Estimated cooling load (W)	Experimental error (%)	Estimated uncertainty (%)	CHP energy efficiency (%)
59.1	62	1.307	264.06	243.54	7.77	±9.85	76.90
58.9	61.8	1.208	244.06	238.74	2.18	±9.83	75.58
59	61.9	1.199	242.24	241.29	0.39	±9.84	74.04
58.7	61.8	1.081	233.46	237.69	-1.81	±9.20	74.70
59	61.9	1.051	212.34	234.54	-10.46	±9.84	73.00
59.2	62.4	1.134	252.81	240.09	5.03	±8.95	76.95
58.9	62.2	1.084	249.21	246.39	1.13	±8.67	74.58
59	62.1	1.113	240.37	234.84	2.30	±9.22	74.77
58.6	62	1.076	254.87	234.24	8.09	±8.40	78.69
58.7	61.9	1.009	224.94	239.94	-6.67	±8.92	73.58

Table A- 34. 500 W BSC PEM fuel cell cooling load measurements at 15 A; Operating temperature ~60 °C, exit air 30 kPa, air stoichiometry 2, inlet hydrogen ~20-30 kPa

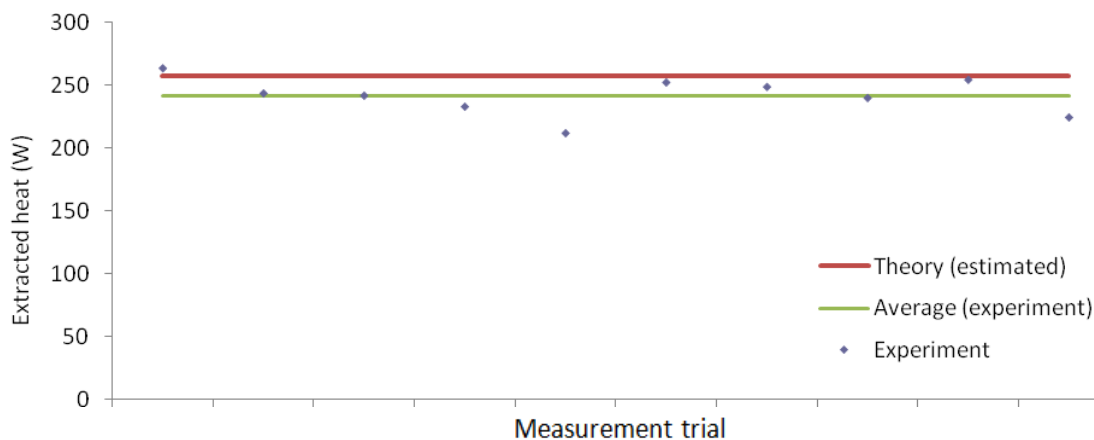


Figure A- 110. 500 W BSC PEM fuel cell cooling load measurements at 15 A; Operating temperature ~60 °C, exit air 30 kPa, air stoichiometry 2, inlet hydrogen ~20-30 kPa

15 A/330 W operating point/ Power measurement

- Operating temperature 60 °C, exit air 30 kPa, air stoichiometry 4, inlet hydrogen ~20-30 kPa
- Theoretical hydrogen consumption if fuel cell hydrogen utilisation coefficient is 100% ideally: 3.67 slpm
- Assumed hydrogen consumption rate for the theoretical calculations: 4.4 slpm (based on 20% extra hydrogen fed into the fuel cell)
- Expected power (manufacturer manual): 330 W
- Maximum uncertainty associated with the measurement instrument for voltage readings when the error for Current adjustment (15 A) is taken into account: 0.6%
- Maximum uncertainty associated with hydrogen flow meter: 1%
- Energy efficiency assumed for the theoretical calculation:38.74%
- Hydrogen utilisation coefficient assumed in the theoretical calculations: ~85%

Voltage (V)	% of uncertainty for the voltage measurement	Power output (W)	Hydrogen consumption (slpm)	% of uncertainty for the hydrogen consumption measurement	Hydrogen utilisation coefficient (%)	Electrical energy efficiency (%)
21.34	±0.24	320.1	3.781	±0.18	97.06	43.74
21.44	±0.24	321.6	3.828	±0.17	95.87	43.40
21.49	±0.24	322.35	3.767	±0.18	97.43	44.21
21.07	±0.24	316.05	3.826	±0.17	95.92	42.68
21.19	±0.24	317.85	3.795	±0.18	96.71	43.27
21.38	±0.24	320.7	3.798	±0.18	96.63	43.62
21.39	±0.24	320.85	3.761	±0.18	97.58	44.07
21.46	±0.24	321.9	3.794	±0.18	96.73	43.83
21.59	±0.24	323.85	3.792	±0.18	96.78	44.12
21.15	±0.24	317.25	3.782	±0.18	97.04	43.34
21.19	±0.24	317.85	3.827	±0.17	95.90	42.91
21	±0.24	315	3.822	±0.17	96.02	42.58
21.11	±0.24	316.65	3.829	±0.17	95.85	42.72

Table A- 35. 500 W BSC PEM fuel cell power and hydrogen consumption measurement at 15 A; Operating temperature ~60 °C, exit air 30 kPa, air stoichiometry 4, inlet hydrogen ~20-30 kPa

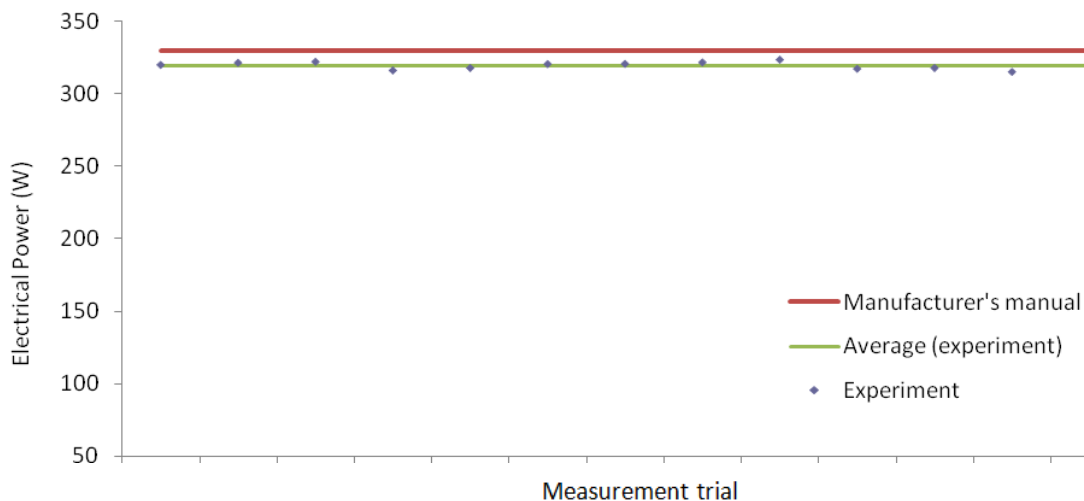


Figure A- 111. 500 W BSC PEM fuel cell power measurements at 15 A; Operating temperature ~60 °C, exit air 30 kPa, air stoichiometry 4, inlet hydrogen ~20-30 kPa

15 A/330 W operating point/ Cooling load measurement

- Operating temperature 60 °C, exit air 30 kPa, air stoichiometry 4, inlet hydrogen ~20-30 kPa
- Theoretically estimated cooling load at the ideal operating condition recommended by the manufacturer: 257.39 W

Note:

- The estimated cooling load at the experimental operating condition (the following table) is found by considering: fuel cell heat used for water evaporation, heat removal by the extra reactants, the convection heat transfer from the body of the fuel cell, and the power drop compared to the ideal condition

Fuel cell inlet water temperature (°C)	Fuel cell exit water temperature (°C)	Water flow rate (litre/min)	Measured cooling load (W)	Estimated cooling load (W)	Experimental error (%)	Estimated uncertainty (%)	CHP energy efficiency (%)
58.1	60.8	1.108	208.41	219.29	-5.22	±10.48	72.21
58.2	61	1.061	206.97	217.79	-5.23	±10.12	71.33
58.3	60.9	1.119	202.69	217.04	-7.08	±10.89	72.00
58	60.9	1.072	216.58	223.34	-3.12	±9.76	71.92
58.4	61	1.083	196.17	221.54	-12.93	±10.90	69.97
58.1	61.1	1.043	217.99	218.69	-0.32	±9.45	73.27
58.3	60.9	1.093	197.98	218.54	-10.39	±10.89	71.27
58.1	61	1.006	203.25	217.49	-7.01	±10.49	71.51
58.1	61.1	1.029	215.06	215.54	-0.22	±10.14	73.42
58.2	61.1	1.015	205.06	222.14	-8.33	±9.78	71.35
58.3	61	1.108	208.41	221.54	-6.30	±9.77	71.04
58.4	61.2	1.113	217.11	224.39	-3.35	±9.45	71.92
58.2	61.1	1.027	207.49	222.74	-7.35	±9.78	70.72

Table A- 36. 500 W BCS PEM fuel cell cooling load measurements at 15 A; Operating temperature ~60 °C, exit air 30 kPa, air stoichiometry 4, inlet hydrogen ~20-30 kPa

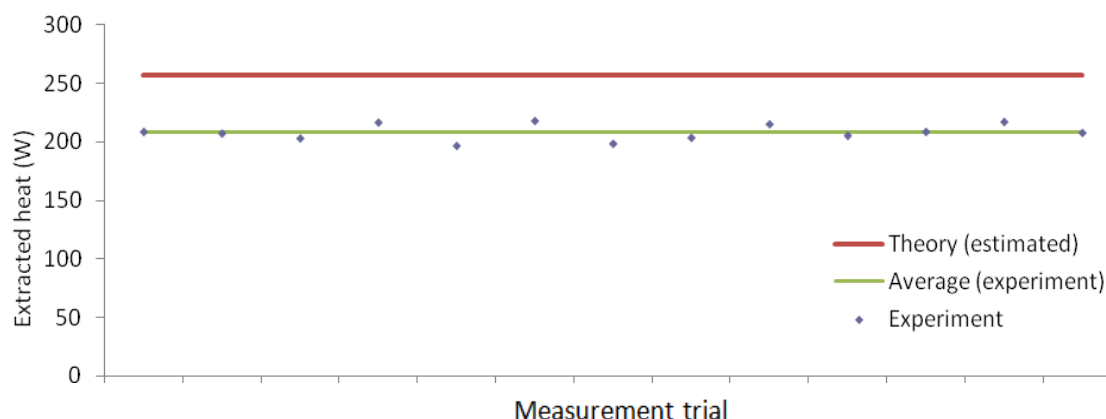


Figure A- 112. 500 W BCS PEM fuel cell cooling load measurements at 15 A; Operating temperature ~60 °C, exit air 30 kPa, air stoichiometry 4, inlet hydrogen ~20-30 kPa

20 A/420 W operating point/ Power measurement

- Operating temperature 40 °C, exit air 30 kPa, air stoichiometry 2, inlet hydrogen ~20-30 kPa
- Theoretical hydrogen consumption if fuel cell hydrogen utilisation coefficient is 100% ideally: 4.89 slpm
- Assumed hydrogen consumption rate for the theoretical calculations: 5.87 slpm (based on 20% extra hydrogen fed into the fuel cell)
- Expected power (manufacturer manual): 420 W
- Maximum uncertainty associated with the measurement instrument for voltage readings when the error for Current adjustment (20 A) is taken into account: 0.6%
- Maximum uncertainty associated with hydrogen flow meter: 1%
- Energy efficiency assumed for the theoretical calculation: 38.24%
- Hydrogen utilisation coefficient assumed in the theoretical calculations: ~85%

Voltage (V)	% of uncertainty for the voltage measurement	Power output (W)	Hydrogen consumption (slpm)	% of uncertainty for the hydrogen consumption measurement	Hydrogen utilisation coefficient (%)	Electrical energy efficiency (%)
17.43	±0.50	348.6	4.93	±0.40	99.19	36.50
16.93	±0.51	338.6	4.96	±0.40	98.59	35.24
16.99	±0.51	339.8	5.13	±0.39	95.32	34.20
16.71	±0.52	334.2	4.94	±0.40	98.99	34.93
16.99	±0.51	339.8	4.93	±0.40	99.19	35.58
16.86	±0.51	337.2	4.98	±0.40	98.19	34.96
17.39	±0.50	347.8	4.99	±0.40	98.00	35.98
17.27	±0.50	345.4	4.96	±0.40	98.59	35.95
16.84	±0.51	336.8	4.97	±0.40	98.39	34.99
16.67	±0.52	333.4	5.09	±0.39	96.07	33.82
16.57	±0.52	331.4	5.03	±0.39	97.22	34.01

Table A- 37. 500 W BSC PEM fuel cell power and hydrogen consumption measurement at 10 A; Operating temperature ~40 °C, exit air 30 kPa, air stoichiometry 2, inlet hydrogen ~20-30 kPa

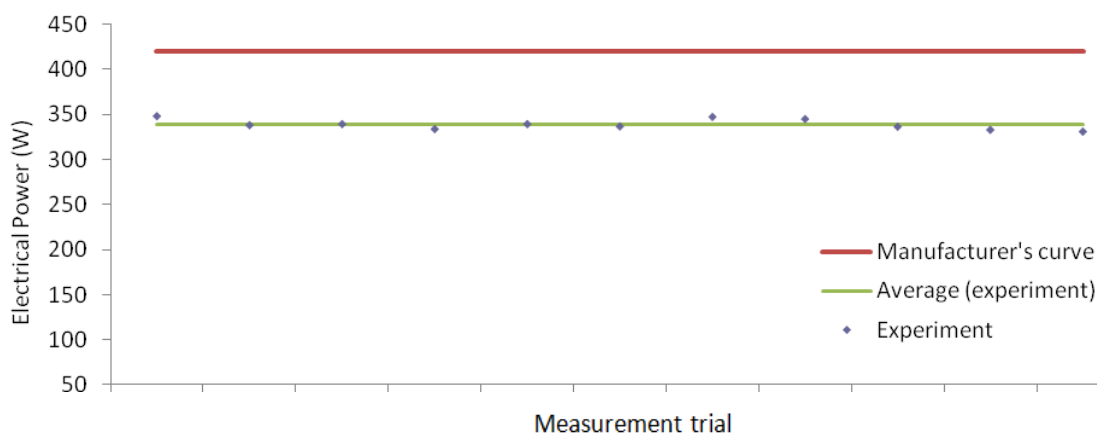


Figure A- 113. 500 W BSC PEM fuel cell power measurements at 20 A; Operating temperature ~40 °C, exit air 30 kPa, air stoichiometry 2, inlet hydrogen ~20-30 kPa

20 A/420 W operating point/ Cooling load measurement

- Operating temperature 40 °C, exit air 30 kPa, air stoichiometry 2, inlet hydrogen ~20-30 kPa
- Theoretically estimated cooling load at the ideal operating condition recommended by the manufacturer: 363.19 W

Note:

- The estimated cooling load at the experimental operating condition (the following table) is found by considering: fuel cell heat used for water evaporation, heat removal by the extra reactants, the convection heat transfer from the body of the fuel cell, and the power drop compared to the ideal condition

Fuel cell inlet water temperature (°C)	Fuel cell exit water temperature (°C)	Water flow rate (litre/min)	Measured cooling load (W)	Estimated cooling load (W)	Experimental error (%)	Estimated uncertainty (%)	CHP energy efficiency (%)
37.8	43.4	1.411	550.48	569.59	-3.47	±4.35	94.15
37.7	43.4	1.501	596.05	579.59	2.76	±4.28	97.28
37.9	43.4	1.458	558.66	578.39	-3.53	±4.43	90.42
38	43.8	1.371	553.98	583.99	-5.42	±4.22	92.82
38.1	43.7	1.386	540.72	578.39	-6.97	±4.36	92.21
38	43.9	1.349	554.48	580.99	-4.78	±4.16	92.44
38.2	44.2	1.383	578.09	570.39	1.33	±4.10	95.79
38.1	43.9	1.375	555.59	572.79	-3.10	±4.23	93.78
38	43.7	1.374	545.62	581.39	-6.56	±4.29	91.66
38.2	43.9	1.395	553.95	584.79	-5.57	±4.30	90.00
38.2	44	1.4	565.69	586.79	-3.73	4.23	92.07

Table A- 38. 500 W BSC PEM fuel cell cooling load measurements at 20 A; Operating temperature ~40 °C, exit air 30 kPa, air stoichiometry 2, inlet hydrogen ~20-30 kPa

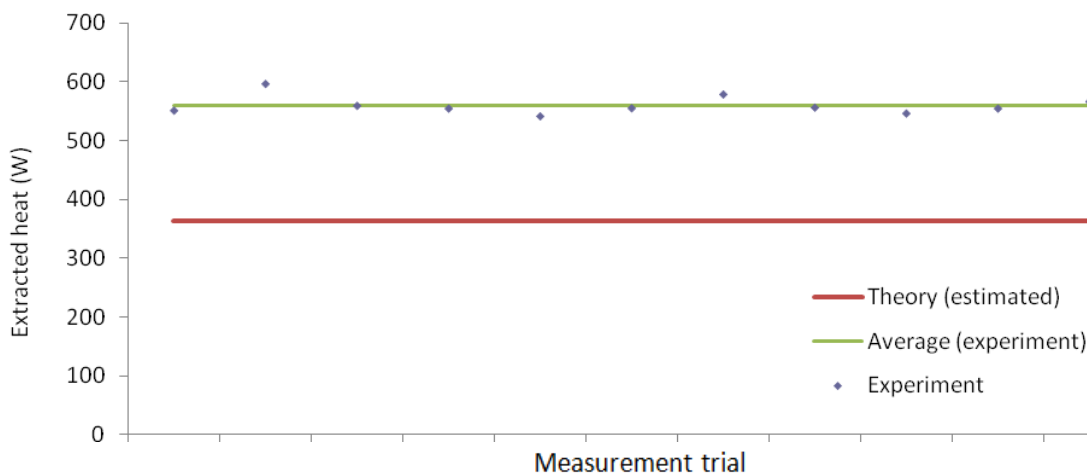


Figure A- 114. 500 W BSC PEM fuel cell cooling load measurements at 20 A; Operating temperature ~40 °C, exit air 30 kPa, air stoichiometry 2, inlet hydrogen ~20-30 kPa

20 A/420 W operating point/ Power measurement

- Operating temperature 50 °C, exit air 30 kPa, air stoichiometry 2, inlet hydrogen ~20-30 kPa
- Theoretical hydrogen consumption if fuel cell hydrogen utilisation coefficient is 100% ideally: 4.89 slpm
- Assumed hydrogen consumption rate for the theoretical calculations: 5.87 slpm (based on 20% extra hydrogen fed into the fuel cell)
- Expected power (manufacturer manual): 420 W
- Maximum uncertainty associated with the measurement instrument for voltage readings when the error for Current adjustment (20 A) is taken into account: 0.6%
- Maximum uncertainty associated with hydrogen flow meter: 1%
- Energy efficiency assumed for the theoretical calculation:38.24%
- Hydrogen utilisation coefficient assumed in the theoretical calculations: ~85%

Voltage (V)	% of uncertainty for the voltage measurement	Power output (W)	Hydrogen consumption (slpm)	% of uncertainty for the hydrogen consumption measurement	Hydrogen utilisation coefficient (%)	Electrical energy efficiency (%)
18.79	±0.24	375.8	4.91	±0.28	99.59	39.51
18.36	±0.25	367.2	4.96	±0.27	98.59	38.22
18.42	±0.25	368.4	4.92	±0.28	99.39	38.66
18.49	±0.25	369.8	4.94	±0.27	98.99	38.65
18.65	±0.25	373	5.09	±0.27	96.07	37.83
18.31	±0.25	366.2	5.01	±0.27	97.60	37.74
18.58	±0.25	371.6	4.96	±0.27	98.59	38.68
18.77	±0.24	375.4	5.02	±0.27	97.41	38.61
18.36	±0.25	367.2	4.99	±0.27	98.00	37.99
18.53	±0.25	370.6	4.98	±0.27	98.19	38.42
18.84	±0.24	376.8	4.99	±0.27	98.00	38.98
18.59	±0.25	371.8	5.04	±0.27	97.02	38.08
18.4	±0.25	368	5.05	±0.27	96.83	37.62
18.47	±0.25	369.4	5.01	±0.27	97.60	38.07

Table A- 39. 500 W BSC PEM fuel cell power and hydrogen consumption measurement at 20 A; Operating temperature ~50 °C, exit air 30 kPa, air stoichiometry 2, inlet hydrogen ~20-30 kPa

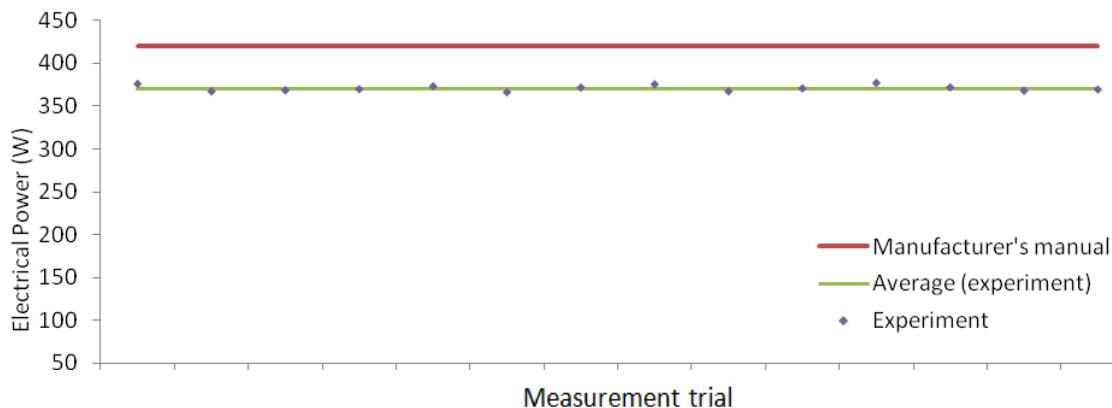


Figure A- 115. 500 W BSC PEM fuel cell power measurements at 20 A; Operating temperature ~50 °C, exit air 30 kPa, air stoichiometry 2, inlet hydrogen ~20-30 kPa

20 A/420 W operating point/ Cooling load measurement

- Operating temperature 50 °C, exit air 30 kPa, air stoichiometry 2, inlet hydrogen ~20-30 kPa
- Theoretically estimated cooling load at the ideal operating condition recommended by the manufacturer: 363.19 W

Note:

- The estimated cooling load at the experimental operating condition (the following table) is found by considering: fuel cell heat used for water evaporation, heat removal by the extra reactants, the convection heat transfer from the body of the fuel cell, and the power drop compared to the ideal condition

Fuel cell inlet water temperature (°C)	Fuel cell exit water temperature (°C)	Water flow rate (litre/min)	Measured cooling load (W)	Estimated cooling load (W)	Experimental error (%)	Estimated uncertainty (%)	CHP energy efficiency (%)
47.1	52.8	1.305	518.22	532.39	-2.74	4.66	94.00
47.2	52.7	1.348	516.51	540.99	-4.74	4.82	91.98
47.2	52.5	1.367	504.74	539.79	-6.94	4.99	91.62
47.3	52.7	1.306	491.32	538.39	-9.58	4.91	89.99
47.4	52.7	1.454	536.87	535.19	0.31	5.00	92.28
47.5	52.9	1.467	551.89	541.99	1.79	4.91	94.60
47.5	53.2	1.374	545.62	536.59	1.65	4.67	95.47
47.7	53.3	1.397	545.02	532.79	2.24	4.76	94.66
47.7	53.3	1.316	513.42	540.99	-5.37	4.76	91.11
47.8	53.6	1.307	528.12	537.59	-1.79	4.61	93.17
47.7	53.4	1.351	536.48	531.39	0.95	4.68	94.49
47.8	53.5	1.302	517.02	536.39	-3.75	4.68	91.04
47.8	53.4	1.308	510.29	540.19	-5.86	4.76	89.79
47.7	53.3	1.282	500.15	538.79	-7.73	4.76	89.60

Table A- 40. 500 W BSC PEM fuel cell cooling load measurements at 20 A; Operating temperature ~50 °C, exit air 30 kPa, air stoichiometry 2, inlet hydrogen ~20-30 kPa

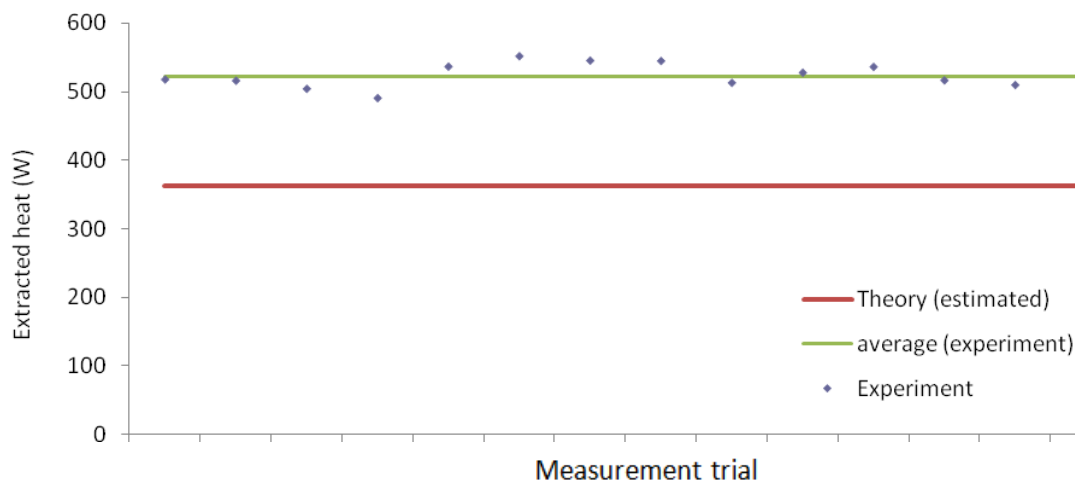


Figure A- 116. 500 W BSC PEM fuel cell cooling load measurements at 20 A; Operating temperature ~50 °C, exit air 30 kPa, air stoichiometry 2, inlet hydrogen ~20-30 kPa

20 A/420 W operating point/ Power measurement

- Operating temperature 60 °C, exit air 30 kPa, air stoichiometry 2, inlet hydrogen ~20-30 kPa
- Theoretical hydrogen consumption if fuel cell hydrogen utilisation coefficient is 100% ideally: 4.89 slpm
- Assumed hydrogen consumption rate for the theoretical calculations: 5.87 slpm (based on 20% extra hydrogen fed into the fuel cell)
- Expected power (manufacturer manual): 420 W
- Maximum uncertainty associated with the measurement instrument for voltage readings when the error for Current adjustment (20 A) is taken into account: 0.6%
- Maximum uncertainty associated with hydrogen flow meter: 1%
- Energy efficiency assumed for the theoretical calculation:38.24%
- Hydrogen utilisation coefficient assumed in the theoretical calculations: ~85%

Voltage (V)	% of uncertainty for the voltage measurement	Power output (W)	Hydrogen consumption (slpm)	% of uncertainty for the hydrogen consumption measurement	Hydrogen utilisation coefficient (%)	Electrical energy efficiency (%)
20.11	±0.43	346.69	4.971	±0.31	98.37	41.77
20.57	±0.42	351.51	4.961	±0.31	98.57	42.81
19.92	±0.43	328.61	5.03	±0.31	97.22	40.89
20.04	±0.43	322.91	5.081	±0.30	96.24	40.72
19.41	±0.44	327.85	5.072	±0.30	96.41	39.51
20.55	±0.42	343.86	4.993	±0.31	97.94	42.50
20.13	±0.43	333.76	4.982	±0.31	98.15	41.72
20.16	±0.43	320.71	5	±0.31	97.80	41.63
20.37	±0.42	355.41	5.09	±0.30	96.07	41.32
20.06	±0.43	330.87	4.968	±0.31	98.43	41.69
19.78	±0.44	336.69	5.112	±0.30	95.66	39.95
19.88	±0.43	326.54	5.102	±0.30	95.84	40.23
20.09	±0.43	344.67	5.003	±0.31	97.74	41.46

Table A- 41. 500 W BSC PEM fuel cell power and hydrogen consumption measurement at 20 A; Operating temperature ~60 °C, exit air 30 kPa, air stoichiometry 2, inlet hydrogen ~20-30 kPa

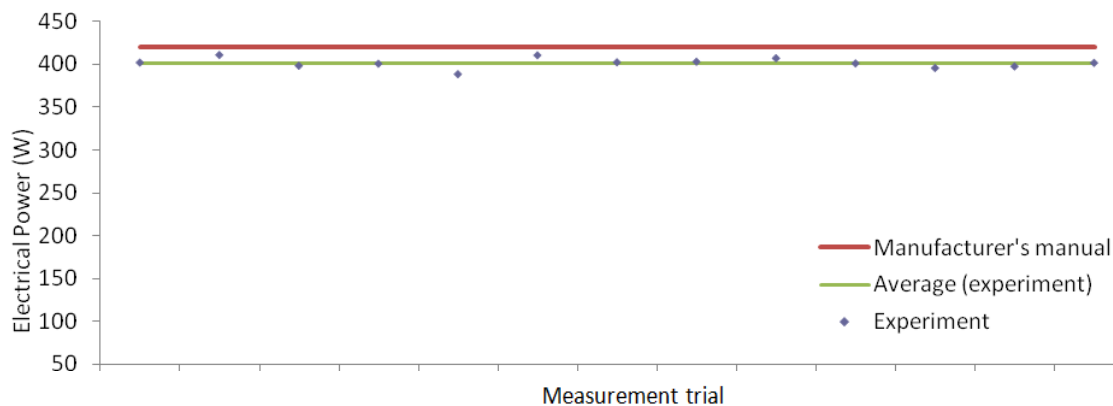


Figure A- 117. 500 W BSC PEM fuel cell power measurements at 20 A; Operating temperature ~60 °C, exit air 30 kPa, air stoichiometry 2, inlet hydrogen ~20-30 kPa

20 A/420 W operating point/ Cooling load measurement

- Operating temperature 60 °C, exit air 30 kPa, air stoichiometry 2, inlet hydrogen ~20-30 kPa
- Theoretically estimated cooling load at the ideal operating condition recommended by the manufacturer: 363.19 W

Note:

- The estimated cooling load at the experimental operating condition (the following table) is found by considering: fuel cell heat used for water evaporation, heat removal by the extra reactants, the convection heat transfer from the body of the fuel cell, and the power drop compared to the ideal condition

Fuel cell inlet water temperature (°C)	Fuel cell exit water temperature (°C)	Water flow rate (litre/min)	Measured cooling load (W)	Estimated cooling load (W)	Experimental error (%)	Estimated uncertainty (%)	CHP energy efficiency (%)
58.6	61.2	1.914	346.69	345.99	0.20	±10.92	77.78
58.5	61.3	1.802	351.51	336.79	4.19	±10.14	79.39
58.5	61.2	1.747	328.61	349.79	-6.45	±10.51	74.62
58.6	61.1	1.854	322.91	347.39	-7.58	±11.34	73.53
58.7	61.3	1.81	327.85	359.99	-9.80	±10.93	72.88
58.5	61.4	1.702	343.86	337.19	1.94	±9.80	78.05
58.4	61.2	1.711	333.76	345.59	-3.54	±10.14	76.31
58.6	61.3	1.705	320.71	344.99	-7.57	±10.52	74.74
58.6	61.4	1.822	355.41	340.79	4.11	±10.15	77.37
58.5	61.2	1.759	330.87	346.99	-4.87	±10.51	76.07
58.4	61.2	1.726	336.69	352.59	-4.72	±10.14	73.95
58.3	61	1.736	326.54	350.59	-7.36	±10.49	73.27
58.3	61.2	1.706	344.67	346.39	-0.50	±9.79	77.03

Table A- 42. 500 W BSC PEM fuel cell cooling load measurements at 20 A; Operating temperature ~60 °C, exit air 30 kPa, air stoichiometry 2, inlet hydrogen ~20-30 kPa

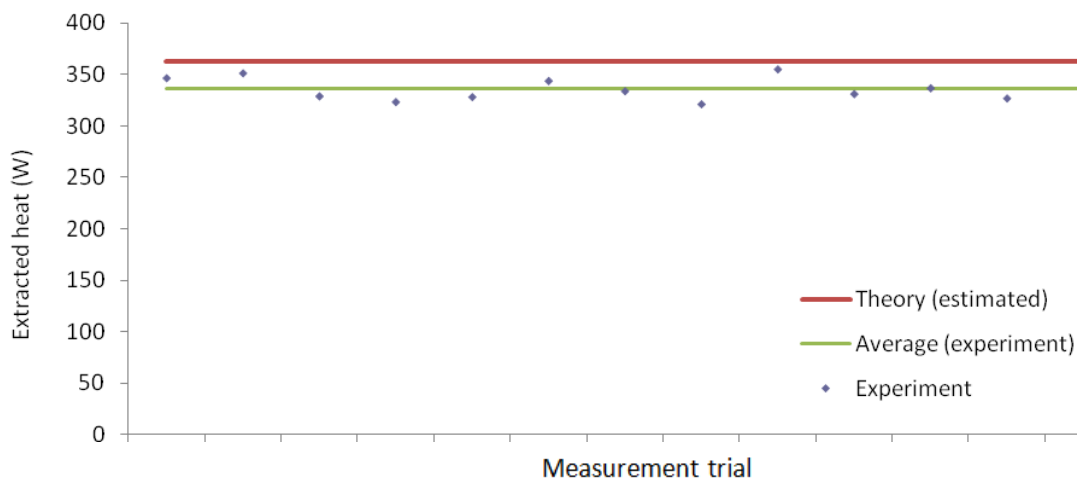


Figure A- 118. 500 W BSC PEM fuel cell cooling load measurements at 20 A; Operating temperature ~60 °C, exit air 30 kPa, air stoichiometry 2, inlet hydrogen ~20-30 kPa

25 A/500 W operating point/ Power measurement

- Operating temperature 40 °C, exit air 30 kPa, air stoichiometry 2, inlet hydrogen ~20-30 kPa
- Theoretical hydrogen consumption if fuel cell hydrogen utilisation coefficient is 100% ideally: 6.11 slpm
- Assumed hydrogen consumption rate for the theoretical calculations: 7.34 slpm (based on 20% extra hydrogen fed into the fuel cell)
- Expected power (manufacturer manual): 500 W
- Maximum uncertainty associated with the measurement instrument for voltage readings when the error for Current adjustment (25 A) is taken into account: 0.6%
- Maximum uncertainty associated with hydrogen flow meter: 1%
- Energy efficiency assumed for the theoretical calculation: 35.15%
- Hydrogen utilisation coefficient assumed in the theoretical calculations: ~85%

Voltage (V)	% of uncertainty for the voltage measurement	Power output (W)	Hydrogen consumption (slpm)	% of uncertainty for the hydrogen consumption measurement	Hydrogen utilisation coefficient (%)	Electrical energy efficiency (%)
16.47	±0.32	411.75	6.18	±0.20	98.87	34.38
16.05	±0.33	401.25	6.27	±0.20	97.45	33.02
16.12	±0.33	403	6.19	±0.20	98.71	33.60
15.93	±0.33	398.25	6.23	±0.20	98.07	32.99
16.28	±0.33	407	6.29	±0.20	97.14	33.39
15.99	±0.33	399.75	6.25	±0.20	97.76	33.01
15.92	±0.33	398	6.17	±0.20	99.03	33.29
16.32	±0.32	408	6.25	±0.20	97.76	33.69
16.28	±0.33	407	6.27	±0.20	97.45	33.50
16.08	±0.33	402	6.22	±0.20	98.23	33.35
16.11	±0.33	402.75	6.19	±0.20	98.71	33.58

Table A- 43. 500 W BSC PEM fuel cell power and hydrogen consumption measurement at 10 A; Operating temperature ~40 °C, exit air 30 kPa, air stoichiometry 2, inlet hydrogen ~20-30 kPa

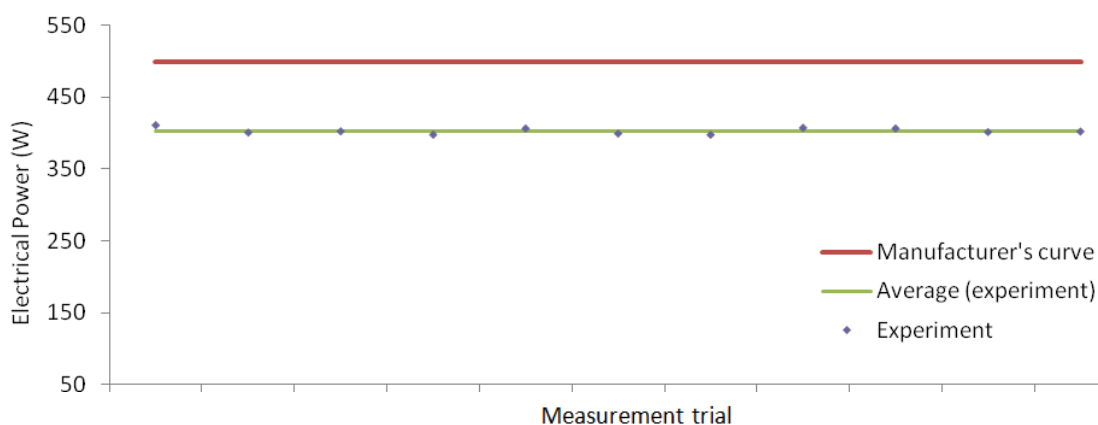


Figure A- 119. 500 W BSC PEM fuel cell power measurements at 25 A; Operating temperature ~40 °C, exit air 30 kPa, air stoichiometry 2, inlet hydrogen ~20-30 kPa

25 A/500 W operating point/ Cooling load measurement

- Operating temperature 40 °C, exit air 30 kPa, air stoichiometry 2, inlet hydrogen ~20-30 kPa
- Theoretically estimated cooling load at the ideal operating condition recommended by the manufacturer: 478W

Note:

- The estimated cooling load at the experimental operating condition (the following table) is found by considering: fuel cell heat used for water evaporation, heat removal by the extra reactants, the convection heat transfer from the body of the fuel cell, and the power drop compared to the ideal condition

Fuel cell inlet water temperature (°C)	Fuel cell exit water temperature (°C)	Water flow rate (litre/min)	Measured cooling load (W)	Estimated cooling load (W)	Experimental error (%)	Estimated uncertainty (%)	CHP energy efficiency (%)
38.1	42.6	2.455	769.64	739.25	3.92	5.35	94.65
38.1	42.9	2.407	804.90	749.75	6.83	5.04	95.27
38	42.8	2.301	769.45	748	2.76	5.03	93.75
38.2	42.9	2.203	721.34	752.75	-4.38	5.14	88.74
38.2	43	2.287	764.77	744	2.69	5.04	92.14
38.4	42.9	2.311	724.50	751.25	-3.72	5.37	88.83
37.9	42.8	2.296	783.78	753	3.90	4.85	94.84
38.1	42.9	2.209	738.69	743	-0.61	4.93	90.68
37.9	42.8	2.201	751.35	744	0.95	4.93	91.34
38.1	43.1	2.233	777.83	749	3.68	4.93	93.89
38	42.9	2.324	793.34	748.25	5.66	5.04	95.72

Table A- 44. 500 W BCS PEM fuel cell cooling load measurements at 25 A; Operating temperature ~40 °C, exit air 30 kPa, air stoichiometry 2, inlet hydrogen ~20-30 kPa

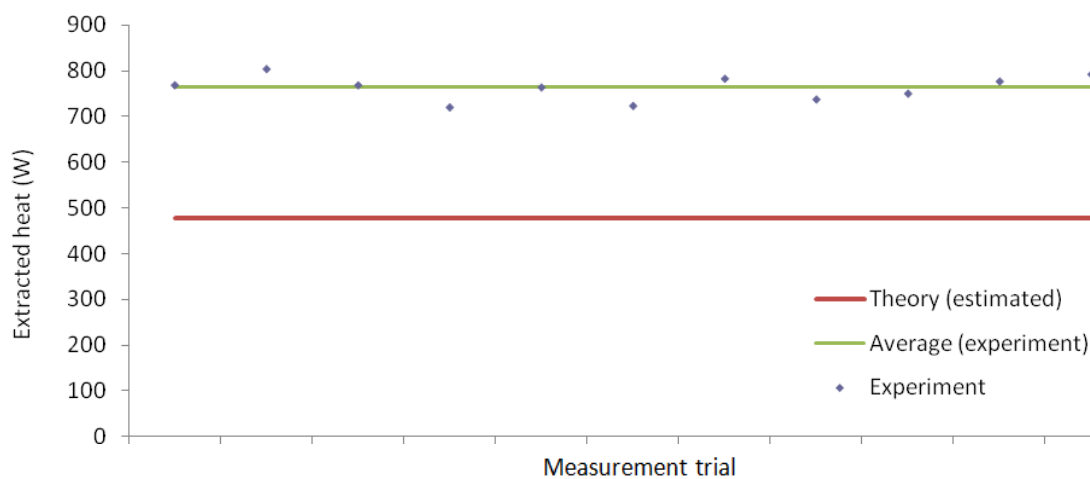


Figure A- 120. 500 W BCS PEM fuel cell cooling load measurements at 25 A; Operating temperature ~40 °C, exit air 30 kPa, air stoichiometry 2, inlet hydrogen ~20-30 kPa

25 A/500 W operating point/ Power measurement

- Operating temperature 50 °C, exit air 30 kPa, air stoichiometry 2, inlet hydrogen ~20-30 kPa
- Theoretical hydrogen consumption if fuel cell hydrogen utilisation coefficient is 100% ideally: 6.11 slpm
- Assumed hydrogen consumption rate for the theoretical calculations: 7.34 slpm (based on 20% extra hydrogen fed into the fuel cell)
- Expected power (manufacturer manual): 500 W
- Maximum uncertainty associated with the measurement instrument for voltage readings when the error for Current adjustment (25 A) is taken into account: 0.6%
- Maximum uncertainty associated with hydrogen flow meter: 1%
- Energy efficiency assumed for the theoretical calculation: 35.15%
- Hydrogen utilisation coefficient assumed in the theoretical calculations: ~85%

Voltage (V)	% of uncertainty for the voltage measurement	Power output (W)	Hydrogen consumption (slpm)	% of uncertainty for the hydrogen consumption measurement	Hydrogen utilisation coefficient (%)	Electrical energy efficiency (%)
18.08	±0.33	452	6.25	±0.18	97.76	37.32
17.99	±0.33	449.75	6.2	±0.18	98.55	37.43
17.89	±0.33	447.25	6.28	±0.18	97.29	36.75
17.51	±0.34	437.75	6.27	±0.18	97.45	36.03
17.92	±0.33	448	6.23	±0.18	98.07	37.11
17.47	±0.34	436.75	6.2	±0.18	98.55	36.35
17.97	±0.33	449.25	6.27	±0.18	97.45	36.98
18.15	±0.33	453.75	6.3	±0.18	96.98	37.17
17.85	±0.33	446.25	6.24	±0.18	97.92	36.90
17.73	±0.34	443.25	6.32	±0.18	96.68	36.19
17.56	±0.34	439	6.25	±0.18	97.76	36.25
18.17	±0.33	454.25	6.21	±0.18	98.39	37.75
17.94	±0.33	448.5	6.19	±0.18	98.71	37.39
17.87	±0.33	446.75	6.18	±0.19	98.87	37.30

Table A- 45. 500 W BSC PEM fuel cell power and hydrogen consumption measurement at 25 A; Operating temperature ~50 °C, exit air 30 kPa, air stoichiometry 2, inlet hydrogen ~20-30 kPa

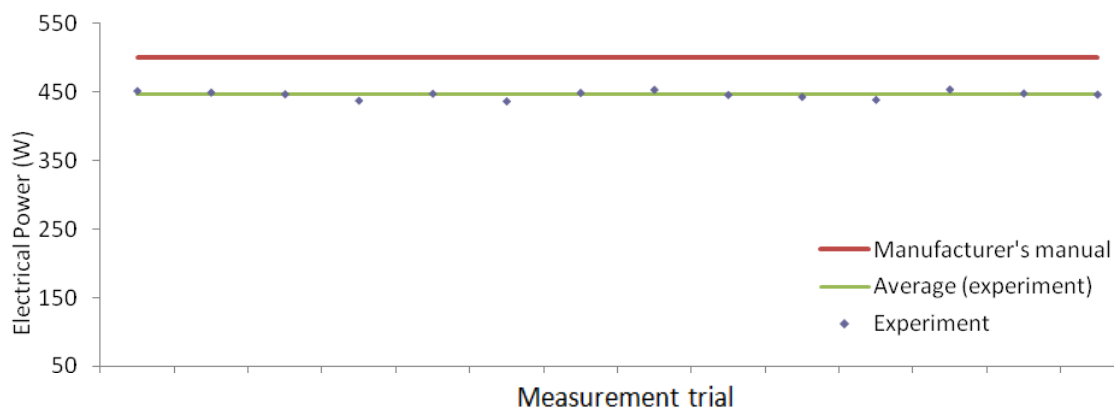


Figure A- 121. 500 W BSC PEM fuel cell power measurements at 25 A; Operating temperature ~50 °C, exit air 30 kPa, air stoichiometry 2, inlet hydrogen ~20-30 kPa

25 A/500 W operating point/ Cooling load measurement

- Operating temperature 50 °C, exit air 30 kPa, air stoichiometry 2, inlet hydrogen ~20-30 kPa
- Theoretically estimated cooling load at the ideal operating condition recommended by the manufacturer: 478W

Note:

- The estimated cooling load at the experimental operating condition (the following table) is found by considering: fuel cell heat used for water evaporation, heat removal by the extra reactants, the convection heat transfer from the body of the fuel cell, and the power drop compared to the ideal condition

Fuel cell inlet water temperature (°C)	Fuel cell exit water temperature (°C)	Water flow rate (litre/min)	Measured cooling load (W)	Estimated cooling load (W)	Experimental error (%)	Estimated uncertainty (%)	CHP energy efficiency (%)
48	52.6	2.204	706.31	689	2.45	±5.74	95.64
48.3	52.8	2.264	709.76	691.25	2.61	±5.88	96.51
48.2	52.9	2.284	747.86	693.75	7.24	±5.63	98.21
48.1	52.8	2.198	719.70	703.25	2.29	±5.63	95.26
48.3	52.8	2.128	667.13	693	-3.88	±5.88	92.37
48.1	52.6	2.126	666.50	704.25	-5.66	±5.87	91.83
47.9	52.9	2.084	725.93	691.75	4.71	±5.30	96.72
48	53	2.005	698.41	687.25	1.60	±5.31	94.38
47.9	53	1.917	681.11	694.75	-2.00	±5.20	93.23
47.9	52.8	2.018	688.88	697.75	-1.29	±5.40	92.44
48	53.1	1.924	683.60	702	-2.69	±5.21	92.69
48.3	53.2	1.921	655.77	686.75	-4.72	±5.42	92.24
48.4	53.3	2.078	709.36	692.5	2.38	±5.43	96.53
47.9	53	1.905	676.85	694.25	-2.57	±5.20	93.82

Table A- 46. 500 W BSC PEM fuel cell cooling load measurements at 25 A; Operating temperature ~50 °C, exit air 30 kPa, air stoichiometry 2, inlet hydrogen ~20-30 kPa

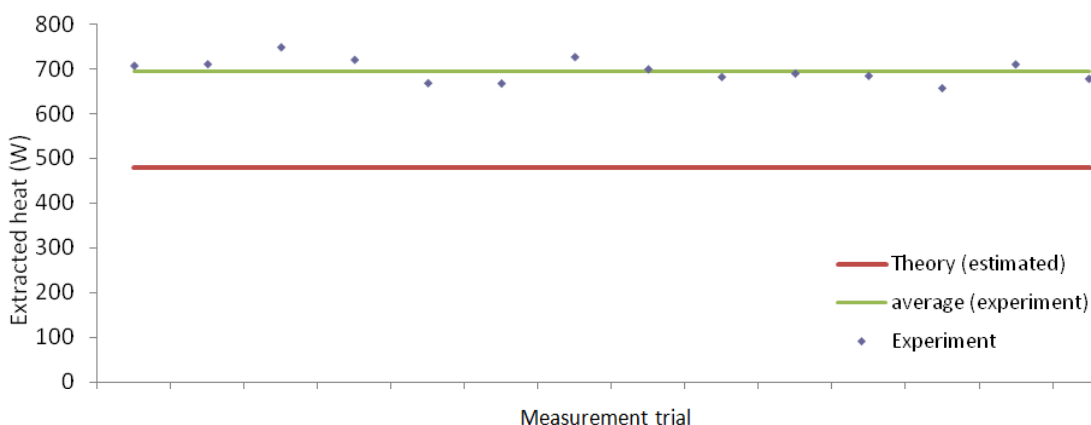


Figure A- 122. 500 W BSC PEM fuel cell cooling load measurements at 25 A; Operating temperature ~50 °C, exit air 30 kPa, air stoichiometry 2, inlet hydrogen ~20-30 kPa

25 A/500 W operating point/ Power measurement

- Operating temperature 60 °C, exit air 30 kPa, air stoichiometry 2, inlet hydrogen ~20-30 kPa
- Theoretical hydrogen consumption if fuel cell hydrogen utilisation coefficient is 100% ideally: 6.11 slpm
- Assumed hydrogen consumption rate for the theoretical calculations: 7.34 slpm (based on 20% extra hydrogen fed into the fuel cell)
- Expected power (manufacturer manual): 500 W
- Maximum uncertainty associated with the measurement instrument for voltage readings when the error for Current adjustment (25 A) is taken into account: 0.6%
- Maximum uncertainty associated with hydrogen flow meter: 1%
- Energy efficiency assumed for the theoretical calculation: 35.15%
- Hydrogen utilisation coefficient assumed in the theoretical calculations: ~85%

Voltage (V)	% of uncertainty for the voltage measurement	Power output (W)	Hydrogen consumption (slpm)	% of uncertainty for the hydrogen consumption measurement	Hydrogen utilisation coefficient (%)	Electrical energy efficiency (%)
18.39	±0.42	459.75	6.28	±0.14	97.29	37.78
18.51	±0.42	462.75	6.23	±0.14	98.03	38.31
18.03	±0.43	450.75	6.27	±0.14	97.53	37.13
18.47	±0.42	461.75	6.26	±0.14	97.54	38.04
18.66	±0.41	466.5	6.25	±0.14	97.74	38.51
18.43	±0.42	460.75	6.23	±0.14	98.01	38.14
18.34	±0.42	458.5	6.30	±0.14	97.06	37.59
17.83	±0.43	445.75	6.23	±0.14	98.01	36.90
18.32	±0.42	458	6.30	±0.14	96.97	37.51
18.49	±0.42	462.25	6.30	±0.14	97.03	37.88

Table A- 47. 500 W BSC PEM fuel cell power and hydrogen consumption measurement at 25 A; Operating temperature ~60 °C, exit air 30 kPa, air stoichiometry 2, inlet hydrogen ~20-30 kPa

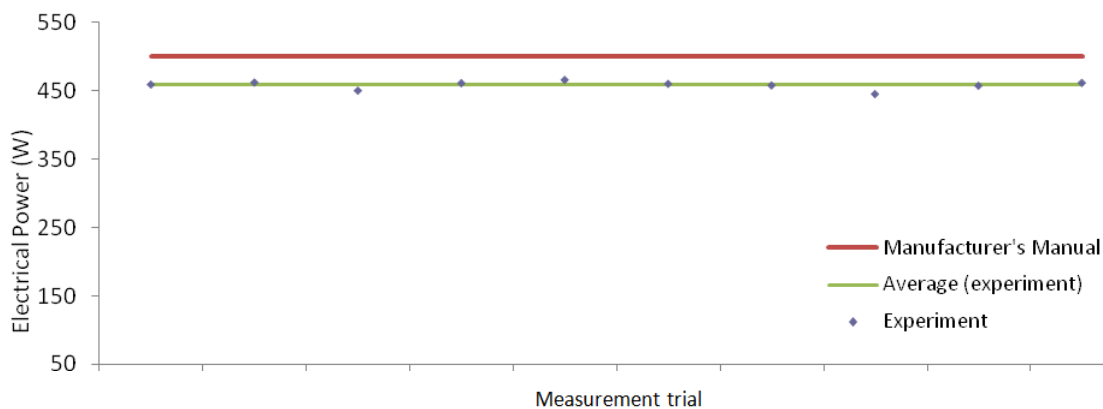


Figure A- 123. 500 W BSC PEM fuel cell power measurements at 25 A; Operating temperature ~60 °C, exit air 30 kPa, air stoichiometry 2, inlet hydrogen ~20-30 kPa

25 A/500 W operating point/ Cooling load measurement

- Operating temperature 60 °C, exit air 30 kPa, air stoichiometry 2, inlet hydrogen ~20-30 kPa
- Theoretically estimated cooling load at the ideal operating condition recommended by the manufacturer: 478W

Note:

- The estimated cooling load at the experimental operating condition (the following table) is found by considering: fuel cell heat used for water evaporation, heat removal by the extra reactants, the convection heat transfer from the body of the fuel cell, and the power drop compared to the ideal condition

Fuel cell inlet water temperature (°C)	Fuel cell exit water temperature (°C)	Water flow rate (litre/min)	Measured cooling load (W)	Estimated cooling load (W)	Experimental error (%)	Estimated uncertainty (%)	CHP energy efficiency (%)
59.1	62.4	2.128	489.23	483.25	1.22	±8.68	77.98
59.4	62.7	2.101	483.02	480.25	0.57	±8.70	78.30
59.2	62.6	2.144	507.84	492.25	3.07	±8.44	78.96
59.3	62.3	2.175	454.58	481.25	-5.87	±9.54	75.49
59	62.4	2.163	512.34	476.5	7.00	±8.43	80.81
59.2	62.3	2.078	448.78	482.25	-7.46	±9.24	75.29
59.2	62.7	2.001	487.91	484.5	0.70	±8.21	77.58
59.1	62.5	2.182	516.84	497.25	3.79	±8.43	79.68
59.4	62.6	2.123	473.29	485	-2.47	±8.97	76.27
59.2	62.8	2.113	529.94	480.75	9.28	±7.99	81.31

Table A- 48. 500 W BSC PEM fuel cell cooling load measurements at 25 A; Operating temperature ~60 °C, exit air 30 kPa, air stoichiometry 2, inlet hydrogen ~20-30 kPa

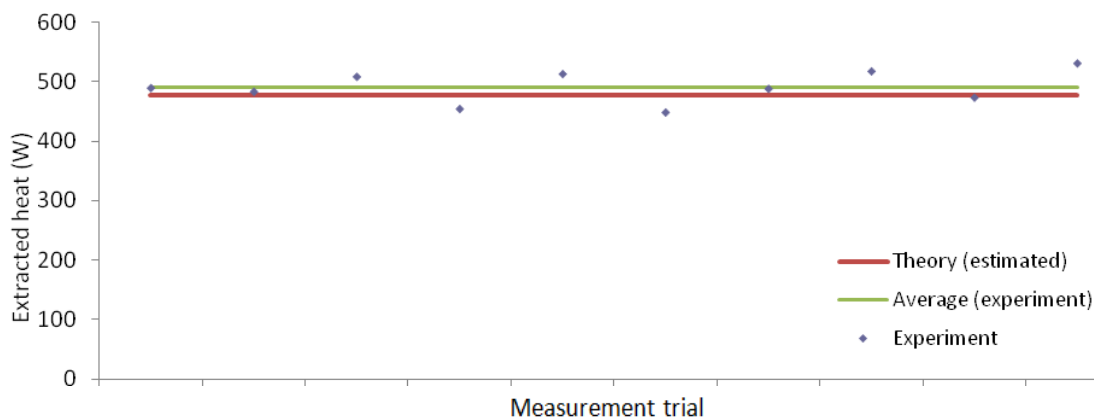


Figure A- 124. 500 W BSC PEM fuel cell cooling load measurements at 25 A; Operating temperature ~60 °C, exit air 30 kPa, air stoichiometry 2, inlet hydrogen ~20-30 kPa

Appendix 3: Equipment datasheets

1- SX320 bp solar datasheet



SX 320

20 Watt Photovoltaic Module

High-efficiency photovoltaic module using silicon nitride multicrystalline silicon cells.

Performance

Rated power (P_{max})	20W
Power tolerance	± 10%
Nominal voltage	12V
Limited Warranty ¹	12 years

Configuration

- M** Multimount frame with lo-pro J-Box and output cable
- J** Clear universal frame and standard J-Box

Electrical Characteristics²

SX320

Maximum power (P_{max}) ³	20W
Voltage at Pmax (V_{mp})	16.8V
Current at Pmax (I_{mp})	1.19A
Warranted minimum P_{max}	18W
Short-circuit current (I_{sc})	1.29A
Open-circuit voltage (V_{oc})	21.0V
Temperature coefficient of I_{sc}	(0.065±0.015)%/ °C
Temperature coefficient of V_{oc}	-(80±10)mV/°C
Temperature coefficient of power	-(0.5±0.05)%/ °C
NOCT (Air 20°C; Sun 0.8kW/m ² ; wind 1m/s)	47±2°C
Maximum series fuse rating	3A
Maximum system voltage	50V (US NEC rating) 50V (IEC 61215 rating)


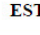




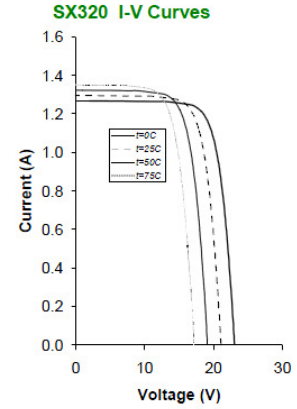
Mechanical Characteristics

Dimensions	M	Length: 421mm (16.6")	Width: 501mm (19.7")	Depth: 23mm (0.9")
	J	Length: 425mm (16.7")	Width: 502mm (19.7")	Depth: 50mm (1.97")
Weight	M	2.5 kg (5.5 pounds)		
	J	3.0 kg (6.6 pounds)		
Solar Cells	36 cells (38mm x 114mm) in a 4x9 matrix connected in series			
Junction Box	J	J-Version junction box with 4-terminal connection block; IP 65, accepts PG 13.5, M20, ½ inch conduit, or cable fittings accepting 6-12mm diameter cable. Terminals accept 2.5 to 10mm ² (8 to 14 AWG) wire		
Output Cables	M	AWG# 18 (0.75mm ²) 2 core ITC/PLTC; length - 4572mm		
Construction	Front: High-transmission 3mm (1/8 th inch) tempered glass; Back: Polyester; Encapsulant: EVA			
Frame	M	Clear anodized aluminum alloy type 6063T6 Multimount frame; Color: silver		
	J	Clear anodized aluminum alloy type 6063T6 Universal frame; Color: silver		

- Module Warranty: 12-year limited warranty of 90% power output; 2-year limited warranty of materials and workmanship. See your local representative for full terms of these warranties.
- These data represent the performance of typical BP modules, and are based on measurements made in accordance with ASTM E1036 corrected to SRC (STC).
- During the stabilization process that occurs during the first few months of deployment, module power may decrease by approx. 1% from typical P_{max} .

Quality and Safety

	Manufactured in ISO 9001-certified factories; conforms to European Community Directives; certified to IEC 61215
	Module power measurements calibrated to World Radiometric Reference through ESTI (European Solar Test Installation at Ispra, Italy)
	Listed by Underwriter's Laboratories for electrical and fire safety (Class C fire rating)
	Approved by Factory Mutual Research in NEC Class 1, Division 2, Groups C & D hazardous locations.

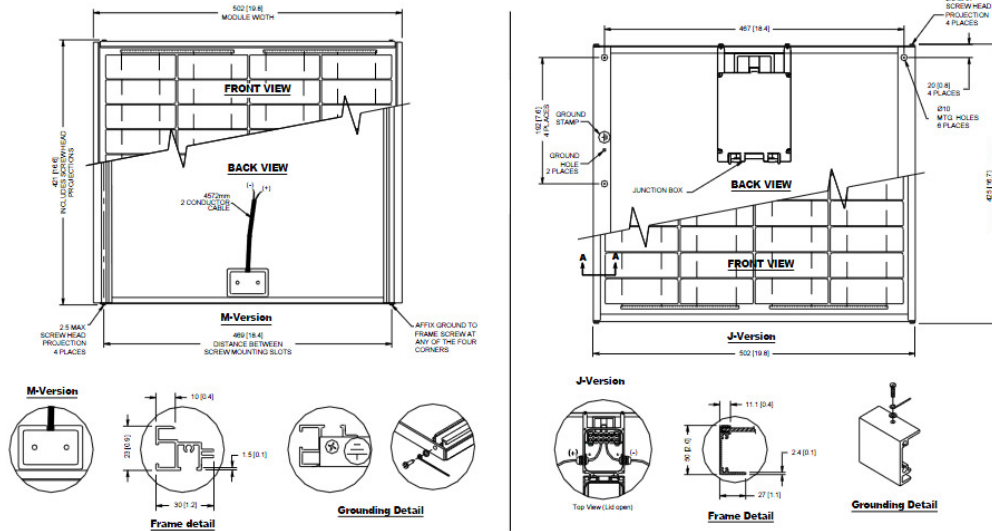


Qualification Test Parameters

Temperature cycling range	-40°C to +85°C (-40°F to 185°F)
Humidity freeze, damp heat	85% RH
Static load front and back (e.g. wind)	2,400 pa (50psf)
Front loading (e.g. snow)	5,400 pa (113psf)
Hailstone impact	25mm Ø (1 inch) at 23 m/s (52mph)

Module Diagram

Dimensions in brackets are in inches. Un-bracketed dimensions are in millimeters. Overall tolerances ±3mm (1/8")



Included with each module: self-tapping grounding screw (J-Version), instruction sheet, and warranty document.

Note: This publication summarizes product warranty and specifications, which are subject to change without notice. Additional information may be found on our web site: www.bpsolar.com



2- bp275 PV module datasheet



BP SOLAR

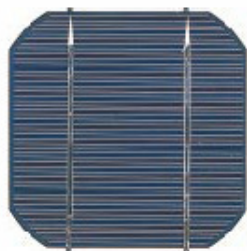
SOLAR MODULES

BP280F & BP275F

SOLAR MODULES

PRODUCT FEATURES

- High efficiency monocrystalline silicon cells.
- Designed for maximum reliability and minimum maintenance.
- Produced using in-house technology in cell manufacturing and encapsulation.
- Highly resistant to water, abrasion, hail impact and other environmental factors.
- Lightweight anodised aluminium frame or laminate version only.
- All proven products. Only materials with extensive field experience used.
- Designed and manufactured to comply with European and International standards. European specification EST1503.
- 20 year product warranty



CELL SPECIFICATIONS

36 series connected, 125 mm monocrystalline silicon pseudo square cells.



APPLICATIONS

GRID-CONNECT

- Rain-screen Facades
- Sun-shade & Balcony Products
- Roofing Products
- Domestic/Residential Roof Products
- Multi-Kilowatt and Megawatt Power Stations
- Generator-type Power for centralised locations.

TELECOMS

- Microwave Repeaters and Terminals
- VHF/UHF Radio Systems and Repeaters
- Mobile Radio Systems
- HF/SB Radio Transceivers
- TV Translators
- Radio Telephones & Telemetry
- Radio Navigational Aids
- Fibre Optic Repeaters
- Miscellaneous Packages DC Loads

RURAL INFRASTRUCTURE

- Community/Village Water Pumping
- Community/Village Water Purification
- Community/Village Refrigeration, Medical and Domestic
- Community/Village Lighting
- Community/Village Television & Video
- Individual House Power
- Community/Village Power

SPECIALIST

- Cathodic Protection
- Aircraft Obstruction Lighting
- Lighthouse Lighting Systems
- Racon Systems
- Beacon Buoy Lighting Systems
- Fog Warning Systems

TECHNICAL SPECIFICATIONS

Module Catalogue Number	BP280	BP275
Nominal Peak Power (Pmax)	80.00W	75.00W
Voltage @ maximum power (V mp)	17.00V	17.00V
Current @ maximum power (I mp)	4.70A	4.45A
Short-circuit current (I sc)	5.0A	4.75A
Open-circuit Voltage (V oc)	21.8V	21.40V

Dimensions		F=Framed L=Laminate
BP275/280F	Length 1188 mm	Width 530 mm
	Depth 43.5 mm	Weight 7.5 kg
BP275/280L	Length 1183 mm	Width 525 mm
	Depth 4 mm (±1 mm)	Weight 5.5 kg



HIGH EFFICIENCY BP280F/BP275F MODULES

POWER SPECIFICATIONS

All performance specifications given are as measured at the standard test conditions.

VOLTAGE/CURRENT CURVE (Nominal)

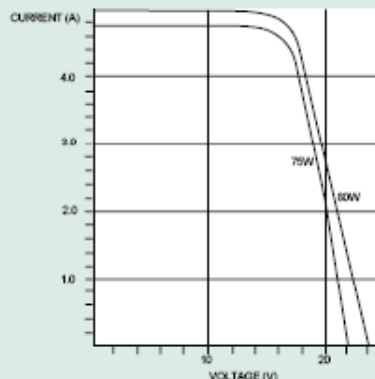
The graph below details module performance at an insolation of 1000 W/m², air mass 1.5 D

Standard Test Conditions

Description	Parameter	Value
Intensity of Illumination	Insolation (W/m ²)	1000
Spectral Density	Air Mass (AM)	1.5
Operating Temperature	Cell Temperature (°C)	25

Description of performance parameters

P _{max}	Maximum power of a module. The point on the curve where the IV is at a maximum
V _{mp}	Voltage at the maximum power point
I _{mp}	Current at the maximum power point
I _{sc}	The short circuit current of a PV module
V _{oc}	The open circuit voltage of a PV module
P _{min}	Minimum guaranteed power of a module



Tolerance – Minimum power, the peak power of all high power modules is normally supplied within minus 5watts actual of the nominal value, for further details contact BP Solar.

Coefficient of Voltage -0.0022 V/cell/°C

Coefficient of Current 8.9 mA/km²/°C

CEC APPROVAL SPECIFICATION NO.503

BP Solar modules have been tested and qualified to the Commission of European Communities specification number 503 at the CEC Joint Research Centre in Ispra, Italy. The qualification tests are designed to demonstrate the module's suitability for use in field conditions.

- 200 thermal cycles from -40°C to 85°C.
- 10 humidity/freeze cycles from 85°C at 85% relative humidity to -40°C.
- Ice ball impact test.
- Ultra violet exposure.
- Outdoor exposure.
- Damp heat.
- Hot spot endurance (to simulate partial shading).
- Mechanical endurance, to simulate wind loads of up to 225 km/h.

Power specifications are measured at Standard BP Solar Test Conditions. For further information on module performance contact BP Solar.

Approved by TÜV Rheinland Group for use as Class II equipment, Schutzklasse II.

CONSTRUCTION

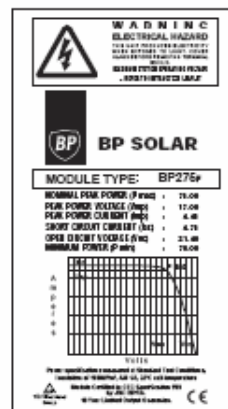
BP280 & BP275 modules are manufactured using industry-standard materials and lamination techniques. Stainless steel fasteners are used throughout. The junction box is bonded directly to the laminate to facilitate both framed and laminate only module products.

Materials are as follows:

- Front Cover: Toughened glass, 3mm, high light transmission (c 92%)
- Encapsulant: Ethylene-vinyl-acetate (EVA)
- Rear Cover: Tri-laminate of PVF/Polyester/PVF
- Frame: Extruded Aluminium, Anodised
- Frame Sealant: High strength bonding tape
- Junction Box: Glass filled polycarbonate

Electrical connections to the module are made via screw terminals within the junction box. One cable gland is fitted and 3 further knockouts (suitable for glands or conduit) are provided to facilitate series and/or parallel connection.

Rear Module Label



Home

Branches

Catalogue



Appendix 4: Solar geometry angles

1- Declination angle (δ)

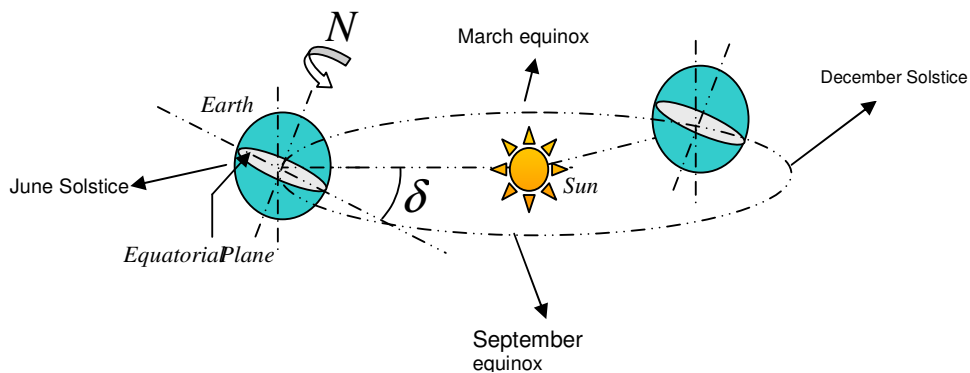


Figure A- 125. Declination angle

2- Solar altitude (a) and solar azimuth (α) angles

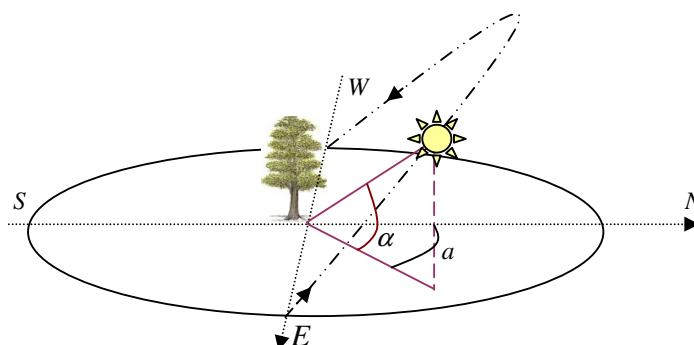


Figure A- 126. Solar altitude and azimuth

3- Array slope angle (β) and array azimuth angle (a_p)

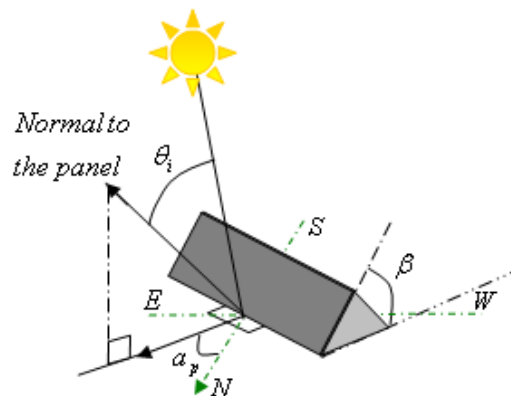


Figure A- 127. Array azimuth and slope angles

Appendix 5: Thermodynamic properties as functions of temperature

	Molar specific heat (J/mol. °K)	Accuracy
Water (Steam)	$\bar{c}_{p,H_2O} = 143.05 - 58.040T^{0.25} + 8.2751T^{0.5} - 0.036989T$	0.43% 300-3500°K
Hydrogen	$\bar{c}_{p,H_2} = 56.505 - 22222.6T^{-0.75} + 116500T^{-1} - 560700T^{-1.5}$	0.6 % 300-3500 °K
Oxygen	$\bar{c}_{p,O_2} = 37.342 + 2.0102 \times 10^{-5}T^{1.5} - 178570T^{-1.5} + 2368800T^{-2}$	0.3 % 300-3500 °K
Nitrogen	$\bar{c}_{p,N_2} = 39.060 - 512790T^{-1.5} + 10727000T^{-2} - 820400000T^{-3}$	0.43 % 300-3500 °K

Table A- 49. Molar specific heat functions for water, hydrogen, oxygen and nitrogen (Sonntag *et al.* 2003)

	Enthalpy of formation (J/mole)
Water (Steam)	$\bar{h}_{f,H_2O} = 143.05T - 46.432T^{1.25} + 5.5167T^{1.5} - 0.01849T^2 - 253719.49$
Hydrogen	$\bar{h}_{f,H_2} = 56.505T - 88890.4T^{0.25} + 116500LnT + 1121400T^{-0.5} - 376189.944$
Oxygen	$\bar{h}_{f,O_2} = 37.342T + 8.0408 \times 10^{-6}T^{2.5} + 357140T^{-0.5} - 2368800T^{-1} - 23884.22$
Nitrogen	$\bar{h}_{f,N_2} = 39.060T + 1025580T^{-0.5} - 10727000T^{-1} + 410200000T^{-2} - 39677.027$

Table A- 50. Enthalpy of formation functions for water, hydrogen, oxygen and nitrogen (Sonntag *et al.* 2003)

	Enthalpy of formation (J/mole. °K)
Water (Steam)	$\bar{s}_{H_2O} = 63.75 + 143.05 \ln T - 232.16T^{0.25} + 16.55T^{0.5} - 0.036989T$
Hydrogen	$\bar{s}_{H_2} = -286.76 + 56.505 \ln T + 29630.13T^{-0.75} - 116500T^{-1} + 373800T^{-1.5}$
Oxygen	$\bar{s}_{O_2} = 37.342 \ln T + 1.34013 \times 10^{-5}T^{1.5} + 119046.667T^{-1.5} - 1184400T^{-2} - 17.48$

Table A- 51. Molar entropy of the contributing components water, hydrogen, and oxygen (Sonntag *et al.* 2003)

Appendix 6: Error analysis

➤ Fuel cell voltage

Below is an example of calculating the uncertainties for the fuel cell voltage measurements and comparing the results with the accuracy range of the measurement instrument:

15 A operating point, operating temperature 50 °C, exit air pressure 30 kPa, air stoichiometry 2, inlet hydrogen pressure 20-30 kPa

Measured voltage (V)	19.84	19.55	19.49	19.66	19.61	19.5	19.48	19.65	19.58	19.6

$$u(V)\% = \frac{u(V)}{\bar{V}} = \frac{\pm \sqrt{\frac{\sum_{i=1}^n (V_i - \bar{V})^2}{n(n-1)}}}{\bar{V}} = \pm 0.17\%$$

Comparing this with the figure given in table 5-6 ($\pm 0.2\%$) it is found that the obtained uncertainty calculated using the experimental data at this operating point (15 A) and condition is within the range of the accuracy given for the electronic load in its manual (table 5-6).

➤ Hydrogen utilisation coefficient/hydrogen consumption rate

Below is an example of calculating the uncertainty percentage of hydrogen flow rate (hydrogen utilisation coefficient).

5A operating point, operating temperature 40 °C, exit air pressure 30 kPa, air stoichiometry 4, inlet hydrogen pressure 20-30 kPa

Measured hydrogen flow rate (slpm)	1.32	1.33	1.35	1.32	1.354	1.335	1.32	1.336	1.33

$$\bar{V}^{\bullet} = 1.333 \text{ slpm}$$

$$u(V^{\bullet}) = \pm \sqrt{\frac{\sum_{i=1}^n (V_i^{\bullet} - \bar{V}^{\bullet})^2}{n(n-1)}} = \pm \sqrt{\frac{\sum_{i=1}^n (V_i^{\bullet} - 1.333)^2}{9(9-1)}} = \pm 0.004196 \text{ or } \pm 0.004$$

Then the percentage of the uncertainty for the mean value is:

$$u(V^{\bullet})\% = \frac{u(V^{\bullet})}{V^{\bullet}} = \frac{\pm 0.004196}{1.333} = \pm 0.31\%$$

This is well within the $\pm 1\%$ range of error (table 5-1), given in the manufacturer's manual of the flow meter. The errors associated with the other measured points are also within this $\pm 1\%$ accuracy range.

➤ *Cooling load*

The cooling load is not measured directly by a particular measurement instrument and it is calculated using a few other measured values including the fuel cell inlet and exit coolant temperatures and the coolant flow rate. That is why for the fuel cell cooling load at different operating points and conditions the combined uncertainty is calculated. Below is an example to show how the accuracies of the measurements are calculated for the case of the fuel cell experimental cooling load at 5A operating point when the operating temperature is about 40 °C, the exit air pressure is 30 kPa, the air stoichiometry is 4, and the inlet hydrogen pressure is about 20-30 kPa (Table A- 52).

Fuel cell inlet temperature (°C)	Fuel cell exit temperature (°C)	Cooling water flow rate (litre/min)	Experimental Cooling load (W)	Experimental Error (%)	Estimated Max Uncertainty (%)
40.8	42.5	0.874	103.51	2.91	±14.12
40.4	42.3	0.801	106.02	6.96	±12.61
40	41.8	0.821	102.95	4.57	±13.24
39.9	41.7	0.813	101.95	4.07	±13.23
39.8	41.5	0.824	97.58	-0.78	±13.98
39.6	41.3	0.874	103.51	4.36	±13.96
39.5	41.2	0.846	100.19	2.09	±13.94
39.4	41.1	0.857	101.49	3.94	±13.93
39.5	41.2	0.839	99.36	-0.84	±13.94

Table A- 52. Measured values to calculate the cooling load of the fuel cell at 5A operating point when the operating temperature is about 40 °C, the exit air pressure is 30 kPa, the air stoichiometry is 4, and the inlet hydrogen pressure is 20-30 kPa

Sample calculation:

This sample calculation is for the first row of the measured data in Table A- 52. The involving parameters here are:

$x_1 = \text{Fuel cell inlet temperature } (^\circ\text{C})$

$x_3 = \text{Fuel cell coolant flow rate (litre / min)}$

$x_2 = \text{Fuel cell exit temperature } (^\circ\text{C})$

Q is the heat extracted from the fuel cell through the water cooling system (fuel cell cooling load). Q is a function of the above-mentioned parameters (1 litre of water = 1 kg):

$$Q = f(x_1, x_2, x_3) = \frac{x_3}{60} \times 4180 \times (x_2 - x_1)$$

Table A- 52 (the measured data) and table 5-4 (the accuracy of the concerned measurement instruments) are used to calculate the uncertainties associated with each of the contributing parameters:

$$u(x_1) = \pm(0.1 + 0.00167 x_1) ^\circ\text{C} = \pm 0.168 ^\circ\text{C}$$

$$u(x_2) = \pm(0.1 + 0.00167 x_2) ^\circ\text{C} = \pm 0.17 ^\circ\text{C}$$

$$u(x_3) = \frac{1}{100} x_3 = \pm 0.009 \text{ litre / min}$$

By substituting these uncertainties into the equation (5-3) the combined uncertainty associated with the calculated heat load is:

$$u(Q) = \pm \sqrt{\sum_{i=1}^N \left[\left(\frac{\partial f}{\partial x_i} \right)^2 \cdot u^2(x_i) \right]}$$

$$u(Q) = \pm \sqrt{\left(\frac{4180}{60} \right)^2 \left[(-x_3)^2 \cdot u^2(x_1) + x_3^2 \cdot u^2(x_2) + (x_2 - x_1)^2 \cdot u^2(x_3) \right]}$$

$$u(Q) = \pm \sqrt{\left(\frac{4180}{60} \right)^2 \left[(-0.874)^2 \times 0.0282 + 0.874^2 \times 0.0289 + (42.5 - 40.8)^2 \times 0.00008 \right]}$$

$$u(Q) = \pm 69.6 \times \sqrt{0.02155 + 0.02207 + 0.0002312} = \pm 14.57 \text{ W}$$

So the percentage of uncertainty comes to:

$$u(Q)\% = \frac{u(Q)}{Q} = \pm \frac{14.57}{103.51} = \pm 14.1\%$$

Obviously the low accuracy of the temperature probes relative to the flow meter accounts for the lion share of this uncertainty. Also the calibration of the digital display connected to the flow meter is another obvious source of error for the readings. The above-obtained uncertainty figure explains the difference between the theoretical and experimental values obtained/calculated for the cooling load of the fuel cell. In most measured points this difference is well within the predicted range of uncertainty. For the given example, the difference between the theoretical and the experimental cooling load is 9.8 W. It has to be noted that an approximate heat transfer from the body of the fuel cell was considered, the experimental fuel cell polarisation curve was fed into the model to estimate the cooling load, the heat removal from the fuel cell through the excess flow of reactants was taken into account, and the water product was assumed to be in liquid form at such a low operating temperature. This difference (9.8 W) agrees with 14.6 W, the maximum uncertainty calculated for this point.

Appendix 7: Components used in the 500-W fuel cell experimental rig

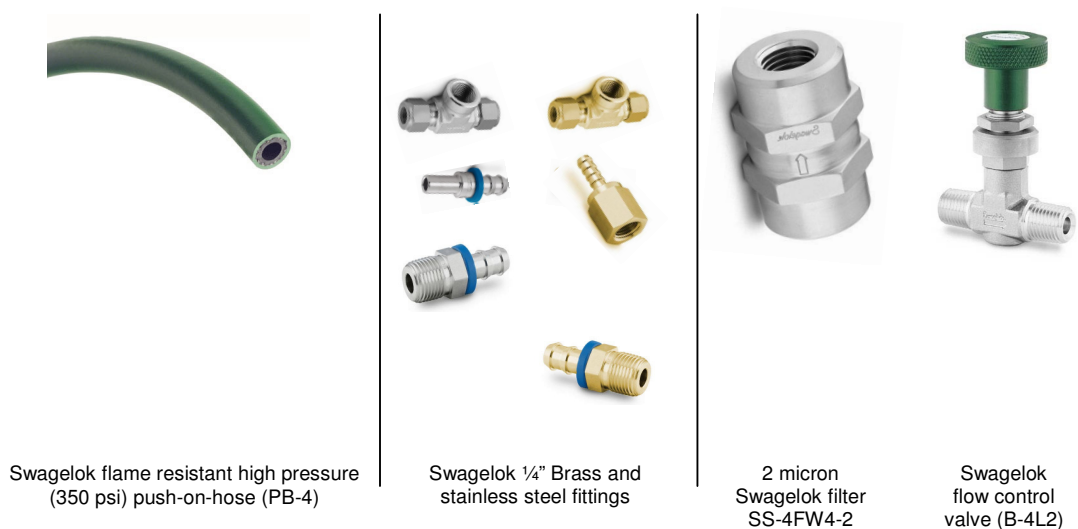


Figure A- 128. Swagelok parts used for putting the hydrogen line together (Swagelok 2008)



Direct acting 2//2-way normally closed solenoid valve
 For use with neutral and aggressive gases and fluids e.g. compressed air, town and natural gas, water, hydraulic oil, vacuum
 Coil orientation can be varied through 360° to facilitate wiring. Installation preferable with coil uppermost
 Moulded-in cable - 3m length
 Protective rating: IP65
 Maximum viscosity: 21mm²/s

Figure A- 129. Stainless steel 24V AC/DC, 0-1000 kPa intrinsically safe solenoid valve, type 6013 ATEX - Supplier: RS Australia, RS stock number: 410-5165 (RSAustralia 2009)



Figure A- 130. Handheld hydrogen detector to check the hydrogen line for leakage (Fuelcellstore 2009)



Figure A- 131. Oil-free Swagelok pressure gauge (Swagelok 2008) - Part No: PGI-50M-PG30-LAOX



Figure A- 132. C100 model mass flow controller from Procon Instrument Technology (Sierra) used in the hydrogen line (C100 user manual)

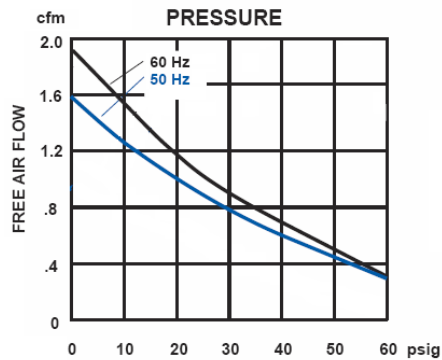


Figure A- 133. Cole-Parmer oil-less air compressor , model : CZ-07054-23 used for supplying air to the 500 W fuel cell (ColeParmer 2009)



Figure A- 134. 810C model Procon Instrument Technology (Sierra) mass flow meter and controller used in the air line (McMillan 2009)

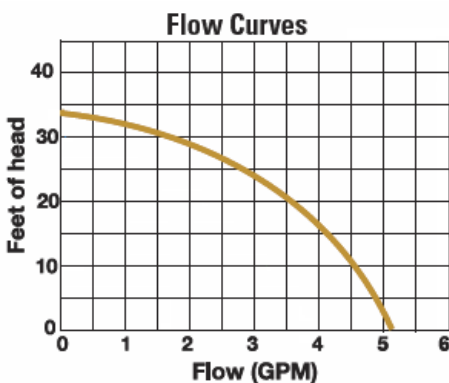


Figure A- 135. The water pump (Cole Parmer Catalogue: 72008-30), used in the fuel cell cooling system (ColeParmer 2009)



Figure A- 136. Flow meters for measuring the fluid flow rates of the heat exchanger (left) (ColeParmer 2009) and 220 Mcmillan model display (right) (McMillan 2009)

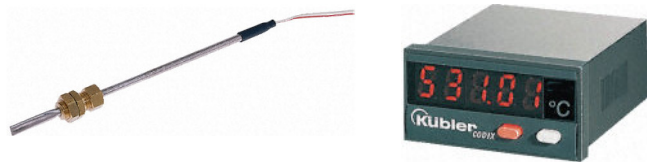


Figure A- 137. Pt100 temperature probe (left); Kubler temperature display (right); used for temperature reading (RSAustralia 2009)

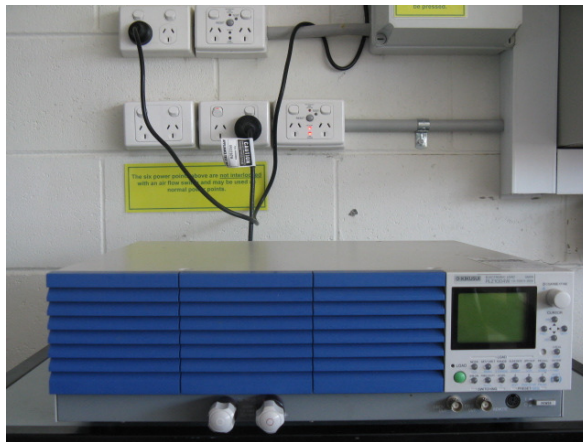


Figure A- 138. Kikusui PLZ1004W electronic load